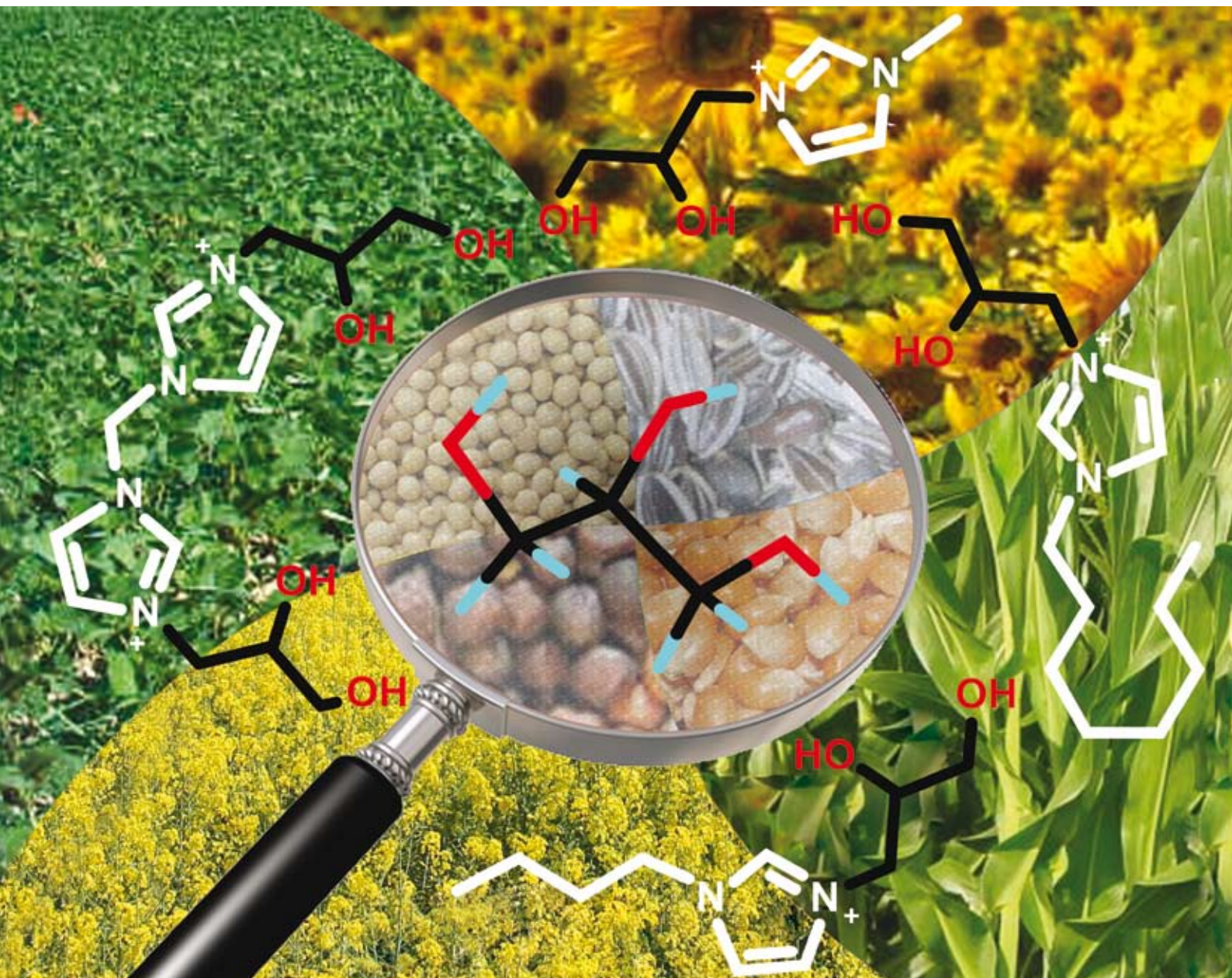


Green Chemistry

Cutting-edge research for a greener sustainable future

www.rsc.org/greenchem

Volume 11 | Number 5 | May 2009 | Pages 593–740



Themed Issue: Green Solvents - Progress in Science and Application

ISSN 1463-9262

Chiappe *et al.*
Glycerylimidazolium based ionic liquids

Behr and Leschinski
Application of water in two-phase
telomerisation

Gubicza *et al.*
Microwave assisted enzymatic
esterification
Thomas *et al.*
Dynamic kinetic resolution of
rac-1-phenylethanol in scCO_2

RSC Publishing



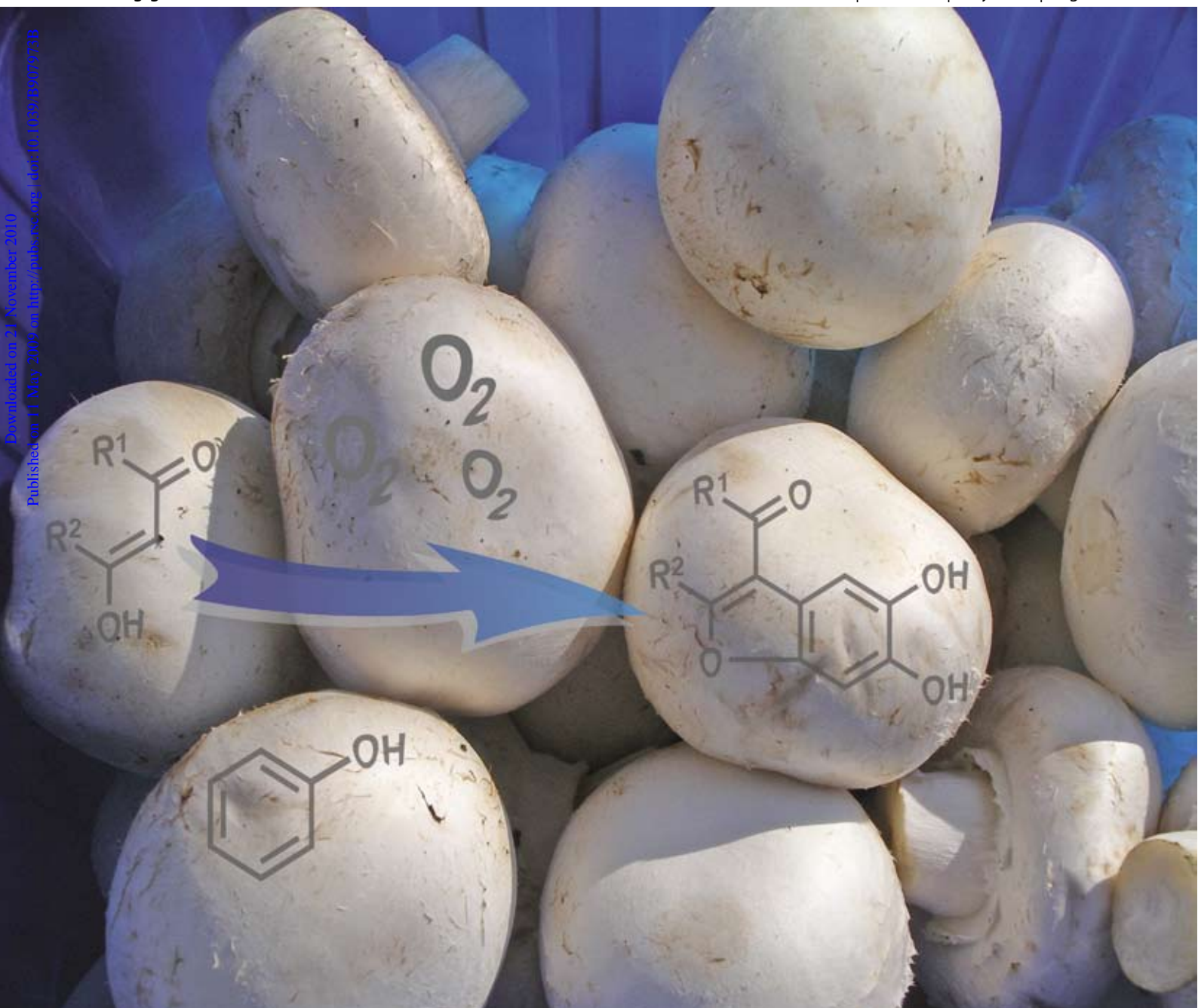
1463-9262(2009)11:3;1-B

Green Chemistry

Cutting-edge research for a greener sustainable future

www.rsc.org/greenchem

Volume 11 | Number 5 | May 2009 | Pages 593–740



Downloaded on 21 November 2010
Published on 11 May 2009 on http://pubs.rsc.org | doi:10.1039/B907973B

ISSN 1463-9262

RSC Publishing

Beifuss *et al.*
Domino reaction catalyzed by *Agaricus bisporus*
Ley *et al.*
Transfer hydrogenation of ketones as a continuous flow process

Dorgan *et al.*
Surface esterification of nanoparticles
Franco *et al.*
New green lubricating grease formulations

Green Chemistry

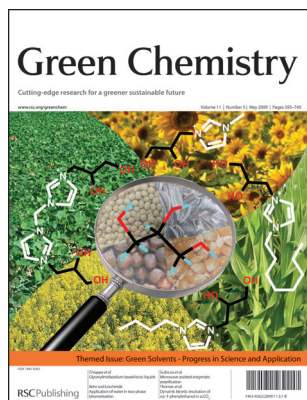
Cutting-edge research for a greener sustainable future

www.rsc.org/greenchem

RSC Publishing is a not-for-profit publisher and a division of the Royal Society of Chemistry. Any surplus made is used to support charitable activities aimed at advancing the chemical sciences. Full details are available from www.rsc.org

IN THIS ISSUE

ISSN 1463-9262 CODEN GRCHFJ 11(5) 593–740 (2009)



Cover

See Chiappe *et al.*, pp. 622–629. Illustration shows different sources of glycerol from which a promising class of task-specific ionic liquids can be obtained. Image reproduced with permission from Cinzia Chiappe from *Green Chem.*, 2009, **11**, 622.



Inside cover

See Beifuss *et al.*, pp. 676–679. *Agaricus bisporus* as a cheap source of tyrosinase and laccase to be used in combination for the catalysis of oxidative domino processes. Image reproduced with permission from Uwe Beifuss from *Green Chem.*, 2009, **11**, 676.

CHEMICAL TECHNOLOGY

T33

Drawing together research highlights and news from all RSC publications, *Chemical Technology* provides a 'snapshot' of the latest applications and technological aspects of research across the chemical sciences, showcasing newsworthy articles and significant scientific advances.

Chemical Technology

May 2009/Volume 6/Issue 5

www.rsc.org/chemicaltechnology

EDITORIAL

603

Green Solvents—Progress in science and application

Walter Leitner, Scientific Editor, introduces the themed issue based on the "Green Solvents—Progress in science and application" conference held in Friedrichshafen, Germany, from 28 September to 2 October 2008.



EDITORIAL STAFF

Editor

Sarah Ruthven

Assistant editors

Sarah Dixon, Katie Dryden-Holt

Publishing assistant

Jessica-Jane Doherty

Team leader, Informatics

Stephen Wilkes

Technical editor

Edward Morgan

Production administration coordinator

Sonya Spring

Administration assistants

Aliya Anwar, Jane Orchard, Julie Thompson

Publisher

Emma Wilson

Green Chemistry (print: ISSN 1463-9262; electronic: ISSN 1463-9270) is published 12 times a year by the Royal Society of Chemistry, Thomas Graham House, Science Park, Milton Road, Cambridge, UK CB4 0WF.

All orders, with cheques made payable to the Royal Society of Chemistry, should be sent to RSC Distribution Services, c/o Portland Customer Services, Commerce Way, Colchester, Essex, UK CO2 8HP. Tel +44 (0) 1206 226050; E-mail sales@rscdistribution.org

2009 Annual (print + electronic) subscription price: £1027; US\$2013. 2009 Annual (electronic) subscription price: £924; US\$1811. Customers in Canada will be subject to a surcharge to cover GST. Customers in the EU subscribing to the electronic version only will be charged VAT.

If you take an institutional subscription to any RSC journal you are entitled to free, site-wide web access to that journal. You can arrange access via Internet Protocol (IP) address at www.rsc.org/ip. Customers should make payments by cheque in sterling payable on a UK clearing bank or in US dollars payable on a US clearing bank. Periodicals postage paid at Rahway, NJ, USA and at additional mailing offices. Airfreight and mailing in the USA by Mercury Airfreight International Ltd., 365 Blair Road, Avenel, NJ 07001, USA.

US Postmaster: send address changes to Green Chemistry, c/o Mercury Airfreight International Ltd., 365 Blair Road, Avenel, NJ 07001. All despatches outside the UK by Consolidated Airfreight.

PRINTED IN THE UK

Advertisement sales: Tel +44 (0) 1223 432246; Fax +44 (0) 1223 426017; E-mail advertising@rsc.org

For marketing opportunities relating to this journal, contact marketing@rsc.org

Green Chemistry

Cutting-edge research for a greener sustainable future

www.rsc.org/greenchem

Green Chemistry focuses on cutting-edge research that attempts to reduce the environmental impact of the chemical enterprise by developing a technology base that is inherently non-toxic to living things and the environment.

EDITORIAL BOARD

Chair

Professor Martyn Poliakoff
Nottingham, UK

Scientific Editor

Professor Walter Leitner
RWTH-Aachen, Germany

Associate Editors

Professor C. J. Li
McGill University, Canada

Members

Professor Paul Anastas
Yale University, USA
Professor Joan Brennecke
University of Notre Dame, USA
Professor Mike Green
Sasol, South Africa
Professor Buxing Han
Chinese Academy of Sciences,
China

Professor Shu Kobayashi,
University of Tokyo, Japan
Dr Alexei Lapkin
Bath University, UK
Professor Steven Ley
Cambridge, UK
Dr Janet Scott
Unilever, UK
Professor Tom Welton
Imperial College, UK

ADVISORY BOARD

James Clark, York, UK
Avelino Corma, Universidad
Politécnica de Valencia, Spain
Mark Harmer, DuPont Central
R&D, USA
Herbert Hugl, Lanxess Fine
Chemicals, Germany
Roshan Jachuck,
Clarkson University, USA
Makoto Misono, nite,
Japan

Colin Raston,
University of Western Australia,
Australia
Robin D. Rogers, Centre for Green
Manufacturing, USA
Kenneth Seddon, Queen's
University, Belfast, UK
Roger Sheldon, Delft University of
Technology, The Netherlands
Gary Sheldrake, Queen's
University, Belfast, UK

Pietro Tundo, Università ca
Foscari di Venezia, Italy

INFORMATION FOR AUTHORS

Full details of how to submit material for publication in Green Chemistry are given in the Instructions for Authors (available from <http://www.rsc.org/authors>). Submissions should be sent via ReSource: <http://www.rsc.org/resource>.

Authors may reproduce/republish portions of their published contribution without seeking permission from the RSC, provided that any such republication is accompanied by an acknowledgement in the form: (Original citation) – Reproduced by permission of the Royal Society of Chemistry.

© The Royal Society of Chemistry 2009. Apart from fair dealing for the purposes of research or private study for non-commercial purposes, or criticism or review, as permitted under the Copyright, Designs and Patents Act 1988 and the Copyright and Related Rights Regulations 2003, this publication may only be reproduced, stored or transmitted, in any form or by any means, with the prior permission in writing of the Publishers or in the case of reprographic reproduction in accordance with the terms of licences issued by the Copyright Licensing Agency in the UK. US copyright law is applicable to users in the USA.

The Royal Society of Chemistry takes reasonable care in the preparation of this publication but does not accept liability for the consequences of any errors or omissions.

☞ The paper used in this publication meets the requirements of ANSI/NISO Z39.48-1992 (Permanence of Paper).

Royal Society of Chemistry: Registered Charity No. 207890

THEMED ISSUE ARTICLES

NEWS

604

Conference report: Lake Constance turns green

Gabriela Adamová, Jamie L. Ferguson, Shieling Ng,
Alberto V. Puga, Héctor Rodríguez, Sandra M. Rountree,
Kenneth R. Seddon and Alina A. Tomaszowska

Highlights from the Green Solvents—Progress in Science and Application Conference in Friedrichshafen, Germany are presented.



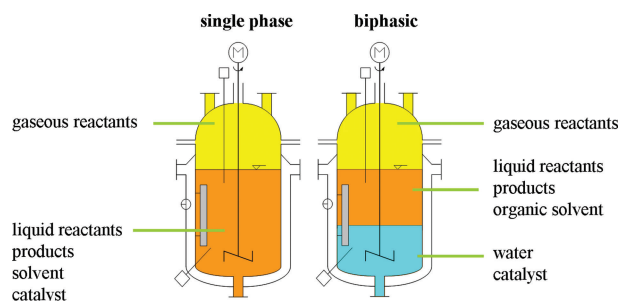
PERSPECTIVE

609

Application of the solvent water in two-phase telomerisation reactions and recycling of the homogeneous palladium catalysts

Arno Behr and Julia Leschinski

This article shows how versatile water can be, used as a solvent in homogeneously catalysed processes, for example, telomerisation reactions with methanol, diethylamine, ethylene glycol and glycerol.



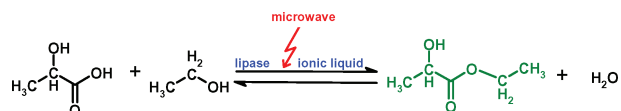
COMMUNICATIONS

614

Microwave assisted enzymatic esterification of lactic acid and ethanol in phosphonium type ionic liquids as co-solvents

Brigitta Major, Ilona Kelemen-Horváth, Zsófia Csanádi,
Katalin Bélafi-Bakó and László Gubicza*

Enzyme catalytic esterification of lactic acid and ethanol in P-containing ionic liquids as co-solvent was studied to synthesize natural ethyl lactate using microwave irradiation. It was found that microwave heating has a beneficial effect on the reaction yield.

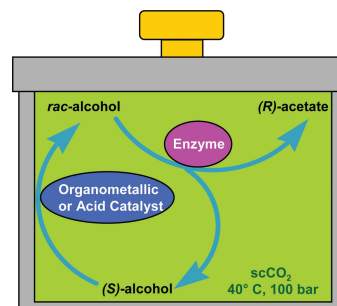


617

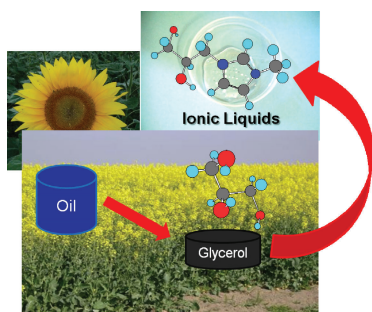
Dynamic kinetic resolution of *rac*-1-phenylethanol in supercritical carbon dioxide

Karima Benaissi, Martyn Poliakoff and Neil R. Thomas*

Pseudomonas (Burkholderia) cepacia lipase in combination with either [Ru(*p*-cymene)Cl₂]₂ or Nafion SAC 13 is shown to catalyse the dynamic kinetic resolution of *rac*-1-phenylethanol in supercritical carbon dioxide.



622

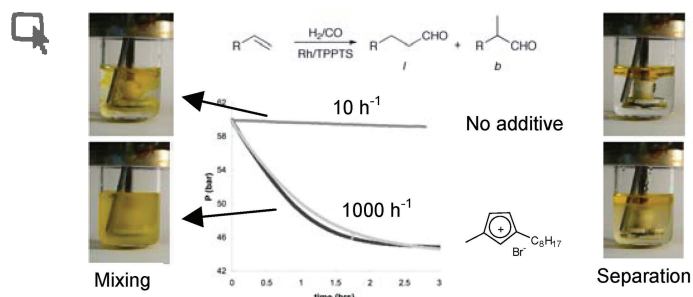


Synthesis and properties of glycerylimidazolium based ionic liquids: a promising class of task-specific ionic liquids

Fabio Bellina,* Alessandra Bertoli, Bernardo Melai, Francesca Scalesse, Francesca Signori and Cinzia Chiappe*

A series of task-specific ionic liquids (TSILs) based on glycerylimidazolium cations have been prepared. The ability of these ILs to act as ligands for transition metal catalyzed reactions has been evidenced.

630

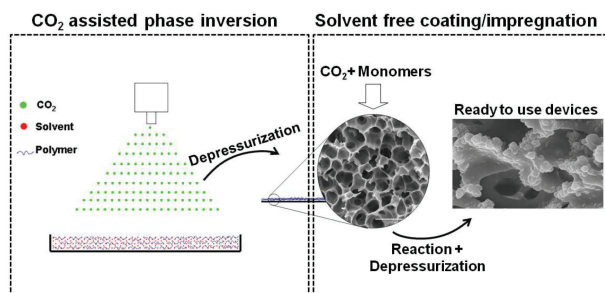


Aqueous-biphasic hydroformylation of alkenes promoted by “weak” surfactants

Simon L. Desset, Simon W. Reader and David J. Cole-Hamilton*

Addition of 1-octyl-3-methyl imidazolium bromide to the aqueous-biphasic hydroformylation of 1-octene catalysed by Rh/TPPS complexes leads to dramatic rate increases with rapid phase separation and good retention of rhodium into the aqueous phase (<0.5 ppm Rh leaching).

638

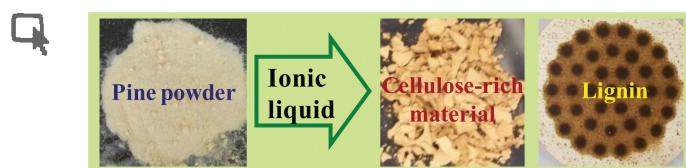


Development and characterization of a thermoresponsive polysulfone membrane using an environmental friendly technology

Márcio Temtem, Daniel Pompeu, Telma Barroso, João Fernandes, Pedro C. Simões, Teresa Casimiro, Ana M. Botelho do Rego and Ana Aguiar-Ricardo*

“Smart” polysulfone membranes with a *T*-switchable microscale structure can be prepared using supercritical CO₂-assisted technology. These membranes exhibited a good performance in terms of on-off valve pore aperture.

646



Complete dissolution and partial delignification of wood in the ionic liquid 1-ethyl-3-methylimidazolium acetate

Ning Sun, Mustafizur Rahman, Ying Qin, Mirela L. Maxim, Héctor Rodríguez and Robin D. Rogers*

Carbohydrate-free lignin and cellulose-rich material can be obtained by complete dissolution of softwood and hardwood in the ionic liquid 1-ethyl-3-methylimidazolium acetate followed by separation.

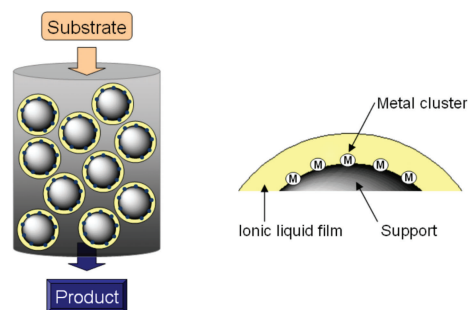
PAPERS

656

Impact of supported ionic liquids on supported Pt catalysts

Richard Knapp, Andreas Jentys and Johannes A. Lercher*

The novel concept of supported ionic liquid mediated metal nanoparticles, which allows combining different functionalities in a single catalytically active material is introduced, with particular focus on the interaction between metal clusters and ionic liquid.

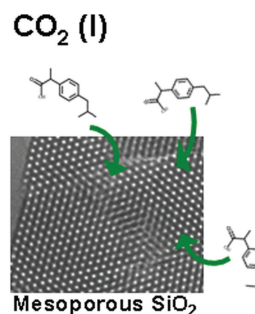


662

Ibuprofen loading into mesostructured silica using liquid carbon dioxide as a solvent

Anna Hillerström,* Jan van Stam and Martin Andersson

A high loading capacity (300 mg Ibuprofen/g SiO₂) was achieved when Ibuprofen was loaded into mesostructured silica using liquid carbon dioxide as the solvent.

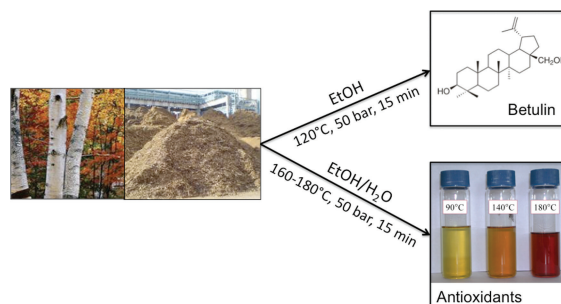


668

Pressurized liquid extraction of betulin and antioxidants from birch bark

Michelle Co, Pirjo Koskela, Peter Eklund-Åkergren, Keerthi Srinivas, Jerry W. King, Per J. R. Sjöberg and Charlotta Turner*

Betulin and antioxidants were extracted from birch bark in a rapid process using pressurized hot water and ethanol as solvents.



REGULAR RESEARCH ARTICLES

EDITORIAL

675

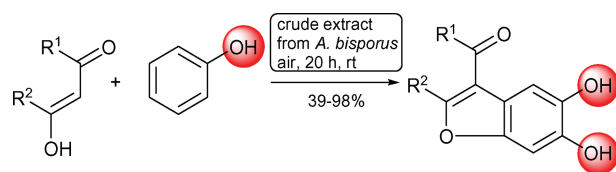
Green chemistry at ACHEMA 2009—from mnemonics to success stories

Kurt Wagemann discusses ACHEMA 2009, to be held in Frankfurt from 11th May 2009, and its links to green chemistry and green engineering.



COMMUNICATIONS

676

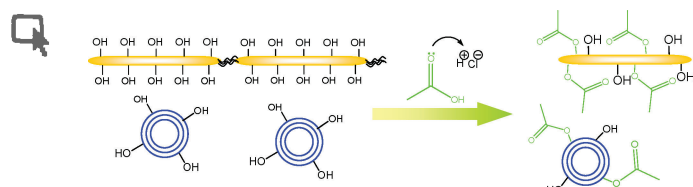


Combined action of enzymes: the first domino reaction catalyzed by *Agaricus bisporus*

Heiko Leutbecher, Szilvia Hajdok, Christina Braunberger, Melanie Neumann, Sabine Mika, Jürgen Conrad and Uwe Beifuss*

The enzymes from a crude extract of the button mushroom (*Agaricus bisporus*) catalyze the domino reaction between phenol and various cyclic 1,3-dicarbonyls using atmospheric oxygen in a highly efficient and sustainable manner.

680

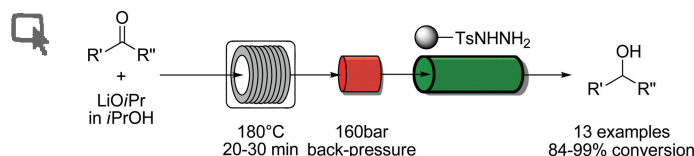


Decorating in green: surface esterification of carbon and cellulosic nanoparticles

Margaret J. Sobkowicz, Birgit Braun and John R. Dorgan

Fischer esterification of surface hydroxyl groups on multiwalled carbon nanotubes, carbon nanospheres, and cellulosic nanowhiskers using acetic and butyric acid is presented as a green approach to decorate the surfaces of nanoparticles.

683



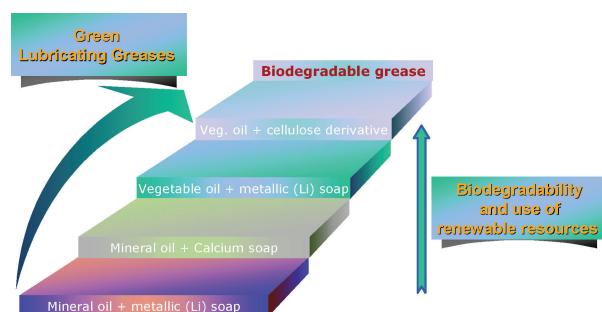
An efficient and transition metal free protocol for the transfer hydrogenation of ketones as a continuous flow process

Jörg Sedelmeier, Steven V. Ley* and Ian R. Baxendale

An efficient and transition metal free transfer hydrogenation protocol for use in flow mode delivering secondary alcohol products in high yields and excellent purities is reported.

PAPERS

686



Development of new green lubricating grease formulations based on cellulosic derivatives and castor oil

R. Sánchez, J. M. Franco,* M. A. Delgado, C. Valencia and C. Gallegos

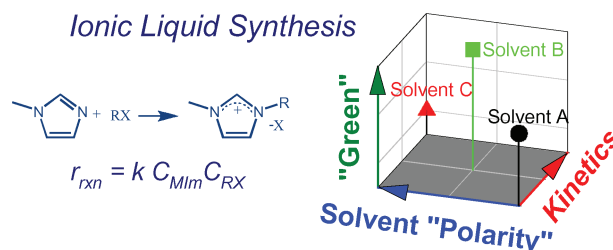
The suitability of cellulose derivatives to form oleogels in a castor oil continuous phase, in order to obtain new biodegradable lubricating grease formulations completely based on natural products, was investigated. Thermal and thermo-rheological behaviours of these biogreases are reported.

694

Kinetics and solvent effects in the synthesis of ionic liquids: imidazolium

Jay C. Schleicher and Aaron M. Scurto*

This investigation illustrates the kinetics and large solvent effects in the synthesis of 1-hexyl-3-methyl-imidazolium bromide in 10 different solvents.

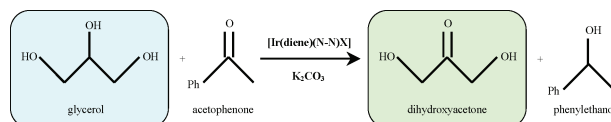


704

A novel glycerol valorization route: chemoselective dehydrogenation catalyzed by iridium derivatives

Erica Farnetti, Jan Kašpar and Corrado Crotti*

Dehydrogenation of glycerol to dihydroxyacetone is catalyzed by Ir(diene)(N-N)X (diene = 1,5-hexadiene, 1,5-cyclooctadiene; N-N = 1,10-phenanthroline, 2,2'-bipyridine and substituted derivatives; X = Cl, I). The reactions are performed under hydrogen transfer conditions, using acetophenone as the hydrogen acceptor.

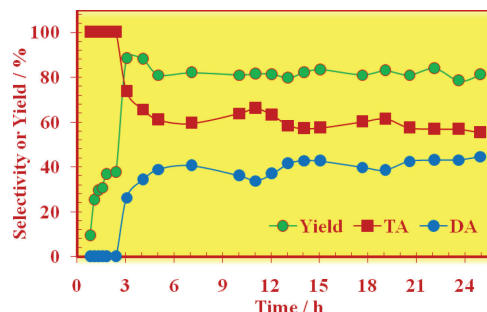


710

Continuous synthesis of glycerol acetates in supercritical carbon dioxide using Amberlyst 15®

Marzieh Rezayat and Hassan S. Ghaziaskar*

Continuous and selective esterification of glycerol with acetic acid to produce triacetin (TA) and diacetin (DA) was performed in supercritical carbon dioxide using Amberlyst 15® with about 4.6 times more selectivity for TA compared to the reaction under reflux conditions.

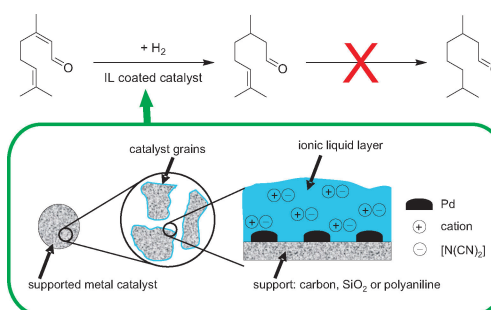


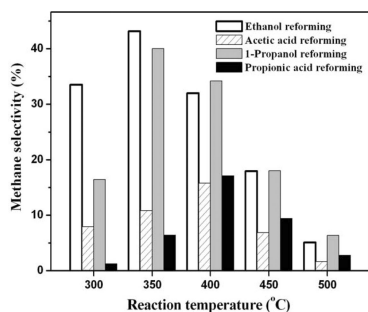
716

Regioselective catalytic hydrogenation of citral with ionic liquids as reaction modifiers

Jürgen Arras, Martin Steffan, Yalda Shayeghi, Dominik Ruppert and Peter Claus*

Modifying supported metal catalysts with ionic liquids shows remarkable effects on their selectivity pattern. With dicyanamide based ionic liquids as reaction modifier, quantitative yields of citronellal are possible through heterogeneously catalyzed citral hydrogenation.

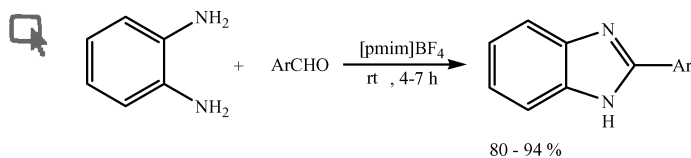




Inhibition of methane formation in steam reforming reactions through modification of Ni catalyst and the reactants

Xun Hu and Gongxuan Lu*

Although steam reforming of the neutral fuels (ethanol, 1-propanol) produced much higher amounts of methane than those of acidic fuels (acetic acid, propanoic acid), the modification of the neutral alcohols with nitric acid could remarkably suppress methane formation.



Remarkable influence of substituent in ionic liquid in control of reaction: simple, efficient and hazardous organic solvent free procedure for the synthesis of 2-aryl benzimidazoles promoted by ionic liquid, [pmim]BF₄

Debasree Saha, Amit Saha and Brindaban C. Ranu*

An easily accessible ionic liquid, [pmim]BF₄ efficiently catalyzes the condensation of *o*-phenylenediamine and aromatic aldehydes at room temperature in open air to produce a variety of structurally diverse 2-arylbenzimidazoles avoiding use of any hazardous organic solvent.

AUTHOR INDEX

Adamová, Gabriela, 604
 Aguiar-Ricardo, Ana, 638
 Andersson, Martin, 662
 Arras, Jürgen, 716
 Barroso, Telma, 638
 Baxendale, Ian R., 683
 Behr, Arno, 609
 Beifuss, Uwe, 676
 Bélafi-Bakó, Katalin, 614
 Bellina, Fabio, 622
 Benaissi, Karima, 617
 Bertoli, Alessandra, 622
 Botelho do Rego, Ana M., 638
 Braun, Birgit, 680
 Braunberger, Christina, 676
 Casimiro, Teresa, 638
 Chiappe, Cinzia, 622
 Claus, Peter, 716
 Co, Michelle, 668
 Cole-Hamilton, David J., 630
 Conrad, Jürgen, 676
 Crotti, Corrado, 704

Csanádi, Zsófia, 614
 Delgado, M. A., 686
 Desset, Simon L., 630
 Dorgan, John R., 680
 Eklund-Åkergren, Peter, 668
 Farnetti, Erica, 704
 Ferguson, Jamie L., 604
 Fernandes, João, 638
 Franco, J. M., 686
 Gallegos, C., 686
 Ghaziaskar, Hassan S., 710
 Gubicza, László, 614
 Hajdok, Szilvia, 676
 Hillerström, Anna, 662
 Hu, Xun, 724
 Jentys, Andreas, 656
 Kašpar, Jan, 704
 Kelemen-Horváth, Ilona, 614
 King, Jerry W., 668
 Knapp, Richard, 656
 Koskela, Pirjo, 668
 Lercher, Johannes A., 656

Leschinski, Julia, 609
 Leutbecher, Heiko, 676
 Ley, Steven V., 683
 Lu, Gongxuan, 724
 Major, Brigitta, 614
 Maxim, Mirela L., 646
 Melai, Bernardo, 622
 Mika, Sabine, 676
 Neumann, Melanie, 676
 Ng, Shieling, 604
 Poliakoff, Martyn, 617
 Pompeu, Daniel, 638
 Puga, Alberto V., 604
 Qin, Ying, 646
 Rahman, Mustafizur, 646
 Ranu, Brindaban C., 733
 Reader, Simon W., 630
 Rezayat, Marzieh, 710
 Rodríguez, Héctor, 604, 666
 Rogers, Robin D., 646
 Rountree, Sandra M., 604
 Ruppert, Dominik, 716

Saha, Amit, 733
 Saha, Debasree, 733
 Sánchez, R., 686
 Scalesse, Francesca, 622
 Schleicher, Jay C., 694
 Scurto, Aaron M., 694
 Seddon, Kenneth R., 604
 Sedelmeier, Jörg, 683
 Shayeghi, Yalda, 716
 Signori, Francesca, 622
 Simões, Pedro C., 638
 Sjöberg, Per J. R., 668
 Sobkowitz, Margaret J., 680
 Srinivas, Keerthi, 668
 Steffan, Martin, 716
 Sun, Ning, 646
 Temtem, Márcio, 638
 Thomas, Neil R., 617
 Tomaszowska, Alina A., 604
 Turner, Charlotta, 668
 Valencia, C., 686
 van Stam, Jan, 662

FREE E-MAIL ALERTS AND RSS FEEDS

Contents lists in advance of publication are available on the web *via* www.rsc.org/greenchem – or take advantage of our free e-mail alerting service (www.rsc.org/ej_alert) to receive notification each time a new list becomes available.

 Try our RSS feeds for up-to-the-minute news of the latest research. By setting up RSS feeds, preferably using feed reader software, you can be alerted to the latest Advance Articles published on the RSC web site. Visit www.rsc.org/publishing/technology/rss.asp for details.

ADVANCE ARTICLES AND ELECTRONIC JOURNAL

Free site-wide access to Advance Articles and the electronic form of this journal is provided with a full-rate institutional subscription. See www.rsc.org/ejs for more information.

* Indicates the author for correspondence: see article for details.

 Electronic supplementary information (ESI) is available *via* the online article (see <http://www.rsc.org/esi> for general information about ESI).

Chemical Technology

Snowblower-like beams mix and sort microparticles

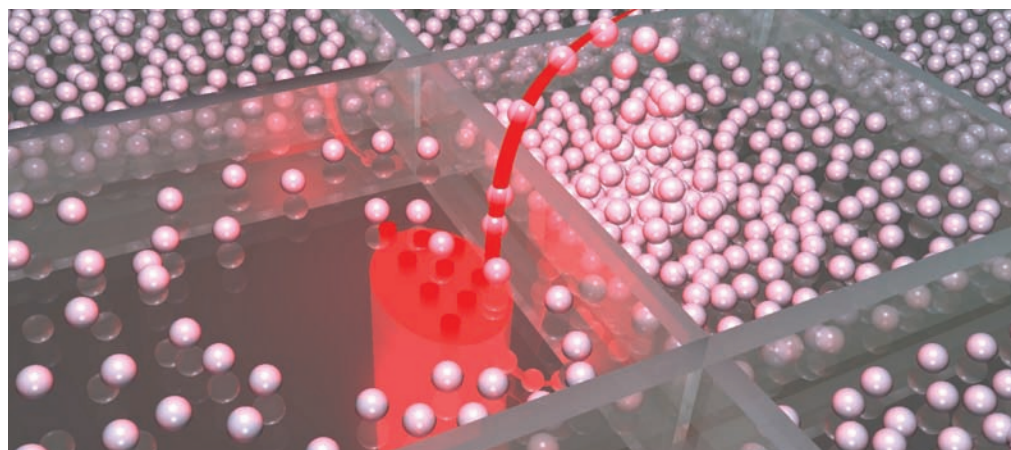
Lasers blow cells over microwalls

Scientists have used the unusual curving properties of laser beams to hurl microparticles and cells over walls.

Jörg Baumgartl, at the University of St Andrews, UK, and colleagues used non-diffracting laser beams to transport particles between microwells. Baumgartl likens the laser beams to micrometre-sized snowblowers. The microparticles and cells are attracted to the bottom of the chip and then 'blown' upwards in an arc by the laser, he says.

Normal laser beams travel in a straight line and their light spreads out over distances. 'For instance, the beam emitted by a laser pointer would have the size of several hundred kilometres were it to reach the Moon,' explains Baumgartl. However, the non-diffracting laser beams he used travel in a curve without spreading out.

In most microfluidic studies, scientists move particles between chambers using a liquid flow. 'Our method opens an alternative route to transport, mix or sort



microparticles and cells within the same microfluidic chip,' says Baumgartl.

'This is an important step forward in increasing the functionality of microfluidic environments by allowing particles to be transferred between different media,' comments Ewan Wright, an expert in optical sciences and physics at the University of Arizona, Tucson, US. 'It is a wonderful example of how,

The laser beam 'blows' particles from one microwell to another

Reference
J Baumgartl *et al*, *Lab Chip*, 2009, DOI: 10.1039/b901322a

over time, fundamental research, here on novel laser fields, can bring about highly innovative results in applied science.'

Baumgartl anticipates the method will lead to high-throughput, automated chips that will mix and sort microparticles and cells or mediate chemical reactions. It could be used to study cell processes and selectively expose cancer cells to drugs, he adds. *Sarah Corcoran*

In this issue

A new twist on actuator architecture

Spiral opals change colour and shape in response to their chemical environment

Lab on ice

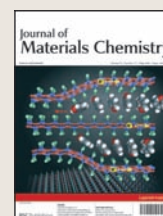
Light-guiding chip is a 'cool' new use for frozen water

Interview: Seeking the killer application

Abe Lee discusses microfluidics and lab-on-a-chip devices

Instant insight: Nothing but surface

Find out why the chemical industry is so interested in metal-organic frameworks



The latest applications and technological aspects of research across the chemical sciences

Application highlights

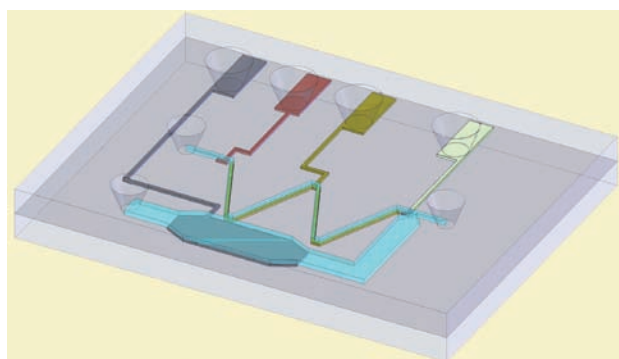
Microreactor enables faster and easier drug analysis

Chip mimics metabolism

Drug metabolism studies can be conducted on smaller samples than before thanks to an on-chip electrochemical cell designed by European scientists.

Electrochemical cells can mimic the oxidative metabolism of drugs within the body. By coupling them to mass spectrometers or liquid chromatographs, scientists can detect and identify the metabolites.

Mathieu Odijk, at the University of Twente, Enschede, the Netherlands, and colleagues made a glass chip containing the usual three electrodes found in an electrochemical cell – the working, reference and counter electrodes – plus an extra sensing electrode to detect generated species. They then connected the chip to a liquid chromatography-mass



spectrometry (LC-MS) system and injected a solution of amodiaquine, an antimalarial drug, through the chip. They showed that the cell oxidised the drug, forming all its major metabolites, which were detected by LC-MS.

Other electrochemical cells are commercially available but Odijk

The chip contains four electrodes: the working electrode (khaki green), the reference electrode (red), the extra sensing electrode (pale green) and, in the separate channel, the counter electrode (pale blue)

explains his uses much smaller sample volumes. 'With this chip, new drugs can be studied faster and with more ease,' he says. He adds that the counter electrode is located in a separate side-channel from the other electrodes, which prevents unwanted side products appearing in the measured spectrograms.

'This chip is used in combination with tools like LC and electrospray-MS. A very logical but technically challenging next step is to combine these three tools on to a single lab-on-a-chip, while keeping the fabrication costs within acceptable limits,' says Odijk.

Madelaine Chapman

Reference

M Odijk *et al*, *Lab Chip*, 2009
DOI: 10.1039/b822962g

Microbes use carbon dioxide in wastewater to produce electricity

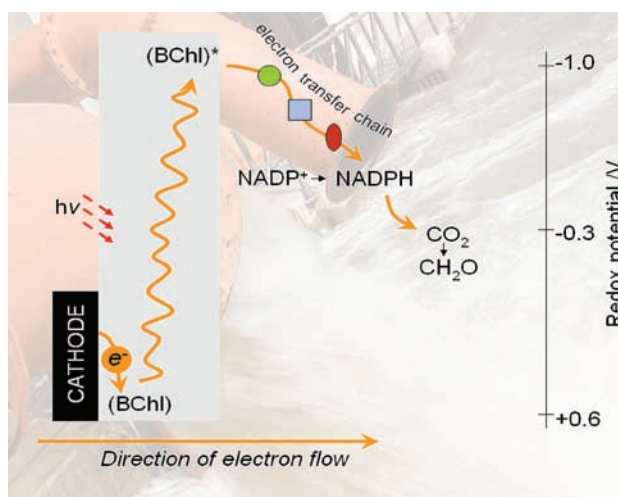
Bacteria generate cleaner power and water

Microbial fuel cells can store away carbon dioxide as well as produce electricity, according an international team of scientists.

Microbial fuel cells offer a clean and efficient way of producing energy because the microbes that power them can feed off almost any organic waste. Xia Huang and colleagues at Tsinghua University, Beijing, China, and Ghent University, Belgium, demonstrated that sunlight helps microbes use dissolved CO₂ (bicarbonate) in wastewater to produce electricity.

Huang showed that when she inoculated a cathode with a mixture of aerobic and anaerobic bacteria and shone a light on it, the biocathode reduced bicarbonate, generating electricity and increasing bacterial growth (biomass). But in the dark, power generation decreased rapidly, indicating that light is needed to supply energy to the fuel cell.

'The process it uses to generate power is different from a typical microbial fuel cell, which uses



precious metal catalysts to chemically reduce oxygen at the cathode,' explains co-worker Xiaoxin Cao. 'Using oxygen reduction to provide power is not ideal because it requires the water to be aerated – a very energy intensive process.' Typical wastewater has a high CO₂ concentration, he adds.

Sunlight drives CO₂ reduction at the cathode

Frédéric Barrière, who studies microbial fuel cells at the University of Rennes 1, France, describes the work as exciting. 'This integration of microorganisms as biocatalysts at the cathode and anode predicts that the microbial fuel cell is sustainable, even if the reported power output is still too low for practical applications.'

Cao acknowledges that increasing the power output is desirable. 'Improving the power output can be done by decreasing ohmic resistance – the focus of research for the last five years – or, more challengingly, by investigating the mechanism of microbe–electrode interaction,' says Cao. 'If this mechanism can be figured out then both the microbial community and the biofilm structure can be optimised and the performance improved.'

Janet Crombie

Reference

Xiaoxin Cao *et al*, *Energy Environ. Sci.*, 2009,
DOI: 10.1039/b901069f

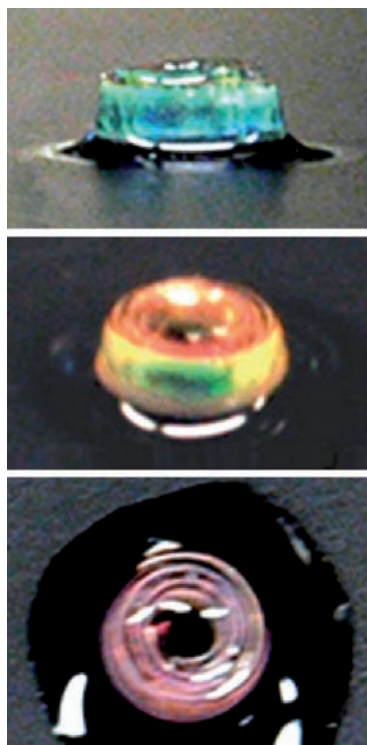
Spiral opals change colour and shape in response to their chemical environment

A new twist on actuator architecture

Scientists have built a novel type of actuator – a device that converts energy into motion – with an artificial opal embedded in it.

To make the actuator, Kwang-Un Jeong at Chonbuk National University, Jeonju, South Korea, and colleagues put colloidal silica in water, where it formed a strip of single crystalline opal one tenth of a millimetre thick. They embedded the strip in a layer of poly(dimethylsiloxane) polymer and then added a layer of polyurethane (PU)/2-hydroxyethyl methacrylate polymer on top. Finally, they sealed the bi-layer strip inside a layer of glass.

The team placed the strip in different solvents and found that it responded differently depending on the solvent's hydrophobicity. The strip curled up to form a right-handed spiral in hydrophilic solvents, such as acetic acid, and a left-handed spiral in hydrophobic solvents, such as hexane. The curling effect is due to the difference in swelling ratios between the two polymer layers,



Reference

K-U Jeong *et al.*, *J. Mater. Chem.*, 2009, 19, 1956 (DOI:10.1039/b822980p)

The spiral actuator changes colour when viewed at different angles

explains Jeong. He showed that the right-handed spirals display different colours depending on the angle they are viewed from but the left-handed spirals do not.

‘Using a bilayer polymer photonic system to create colour-tunable spiral photonic actuators is a simple and elegant idea,’ says Christopher Li, an expert in soft matter and hybrid materials at Drexel University, Philadelphia, US. ‘Being able to control the macroscopic handedness of the spiral is fascinating. Slightly changing the sample architecture could lead to profound shapes, such as a helix.’

According to Jeong, the actuators even respond to gaseous solvents. He says that the device may have varied applications: ‘These colour-tunable, reversible spiral photonic switches can be useful as mechanical actuators and electrical devices, as well as optical components. Our ultimate goal is to construct complicated 3D objects from programmed 2D structures.’
James Hodge

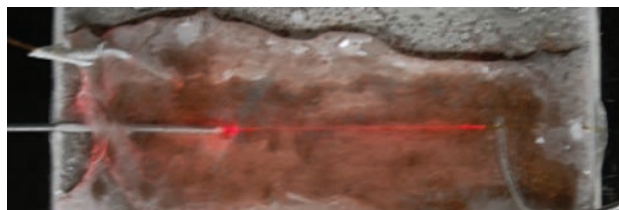
Light-guiding chip is a ‘cool’ new use for frozen water

Lab on ice

Experimental apparatus made from ice can be used as detecting systems for solvent extraction and chromatography, claim Japanese scientists. The apparatus is cheaper, more readily available and more environmentally friendly than current equipment, they say.

Tetsuo Okada and colleagues at the Tokyo Institute of Technology used ice to make a liquid-core waveguide, a device for guiding light through liquid-filled channels. Guiding light through liquids is difficult because they have low refractive indices, meaning that they slow down the speed of light. But if the liquid is surrounded by cladding with a lower refractive index, the cladding reflects the light back into the liquid, keeping it on course through the channel without significant loss of intensity.

‘Most current liquid-core



waveguides are fabricated with Teflon AF-2400 [a fluoropolymer plastic] but it adsorbs various substances on its surface and is damaged even by weak mechanical contact. It also has a high cost,’ explains Okada. ‘Water-ice is much less expensive and, of course, is environmentally friendly.’

Okada made an ice chip with a thin tunnel running through it. He injected a liquid into the tunnel and shone light through it. He showed that the ice cladding, which has a lower refractive index than most

The ice cladding keeps the light on course through the channel

solvents, was better at guiding light than a previously reported Teflon AF-coated glass microchip.

Purnendu Dasgupta, an expert in analytical chemistry at the University of Texas at Arlington, US, describes the study as ‘a fascinating piece of work’. ‘It makes one wonder what the refractive index properties of some other frozen liquids may be,’ he comments.

Okada used the waveguide for ice chromatography, where different compounds in a sample separate out according to their affinity for ice. However, he found that the aqueous core caused the light intensity to fluctuate. ‘To prevent such instability, the experimental conditions, such as the type of liquid in the core, its concentration, and working temperature, should be carefully optimised,’ says Okada.
Colin Batchelor

Reference

K Sugiyama, M Harada and T Okada, *Lab Chip*, 2009, 9, 1037 (DOI: 10.1039/b821382h)

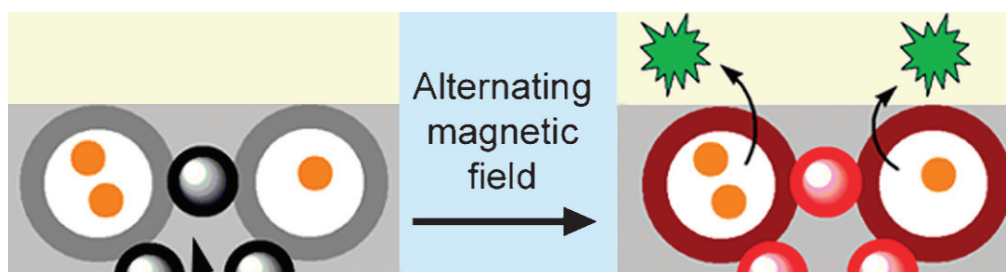
Nanoparticle-glued vesicles deposit contents on demand

Magnets control drug release...

A smart, tissue-like biomaterial that can release drugs in response to a magnetic trigger has been created by UK scientists.

Simon Webb and colleagues from the University of Manchester used magnetic nanoparticles to glue together dye-containing vesicles and then embedded them in a hydrogel. The vesicles were positioned within the hydrogel using magnetism and the dye released using an alternating magnetic field as a trigger. Webb says this indicates that the tissue-like gel could be used to store drugs and deliver them to the site of disease without affecting the surrounding tissue.

Although the group have previously used vesicles to mimic cells sticking together, Webb explains that the magnetic particles and hydrogel matrix strengthen the assemblies and make them easier to control. 'Gratifyingly, this



combination has provided robust materials that can be patterned and release biochemicals in response to a magnetic trigger,' he adds.

'The clever part of all this is the way in which the authors interface their magnetic triggers with vesicles using precisely controlled non-covalent interactions,' says David Smith, who investigates nanoscale gel-phase materials at the University of York, UK. 'Embedding the resulting triggered-release system within a

Magnetic nanoparticle-vesicle assemblies embedded within a hydrogel release their contents in response to a remote magnetic trigger

hydrogel then generates the kind of material which could be used for drug delivery.' He adds that an alternating magnetic field is ideal for clinical use as it does not adversely affect healthy tissue.

Webb says they are working to create smaller patterns in the hydrogel matrix and to magnetically trigger the release of cell messenger molecules, such as growth factors, so the technology can be used for biomedical applications.

Rachel Cooper

Reference

R J Mart, K P Liem and S J Webb, *Chem. Commun.*, 2009, DOI: 10.1039/b901472a

Magnetic beads seek out new drugs with the help of modified viruses

...and clean up phage display

Microfluidic washing can improve drug candidate identification, claim US scientists.

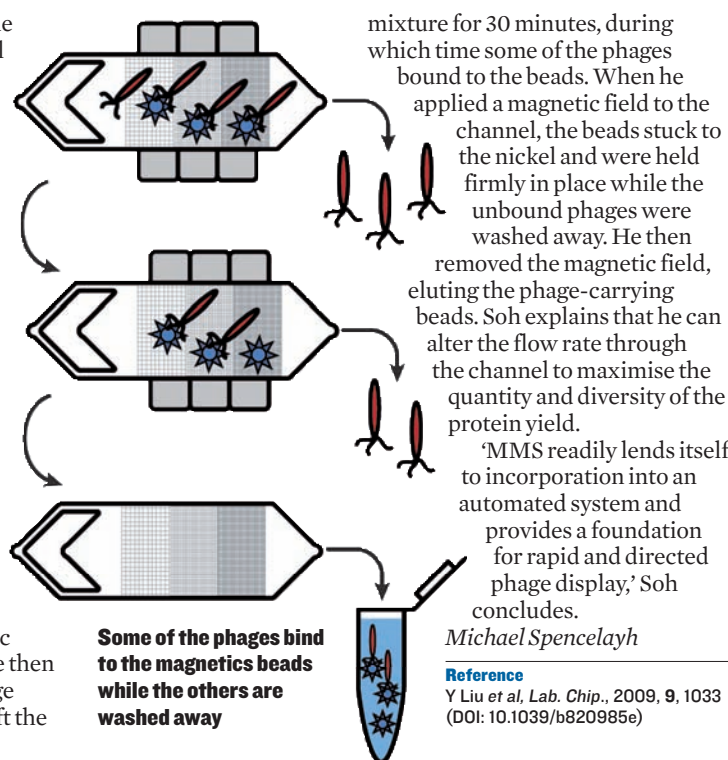
Tom Soh at the University of California, Santa Barbara, and colleagues used micro-magnetic separation (MMS) to standardise the washing step in phage display, a method used to find proteins that interact strongly with disease-causing molecules, such as certain enzymes.

A bacteriophage (phage) is a virus that infects only bacteria. In phage display, scientists insert a new gene into a phage's genetic material. When bacteria process the new gene, they make a new protein, which is exposed on the phage's surface. Using a collection of around a billion phages each with a different inserted gene, scientists can create a library of phages, each displaying a different protein. They then expose the library to the immobilised target molecule. Some of the proteins bind to the target while the unbound

phages are washed away. The bound proteins are potential drug candidates and are studied further.

The process requires a lot of the target molecule, explains Soh, which is problematic when it is in limited supply. It also yields false positives when proteins bind to the target's solid support rather than the target itself. 'It is also challenging to control accurately the stringency of washing in a reproducible way,' Soh adds – using a faster or longer wash flow can strip off bound phages from the target.

Soh's MMS device consists of a glass channel with nickel patterns on its surface. Soh coated magnetic beads with a target molecule then mixed the beads with a phage library in the channel. He left the



Some of the phages bind to the magnetic beads while the others are washed away

mixture for 30 minutes, during which time some of the phages bound to the beads. When he applied a magnetic field to the channel, the beads stuck to the nickel and were held firmly in place while the unbound phages were washed away. He then removed the magnetic field, eluting the phage-carrying beads. Soh explains that he can alter the flow rate through the channel to maximise the quantity and diversity of the protein yield.

'MMS readily lends itself to incorporation into an automated system and provides a foundation for rapid and directed phage display,' Soh concludes.

Michael Spencelayh

Reference

Y Liu et al, *Lab. Chip.*, 2009, 9, 1033 (DOI: 10.1039/b820985e)

Interview

Seeking the killer application

Abe Lee tells Kathleen Too about the fundamentals of micro- and nanofluidics, lab-on-a-chip devices and finding the microfluidics 'killer application'



Abe Lee

Abraham (Abe) Lee is a professor in the departments of biomedical engineering and mechanical and aerospace engineering at the University of California, Irvine, US. He is the director of the Micro/Nano Fluidics Fundamentals Focus (MF3) Center sponsored by companies with funding from the Defense Advanced Research Projects Agency. Professor Lee has developed a series of lab-on-a-chip devices for biomedical and biotechnological applications. His research has contributed to the founding of several start-up companies and he also serves as an advisor to companies and government agencies. He is also a new member of the Lab on a Chip editorial board.

How would you define the terms microfluidics and lab-on-a-chip?

I don't want to reinvent the wheel so this is taken from George Whitesides' paper *The origins and the future of microfluidics*¹ – 'Microfluidics is the science and technology of systems that process or manipulate small (10^{-9} to 10^{-18} litres) amounts of fluids, using channels with dimensions of tens of nanometres to hundreds of microns.' Microfluidics involves the ability to carry out separations and detection with high resolution and sensitivity and the use of very small quantities of samples and reagents. Other advantages are low cost, short times for analysis and small footprints for the analytical devices. I would add that lab-on-a-chip (LOC) is to perform chip-scale chemical or biological assays driven by microfluidics to automate and streamline the different process steps.

Can you tell me about the Micro/Nano Fluidics Fundamentals Focus Center?

The MF3 Center was initiated in 2006 and is based at the University of California with the participation of nine other US universities. The mission of the centre is to create a focused community, composed of academic, government and commercial institutions, dedicated to developing the basic science and technology of micro- and nanoscale fluidics and providing solutions to commercial problems.

In essence, we are attempting to bridge the gap between fundamental research at universities and product-driven research within companies. This is often thought of as the 'valley of death' in terms of technology development. It happens when a brilliant idea is proposed and fundamental research is carried out in an academic environment; yet the timing and relevance to the company's product plans are weak. On the other hand, companies typically don't have the mandate and manpower to carry out the original or fundamental research. Therefore, in order to marry the two sectors, the MF3 Center set out to perform fundamental research driven by industrial needs.

As well as research projects and collaboration, the centre also promotes rapid prototyping and manufacturing of micro- and nanofluidic devices. We have invested in a hot embossing tool that will be used to develop moulds for a reel-to-reel tape

machine that can quickly turn research prototypes into manufacturable products.

What does the future hold for microfluidics and the LOC sector?

I believe the future is bright. We shall see LOC devices instrumental in helping us to live a healthier and higher quality life when microfluidic chips become as ubiquitous as microelectronic chips. We will have access to health indicators to greatly improve diagnostics and therapeutics and truly realise the potential of 'personalised medicine' through the maturation of LOC technologies. Food and water safety, as well as environmental monitoring, will also benefit from low cost, autonomous LOC devices.

Many technologists are now working hard to find a microfluidics 'killer application'. Do you have a feel for what this might be?

Killer applications come from either a great need or a great 'need to have'. They may also come from imposed needs or a disaster-triggered need to prevent future ones. The future is hard to predict but I will go with an application in the food industry either related to testing livestock or testing crops. This gigantic industry is largely untapped by LOC technologies. However, the need to have a 'personal digital health assistant' might also prompt a killer application in genetic testing for various disease susceptibilities or traits by home testing or at local surgeries or pharmacies.

Which historical scientific figure would you most like to have dinner with and why?

Isaac Newton – I am fascinated by how he was able to distil very simple principles of nature from very complex phenomena. An ability to discover regularity and order in a seemingly random universe defines what good scientists do. However, it is almost impossible that one can come up with principles as fundamental as Newton and influence fields as broad as he did (mechanics, optics, mathematics). I would hope that the dinner would enlighten me on how to have a clear mind and focus, as one ages, to still produce and lead important studies.

Reference

1 G M Whitesides, *Nature*, 2006, **442**, 368

Instant insight

Nothing but surface

Alexander Czaja, Natalia Trukhan and Ulrich Müller of BASF SE, Ludwigshafen, Germany, discuss the possible applications of metal-organic frameworks (MOFs) for the chemical industry

New materials are essential for major breakthrough applications that will influence daily life – just think of the success of semiconductors, without which modern life would be unimaginable. There are also less visible, but nevertheless important, breakthroughs, such as zeolites for fluid catalytic cracking. This process provides the majority of the world's gasoline and without it, the consequences on our lives would be dire.

New materials are also pivotal for the chemical industry. MOFs are an emerging class of materials, the properties of which are exciting industrial chemists.

Scientists have made hundreds of different MOFs by self-assembling simple, molecular building blocks – metal ions and a variety of bridging ligands. The resulting tailored, nanoporous host materials are robust solids with high thermal and mechanical stability. The most striking difference compared to state-of-art materials, such as zeolites, is a MOF's total lack of non-accessible bulk volume – they were once called 'crystals full of nothing' by Omar Yaghi, one of the pioneers in the MOF field. Because MOFs don't have dead volume, they have, in terms of weight, the highest porosities and surface areas of all materials.

The ability to synthesise MOFs on a large scale, sometimes even exceeding zeolite synthesis in terms of efficiency, frees the way for thinking about technical applications. Scientists first examined applications benefiting from a MOF's large surface area, for example gas purification, gas separation and gas storage. In gas purification processes, such as removing the odorant in natural gas to make it usable for fuel cell



applications, MOFs outperform active carbons. In gas separations, for example hydrogen purification, a MOF's pore size distribution becomes advantageous – the small hydrogen molecules enter the MOF's porous structure while larger gas molecules, like nitrogen or carbon dioxide, cannot. This leads to gas separation very similar to what is achieved by classical sieving.

In gas storage, the MOF's high surface area offers plenty of space for gas molecules to interact with surface centres that can weakly bind (physisorb) the gas molecules. A MOF-filled gas cylinder can hold up to 35 per cent more natural gas than the hollow cylinders used at present. And so MOFs could enable higher ranges for cars fuelled by natural gas.

Catalysis is the youngest, least developed field of MOF research. But scientists have already

MOFs can be formed into different shapes to cater for different uses

demonstrated the potential of MOF catalysts and have developed ways to modify MOFs after the actual materials synthesis step, which will speed up catalysis development. The main advantage of a MOF catalyst, however, is its high density of active centres, which are spatially separated from each other and fully exposed.

The chemical industry is really interested in MOF materials, which will ultimately benefit the consumer. The first application will probably come from gas purification, separation or storage. However, due to the fascinating properties of MOFs, research on their catalytic properties will be very interesting in the future.

Read more in 'Industrial applications of metal-organic frameworks' in the MOF theme issue of Chemical Society Reviews (issue 5).

Reference

A U Czaja et al, *Chem. Soc. Rev.*, 2009, DOI: 10.1039/b804680h

Instant insight

Probing radioactive research

Microfluidic reactors have the ability to revolutionise radiopharmaceutical synthesis, according to Arkadij Elizarov from Siemens Molecular Imaging Biomarker Research, Los Angeles, US. He analyses the advantages and drawbacks of this potentially life-saving technology

Positron emission tomography (PET) is a powerful diagnostic tool used for assessing a wide range of disorders in areas such as cancer, neurology, cardiology and inflammation. It relies on radiopharmaceuticals labelled with short-lived radioisotopes, such as fluorine-18 or carbon-11. The radiopharmaceutical is injected into the patient's body where it concentrates in the tissues of interest. Scientists then monitor its radioactive decay using an imaging scanner.

Radiopharmaceutical synthesis is a multi-step process that starts with the particle accelerator, known as the cyclotron, producing the raw isotope. The steps that follow include isotope concentration, solvent exchange, the radiolabelling reaction, other chemical transformations and purification. Radiopharmaceuticals must be produced rapidly and in high yield, immediately before being injected into the patient. The synthesis also has to be operated remotely to protect the user from radiation. Clearly, the synthetic chemist's traditional tools are insufficient. Scientists prepare radiopharmaceuticals using relatively large-scale automated synthesis modules. But these modules significantly dilute the labelling agents and reduce reaction rates.

Microfluidics could be the solution to radiosynthesis' deficiencies.

Reactions in microfluidic devices are often rapid and high yielding and can be easily automated. Scientists have investigated multiple approaches but they can be classified into two main categories: continuous flow reactors and batch reactors. In flow reactors, reactions take place in running solutions. Their high surface-to-volume ratios and rapid heat and mass transfer increase the reaction rates while minimising the amount of radioactivity present at any given point in the system. (A high concentration of radioactivity may decompose some species over time.) Batch reactors use fixed amounts of reagents in each synthetic step. They use higher reagent concentrations, which improves reaction rates, but the high radioactivity concentration is a concern. This is lessened by minimising the time spent by reagents in a concentrated state.

Flow reactors are better understood and accepted – they have a massive amount of data from non-radioactive applications as a reference. Batch reactors explore new areas and often do not have non-radioactive analogues. Both technologies have improved the reaction times and yields of certain radiosynthesis steps. However, despite many published reports, microfluidic instruments have yet to make a revolutionary impact in the field of PET.

Reference

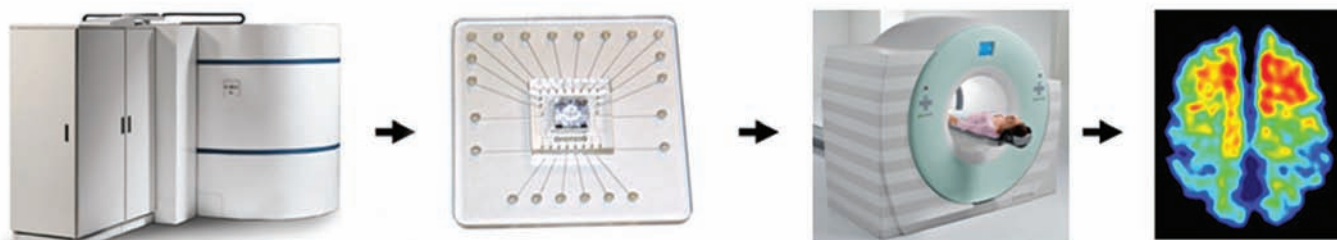
A M Elizarov, *Lab Chip*, 2009, DOI: 10.1039/b820299K

None of the approaches contains a complete solution that can integrate the entire process, starting with raw radioisotope and yielding an injectable dose of radiopharmaceutical. The advantages of microfluidics in radiosynthesis have to be balanced against its drawbacks, such as material incompatibility or the inability to perform solvent exchange.

Many reports have concentrated on performing the radiolabelling reaction alone. While it is the most critical step of radiosynthesis, the steps before and after it have to occur without loss of reagent, product or time. Thus, the first system that draws on all reported advantages of microfluidics, addresses all the issues and enables total process integration should be a blockbuster. Several groups are pursuing this goal. When realised, it will not only open up a path for more efficiently producing known radiopharmaceuticals, but will enable scientists to develop and use new, more potent PET probes, which are being held back solely on the basis of their inefficient synthesis. Such technology, enabling earlier diagnosis of many diseases, will save hundreds of lives.

Read more in 'Microreactors for radiopharmaceutical synthesis' in issue 10 of *Lab on a Chip*.

Raw isotope from the cyclotron (far left) must be quickly converted into a radiopharmaceutical before being injected into a patient



Essential elements

Lab on a Chip goes YouTube™

Are you interested in watching the latest advances in microfluidics on video? The new *Lab on a Chip* YouTube™ video channel makes it possible by visualising all the latest scientific research in the field of miniaturisation. 'Many of the articles we receive for *Lab on a Chip* include video footage. These videos are currently captured on our journal website together with the scientific article, but we felt it was essential to share all this interesting information, not only with the scientists who regularly read *Lab on a Chip* but with the wider scientific community,' states Harp Minhas, editor of the journal.

One of the videos included

illustrates how researchers at the University of St Andrews, UK, use the unusual curving properties of laser beams to hurl microparticles and cells over walls. The scientists were looking into optically redistributing of microparticles and cells between microwells.



'I think it is a great idea to establish such a video channel, in particular within the field of microfluidics where the vast majority of results are recorded

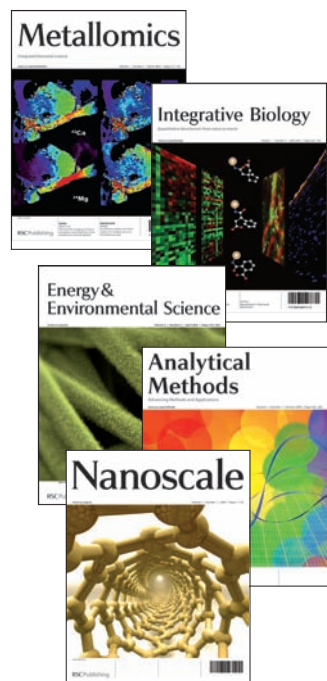
and presented as video files,' comments Jörg Baumgartl who led the research. The associated article is published in *Lab on a Chip* as an advance article at www.rsc.org/loc.

'All scientists are keen to increase the visibility and impact of their work and this ties in with the RSC goal to communicate the chemical sciences as widely as possible and engage a wide audience,' adds Harp Minhas. 'Videos are a universal language and aid the understanding of scientific work on an international level. YouTube™ represents the perfect medium to help us achieve this goal.'

To find out more go to www.youtube.com/labonachipvideos

Did you know...

RSC Publishing offers FREE online institutional access for a number of new RSC journals. You could already be enjoying free access to *Metallomics* and *Integrative Biology*.



Don't miss out on the last months of *Energy & Environmental Science's* free access period which expires at the end of 2009. In addition, RSC Publishing's two new journals, *Analytical Methods* and *Nanoscale*, will have free access until the end of 2010!

To register couldn't be easier. Just fill in our online form at www.rsc.org/free_access_registration and start receiving the latest new journal issues today.

Out and about

The Third *ChemComm* International Symposium on Organic Chemistry was held in February in China. The RSC partnered with three universities – Peking University, Sichuan University and the Shanghai Institute of Organic Chemistry – to host the three one-day meetings. With over 700 delegates attending and key speakers from across the world, the symposium was a huge success.

Sarah Thomas, editor of *ChemComm* comments: 'The lectures presented during the symposium were of outstanding quality and covered the whole breadth of organic chemistry from transition metal asymmetric catalysis, organocatalysis,

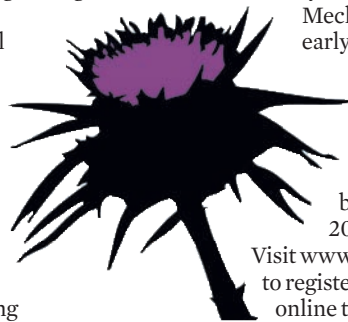
mechanistic studies to the synthesis of both natural and non-natural products.' Abstracts of the research presented at the symposium, and biographies of the presenters can be found at www.rsc.org/chemcommsymposia

The RSC is also organising the 42nd IUPAC Congress which will be held in Glasgow, UK, in August. The programme features around 50 symposia, which will demonstrate the impact of the chemical sciences, highlighting

exciting innovations with an overall focus on 'Chemistry Solutions'. Key themes for this event are: Analysis & Detection, Chemistry for Health, Communication & Education, Energy & Environment, Industry & Innovation, Materials and

Synthesis & Mechanism. An early bird discount of £50 is available for those who register for the meeting before 5 June 2009.

Visit www.iupac2009.org to register your place online today!



Chemical Technology (ISSN: 1744-1560) is published monthly by the Royal Society of Chemistry, Thomas Graham House, Science Park, Milton Road, Cambridge UK CB4 0WF. It is distributed free with *Chemical Communications*, *Journal of Materials Chemistry*, *The Analyst*, *Lab on a Chip*, *Journal of Atomic Absorption Spectrometry*, *Green Chemistry*, *CrystEngComm*, *Physical Chemistry Chemical Physics*, *Energy & Environmental Science* and *Analytical Abstracts*. *Chemical Technology* can also be purchased separately. 2009 annual subscription rate: £199; US \$396. All orders accompanied by payment should be sent to Sales and Customer Services, RSC (address above). Tel +44 (0) 1223 432360, Fax +44 (0) 1223 426017 Email: sales@rsc.org

Editor: Joanne Thomson
Deputy editor: Sarah Dixon
Associate editors: Celia Gitterman, Elinor Richards
Interviews editor: Ruth Doherty
Web editors: Nicola Convine, Michael Townsend, Debora Giovannelli
Essential elements: Kathrin Hilpert and Christine Hartshorne
Publishing assistant: Jackie Cockrill
Publisher: Graham McCann

Apart from fair dealing for the purposes of research or private study for non-commercial purposes, or criticism or review, as permitted under the Copyright, Designs and Patents Act 1988 and the copyright and Related Rights Regulations 2003, this publication may only be reproduced, stored or transmitted, in any form or by any means, with the prior permission of the Publisher or in the case of reprographic reproduction in accordance with the terms of licences issued by the Copyright Licensing Agency in the UK. US copyright law is applicable to users in the USA.

The Royal Society of Chemistry takes reasonable care in the preparation of this publication but does not accept liability for the consequences of any errors or omissions. The RSC is not responsible for individual opinions expressed in *Chemical Technology*. Content does not necessarily express the views or recommendations of the RSC.

Royal Society of Chemistry: Registered Charity No. 207890.

RSC Publishing

Green Solvents—Progress in science and application

DOI: 10.1039/b907013n

The use of organic solvents remains a major source for VOC emissions from the chemical industry. As shown in Fig. 1, VOC emissions in Germany were cut down by almost 50% percent within the period of 1990 to 2000. However, the reduction was mainly achieved within the transportation and fuel sector, whereas the total emission from solvent uses remained almost stagnant at approximately 1000 kT per year. This reflects at least partly the fact that emission can be controlled in transportation by increased engine efficiency and other technical measures, but reduction requires replacement of existing solvent technologies in the processing sector. The implementation of Green Solvents thus has still a large potential to contribute to more sustainable processes in chemical, pharmaceutical and processing industries.

industrial sectors, as they can lead to improvements and innovations in reaction and processing technologies beyond the replacement of conventional solvents in existing processes. The biennial conference “Green Solvents” focuses on the use of such media in chemical synthesis, catalysis, material sciences, and separation processes. The present issue of *Green Chemistry* features a number of contributions that are based on presentations given at the latest, fourth edition, of this symposium, held in Friedrichshafen at the beautiful shores of Lake Constance, Germany, from 28 September to 2 October 2008. Professor **Istvan Horvath** gave the *Green Chemistry* sponsored lecture at this meeting as part of the celebrations for the 10th year of publishing of the Journal, and a perspective based on the his lecture was published in Issue 11, 2008

- The use of green solvents can provide additional control factors over activity and selectivity in all areas of catalysis, including heterogeneous, homogeneous and bio-catalysis.

- The preparation of catalysts and materials holds many opportunities for the application of advanced fluids.

- The principal requirements of solution phase processes in the utilization and transformation of biomass opens a wide field of enormous potential impact for green solvents in the supply chain of fuels and chemicals.

Another interesting aspect that has been prolific in this area over the years is the complementary and synergistic research on chemical processes with other fields of applications requiring fluid phases. Recently, this has been most pronounced for ionic liquids, where applications as diverse as compressor fluids, solar cells, or electro plating are progressing rapidly. As a result, two types of conferences, which are held in alternating years, have emerged: The “Green Solvents” conference, where typical solvent and solution phase processes can be discussed in direct comparison to the concepts based on other advanced fluids, and the “International Conference on Ionic Liquids” (COIL, to be held this year for third time from 31 May–4 June 2009, in Cairns, Australia) where the latest developments on ILs are discussed all across the various areas of applications.

The 2008 edition of the Green Solvents conference was entitled “Progress in Science and Application”. Albeit the meeting showed that significant progress has been made over the last 5–10 years, it also demonstrated that many fundamental questions are yet to be answered and numerous applications are still to be developed. It is thus more than likely, that we will meet again in 2010.

Walter Leitner

RWTH-Aachen, Germany

Scientific Editor, *Green Chemistry*

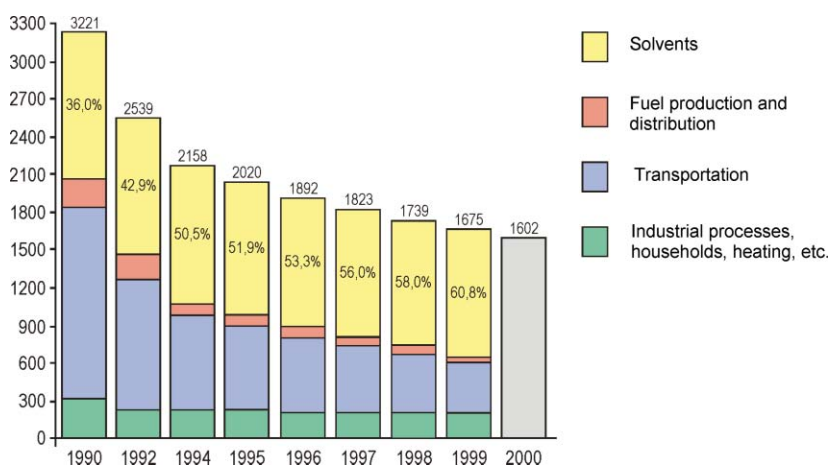


Fig. 1 Reduction of VOC emissions from various sources in Germany during the period of 1990 to 2000. (Graphics reproduced from: Umweltdaten Deutschland 2002, www.umweltbundesamt.de.)

The pharmaceutical industry, for example, has made significant steps towards identifying organic solvents with a reduced ecological footprint compared to traditional reaction and separation media (*1st generation green solvents*). *Advanced fluids* or *2nd generation green solvents*, such as water, liquid polymers, ionic liquids, and supercritical fluids, hold considerable additional promise for this and other

(*Green Chem.*, 2008, **10**, 1024–1028, DOI: 10.1039/b812804a).

From the presentations and discussions at this conference several trends can be deduced, which are also reflected in the contributions to this volume.

- The integration of reaction and separation for process intensification continues to be a major driving force for the research in this field.

Conference report: Lake Constance turns green†

DOI: 10.1039/b822925m

On the shores of Lake Constance (Fig. 1), overlooking the Swiss Alps and Austria, Friedrichshafen (Germany, home of the Zeppelin) hosted the 2008 manifestation of the biannual DECHEMA Green Solvents Conference. This year's theme, *Progress in Science and Application*, followed previous years' themes: *Catalysis* (2002), *Synthesis* (2004), and *Processes* (2006). The organising committee comprised Prof. Walter Leitner, Prof. Kenneth Seddon, Prof. Peter Wasserscheid, Dr Dana Demtröder and Ms Barbara Feißt. Out of one hundred and fifty-one participants, ninety-five percent were associated with European institutions and companies (over half, German), and a few hailed from the USA, Japan and South Africa. Altogether, the conference drew a thorough mix of academics and industrialists, students, chemists and chemical engineers. The whole critical discussion was concentrated around three currently “big” solvent topics: water, CO₂ and ionic liquids.

Water and CO₂ are benign substances in nature and by nature; at near- or supercritical conditions, their properties can change substantially with relatively small changes in temperature and pressure. Likewise, the physical properties (*e.g.* density, viscosity) of gas (CO₂ or other)-expanded liquids can vary substantially with small changes in composition. Such flexibility of the solvents *in situ* allow, for example, the efficiencies of a homogeneous reaction combined with the easy recovery of a catalyst or product. Ionic liquids, while not necessarily benign, are inherently “tuneable”, by the choice of functionality built into the cation and anion.

Prof. Leitner (RWTH Aachen; see Fig. 2), as conference chairman, foreshad-



Fig. 1 Lake Constance adopts a green policy.



Fig. 2 Walter Leitner illustrates the drawbacks of conventional solvent processes.

owed these and other points of potential discussion; he showed the seriousness of

the issues by overviewing the level of emissions, which are currently occurring to the atmosphere, and highlighting that the chemicals industry was the worst, and most persistent, source of volatile organic compounds (VOCs); see Fig. 3. Prof. Leitner then handed the floor to Prof. Horváth (Eötvös University, Budapest) for the opening lecture, which was sponsored by this journal.

István Horváth highlighted one of the key principles of green chemistry—the elimination of solvents in chemical processes or replacement of hazardous solvents. He discussed all the examples that he had experienced in his scientific career,

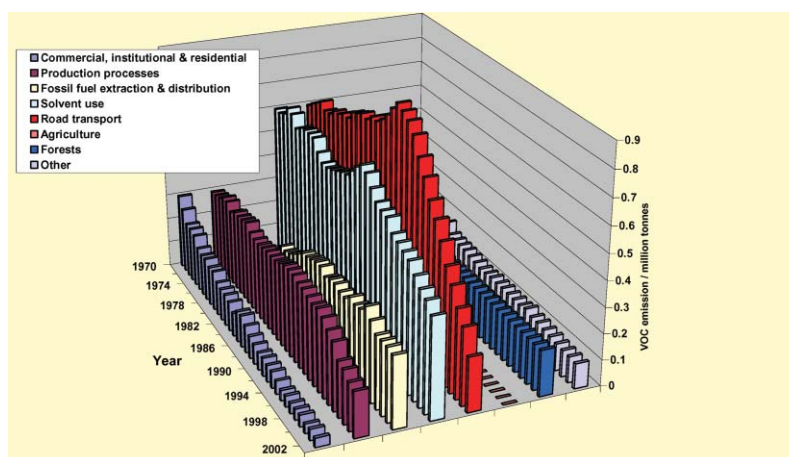


Fig. 3 UK VOC emissions (1970–2002). Note the predominance of emissions from solvent usage in the latest data.

† This paper was published as part of the themed issue of contributions from the Green Solvents – Progress in Science and Application conference held in Friedrichshafen, September 2008.

including water, alcohols, acids, fluorosolvents, ionic and bio-ionic liquids, as a demonstration not just of how solvents can be environmentally friendly, but also that they are an integral part of the solution to a whole spectrum of chemical challenges. In his conclusion, Horváth addressed the global initiative to steer away from a petroleum-based economy towards a renewables-based one, presenting γ -valerolactone (see Fig. 4) as a suitable plant-derived molecule for the production of both energy and carbon-based consumer products.¹ It is a five-carbon, five-membered cyclic ester with low vapour pressure, low melting point, high boiling and flash points, which is relatively safe for transport on large scale. Blended 10% v/v with 95-octane gasoline, it performs very similarly to ethanol. It does not form azeotropes with water, hence its isolation *via* distillation from an aqueous solution is less energy-intensive than isolation of bioethanol. Horváth was not the only speaker to mention γ -valerolactone, but his presentation prompted an energetic discussion afterwards.

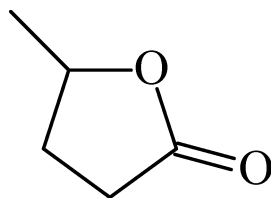


Fig. 4 γ -Valerolactone

Neil Thomas (University of Nottingham) gave a comprehensive talk on biocatalysis in green solvents, using enzymes as homogeneous catalysts in fluorosolvents and supercritical fluids. Virtually water-immiscible fluorosolvents readily dissolve in gases like CO_2 and O_2 and have temperature-controlled miscibility with organic solvents. Enzymes could be solubilised in a fluorosolvent phase by coating with a fluorosoluble hydrophobic surfactant (*e.g.* Krytox). This technique, referred to as hydrophobic ion pairing, is inexpensive, reversible, and applicable to most enzymes. Thomas verified that enzymes were suspended singularly, not as aggregates or in aqueous micelles. Hydrophobic ion pairing could be used to dissolve enzymes in supercritical CO_2 as well, but with the limitation that wet supercritical CO_2 is

acidic and can form (reversible) carbamates with amine side chains. Thomas showed use of hydrophobic ion pairing for biphasic dynamic kinetic resolutions of chiral substrates, with enzyme catalysts dissolved in either supercritical CO_2 or fluorosolvent and substrate dissolved in an organic phase. The mixture could be warmed into a single phase, then cooled after the reaction to separate products (organic phase) from catalyst (fluorosolvent phase).

From an industrial perspective, Andrew Wells (AstraZeneca) stressed that improving the sustainability of solvent systems is essential because of factors such as regulatory constraints, safety, and environmental impact. In the pharmaceutical industry, solvents constitute a high proportion of the total waste produced, energy and natural resources used, and cost. Wells exemplified these concepts through a series of processes which have been modified to be more sustainable: a revision of the commercial synthesis of Lipitor[®] allowed the replacement of triethylborane with alcohol dehydrogenase in water as a reducing agent at room temperature rather than at $-78\text{ }^\circ\text{C}$. The advantages of supercritical CO_2 in continuous-flow reactors or for chromatographic processes were also outlined. Finally, he showed that cleaning reactors, an operation classically consuming large amounts of volatile organic compounds, can be done more efficiently with detergents in water and careful monitoring.

Uwe Vagt (BASF) talked about challenges in the commercialisation of ionic liquids, including price, purity, low toxicity, reliable supply, and recovery from catalytic processes. Therefore, high priority is placed upon such properties as material compatibility (corrosion behaviour) and environmental aspects (toxicity, biodegradability). He listed a few examples of cations chosen for specific purposes: ammonium/pyrrolidinium for electrolytes, cholinium for biodegradability, or imidazolium for its broad applications and low viscosity. BASF's range of interests includes ionic liquid synthesis, chemical processes, separation technology, engineering and functional fluids, dye-sensitised solar cells, and polymer and metal processing.

The applications of ionic liquids as electrolytes in fuel cells, batteries, sensors, super-capacitors, and dye-sensitised solar

cells were stressed by Thomas Schubert (IoLiTec). IoLiTec has developed a series of electrolytes in collaboration with several partners for applications in dye-sensitised solar cells. Ionic liquids also have applications for metal deposition and metal finishing. The metal can either be deposited pure from the ionic liquid (most metals) or as an alloy (Cr, Mn and Mo). A problem in the case of aluminium deposition is that the chloroaluminate ionic liquids used are not water-stable. Alternative aluminium salts were screened, but none were found to be better. However, various additives were explored with some success (*e.g.* LiF for good surface adhesion, and toluene for smooth deposition).

Matthias Seiler (Evonik Degussa) described refrigerant/sorbent cooling and heating systems: absorption chillers are cooling machines that use heat as the primary source of energy to drive a refrigeration cycle. The choice of the working pair of fluids used is crucial: the two pairs which are currently commercially viable are $\text{NH}_3/\text{H}_2\text{O}$ (refrigeration) and $\text{H}_2\text{O}/\text{LiBr}$ (water chillers). Seiler compared the disadvantages of the $\text{H}_2\text{O}/\text{LiBr}$ system (corrosivity and crystallisation of refrigerant) and the $\text{NH}_3/\text{H}_2\text{O}$ system (toxicity, high working pressure, and need for rectification) and proposed the use of an ionic liquid with H_2O or CO_2 as refrigerant.

An interesting twist on natural products was Cinzia Chiappe's (University of Pisa) talk on the use of natural renewable starting materials to generate ionic liquids. Currently, most room-temperature ionic liquids are from petrochemical-derived products. Chiappe illustrated ionic liquids based on amino acids, fructose, choline, or ascorbic acid. Though most were quite viscous, these could offer advantages such as chirality (*e.g.* for use in enantioselective reactions). Chiappe also discussed glycerol as a precursor for a wide range of chemicals. Strongly Brønsted acidic salts, such as bis(glycerato)borate acids, were reported to be liquids at room temperature. Denise Reinhardt (Friedrich-Schiller University of Jena) showed that some mixed systems, such as fructose/urea melts, could be promising sustainable solvents, being non-toxic, biodegradable, and available from renewable resources.

Robin Rogers (QUILL) outlined the mechanism for cellulose dissolution in

the ionic liquids [C₂mim]Cl and [C₂mim]-[ethanoate] (where C₂mim = 1-ethyl-3-methylimidazolium) and expounded upon a variety of other feedstocks being dissolved in ionic liquids—[C₂mim]-[ethanoate] dissolved pine (up to 92.6%) and oak (99.5%), taking one to two days for dissolution, separation, and fragmentation. Mild grinding led to complete and faster dissolution. Rogers suggested uses for dissolved lignocellulosic materials in *e.g.* fibres, sensor supports, and composite materials. As with all green technologies, Rogers stressed that there needs to be clear communication between universities, industry, and government for these applications to be realised and utilised. Tadafumi Adschiri (Tohoku University) used high-temperature water to dissolve cellulose in a pre-treatment for biodegradation to glucose. Like [C₂mim]Cl and [C₂mim][ethanoate], high-temperature water dissociates the polymer's hydrogen bonds. Once cellulose in its naturally-occurring crystalline form, cellulose I, is dissolved in supercritical water, it reprecipitates slowly as cellulose II, which undergoes enzyme hydrolysis twice as fast as cellulose I. Further reactions on glucose (*e.g.* retro-aldol or dehydration) can lead then to a number of useful chemicals. In addition, Adschiri described how he synthesised organic/inorganic hybrid nanoparticles of well-controlled size and shape in supercritical water. Moreover, Michal Roth (Academy of Science of the Czech Republic) used near-critical water for the extraction of solid hydrocarbons, tuning the solubility of these hydrophobic solutes by variance in temperature and pressure. The cohesive energy density of water, he explained, falls steeply, going from ambient water toward supercritical.

Alexei Lapkin (University of Bath) wanted to use plants as natural factories for making complex functional molecules. In a case study with the plant *Artemisia annua*, he discussed the use of various (conventional) solvents to extract different high-value products. More interestingly, his talk drove home how the commercial viability of natural product extraction, from cultivation to final product isolation, is very sensitive to the global market price for the main extraction product (here, an anti-malarial molecule). On the premise of the food industry's strong preference for using benign solvents, Charlotte Turner

(Uppsala University) used near-critical water to successfully extract high-value products (such as quercetin and betolin) from plant matter (onion waste and birch bark, respectively).

Andy Cooper (University of Liverpool) presented emulsion templated meso- and nanoporous polymeric materials which can be prepared from liquid or supercritical CO₂. The stability of the emulsion is improved by introduction of carbonate groups in the monomer and/or by lowering the temperature. It was the second part of Cooper's lecture that proved even more fascinating to the audience, however, showing how a simple water/silica blend (95:5 by weight), so-called "dry water", is able to store large amounts of methane. The gas is encapsulated in a clathrate fashion in the structure of water droplets, stabilised by silica sitting in the water-air interface. Thus, the capacity for methane storage is strikingly high (175:1 v/v), but the material requires high pressures and/or low temperatures to be stabilised. The inclusion of a tetraalkylammonium bromide, although decreasing the capacity to 50:1 v/v, greatly enhances the stability of the gas-loaded material, which does not show any methane release at ambient conditions.

Liquid CO₂ can be utilised as a carrier solvent for the impregnation of drug molecules into a mesoporous material, as reported by Anna Hilleström (YKI, Institute for Surface Chemistry, Stockholm). The aim of this project was to optimise the loading capacity of ibuprofen (extensively used as anti-inflammatory drug) into meso-structured silica. Some advantages of using liquid CO₂, instead of organic solvents, are that no residues are observed in the final material, no drying step is required, it provides tunable solubility (changing pressure, temperature or presence of co-solvent), and it is harmless and inexpensive. In addition, a high loading capacity of ibuprofen into mesoporous silica can be achieved, due to the solvophobicity of the drug in liquid CO₂.

Ana Aguiar-Ricardo (Universidade Nova de Lisboa) explained how she used supercritical CO₂ in the preparation of switchable "smart" biomaterials, which can change their structures upon different stimuli, such as temperature or pH. For example, porous polysulfone can be impregnated with a thermore-

sponsive polymer, which would fill the pores below its low critical solution temperature, preventing water flow through them.

Marijke Aerts (Eindhoven University of Technology) showed how residual monomers could be extracted from polymer latexes using supercritical CO₂ and water. This is an important purity issue regarding environmental regulations on commercial polymers. In a system of latex-in-water droplets, dispersed in supercritical CO₂, the supercritical CO₂ plasticised the polymer at the droplet surface and allowed styrene to diffuse out quickly. Joachim Karthäuser (SiOx Machines) proposed high-pressure liquid CO₂ as a versatile extraction and cleaning solvent for leather, plastics, and metal. The equipment developed by SiOx Machines for such applications was described. His talk illustrated how the resistance of the market towards new technologies, even very promising ones, could significantly delay the time from discovery to commercialisation.

Richard Noble (University of Colorado) presented a successful method of separating CO₂ from N₂, *via* selective absorption with basic ionic liquids having pendant amino groups. Their high viscosity discourages their use as pure solvents, but they can be mixed with amines or other ionic liquids to reduce viscosity without loss of CO₂ affinity. Patricia de Luis (University of Cantabria) replaced a volatile, dispersed absorbent (*N,N*-dimethylaniline) with an ionic liquid in a ceramic hollow fibre membrane to recover SO₂ from a manufacturing process of ZnO and SO₂. Her final choice of [C₂mim][EtSO₄] was a compromise of price, viscosity, toxicity, affinity for SO₂, and availability. Anders Riisager (Denmark University of Technology) also discussed the use of supported ionic liquid phase (SILP) absorbents for SO₂ and CO₂. Riisager showed that SILPs could even be made catalytically active, either by containing dissolved metal complexes or by the ionic liquids themselves having intrinsic catalytic activity. Alkene hydroformylation or hydrogenation reactions, and production of N₂ from NO_x, using NH₃ and O₂ with his method, were demonstrated. Pertinent to gas absorption in ionic liquids, Aaron Scurto (University of Kansas) presented some of the first studies of interfacial mass transfer for biphasic

systems with ionic liquids. As a tool for “tuneability”, gas-expansion of both ionic and molecular liquids can substantially change their physical properties (viscosity, diffusivity). The beneficial effect of dissolved CO₂ on the mass transport properties of ionic liquids was illustrated in rhodium-catalysed hydrogenation and hydroformylation of 1-octene in a biphasic ionic liquid/CO₂ system.

There are no prior examples of chiral ionic liquids having been used to stabilise nanoparticles. Alexander Kraynov (RWTH Aachen) claimed that chiral tetraalkylammonium tartrates can stabilise various catalysts (Raney Ni, Cu, *etc.*) and, at the same time, transfer the chirality to the products in hydrogenation reactions. Higher stability and high catalytic activity were shown. Similarly, metal clusters supported on nanoparticles coated with ionic liquids were reported by Richard Knapp (Munich University of Technology). The ionic liquid acts as a surface mediator (tunable solubility of the reactants), reaction medium, and stabilising agent, preventing the metal particles from oxidation. The coated catalyst shows higher activities at lower temperatures when compared to uncoated.

David Cole-Hamilton (University of St. Andrews) discussed aqueous biphasic hydroformylation of medium chain alkenes. The use of 1-methyl-3-octylimidazolium bromide ([C₈mim]Br) as an additive increases the turnover frequency, presumably by acting as a weak surfactant stabilising micelles, thus increasing the contact surface of the organic and water phases, though allowing fast phase separation and good catalyst recovery. An alternative solution is to use a biphasic system with a catalyst switching between phases. The catalyst is soluble in the organic phase during reaction, but switches to the aqueous phase when bubbling CO₂. The catalyst will go back to the organic phase when bubbling N₂. Julia Leschinski (Dortmund University of Technology) showed the effectiveness of water in the recycling of homogeneous transition metal catalysts, exemplified in the telomerisation of butadiene.

Jörg Sundermeyer (Philipps University, Marburg) presented two oxidation processes catalysed by copper compounds. Firstly, the ring oxidation of phenols to quinones by molecular oxygen was

described, using copper salt/ionic liquid mixtures. An oxotetracuprate cluster was identified and believed to be the actual catalytically active species. Optimisations were carried out using different ratios of CuCl₂ to ionic liquid at 10 bar of O₂. It was found that a 1:1 ratio was best, producing 100% conversion of the phenol and 94% selectivity to the quinone. The second transformation discussed was the oxidative carbonylation of methanol with dioxygen and CO to yield dimethyl carbonate and water (ENICHEM Process). A variety of copper-containing hydrophobic ionic liquids were tested, and the best was found to be [Cu(C₁₂im)₄][PF₆] (where C₁₂im = 1-dodecylimidazole), giving 60% conversion and 78–89% selectivity.

For the preparation of polyethylene nanoparticles, Stefan Mecking (University of Konstanz) replaced the currently-used Ziegler and Phillips catalysts (which requires anhydrous conditions) with aqueous-phase Ni(II) catalysts. The structure of the product—linear *vs.* branched polyethylene—can be controlled by the choice of catalyst ligands. M. G. Finn (Scripps Research Inst.) also spoke on aqueous-phase reactions under *ambient* conditions. He demonstrated so-called “click reactions” (*e.g.* an azide with an alkyne to form a triazole ring), which are highly energetically favourable, highly selective reactions, assumed to have a narrow transition state. These are often best carried out in water. Finn then discussed why some reactions of hydrophobic substrates are faster in water. One explanation could be ground state destabilisation in water, the classic “hydrophobic effect”. Another could be cohesive energy density: reactions which are accelerated by pressure could be accelerated in water, due to its (ambient) cohesive energy density being far greater than that of any other common solvent. Finally, a reaction could occur “on water”, analogous to a surface reaction at an oil-water interface. The structure of water at the interface is such that many water molecules (about one in four) have a hydroxyl group protruding into the organic phase. These groups may stabilise the transition state through hydrogen bonding and thus catalyse a reaction.

The series of talks was well complemented by over sixty posters. The poster session (Fig. 5) formed the heart of the



Fig. 5 The poster session.

conference, and proved to be a productive time for interaction. More than two-thirds of the posters were related to ionic liquids, mostly to their use as solvents for reactions and catalytic processes. The remainder were presenting supercritical fluids, water and other potentially green solvents, as well as binary solvent systems, *e.g.* ionic liquids and supercritical CO₂. Besides reactions and catalysis, topics such as extraction, polymer science, and fundamental issues were also represented.

The quality and diversity of the science and application found in this year's posters were reflected in the poster prize winners. All three related to catalytic reactions, but with different approaches. First prize went to a poster by Marion Stricker and Jörg Sundermeyer (University of Marburg, Germany) on copper-based catalytic ionic liquids in the synthesis of dimethyl carbonate. Second went to Benjamin Schaffner and co-workers at the University of Rostok (Germany) and University Claude Berard of Lyon (France), for work on metal-catalysed reactions in propylene carbonate. The third prize travelled to Japan, to reward the efforts of Masaru Watanabe and co-workers (from Tohoku University) on the investigation of microwave-assisted heterogeneous catalytic conversion of glucose and fructose to 5-hydroxymethylfurfural in near-critical water.

It was a major success of the *Green Solvents: Progress in Science and Application* conference to programme a multidisciplinary sequence of lectures, avoiding topic segregation of the sessions. Industrialists, chemical engineers, and students were all reporting excellent research from different fields, allowing interesting discussions to be held and cross-fertilisation of ideas to arise. Some people argue that

green chemistry is simply more efficient chemistry. If one can tune the properties of a solvent to one's process, the solvent can be a green feature of the process. From the variety and scope of this year's presentations, we can look forward to the 2010 meeting being dominated by a deeper understanding of this tuneability,

and more processes which have been designed rather than discovered.

Gabriela Adamová, QUILL, The Queen's University of Belfast, Belfast, BT9 5AG, United Kingdom. E-mail: quill@qub.ac.uk, **Jamie L. Ferguson**, **Shieling Ng**, **Alberto V. Puga** ‡, **Héctor**

Rodríguez, **Sandra M. Rountree**, **Kenneth R. Seddon** and **Alina A. Tomaszowska**

Reference

- 1 I. T. Horváth, H. Mehdi, V. Fábos, L. Boda and L. T. Mika, *Green Chem.*, 2008, **10**, 238–242.

‡ né Alberto Vaca

Application of the solvent water in two-phase telomerisation reactions and recycling of the homogeneous palladium catalysts†

Arno Behr and Julia Leschinski

Received 13th November 2008, Accepted 9th January 2009

First published as an Advance Article on the web 17th February 2009

DOI: 10.1039/b820305a

In the chemical industry organic solvents should be avoided wherever possible. They are often toxic to marine organisms and plants as well as to higher organisms and humans. Moreover, volatile organic compounds (VOC) cause air pollution which leads to the necessity of expensive separation technologies like waste water or exhaust gas treatments. Solutions for these problems are either the development of processes without the use of any solvent or the use of environmentally benign solvents such as water. In this contribution it is shown how versatile water can be, used as a solvent in homogeneously catalysed processes, for example, telomerisation reactions with methanol, diethylamine, ethylene glycol and glycerol. In this context another positive effect of the solvent water is the ecologically and economically required retention of the transition metal catalyst inside the process. Furthermore, different reactor types, a loop reactor and a mixer-settler reactor, are presented to cope with the challenges of mass transport limitations and selectivity control in aqueous biphasic systems.

1 Introduction

A transition metal homogeneously catalysed reaction in one single liquid phase with gaseous reactants leads to some challenges (Fig. 1a). Firstly, the catalyst must be separated after the reaction to avoid heavy metal contamination of the reaction products. Moreover, a recycling method for the catalyst is required in terms of cost reduction. In the case of gaseous reactants there can be a mass transport limitation between the gaseous and liquid phase which can lead to low reaction rates.

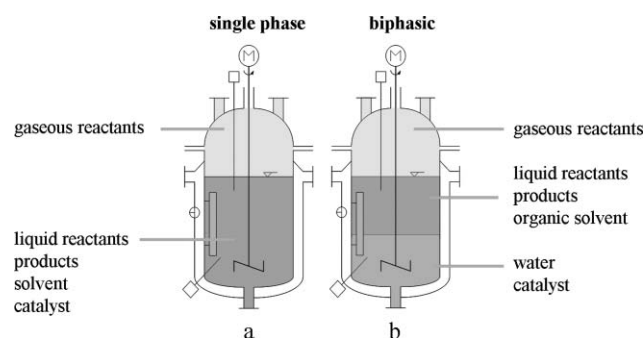


Fig. 1 Homogeneous catalysis in single phase and biphasic mode.

The catalyst separation and recycling can be implemented by using the aqueous biphasic technique (Fig. 1b). The main advantage is the easy catalyst separation but often the main

disadvantage is the increase of mass transport limitations due to the additional liquid phase. This problem has to be solved by special reactor and process design.

In an aqueous catalyst phase a polar soluble catalyst is needed. One famous example is triphenylphosphine trisulfonate (TPPTS) (Fig. 2) which is used in the Ruhrchemie-Rhône-Poulenc-process¹ and has also been patented for the use in telomerisation reactions.²

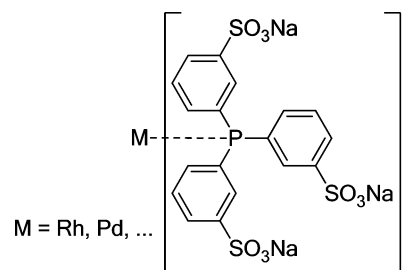


Fig. 2 Water soluble transition metal catalyst with the ligand triphenylphosphine trisulfonate (TPPTS).

If this ligand is used, catalyst separation and recycling can be done by simple phase separation and recycling of the aqueous phase. Moreover, polar reactants can also be separated and recycled in this way.

The telomerisation is defined as the dimerisation of 1,3-dienes with simultaneous addition of a nucleophile such as water or alcohols. In Fig. 3 the telomerisation reaction and potential reactants and products are shown.³

It is obvious that the telomerisation is a direct and atom economic way to unsaturated aliphatic products with interesting applications. In the following, telomerisation reactions of butadiene with different nucleophiles are presented.

Department of Biochemical and Chemical Engineering, Technical Chemistry A, Technische Universität Dortmund, D-44227, Dortmund, Germany

† This paper was published as part of the themed issue of contributions from the Green Solvents - Progress in Science and Application conference held in Friedrichshafen, September 2008.

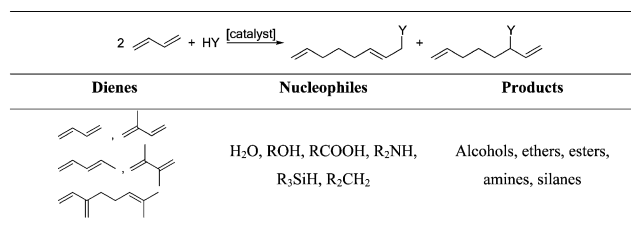


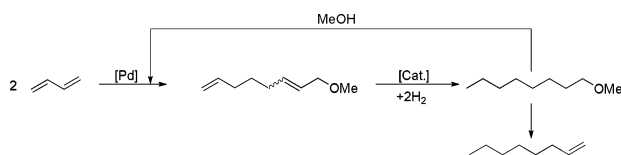
Fig. 3 Telomerisation reactions.

2 Results and discussion

In this contribution we will present reactions of 1,3-butadiene with mono-functionalised nucleophiles such as mono-alcohols and secondary amines which were conducted in a jet loop reactor. Moreover, reactions with multi-functionalised alcohols in mixer-settler-units will be shown. A detailed discussion of various nucleophiles and dienes can be found in our latest review on telomerisation.⁴

2.1 Telomerisation of butadiene with methanol

The telomerisation with methanol leads to methoxyoctadienes which can be used as intermediates in the production of 1-octene as a comonomer in the production of LLDPE (Fig. 4).⁵⁻⁷

Fig. 4 Production of 1-octene *via* telomerisation.

If the reaction is conducted with gaseous butadiene in an aqueous catalyst phase (>10 wt% water) containing palladium and the ligand TPPTS, there are three phases in total. The reaction products (telomers) form a second liquid phase. To enhance mass transport, a continuously operated loop reactor was used^{8,9} as shown in Fig. 5.

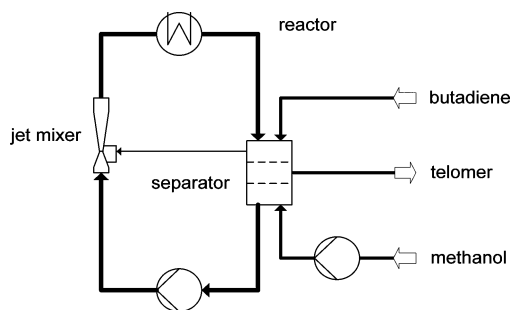


Fig. 5 Loop reactor for telomerisation.

Gaseous and liquid reactants as well as the catalyst phase are mixed intensively inside a jet mixer. They react inside the heated loop and the phases can be separated by simple phase separation. The mixing behaviour is excellent and reaction and product separation are continuously operated. Moreover, catalyst and reactants can be recycled and the chemoselectivity was above 99% for more than 50 h. The regioselectivity was also very high

(96% linear telomer) at a moderate palladium leaching of 35–65 ppm in the product phase. Because of the excellent mass transport conditions a space-time-yield of $160 \text{ kg m}^{-3} \text{ h}^{-1}$ during a reaction period of 56 h could be achieved.⁹

2.2 Telomerisation of butadiene with diethylamine

The telomerisation of butadiene with ammonia was already done in aqueous biphasic systems to control consecutive reactions.¹⁰⁻¹² Telomerisation reactions with secondary amines can even be conducted in methanol without any methanol conversion.¹³ For example diethylamine is highly active in the telomerisation of butadiene (Fig. 6) also in the solvent methanol.

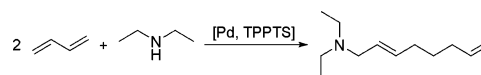
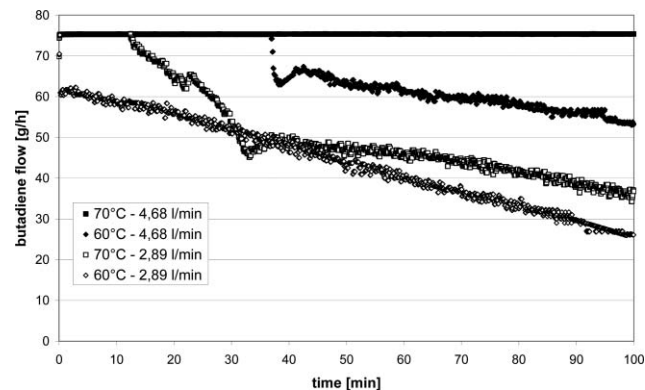


Fig. 6 Telomerisation of butadiene with diethylamine.

This reaction showed a mass transfer limitation in an aqueous biphasic system in semi-batch experiments in a stirred tank reactor,¹⁴ where the reaction rate increased with increasing stirrer velocity. Because of this restriction the reaction was conducted in the loop reactor which was already used in the telomerisation with methanol (Fig. 5). In this reactor type the butadiene intake was very high and could be further increased by increasing temperature and volume flow through the loop (Fig. 7).

Fig. 7 Butadiene intake in the continuous telomerisation with diethylamine.¹⁴

The application of the loop reactor led to an increase of space-time-yield from $45 \text{ kg m}^{-3} \text{ h}^{-1}$ to $152 \text{ kg m}^{-3} \text{ h}^{-1}$ at a catalyst concentration of only 0.005 mol% palladium at 60 °C.

2.3 Telomerisation of butadiene with ethylene glycol

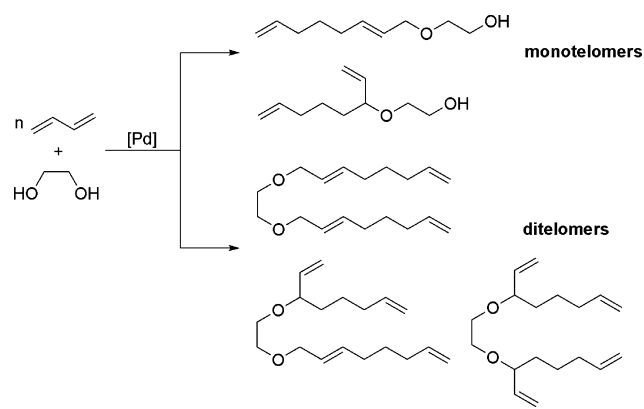
If multifunctional nucleophiles are used, control of selectivity is a major challenge. Due to various possibilities of functionalisation the product distribution is rather broad, especially if the reaction is carried out in monophasic systems.¹⁵ Fig. 8 shows the possibility of undesired consecutive reactions of the monotelomers to ditelomers for the example of ethylene glycol.

To increase the selectivity towards the monotelomers, the aqueous biphasic technique could be applied to utilise the *in situ* extraction effect. The monotelomers are extracted into the organic phase formed by liquid butadiene and are therefore separated from the aqueous catalyst phase avoiding consecutive

Table 1 Comparison of the monophasic and biphasic telomerisation of butadiene with ethylene glycol¹⁵

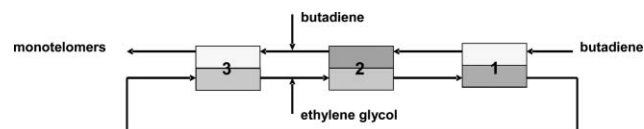
Products	Yield %	
	Single liquid phase	Aqueous biphasic catalysis
monotelomers	60	80
ditelomers	20	<1
dimers	10	<1

^a T = 80 °C, t = 4 h.

**Fig. 8** Telomerisation of butadiene with ethylene glycol.

reactions to the ditelomers. Table 1 shows that by using aqueous biphasic catalysis the yield of monotelomers increases from 60% to 80% whereas the yield of ditelomers decreases from 20% to nearly 0%.

Due to the biphasic system the reaction proceeds more selectively, however the reaction rate is decreased due to mass transport limitations. Therefore, a three-step mixer-settler-process was developed^{16–18} to overcome this problem (Fig. 9). In the first and the last step separation properties are the most

**Fig. 9** Cross-counter-current mode in the telomerisation with ethylene glycol.^{16,17}

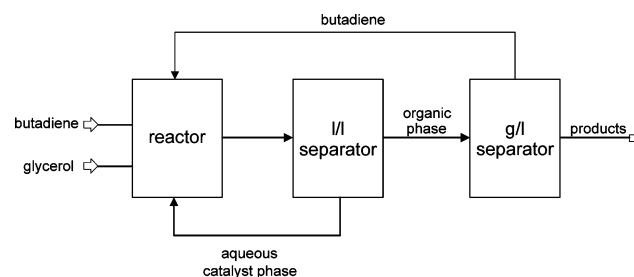
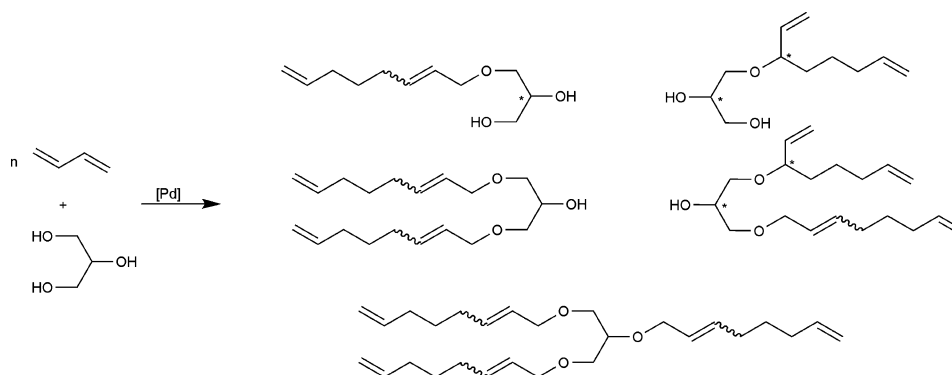
important features so that the polarity differences between the two phases should be as high as possible. The reaction should take place in the middle step of the reactor cascade so that a decreased polarity difference is beneficial.

In the so-called “cross-counter-current-mode” of the mixer-settler-cascade butadiene is added directly before the separation of the product (step 3) to increase the polarity difference again. During the reaction, ethylene glycol is converted so that the aqueous phase leaving step 3 is very polar. However, also the product phase is more polar due to the product formation. That is the reason why additional butadiene is added before step 3. In the reaction step (step 2) ethylene glycol is added to decrease the polarity of the catalyst phase thus also decreasing mass transport limitations. Fresh butadiene is also added in step 1 where the catalyst is separated to increase the separation quality here. The process was run continuously for more than 30 h with a yield of 75% of monotelomer at a palladium leaching of only 19 ppm.

Table 2 Comparison of the monophasic and biphasic telomerisations of butadiene with glycerol^{23,24}

Products	Yield ^a %	
	Single liquid phase ^b	Aqueous biphasic catalysis ^c
monotelomers	45	70
ditelomers	30	1
octadienols	—	<5

^a T = 90 °C, 600 min⁻¹, n_{butadiene}/n_{glycerol} = 2. ^b t = 60 min, solvent: isopropanol. ^c 6 h.

**Fig. 11** Flow diagram for the continuous telomerisation of butadiene with glycerol.**Fig. 10** Telomerisation of butadiene with glycerol.

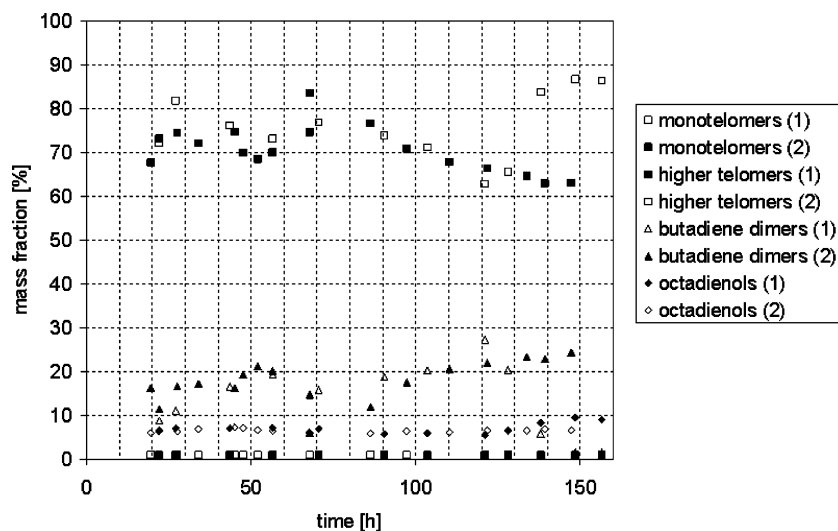


Fig. 12 Continuous telomerisation of butadiene with glycerol ($T = 90\text{ }^{\circ}\text{C}$, 1000 min^{-1} , $0.077\text{ mol}\%$ Pd, $0.03\text{ mol}\%$ inhibitor, $0.13\text{ mol}\%$ phosphonium salt, $m(\text{But}) = 20\text{ g/h}$, $m(\text{Gly})/m(\text{Water}, t = 0) = 1$, $P/\text{Pd} = 7$).²⁹

2.4 Telomerisation of butadiene with glycerol

The use of glycerol as a nucleophile leads to numerous products which are shown in Fig. 10.

Besides linear and branched monotelomers there can also be consecutive reactions towards di- and tritelomers especially in monophasic systems.^{19,20} Monotelomers are valuable intermediates in the production of surfactants or defoaming agents,^{21,22} so that a high selectivity towards these products is highly desirable. Once again, an aqueous biphasic reaction leads to an increased selectivity towards the mono-substituted products (Table 2).^{23,24}

As in the reaction with ethylene glycol, the monotelomers are extracted by the organic phase containing liquid butadiene and consecutive reactions are avoided. In the aqueous biphasic reaction there is the possibility of 2,7-octadienol formation, which is the telomer of butadiene and water,²⁵ but Table 2 shows that this product is formed in yields below 5%. Further by-products which are undesired especially in technical processes are butadiene dimers, oligomers and polymers which cause fouling inside the process equipment. A further requirement for an economic technical process is the catalyst stability, which has to be enhanced to save catalyst costs. In order to analyse these aspects, a continuous process was developed (Fig. 11)^{26,27} and realised in a miniplant.^{28,29}

Liquid butadiene and glycerol are mixed in a reaction step followed by liquid/liquid-phase separation, where the catalyst and unconverted glycerol are recycled to the reactor. The organic phase is fed into a flash-unit where unconverted butadiene evaporates and the liquid products can be removed. Butadiene is liquefied and fed into the reactor.

Due to the application of stabilising agents such as phosphonium salts³⁰ and polymerisation inhibitors (radical interceptors) the process could be run for more than 250 h with a constantly high product quality and leaching values below 20 ppm. In Fig. 12 two continuous runs are shown.

It becomes obvious that butadiene dimers are the main by-products and that their formation is increased by decreasing catalyst activity. The formation of the telomers decreases if the catalyst is deactivated and dimers are formed instead. All

recycling loops were closed so that unconverted substrates could be reused.

3 Conclusions

The green solvent water is a perfect solvent in liquid–liquid–two-phase catalysis. This technique could be applied at different telomerisation reactions in a mixer-settler-arrangement as well as in a loop reactor. The processes were run continuously at low palladium leaching and unconverted substrates were recycled which leads to very economic processes. Moreover, mass transport limitations and selectivity could be controlled by choosing the right reactor and process concepts. All processes were conducted without additional organic solvents so that costs for waste water treatment or solvent recovery could be saved and the environment is not polluted.

Acknowledgements

We would like to thank Umicore AG & Co. KG, especially Dr. Ralf Karch, for providing noble metal catalysts and OXEA-group for TPPTS as well as Cognis Oleochemicals, especially Dr. Alfred Westfechtel, for providing glycerol as well as financial and scientific support. Moreover, we would like to thank the German Federal Ministry of Food, Agriculture and Consumer Protection, Deutsche Forschungsgemeinschaft (German Research Foundation) and Fonds der Chemischen Industrie for financial support of the projects.

References

- 1 A. Behr, *Angewandte Homogene Katalyse*, Wiley-VCH, Weinheim, 2008.
- 2 E. Kuntz, (Rhône-Poulenc), DE2733516, 1978.
- 3 A. Behr, in *Aspects Homogeneous Catal.*, Vol. 5 (Ed.: R. Ugo), Springer Verlag, 1984, 3-73.
- 4 A. Behr, M. Becker, T. Beckmann, L. Johnen, J. Leschinski and S. Reyer, *Angew. Chem.*, in print.
- 5 R. C. Bohley, G. B. Jacobsen, H. L. Pelt, B. J. Schaart, M. Schenk and D. A. G. van Oeffelen, (Dow Benelux), WO9210450 A1, 1992.
- 6 C. L. Edwards, (Shell), WO2005019139, 2005.

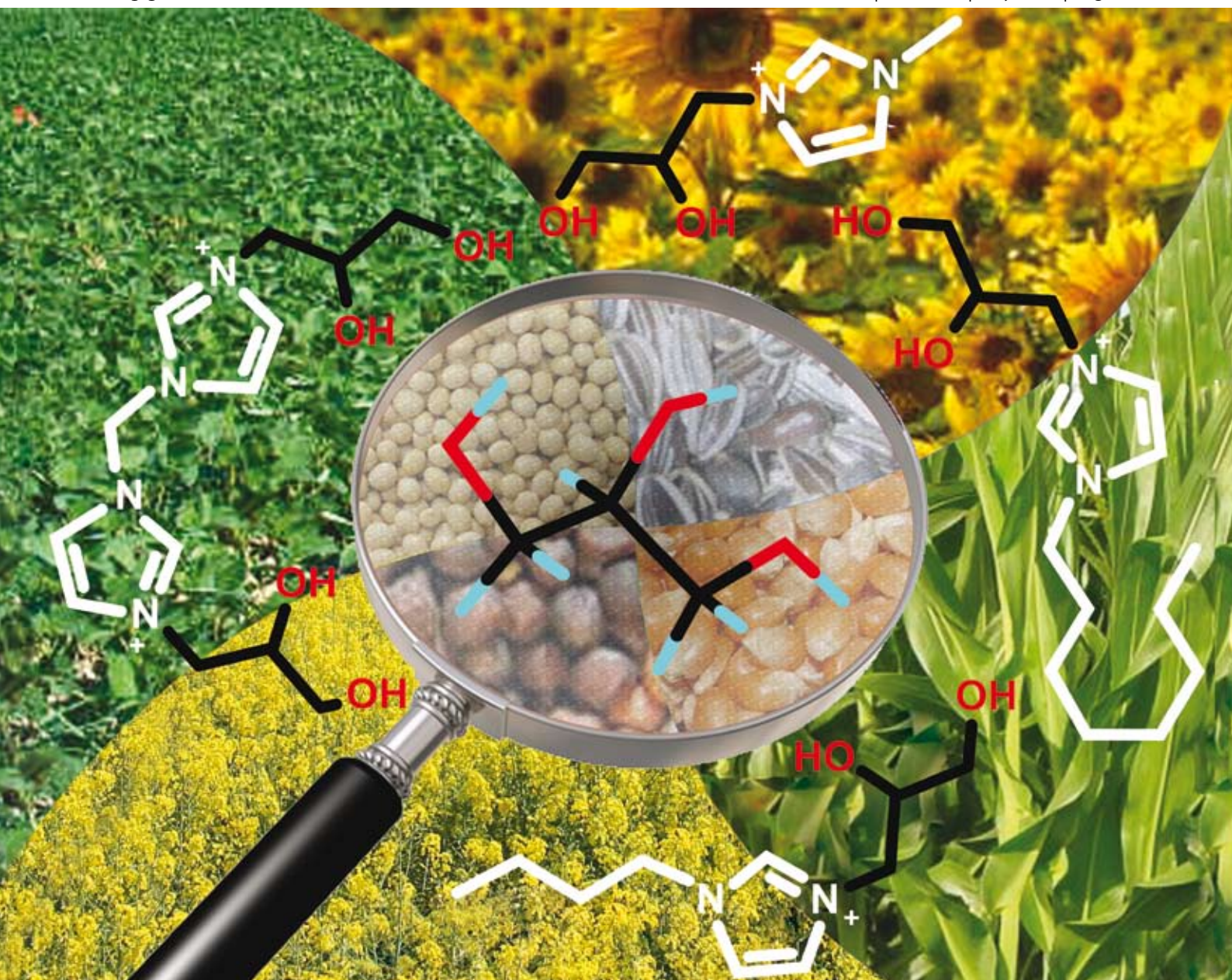
- 7 D. Röttger and A. Tuchlenski, (Oxeno), US2004059170, 2004.
- 8 A. Behr and D. Dehn, *Chem. Ing. Tech.*, 2008, **80**, 1509–1517.
- 9 D. Dehn, PhD thesis, Technische Universität Dortmund, 2008.
- 10 T. Prinz, W. Keim and B. Drießen-Hölscher, *Chem.-Eur. J.*, 1999, **5**, 2069.
- 11 T. Prinz, W. Keim and B. Drießen-Hölscher, *Angew. Chem. Int. Ed.*, 1996, **35**, 1708.
- 12 B. Drießen-Hölscher, in *Synthetic methods of organometallic and inorganic chemistry*, Vol. 10 (Eds.: W. A. Herrmann, G. Brauer), Thieme, Stuttgart, 2002.
- 13 M. Beller, N. D. Clement, L. Routaboul, A. Grotevendt and R. Jackstell, *Chem. Eur. J.*, 2008, **14**, 7408–7420.
- 14 T. Beckmann, PhD thesis, Technische Universität Dortmund, 2009.
- 15 A. Behr and M. Urschey, *J. Mol. Catal. A: Chem.*, 2003, **197**, 101–113.
- 16 A. Behr and J. Seuster, in *Multiphase Homogeneous Catalysis* (Eds.: B. Cornils, H. Olivier-Bourbigou), Wiley-VCH, Weinheim, 2005, 114–122.
- 17 J. Seuster, PhD thesis, Technische Universität Dortmund, 2008.
- 18 A. Behr, J. Seuster, *Chem. Ing. Tech.*, in print.
- 19 R. Palkovits, I. Nieddu, R. J. M. Klein Gebbink and B. M. Weckhuysen, *ChemSusChem*, 2008, **1**, 193–196.
- 20 R. Palkovits, I. Nieddu, C. A. Kruithof, R. J. M. Klein Gebbink and B. M. Weckhuysen, *Chem.-Eur. J.*, 2008, **14**, 8995–9005.
- 21 R. Bunte, B. Gruber and J. Tucker, (Henkel), DE4021511,90-4021511, 1992.
- 22 K. Hill and U. Mahler, (Henkel), WO9202284 A1, 1992.
- 23 A. Behr and J. Leschinski, in 40. Jahrestreffen Deutscher Katalytiker, Weimar, 2007.
- 24 A. Behr, J. Leschinski, C. Awungacha, S. Simic and T. Knoth, *Chem. Sus. Chem.*, DOI: 10.1002/cssc.200800197.
- 25 Y. Tokitoh, T. Higashi, K. Hino, M. Murasawa and N. Yoshimura, (Kuraray Co., Ltd.), EP0436226, 1990.
- 26 A. Behr and J. Leschinski, (Cognis Oleochemicals), DE 10 2008 023 015.4, 2008.
- 27 A. Behr and J. Leschinski, (Cognis Oleochemicals), DE 10 2008 023 016.2, 2008.
- 28 J. Leschinski, PhD thesis, Technische Universität Dortmund, 2009.
- 29 A. Behr, J. Leschinski, A. Prinz and M. Stoffers, *Chem. Eng. Proc.*, submitted.
- 30 T. Maeda and Y. Tokitoh, (Kuraray), US5100854, 1992.

Green Chemistry

Cutting-edge research for a greener sustainable future

www.rsc.org/greenchem

Volume 11 | Number 5 | May 2009 | Pages 593–740



Themed Issue: Green Solvents - Progress in Science and Application

ISSN 1463-9262

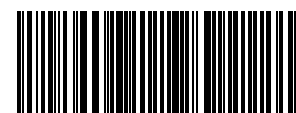
RSC Publishing

Chiappe *et al.*
Glycerylimidazolium based ionic liquids

Behr and Leschinski
Application of water in two-phase
telomerisation

Gubicza *et al.*
Microwave assisted enzymatic
esterification

Thomas *et al.*
Dynamic kinetic resolution of
rac-1-phenylethanol in scCO_2



1463-9262(2009)11:3;1-B

Microwave assisted enzymatic esterification of lactic acid and ethanol in phosphonium type ionic liquids as co-solvents†

Brigitta Major, Ilona Kelemen-Horváth, Zsófia Csanádi, Katalin Bélafi-Bakó and László Gubicza*

Received 19th November 2008, Accepted 19th January 2009

First published as an Advance Article on the web 26th January 2009

DOI: 10.1039/b820575b

Microwave heating was found to have a beneficial effect on the enzymatic esterification of lactic acid (LA) with ethanol in Cyphos 202 ionic liquid (IL) medium. Microwave irradiation caused hydrolysis of lactoyllactic acid (the linear dimer of LA) during the reaction, thus, as a result, more lactic acid was available as substrate and a higher ester yield was achieved in the esterification.

Introduction

The group of lactate esters is one of the most important derivatives of LA.¹ Lactate esters can be used in the composition or production of multitude products, including packaging, paints, grease removers and cleansers. Low-cost lactate esters, which can potentially be used to produce other chemicals such as copolymers of biodegradable plastics, acrylates, glycol and other specialty chemicals, are intermediate products. Ethyl lactate is a natural flavouring compound, therefore a valuable food and perfumery additive.² Natural LA can be produced by bioconversion, which is, however, not as widely used as could be because of its costly recovery and purification steps. Several downstream processes have been developed such as reactive distillation, reactive extraction, electrodialysis, adsorption and esterification.³ One of the latest methods is the extraction by phosphonium type ILs containing hydrophobic anions. These ILs are proper extracting agents for LA since they form complexes with it.⁴ On the other hand, ILs may be suitable media for biocatalytic synthesis because of their enzyme stabilization effect, reusability and negligible vapour pressure.^{5,6} For that reason esterification reactions might be carried out in the extracting agent. Avoiding an expensive separation process would help to produce valuable products with reduced cost.

Recently, the use of microwave irradiation is spreading in the field of organic chemistry, since it is a cleaner and more efficient energy source than the traditional convective heating.⁷ The effect of microwave irradiation was studied in the conversion of fructose into 5-hydroxymethylfurfural (HMF)—as one of the latest examples—and it turned out that fructose conversion and HMF yields by microwave heating were higher than those by sand bath heating.⁸ Moreover, microwave conditions are able to increase the reaction rate of enzymatic esterification processes

in organic solvents.⁹ The stability of *Candida antarctica* lipase B (CALB) in an organic solvent¹⁰ and solvent-free system¹¹ was found to be higher under microwave heating than under conventional heating.

Although both microwave irradiation and ILs provide several advantages in the case of esterification reactions, only one report describes an enzymatic acylation using the two special conditions simultaneously.¹² Therefore our goal was to test the influence of microwave energy on the enzymatic synthesis of ethyl lactate in ILs. The reason for choosing LA to investigate the esterification is that it has so far only been tested in organic solvents, in toluene¹³ and recently in some hydrophobic ethers and ketones.¹⁴ Carrying out this synthesis in ILs is a novel process itself.

Results and discussion

Several ILs were tested to find an appropriate medium for the ethyl lactate synthesis. It was found that the reaction can be carried out in Cyphos 104 and Cyphos 202, which consist of the same cation with different anions (see Fig. 1) and were also tested as extracting agents in the case of LA.⁴ Although these ILs are somewhat more viscous than typical imidazolium salts, when organic substrates are added the viscosity may decrease by an order of magnitude.¹⁵

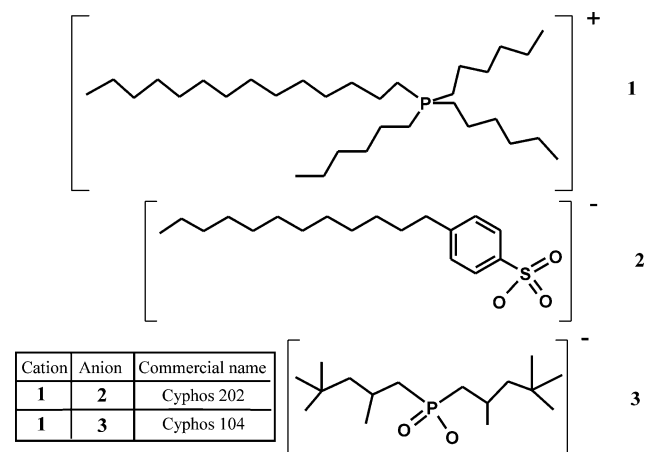


Fig. 1 The structure of Cyphos 104 (trihexyl-tetradecyl-phosphonium-bis(2,4,4-trimethylpentyl)-phosphinate) and Cyphos 202 (trihexyl-tetradecyl-phosphonium-dodecylbenzene-sulfonate) ILs.

The investigated ILs gave a one-phase system with the substrates and products and they were found to be a suitable media for the enzymatic reaction.

Research Institute of Chemical and Process Engineering, University of Pannonia, Egyetem u 10, 8200, Veszprém, Hungary. E-mail: gubicza@mukki.richem.hu; Fax: +36 88-624038; Tel: +36 88-624044

† This paper was published as part of the themed issue of contributions from the Green Solvents – Progress in Science and Application conference held in Friedrichshafen, September 2008.

In order to define the optimal reaction parameters of the synthesis, we need to determine the minimal amount of IL for the reaction under conventional conditions. Varying the concentration of IL in the range of 155 g dm^{-3} (0.20 mol dm^{-3}) to 346 g dm^{-3} (0.44 mol dm^{-3}) the ethyl ester yield increased extensively. Further addition of IL had no significant influence on it. The optimal LA/ethanol molar ratio was found to be 1:7. The amount of immobilised CALB was varied between 12.5 and 50 mg mmol^{-1} LA depending on the required reaction time. Using the smallest amount, the reaction was complete in 24 hours. The highest yield (95%) (correlating to the amount of monomer LA) was achieved in the case of 2 w/w% initial water content in Cyphos 104.

Control reactions were carried out to study the influence of microwave irradiation on CALB and ILs. In these experiments, different systems (ILs; CALB; CALB with ILs and ethanol) were irradiated by microwave energy for 2 hours at 40°C . After this treatment, reactions were started in a shaking incubator and the observed yields were compared. According to the obtained data, the incubation of ILs had no effect on the ester yield. The irradiated pure enzyme reached only 72% of the expected yield. The reason for this decreased activity was presumably not the microwave irradiation but the fact that enzymes are not really stable without a solvent. In our experiments, a mixture of IL and ethanol was used as solvent. The microwave assisted incubation resulted in the same yield as its control reaction under conventional heating (2 hours, 40°C in a shaking incubator). Although ethanol itself slightly damages the enzyme, its use in excess was necessary to solve the mixing problems of the viscous IL. Consequently, microwave irradiation harms neither CALB nor Cyphos type ILs.

The esterification reaction in the mentioned ILs was tested under microwave conditions. In the case of Cyphos 202, the reaction rate increased while in Cyphos 104 the results remained at the same level as in the shaking incubator. Further reactions were carried out in Cyphos 202 because it was the only medium where microwave irradiation had a positive effect on the reaction rate.

Since the influence of water content is very important in esterification reactions¹⁶ and the polar water molecules can effect the energy dissipation under microwave conditions,¹⁷ the most important reaction parameter is the optimal initial water content. A constant water level in the reaction mixture containing the ionic liquid as solvent can be maintained by pervaporative removal of the water formed continuously.^{18,19}

In this study, in both cases (conventional and microwave heating) low (2 w/w%) initial water content resulted in low yields. Under conventional conditions (convective heating), the highest ethyl lactate content was achieved at 4 w/w% initial water content, while under microwave conditions 3 w/w%. The ester yield was 105% (Fig. 2) in both cases. Using conventional heating, 24 hours reaction time was needed to carry out the reaction, while under microwave conditions 7 hours were enough.

As Fig. 2 shows, in some cases ester yield exceeded the maximal level calculated on the initial monomer LA content of the reaction mixture. The reason for this increased yield is that the lactoyllactic acid (open chain dimer of LA) is able to decompose to monomers and form ethyl lactate. Engin

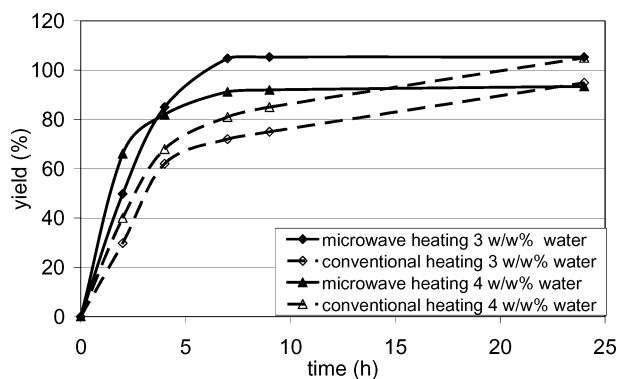


Fig. 2 The effect of conventional and microwave heating on the ethyl lactate synthesis in Cyphos 202 IL using 3 and 4 w/w% initial water content, respectively (2 mmol LA, 14 mmol ethanol, 0.77 mmol Cyphos 202 IL and 12.5 mg *Candida antarctica* lipase B).

*et al.*²⁰ report that neither temperature change nor catalyst addition alter the dynamic equilibrium between LA, lactoyllactic acid and water, but in an esterification reaction the formation of water causes the hydrolysis of the lactoyllactic acid. It was found that its hydrolysis is a very slow reaction under conventional heating and may be a rate-limiting step in ethyl lactate formation. However, in our experiments using microwave irradiation, an enhanced hydrolysis of lactoyllactic acid was observed. According to the results of HPLC analysis (Fig. 3) the lactoyllactic acid content of the reaction mixture decreases providing fresh substrate (LA) for the reaction. The amount of lactide, the cyclic di-ester of lactic acid, remained practically constant during the reaction.

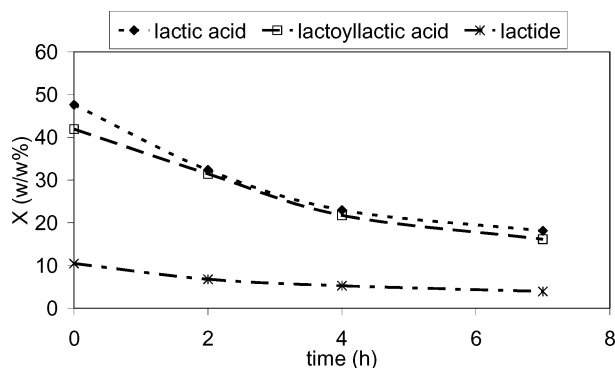


Fig. 3 Composition of the LA solution in the reaction mixture vs. reaction time under microwave conditions (reaction conditions: see Fig. 2).

While the ester yield increases to 105%, the composition of LA/lactoyllactic acid remains stable (Fig. 4) (about 47 w/w% LA, 43 w/w% lactoyllactic acid). In this case, the rate of the esterification reaction is comparable with the rate of the decomposition of lactoyllactic acid. Since microwave irradiation accelerates the hydrolysis of the dimer, it is not a rate limiting step any longer. Using microwave irradiation, this influence results in shorter reaction time than under conventional conditions and this may be the reason for the faster reaction using a higher amount of initial water content. The application of IL, as a co-solvent used for the extraction of lactic acid, thus increases the ester yield.

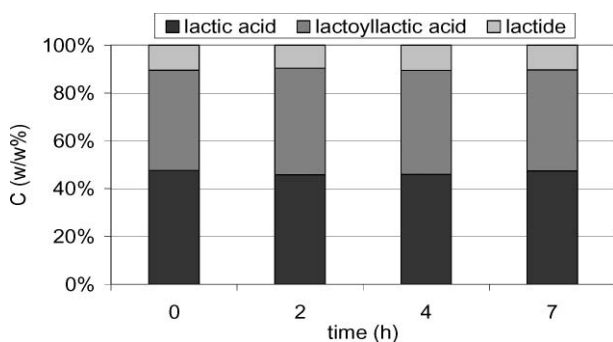


Fig. 4 Composition of the unreacted compounds in the reaction mixture during reaction under microwave conditions (reaction conditions: see Fig. 2).

Conclusions

The enzymatic synthesis of ethyl lactate was successfully achieved in Cyphos 104 and Cyphos 202 ILs. These media have also been applied to extract LA from the fermentation broth, thus the same media can be used for both extraction and reaction.⁴ Further improvement of the esterification reaction is possible using microwave heating instead of conventional conditions. According to our results, microwave irradiation enhanced the ethyl lactate production accelerating the hydrolysis of lactoyllactic acid. Based on our findings, combining the advantage of microwave treatment with the esterification in the extracting agent as co-solvent can result in a reaction with enhanced yields and higher rate.

Experimental

Materials

Immobilized CALB (Novozym 435[®]) was received from Novozymes (Bagsvaerd, Denmark) as a gift. Cyphos 104 (purity >95 w/w%) and 202 ILs were purchased from IoLiTec GmbH, Germany. Ethanol (absolute) and lactic acid (90 w/w% solution) were purchased from Spektrum 3D, Hungary. All the organic solvents of analytical grade were received from Scharlau, Spain.

The exact composition of the LA solution (53 w/w% LA, 26 w/w% lactoyllactic acid, 7 w/w% lactide and 14 w/w% water) was determined by acid–base titration and Karl Fisher titrator.

Experimental setup using conventional heating

The reactions using conventional heating were carried out in a GFL 3031 shaking incubator on 40 °C, at 150 rpm.

In a typical experiment a solution of the substrates consisting of 340 mg LA solution (containing 2 mmol LA), 14 mmol ethanol, 0.77 mmol IL and 25 mg enzyme were prepared and reacted. 50 μ L samples were taken and extracted by 4 \times 80 μ L hexane before GC analysis. As a preparation for HPLC analysis the samples were diluted in 5 ml phosphate buffer (pH: 2.3, 6% acetonitrile content).

Experimental setup using microwave heating

Tests under microwave conditions were performed in commercial microwave equipment (Discover series, BenchMate model, CEM Corporation, USA) with a capacity of 4 ml. It was equipped with a magnetic stirrer and a fibre-optic sensor to monitor the temperature, which was set by varying the microwave power. For the esterification reactions of LA, 10 W energy was used to hold the reaction temperature on 40 °C. The volume and the composition of the reaction mixture was the same as under conventional conditions.

Analytical methods

Water content of the substrates and the reaction mixture was measured by a Mettler Toledo DL31 type Karl Fisher titrator. The product samples were analysed by a HP 5890A gas chromatograph with a HP-FFAP column and FID detector. The HPLC analyses were carried out on MERC type equipment with a Zorbax SB-Aq 76 column and L-7450 detector. The monitoring wavelength was 215 nm. All reactions were carried out in triplicate and the average error was less than 6%.

Acknowledgements

This work was partly supported by the Hungarian–Slovak Science and Technology Cooperation (Project No. SK-03/2006).

Notes and references

- 1 R. Datta and M. Henry, *J. Chem. Technol. Biot.*, 2006, **81**, 1119–1129.
- 2 S. Aparicio and R. Alcalde, *Green Chem.*, 2009, **11**, 65–78.
- 3 H. G. Joglekar, I. Rahman, S. Babu, B. D. Kulkarni and A. Joshi, *Sep. Purif. Technol.*, 2006, **52**, 1–17.
- 4 J. Marták and Š. Schlosser, *Sep. Purif. Technol.*, 2007, **57**, 438–494.
- 5 E. Fehér, V. Illeova, I. Kelemen-Horváth, K. Bélafi-Bakó, M. Polakovic and L. Gubicza, *J. Mol. Catal. B: Enzym.*, 2008, **50**, 28–32.
- 6 S. Cantone, U. Hanefeld and A. Basso, *Green Chem.*, 2007, **9**, 945–971.
- 7 D. Bogdal, *Microwave-assisted Organic synthesis: One Hundred Reaction Procedures*, Elsevier Sciences, 2005.
- 8 W. Qi, M. Watanabe, T. M. Aida and R. L. Smidt, Jr., *Green Chem.*, 2008, **10**, 799–805.
- 9 D. Yu, Z. Wang, P. Chen, L. Jin, Y. Cheng, J. Zhou and S. Cao, *J. Mol. Catal. B: Enzym.*, 2007, **48**, 51–57.
- 10 B. Réjasse, S. Lamare, M.-D. Legoy and T. Besson, *Org. Biomol. Chem.*, 2004, **2**, 1086–1089.
- 11 B. Réjasse, T. Besson, M.-D. Legoy and S. Lamare, *Org. Biomol. Chem.*, 2006, **4**, 3703–3707.
- 12 K. Lundell, T. Kurki, M. Lindroos and L. T. Kanerva, *Adv. Synth. Catal.*, 2005, **347**, 1110–1118.
- 13 S. Parida and J. S. Dordick, *J. Am. Chem. Soc.*, 1991, **113**, 2253–2259.
- 14 S. Hasegawa, M. Azuma and K. Takahashi, *Enzyme Microb. Technol.*, 2008, **43**, 309–316.
- 15 K. R. Seddon, A. Stark and M. J. Torres, *Pure Appl. Chem.*, 2000, **72**, 2275–2287.
- 16 M. D. Romero, L. Calvo, C. Alba, A. Daneshfar and H. S. Ghaziaskar, *Enzyme Microb. Technol.*, 2005, **37**, 42–48.
- 17 W. Huang, Y.-M. Xia, H. Gao, Y.-J. Fang, Y. Wang and Y. Fang, *J. Mol. Catal. B: Enzym.*, 2005, **35**, 113–116.
- 18 L. Gubicza, N. Nemestóthy, T. Fráter and K. Bélafi-Bakó, *Green Chem.*, 2003, **5**, 236–239.
- 19 L. Gubicza, K. Bélafi-Bakó, E. Fehér and T. Fráter, *Green Chem.*, 2008, **10**, 1284–1287.
- 20 A. Engin, H. Haluk and K. Gurkan, *Green Chem.*, 2003, **5**, 460–466.

Dynamic kinetic resolution of *rac*-1-phenylethanol in supercritical carbon dioxide†

Karima Benaissi,^{a,b} Martyn Poliakoff^a and Neil R. Thomas^{*a,b}

Received 12th December 2008, Accepted 16th March 2009

First published as an Advance Article on the web 25th March 2009

DOI: 10.1039/b822349a

The kinetic resolution (KR) and dynamic kinetic resolution (DKR) of racemic 1-phenylethanol with the acyl donor vinyl acetate catalysed by *Pseudomonas cepacia* lipase ATCC 21808 (PCL) (this has recently been reclassified as *Burholderia cepacia* lipase), either as the suspended native protein (PCL) or immobilised on ceramic particles (commercial lipase Amano PS CI) has been examined, as batch reactions, in supercritical carbon dioxide (scCO₂). The yields and enantioselectivities achieved in these reactions were comparable to experiments conducted in hexane. The immobilised lipase PS CI displayed excellent yields (48–49%) and enantioselectivities (98–99%) to give (*R*)-phenylethyl acetate after 2.5 hours reaction at 40 °C in scCO₂. The acylated product was obtained in higher yield in scCO₂ compared to the reaction carried out in hexane (yield 30–35%; ee 98–99%) under comparable conditions. Unlike PCL, the immobilised lipase PS CI could then be successfully reused with no loss of activity or selectivity observed over four reaction cycles. Combining lipase PS CI with a chemical catalyst (either the metal catalyst [Ru(*p*-cymene)Cl₂]₂ or the acid catalyst Nafion SAC 13) to catalyse the racemisation of the unreacted alcohol caused an increase in the yield of the (*R*)-acyl phenylethanol product to 70 and 85%, respectively, in scCO₂ indicating a viable dynamic kinetic resolution system had been established. The enantioselectivities of the products in these reactions were slightly higher in scCO₂ (96% Ru-catalyst; 85% Nafion) compared to those observed in hexane (91%; 81%). The lower enantioselectivity with the acidic Nafion SAC 13 catalyses indicates that some non-enzymic acid catalysed esterification was occurring.

Introduction

The identification of efficient methods for synthesizing enantiomerically pure compounds or separating racemic mixtures has been very active in recent years due to the emergence of new regulations restricting the utilisation of racemic mixtures

as pharmaceuticals.¹ The resolution of racemates is currently the most widely used approach. A variety of catalysts (metal, enzymes, whole cells) have been identified that can be used to resolve alcohols, amines, acids and other key building blocks. In order to increase the commercial scope of these reactions, here we demonstrate that dynamic kinetic resolution of *rac*-1-phenylethanol is achievable using a combination of enzyme and either organometallic or acidic catalysis solely in scCO₂ for the first time.²

Enzymes immobilised on solid supports have been shown to offer good stability in non-aqueous media and can easily be recycled, hence these were chosen for enantioselective heterogeneous catalysis in supercritical carbon dioxide (scCO₂).¹ The kinetic resolution (KR) of *rac*-1-phenylethanol catalysed by enzymes has been shown to be very efficient;^{1,3} however the drawback of this type of reaction is the limitation in yield to 50% of the desired enantiomer.^{1,3} Dynamic kinetic resolution (DKR) overcomes this problem by racemising the undesired enantiomer so that it becomes an acceptable substrate for the enzyme such that >50% of the substrate can be resolved.^{1,3,4} The unreacted enantiomer is continuously isomerised during the resolution process leading potentially to an efficient conversion of all the starting material to the desired product.⁵

For efficient chemoenzymatic DKR, several conditions are required.⁵ For a one pot reaction, enzyme and chemical catalysts should be compatible. Enzymes usually work under mild conditions of temperature and pressure while metal catalysts are quite often most efficient at temperatures higher than 80 °C, so a compromise in conditions is often required.^{1,4,5} Parameters such as the nature of the solvent need to be optimised as this can significantly influence the activity of the enzyme and the solubility and reactivity of the metal catalyst, thereby changing its activity for the racemisation.⁶ For DKR to be achieved it is crucial for the rate of the racemisation step to be the same or higher than the rate of removal of one enantiomer from the system by enzymic resolution, such that high conversions and enantioselectivities of the desired product are achieved.^{1,3,5,6} In other words, for efficient DKR, racemisation should proceed faster than the kinetic resolution.^{5,7} The choice of the racemisation method depends on the nature of the substrate that is to be racemised and the most commonly used racemisation catalysts have involved bases, enzymes and transition metals.⁴

The use of transition metals^{4,6} for the racemisation of alcohols is based on the occurrence of hydrogen-transfer mechanisms⁸ and has been widely developed in recent years.⁴ Different transition metals (palladium, rhodium, iridium, ruthenium) have been tested for the racemisation step^{4,5} but more and

^aSchool of Chemistry, The University of Nottingham, Nottingham, UK NG7 2RD

^bCentre for Biomolecular Sciences, The University of Nottingham, Nottingham, UK NG7 2RD. E-mail: Neil.Thomas@nottingham.ac.uk; Fax: +44 (0)115 951 3565; Tel: +44 (0)115 951 3564

† This paper was published as part of the themed issue of contributions from the Green Solvents – Progress in Science and Application conference held in Friedrichshafen, September 2008.

more studies focus on ruthenium metal catalysts^{1,3,6,8} since they have shown high activities for the racemisation of a wide range of substrates at low temperatures in organic media,^{1,3} as required for compatible enzyme–metal catalysed DKR.^{7,9} For instance, Riermeier *et al.* have optimised¹⁰ the DKR of aromatic secondary alcohols using a ruthenium-based catalyst activated with chelating aliphatic diamines.

Alternatively, one of the other emerging methods for catalyzing the racemisation of alcohols is the use of acid resins such as Amberlyst 15 or Nafion SAC 13.¹¹ The racemisation of alcohols by means of an acid catalyst has been shown to proceed by a dehydration–rehydration mechanism leading to the formation of a carbocation intermediate.¹¹ Solid acid catalysts have previously been shown to efficiently racemise secondary alcohols in aqueous conditions.¹¹ As these are insoluble, they can be rapidly separated from the reaction and recycled.¹¹ Only a few examples of DKR carried out involving scCO₂ have been reported. However, high temperatures and long reaction times are often required. Recently, Lozano *et al.* have employed a combination of immobilised enzyme and acid catalyst for the continuous DKR of *rac*-1-phenylethanol in a scCO₂/ionic liquid biphasic system in which the reaction occurs in the ionic liquid and the scCO₂ is used to extract the reaction product, resulting in high yields and good enantioselectivities.^{12,13}

Here we describe DKR in a system that uses scCO₂ as the reaction solvent combining the kinetic resolution of *rac*-1-phenylethanol through an enzymic acylation reaction with simultaneous racemisation involving either a metal catalyst or an acid catalyst. The feasibility of this chemo-enzymatic DKR in scCO₂ was compared to that in hexane. scCO₂ offers a number of advantages as a reaction solvent in that it is environmentally benign, can be easily separated from the products dissolved in it through a change in pressure, simplifying product isolation, and therefore the CO₂ can be repeatedly recycled especially if used with immobilised catalysts that give near quantitative conversions.

Results and discussion

Kinetic resolution of *rac*-1-phenylethanol

The ability of PS CI immobilised enzyme to catalyse the kinetic resolution (KR) of *rac*-1-phenylethanol was examined in both scCO₂ and hexane using a reaction time of 2.5 hours. The catalytic activity of the native enzyme (PCL) was also studied and, as can clearly be seen in Fig. 1, the latter had significantly lower catalytic activity whilst the immobilised enzyme PS CI exhibited high activity and enantioselectivity for the kinetic resolution of *rac*-1-phenylethanol with vinyl acetate at 40 °C in both solvents and was easily recycled.

Excellent yields of the acetyl-(1*R*)-phenylethanol (48%) were obtained after only 2.5 hours in scCO₂ whereas only 33% of the ester was produced under comparable conditions in hexane. Whilst similar levels of conversion were observed for the native enzyme (PCL) in both hexane and scCO₂, the higher yield observed with PS CI is due to both the immobilisation of the enzyme preventing its aggregation, which would reduce the accessibility of the substrates to the enzyme active sites, and the additional conversion in scCO₂ over that in hexane that may be

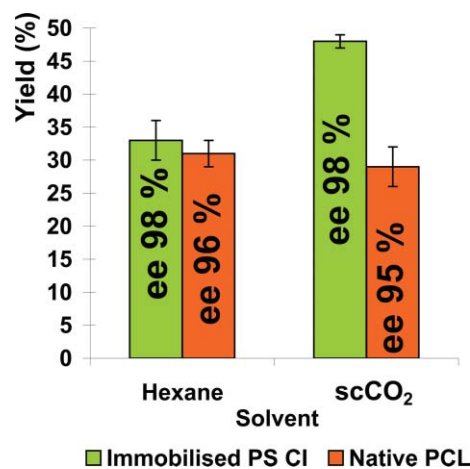


Fig. 1 KR of *rac*-1-phenylethanol (0.14 M) with vinyl acetate (0.28 M) catalysed by PCL (1 U mL⁻¹) using either immobilised (PS CI) or suspended enzyme (PCL) in hexane at atmospheric pressure or scCO₂ at 100 bar (40 °C for 2.5 hours). Yields and (*R*)-ester enantiomeric excesses (ee) were estimated by GLC using a chiral Betadex 110 column.

due to the lower viscosity of the supercritical fluid, thus leading to better penetration of the ceramic supporting enzyme and hence flux of substrates to the enzyme active sites.²

The reusability of the immobilised lipase PS CI for the KR of *rac*-1-phenylethanol catalysed in scCO₂ was also investigated. The activity and enantioselectivity of the enzyme was compared to that of the suspended native enzyme and results are shown in Fig. 2. Unlike the suspended native PCL, the immobilised lipase PS CI displayed excellent stability in both hexane and scCO₂ since it was successfully reused for the KR of *rac*-1-phenylethanol over four cycles. It is also worth noting that both the activity and the enantioselectivity of the immobilised lipase did not appear to be significantly affected by the pressurisation and depressurisation procedures for the reaction carried out in scCO₂.

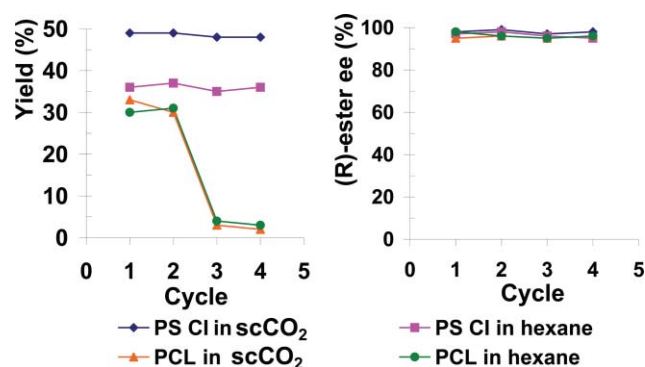


Fig. 2 Recycling of PCL either immobilised PS CI or native PCL for the KR of *rac*-1-phenylethanol in hexane and in scCO₂ 100 bar at 40 °C for 2.5 hours. Yields (left) and (*R*)-ester enantiomeric excesses (ee) (right) were determined by GLC using a chiral Betadex 110 column.

Dynamic kinetic resolution of *rac*-1-phenylethanol

The dynamic kinetic resolution (DKR) of *rac*-1-phenylethanol was investigated using the lipase PS CI in combination with either a metal catalyst or an acid catalyst. Different parameters

(such as nature of the solvent, temperature, reaction time and amount of catalyst) were investigated and the best conditions identified; the experimental results observed are summarized in Fig. 3.

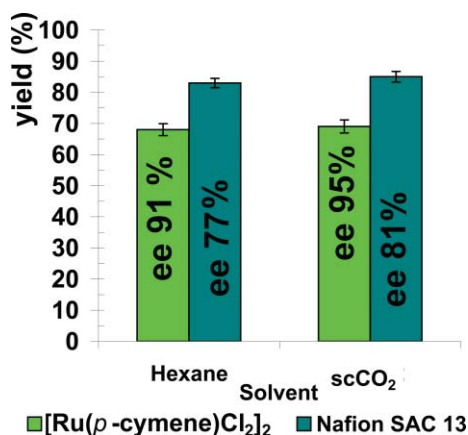


Fig. 3 DKR of *rac*-1-phenylethanol (0.14 M) with either vinyl acetate (Ru-catalyst) or phenyl acetate (Nafion) (0.28 M) catalysed by a combination of immobilised lipase PS CI (5 U mL⁻¹) and either [Ru(*p*-cymene)Cl₂]₂ (4.1 mM) or Nafion SAC 13 (0.02 mM) for the temperature and period of time indicated in hexane and scCO₂ 100 bar. Yields and (*R*)-ester enantioselective excesses (ee) were estimated by GLC equipped with chiral Betadex 110 column.

DKR using a combination of lipase and metal catalyst

The activity of [Ru(*p*-cymene)Cl₂]₂ was investigated for the racemisation of (*S*)-1-phenylethanol in organic solvents (hexane, toluene) at different temperatures (40, 55 °C). The metal catalyst was poorly active at 40 °C in both organic solvents tested, probably because dimeric metal catalysts are usually active at higher temperatures once they have fragmented into monomeric species.⁴ Promising results were obtained at 55 °C and the rate of racemisation was observed to be faster in toluene than that in hexane. We believe this is due to the higher solubility of the ruthenium catalyst in toluene compared to hexane, thus increasing the contact with the substrate.¹⁰

DKR has been investigated using a combination of a lipase and [Ru(*p*-cymene)Cl₂]₂ at 55 °C, and the nature of the acetate donor and addition of acetophenone as a sacrificial hydride acceptor have been examined.¹⁰ Racemisation using ruthenium catalysts proceeds through hydrogen transfer to the substrate. When using alkenyl acetates such as vinyl acetate, the aldehyde generated during the resolution step inhibits the activity of the metal catalyst by competing with the oxidized substrate during hydrogenation.¹ Unlike vinyl acetate, phenyl acetate forms a ketone which does not interfere with the racemisation catalyst, hence leading to higher enantioselectivities of the desired product. When using the ruthenium catalyst, acetophenone was also added to the reaction as it was shown to speed up the racemisation step.¹

The DKR of *rac*-1-phenylethanol with phenyl acetate was investigated at 55 °C with a reaction time of 6 days in both hexane and scCO₂. The results (see Fig. 3) achieved for the DKR were encouraging, since more than 50% yield (68–69%) and high enantioselectivities (91–95%) were achieved using PS CI/[Ru(*p*-

cymene)Cl₂]₂ as catalysts in both media investigated. Also the enantioselectivity of the reaction seemed to be slightly increased in scCO₂ (95%) compared to the reaction in hexane (91%) which was encouraging. The [Ru(*p*-cymene)Cl₂]₂ was shown to convert (*S*)-1-phenylethanol to a 56 : 44 (*S*) : (*R*) mixture after 3 days at 40 °C in hexane, suggesting that the racemisation step becomes rate limiting if excess enzyme is used.

Long reaction times (3 to 6 days) were required in both media investigated due to the moderate activity of the ruthenium catalyst at 55 °C, as fragmentation of the dimeric metal-catalyst is inefficient at this temperature compared to that at 80 °C used in the absence of enzymes.^{1,3,6,8} Hence, a different type of racemising catalyst was investigated.

DKR using a combination of lipase and an acid catalyst

The DKR of *rac*-1-phenylethanol was catalysed by a combination of lipase PS CI and Nafion SAC 13 for five hours at 40 °C in hexane and scCO₂ (100 bar).

Acid catalysts, such as Nafion, are believed to work through a hydration/dehydration process, hence they have been successfully used in the past for dehydration reactions.¹¹ Their use as racemisation catalysts, however, is rather new. Acid catalysts Amberlyst 15, Amberlite XN 1010, Amberlyst XR 120 and Nafion SAC 13 were tested for the racemisation of (*S*)-1-phenylethanol at 40 °C in hexane. Nafion SAC 13 and Amberlyst 15 were observed to be the most efficient at racemising (*S*)-1-phenylethanol. Exposure of (*S*)-1-phenylethanol to Nafion SAC 13 for 6 hours in hexane produced a racemic product whilst Amberlyst 15 gave a ratio of 41 : 59 (*R*) : (*S*) 1-phenylethanol with evidence of some dehydration product. Nafion SAC 13 was hence selected to catalyse the DKR of the secondary alcohol in scCO₂. The results (shown in Fig. 3) obtained for the DKR using PS CI and Nafion SAC 13 as catalysts were very encouraging, since good conversions (77–85%) and enantioselectivities (77–81%) were achieved after only five hours at 40 °C in either solvent. Again, the enantioselectivity of the reaction appeared to be marginally better in scCO₂ (81%) compared to that in hexane (77%). The moderate enantioselectivities (81–85%) achieved in both solvents are very likely to be due to the chemical esterification of the substrates catalysed by the acid Nafion SAC 13. A physical separation of the enzyme and the metal catalyst and the use of a continuous flow system might help in preventing this undesirable side reaction occurring.

Experimental

Safety note

Experiments with scCO₂ involve high pressures and should only be carried out in equipment with the appropriate pressure rating.

Materials

Lipase from *Pseudomonas (Burkholderia) cepacia* (PCL, 40 U mg⁻¹) was purchased from BioChemika. Lipase from *Pseudomonas cepacia* immobilised on ceramic particles (Amano PS CI 1000 U g⁻¹) and Nafion SAC 13 acid catalyst (13% w/w Nafion in silica matrix, surface area 200 m² g⁻¹, 0.15 mEq of –SO₃H acid loading) were obtained from Aldrich. Chemicals:

rac-1-phenylethanol, dodecane and *N,N,N',N'*-tetramethylpropane diamine (TMPDA), were purchased from Aldrich; vinyl acetate, phenyl acetate and acetophenone were purchased from Fluka. The ruthenium catalyst, $[\text{Ru}(p\text{-cymene})\text{Cl}_2]$ was purchased from Lancaster Synthesis. All organic solvents were purchased at the highest purity available from Aldrich. All commercially available reagents and solvents were used without further purification. High purity carbon dioxide was purchased from CryoService. Gases hydrogen, helium and air were purchased from BOC Gases.

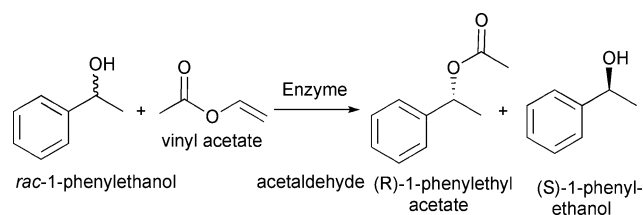
Methods

Enzymatic reactions in organic solvents were carried out in 5 mL septum-sealed Supelco glass micro reaction vessels equipped with a magnetic stirrer under stirring at 500 rpm in a silicon oil bath thermostatted to the indicated temperature using a Yellowline MST basic hot plate equipped with a Yellowline TC1 thermostat. Reactions in scCO_2 were performed in a stainless-steel high pressure batch reactor specially designed at the University of Nottingham.¹⁴ The batch reactor (autoclave) equipped with a magnetic stirrer had an internal volume of 8.5 mL and was placed on an IKA Labortechnik RCT basic stirring plate. Solid substrates and reactants and stirrer bar were added into the reactor prior to sealing using a clamp. Liquid substrates and reactants were added using a Gilson Pipetman micropipette into the autoclave, which was then sealed using a safety valve. The band heater, thermocouple, CO_2 supply and exhaust tubing were then connected to the autoclave. The system was then heated to the desired temperature and liquid CO_2 was pumped into the reactor using high pressure NWA PM-101 Pickel pump until the desired pressure was achieved. The reaction mixture was stirred for the period of time indicated and the system was then depressurised with dry ice and acetone. The resulting mixture was dissolved in acetone (3 mL) and centrifuged for two min at 8000 rpm. Aliquots (50 μL) were diluted in acetone (1 mL) and substrates and products were analyzed by gas-liquid chromatography (GLC) using a Shimadzu GC 2010 chromatograph equipped with a Shimadzu AOC-20Si autosampler and using helium as a carrier gas.

The structure of products was further identified using GLC and GLC-MS by comparing the retention times and fragmentation patterns with those of authentic samples. GLC-MS was performed using a thermo Finnegan Polaris-Q trap GC-MS equipped with a DB-5 (30 \times 0.25 \times 0.25 μm film thickness) fused silica column. Helium was used as a carrier gas and sample ionisation was carried out using electron impact (EI) at 70 eV.

Kinetic resolution of *rac*-1-phenylethanol

The transesterification of *rac*-1-phenylethanol with vinyl acetate catalysed by *Pseudomonas (Burholderia) cepacia* lipase (PCL, MW = 39 000) to give (*R*)-1-phenylethyl acetate and acetaldehyde was studied at 40 °C for 2.5 hours in scCO_2 and compared to that in hexane. The reaction studied is shown in Scheme 1. Substrates *rac*-1-phenylethanol (1.2 mmol, 142 μL) and vinyl acetate (2.4 mmol, 220 μL) were added to the immobilised enzyme PS CI (8.5 U, 8.5 mg) in the batch reactor (8.5 mL) then pressurised with CO_2 to 100 bar. The system was then heated to 40 °C and the reaction mixture stirred for 2.5 hours. Comparable



Scheme 1 KR of *rac*-1-phenylethanol (0.14 M) with vinyl acetate (0.28 M) catalysed by *Pseudomonas cepacia* lipase PCL (1 U mL^{-1}) to produce (*R*)-1-phenylethyl acetate, (*S*)-1-phenylethanol and acetaldehyde in scCO_2 (8.5 mL) and hexane (5 mL) at 40 °C for 2.5 hours.

reactions were set up in hexane (5 mL) and all experiments were performed in triplicate. Aliquots were collected and analyzed as described above. Yields and enantioselective excesses (ee) of substrates and products were estimated using GLC equipped with a Supelco Betadex 110 (30 m \times 0.25 mm \times 0.25 μm film thickness) chiral column.

Dynamic kinetic resolution of *rac*-1-phenylethanol

Lipase-metal catalysed DKR of *rac*-1-phenylethanol with vinyl or phenyl acetate, catalysed by a combination of the immobilised lipase PS CI and a chemical catalyst ($[\text{Ru}(p\text{-cymene})\text{Cl}_2]_2$ metal catalyst or Nafion SAC 13 acid catalyst (structures of which are shown in Fig. 4), was investigated at 40 and 55 °C in both hexane and scCO_2 . The reaction studied is shown in Scheme 2.

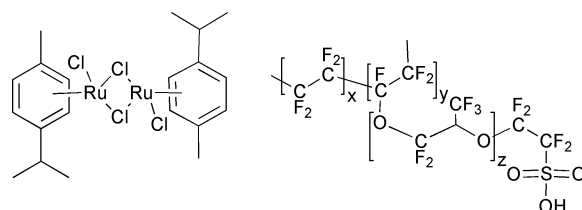
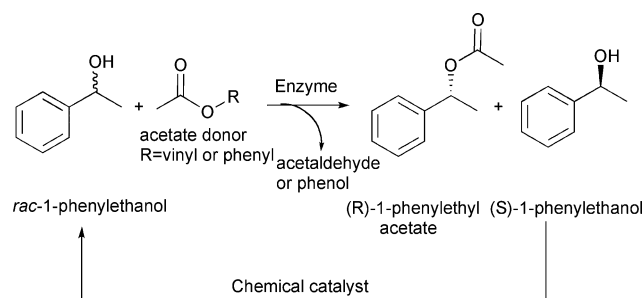


Fig. 4 Structures of $[\text{Ru}(p\text{-cymene})\text{Cl}_2]_2$ metal catalyst (left) and Nafion SAC 13 acid catalyst (right).



Scheme 2 Dynamic kinetic resolution of *rac*-1-phenylethanol (0.14 M) with different acetate donors (0.28 M) was catalysed using a combination of immobilised lipase PS CI (5 U mL^{-1}) and chemical catalyst, either $[\text{Ru}(p\text{-cymene})\text{Cl}_2]_2$ metal catalyst (4.1 mM) at 55 °C for 6 days or Nafion SAC 13 acid catalyst (0.02 mM) at 40 °C for 5 hours, in scCO_2 (8.5 mL) or hexane (5 mL).

Catalysts $[\text{Ru}(p\text{-cymene})\text{Cl}_2]_2$ (0.035 mmol, 15 mg), lipase PS CI (5 U, 26 mg), and substrates and reactants *rac*-1-phenylethanol (1.2 mmol, 142 μL), phenyl acetate (2.4 mmol, 284 μL), acetophenone (0.6 mmol, 71 μL), *N,N,N',N'*-tetramethylpropane diamine (0.35 mmol, 4 μL) and dodecane

(34 μL , internal standard) were used and the reaction studied at 55 $^{\circ}\text{C}$ for 6 days.

Catalysts Nafion SAC 13 (0.02 mmol, 8.5 mg), PS CI (5 U, 26 mg), and substrates and reactants *rac*-1-phenylethanol (1.2 mmol, 142 μL), vinyl acetate (2.4 mmol, 284 μL) and dodecane (34 μL , internal standard) were used and the reaction was studied at 40 $^{\circ}\text{C}$ for 5 hours.

Using both acid and metal catalysts tested, reactions were investigated in a scCO_2 batch reactor (8.5 ml) pressurised with CO_2 to 100 bar, and comparable reactions were set up in hexane (5 mL). The system was then heated to the indicated temperature and the reaction mixture stirred for the indicated period of time. All experiments were performed in triplicate. Aliquots were collected and analyzed as described above. Yields and enantioselective excesses (ee) of substrates and products were estimated using GLC equipped with a Supelco Betadex 110 (30 m \times 0.25 mm \times 0.25 μm film thickness) chiral column.

Conclusions

The kinetic resolution of *rac*-1-phenylethanol catalysed by immobilised enzymes was investigated in scCO_2 . Excellent conversions and enantioselectivities were achieved using the immobilised lipase PS CI at 40 $^{\circ}\text{C}$ in 2.5 hours in scCO_2 . Under comparable conditions, the conversions and enantioselectivities of the reaction in scCO_2 were significantly higher than the ones in hexane. Efficient DKR of *rac*-1-phenylethanol was achieved using the immobilised lipase PS CI and $[\text{Ru}(p\text{-cymene})\text{Cl}_2]_2$ as catalysts. In the presence of acetophenone as a hydrogen acceptor and phenyl acetate as the acetate donor, good conversions and enantioselectivities were achieved in either hexane or scCO_2 after six days reaction at 55 $^{\circ}\text{C}$. A combination of PS CI and Nafion SAC 13 acid-catalyst has been used to demonstrate that the DKR of *rac*-1-phenylethanol with vinyl acetate at 40 $^{\circ}\text{C}$ is achievable in only five hours in scCO_2 . With both chemical

catalysts tested, the enantiomeric excesses of the products in the DKR were observed to be slightly higher in scCO_2 compared to reactions in hexane.

Acknowledgements

We would like to thank all our colleagues in the Clean Technology Group at the University of Nottingham for their invaluable help and support. We also would like to address many thanks to the Workshop, Mark Guyler and Paul Hamley for their invaluable help and technical support. Finally we thank the Marie Curie Programme and SubClean Probiomat (MEST-CT-2004-007767) for funding.

References

- 1 M. Eckert, A. Brethon, Y. X. Li, R. A. Sheldon and I. Arends, *Adv. Synth. Catal.*, 2007, **349**, 2603–2609.
- 2 H. R. Hobbs and N. R. Thomas, *Chem. Rev.*, 2007, **107**, 2786–2820.
- 3 K. Bogar, B. Martin-Matute and J. E. Bäckvall, *Beilstein J. Org. Chem.*, 2007, **3**.
- 4 H. Pellissier, *Tetrahedron*, 2008, **64**, 1563–1601.
- 5 Y. Ahn, S. B. Ko, M. J. Kim and J. Park, *Coord. Chem. Rev.*, 2008, **252**, 647–658.
- 6 S. B. Ko, B. Baburaj, M. J. Kim and J. Park, *J. Org. Chem.*, 2007, **72**, 6860–6864.
- 7 O. Pamies and J. E. Bäckvall, *Chem. Rev.*, 2003, **103**, 3247–3261.
- 8 B. Martin-Matute and J. E. Bäckvall, *Curr. Opin. Chem. Biol.*, 2007, **11**, 226–232.
- 9 H. Pellissier, *Tetrahedron*, 2003, 8291–8327.
- 10 T. H. Riermeier, P. Gross, A. Monsees, M. Hoff and H. Trauthwein, *Tetrahedron Lett.*, 2005, **46**, 3403–3406.
- 11 S. Wuyts, K. De Temmerman, D. E. De Vos and P. A. Jacobs, *Chem.–Eur. J.*, 2005, **11**, 386–397.
- 12 P. Lozano, T. De Diego and J. L. Iborra, *Chim. Oggi*, 2007, **25**, 76–79.
- 13 P. Lozano, T. De Diego, M. Larnicol, M. Vaultier and J. L. Iborra, *Biotechnol. Lett.*, 2006, **28**, 1559–1565.
- 14 S. M. Howdle, P. Grebenik, R. N. Perutz and M. Poliakoff, *J. Chem. Soc., Chem. Commun.*, 1989, 1517–1519.

Synthesis and properties of glycerylimidazolium based ionic liquids: a promising class of task-specific ionic liquids†

Fabio Bellina,^{*a} Alessandra Bertoli,^b Bernardo Melai,^b Francesca Scalesse,^a Francesca Signori^c and Cinzia Chiappe^{*a,b}

Received 8th December 2008, Accepted 27th January 2009

First published as an Advance Article on the web 25th February 2009

DOI: 10.1039/b821927c

A series of task-specific ionic liquids (TSILs) based on glycerylimidazolium cations have been prepared by reaction of 1-chloropropanediol, a compound obtainable from glycerol (a widely available and in-expensive waste product), with the appropriate base (1-*H*-imidazole, 1,2-dimethylimidazole and 1-methyl-1-*H*-imidazole). The reaction of 3-(1*H*-imidazol-1-yl)propane-1,2-diol with chloroalkanes, bromoalkanes and alkyl mesylates gave the corresponding salts which were characterized. The possibility to use these ILs in palladium catalyzed reactions was evaluated, evidencing good catalyst stability and a high recyclability.

Introduction

Currently, ionic liquids (ILs) are receiving great attention for application as innovative solvents or additives in a variety of different areas reaching from material synthesis to separation science as well as alternative reaction media.¹ However, despite promising results evidenced by the many studies in which they have been used as solvents, evidencing unique properties, their widespread application in process chemistry is still hampered by doubts generally related to some practical drawbacks: (i) cost and possible toxicological concerns, (ii) problems related to product isolation, and (iii) catalyst recovery. To overcome at least some of these drawbacks more recently functionalized ILs, the so-called Task-Specific ILs (TSILs), have been synthesized.² A range of different functional groups providing properties similar or identical to those of the major classes of organic solvents has been incorporated into IL cations, including vinyl and allyl, amine, amide, ether and alcohol, acid, urea and thiourea, fluorinated chains, alkyne, phosphoryl, nitrile, thiols, and ferrocenyl groups. The functionalization of the anion has been also performed, and ILs based on metal carbonyls, alkylselenites, and functionalized borates were synthesized.³ Some of these ILs have been used as solvents in selected metal catalyzed reactions,⁴ evidencing that TSILs can favor the activation of the catalyst, generate new catalytic species, improve the stability of the catalyst. Moreover, properly designed TSILs are able to optimize immobilization and recyclability,

facilitate product isolation, and influence the selectivity of the reaction.

On the other hand, the unique physico-chemical properties of these salts,⁵ and in particular their solubility or insolubility in organic and aqueous media, has suggested the possibility of using TSILs as soluble supports for organic synthesis. This novel liquid-phase strategy could embrace several possibilities: (a) supported catalysts, (b) supported reagents, and (c) supported substrates.⁶ In particular, the alcohol-functionalized TSILs have been extensively studied as replacements for solid polymer supports in the heterogeneous-phase synthesis of organic molecules. Bazureau *et al.*⁷ synthesized various polyoxy-alcohol-functionalized TSILs evidencing the potential of these salts as liquid supports in ionic liquid-phase Knoevenagel reactions, 1,3-dipolar cycloaddition and in the generation of a small library of thiazolidines and 2-thioxotetrahydropyrimidin-4-(1*H*)-ones.⁸ Similarly, Miao and Chan utilized these TSILs as liquid supports for Suzuki coupling reactions, and demonstrated their advantage over conventional solution phase synthesis.⁹ Interestingly, recent investigations evidence that the introduction of a hydroxyl group on the longer alkyl chain of the imidazolium cation decreases toxicity towards aquatic species.¹⁰

As an extension of our research into ionic liquid systems arising from low cost renewable resources (possibly, from waste materials) we became interested in the use of ionic liquids containing two vicinal hydroxyl groups in reaction media and additives. These TSILs can be prepared by reaction of a proper base with 1-chloropropanediol, a commercial compound obtainable, as evidenced by a recent patent,¹¹ from glycerol. Nowadays, glycerol is generated as a by-product in the production of bio-diesel and it is estimated that if production of biodiesel increases as projected, glycerol will become widely available and inexpensive (eventually, even a possible waste product).¹²

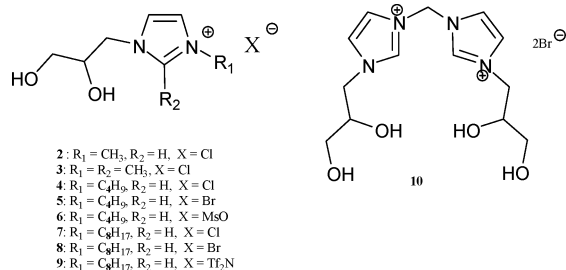
Herein, we wish to report a series of imidazolium based ILs (2–10) functionalized by a 2,3-dihydroxypropyl group evidencing their potential uses as ligands and solvents for palladium(II)-catalyzed reactions.

^aDipartimento di Chimica e Chimica Industriale, via Risorgimento 35, 56126, Pisa, Italy. E-mail: bellina@dcci.unipi.it; Fax: +39 050 2219260; Tel: +39 050 2219334

^bDipartimento di Chimica Bioorganica e Biofarmacia, via Bonanno 33, 56126, Pisa, Italy. E-mail: cinziac@farm.unipi.it; Fax: +39 050 2219660; Tel: +39 050 2219669

^cCNR-INFM PolyLab, via Risorgimento 35, I-56126, Pisa

† This paper was published as part of the themed issue of contributions from the Green Solvents – Progress in Science and Application conference held in Friedrichshafen, September 2008.



Experimental

Melting points are uncorrected. NMR spectra were recorded at room temperature at 200 (^1H), 250 (^1H) or 300 MHz (^1H) and 50.3 (^{13}C), 67.5 (^{13}C) or 75.7 MHz (^{13}C). The NMR spectra were recorded using $\text{DMSO}-d_6$, CDCl_3 or D_2O . FT-IR spectra were taken on pure compounds using a Perkin Elmer Spectrum One FTIR-ATR (400–4000 cm^{-1}). Differential scanning calorimetry (DSC) measurements were performed on 7–10 mg samples under nitrogen atmosphere by using a Mettler Toledo 822e instrument. The samples were sealed in aluminium pans under an inert atmosphere, and the temperature was calibrated using indium and stannous calibration standards. Samples were heated from 30 °C to the set high temperature, 230 °C, at 20 °C min^{-1} (1st heating), cooled to the set low temperature (–50 °C) at the same rate scan (1st cooling), then heated again to the set high temperature at 20 °C min^{-1} (2nd heating). Glass transition temperatures were measured from the inflection point in the second heating curve. Crystallization and melting enthalpies were evaluated from the integrated areas of melting peaks. Conductance measurements were performed using a CON 510 bench meter supplied with conductivity/TDS electrode. This electrode comes with a stainless steel ring, a cell constant of $K = 1.0$ and an inbuilt temperature sensor for automatic temperature compensation. GC-analyses were carried out using an Alltech AT-35 bonded FSOT column (30 m \times 0.25 mm id) and an Alltech AT-1 bonded FSOT column (30 m \times 0.25 mm id). ESI-MS analyses were performed on a Finnigan LCQ Advantage (Thermo Finnigan, San Jose, CA, USA) ion trap instrument equipped with Excalibur software.

All reactions were performed under argon, by standard syringe, cannula and septa techniques. 1-Methyl-1*H*-imidazole, 1,2-dimethyl-1*H*-imidazole, 1-chlorobutane, 1-bromobutane, 1-chlorooctane, 1-bromooctane, ethyl acrylate and iodobenzene were commercially available and were freshly distilled. All the other chemicals used in the reactions were reagent grade and used as purchased. 1-Butyl methanesulfonate was prepared according to reported procedures.¹³

3-(1*H*-imidazol-1-yl)propane-1,2-diol (1)

To a suspension of NaH (60% dispersion in mineral oil, 4.80 g, 120 mmol) in 60 mL of anhydrous DMF (Aldrich cat. 22.705–6) a solution of 1*H*-imidazole (6.81 g, 100 mmol) in 40 mL of anhydrous DMF was added dropwise. The resulting pale yellow mixture was stirred at room temperature for 3 h, then a solution of 3-chloro-1,2-propanediol (9.20 mL, 12.16 g, 120 mmol) in 20 mL of anhydrous DMF was added dropwise and the resulting colorless suspension was stirred at 70 °C for 24 h. The reaction

mixture was cooled to room temperature and filtered, and the solvent was removed *in vacuo*. The resulting viscous yellow oil was suspended in MeCN (60 mL), refluxed for 24 h and then rapidly filtered. The clear solution obtained was cooled to room temperature and successively to 0 °C, affording 3-(1*H*-imidazol-1-yl)propane-1,2-diol (1) (9.63 g, 68%) as a colorless solid: m.p. 76–78 °C (ref. 14 m.p. 77–78 °C). EI-MS m/z 142 (27), 117 (37), 89 (17), 82 (100), 68 (16), 55 (12). $^1\text{H-NMR}$ (200 MHz, $\text{DMSO}-d_6$): 7.56 (1H, s), 7.12 (1H, s), 6.86 (1H, s), 5.12 (1H, d, $J = 5.1$ Hz), 4.87 (1H, t, $J = 5.5$ Hz), 4.08 (1H, m), 3.84 (1H, m), 3.68 (1H, m), 3.28 ppm (2H, m). $^1\text{H-NMR}$ (300 MHz, D_2O): 7.61 (1H, s), 7.11 (1H, s), 6.96 (1H, s), 4.02 (4H, m), 3.50 (3H, m). The ^1H NMR data of this compound were in agreement with those reported in the literature.¹⁴

1-(2,3-Dihydroxypropyl)-3-methyl-1*H*-imidazolium chloride (2) ([GLYMIM]Cl)¹⁵

A solution of 1-methyl-1*H*-imidazole (12 mL, 14.32 g, 150 mmol) and 3-chloro-1,3-propanediol (4.2 mL, 5.53 g, 50 mmol) was stirred at 80 °C for 70 h. The crude reaction mixture was washed with AcOEt (4 \times 10 mL) and the resulting yellow oil was heated at 100 °C and stirred under vacuum (0.1 bar) for 24 h. [GLYMIM]Cl (2) was obtained as a viscous pale yellow oil (9.11 g, 95%). IR (neat): 3281, 3239 (OH). $^1\text{H-NMR}$ (250 MHz, D_2O): 8.75 (1H, s), 7.49 (1H, s), 7.45 (1H, s), 4.30 (1H, dd, $J = 13.9$ Hz, $J = 2.7$ Hz), 4.02 (1H, dd, $J = 13.9$ Hz, $J = 5.7$ Hz), 3.98 (1H, m), 3.90 (3H, s), 3.61 ppm (2H, d, $J = 8.04$ Hz). $^{13}\text{C-NMR}$ (67.5, D_2O): 136.6 (CH), 123.5 (CH), 122.9 (CH), 69.8 (CH), 62.4 (CH_2), 51.7 (CH_2), 35.8 (CH_3) ppm.

1-(2,3-Dihydroxypropyl)-2,3-dimethyl-1*H*-imidazolium chloride (3) ([GLYDIMIM]Cl)

A solution of 1,2-dimethyl-1*H*-imidazole (17.7 mL, 19.23 g, 200 mmol) and 3-chloro-1,3-propanediol (16.7 mL, 22.11 g, 200 mmol) was stirred at 80 °C for 72 h. The crude reaction mixture (an yellow oil) was washed with AcOEt (5 \times 25 mL) obtaining a solid which was recovered by filtration, washed with Et_2O (5 \times 60 mL), THF (2 \times 40 mL), Et_2O (2 \times 60 mL) and dried under vacuum (0.1 bar) for 24 h. [GLYDIMIM]Cl (3) (27.81 g, 67%) was obtained as a pale yellow solid: m.p. 24 °C. IR (neat) 3349, 3208 (OH). $^1\text{H-NMR}$ (250 MHz, D_2O): 7.35 (1H, d, $J = 2.0$ Hz), 7.31 (1H, d, $J = 2.0$ Hz), 4.27 (1H, dd, $J = 14$ Hz, $J = 2.7$ Hz), 4.08 (1H, dd, $J = 14$ Hz, $J = 5.7$ Hz), 4.02 (1H, m), 3.70 (3H, m), 3.65 (2H, d, $J = 8.0$ Hz), 2.61 (3H, s). $^{13}\text{C-NMR}$ (67.5, D_2O): 145.1 ($>\text{C}<$), 122.2 (CH), 121.3 (CH), 71.1 (CH), 62.4 (CH_2), 51.7 (CH_2), 32.5 (CH_3), 9.10 (CH_3) ppm.

3-Butyl-1-(2,3-Dihydroxypropyl)-1*H*-imidazolium chloride (4) ([GLYBIM]Cl)

A mixture of 3-(1*H*-imidazol-1-yl)propane-1,2-diol (1) (14.20 g, 100 mmol) and 1-chlorobutane (31.6 mL, 27.77 g, 300 mmol) was refluxed (85 °C, oil bath temperature) for 72 h. The crude reaction mixture was washed with AcOEt (6 \times 25 mL), heated at 75 °C and stirred under vacuum (0.1 bar) for 24 h. [GLYBIM]Cl (4) (21.53 g, 92%) was obtained as a pale yellow oil. IR (neat): 3253 (OH). $^1\text{H-NMR}$ (250 MHz, D_2O): 8.81 (1H, s), 7.51 (2H, br s), 4.38 (1H, dd, $J = 14$ Hz, $J = 2.7$ Hz), 4.21 (1H, $J = 14$ Hz,

$J = 7.7$ Hz), 4.04 (1H, m), 3.60 (2H, d, $J = 6.5$ Hz), 1.84 (2H, *pseudo*-quint, $J = 7.5$ Hz), 1.29 (2H, *pseudo*-sext, $J = 7.5$ Hz), 0.89 ppm (3H, t, $J = 7.5$ Hz). ^{13}C -NMR (67.5, D_2O): 135.9 (CH), 123.0 (CH), 122.3 (CH), 69.8 (CH), 62.4 (CH_2), 51.8 (CH_2), 49.4 (CH_2), 31.2 (CH_2), 18.7 (CH_2), 12.6 (CH_3) ppm.

3-Butyl-1-(2,3-dihydroxypropyl)-1H-imidazolium bromide (5) ([GLYBIM]Br)

A mixture of 3-(1H-imidazol-1-yl)propane-1,2-diol (**1**) (14.20 g, 100 mmol) and 1-bromobutane (16.1 mL, 20.56 g, 150 mmol) was stirred at 40 °C for 70 h. The top layer of the biphasic crude reaction mixture, which contained unreacted starting material, was decanted and the bottom layer was washed with Et_2O (6 × 25 mL), heated at 70 °C and stirred under vacuum (0.1 bar) for 24 h. [GLYBIM]Br (**5**) (26.08 g, 93%) was obtained as a pale orange oil. IR (neat): 3295 (OH). ^1H -NMR (250 MHz, D_2O): 8.85 (1H, s), 7.55 (2H, br s), 4.41 (1H, dd, $J = 14$ Hz, $J = 2.9$ Hz), 4.21 (2H, dd, $J = 14$ Hz, $J = 6.7$ Hz), 4.10 (1H, m), 3.63 (2H, d, $J = 5.5$ Hz), 1.87 (2H, *pseudo*-quint, $J = 7.0$ Hz), 1.30 (2H, *pseudo*-sext, $J = 7.0$ Hz), 0.92 ppm (3H, t, $J = 7.0$ Hz). ^{13}C -NMR (67.5, D_2O): 135.9 (CH), 123.0 (CH), 122.4 (CH), 69.9 (CH), 62.5 (CH_2), 51.8 (CH_2), 49.5 (CH_2), 31.3 (CH_2), 18.8 (CH_2), 12.7 (CH_3) ppm.

3-Butyl-1-(2,3-dihydroxypropyl)-1H-imidazolium methanesulfonate (6) ([GLYBIM][OMs])

A mixture of 3-(1H-imidazol-1-yl)propane-1,2-diol (**1**) (15.08 g, 66 mmol) and butyl methanesulfonate (15.08 g, 99 mmol) was stirred at 80 °C for 70 h. The crude reaction mixture was washed with Et_2O (5 × 15 mL), THF (6 × 20 mL), heated at 50 °C and stirred under vacuum (0.1 bar) for 24 h. [GLYBIM][OMs] (**6**) (26.08 g, 93%) was obtained as a pale yellow oil. IR (neat): 3338 (OH). ^1H -NMR (250 MHz, D_2O): 8.79 (1H, s), 7.51 (2H, br s), 4.37 (1H, dd, $J = 14$ Hz, $J = 1.7$ Hz), 4.20 (1H, dd, $J = 14$ Hz, $J = 7.7$ Hz), 4.03 (1H, m), 3.59 (2H, d, 5.1 Hz), 2.78 (3H, s), 1.84 (2H, *pseudo*-quint, $J = 7.2$), 1.30 (2H, *pseudo*-sext, $J = 7.2$), 0.90 ppm (3H, t, $J = 7.2$). ^{13}C -NMR (67.5, D_2O): 135.9 (CH), 123.0 (CH), 122.3 (CH), 69.8 (CH), 62.4 (CH_2), 51.7 (CH_2), 49.4 (CH_2), 38.5 (CH_3), 31.1 (CH_2), 18.7 (CH_2), 12.6 (CH_3) ppm.

1-(2,3-Dihydroxypropyl)-3-octyl-1H-imidazolium chloride (7) ([GLYOCTIM]Cl)

A mixture of 3-(1H-imidazol-1-yl)propane-1,2-diol (**1**) (8.87 g, 62 mmol) and 1-chlorooctane (31.8 mL, 27.65 g, 186 mmol) was stirred at 95 °C for 90 h. The top layer of the biphasic crude reaction mixture, which contained unreacted starting material, was decanted and the bottom layer was washed with AcOEt (5 × 20 mL), Et_2O (6 × 20 mL), heated at 100 °C and stirred under vacuum (0.1 bar) for 24 h. [GLYOCTIM]Cl (**7**) (15.51 g, 92%) was obtained as a pale orange oil. IR (neat) 3279 (OH). ^1H -NMR (250 MHz, D_2O): 8.90 (1H, s), 7.58 (1H, s), 7.55 (1H, s), 4.40–4.26 (2H, m), 4.07 (1H, m), 3.61 (2H, d, $J = 5$ Hz), 1.87 (2H, m), 1.26 (12H, m), 0.80 ppm (3H, m). ^{13}C -NMR (67.5, D_2O): 136.0 (CH), 123.2 (CH), 122.3 (CH), 69.8 (CH), 62.4 (CH_2), 51.9 (CH_2), 49.7 (CH_2), 31.3 (CH_2), 29.4 (CH_2), 28.6 (CH_2), 28.4 (CH_2), 25.6 (CH_2), 22.2 (CH_2), 13.6 (CH_3) ppm.

1-(2,3-Dihydroxypropyl)-3-octyl-1H-imidazolium bromide (8) ([GLYOCTIM]Br)

A mixture of 3-(1H-imidazol-1-yl)propane-1,2-diol (**1**) (14.20 g, 100 mmol) and 1-bromooctane (26.1 mL, 28.97 g, 150 mmol) was stirred at 80 °C for 69 h. The crude reaction mixture was washed with Et_2O (8 × 20 mL), THF (3 × 20 mL) and heated at 75 °C and stirred under vacuum (0.1 bar) for 24 h. [GLYOCTIM]Br (**8**) (30.90 g, 92%) was obtained as a pale yellow oil. IR (neat): 3305 (OH). ^1H -NMR (250 MHz, D_2O): 8.90 (1H, s), 7.57 (2H, s), 4.37 (1H, dd, $J = 14$ Hz, $J = 2.7$ Hz), 4.22 (1H, dd, $J = 14$ Hz, $J = 7.7$ Hz), 4.07 (1H, m), 3.62 (2H, d, $J = 5.7$), 1.87 (2H, m), 1.26 (12H, m), 0.80 ppm (3H, m). ^{13}C -NMR (67.5, D_2O): 136.0 (CH), 123.2 (CH), 122.3 (CH), 69.8 (CH), 62.4 (CH_2), 51.9 (CH_2), 49.7 (CH_2), 31.3 (CH_2), 29.4 (CH_2), 28.5 (CH_2), 28.4 (CH_2), 25.6 (CH_2), 22.2 (CH_2), 13.6 (CH_3) ppm.

1-(2,3-dihydroxypropyl)-3-octyl-1H-imidazolium bis(trifluoromethanesulfonyl)imide (9) ([GLYOCTIM][NTf₂])

A mixture of [GLYOCTIM]Br (**8**) (6.82 g, 20.35 mmol) and lithium bis(trifluoromethanesulfonyl)imide (5.86 g, 20.35 mmol) in 35 mL of H_2O were stirred at 70 °C for 1 h. The resulting biphasic colorless mixture was allowed to cool to room temperature and stirred for 22 h. The crude reaction mixture was diluted with H_2O and acetone, and the solvents were removed *in vacuo*. The resulting yellow oil was diluted with acetone, filtered and concentrated, and this operation was repeated twice. The resulting crude product was then washed with H_2O (6 × 20 mL) and then heated at 80 °C and stirred under vacuum (0.1 bar) for 4 h. [GLYOCTIM][NTf₂] (**9**) (9.41 g, 92%) was obtained as a pale yellow oil. IR (neat): 3520 (OH). ^1H -NMR (250 MHz, CDCl_3): 8.65 (1H, br s), 7.45 (1H, br s), 7.28 (1H, br s), 4.4–3.96 (3H, m, ABM system), 3.66–3.50 (2H, AB system), 1.83 (2H, m), 1.25 (12H, br s), 0.86 ppm (3H, t, $J = 6.4$ Hz). ^{13}C -NMR (67.5, CDCl_3): 136.0 (CH), 123.2 (CH), 122.3 (CH), 69.8 (CH), 63.1 (CH_2), 51.9 (CH_2), 50.2 (CH_2), 31.7 (CH_2), 30.0 (CH_2), 29.0 (CH_2), 28.8 (CH_2), 26.1 (CH_2), 22.6 (CH_2), 14.0 (CH_3) ppm.

3,3'-Methylenebis(1-(2,3-dihydroxypropyl)-1H-imidazolium dibromide (10) ([MEBISGLYIM]Cl)

A mixture of 3-(1H-imidazol-1-yl)propane-1,2-diol (**1**) (20 g, 141 mmol) and dibromomethane (50 mL, 124.75 g, 718 mmol) was stirred at 80 °C for 72 h. The top layer of the biphasic crude reaction mixture, which contained unreacted starting material, was decanted and the bottom layer was washed with Et_2O (3 × 50 mL), THF (4 × 50 mL), heated at 85 °C and stirred under vacuum (0.1 bar) for 24 h. [MEBISGLYIM]Cl (**10**) (30.90 g, 96%) was obtained as a pale yellow oil. IR (neat): 3306 (OH). ^1H -NMR (250 MHz, D_2O): 9.40 (2H, s), 7.89 (2H, s), 7.72 (2H, s), 6.80 (2H, s), 4.51 (2H, dd, $J = 14$ Hz, $J = 2.7$ Hz), 4.31 (2H, dd, $J = 14$ Hz, $J = 8$ Hz), 4.13 (2H, m), 3.67 ppm (4H, d, $J = 5.5$ Hz). ^{13}C -NMR (67.5, D_2O): 137.6 (CH), 124.5 (CH), 122.1 (CH), 69.6 (CH), 62.5 (CH_2), 59.0 (CH_2), 52.0 (CH_2) ppm.

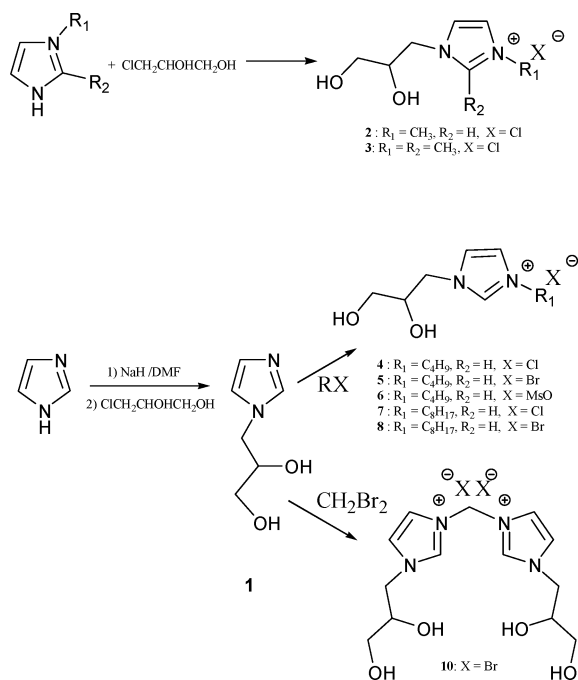
ILs **2–10** appeared pure at ^1H NMR and ESI-MS analysis.

General procedure for the Heck reactions

The selected GLY-based TSIL (1 mL), sodium acetate (90.2 mg, 1.1 mmol) and palladium (II) chloride (8.9 mg, 0.05 mmol) were placed in a 10 mL Schlenk tube fitted with a silicon septum and equipped with a magnetic stirring bar. The reaction tube was evacuated and back-filled with argon, and this sequence was repeated four times. Deaerated ethyl acrylate (0.15 mL, 0.14 g, 1.4 mmol) and iodobenzene (0.11 mL, 0.20 g, 1.0 mmol) were then added by syringe into the tube. The resulting mixture was stirred vigorously at 100 °C for 1 h. After this period of time the dark brown crude reaction mixture was cooled to room temperature and the product extracted with petroleum ether (10–15 × 2 mL), naphthalene was added as an internal standard and the GLC yield (%) of ethyl cinnamate was determined. The results are reported in Table 4. The TSIL phase containing the palladium catalyst was placed under vacuum for 4 h, and reused for the next runs under identical reaction conditions.

Results and discussion

The synthetic pathways for ionic liquids **2–10** are reported in Scheme 1.



Scheme 1 Reaction pathways.

1-(2,3-Dihydroxypropyl)-3-methyl-1*H*-imidazolium chloride (**2**, [GLYMIM]Cl) and 1-(2,3-dihydroxypropyl)-2,3-dimethyl-1*H*imidazolium chloride (**3**, [GLYDIMIM]Cl) were prepared by reaction of 1-methyl-1*H*-imidazole or 1,2-dimethyl-1*H*-imidazole with 3-chloro-1,3-propanediol. All the other salts were prepared using 3-(1*H*-imidazol-1-yl)propane-1,2-diol (**1**) as starting material.¹⁶ The appropriate alkyl halides or mesylate are reacted in the absence of solvent at temperatures ranging from 80 to 95 °C to afford the corresponding salts, **4–6** and **7–8**. Subsequent metathesis of **8** in water with lithium

bis(trifluoromethanesulfonyl)imide in equimolar amount, afford the bis(trifluoromethanesulfonyl)imide salt **9**.

Finally, 3,3'-methylenebis(1-(2,3-dihydroxypropyl)-1*H*-imidazolium dibromide (**10**, [MBISGLYIM]Cl) was prepared by reaction of **1** with dibromomethane. It should be noted that salt **2** has been reported previously although their physical properties were not described in detail.¹⁷ With the exception of **9**, all of the ionic liquids are soluble in water, but they are immiscible with solvents of low polarity, such as ethyl ether and alkanes.

Salts **2–10** were characterized using electrospray ionization mass spectrometry (ESI-MS), IR, ¹H and ¹³C NMR. The ¹H and ¹³C NMR spectra of **2–10** in D₂O or DMSO are as expected with little change in the spectra as the anion is varied.

The positive ion ESI mass spectra of **2–9** exhibit parent peaks respectively at *m/z* 157, 171, 199 and 255 corresponding to the expected cations, whereas IL **10**, bearing a double charged cation, shows a parent peak at *m/z* 149. In negative mode intense peaks due to the [MsO]⁻ and [Tf₂N]⁻ anions were observed. Moreover, aggregates based on small cation–anion clusters, which are reduced in intensity as the concentration of TSIL solution is reduced, characterized the spectra of all examined ILs (Fig. 1). Since the spectra have been registered under identical conditions (solvent, concentration, ionization energy, *etc.*), the comparison of the cluster peak distributions characterizing the spectra both in positive and negative mode (generally, in negative mode clusters are more evident), can give a semi-quantitative evaluation of the strength of the anion–cation interaction.¹⁸ On the basis of the data reported in Table 1, it is evident that this ability strongly depends on the anion and increases in the order [Tf₂N]⁻ <<[OMs]⁻ < Br⁻ < Cl⁻. Thus, data here reported confirm the very low tendency of the [Tf₂N]⁻ anion to give clusters in ESI-MS (*in vacuo*), and probably in pure liquid, and the ability of halides to give three-dimensional networks of anions–cations under both these conditions. It is noteworthy that also IL **3**, bearing a methyl group at the C-2 position, gives a significant number of clusters both in negative and positive mode (Table 1). This is in contrast with the situation evidenced¹⁸ with the corresponding unfunctionalized imidazolium cation, [bdmim]⁺, which presented a reduced ability to give clusters. Probably, the introduction of two OH groups increases the anion–cation interaction sites, in particular when coordinating anions such as chloride are used.

The different ability of anions and cations to give ionic three-dimensional networks can also be envisaged from the IR spectra. The main feature in the IR spectra of the pure ILs **2–10** is the characteristic OH stretching vibration(s), whose frequency significantly depends on anion and alkyl chain length, ranging from 3239 to 3520 cm⁻¹. In particular, the IR spectrum of IL **9**, bearing the low basic and weakly coordinating [Tf₂N]⁻ anion, is characterized by a broad band around 3520 cm⁻¹. At variance, in salts **2–8** having more coordinating anions (chloride, bromide and mesylate) the OH stretching vibration is stronger and significantly red-shifted. Since the red-shift and the intensity increase of OH stretching mode is normally a consequence of the hydrogen-bonding, these data strongly suggest that in the pure liquid the hydroxyl group(s) interact with the anion, in particular when the anion is able to give hydrogen bonding.

The key criterion for evaluation of an ionic liquid is its melting point. For the imidazolium-based salts, the influence

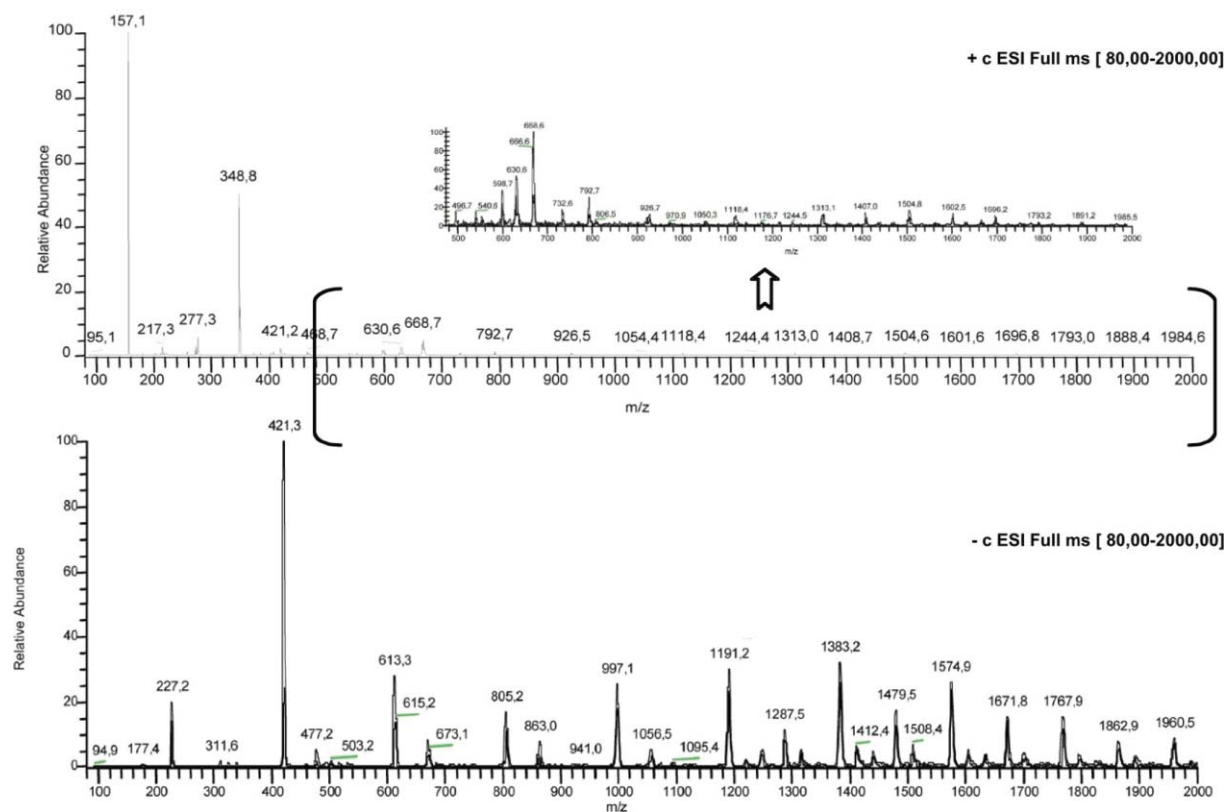


Fig. 1 ESI-MS analysis of IL **2** (10 ppm, CH₃CN) in positive (in window, zoom of the region between 500 and 2000 *m/z*) and negative mode.

of structural variation of the cation and/or anion on the melting point has been extensively investigated. Generally, low symmetry, weak intermolecular interactions and a good charge distribution over the cation and/or anion tend to produce salts with lower melting points. The effect of alkyl chain length and anion structure on the thermal properties of ILs **2–10** was investigated using differential scanning calorimetry (DSC). Typical DSC thermograms for glycerylimidazolium based ILs are reported in Fig. 2, data related to ILs **2–10** are plotted in Table 2.

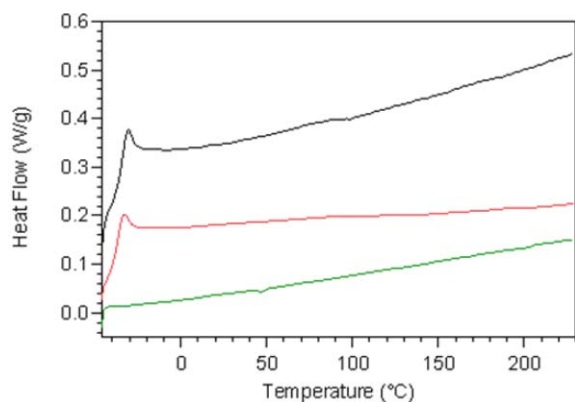


Fig. 2 DSC traces of ILs **7** (black), **8** (red) and **9** (green).

No melting point was evidenced in the DSC thermograms. The glass transition temperatures (T_g) of glycerylimidazolium based ILs decrease with increasing alkyl chain length within chloride and bromide salts series.

This trend is analogous to that observed for methyl substituted imidazolium salts, for which the increase of length and flexibility of the other alkyl group results in lower melting points. With a constant butyl substituent, varying the anion from chloride to bromide to mesylate glass transition temperatures change from -28 to *ca.* -40 °C. Analogously, in the octyl series, glass transition temperatures decrease changing the anion from chloride to bromide and to bistriflimide. It is noteworthy that, while the melting point of a species is affected both by features that are present in liquid and solid states, the T_g is determined by the physical properties of the liquid only; *i.e.* increased hydrogen bonding, thus T_g rises. In agreement with this statement, the T_g values follow the above mentioned trend (chloride > bromide >> [Tf₂N⁻]) and a correlation may be found between the T_g and the OH stretching vibration (Table 2).

Ionic conductivity is one of the most important properties of ionic liquids considered as electrolytes. As expected, salts **2–9** present moderate conductivities (up to 0.147 mS cm⁻¹). In agreement with the other physico-chemical properties, conductivity depends primarily on the anion and IL **9**, [GLYOCTMIM][Tf₂N], presents the higher value, although also the variation of alkyl chain length affects this parameter.

Temperature dependency of ionic conductivity for five ILs is shown in Fig. 3. Considering the high viscosity of these salts, the conductivities of these salts exhibit non-Arrhenius behavior. Therefore, the Vogel–Tammann–Fulcher (VTF) equation was used to represent the temperature dependence of conductivity. In Fig. 3, the variation of $\lg(k)$ versus $1/(T-T_0)$ is plotted. The best fit values for k_0 (S cm⁻¹), B' (K) and T_0 (K) are given in Table 3.

Table 1 ESI-MS analysis by direct infusion in positive and negative mode

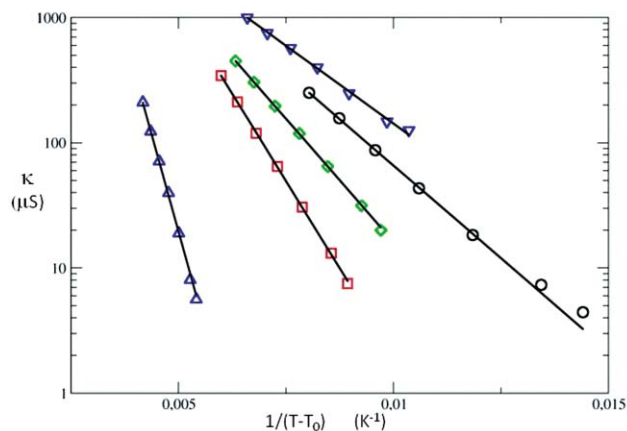
IL	Clusters															
	C ⁺ ^a	C ₂ A ⁺	C ₃ A ⁺	C ₄ A ⁺	C ₅ A ⁺	C ₆ A ⁺	A ⁺	CA ⁻	C ₂ A ⁻	C ₃ A ⁻	C ₄ A ⁻	C ₅ A ⁻	C ₆ A ⁻	C ₇ A ⁻	C ₈ A ⁻	C ₉ A ⁻
2	157.7 (100) ^b	348.9 (54)	582.7 (2)	788.7 (2)	996.1 (1)	1202.4 (1)		227.2 (21)	421.2 (100)	613.1 (29)	861.2 (7)	997.1 (28)	1191.4 (36)	1381.9 (26)	1577.2 (25)	
3	171.1 (100)	376.8 (5)						240.9 (20)	448.7 (100)	655.2 (50)	974.2 (8)	1206.7 (9)				
4	199.2 (100)	432.8 (57)						269.4 (53)	506.9 (100)	739.1 (20)	1194.4 (9)					
5	199.2 (100)	478.9 (20)					95.3 (44)	359.6 (50)	637.1 (100)	918.7 (12)						
6	199.2 (100)	493.8 (5)						389.7 (53)	683.0 (100)	997.8 (5)						
7	255.2 (100)	546.9 (26)						327.5 (13)	617.5 (100)	907.1 (27)						
8	255.2 (100)	590.9 (48)							415.7 (28)	751.4 (100)						
9	255.2 (100)						280 (100)		415.7 (28)	751.4 (100)						
10	297.1 (5)	149.2 (100)	378.8 (53)	836.8 (15)	1292.6 (10)	1754 (5)			CA ⁻	C ₃ A ⁻	C ₃ A ⁻	C ₃ A ⁻	1486.6 (6)	1777.9 (5)		
									538.8 (5)	996.7 (94)	814.5 (7)	1348.7 (1)	1421.8 (9)	1757.1		

^a C = cation; A = anion. ^b Relative abundance.**Table 2** Physico-chemical properties of ILs 2–10

IL	T_g		T_{cc}	T_m	κ	ν OH
	$T/^\circ\text{C}$	$\Delta C_p/\text{J g}^{-1} \text{ }^\circ\text{C}$				
2	-23	0.289	nd	nd	—	3239; 3281
4	-28	0.423	nd	nd	7.32	3253
5	-30	0.368	nd	nd	13.10	3295
6	≡ -40	nd	nd	nd	31.50	3338
7	-33	0.271	nd	nd	—	3279
8	-36	0.249	nd	nd	8.03	3305
9	nd	nd	nd	nd	147.6	3520
10	21	0.49	nd	nd	—	3306

 T_g : Glass transition temperature, T_{cc} : temperature of cold crystallization (crystallization during heating); κ , ionic conductivity at 25 °C; nd, not determined.**Table 3** VFT Equation parameters for ionic conductivity

IL	T_0/K	$\kappa_0/\text{S cm}^{-1}$	B'/K	R^{2a}
4	223.7	0.0601	682	0.9916
5	181.2	0.7590	1285	0.9944
6	190.1	0.1389	906	0.9928
8	108.4	32.300	2864	0.9909
9	196.6	0.0432	571	0.9939

^a Correlation coefficients.**Fig. 3** Temperature dependency of ionic conductivity for ILs 4 (○), 5 (□), 6 (◇), 8 (△) and 9 (▽) to the Vogel–Tammann–Fulcher (VTF) equation.

Palladium-catalyzed cross-coupling reactions in ILs

Palladium-catalyzed carbon–carbon bond forming reactions have contributed remarkably to synthetic organic chemistry.¹⁹ Among these reactions, the Heck reaction and its related reactions have been extensively utilized in preparing a wide variety of olefinic compounds.²⁰ In view of the increasing demand for environmental benign reaction processes, a particular effort has been put towards investigating the Heck reaction, including searching for phosphine-free methods. In particular, recently phosphine-free palladium catalysts have been successfully employed in carrying out the Heck coupling in ionic liquids.^{4d,21} In fact, it has been shown that, depending on their structural features, ILs can act not only as solvents, but also as ligands or ligand precursors for transition-metal complexes, increasing

their thermal stability and catalytic activity. Moreover, ILs can act as “liquid” immobilizing supports for metal catalysts, allowing an easy recovery of the products from the reaction mixture and the recycling of the catalyst system. In this study, we performed a Heck coupling by reacting iodobenzene and ethyl acrylate (1.4 equiv.) in glycerylimidazolium-based ionic liquids **2–8** at 100 °C in the presence of 5 mol % palladium chloride as the catalyst precursor and AcONa (1.1 equiv.) as the base (Fig. 4).

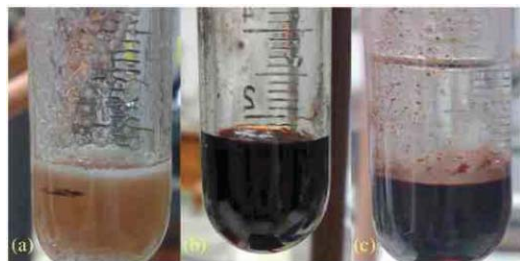


Fig. 4 Heck reaction in [GLYOCTIM]Cl **7**. (a) Reaction mixture before heating. (b) and (c) reaction mixture after 1 h at 100 °C before and after the addition of petroleum ether, respectively.

The coupling was stopped after 1 h and *trans*-ethyl cinnamate, which was formed as the only product in all reactions (no biphenyl could be detected), was recovered by extraction with petroleum ether and quantified by GC after addition of naphthalene as an internal standard (Table 4).

The glycerylimidazolium-based liquid phase containing the active catalyst resulting from the extraction of the coupling product was dried under vacuum before new substrates were charged.

Generally, reuse of the IL systems was not very encouraging, due to the progressive loss of activity, in particular in [GLYOCTIM]Cl **7**. In the investigated ILs, reaction yield increases on increasing the alkyl chain on cation, that is on their increasing lipophilicity: [GLYOCTIM]Cl > [GLYBIM]Cl > [GLYMIM]Cl, and [GLYOCTIM]Br > [GLYBIM]Br. The very low yield obtained by using IL **3** as a solvent suggests that imidazolium carbenes, formed by reaction of the base with the acidic C(2)–H bond of the [GLYIM⁺] cations, might be actively implicated in these reactions. In fact, Pd-carbene complexes have been isolated when PdCl₂²² or Pd(OAc)₂^{21a} (which in our case

may arise from PdCl₂ by ligand exchange with AcONa) were heated in imidazolium-based ILs. It has been also reported that the formation of carbenes in imidazolium-based ILs is favoured by the basicity of the counteranion,^{21a,23} which helps to explain the observed experimental results: bromides gave lower conversions than chlorides and practically no reaction was observed in [GLYBIM][OMs], **6**.

Finally, it is interesting to note that the use of this new class of TSILs appears more favourable in comparison with the “classical” ionic liquids such as BMIM-based ones. In fact, our protocol does not require the addition of any metal ligand²⁴ or the use of preformed Pd complexes²⁵ and, at least for **7**, it competes in terms of chemical yield and reaction time even with protocols that use MW heating.²⁶

Conclusions

Introduction of the 2,3-dihydroxypropyl group on the imidazolium ring yields an interesting series of ILs. This group is able to hydrogen bond the anion, giving salts which are liquid at room temperature whose glass transition temperature increases on increasing hydrogen bonding ability of the anion. The strong interactions among ions evidenced by the tendency to give clusters in the ESI-MS spectra determine the low ionic conductivity. On the other hand, the presence of the hydroxyl groups on the cation, which can act as ligands for transition metals, also affects the applicability of these functionalized ILs in metal-catalyzed reactions.

Acknowledgements

We thank Fondazione Caripi for the financial support.

Notes and references

- Ionic Liquids IIIB: Fundamentals, Progress, Challenges, and Opportunities – Transformations and Processes*, ed. R. D. Rogers, and K. R. Seddon, ACS Symp. Ser., vol. 902, American Chemical Society, Washington D.C., 2005; *Ionic Liquids IIIA: Fundamentals, Progress, Challenges, and Opportunities – Properties and Structure*, ed. R. D. Rogers, and K. R. Seddon, ACS Symp. Ser., vol. 901, American Chemical Society, Washington D. C., 2005; *Ionic Liquids in Synthesis*, ed. P. Wasserscheid, and T. Welton, Wiley-VCH, Weinheim, 2nd edn, 2007.
- W. Chen and F. Liu, *J. Organomet. Chem.*, 2003, **673**, 5; M. Sorm and S. Nespurek, *Acta Polym.*, 1985, **36**, 433; D. Zhao, Z. Fei, T. J. Geldbach, R. Scopelliti, G. Laurenczy and P. J. Dyson, *Helv. Chim. Acta*, 2005, **88**, 665; F. Mazille, Z. Fei, D. Kuang, D. Zhao, S. M. Zakeeruddin, M. Gratzel and P. J. Dyson, *Inorg. Chem.*, 2006, **45**, 1585; K. M. Lee, Y. T. Lee and Y. J. B. Lin, *J. Mater. Chem.*, 2003, **13**, 1079; L. C. Branco, J. N. Rosa, J. J. Moura Ramos and C. A. M. Afonso, *Chem.–Eur. J.*, 2002, **8**, 3671; A. P. Abbott, G. Capper, D. L. Davies and R. Rasheed, *Inorg. Chem.*, 2004, **43**, 3447; A. C. Cole, J. L. Jensen, I. Ntai, K. L. T. Tran, K. J. Weaver, D. C. Forbes and J. H. Jr Davis, *J. Am. Chem. Soc.*, 2002, **124**, 5962; J. D. Holbrey, W. M. Reichert, I. Tkatchenko, E. Bouajila, O. Walter and I. Tommasi, *Chem. Commun.*, 2003, 28; N. Brausch, A. Metlen and P. Wasserscheid, *Chem. Commun.*, 2004, 1552; Z. Fei, D. Zhao, T. J. Geldbach, R. Scopelliti and P. J. Dyson, *Chem. Eur. J.*, 2004, **10**, 4886; D. Li, F. Shi, J. Peng, S. Guo and Y. Deng, *J. Org. Chem.*, 2004, **69**, 3582; Z. Fei, W. H. Ang, T. J. Geldbach, R. Scopelliti and P. J. Dyson, *Chem. Eur. J.*, 2006, **12**, 4014; Y. R. Mirzaei, H. Xue and J. M. Shreeve, *Inorg. Chem.*, 2004, **43**, 361; Z. Mu, W. Liu, S. Zhang and F. Zhou, *Chem. Lett.*, 2004, **33**, 524.
- R. J. C. Brown, P. J. Dyson, P. J. Ellis and T. Welton, *Chem. Commun.*, 2001, 1862; P. J. Dyson, J. S. McIndoe and D. Zhao, *Chem. Commun.*,

Table 4 Heck Coupling in ILs

Entry	IL	GLC Yield (%) ^a		
		First recycle	Second recycle	Third recycle
1	[GLYMIM]Cl, 2	13	11	15
2	[GLYBIM]Cl, 4	37	66	46
3	[GLYOCTIM]Cl, 7	87	65	35
4	[GLYBIM]Br, 5	28	22	21
5	[GLYOCTIM]Br, 8	49	48	15
6	[GLYBIM][OMs], 6	3	—	—
7	[GLYDIMIM]Cl, 3	3	—	—

^a Determined using naphthalene as an internal standard.

- 2003, 508; H. S. Kim, Y. J. Kim, J. Y. Bae, S. J. Kim, M. S. Lah and C. S. Chin, *Organometallics*, 2003, **22**, 2498; D. Zhao, Z. Fei, C. A. Ohlin, G. Laurency and P. J. Dyson, *Chem. Commun.*, 2004, 2500.
- 4 Z. Fei, T. J. Geldbach, D. Zhao and P. J. Dyson, *Chem. Eur. J.*, 2006, **12**, 2122; S. Lee, *Chem. Commun.*, 2006, 1049; C. Chiappe, D. Pieraccini, D. Zhao, Z. Fei and P. J. Dyson, *Adv. Synth. Cat.*, 2006, **348**, 68; Z. Fei, D. Zhao, D. Pieraccini, W. H. Ang, T. J. Geldbach, R. Scopelliti, C. Chiappe and P. J. Dyson, *Organometallics*, 2007, **26**, 1588.
- 5 C. Chiappe and D. Pieraccini, *J. Phys. Org. Chem.*, 2005, **18**, 275.
- 6 W. Miao and T. A. Chan, *Acc. Chem. Res.*, 2006, **39**, 897–908.
- 7 J. Fraga-Dubreuil, M.-H. Famelart and J. P. Bazureau, *Org. Process Res. Dev.*, 2002, **6**, 374.
- 8 (a) J. Fraga-Dubreuil and J. P. Bazureau, *Tetrahedron Lett.*, 2001, **42**, 6097; (b) J. Fraga-Dubreuil and J. P. Bazureau, *Tetrahedron*, 2003, **59**, 6121; (c) H. Hakkou, J. J. V. Eynde, J. Hamelin and J. P. Bazureau, *Tetrahedron*, 2004, **60**, 3745; (d) H. Hakkou, J. J. V. Eynde, J. Hamelin and J. P. Bazureau, *Synthesis*, 2004, 1793.
- 9 W. Miao and T. H. Chan, *Org. Lett.*, 2003, **5**, 5003.
- 10 C. Pretti, C. Chiappe, I. Baldetti, S. Brunini, G. Monni and L. Intorre, *Ecotoxicol. Environ. Saf.*, 2008, DOI: 10.1016/j.ecoenv.2008.09.010.
- 11 A. Ten Kate, M. J. J. Mayer, C. J. G. Cornelis, B. Kuzmanovic, C. A. M. C. Dirix, PCT Int. Appl. (2008), WO 2008074733 A1 200880626.
- 12 C. H. Christensen, J. Rass-Hansen, C. C. Marsden, E. Taarning and K. Egeblad, *ChemSusChem*, 2008, **1**, 283.
- 13 (a) S. Ahmed, C. P. Owen, K. James, C. K. Patel and L. Sampson, *J. Steroid Biochem. Mol. Biol.*, 2002, 429; (b) S. Chatti, M. Bortolussi and A. Loupy, A., *Tetrahedron*, 2001, 4365.
- 14 N. Ueda, T. Kawabata and K. Takemoto, *J. Heterocyclic Chem.*, 1971, **8**, 827.
- 15 K.-S. Kim, D. Demberelnyamba and H. Lee, *Langmuir*, 2004, **20**, 556.
- 16 N. Ueda, T. Kawabata and K. Takemoto, *J. Heterocyclic Chem.*, 1971, **8**, 827.
- 17 K.-S. Kim, D. Demberelnyamba and H. Lee, *Langmuir*, 2004, **20**, 556.
- 18 R. Bini, O. Bortolini, C. Chiappe, D. Pieraccini and T. Siciliano, *J. Phys. Chem. B*, 2007, **111**, 598.
- 19 J. Tsuji, *Palladium reagents and catalysts*, John Wiley, New York, 1996.
- 20 I. P. Beletskaya and A. V. Cheprakov, *Chem. Rev.*, 2000, **100**, 3009.
- 21 (a) L. Xu, W. Chen and J. Xiao, *Organometallics*, 2000, **19**, 1123; (b) H. Hagiwara, Y. Shimizu, T. Hoshi, T. Suzuki, M. Ando, K. Okhubo and C. Yokoyama, *Tetrahedron Lett.*, 2001, **42**, 4349; (c) V. Calò, A. Nacci, A. Monopoli, S. Laera and N. Cioffi, *J. Org. Chem.*, 2003, **68**, 2929; (d) V. Calò, A. Nacci and A. Monopoli, A., *J. Mol. Catal. A: Chem.*, 2004, **214**, 45; (e) L. Wang, H. Li and P. Li, *Tetrahedron*, 2009, **65**, 264.
- 22 J. E. L. Dullius, P. A. Z. Suarez, S. Einloft, S. R. F. de Souza, J. Dupont, J. Fischer and A. De Cian, A., *Organometallics*, 1998, **17**, 815.
- 23 R. Sheldon, *Chem. Commun.*, 2001, 2399.
- 24 S. A. J. Carmichael, M. J. Earle, J. D. Holbrey, P. B. McCormac and K. R. Seddon, *Org. Lett.*, 1999, **1**, 997.
- 25 S. B. Park and H. Alper, *Org. Lett.*, 2003, **5**, 3209.
- 26 K. S. A. Vallin, P. Emilsson, M. Larhed and A. Hallberg, *J. Org. Chem.*, 2002, **67**, 6243.

Aqueous-biphasic hydroformylation of alkenes promoted by “weak” surfactants†‡

Simon L. Desset, Simon W. Reader and David J. Cole-Hamilton*

Received 10th December 2008, Accepted 17th February 2009

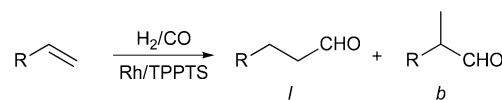
First published as an Advance Article on the web 6th March 2009

DOI: 10.1039/b822139a

The aqueous-biphasic hydroformylation of higher alkenes catalyzed by Rh/TPPTS has been carried out in the presence of imidazolium, pyridinium and triethylammonium salts. High reaction rates are achieved with imidazolium and triethylammonium salts provided that their alkyl “tail” is $\geq C_8$. Fast and complete phase separation, and good retention of the metal in the aqueous phase could be achieved with an octyl “tail”. Imidazolium salts were found to give the highest rate enhancement. The nature of the anion showed a moderate influence on the reaction. Evidence suggests that the additive can act as weak surfactant allowing emulsions to be formed and broken by simply switching the stirring on and off.

Introduction

The use of catalysts that allow the selective production of the desired product under mild conditions has been recognized as one of the main requirements for sustainable chemical development.¹ To achieve this aim, homogeneous catalyst are tools of choice, since they display high activity and their selectivity can be tailored through the use of specially designed ligands. Unfortunately, the catalyst being dissolved in the reaction medium makes its separation from the products often a challenging task. Beside economic considerations, the loss of catalyst in the product is not acceptable for environmental and toxicological reasons. Different strategies have thus been developed to tackle this problem.² Among them, aqueous-biphasic catalysis constitutes a very elegant approach.³ By using water, a benign solvent, as a catalyst immobilizing phase, non-polar products are present in a different phase from the catalyst and can be simply removed by decantation. This methodology has proven its viability with the industrial Ruhr Chemie–Rhône Poulenc process, in which the rhodium catalyzed hydroformylation of propene or butene has been conducted since 1984 producing 800 000 t y⁻¹ of C₄ and C₅ aldehydes (Scheme 1).⁴ In this process, the rhodium catalyst is efficiently anchored in the aqueous phase *via* the water soluble ligand P(3-C₆H₄SO₃Na)₃, TPPTS, leading to very low metal leaching, *i.e.* ppb scale.⁵ However, the scope of this methodology is greatly reduced by the low solubility of the substrate in the aqueous phase.



Scheme 1 The hydroformylation of alkenes catalyzed by a Rh/TPPTS complex under aqueous-biphasic conditions (R = CH₃: propene, R = C₄H₉: 1-hexene, R = C₆H₁₃: 1-octene and R = C₈H₁₇: 1-decene; *l* = linear, *b* = branched).

Poorly water soluble substrates react far too slowly under aqueous biphasic conditions for economically viable industrial application.

Numerous studies have been aimed at extending the scope of the aqueous-biphasic methodology to more hydrophobic substrates. Ligands for which the solubility can be reversibly switched by pH or temperature variation, or by addition/removal of CO₂ have been used to transfer the catalyst between the aqueous and the organic phase.^{6–8} This allows the reaction to be carried out under homogeneous conditions, *i.e.* without mass transfer limitation, while transferring the catalyst to the aqueous phase after reaction for easy separation by decanting. Supporting the aqueous phase onto porous oxide supports has been used to develop heterogeneous-like catalysts.⁹ With those catalysts, the reaction rate was shown to be independent of the substrate water solubility.¹⁰ A new reactor design has also been shown to enhance reaction rates for poorly water soluble substrates.¹¹ All these elegant new approaches show very promising results. However, they require a significant redesign of the process which makes them unsuitable for a rapid wider application of the aqueous-biphasic methodology.

Additives have also been used to improve the solubility of the substrate in the catalyst phase without the need for a complete change in the process. Cosolvents, such as lower alcohols, have been shown to increase the reaction rate for aqueous-biphasic hydroformylation.¹² However, they induce side reactions, such as acetal formation, and leaching of the cosolvent into the product phase complicates the product separation. Inverse phase transfer catalysts, such as modified cyclodextrins and calixarenes, were shown to enhance reaction rates in various reactions under

EaStCHEM, School of Chemistry, University of St Andrews, The Purdie Building, North Haugh, St Andrews, Fife, UK KY16 9ST.
E-mail: djc@st-andrews.ac.uk; Fax: +44 (0)1334 463808;
Tel: +44 (0)1334 463805

† This paper was published as part of the themed issue of contributions from the Green Solvents – Progress in Science and Application conference held in Friedrichshafen, September 2008.

‡ Electronic supplementary information (ESI) available: Videos of the mixing and phase separation in the presence and absence of [OctMim]Br. See DOI: 10.1039/b822139a

aqueous-biphasic conditions.¹³ Cationic surfactants can greatly enhance the reaction rate in aqueous-biphasic systems.¹⁴ However, phase separation can become troublesome, since these systems are prone to emulsion.¹⁵

In a preliminary communication, we have described the use of imidazolium salts as promoters for aqueous-biphasic hydroformylation of higher alkenes catalyzed by Rh/TPPTS.¹⁶ In this paper we describe details of that system and discuss the influence of the additive structure on the reaction (Fig. 1), especially the influence of the apolar tail of the cationic group and the ionic head group, as well as the influence of the anion. Moreover, we provide further evidence of the additive acting as a “weak” surfactant.

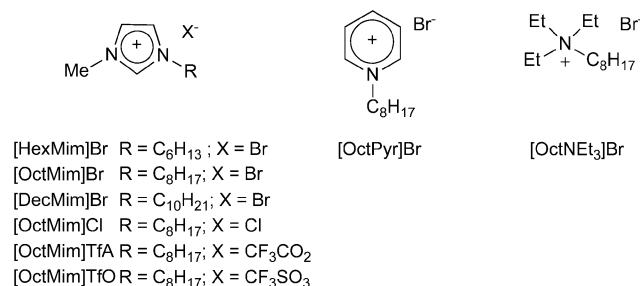


Fig. 1 Structure of the different additives used in this study.

Results and discussion

Use of [OctMim]Br in the aqueous-biphasic hydroformylation of alkenes

In the absence of additives, the hydroformylation of medium chain alkenes is very slow (see Fig. 2). For example, 1-octene gives only 1.9% conversion to aldehydes in 3 h (initial turnover frequency, TOF = 10 h⁻¹, under the conditions of Table 1). On adding [OctMim]Br, the rate increases dramatically above 0.033 mol dm⁻³ (Fig. 3), reaching 1100 h⁻¹ at a concentration of 0.5 mol dm⁻³ with a decrease of linear selectivity (linear

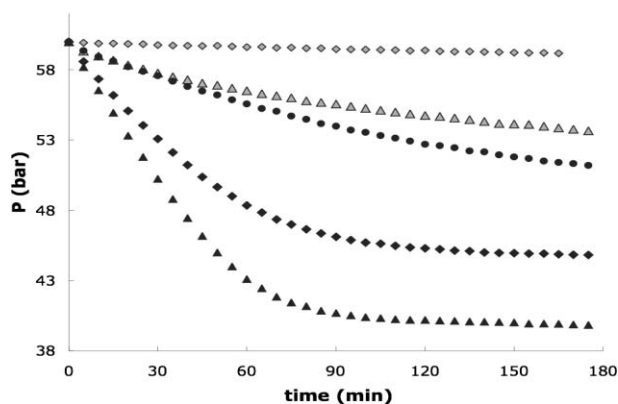


Fig. 2 Gas uptake plots from a ballast vessel for the hydroformylation of various alkenes in the absence (grey) and presence (black) of [OctMim]Br (0.5 mol dm⁻³). ▲ 1-Hexene, ◆ 1-octene, ● 1-decene (for conditions see Table 1 footnote a, P/Rh = 10).

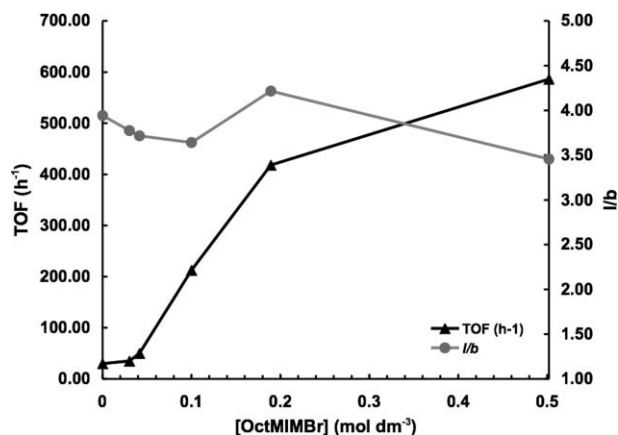


Fig. 3 Effect of the concentration of [OctMim]Br on the average TOF and the *l/b* ratio for the hydroformylation of 1-octene (closed reactor).

to branched ratio (*l/b*) = 2.9 vs. 4.9 in the absence of additive) (Table 1). Importantly, on opening the autoclave the two phases were fully separated and clear, the lower aqueous

Table 1 Aqueous-biphasic hydroformylation of alkenes in the presence of different 1-alkyl-3-methyl-imidazolium salts^a

Entry	Alkene	Additive	P/Rh	Aldehydes (%)	Isomerised Alkenes (%)	<i>l/b</i> ^b	TOF ₀ /h ^{-1c}	[Rh] _{org} (ppm) ^d	Phase separation
1	1-Octene	—	10	2	1.5	4.9	10	n.d. ^f	<10 min ^e
2	1-Octene	[HexMim]Br	50	8	2	8.7	47	0.13	<10 min ^e
3	1-Octene	[OctMim]Br	10	92	6	2.9	1100	126	<10 min ^e
4	1-Octene	[OctMim]Br	50	92	3	3.2 ^g	900	0.49	<10 min ^e
5	1-Octene	[DecMim]Br	50	94	1.4	3.0 ^g	1200	0.31	stable emulsion
6	1-Hexene	—	10	38	4	4.5	300	n.d. ^f	<10 min ^e
7	1-Hexene	[HexMim]Br	10	20	0	7.8	150	0.30	<10 min ^e
8	1-Hexene	[HexMim]Br	50	37	0	13.7	200	0.21	<10 min ^e
9	1-Hexene	[OctMim]Br	10	90	9	2.8 ^h	1550	27	<10 min ^e
10	1-Octene	[OctMim]Cl	50	81	3	3.2	650	n.d.	<10 min ^e
11	1-Octene	[OctMim]TfA	50	83	4	3.1	650	0.13	<10 min ^e
12	1-Decene	—	10	1	30 ⁱ	3.1	n.d. ^j	n.d. ^f	<10 min ^e
13	1-Decene	[OctMim]Br	10	63	18 ⁱ	2.5	340	23	<10 min ^e

^a Reaction conditions: *T* = 100 °C; *P* = 20 bar (CO/H₂ = 1 : 1); stirring rate = 1000 rpm; 3 h; [additive]_{aq} = 0.5 mol dm⁻³; [Rh]_{aq} = 1.25 × 10⁻³ mol dm⁻³; alkene: 2 cm³; H₂O: 8 cm³. ^b Mole of linear aldehyde/mole of all the branched aldehydes. ^c Initial turnover frequency (mole of alkene converted per mole of rhodium per hour); calculated from the tangent at the origin of the gas uptake curve obtained. ^d Concentration of rhodium detected in the organic phase by ICP-MS. ^e The phases were fully separated by the time the autoclave was vented and opened, ca. 10 min after the reaction was stopped. ^f Not determined. ^g 2-Ethylheptanal detected. ^h 2-Ethylpentanal detected. ⁱ Including 12% of isomers present in the starting material. ^j The reaction is too slow for the gas uptake to be measured.

phase being orange and the organic phase being colourless (see Fig. 4).



Fig. 4 Photograph of the separated phases after hydroformylation of 1-octene in the presence of [OctMim]Br (0.5 mol dm^{-3}).

Analysis of the organic phase by ICP-MS showed that, despite the lack of colour, the organic phase contained 126 ppm of rhodium—an unacceptable level of leaching. These reactions were carried out with a P : Rh ratio of 10, whilst commercial processes operate with very much higher ratios (>100). Reasoning that a higher ratio might improve the l/b ratio, but might also enhance the catalyst retention, we carried out a reaction with P/Rh = 50. The reaction rate was not much affected, but the l/b ratio increased to 3.2. Crucially, the [Rh] in the organic phase dropped dramatically to 0.49 ppm. These results are summarised in Fig. 5.

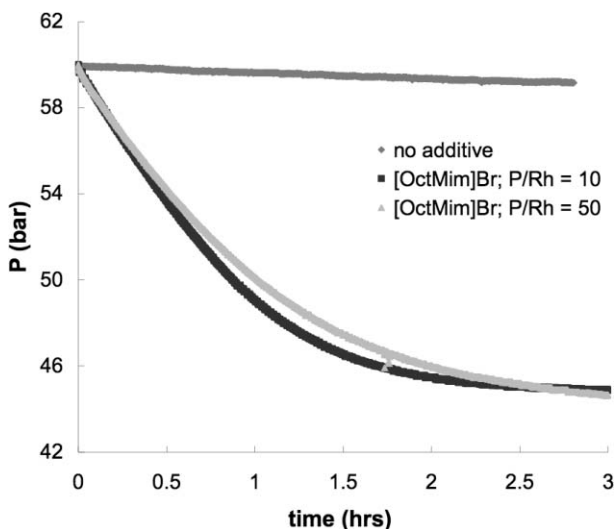


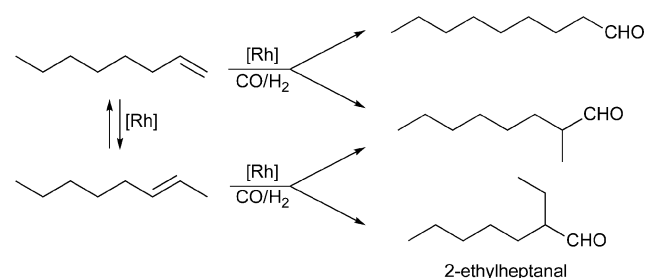
Fig. 5 Effect of the presence of [OctMim]Br and different P/Rh ratio on the gas uptake from a ballast vessel during the aqueous-biphasic hydroformylation of 1-octene (for conditions see Table 1 footnote *a*).

Similar improvements were obtained using 1-hexene and 1-decene (Table 1 and Fig. 2). For the former, the reaction was complete in <1.5 h (compared to 38% conversion after 3 h in the absence of additive); whilst for 1-decene there was no observable gas uptake in the absence of additive, but the reaction to aldehydes had proceeded to 71.4% in 3 h, allowing for the isomerised alkenes in the starting 1-decene, in the presence of [OctMim]Br (0.5 mol dm^{-3}).

In all cases, the observed amount of isomerised alkene was enhanced by the presence of the additive, but not relative to the amount of aldehyde formed. For 1-octene and 1-decene, isomerisation was suppressed relative to hydroformylation. For 1-hexene and for 1-octene with Rh/P = 10, the gas uptake plots from a ballast vessel (Fig. 2 and 5) were linear over substantial parts of the reaction. This is probably because the gas transfer became rate determining. This would also explain why the initial rate of hydroformylation of 1-octene is only slightly different when using Rh/P = 10 or 50. Normally, hydroformylation reactions are inhibited by the presence of excess phosphine (negative order in [P]), but, if the reaction is gas transport limited, this order will not be observed. The gas uptake curve for 1-octene with P/Rh = 50 fits to first order kinetics, so the reaction is probably limited by the intrinsic kinetics, rather than by mass transport, at the higher loading of phosphine.

Variation of the apolar chain on the additive

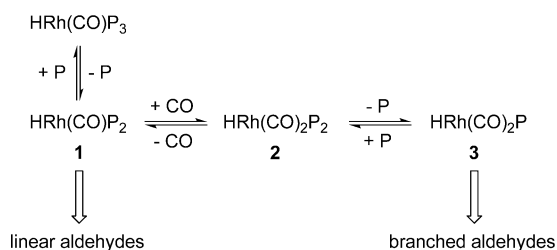
In order to try to understand the origin of the dramatic rate increase for the 1-octene hydroformylation when using [OctMim]Br as additive, as well as to see whether further improvements are possible, we studied the effect of varying the chain length of the alkyl substituent on the methyl imidazolium salt. [DecMim]Br, having a C_{10} side chain, enhances the reaction rate even further but leads to the formation a stable emulsion (Table 1, entry 5). The effect of [HexMim]Br, bearing a slightly shorter chain, C_6 , is intriguing. It shows little influence on the reaction rate. However, it has a dramatic effect on the linear selectivity (Table 1, entries 1–2). The l/b ratio for the C_9 aldehyde reaches 8.7 in the presence of [HexMim]Br albeit with a 50 fold excess of ligand. This marked difference in linear selectivity can be attributed to different parameters. When comparing [HexMim]Br with [OctMim]Br it should be kept in mind that the linear selectivities are observed at very different conversion. At low conversion, the linear alkenes are mainly transformed, yielding linear aldehydes if the catalyst is selective. On the other hand, internal alkenes, which build up in the reaction mixture due to competitive isomerisation (Scheme 2), are hydroformylated to yield branched products when high conversion is reached, and only small amounts of terminal alkenes remain in the reaction mixture. This may explain the low linear selectivity observed in presence of [OctMim]Br and [DecMim]Br (Table 1, entries 4–5). Supporting this, 2-ethylheptanal arising from the hydroformylation of 2-octene (Scheme 2), was detected in reactions carried out to high conversion. However, when the reaction in the presence of [OctMim]Br was run for a shorter time (1.2 h), *i.e.* to lower conversion (58.7% aldehydes), the



Scheme 2 Hydroformylation–isomerisation of 1-octene.

l/b ratio was 3.3. This suggests that the low linear selectivity is due to a poorer selectivity of the catalytic system in the presence of [OctMim]Br, rather than to the hydroformylation of isomerised alkenes. Thus, the difference in linear selectivity observed between [OctMim]Br and [HexMim]Br seems genuine and does not arise from a conversion artefact.

In order to assess the influence of [HexMim]Br on the reaction selectivity at higher conversion, we investigated the hydroformylation of 1-hexene, which shows some activity even in the absence of additive. For this substrate, [HexMim]Br showed an inhibition effect on the reaction rate, but again led to higher linear selectivity compared with the neat biphasic system at similar conversion (Table 1, entries 6–7). Moreover, no isomerised alkenes were detected in the reaction mixture. When using a larger ligand excess, the l/b ratio increased to 13.7. Surprisingly, the reaction rate also increased, whereas excess ligand usually has an inhibiting effect on the reaction rate. When using [OctMim]Br, high reaction rate could be achieved but with poor linear selectivity and significant isomerisation of the substrate. The high linear selectivity observed for the hydroformylation of 1-hexene seems very likely to be due to the presence of [HexMim]Br. One explanation for this could be the increase of the ionic strength of the aqueous phase in the presence of [HexMim]Br. Hanson and coworkers reported that the linear selectivity of the aqueous-biphasic hydroformylation of 1-octene catalyzed by Rh/TPPTS can be improved upon addition of Na_2HPO_4 (0.5 mol dm^{-3}).¹⁷ They showed by variable temperature ³¹P-NMR studies that the dissociation energy of TPPTS from $[\text{HRh}(\text{CO})(\text{TPPTS})_3]$ increases with the ionic strength of the solution. Dissociation of TPPTS is required to form the low phosphine coordinated complex **3** responsible for the formation of branched aldehydes (Scheme 3). Therefore, in aqueous media with high ionic strength the equilibria lie in favour of **1**, leading to a higher proportion of linear products. In our system, [HexMim]Br, presumably dissociated in the water phase, may increase the ionic strength, which would explain its effect on the reaction selectivity, although we note that [HexMim]Br is not expected to be as structure directing towards the water as is Na_2HPO_4 . The low linear selectivity observed with [OctMim]Br and [DecMim]Br may be due to the formation of micelles. Conductivity measurements show that [OctMim]Br has a critical micelle concentration (CMC) of $2.16 \times 10^{-2} \text{ mol dm}^{-3}$ at 25 °C, *i.e.* well below the concentration used in the catalytic experiments. These longer chain additives, which form aggregates under the reaction conditions, do not significantly increase the ionic strength of the water and, hence, have no promoting effect on the linear selectivity. The increased ionic strength might also possibly be responsible



Scheme 3 Equilibria involved in the formation of the different active catalytic species.

for the lower rate obtained when using [HexMim]Br and 1-hexene, since this would reduce the solubility of 1-hexene in the aqueous phase. However, the slight increase in rate at high phosphine loadings would not be accounted for by this explanation.

Variation of the “ionic head”

Having established that, in our system, the optimum balance between high reaction rate and good phase separation is obtained with an additive bearing a C_8 alkyl chain, we investigated the effect of structural variation of the additive “ionic head” while keeping the length of the “tail” to 8 carbon atoms. We investigated the use of water soluble *N*-octylpyridinium bromide, [OctPyr]Br, and *N*-octyl-*N,N,N*-triethylammonium bromide, [OctNEt₃]Br, as additives for the aqueous-biphasic hydroformylation of 1-octene with a 50 fold excess of TPPTS over rhodium (Fig. 6). From the gas uptake curves obtained, it appears that changing the structure of the “ionic” head of the additive dramatically changes its influence on the reaction rate. Surprisingly, [OctPyr]Br showed very little effect on the reaction rate. Moreover, opposite to what was observed with [HexMim]Br, it also had almost no influence on the regioselectivity, the l/b values observed being typically 4.1. On the other hand, the addition of [OctNEt₃]Br to the system allowed 1-octene to be transformed with a TOF₀ of 350 h⁻¹ and a l/b value of *ca.* 3.0. None of those additives showed detrimental effects on the phase separation. The phases were fully separated by the time the autoclave was opened, *ca.* 10 min after the reaction was stopped. The smaller effect on the reaction rate observed for [OctNEt₃]Br compared with [OctMim]Br may arise from steric interactions. We propose (see below) that the accelerating effect observed with [OctMim]Br arises from the formation of an emulsion. Li has attributed the increased rate of hydroformylation reactions in the presence of cationic surfactants to the high concentration of Rh/TPPTS at the positively charged surface of the micelle.¹⁴ This brings the catalyst and the substrate, solubilised in the core of the micelles, in close proximity and, hence, accelerates the reaction through a local concentrating effect. When using [OctNEt₃]Br, the ethyl groups may lead to a more sterically crowded micelle surface than the

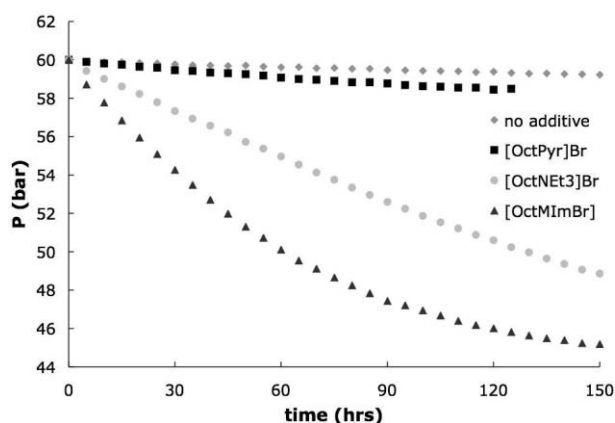


Fig. 6 Effect of the variation of the additive ionic “head” on the gas uptake from a ballast vessel during the aqueous-biphasic hydroformylation of 1-octene. (for conditions see Table 1 footnote *a*).

planar imidazolium cation and, thus, hinder the contact between the substrate and the catalyst.

Variation of the anion

Having investigated some of the possible structural variations of the cationic part of the additive, we tested the effect of changing the nature of the anion. It is well established that the nature of the anion has a dramatic impact on the water solubility of 1-alkyl-3-methylimidazolium salts. We synthesized 1-octyl-3-methylimidazolium salts with bromide, chloride, trifluoroacetate and triflate anions, since they are likely to yield water soluble salts. Unfortunately, the triflate salt, [OctMim]TfO, proved to be insoluble in water and therefore unsuitable for our purpose. All the other salts were fully miscible with water at the investigated concentrations. [OctMim]Cl and [OctMim]TfA both led to higher reaction rates compared to the reactions carried out without additive. However, they were less efficient than their bromide analogues in speeding up the reaction (Table 1, entries 4, 10 and 11). The reaction selectivities were similar to those observed in the presence of [OctMim]Br. The rhodium leaching was found to be very low when using [OctMim]TfA. However, the crude reaction solution obtained in the presence of this additive had a strong “vinegary” smell, presumably arising from the hydrolysis of the CF_3CO_2 anion.

Origin of the promoting effect

Based on the comparison of the results regarding rate improvement, phase separation and rhodium leaching obtained for the hydroformylation of 1-octene in the presence of [HexMim]Br, [OctMim]Br and [DecMim]Br, we proposed that the rate improvement most probably arises because the additive is acting as a surfactant.¹⁶ To test this hypothesis further, we visualised the mixing behaviour of aqueous-octene biphasic systems with and without added [OctMim]Br at room temperature and atmospheric pressure, using a yellow dye to colour the organic phase (Fig. 7). From the photographs and the videos available in the ESI[†] it can be seen that, while the system is poorly mixed without additive, a much more homogeneous system is obtained in the presence of [OctMim]Br after only 6 s of stirring. When the stirring is stopped, the phases instantly separate when no additive is present. In the presence of [OctMim]Br, the two phases take longer to separate, but after 20 s a biphasic system is obtained with a clear interface. The persisting yellow coloration

of the aqueous phase indicates that some of the 1-octene dyed phase remains trapped in the water.

These results, together with those obtained using different alkyl chains on the imidazolium salt, support our proposal that [OctMim]Br acts as a weak surfactant. It promotes the formation of an emulsion whilst being stirred but the emulsion is too unstable and breaks quickly after the stirring is stopped. Consistent with this hypothesis, the effect of the additive is only noticeable above the CMC (Fig. 3).

Conclusions

We have studied the use of several structurally related additives in the aqueous-biphasic hydroformylation of higher alkenes. By careful choice of the cationic head group and its alkyl side chain, high reaction rates can be obtained without impairing the phase separation or the metal retention. These additives could greatly improve the scope of the aqueous-biphasic methodology. The structural features of the additive play an important role. The length of the side chain appears to be the most critical feature. The nature of the cationic head group also has an important influence on the reaction rate, but for reasons that remain rather unclear at the moment. Regarding the anion, its effect is less marked, although care should be taken with regard to its stability under the reaction conditions. The most promising additive is based on the 1-octyl-3-methylimidazolium cation. We propose that it affects the reaction by forming emulsions with poor stability that improve the contact between the catalyst and the substrate, but break after settling for a short time. These unstable emulsions seem to be very promising media for aqueous-biphasic systems, since switching between a pseudo monophasic system (good for high reaction rates) and a biphasic system (good for catalyst product separation) is just a matter of switching the stirrer on and off.

Experimental

General

All experiments were carried out under dry argon on a vacuum line using standard Schlenk techniques.

Gases, argon and syngas, were purchased from BOC gases. Water was distilled, degassed by vacuum, and stored under argon. Triphenylphosphine trisulfonate sodium salt, TPPTS,

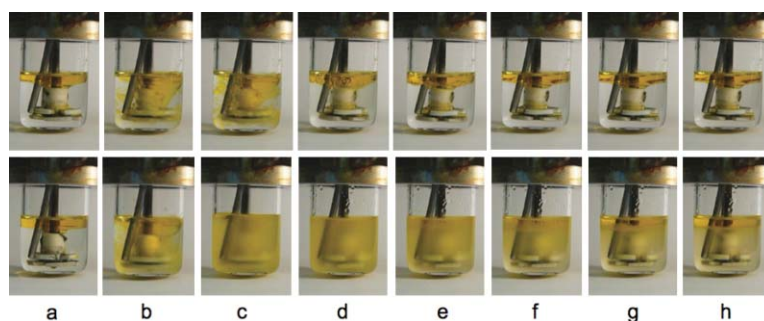


Fig. 7 Photographs of an octene–water biphasic system (octene: 2 cm^3 , dyed; water: 8 cm^3) without additive (top line) and with [OctMim]Br (0.5 mol dm^{-3} , bottom line). (a) At $t = 0\text{ s}$; (b) after 2 s stirring; (c) after 6 s stirring; (d) after 12 s stirring (stirring is stopped); (e) after 2 s settling; (f) after 6 s settling; (g) after 12 s settling and (h) after 20 s settling (stirring rate = 1000 rpm). Videos are available in the ESI.[†]

(Aldrich, 96% or prepared according to ref. 18), [Rh(acac)(CO)₂] (Strem chemical, 99%), deuterium oxide (Aldrich, 99.9 atom% D) and silver trifluoroacetate (Aldrich, 98%) were used as received. Alkenes, 1-hexene (Aldrich, 99%), 1-octene (Aldrich, 98%) and 1-decene (Aldrich, 95%) were purified from peroxide by extraction with aqueous (NH₄)₂Fe(SO₄)₂·6H₂O followed by filtration through basic alumina and stored in the dark under argon.

Ethyl acetate (Fischer, technical grade) was dried over magnesium sulfate and distilled over P₂O₅. Acetonitrile (Fischer, technical grade) was distilled over CaH₂. *N*-methylimidazole (Acros Organics, 99%) was distilled over sodium. Pyridine (Aldrich, 99%) was distilled over KOH. Triethylamine (Aldrich 98%) was refluxed overnight with KOH and then distilled. 1-Bromohexane (Aldrich, 98%) was dried over CaH₂ and distilled over P₂O₅. 1-Bromooctane (Aldrich, 99%) was distilled over K₂CO₃. 1-Chlorooctane (Aldrich, 99%) was distilled over CaH₂ under vacuum. 1-Bromodecane (Aldrich, 98%) was dried over CaH₂ and distilled over P₂O₅ under vacuum.

Gas chromatography analyses were carried out using a Hewlett-Packard 5890 series gas chromatograph equipped with a flame ionisation detector (FID) fitted with a Supelco MDN-35 (35% phenyl-/65% methyl-polysiloxane) capillary column for quantitative analysis. The temperature programme used was: 50 °C (4 min), Δ 20 °C min⁻¹ to 130 °C (2 min), Δ 20 °C min⁻¹ to 260 °C (13.5 min). The temperature of the injector and the detector were both 250 °C. The split ratio used was 100 : 1. Helium was used as the carrier gas with a flow of 1 ml min⁻¹.

¹³C, ¹H and ³¹P NMR spectra were recorded on Bruker AM 300/400 NMR spectrometers or a Varian 300 NMR spectrometer. Broadband decoupling was used for ¹³C and ³¹P NMR spectra. ¹H and ¹³C NMR spectra were referenced internally to deuterated solvents; which were referenced relative to TMS, δ = 0 ppm, CDCl₃, δ_H = 7.27 ppm and δ_C = 77.23 ppm, and D₂O δ_H = 4.53 ppm. ³¹P NMR spectra were referenced externally to 85% H₃PO₄. Coupling constants are given in Hz.

Catalyst preparation

Catalyst solutions were prepared as follows: weighed amounts of [Rh(acac)(CO)₂] and TPPTS were dissolved in a known volume of water containing the additive at the desired concentration. CO/H₂ was then gently bubbled through the resulting yellow solution at 60 °C for 1 h. δ_P (300 MHz; D₂O) -4.55 (br s).

To check that the procedure was efficient to form the catalytically active complex *in situ*, the same procedure was followed but with higher concentration to allow detection by ³¹P{¹H} NMR spectroscopy. δ_P (300 MHz; D₂O) -4.55 (br s) and 44.78 (d, ¹J_{P-Rh} 155). Literature values: δ_P (D₂O) 42.8 (d, ¹J_{P-Rh} 156)^{19a} and δ_P (300 MHz; D₂O) -5.7 (s) 44.7 (d, ¹J_{P-Rh} 156).^{19b}

Hydroformylation of alkenes

Typical procedure for the hydroformylation of alkenes at constant pressure: an autoclave fitted with a mechanical stirrer, thermocouple pocket and pressure transducer, and attached to

a ballast vessel *via* a catalyst injector and a mass flow controller, was degassed by pressurizing three times with CO/H₂ and releasing the pressure. Catalyst solution (8 cm³) was transferred into the autoclave and degassed by pressurizing three times with CO/H₂ and releasing the pressure. The autoclave was pressurized with CO/H₂ (1 : 1, 16 bar) and heated to 100 °C (Stirrer speed = 1000 rpm). Meanwhile, the substrate injector was charged with the substrate (2 cm³). Once the reactor had reached 100 °C, the substrate was injected using an overpressure of CO/H₂ and the pressure was brought to 20 bar. CO/H₂ was then fed from the ballast vessel to maintain the pressure in the autoclave at 20 bar, and the pressure in the ballast vessel was monitored electronically. At the end of the reaction the autoclave was quickly cooled and depressurized. The content of the autoclave was transferred to a vial for visual inspection of the phase separation. The organic phase was analysed by GC for organics and by ICP-MS for rhodium. The results presented (Fig. 2, 5, and 6 and Table 1) are the average of at least 3 runs under each set of conditions.

Typical procedure for hydroformylation of 1-octene in a closed reactor: an autoclave, fitted with a mechanical stirrer, thermocouple pocket, pressure transducer, gas inlet and injection port, was degassed by 3 alternate vacuum-N₂ cycles. The stock catalyst solution (8 cm³) and 1-octene (2 cm³) were transferred into the autoclave. The autoclave was purged three times with pressurised CO/H₂. The autoclave was pressurized with CO/H₂ (1 : 1, 20 bar) and heated, with stirring, to 100 °C. After 2 h, the autoclave was quickly cooled depressurised and the content analysed using GC for the organic products. The results presented (Fig. 3) are the average of at least 3 runs under each set of conditions.

Synthesis of the additives

1-Hexyl-3-methylimidazolium bromide, [HexMim]Br. *N*-Methylimidazole (10 cm³, 10.30 g, 0.125 mol), 1-bromohexane (21 cm³, 24.70 g, 0.150 mol) and ethyl acetate (30 cm³) were heated under reflux for 24 h in an atmosphere of argon. The biphasic system obtained was separated and the upper organic phase discharged. The bottom product phase was washed with ethyl acetate (3 × 30 cm³), and dried under vacuum (0.01 mbar) at 50 °C to give 1-octyl-3-methylimidazolium bromide (23.47 g, 75%) as a colourless liquid. δ_H(300 MHz, CDCl₃) 0.21 (3H, t, ³J 6.7, NC₇H₁₄CH₃), 0.55–0.78 (6H, m, CH₂), 1.30 (2H, quintet, ³J 6.9 NCH₂CH₂), 3.52 (3H, s, NCH₃), 3.74 (2H, t, ³J 7.4, NCH₂), 7.14 (1H, t, ⁴J 1.7, NCHCHN), 7.25 (1H, t, ⁴J 1.7, NCHCHN) and 9.59 (1H, s, NCHN).

1-Octyl-3-methylimidazolium bromide, [OctMim]Br. *N*-Methylimidazole (29 cm³, 29.87 g, 0.364 mol), 1-bromooctane (69 cm³, 77.14 g, 0.399 mol) and ethyl acetate (100 cm³) were heated under reflux for 16 h in an atmosphere of argon. The biphasic system obtained was separated and the upper organic phase discharged. The bottom product phase was washed with ethyl acetate (3 × 100 cm³), and dried under vacuum (0.01 mbar) at 50 °C to give 1-octyl-3-methylimidazolium bromide (87.16 g, 87%) as a colourless liquid. δ_H(400 MHz, CDCl₃) 0.65 (3H, t, ³J 6.9, NC₇H₁₄CH₃), 0.99–1.16 (10H, m, CH₂), 1.71 (2H, quintet, ³J 7.2 NCH₂CH₂), 3.93 (3H, s, NCH₃), 4.13 (2H, t, ³J

7.4, NCH₂), 7.37 (1H, t, ⁴J 1.8, NCHCHN), 7.56 (1H, t, ⁴J 1.8, NCHCHN) and 9.97 (1H, s, NCHN)

1-Decyl-3-methylimidazolium bromide, [DecMim]Br. *N*-Methylimidazole (10 cm³, 10.30 g, 0.125 mol), 1-bromodecane (29 cm³, 77.14 g, 0.140 mol) and ethyl acetate (40 cm³) were heated under reflux for 28 h in an atmosphere of argon. The biphasic system obtained was separated and the upper organic phase discharged. The bottom product phase was washed with ethylacetate (3 × 40 cm³), and dried under vacuum (0.01 mbar) at 50 °C to give 1-decyl-3-methylimidazolium bromide (33.74 g, 89%) as a colourless viscous liquid. δ_H(300 MHz, CDCl₃) 0.69 (3H, t, ³J 6.7, NC₇H₁₄CH₃), 0.99–1.22 (14H, m, CH₂), 1.75 (2H, quintet, ³J 7.2 NCH₂CH₂), 3.97 (3H, s, NCH₃), 4.16 (2H, t, ³J 7.4, NCH₂), 7.40 (1H, t, ⁴J 1.8, NCHCHN), 7.59 (1H, t, ⁴J 1.8, NCHCHN) and 10.08 (1H, s, NCHN)

1-Octyl-3-methylimidazolium chloride, [OctMim]Cl. *N*-Methylimidazole (40 cm³, 41.2 g, 0.502 mol), 1-chlorooctane (103 cm³, 89.52 g, 0.602 mol) and ethyl acetate (100 cm³) were heated under reflux for 5 days in an atmosphere of argon. The biphasic system obtained was separated and the upper organic phase discharged. The bottom product phase was washed with ethyl acetate (3 × 50 cm³), and dried under vacuum (0.01 mbar) at 50 °C to give 1-octyl-3-methylimidazolium chloride (63.0 g, 54%) as a pale yellow liquid. δ_H(300 MHz, CDCl₃) 0.69 (3H, t, ³J 6.8, NC₇H₁₄CH₃), 1.12 (10H, m, CH₂), 1.75 (2H, quintet, ³J 7.3 NCH₂CH₂), 3.97 (3H, s, NCH₃), 4.18 (2H, t, ³J 7.7, NCH₂), 7.39 (1H, t, ³J 1.7, NCHCHN), 7.63 (1H, t, ³J 1.7, NCHCHN) and 10.42 (1H, s, NCHN).

1-Octyl-3-methylimidazolium trifluoroacetate, [OctMim]TfA. 1-Octyl-3-methylimidazolium chloride (7.48 g, 0.032 mol) in solution in water (25 cm³) was added to a suspension of silver trifluoroacetate (7.42 g, 0.034 mol) in water (25 cm³) and the mixture was stirred overnight. The silver chloride precipitate was removed by filtration and the aqueous phase was extracted with dichloromethane (4 × 25 cm³). The organic phases were combined and washed with small portions of water (10 cm³) until silver nitrate test on the washings gave no precipitate. The solvent was evaporated, and further drying under vacuum (0.01 mbar) gave 1-octyl-3-methylimidazolium trifluoroacetate (3.2 g, 31%) as a colourless liquid. δ_H(400 MHz, CDCl₃) 0.81 (3H, t, ³J 6.9, NC₇H₁₄CH₃), 1.27 (10H, m, CH₂), 1.88 (2H, quintet, ³J 7.2 NCH₂CH₂), 4.04 (3H, s, NCH₃), 4.24 (2H, t, ³J 7.4, NCH₂), 7.27 (1H, t, ⁴J 1.7, NCHCHN), 7.33 (1H, t, ⁴J 1.7, NCHCHN) and 10.36 (1H, s, NCHN).

***N*-Octylpyridinium bromide, [OctPyr]Br.** Pyridine (10 cm³, 9.78 g, 0.124 mol), 1-bromooctane (24 cm³, 26.83 g, 0.139 mol) and ethyl acetate (30 cm³) were stirred under reflux for 14 h in an atmosphere of argon. The biphasic system obtained was separated and the upper organic phase discharged. The bottom product phase was washed with ethyl acetate (3 × 30 cm³), and dried under vacuum (0.01 mbar) at 50 °C to give *N*-octylpyridinium bromide (26.1 g, 77%) as a colourless liquid. δ_H(300 MHz, CDCl₃) 0.66 (3H, t, ³J 6.8, NC₇H₁₄CH₃), 0.96–1.26 (10H, m, CH₂), 1.89 (2H, quintet, ³J 7.3 NCH₂CH₂), 4.83 (2H, t, ³J 7.5, NCH₂), 8.04 (2H, t, ³J 7.2, CHCHCH), 8.42 (1H,

tt, ³J 7.8, ⁴J 1.2, CHCHCH) and 9.46 (2H, dd, ³J 6.7, ⁴J 1.2, CHNCH).

***N*-Octyl-*N,N,N*-triethylammonium bromide, [OctNEt₃]Br.** Triethylamine (12 cm³, 8.71 g, 0.086 mol), 1-bromooctane (12 cm³, 13.41 g, 0.069 mol) and acetonitrile (25 cm³) were heated under reflux for 18 h in an atmosphere of argon. The mixture obtained was cooled to 0 °C and ethyl acetate was added in portions until precipitation of a white solid. The cold suspension was filtered, the solid collected, washed with ethyl acetate (3 × 30 cm³) and dried under vacuum (0.01 mbar) to give *N*-octyl-*N,N,N*-triethylammonium bromide (15.12 g, 74%) as a white solid. δ_H(300MHz; CDCl₃) 0.87 (3H, t, ³J 6.8, NC₇H₁₄CH₃), 1.21–1.44 (19H, m, CH₂ and NCH₂CH₃), 1.70 (2H, quintet, ³J 7.1, NCH₂CH₂), 3.24–32.27 (2H, m, NCH₂C₇H₁₅) and 3.52 (6H, q, ³J 7.3, NCH₂CH₃); *m/z* (ESI) 214 (M⁺, 100%).

Acknowledgements

We thank Sasol Technology (UK) Ltd for partial funding of a studentship (SLD).

Notes and references

- 1 P. Anastas, and J. Warner, *Green Chemistry: Theory and practice*, Oxford University Press, USA, 1998.
- 2 For different methods of catalyst recycling, see (a) D. J. Cole-Hamilton, *Science*, 2003, **299**, 1702; (b) *Catalyst Separation, Recovery and Recycling: Chemistry and Process Design*, ed. D. J. Cole-Hamilton and R. P. Tooze, Springer, Dordrecht, 2005.
- 3 For review, see *Aqueous-Phase Organometallic Catalysis*, ed. B. Cornils and W. A. Herrmann, Wiley-VCH, Weinheim, 2nd edn, 2004.
- 4 H.-W. Bohnen and B. Cornils, *Adv. Catal.*, 2002, **47**, 1.
- 5 B. Cornils, *Org. Process Res. Dev.*, 1998, **2**, 121.
- 6 (a) A. Buhling, P. C. J. Kamer and P. W. N. M. van Leeuwen, *J. Mol. Catal. A: Chem.*, 1995, **98**, 69; (b) A. Buhling, J. W. Elgersma, P. C. J. Kamer, and P. W. N. M. van Leeuwen, *J. Mol. Catal. A: Chem.*, 1997, **116**, 297; (c) M. Karlsson, M. Johansson and C. Andersson, *J. Chem. Soc., Dalton Trans.*, 1999, 4187.
- 7 (a) Z. Jin, X. Zheng and B. Fell, *J. Mol. Catal. A: Chem.*, 1997, **116**, 55; (b) F. Wen, H. Bönemann, J. Jiang, D. Lu, Y. Wang and Z. Jin, *Appl. Organomet. Chem.*, 2005, **19**, 81; (c) H. Azoui, K. Baczkko, S. Cassel and C. Larpent, *Green Chem.*, 2008, **10**, 1197.
- 8 (a) A. Andreotta, G. Barberis and G. Gregorio, *Chim. Ind.*, 1978, **60**, 887; (b) S. L. Desset and D. J. Cole-Hamilton, *Angew. Chem., Int. Ed.*, 2009, **48**, 1472.
- 9 M. E. Davis, Transition to heterogeneous techniques (SAPC and variations), in *Aqueous Phase Organometallic Catalysis*, ed. B. Cornils and W. A. Herrmann, Wiley-VCH, Weinheim, 2nd edn, 2004.
- 10 I. T. Horvath, *Catal. Lett.*, 1990, **6**, 43.
- 11 K.-D. Wiese, O. Möller, G. Protzmann and M. Trocha, *Catal. Today*, 2003, **79–80**, 97–103.
- 12 (a) P. Purwanto and H. Delmas, *Catal. Today*, 1995, **24**, 135; (b) H. Ding, B. E. Hanson, T. Bartik and B. Bartik, *Organometallics*, 1994, **13**, 3761.
- 13 (a) E. Monflier, G. Fremy, Y. Castanet and A. Mortreux, *Angew. Chem., Int. Ed. Engl.*, 1995, **34**, 2269; (b) S. Tilloy, F. Bertoux, A. Mortreux and E. Monflier, *Catal. Today*, 1999, **48**, 245; (c) L. Leclercq, F. Hapiot, S. Tilloy, K. Ramkisoening, J. N. H. Reek, P. W. N. M. vanLeeuwen and E. Monflier, *Organometallics*, 2005, **24**, 2070; (d) D. Kirschner, T. Green, F. Hapiot, S. Tilloy, L. Leclercq, H. Bricout and E. Monflier, *Adv. Synth. Catal.*, 2006, **348**, 379; (e) E. Karakhanov, T. Buchneva, A. Maximov and M. Zavertyaeva, *J. Mol. Catal. A: Chem.*, 2002, **184**, 11.
- 14 (a) H. Chen, Y. Li, J. Chen, P. Cheng, Y.-E. He and X. Li, *J. Mol. Catal. A: Chem.*, 1999, **149**, 1; (b) L. Wang, H. Chen, Y.-E. He,

- Y. Li, M. Li and X. Li, *Appl. Catal., A*, 2003, **242**, 85; (c) H. Fu, M. Li, H. Chen and X. Li, *J. Mol. Catal. A: Chem.*, 2006, **259**, 156.
- 15 (a) C. Yang, X. Bi and Z.-S. Mao, *J. Mol. Catal. A: Chem.*, 2002, **187**, 35; (b) H. Bahrman, S. Bogdanovic and P. W. N. M. van Leeuwen, Higher Alkenes. in *Aqueous Phase Organometallic Catalysis*, ed. B. Cornils and W. A. Herrmann, Wiley-VCH, Weinheim, 2nd edn, 2004.
- 16 S. L. Desset, D. J. Cole-Hamilton and D. F. Foster, *Chem. Commun.*, 2007, 1933.
- 17 H. Ding, B. E. Hanson and T. E. Glass, *Inorg. Chim. Acta*, 1995, **229**, 329.
- 18 W. A. Herrmann, and C. W. Kohlpaintner, Synthesis of water-soluble phosphines and their transition metal complexes in *Inorganic Synthesis*, ed. M. Y. Darensbourg, Wiley, New-York, 1998, vol. 32, ch. 1, pp 8-25.
- 19 (a) I. T. Horvath, R. V. Kastrup, A. A. Oswald and E. J. Mozeleski, *Catal. Lett.*, 1989, **2**, 85–90; (b) E. Monflier, H. Bricout, F. Hapiot, S. Tilloy, A. Aghmiz and A. M. Masdeu-Bulto, *Adv. Synth. Catal.*, 2004, **346**, 425–431.

Development and characterization of a thermoresponsive polysulfone membrane using an environmental friendly technology†

Márcio Temtem,^a Daniel Pompeu,^a Telma Barroso,^a João Fernandes,^a Pedro C. Simões,^a Teresa Casimiro,^a Ana M. Botelho do Rego^b and Ana Aguiar-Ricardo^{*a}

Received 2nd December 2008, Accepted 18th February 2009

First published as an Advance Article on the web 11th March 2009

DOI: 10.1039/b821495f

A new and environmentally friendly technology has been used successfully to produce thermoresponsive polysulfone membranes with good performance in terms of valve mechanism in the pores, with a complete on-off control of water permeability. Membranes were prepared using a CO₂-assisted phase inversion method and their pores were coated/impregnated with a thermoresponsive polymer – poly(*N*-isopropylacrylamide) – using a new methodology for the preparation of these type of structures. The coating/impregnation efficiency was assessed by SEM and XPS analysis that confirmed the presence of nitrogen due to the thermoresponsive hydrogel. Contact angle measurements and phosphate buffer solution permeability were determined in order to characterize the structure hydrophobicity variations with temperature. The on-off mechanism was tested using a model protein (BSA) as a proof of concept for the ability to control pore apertures by temperature stimulus. A diffusion model based on Fick's law and Langmuir adsorption was developed.

Introduction

Stimuli-responsive polymeric-based membranes have received a lot of interest over the last decade from various scientific fields because their permeation properties can be controlled or adjusted according to external chemical and physical stimuli, such as pH,¹ temperature,² electric field,³ concentration of chemical species, light,⁴ or ionic strength⁵ of their environments. They have found a broad range of applications, as controlled drug delivery devices,⁶ in bioseparation processes,⁷ chemical separation, water treatment, chemical sensors⁸ and tissue engineering applications.^{9,10}

A special interest has been given to thermoresponsive membranes since, in many cases, environmental temperature fluctuations occur naturally and because temperature stimuli can be easily designed and artificially controlled. Several techniques have been used to prepare temperature sensitive polymeric-based membranes such as the vacuum filtration method,¹¹ the adsorption method,¹² the coating method,¹³ by the introduction of nanosized thermoresponsive particles into the membranes¹⁴ or by simply grafting thermoresponsive polymers onto porous membranes substrates by different grafting techniques.¹⁵ An

advantage of such membranes is that the porous substrate acts as a dimensionally stable matrix for mechanical support, while the conformational changes of the graft thermoresponsive polymer induced by environmental stimuli lead to permeability changes. Temperature^{16–18} or pH¹⁶ polymers have been grafted onto porous substrates. The grafted polymers may be located mainly on the external membrane surface or be homogeneously distributed inside the pores. In some reports of plasma-induced graft polymerisation, active species are generated mainly near the membrane surface.¹⁹

In a recent work, a new strategy was proposed²⁰ for the solvent-free impregnation/coating of polymeric surfaces and porous structures with thermoresponsive polymers. It was proved that supercritical carbon dioxide (scCO₂) can be used as a carrier to homogeneously distribute the monomer, initiator and cross-linker within the micropores of a polymeric substrate and act as reaction medium for the polymerisation reaction using the pores as microreactors. We strongly believe that this technique can be used to prepare membranes with high response performance to environment stimulus for advanced purification/separation applications or systems for switchable release of molecules.

Poly(*N*-isopropylacrylamide) (PNIPAAm) is the most studied temperature-responsive polymer because it has a low-critical solution temperature (LCST) – a phenomenon that is thermodynamically similar to that causing temperature-induced protein folding – that occurs around 32 °C in aqueous solution,^{21,22} close to body temperature. It dissolves in water below the LCST and precipitates from the aqueous solution above the LCST due to the disruption of hydrogen bonding with water and the increasing hydrophobic interactions among isopropyl groups.

The phase behaviour of PNIPAAm in aqueous solutions was studied with several techniques, including turbidity,²³

^aREQUIMTE/CQFB, Departamento de Química, Faculdade de Ciências e Tecnologia, Universidade Nova de Lisboa, 2829-516, Caparica, Portugal. E-mail: aar@dq.fct.unl.pt; Fax: +351 212948385; Tel: +351 21 2949648

^bCentro de Química-Física Molecular (CQFM) and Institute of Nanoscience and Nanotechnology (IN), Departamento de Engenharia Química e Biológica, Instituto Superior Técnico – Universidade Técnica de Lisboa, Lisboa, Portugal

† This paper was published as part of the themed issue of contributions from the Green Solvents – Progress in Science and Application conference held in Friedrichshafen, September 2008.

light scattering²⁴ and IR spectroscopy.²⁵ The vast majority of these studies confirmed that free PNIPAAm chains have a hydrophilic–hydrophobic phase transition (LCST in water at 32 °C) and that this transition is a very sharp transition (about 5 °C). Grafted chains of PNIPAAm have shown promise for creating responsive surfaces. Conformational changes of the polymer are likely to play a role in some of these applications, in addition to changes in local interactions. However, the conformational change of the grafted PNIPAAm brushes varies greatly with molecular weight and grafting density. The maximum conformational change was observed for PNIPAAm brushes with high molecular weight and intermediate grafting density.²⁶ This trend was also predicted with a self-consistent-field calculation by Mendez and coworkers.²⁷ More recent experimental findings show that, under some grafting conditions, end-anchored PNIPAAm does not become insoluble and does not collapse above 32 °C.

In order to address the issue of temperature-responsive behaviour in PNIPAAm coated microporous substrates, we explored the ability of supercritical CO₂-assisted technology to produce “smart” polysulfone membranes. Our focus was to evaluate the temperature response performance of membranes that were coated/impregnated with PNIPAAm chains produced by *in situ* polymerisation in comparison to the PNIPAAm chains grafted to membranes in advanced purification/separation applications. The procedure developed is schematically represented in Fig. 1. In a first step, the matrices, porous membranes of polysulfone (PS), were prepared using a “green” methodology – scCO₂ induced phase inversion method, as described by Temtem *et al.*²⁸ Besides its environmental advantages this methodology introduces additional parameters that can be used to control membrane morphology (pressure, temperature, depressurization rate). Secondly, the PS membranes with well defined pores in the micrometre range are coated/impregnated by *in situ* *N*-isopropylacrylamide (NIPAAm) polymerisation in scCO₂. The monomer is highly soluble in scCO₂ and thus the reaction can be performed without any surfactants. To avoid compromising the integrity of the “smart” surface coating, PNIPAAm synthesis

can be done in the presence of a cross-linking agent, *N,N*-methylenebisacrylamide (MBAM),²⁹ to allow the system to swell in aqueous media and to open and close the pores, without dissolving the thermoresponsive polymer. The use of scCO₂ as the polymerisation medium offers many advantages when compared with conventional polymerisation since there is no need for an intensive drying action before further processing or characterization steps and it is possible to easily separate the solvent from the engineered matrix, leading to highly pure materials.

In addition, permeation of bovine serum albumin (a model protein) through the thermoresponsive porous PS membranes was investigated. Protein diffusion was selected as a case study because of its applications in biotechnology and food industries with unlimited business opportunities.³⁰ This is also a demanding process due to the complexity of proteins themselves and their biological environments.

Experimental

Materials

Polysulfone (PS) ($M_w = 67000 \text{ g mol}^{-1}$) in pellet form, *N*-isopropylacrylamide (NIPAAm, purity $\geq 97\%$), *N,N*-methylenebisacrylamide (MBAM, purity $\geq 98\%$), *N,N*-dimethylpropionamide (purity $\geq 98\%$), *N,N*-dimethylacetamide (purity $\geq 98\%$) and bovine serum albumin (BSA) ($M_w = 66000 \text{ g mol}^{-1}$, purity $\geq 98\%$) were obtained from Sigma–Aldrich and *N,N*-dimethylformamide (purity $\geq 95\%$) from May & Baker. CO₂ was obtained from Air Liquide with purity higher than 99.998%.

Membrane production

Polysulfone membranes were prepared following the procedure described in detail by Temtem *et al.*^{28,31} using an optimized high-pressure cell for membrane preparation with the scCO₂ induced phase inversion method³² and a supporting disk for the casting solution with 1 mm of thickness. The casting solution

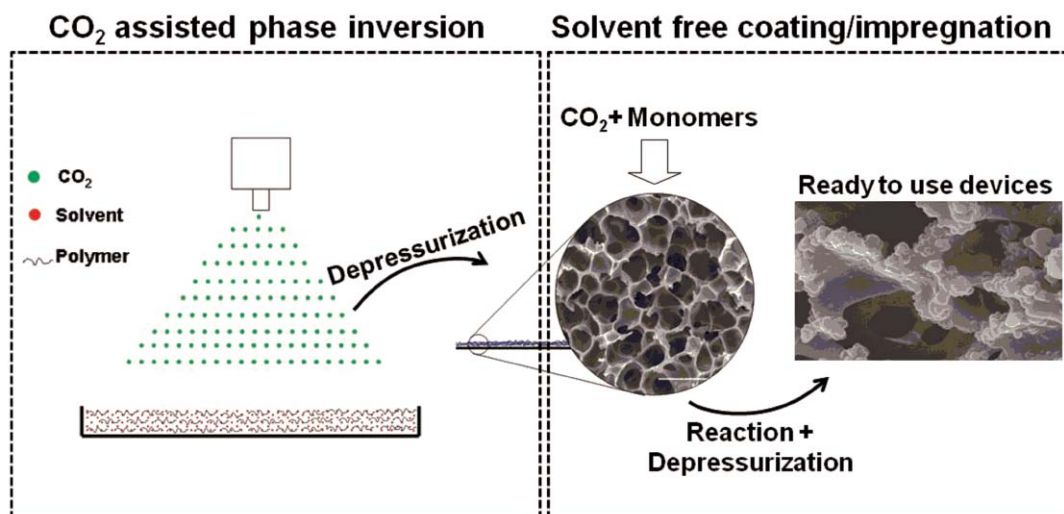


Fig. 1 Schematic description of thermoresponsive membranes preparation methodology.

was prepared by solubilising a certain amount of polymer into a specific solvent (dimethylformamide, dimethylacetamide or dimethyl propionamide) in order to prepare a 15% w/w solution. In a typical procedure CO₂ is added until the desired pressure, with an exact flow, using a Gilson 305 piston pump. After reaching the normal operational pressure, the supercritical solution passes through a back pressure regulator (Jasco 880–81) which separates the CO₂ from the solvent.

All the experiments were performed at 18.6 ± 0.7 MPa with a CO₂ flow of 9.8 g min⁻¹ for 2 hours. At the end the system is depressurized (1 min) and a thin homogeneous membrane is obtained.

Polymerisation of PNIPAAm within porous membranes

In a typical procedure, the *in situ* polymerisation of PNIPAAm within the membrane pores is performed by loading the membranes and reactants, monomer, cross-linking agent (1 wt%) and initiator (2 wt%), into the high-pressure cell. The reactor is then sealed and nitrogen is added to purge the cell and test for leaks. The nitrogen is slowly released and liquid carbon dioxide is loaded into the cell using a high-pressure compressor. The cell is immersed in the water bath and temperature and pressure are allowed to rise to the required experimental conditions. Additional CO₂ may be added to reach the exact desired pressure. The reactions were performed at 65 °C and 20 MPa, as reported in a previous work from our group²⁰ and proceeded for 24 hours under stirring. The reactions were carried out in a high-pressure apparatus already described elsewhere.³³

Membranes characterization

Scanning Electron Microscopy (SEM) was performed in a Hitachi S-2400, with an accelerating voltage set to 15 kV. For cross-section analysis the membrane samples were frozen and fractured in liquid nitrogen. All samples were coated with gold before analysis.

X-ray photoelectron spectroscopy (XPS) analyses were performed on a XSAM800 X-ray spectrometer, operated in the fixed analyser transmission (FAT) mode, with a pass energy of 20 eV, a power of 130 W and using a non-monochromatic radiation from Mg anode ($h\nu = 1253.6$ eV). Spectra were collected with a step of 0.1 eV, and 60 s of acquisition by sweep, using a Sun SPARC Station 4 with Vision software (Kratos). The curve fitting for component peaks was carried out with a non-linear least-squares algorithm using a mixture of Gaussian and Lorentzian peak shapes. Sensitivity factors used were: C 1s – 0.25, O 1s – 0.66, N 1s – 0.44 and S 2p – 0.54.

Membrane porosity and pore size distribution were determined by mercury porosimetry (Micromeritics, autopore IV). Membrane hydrophobicity was evaluated through the measurement of the contact angle of Millipore water droplets in a KSV Goniometer model CAM 100 at two different temperatures 20 and 40 °C.

The permeability to pure water was determined by measuring the water flux through the membranes using a 10 mL filtration unit (Amicon Corp., model 8010) with an effective area of 4.1 cm². All the experiments were carried out varying the applied hydrostatic pressure from 0 to 0.50 MPa.

Protein diffusion

A stirred cell consisting of two identical cylindrical chambers, with 50 cm³, was used (Fig. 2). A thermoresponsive membrane with 4.1 cm² was clamped between the chambers and temperature was controlled by means of a thermostatted water bath. In a typical procedure, one of the chambers is filled with a protein in phosphate buffer solution (PBS) (3 mg mL⁻¹), at a certain temperature. The receptor chamber was filled with PBS at the beginning of the experiment. 1 mL aliquots were withdrawn periodically from the solutions and collected in eppendorfs. Vigorous stirring of each cell compartment was carried out to eliminate the thermo convective effect on permeation. BSA was quantified by UV spectroscopy (Helios Alpha Double-Beam UV/VIS Spectrophotometer) at a wavelength of 280 nm. To relate the absorbency to the concentration of the BSA, calibration measurements were performed.

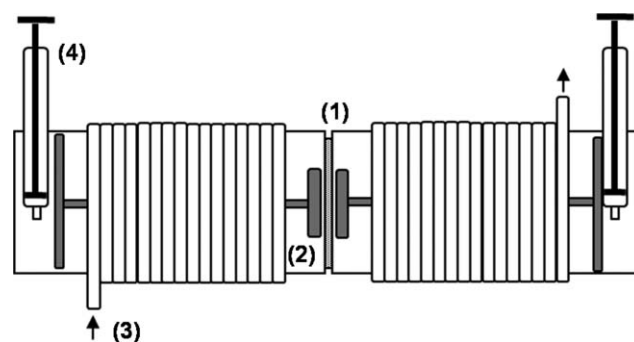


Fig. 2 Schematic representation of the filtration cell. (1) – Thermoresponsive membrane; (2) – magnetic stirrer; (3) – water recirculation; (4) – syringe for sampling.

Modelling experiments

To predict the diffusion of BSA through the pores at two different temperatures (above and below the LCST) a simple model was developed.

The protein flux through the membrane is the result of two different types of transport: diffusion and convection. The first one corresponds to the diffusion flow and can be calculated from the first Fick's law (eqn (1)) while the contribution of convection J_s (solute flow) is assumed to be the protein that is transported due to the osmotic pressure difference

$$J_{diff} = -D \frac{\partial c_{mx}}{\partial x} \quad (1)$$

where J_{diff} is the diffusion flux (kg m⁻² s⁻¹), D is the diffusion coefficient (m² s⁻¹), c_{mx} is the concentration across the membrane (in kg m⁻³) and x is the perpendicular distance to the membrane surface (m).

The flux of water (J_w) and solute (J_s) are given by:

$$J_w = -L_p(\sigma\Delta\pi) \quad (2)$$

$$J_s = -(1 - \sigma) J_w \quad (3)$$

where L_p (m s⁻¹ Pa⁻¹), $\Delta\pi$ (Pa) and σ are the pure water permeability, osmotic pressure, and selectivity, respectively. The

osmotic pressure of BSA was obtained from the following correlation:³⁴

$$\Delta\pi = 204.78 \times \frac{\partial c_{\text{mx}}}{\partial x} + 2 \times \frac{\partial c_{\text{mx}}^2}{\partial x} + 8.44 \times 10^{-3} \times \frac{\partial c_{\text{mx}}^3}{\partial x} \quad (4)$$

In many protein filtration processes the protein adsorption is not negligible. This equilibrium can be represented by the Langmuir equation:

$$q_x = q_m \frac{KC_{\text{mx}}}{1 + KC_{\text{mx}}} \quad (5)$$

where q_m (kg m^{-2}) is the monolayer adsorption capacity and K ($\text{m}^3 \text{kg}^{-1}$) is the Langmuir constant or association constant, which is a measure of the apparent affinity of the protein with the surface.

The total protein permeation can be estimated using the following equation derived from eqn (1) to (5):

$$\frac{\partial c_{\text{mx}}}{\partial t} = D \frac{\partial^2 c_{\text{mx}}}{\partial x^2} + \frac{J_{\text{S}} A_{\text{CP}}}{V_{\text{CP}}} + \frac{\partial q_x}{\partial t} \frac{A_{\text{Pore}}}{V_{\text{Pore}}} \quad (6)$$

with

$$\frac{\partial q_x}{\partial t} = \frac{q_m [K(1 + KC_{\text{mx}}) - K(KC_{\text{mx}})]}{[1 + KC_{\text{mx}}]^2} \quad (7)$$

where A_{CP} (m^2) and V_{CP} (m^3) are the cross section area and volume of a hypothetical cylindrical pore^{35,36} that crosses the membrane and A_{Pore} and V_{Pore} are the volume and internal area of a pore. From mercury intrusion porosimetry (MIP) data a median pore diameter of $0.0119 \mu\text{m}$ was obtained.

The material balance to the amount of protein is defined by:

$$C_{\text{bi}} V_{\text{solution}} = C_{\text{b}} V_{\text{solution}} + C_{\text{p}} V_{\text{solution}} + \sum_0^x C_{\text{mx}} V + \sum_0^x q_x A \quad (8)$$

with C_{bi} (kg m^{-3}), C_{b} , and C_{p} , the bulk initial concentration, the permeate concentration and the bulk concentration, respectively, at the different time points. V_{solution} and V are the volumes of the solution in contact with the membrane and the volume of solution inside the pores with a thickness x and A is the area where the protein is adsorbed, obtained from the MIP ($14.1 \text{ m}^2 \text{ mg}^{-1}$).

The following boundary conditions were used:

$$C_{\text{m}0} = C_{\text{b}} \quad (9)$$

$$C_{\text{m}x} = C_{\text{p}} \quad (10)$$

The system of partial differential equations of the model was solved by uncoupling the spatial and time discretisation; the original partial differential equations of the model were converted into a system of ordinary differential equations (ODEs) using the control volume method, as used elsewhere,³⁷ to which an efficient stiff-integrator was subsequently applied for time integration. The ODE system obtained after spatial discretisation was integrated in time using the commercial process simulation software package gPROMS.³⁸

Results and discussion

In this study, we have applied our group background to the preparation of porous structures and synthesis of temperature responsive polymers to fabricate smart membranes. The thermoresponsive PS membranes were prepared according to Fig. 1: (i) preparation of PS membranes from commercial polysulfone cast in different solutions by scCO_2 induced phase inversion method; (ii) the impregnation/coating of porous PS matrices by *in situ* synthesis of PNIPAAm in supercritical media.

Polysulfone membranes were prepared fixing all the main parameters that influence membrane morphology: depressurization time (1 min); temperature (45°C) and pressure (18.6 MPa). Three casting solutions were prepared, using the following solvents: dimethylformamide (DMF), dimethylacetamide (DMA) and dimethylpropionamide (DMPA) in order to prove our ability to control membrane morphology. In a previous publication²⁸ we have presented the tuning of the water permeability by simply modifying the solvent in the casting solution. The water permeability and the pores increased with the molecular size of the solvents ($\text{DMF} < \text{DMA} < \text{DMPA}$). Due to the intermediate behaviour observed for the membranes prepared with DMA, they were selected in the case study of protein permeation control; nevertheless the results of water permeability will be compared to verify if the pore size diameter is a paramount in the control of the coating/impregnation process.

Microscale manipulation of polysulfone membranes structure was achieved by coating/impregnating membrane pores and surface with PNIPAAm.

Morphological and chemical characterization

Fig. 3 shows the membranes surface and cross-section SEM images before and after the *in situ* PNIPAAm polymerisation.

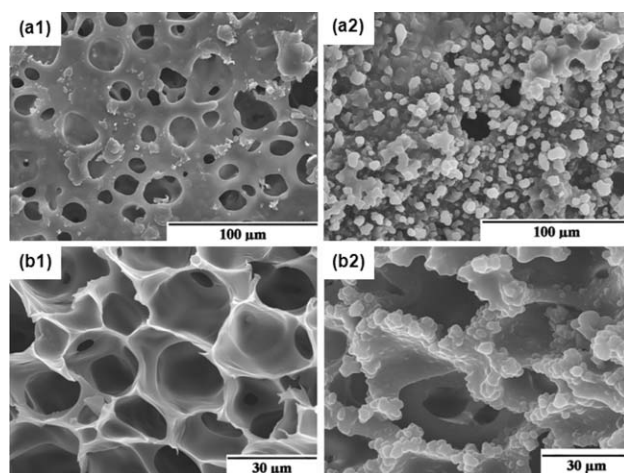


Fig. 3 Scanning electron micrographs of: (a) membrane surface morphology and (b) membrane cross section morphology. (1) unmodified polysulfone membranes and (2) PNIPAAm-coated membrane.

The results showed that the membranes internal and surface microstructures suffered modifications due to the pores and surface filling with PNIPAAm network. Mercury intrusion porosimetry (Fig. 4) confirmed these observations. For the polysulfone membranes an average pore diameter of $23 \mu\text{m}$

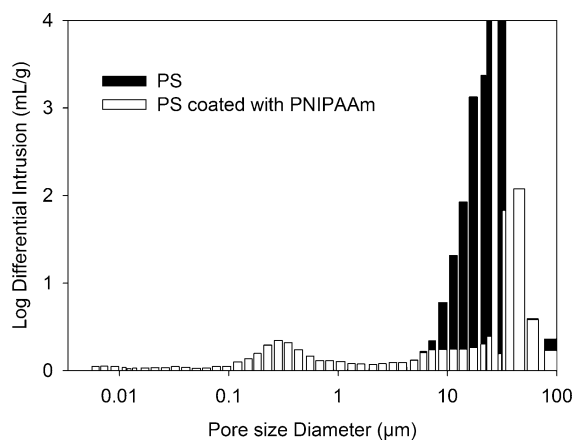


Fig. 4 Pore size distribution of membranes before and after coating with PNIPAAm.

was observed with a porosity of 72%, while for the thermoresponsive membranes these values decreased for 0.36 μm and 57% respectively. The effectiveness of the supercritical assisted polymerisation procedure for coating the pores on membrane surface was also evaluated by XPS analysis. XPS is a technique able to identify and quantify the elemental composition at the surface region with an analysis depth of the order of 3–10 nm. In Fig. 5(a) we could notice the absence of sulfur after PNIPAAm synthesis, despite being present in the polysulfone back bone chain, confirming that the surface was completely coated with the temperature sensitive polymer. The relative amount of nitrogen and carbon existing in the surface of the coated membranes was quantified for different sliced membrane samples. An atomic ratio of $\text{N}/\text{C} = 0.137$ was detected in the surface of the coated membranes, in accordance with PNIPAAm composition. These results are consistent with the nitrogen spectra (N 1s) presented in Fig. 5(b). Moreover, as expected, differences were observed in the carbon (C 1s) spectra in Fig. 5 (a) and (b). For carbon bonded to electron attractive groups, such as the amide group from NIPAAm, a shoulder peak with a higher binding energy would appear beside the position corresponding to C–C and C–H bonds, which was visible in the spectrum of the coated membranes. Simultaneously, the typical $\pi \rightarrow \pi^*$ transition from the aromatic rings of polysulfone disappeared. Another important consideration is the fact that these results revealed that we were able to prepare porous structures without any residues of organic solvents. No contamination from dimethylacetamide was observed.

Membrane hydrophobicity can also be analysed with contact angle measurements. Fig. 6 presents the contact angle variations with temperature for the membranes before and after coating. Unmodified membranes had a constant behaviour at 20 °C and 40 °C with contact angles of 74–70° and 90–80°, respectively. This slight membrane hydrophobic behaviour when prepared by the CO_2 assisted phase inversion method was recently reported.³² These values, somewhat smaller than the ones obtained in other publications,³⁹ are related with the different solvent–non solvent interactions during the phase-inversion process, and as a consequence different chemical groups appear in the surface of the membrane. The addition of PNIPAAm to the membranes increased their hydrophilic character and revealed that the thermoresponsive membranes present different behaviour when

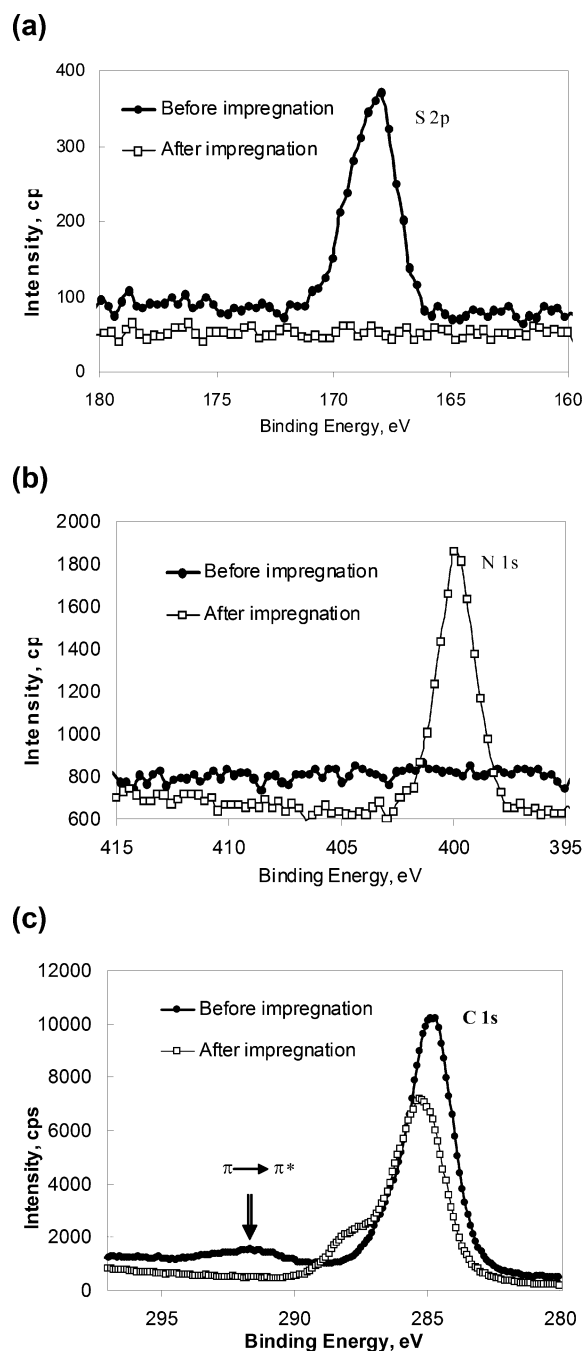


Fig. 5 XPS spectrum of unmodified polysulfone membrane and polysulfone membrane coated with PNIPAAm; (a) sulfur (S 2p) peak, (b) nitrogen (N 1s) peak, (c) carbon (C 1s) peak and $\pi \rightarrow \pi^*$ transition.

the temperature is above or below the LCST. The contact angles presented at 20 °C were slightly smaller than the ones at 40 °C which reflects the interactions with water that occur below the LCST. The decrease in the contact angle is due to the hydrogel nature of PNIPAAm which will allow it to absorb more water, and as a consequence the contact angle decreases.

Temperature dependent water permeability

The incorporation of the thermoresponsive polymer should provide other possibilities to polysulfone membranes including

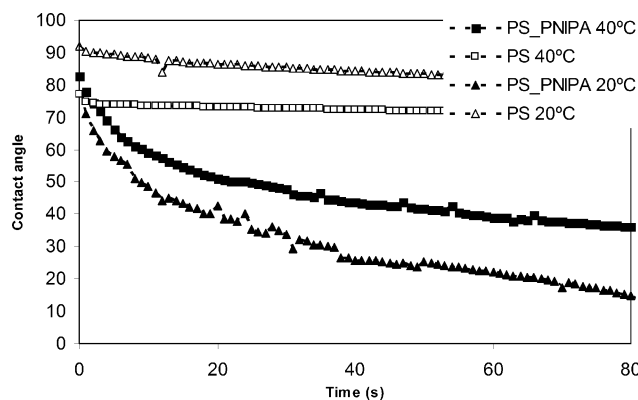


Fig. 6 Temperature dependence for dynamic contact angle changes on unmodified polysulfone (PS) membrane and on PNIPAAm coated PS membrane (PS-PNIPAAm).

improved or switchable release control of bioactive molecules (protein) through membrane pores.

The pure water flux, which is defined as the volumetric flow rate divided by the membrane area and the pressure difference, is an important parameter to characterize. The flux of aqueous solutions through PNIPAAm-coated PS membranes was investigated as a function of temperature (in the range 25–40 °C). The results obtained for membranes prepared from three different casting solutions (DMF, DMA and DMPA) are shown in Fig. 7(a). The temperature-dependent permeability is the direct regulatory effect of the PNIPAAm chains on the membranes and pore surfaces. In all examples, when the temperature is below the LCST only a small amount of water

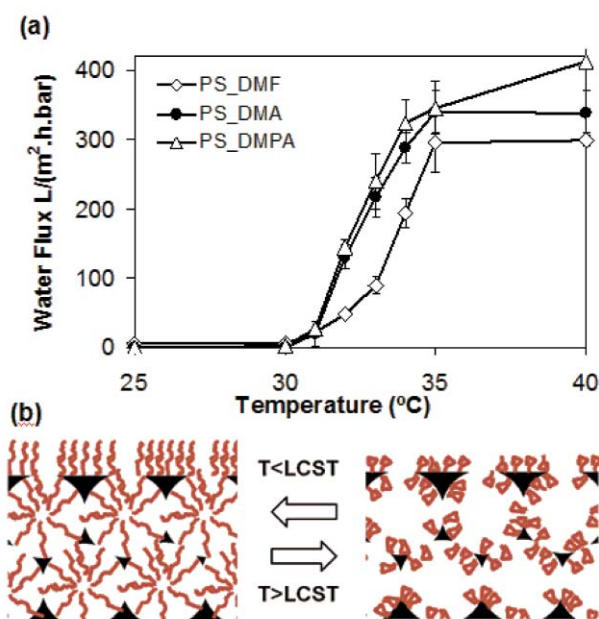


Fig. 7 (a) Phosphate buffer solution flux variation with temperature; (b) a schematic representation of stimuli-responsive porous membrane mechanism to control pore size: at temperatures below the lower critical solution temperature, $T < LCST$, expanded polymer chains close pores and limit water permeability and protein diffusion; at temperatures above the lower critical solution temperature, $T > LCST$, shrunken polymer chains open pores and no longer limit the protein diffusional and convective transport.

is able to cross the membrane (water permeability $\sim 0 \text{ L m}^{-2} \text{ h}^{-1} \text{ bar}^{-1}$), in contrast with the results observed for temperatures above the LCST (water permeability $> 300 \text{ L m}^{-2} \text{ h}^{-1} \text{ bar}^{-1}$). To the best of our knowledge this increase of several orders of magnitude was the biggest on-off ratio for water permeability data upon temperature changes reported in the literature. This means that at the surface densities and molecular weight used in this study, the hydrophilic PNIPAAm chains assume a highly extended conformation below 32 °C, leading to a remarkable reduction of the effective pore size. On the other hand, above the LCST, the chains become less hydrophilic on the membrane and pore surface, assuming a much collapsed conformation resulting in the opening of the pores and hence the observed increase in the permeation rate. The mechanism of on-off valve pore aperture is schematically explained in Fig. 7(b).

These results demonstrate that the supercritical PNIPAAm coating method, although leading to a low molecular weight polymer network, produced a thermoresponsive matrix with a very sharp hydrophilic–hydrophobic phase transition (LCST in water at $32 \pm 5 \text{ }^\circ\text{C}$). Recent experimental findings²⁶ showed that grafted PNIPAAm coatings only show temperature-triggered conformational changes depending on the grafting density and molecular weight. Indeed, it is known that the transition might be suppressed for low molecular weight ($M_w < 75\,000$) end-grafted PNIPAAm. These chains therefore remain swollen above the LCST rather than attract.

It is also interesting to notice the correlation between the mean pore size diameter, the water permeabilities previously reported²⁸ and the tuning in the permeability after coating/impregnation with PNIPAAm. The membranes that presented higher permeability before coating continued to present this behaviour after impregnation.

Protein permeation

Permeation studies were carried out in a two compartment diffusion cell. Two chambers are separated by a circular thermoresponsive membrane having a diameter and thickness of 11 mm and 700 μm , respectively. The bovine serum albumin (BSA) permeation was used for monitoring of the smart PS membrane stimuli-responsive nature. Fig. 8(a) shows the concentration profile of BSA through the coated membrane at two different temperatures: 20 °C and 40 °C, below and above the transition temperature of PNIPAAm, respectively. It is evident that below the LCST the transport is much smaller, in contrast to a high rate above the LCST.

This is also a dynamic mechanism, as we can observe in Fig. 8(b). As the temperature of the solutions surrounding the clamped smart PS membrane was changed, the permeability changed drastically. Inducing temperature pulses from 20–40 °C it is possible to close and open the pores of the membrane for several days. Protein adsorption is also an important factor to take into account. At 20 °C when the PNIPAAm chains are more hydrophilic they will have a higher adsorption capability due to the fact that they are untangled. At 40 °C, due to the more favourable interactions between the polymer chains they will be mostly tangled, decreasing the adsorption capability.⁴⁰

To understand this process a simple mathematical model was developed. The bulk initial concentration, C_{bi} , the monolayer

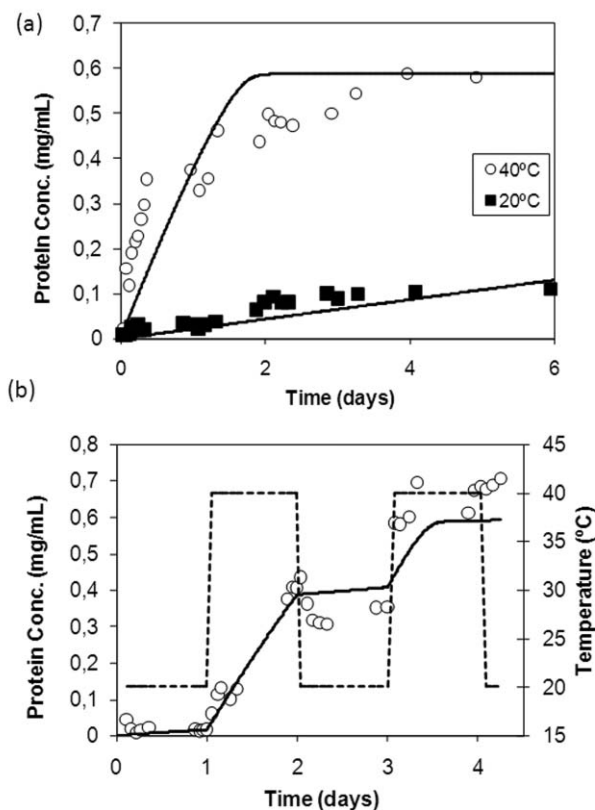


Fig. 8 (a) Diffusion cell experiment with 3 mg mL⁻¹ BSA, pH 7.4 and 0.1M PBS at 20 and 40 °C. (b) Effect of step temperature gradient on protein filtration. The curve fitting was performed according to the mathematical model developed in this work.

adsorption capacity, q_m , and the Langmuir constant or association constant, K , listed in Table 1 constitute the model input parameters along with median pore diameter and total pore area obtained from MIP data.

It was assumed that the protein concentration in the boundary layer next to the membrane was the same as the bulk concentration in both sides of the membrane and that $C_{m,x}$ was in equilibrium with q_x . To adjust the model to the experimental data it was necessary to use higher water permeability values (Table 2) than the ones that were obtained for the pure water system (Fig. 7a). This is related to the introduction of a third compound (BSA) that interferes in the hydrophilic–hydrophobic equilibrium established between water and PNIPAAm. It would be interesting to extend this strategy towards the study of using the smart membranes with surface properties that could

Table 1 Bulk initial concentration, C_{bi} , monolayer adsorption capacity, q_m , and Langmuir constant or association constant, K , used in the model

	$C_{bi}/\text{mg mL}^{-1}$	$q_m/\text{ng m}^{-2}$	$K/\text{mL mg}^{-1}$	$X/\mu\text{m}$
20 °C	3	220	1.36	700 ^b
40 °C	3	150 ^a	27.57	700 ^b
Ref.	—	40	40	—

^a In ref. 40 this value is 188 ± 22 . ^b Measured from the SEM images.

Table 2 Estimated values for protein diffusion coefficient, D , pure water permeability, L_p , and selectivity, σ , in this work

	$D/\text{m}^2 \text{s}^{-1}$	$L_p/\text{m s}^{-1} \text{Pa}^{-1}$	σ
20 °C	1×10^{-11}	7.3×10^{-12}	0.9927
40 °C	7.7×10^{-10}	7.3×10^{-10}	

change with temperature in the separation of different high value bioactive molecules.

Table 2 summarizes the parameters that were optimized in order to adjust the mathematical model to experimental protein diffusion.

The transport mechanism for these membranes is a consequence of two different types of transport: protein diffusion – which is the predominant mechanism when the pores are close below the LCST – and bulk transport of the protein by the solvent, predominant when the pores are open above the LCST. To test the stability of the PNIPAAm-coated membranes, the water and protein permeability measurements were repeated after 2 months and the on-off ratios were reproduced.

Conclusions

This work represents a new “green” alternative for the production of high-tech porous structures, namely thermoresponsive membranes, without any solvent residues. Besides these advantages, the membranes prepared in this work exhibited a good performance in terms of valve mechanism in the pores with a complete on-off control of water permeability. The transport of a model protein was used as a proof of concept and a mathematical model was developed, based on the Fick’s law and in Langmuir adsorption. Protein diffusion at temperatures below and above LCST showed sharp variation, but the on-off control is different from pure water fluxes. This behaviour is due to the PNIPAAm chain conformational changes caused by protein presence in the media introducing different water–protein–PNIPAAm interactions.

The approach used in this work is not merely limited to temperature responsive hydrogels. This concept can also be used to develop smart membranes whose pores can open and close by electronically induced external triggers such as pH, light or electrical field.

Acknowledgements

We thank the financial support from Fundação para a Ciência e Tecnologia (FCT), through contracts PTDC/CTM/70513/2006, SFRH/BD/16908/2004 for M.T., FEDER, FSE, Fundação Calouste Gulbenkian, FLAD and MIT-Portugal Program, Bioengineering Systems Focus Area. We are grateful to J. P. Crespo, A. C. Roque and J. Sotomayor for the helpful discussions.

References

- 1 D. Lee, A. J. Nolte, A. L. Kunz, M. F. Rubner and R. E. Cohen, *J. Am. Chem. Soc.*, 2006, **128**, 8521.
- 2 Y. S. Park, Y. Ito and Y. Imanishi, *Langmuir*, 1998, **14**, 910.
- 3 G. Brisson, M. Britten and Y. Pouliot, *J. Membr. Sci.*, 2007, **297**, 206.
- 4 Y. S. Park, Y. Ito and Y. Imanishi, *Macromolecules*, 1998, **31**, 2606.

- 5 Y. Ito, M. Inaba, D.-J. Chung and Y. Imanishi, *Macromolecules*, 1992, **25**, 7313.
- 6 C. C. Ng, Y.-L. Cheng and B. A. Saville, *J. Sex. Reprod. Med.*, 2001, **1**, 21.
- 7 P. M. Brad, W. Woonton, L. E. Bennett, G. W. Smithers, K. DeSilva and M. T. W. Hearn, *Innov. Food Sci. Emerg. Technol.*, 2008, **9**, 232.
- 8 A. Baldi, Y. Gu, P. S. Lofness, R. A. Seigel and B. Ziaie, *J. Microelectromech. Syst.*, 2003, **12**, 613.
- 9 N. Yamada, T. Okano, H. Sakai, F. Karikusa, Y. Sawasaki and Y. Sakurai, *Makromol. Chem. Rapid Commun.*, 1990, **11**, 571.
- 10 T. Okano, N. Yamada, H. Sakai and Y. Sakurai, *J. Biomed. Mater. Res.*, 1993, **27**, 1243.
- 11 S. Y. Lin, C. J. Ho and M. J. Li, *J. Control. Release*, 2001, **73**, 293.
- 12 S. Y. Lin, H. L. Lin and M. J. Li, *J. Membr. Sci.*, 2003, **225**, 135.
- 13 J. P. Chen, Y. M. Sun and D. H. Chu, *Biotechnol. Prog.*, 1998, **14**, 473.
- 14 K. Zhang and X. Y. Wu, *Biomaterials*, 2004, **25**, 5281.
- 15 L.-Y. Chu, Y. Li, J.-H. Zhu and W.-M. Chen, *Angew. Chem., Int. Ed.*, 2005, **44**, 2124.
- 16 J. Xue, L. Chen, H. L. Wang, Z. B. Zhang, X. L. Zhu, E. T. Kang and K. G. Neoh, *Langmuir*, 2008, **24**, 14151.
- 17 S. J. Lue, J.-J. Hsu, C.-H. Chen and B.-C. Chen, *J. Membr. Sci.*, 2007, **301**, 142.
- 18 A. Kikuchi and T. Okano, *Prog. Polym. Sci.*, 2002, **27**, 1165.
- 19 M. Yang, L.-Y. Chu, Hai-Dong Wang, Rui Xie, Hang Song, and Catherine Hui Niu.
- 20 M. Temtem, T. Casimiro, J. F. Mano and A. Aguiar-Ricardo, *Green Chem.*, 2007, **9**, 75.
- 21 H. G. Schild, *Prog. Polym. Sci.*, 1992, **17**, 163.
- 22 V. V. A. Fernandez, N. Tepale, J. C. Sanchez-Diaz, E. Mendizabal, J. E. Puig and J. F. A. Soltero, *Colloid Polym. Sci.*, 2006, **284**, 387.
- 23 S. Fujishige, K. Kubota and I. Ando, *J. Phys. Chem.*, 1989, **93**, 3311; P. Stayton, T. Shimoboji, C. Long, A. Chilkoti, G. H. Chen, J. M. Harris and A. S. Hoffman, *Nature*, 1995, **378**, 472.
- 24 X. Wang, X. Qiu and C. Wu, *Macromolecules*, 1998, **31**, 2972.
- 25 Y. Katsumoto, T. Tanaka, H. Sato and Y. Ozaki, *J. Phys. Chem.*, 2002, **106**, 3429.
- 26 H. Yim, M. S. Kent, S. Mendez, G. P. Lopez, S. Satija and Y. Seo, *Macromolecules*, 2006, **39**, 3420.
- 27 S. Mendez, J. G. Curro, J. D. McCoy and G. P. Lopez, *Macromolecules*, 2005, **38**, 174.
- 28 M. Temtem, T. Casimiro and A. Aguiar-Ricardo, *J. Membr. Sci.*, 2006, **283**, 244.
- 29 R. Pelton and P. Chibante, *Colloids Surf.*, 1986, **20**, 247.
- 30 A. Shah, *Separation systems for commercial biotechnology*, BCC Research, 2007.
- 31 M. Temtem, L. M. C. Silva, P. Z. Andrade, F. Santos, C. Lobato, J. M. S. Cabral, M. M. Abecasis and A. Aguiar-Ricardo, *J. Supercrit. Fluids*, 2009, DOI: 10.1016/j.supflu.2008.10.020.
- 32 M. Temtem, T. Casimiro, J. F. Mano and A. Aguiar-Ricardo, *J. Supercrit. Fluids*, 2008, **43**, 542.
- 33 T. Casimiro, A. M. Banet-Osuna, A. M. Ramos, M. Nunes da Ponte and A. Aguiar-Ricardo, *Eur. Polym. J.*, 2005, **41**, 1947.
- 34 V. L. Vilker, C. K. Colton and K. A. Smith, *J. Coll. Interf. Sci.*, 1981, **79**, 548.
- 35 S. J. Lue, J.-J. Hsu and T.-C. Wei, *J. Membr. Sci.*, 2008, **321**, 146.
- 36 S. J. Lue, J.-J. Hsu, C.-H. Chen and B.-C. Chen, *J. Membr. Sci.*, 2007, **301**, 142.
- 37 P. C. Simões, J. Fernandes and J. P. B. Mota, *J. Supercrit. Fluids*, 2005, **35**, 167.
- 38 *Process Systems Enterprise, gPROMS v2.0 Introductory User Guide*, Process Systems Enterprise Ltd, London, 2001.
- 39 D. S. Wavhal and E. R. Fisher, *Desalination*, 2005, **172**, 189.
- 40 X. Cheng, H. E. Canavan, D. J. Graham, D. G. Castner and B. D. Ratner, *Biointerphases*, 2006, **1**, 1.

Complete dissolution and partial delignification of wood in the ionic liquid 1-ethyl-3-methylimidazolium acetate†‡

Ning Sun,^a Mustafizur Rahman,^a Ying Qin,^a Mirela L. Maxim,^a Héctor Rodríguez^b and Robin D. Rogers^{*a,b}

Received 17th December 2008, Accepted 23rd February 2009

First published as an Advance Article on the web 13th March 2009

DOI: 10.1039/b822702k

Both softwood (southern yellow pine) and hardwood (red oak) can be completely dissolved in the ionic liquid 1-ethyl-3-methylimidazolium acetate ([C₂mim]OAc) after mild grinding. Complete dissolution was achieved by heating the sample in an oil bath, although wood dissolution can be accelerated by microwave pulses or ultrasound irradiation. It has been shown that [C₂mim]OAc is a better solvent for wood than 1-butyl-3-methylimidazolium chloride ([C₄mim]Cl) and that variables such as type of wood, initial wood load, particle size, *etc.* affect dissolution and dissolution rates; for example, red oak dissolves better and faster than southern yellow pine. Carbohydrate-free lignin and cellulose-rich materials can be obtained by using the proper reconstitution solvents (*e.g.*, acetone/water 1 : 1 v/v) and approximately 26.1% and 34.9% reductions of lignin content in the reconstituted cellulose-rich materials (from pine and oak, respectively) have been achieved in one dissolution/reconstitution cycle. The regenerated cellulose-rich materials and lignin fractions were characterized and compared with the original wood samples and biopolymer standards. For pine, 59% of the holocellulose (*i.e.*, the sum of cellulose and hemicellulose) in the original wood can be recovered in the cellulose-rich reconstituted material; whereas 31% and 38% of the original lignin is recovered, respectively, as carbohydrate-free lignin and as carbohydrate-bonded lignin in the cellulose-rich material.

1. Introduction

With the inevitable depletion of petroleum-based resources, there has been an increasing worldwide interest in finding alternative resources; particularly from renewable resources including biomass. Recently, there has been a tremendous increase of interest in cellulosic biomass for the production of biofuels;^{1–4} however, we wonder about the wisdom of taking Nature's abundant biopolymers: cellulose, hemicellulose, and lignin, chopping one up to create a monomeric fuel (ethanol), and burning the rest. Even though current 'biorefinery' concepts do emphasize other value-added chemicals besides fuel, it is typically the cellulose and hemicellulose which are utilized in producing paper, fibers, membranes, and other commodity materials and chemicals, while lignin is usually burned for energy.⁵ It is gratifying to see recent research now starting to turn to lignin as a source of chemicals, such as binders, dispersants, and emulsifiers,⁶ or lignin used in new processes for the synthesis of biopolymers,^{7,8} biocomposites,^{9–11} and biofuels,¹ as well as a source of carbon fibers.⁶ Nonetheless, there still seems

to be relatively little emphasis on using Nature's biopolymers as polymers rather than a feedstock for producing molecular chemical entities.

One reason for the current biological and chemical approaches being taken to utilize biomass is the difficulty in processing lignocellulosic materials and the energy needed for separation of the components.^{12,13} Lignin (Fig. 1), a three-dimensional amorphous polymer based on methoxylated phenylpropanoid units, is covalently bonded to carbohydrates in the plant, and therefore crosslinks to different polysaccharides, conferring mechanical strength to the cell wall.¹⁴ Dissolution and further separation is difficult because of the complex matrix of carbohydrates inside the plant cell walls.

To date, the over 120 year old Kraft pulping process is the most dominant chemical pulping process practiced on an industrial scale.¹⁵ Kraft pulping liquor contains caustic soda and sodium sulfide. Chemicals used in this process are potential pollutants that need to be recovered, adding costs to the mill investment.⁵ Even after pulping, several purification steps are required, including bleaching and alkali extraction, to develop cellulose products with the desired molecular weight and physical length of the fibers.⁵

New and efficient solvents and process technologies are needed to help unlock the promise of lignocellulosic biomass, and in this regard, perhaps the field of ionic liquids (ILs) might actually live up to its tremendous potential as a new class of designer solvents. It has already been shown that ionic liquids can dissolve a large number of biomacromolecules, such as cellulose,^{16–18} silk fibroin,¹⁹ lignin,²⁰ starch and zein

^aCenter for Green Manufacturing and Department of Chemistry, The University of Alabama, Tuscaloosa, AL 35487, USA

^bQUILL, School of Chemistry and Chemical Engineering, The Queen's University of Belfast, Belfast, UK BT9 5AG

† This paper was published as part of the themed issue of contributions from the Green Solvents – Progress in Science and Application conference held in Friedrichshafen, September 2008.

‡ Electronic supplementary information (ESI) available: Fig. S1–4. See DOI: 10.1039/b822702k

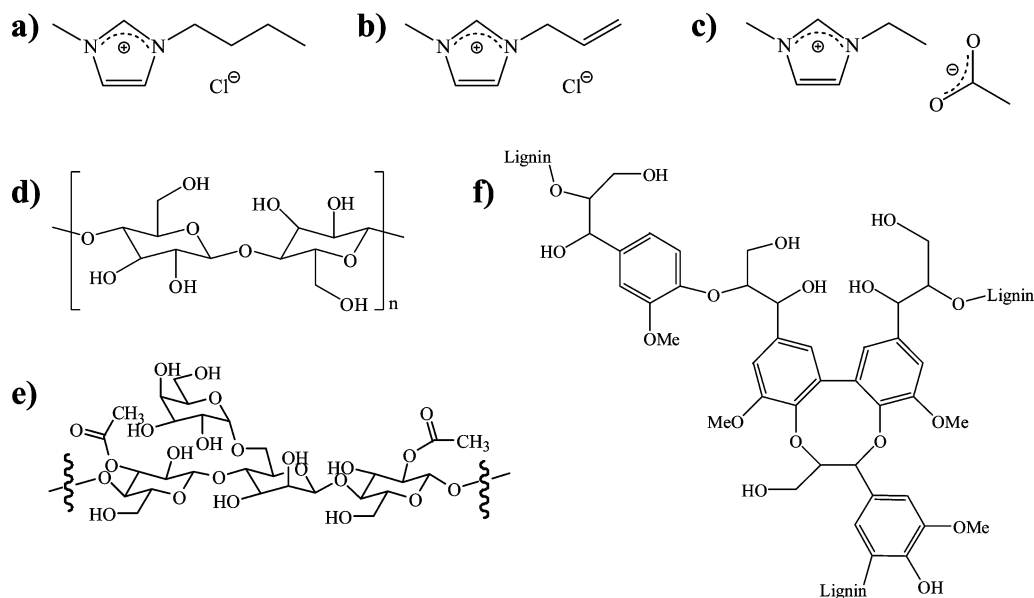


Fig. 1 Structures of the ILs mentioned in this article, as well as of the major constituent biopolymers of wood: (a) 1-butyl-3-methylimidazolium chloride ($[C_4\text{mim}]\text{Cl}$); (b) 1-allyl-3-methylimidazolium chloride ($[\text{Amim}]\text{Cl}$); (c) 1-ethyl-3-methylimidazolium acetate ($[C_2\text{mim}]\text{OAc}$); (d) cellulose; (e) representative structure of hemicellulose (galactoglucomannan, major hemicellulose in softwood); (f) representative structure of lignin.

protein,²¹ chitin/chitosan,^{22,23} wool keratin,²⁴ *etc.*, with high efficiency. Wood dissolution has also been studied in ILs and promising results have been obtained, where it has been shown that both hardwood and softwood can be dissolved, at least partially, in ILs.^{25–27} Thus far, the ILs of choice for most of these studies (Fig. 1) have been 1-butyl-3-methylimidazolium chloride ($[C_4\text{mim}]\text{Cl}$) and 1-allyl-3-methylimidazolium chloride ($[\text{Amim}]\text{Cl}$), but ILs have been recognized as “designer solvents”,²⁸ and it is anticipated that even better solvents will be found.

Dissolution of cellulose, the main component of wood, is based on the disruption of the inter- and intramolecular hydrogen bonding of cellulose and the formation of new hydrogen bonds between the carbohydrate hydroxyl protons and the anions of the IL.^{29,30} Thus, by changing the basicity of the anion and by not introducing hydrogen bond donors in the cation, ILs with different hydrogen bonding basicity can be obtained,³¹ which should exhibit improved solvating power for cellulose. In addition, the 1-alkyl-3-methylimidazolium chloride ILs ($[C_n\text{mim}]\text{Cl}$, where n is the number of carbons in the alkyl chain) typically used to dissolve cellulose are solids at room temperature and the viscosity (after melting) is high.³² Moreover, halogen anions may make these ILs corrosive, toxic, and environmentally unfriendly, although they may still be better than caustic or organic solvents.³³ It has been shown that lower melting points and viscosities can be obtained by substituting the saturated alkyl substituent in the imidazolium cation with an alkenyl substituent (*e.g.*, $[\text{Amim}]\text{Cl}$);¹⁷ but still the problems associated with the presence of the halide anion remain in full.

ILs with carboxylic acid anions or phosphonate anions have been reported to have low melting points, low viscosities, and high hydrogen bonding acceptor abilities; all of which should facilitate the dissolution of biomacromolecules.^{34–36} Wu *et al.* have recently shown higher solvating power of 1-butyl-3-methylimidazolium acetate ($[C_4\text{mim}]\text{OAc}$) for chitin than

$[\text{Amim}]\text{Cl}$ or $[C_4\text{mim}]\text{Cl}$.²³ In particular, BASF, one of the pioneers in industrial usage of ILs, has turned to 1-ethyl-3-methylimidazolium acetate ($[C_2\text{mim}]\text{OAc}$) for dissolution of cellulose, because of its desirable properties such as low toxicity ($\text{LD}_{50} > 2000 \text{ mg kg}^{-1}$), low corrosiveness, low melting point ($< -20 \text{ }^\circ\text{C}$), low viscosity (10 mPa s at $80 \text{ }^\circ\text{C}$), and favorable biodegradability.³⁷

Here, we utilize $[C_2\text{mim}]\text{OAc}$ to demonstrate the complete and direct dissolution of wood after mild grinding and compare the results with the previously studied $[C_4\text{mim}]\text{Cl}$. In addition to achieving complete dissolution of wood, the major biopolymer fractions (lignin and cellulose/hemicellulose) have been partially separated in one cycle simply by choosing proper reconstitution solvents. The characterization of the reconstituted materials and the major parameters which affect the dissolution and dissolution rate are discussed.

2. Experimental

2.1 Materials

Softwood (southern yellow pine) and hardwood (red oak) samples were received from Seaman Timber Co. (Montevallo, AL) as wood shavings (varied sizes, mostly within 0.5–1.0 mm). Microcrystalline cellulose (MCC) with degree of polymerization 270 was purchased from Sigma-Aldrich Inc. (Milwaukee, WI). Indulin AT (lignin from Kraft pulping process) was provided by MeadWestvaco Corporation (Glen Allen, VA) and used herein as a lignin standard. Xylan (from beechwood) was purchased from Sigma-Aldrich Inc. (St. Louis, MO). The ILs $[C_2\text{mim}]\text{OAc}$ and $[C_4\text{mim}]\text{Cl}$ ($\geq 95\%$) were provided by BASF (Ludwigshafen, Germany). Dimethyl sulfoxide (DMSO) (99.9%) was purchased from Sigma-Aldrich (St. Louis, MO). Deuterated DMSO ($\text{DMSO-}d_6$) used for NMR samples was purchased from Cambridge Isotope Laboratories, Inc.

(Andover, MA). Deionized water was obtained from a commercial deionizer by Culligan (Northbrook, IL) with a specific resistivity of 17.25 M Ω cm at 25 °C.

2.2 Wood dissolution and regeneration

Determination of complete dissolution. Wood chips were ground into powder using an electric lab mill (Janke & Kunkel Ika Labortechnik, Wilmington, NC). The chips were ground for 1 min, and powders of different sizes (less than 0.125 mm, 0.125–0.250 mm, 0.250–0.500 mm, and 0.500–1.000 mm) were separated using a series of Brass sieves and then dried overnight in an oven (Precision Econotherm Laboratory Oven) at 90 °C, to avoid influence of the moisture content of the wood source in the results.

In a typical dissolution trial, 0.50 g of wood were added to 10 g of [C₂mim]OAc in a 50 mL beaker. The mixture was then placed into an oil bath (white mineral oil, Fisher Scientific, Fair Lawn, NJ), and heated on a hot plate (Isotemp®, Fisher Scientific) with vigorous magnetic stirring (700 rpm), in the open atmosphere. The selected temperature for dissolution was monitored by a thermometer inside the oil.

To determine the time for achieving complete dissolution, aliquots of the mixture (*ca.* 1 mL each) were taken with a pipette at different time intervals, diluted with 2 mL of DMSO to lower the viscosity without causing precipitation of any dissolved material,²⁵ and placed under a microscope (Reichert Stereo Star Zoom 580) at 25x to detect any undissolved particles. Complete dissolution time is reported as that for which a homogeneous solution, with no undissolved materials, was observed after dilution and centrifugation (Clay Adams® Brand DYNAC centrifuge) at 100 \times g.

Evaluation of variables at fixed cooking times. The effect of the type of IL, wood species, initial wood load, and particle size on the dissolution process was analyzed in experiments with a fixed time of 16 h (see below for the rationale behind this choice). After treatment, *ca.* 10 mL of DMSO were added to the mixture to reduce the viscosity, followed by vigorous vortexing (Thermolyne, type 37600 mixer) and high speed centrifugation (100 \times g) for 10 min. The solution was then separated from the settled residue, which was washed with DMSO (3 \times 10 mL), to strip any dissolved substances adsorbed or trapped within the solid texture. After that, the residue was further washed with deionized water (3 \times 20 mL), dried at 90 °C overnight in the oven, and weighed. The percent of wood dissolved was calculated according to eqn 1:

$$\text{Wood dissolved (\%)} = \frac{m_{\text{ow}} - m_{\text{res}}}{m_{\text{ow}}} \times 100 \quad (1)$$

where m_{ow} represents the mass of the original wood added, and m_{res} is the mass of the residue recovered.

It must be noted that the washing with DMSO described in the paragraph above does not imply further dissolution of wood.²⁵ Although DMSO is a solvent for carbohydrate-free lignin, native lignin in wood has a more complex structure with many linkages between the lignin units and between lignin and carbohydrates, which prevent it from dissolution in DMSO.

Pretreatment with microwaves or ultrasound. The effect of pretreatment with microwaves or ultrasound was also investigated. In each pretreatment experiment, the wood/IL mixtures were subjected to either microwave or ultrasound before being placed into the oil bath for heating. For microwave treatment, the mixtures underwent 30, 60, or 100 pulses of 3 s each, in a domestic microwave (Sharp R-209KK Carousel), with overhead mechanical stirring in between the pulses. After pretreatment, the mixtures were placed in the oil bath with stirring. Ultrasound pretreatment included exposure to irradiation (Fisher Scientific FS30H) at 40 °C for 1 h. These pretreatments were followed by regular oil bath heating until complete dissolution, according to the procedure described above.

Regeneration. For regeneration of the dissolved material, the wood/IL solutions were poured into a 300 mL beaker containing 100 mL of acetone/water (1 : 1 v/v). The beaker was sealed with Parafilm® and the mixture was stirred at room temperature for 1 h. The precipitated cellulose-rich materials were separated from the washing by filtration through a ceramic funnel with nylon filter paper on a Büchner flask under soft vacuum, while the lignin was subsequently precipitated from the filtrate by evaporating the acetone in air, leaving the IL in the remaining aqueous solution. Repeated washing with acetone/water (to ensure that all the carbohydrate-free lignin and IL had been washed out) and subsequent evaporation of the acetone in air (for precipitation of the lignin), were performed. The regenerated lignin was separated from the remaining aqueous solution of IL by vacuum filtration, again using a ceramic Büchner funnel with nylon filter paper. More lignin can be obtained by adjusting the pH of the washing to 2–3, using concentrated H₂SO₄ (96.1%), however, this strategy will pose a problem for the further recycling of the IL.

2.3 Characterization of the wood and regenerated materials

The original wood, regenerated cellulose-rich materials, undissolved residue, Indulin AT and precipitated lignin, obtained as described earlier, were characterized by FT-IR using a PerkinElmer Spectrum 100 FT-IR spectrometer equipped with an attenuated total reflectance (ATR) cell with 4 scans at 2 cm⁻¹ resolution. The IL, MCC, xylan, Indulin AT, original wood, and regenerated cellulose-rich materials were analyzed by NMR using a Bruker Avance 500 NMR spectrometer equipped with a 5 mm BBO probe. IL samples were prepared by mixing the IL with DMSO-*d*₆ in the ratio 85 : 15 (w/w), and the spectra were recorded at room temperature. The wood samples were prepared by adding 15% (w/w) DMSO-*d*₆ to the IL/wood solution,²⁵ whereas cellulose and cellulose-rich materials were prepared by dissolving 5% (w/w) MCC (as cellulose standard) or regenerated cellulose-rich materials in [C₂mim]OAc/DMSO-*d*₆ (85 : 15, w/w) at 90 °C. These spectra were collected at 70 °C due to the high viscosity (in spite of the viscosity modifying effect of DMSO-*d*₆) at room temperature. To get high resolution spectra, a total of 20 000 scans were collected for ¹³C NMR at 125.76 MHz, and the spectra were processed with a 10 Hz line-broadening factor. ¹H NMR spectra were collected with 128 scans at 500.13 MHz. Lignin or xylan samples were prepared by dissolving 5% (w/w) Indulin AT, IL-processed lignin, or xylan directly in DMSO-*d*₆ at 90 °C. Spectra were collected at room

temperature with 5000 scans at 125.76 MHz for ^{13}C NMR, and with 128 scans at 500.13 MHz for ^1H NMR spectra.

The lignin content for original wood and regenerated cellulose-rich materials was determined by TAPPI methods^{38,39} with a scaled down process. Approximately 0.1 g of dried wood or 0.2 g of regenerated material (pulp) were placed into a 20 mL vial, and 1.5 mL (for wood samples) or 4.0 mL (for regenerated materials) of 72% H_2SO_4 aqueous solution were added. The mixture was stirred at room temperature for 2 h and then transferred to a 200 mL round-bottomed flask, diluted with 56 mL (for wood samples) or 150 mL (for regenerated materials) of deionized water, and refluxed for 4 h. The solution was filtered and dried, and acid insoluble lignin was determined gravimetrically. The filtrate was diluted to 100 mL (for wood samples) or 200 mL (for regenerated materials) with deionized water, and acid soluble lignin was calculated from UV absorbance (Cary 3C UV-visible Spectrometer) at 205 nm using an extinction coefficient of $110\text{ L g}^{-1}\text{ cm}^{-1}$.⁴⁰

The crystallinity of the cellulose in wood and regenerated cellulose-rich materials was monitored by powder X-ray diffraction (PXRD), using a Rigaku D/MAX-2BX horizontal X-ray diffractometer equipped with $\text{Cu-K}\alpha$ radiation ($\lambda = 1.5418\text{ \AA}$), at room temperature. The samples were scanned within $5.00\text{--}30.00^\circ 2\theta$ in step mode with a step of 0.01° and a rate of 1° min^{-1} .

Changes in morphology before and after IL treatment were analyzed by scanning electron microscopy (SEM). SEM images were taken at 2000x magnification using a Philips XL30 SEM instrument operated at 5 kV accelerating voltage. Prior to imaging, the samples were sputter-coated with gold to make the fibers conductive, avoiding degradation and build up of charge on the specimen.

3. Results and discussion

3.1 Complete dissolution of hardwood and softwood

The IL $[\text{C}_4\text{mim}]\text{Cl}$ has been reported to partially dissolve wood shavings (with a particle size of *ca.* $5 \times 5\text{ mm}$),²⁵ while Kilpeläinen *et al.* report the complete dissolution of up to 8% wood in both $[\text{C}_4\text{mim}]\text{Cl}$ and $[\text{Amim}]\text{Cl}$ under inert atmosphere, by using wood powder after mechanical pulping.²⁶ Mechanical pulping helps to break some of the lignin-carbohydrate bonds, but consumes considerable amounts of energy and degrades the biopolymers, since it involves high temperatures and pressures as well as long times.⁵⁴¹ We wondered if the greater basicity of $[\text{C}_2\text{mim}]\text{OAc}$, compared with the aforementioned ILs, could dissolve biomass more efficiently, while reducing the mechanical

grinding requirements, thus lowering process energy demand and getting less degraded biopolymers.

Temperature is also an important variable to be considered. In the works reporting wood dissolution in ILs, temperatures from 80 to 130°C have been used.^{25,26} Higher temperature helps dissolution, but at the same time results in more degradation of the cellulose, and indeed, the IL. For the work reported here, we chose a temperature of 110°C as a compromise, between enhanced dissolution and higher energy demand.

Prior to starting the tests, the stability of $[\text{C}_2\text{mim}]\text{OAc}$ under the proposed conditions was studied. ^1H and ^{13}C NMR spectra were recorded for $[\text{C}_2\text{mim}]\text{OAc}$ before and after heating it at 110°C for 48 h, and no significant changes were observed, except for some small extra peaks observed in a magnified view of the 55–110 ppm window of the ^{13}C NMR spectrum, namely at 62.7, 83.6, and 86.2 ppm (see ESI,† Fig. S1–S3). Although these peaks might be related to some incipient decomposition, their intensity is very low and peak integrations of ^1H NMR spectra after the 48 h heating period were unaffected.

As a final test, before conducting our comparative study, we set out to determine if, given enough time, $[\text{C}_2\text{mim}]\text{OAc}$ could completely dissolve our representative softwood (southern yellow pine) and hardwood (red oak). When adding 0.50 g of wood powder (with particle size 0.125–0.250 mm) to 10 g of $[\text{C}_2\text{mim}]\text{OAc}$, complete dissolution of the wood was observed in 46 h for pine and 25 h for oak (see below for additional discussion), although most of the added wood (>90% w/w) was dissolved after only 16 h of heating in both cases. This is indicative of the variability in the rate of dissolution of the biomass, where harder to dissolve fractions may be represented by polymers of higher molecular weights or polymers that are more strongly inter- or intramolecularly bonded or interacting.

It should be also noted that increased degradation of both the IL and cellulose was observed with longer heating time (see ESI,† Fig. S4). We therefore, chose a standard cooking time of 16 h in the tests described below to evaluate the effect of various process variables on dissolution.

3.2 Evaluation of process variables, cooking at 110°C for 16 h

Effect of IL. $[\text{C}_4\text{mim}]\text{Cl}$ and $[\text{C}_2\text{mim}]\text{OAc}$ were tested for their ability to dissolve both hard- and softwood under identical conditions and $[\text{C}_2\text{mim}]\text{OAc}$ was shown to be superior. Dissolution data, expressed as the weight percentage of added wood dissolved, are shown in Table 1. $[\text{C}_4\text{mim}]\text{Cl}$, which has been previously reported as a solvent for wood,^{25,26} dissolved much less than $[\text{C}_2\text{mim}]\text{OAc}$ under the same conditions (Table 1,

Table 1 Percentage of dissolved wood relative to the initial wood load (0.50 g) in 10 g IL after cooking at 110°C for 16 h

Entry	Ionic liquid	Wood	Particle size (mm)	Dissolution (%)
1	$[\text{C}_2\text{mim}]\text{OAc}$	Southern yellow pine	0.500–1.000	92.6
2	$[\text{C}_2\text{mim}]\text{OAc}$	Southern yellow pine	0.250–0.500	93.5
3	$[\text{C}_2\text{mim}]\text{OAc}$	Southern yellow pine	0.125–0.250	98.2
4	$[\text{C}_2\text{mim}]\text{OAc}$	Southern yellow pine	< 0.125	98.5
5	$[\text{C}_4\text{mim}]\text{Cl}$	Southern yellow pine	0.250–0.500	26.0
6	$[\text{C}_4\text{mim}]\text{Cl}$	Southern yellow pine	< 0.125	52.6
7	$[\text{C}_2\text{mim}]\text{OAc}$	Red oak	0.500–1.000	97.8
8	$[\text{C}_2\text{mim}]\text{OAc}$	Red oak	0.250–0.500	98.5
9	$[\text{C}_2\text{mim}]\text{OAc}$	Red oak	0.125–0.250	99.5

entries 2 and 4 vs. entries 5 and 6). One explanation for this is that, as we expected, the increased basicity of the acetate anion makes it more efficient at disrupting the inter- and intramolecular hydrogen bonding in biopolymers than Cl⁻ (whose role in the dissolution of at least cellulose has been reported^{25,34–36}). However, the lower viscosity and melting point of [C₂mim]OAc also facilitate the dissolution and handling of the solution, and thus this IL is better from a process point of view as well.

Kilpeläinen *et al.* have reported dissolution of wood in [C₄mim]Cl of up to 8% (wt% of the solution) in 8 h at 110 °C under inert atmosphere.²⁶ In their work, they used thermomechanical pulp, or ball-milled powder, which probably underwent intense mechanical pulping under high pressure and temperature, resulting in loose wood structure, as well as partial degradation of both cellulose and lignin.⁴¹ It has been reported in the literature that ball milling leads to cleavage of aryl ether linkages (one of the main lignin–carbohydrate linkages) and formation of free phenolic hydroxyl groups.⁴²

Effect of particle size. The data in Table 1 indicate that smaller wood particles are easier to dissolve (entries 1–4, 5–6, and 7–9) in either IL, although the effect is more pronounced for [C₄mim]Cl. This is likely due to a combination of factors including the increased surface area of the smaller particles and the increase in mechanical pulping (breaking down the internal structure) necessary to obtain smaller particles. It is noteworthy, that [C₂mim]OAc dissolves more than 90% of the added wood even for particle sizes as large as 0.5–1.0 mm. This suggests that [C₂mim]OAc would be much more economical to use in a process (all other factors being equal) since the energy needed to reduce the biomass particle size could be minimized.

Effect of wood species. As noted above, red oak took only 25 h to be completely dissolved in [C₂mim]OAc at 110 °C, while southern yellow pine required 46 h. Table 1 also reveals that under our standardized test conditions, red oak shows slightly higher dissolution (entries 7–9) than southern yellow pine (entries 1–3). This might be explained in the compositional differences between hard- and softwoods. Generally, hardwood is of higher density and hardness than softwood,⁴³ however, softwoods actually contain more lignin than hardwoods.⁴⁴ Most of the lignin in wood is bonded to hemicellulose components (mainly through arabinose, xylose, and galactose moieties) like a cementing agent, resulting in a complex and inaccessible structure.⁴³ The differences we observe could also be due to the variations in the lignin–carbohydrate association, the lignin distribution, or the lignin structure itself in hardwoods and softwoods. (Softwood lignin is composed mostly of guaiacyl units, while hardwood lignin contains not only guaiacyl, but also syringyl moieties.⁴⁴)

Effect of initial wood concentration. The effect of initial wood concentration was investigated by loading different amounts of pine sawdust in 10 g of [C₂mim]OAc from 4 parts wood per 100 parts IL to 10 parts per 100 and treating the mixture to the standard cooking time and temperature. The data in Table 2 indicate that as the initial load of wood increases, a lower percentage of the wood added is dissolved. From these results, an optimum wood load would be approximately 5 parts of wood

Table 2 Effect of initial wood load (southern yellow pine sawdust, particle size <0.125 mm) on dissolution in [C₂mim]OAc (110 °C; 16 h)

Entry	Initial wood load/parts per 100 parts of IL	Dissolution (%)
1	4	99.5
2	5	98.5
3	8	46.3
4	10	40.0

Table 3 Effect of pretreatment on the time required to achieve complete dissolution (*t_{cd}*) of 0.50 g of southern yellow pine sawdust (particle size 0.125–0.250 mm) in 10 g of [C₂mim]OAc at 110 °C

Pretreatment method	Pretreatment conditions	<i>t_{cd}</i> (h)
None	None	46
Microwave	30 × 3 s pulses	45
Microwave	60 × 3 s pulses	21
Microwave	100 × 3 s pulses	16
Ultrasound	1 h at 40 °C	23

added to 100 parts of IL, however, such values might vary upon scale up of the final process.

Effect of pretreatment. The effect of microwave or ultrasound pretreatment on the wood/IL mixtures, prior to cooking was studied to determine if the time to complete dissolution could be reduced. As shown in Table 3, accelerated dissolution of wood in [C₂mim]OAc was achieved by applying either pretreatment method. With 60 × 3 s microwave pulses (pulsed in order to prevent overheating and degradation of both the biopolymers and the IL), the complete dissolution time was reduced to less than half that without pretreatment. Ultrasound pretreatment had a similar effect. Both microwave treatment and ultrasound have been reported to enhance the dissolution of cellulose in ILs.^{16,45}

Analysis of the dissolved wood. The major biopolymer components of wood dissolved in the IL have been identified by comparing the ¹³C NMR spectra of standards (Indulin AT for lignin, xylan for hemicellulose, and MCC for cellulose; Fig. 2a–c) with spectra of wood solutions (Fig. 2d–f). In the spectra for dissolved wood the major cellulose peaks at 60.3 ppm (C6), 74.1 ppm (C2), 75.1 ppm (C3), 75.8 ppm (C5), 78.8 ppm (C4), and 102.3 ppm (C1), are clearly visible, as are the characteristic peaks of lignin and hemicellulose at 55.7 ppm and 63.3 ppm, respectively.^{25,46} The spectra with [C₂mim]OAc (Fig. 2d–e) as wood solvent show better resolution and more extracted components compared to the spectra with [C₄mim]Cl (Fig. 2f) as the solvent reflecting the lower viscosity and higher dissolving power of the acetate IL. In addition, the spectrum of dissolved red oak (Fig. 2d) compared to that of southern yellow pine (Fig. 2e) provides further indication of the different concentrations of hemicellulose and lignin in the IL solutions of oak vs. pine.

Spectra c–e in Fig. 2 show the ¹³C NMR spectra of samples containing 5 parts of MCC or wood in 100 parts of [C₂mim]OAc and cooked at 110 °C for 16 h. After this time, some small extra peaks appear at 59.3 ppm, 63.7 ppm, 69.6 ppm, and 70.4 ppm, which belong to cellulose oligomers indicating some

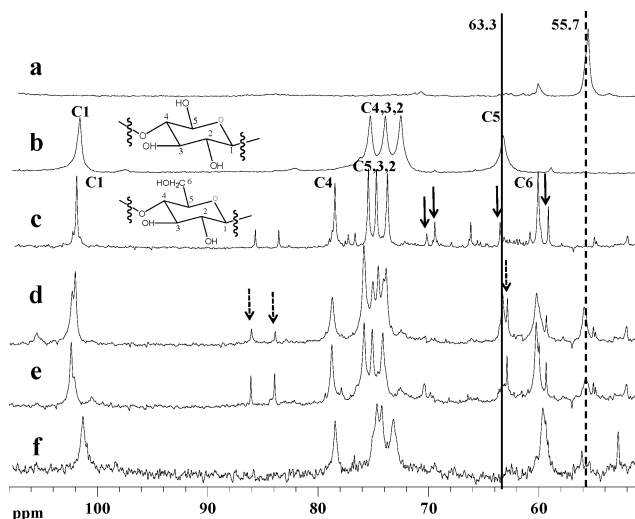


Fig. 2 ^{13}C NMR spectra of biopolymer standards and wood solutions: (a) Indulin AT, directly dissolved in $\text{DMSO-}d_6$; (b) xylan, directly dissolved in $\text{DMSO-}d_6$; (c) MCC, cooked for 16 h at 110°C in $[\text{C}_2\text{mim}]\text{OAc}$, and then diluted with $\text{DMSO-}d_6$; (d) oak, cooked for 16 h at 110°C in $[\text{C}_2\text{mim}]\text{OAc}$, and then diluted with $\text{DMSO-}d_6$; (e) southern yellow pine, cooked for 16 h at 110°C in $[\text{C}_2\text{mim}]\text{OAc}$, and then diluted with $\text{DMSO-}d_6$; and (f) southern yellow pine, cooked for 16 h at 110°C in $[\text{C}_4\text{mim}]\text{Cl}$, and then diluted with $\text{DMSO-}d_6$. Solid and dashed vertical lines mark the distinctive peaks for hemicellulose and lignin, respectively. The structures of xylan and cellulose with labeled carbon atoms have been inserted for facilitation of peak assignment in the corresponding spectra. Peaks belonging to cellulose oligomers resulting from minor degradation of cellulose are indicated with solid arrows in spectrum c. Peaks arising from minor degradation of $[\text{C}_2\text{mim}]\text{OAc}$ are marked with dashed arrows in spectrum d.

minor degradation of cellulose.⁴⁷ Peaks at 62.7 ppm, 83.6 ppm, and 86.2 ppm arise from minor degradation of $[\text{C}_2\text{mim}]\text{OAc}$, and with longer heating time, increase in intensity (see ESI, ‡ Fig. S4). Thus, the improved dissolution capacity provided by operation with longer cooking times is inevitably accompanied by some degradation of the biopolymers dissolved, as well as of the IL. Moderately short dissolution times would be preferred, perhaps even if multiple contacts or cycles were necessary.

3.3 Regeneration of wood solutions with partial separation

A previous study²⁵ showed that carbohydrate-free lignin can be easily dissolved in acetone/water (1:1 v/v), which simultaneously acts as anti-solvent for cellulose and cellulose-rich materials dissolved in an IL. This led us to the development of the process scheme shown in Fig. 3. After cooking, the wood solutions were treated with acetone/water solution precipitating the cellulose-rich solids which were recovered by filtration. The filtrate was collected, the acetone evaporated, and precipitated lignin was obtained leaving the IL in aqueous solution. More lignin could be precipitated by reducing the pH of remaining aqueous solution to 2–3 units (see details in the Experimental section). Each solid fraction was analyzed as discussed below.

The recycling of the IL is indicated with a dashed line in Fig. 3. It was not explicitly investigated or evaluated in the present work, but certainly the viability of the process at a large scale would be conditioned by the existence of an efficient

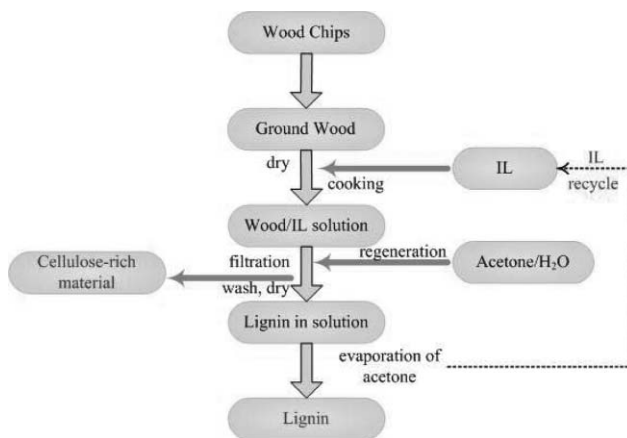


Fig. 3 Flowchart for the process of dissolution and regeneration of wood in IL.

recycling protocol of the IL.²⁵ Concentration of the solution *via* environmentally friendly aqueous biphasic systems could be a strategy to pursue,⁴⁸ compared to the highly energy demanding process of distillation.

Analysis of the reconstituted cellulose-rich material from dissolved wood. After being washed with acetone/water and dried in an oven overnight, the recovered cellulose-rich materials were re-dissolved in $[\text{C}_2\text{mim}]\text{OAc}$ at 110°C for 2 h and then $\text{DMSO-}d_6$ was added into the solution prior to measurement of their ^{13}C NMR spectra (the weight ratio between cellulose-rich materials, $[\text{C}_2\text{mim}]\text{OAc}$, and $\text{DMSO-}d_6$ was 1 : 16 : 3 by weight to get 5% w/w of cellulose-rich materials in solution). MCC was dissolved using the same ratio for comparison. Fig. 4 compares the ^{13}C NMR spectra of reconstituted cellulose-rich materials from two different wood loadings (5 parts or 8 parts of pine per 100 parts of $[\text{C}_2\text{mim}]\text{OAc}$). The reconstituted materials are primarily cellulose, with all major cellulose peaks clearly present. The additional peaks at 55.7 ppm and 63.3 ppm correspond to lignin and hemicelluloses, respectively (compare to Fig. 2).

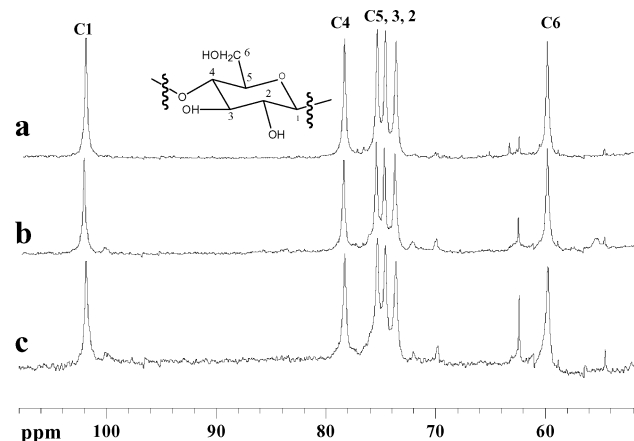


Fig. 4 ^{13}C NMR spectra, in $[\text{C}_2\text{mim}]\text{OAc}/\text{DMSO-}d_6$, of: (a) MCC and regenerated cellulose-rich materials recovered from the dissolution of (b) 0.50 g or (c) 0.80 g southern yellow pine (particle size $<0.125\ \mu\text{m}$) treated with 10 g $[\text{C}_2\text{mim}]\text{OAc}$ for 16 h at 110°C . Both the dissolution of MCC and the re-dissolution of the regenerated materials were carried out at 110°C for 2 h. Spectra b and c correspond to entries 2 and 3, respectively, in Table 2.

Table 4 Lignin content of original wood and regenerated cellulose-rich materials, as determined by the TAPPI 222³⁸ and TAPPI UM 250⁴⁰ methods

Type of wood	Materials	L_K (%)	L_{AS} (%)	L_T (%) ^a
Southern yellow pine	Original wood	31.1	0.7	31.8
	Regenerated material ^b	21.1	2.4	23.5
	Regenerated material ^c	8.2	1.1	9.3
Red oak	Original wood	21.3	2.5	23.8
	Regenerated material ^b	12.1	3.4	15.5

^a Total lignin (L_T) = Klason lignin (L_K) + acid soluble lignin (L_{AS}).

^b Regenerated material from 0.50 g wood in 10 g [C₂mim]OAc with 98.5% dissolution. ^c Regenerated material from 0.80 g wood in 10 g [C₂mim]OAc with 46.3% dissolution.

It is apparent in comparing Fig. 2e to Fig. 4b–c, that after regeneration the cellulose-rich materials contain less lignin than the original wood. In addition, any minor degradation products have been washed out.

It can also be seen in Fig. 4 that, in the regenerated cellulose-rich materials, the lignin peak at 55 ppm is smaller in the sample coming from the dissolution of a higher initial wood load (8 parts of pine per 100 parts of IL, dissolution of 46.3% of added wood) than in that of a lower load (5 parts of wood per 100 parts of IL, dissolution of 98.5% of added wood). This supports the previously discussed difficulty in dissolving native lignin from wood.

A consequence of this is that any carbohydrates not bonded to lignin or with fewer lignin bonds will be preferentially dissolved. With a higher wood load but only 46.3% dissolution, the preferred components (less lignin-bonded carbohydrates) dissolve first. This and a previous finding²⁵ reporting that almost pure cellulose can be separated from wood with incomplete dissolution, suggest that one could consider an alternative process to total dissolution of wood biomass, where more freely soluble cellulose is simply extracted.

Quantification of lignin content. The acid insoluble lignin content of original and regenerated wood fractions was determined using a scaled down TAPPI 222³⁸ procedure. The systematic error caused by scaling down the original procedure was tested by comparing the lignin content results using different amounts of southern yellow pine powder. The results indicated that the error after scaling down the wood content to 0.1 g was negligible. The acid soluble lignin content was determined according to TAPPI Useful Methods, UM 250.⁴⁰

The data for lignin content of both oak and pine before and after dissolution/regeneration are provided in Table 4. All regenerated cellulose-rich materials have a considerably lower lignin content compared to the corresponding original wood samples with reduction in the lignin percentages of 26.1% for pine and 34.9% for oak. The recovery of a more highly delignified material from oak than pine might be expected from the differences in composition and relative dissolution of these two wood species. The lignin content of the regenerated cellulose-rich materials with higher load is much lower than the one with lower load, which is consistent with the analysis of NMR spectra in Fig. 4.

We note that the delignification of wood in the Kraft process is *ca.* 50%.⁴⁹ Here, in a single treatment cycle, the IL has obtained

fairly good delignification at lower temperature and pressure, without the high demand of caustic and other chemicals, and with ready recovery of lignin (*vide infra*). A second cycle, using the regenerated cellulose-rich materials (from softwood) from the first cycle resulted in additional delignification. Upon reconstitution of the cellulose-rich material from the second cycle, an additional 22.3% reduction in lignin content (referred to the content of the original wood) was observed, accounting for an overall reduction of 48.4% with the two cycles combined.

Quantification of recovered lignin and carbohydrates from the original wood. An analysis of the mass and composition of the products has been carried out when using 0.50 g of pine (with a lignin content of 31.8%) in 10 g of [C₂mim]OAc (complete dissolution), in order to develop a proper mass balance. A schematic description of such mass balance is shown in Fig. 5. It was found that 0.26 g (52% of added wood) was recovered as regenerated cellulose-rich material (with a lignin content of 23.5%); whereas 0.03 g (6% of added wood) was obtained in the first cycle as processed lignin by evaporating the acetone, and 0.02 g of additional lignin (4% of added wood) was obtained with adjustment to pH 2–3 (using H₂SO₄), accounting for a total of 0.05 g (10% of added wood) of recovered lignin, totally free of carbohydrates. Overall, 31% of the native lignin present in the original wood was regenerated as carbohydrate-free lignin, and 59% of the native carbohydrates in the original wood were regenerated in the cellulose-enriched material along with 38% of the native lignin still bonded.

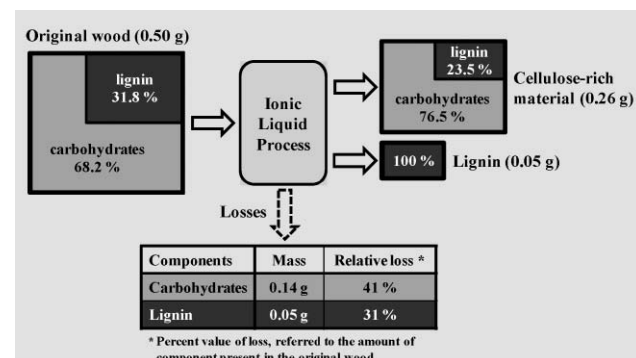


Fig. 5 Mass balance for the process of total dissolution of 0.50 g of southern yellow pine in 10 g of [C₂mim]OAc with subsequent regeneration of materials (including pH adjustment for further recovery of lignin—see main text for details). Losses, which represent 41% of the original carbohydrates and 31% of the original lignin available in the wood, are mainly due to the current process washing steps.

Analysis of the undissolved residues and reconstituted materials from dissolved wood. The FT-IR spectra of the solid cellulose-rich and lignin fractions from dissolution and regeneration of pine and oak, the undissolved residues, and original wood samples were measured and are compared in Fig. 6 and 7. Fig. 6a (pine) and 6b (oak) compare the original ground wood, to the regenerated cellulose-rich material, and to the undissolved residue. The absorbances at 3337–3362 (OH stretch), 2891–2896 (CH stretch), 1729, 1635/1641, 1155, 1028, and 895 cm⁻¹ are associated with native cellulose or hemicellulose.^{50,51}

The band at 1729 cm⁻¹ in the original oak (Fig. 6b, top) comes from a C=O stretching vibration in acetyl groups of

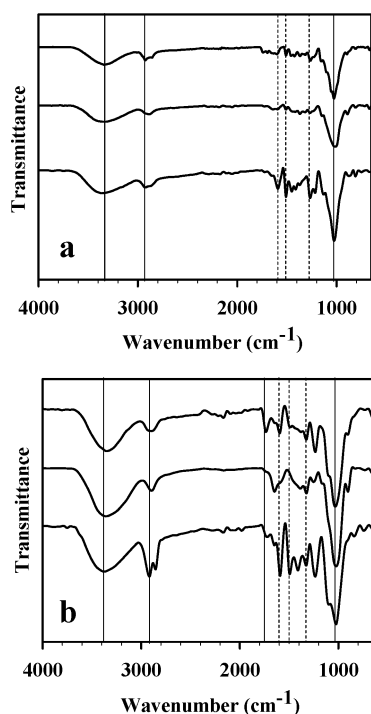


Fig. 6 FT-IR spectra for ground wood (top spectra), regenerated cellulose-rich materials (middle spectra), and undissolved residue (bottom spectra) for 0.250–0.500 mm (a) southern yellow pine and (b) red oak. Vertical solid lines mark characteristic peaks of cellulose/hemicellulose, whereas those of lignin are marked by vertical dashed lines.

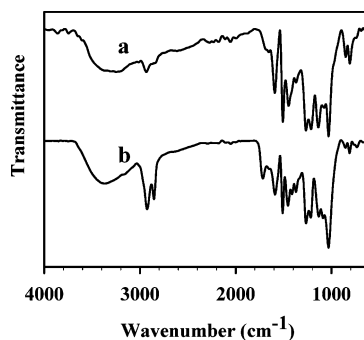


Fig. 7 FT-IR spectra for (a) Indulin AT and (b) lignin recovered from the dissolved wood by addition of acetone/water (1 : 1 v/v) and subsequent evaporation of acetone (according to the process flowchart in Fig. 3).

hemicellulose (it can not be seen for pine because of the presence of different hemicellulose species). After regeneration (Fig. 6b, middle), this band disappears, indicating that some hemicellulose was lost in the washing step. The absorbance bands at 1155 and 895 cm⁻¹, corresponding to C–O–C asymmetric bridge stretching vibration in cellulose/hemicellulose and C–H deformation vibration in cellulose respectively,⁵⁰ were more resolved in both regenerated pine and oak, indicating that the regenerated materials are richer in carbohydrates.

Lignin characteristic peaks at 1590/1509 cm⁻¹ (C=C stretching vibration), 1459 cm⁻¹ (asymmetric bending in CH₃), 1419 cm⁻¹ (C–H deformation), 1320 cm⁻¹ (C–O vibration in the syringyl ring—not present in softwood lignin), and 1261/

1231 cm⁻¹ (guaiacyl/syringyl ring and C–O stretching vibration)^{43,50} were more intense in the spectra of the residues (Fig. 6a/b, bottom), indicating that the residue is enriched in lignin, compared to the regenerated cellulose-rich material and the original wood. In other words, the less lignin-bonded cellulose/hemicellulose in the wood is preferentially dissolved into the IL.

The spectrum of lignin recovered from the dissolution of pine after evaporation of the acetone, is compared to that of Indulin AT in Fig. 7. The close similarity of these two spectra indicates that the recovered material in this step is lignin. Comparison of the ¹³C NMR spectra for the IL-processed lignin and Indulin AT is shown in Fig. 8. The absence of carbohydrate signals and the clear presence of characteristic peaks of lignin, indicate that the lignin isolated in the IL process is free of carbohydrates.

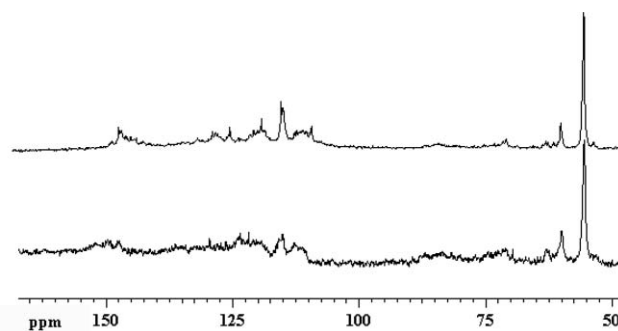


Fig. 8 ¹³C NMR spectra of Indulin AT (top) and IL-processed lignin (bottom) in DMSO-*d*₆.

PXRD and SEM analysis. PXRD spectra were collected for original pine powder and the corresponding regenerated cellulose-rich material and are shown in Fig. 9. In the original wood, cellulose exists in native form, which is cellulose I.⁵² After regeneration as floes, cellulose II of low crystallinity is recovered. The isolation of cellulose II and not cellulose I is further proof of a true dissolution route.

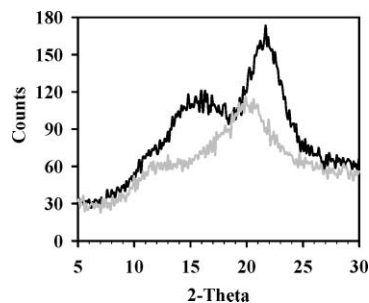


Fig. 9 Diffractograms of southern yellow pine (0.250–0.500 mm particle size; grey) and regenerated cellulose-rich materials from the same particle size (black). The former is consistent with the presence of cellulose I, and the latter with the presence of cellulose II.

SEM images of the morphology of the original pine and regenerated material are shown in Fig. 10. The regenerated cellulose-rich material shows a different morphology compared to the original wood, with a conglomerate texture in which wood fibers are fused into a relatively more homogeneous macrostructure.¹⁶

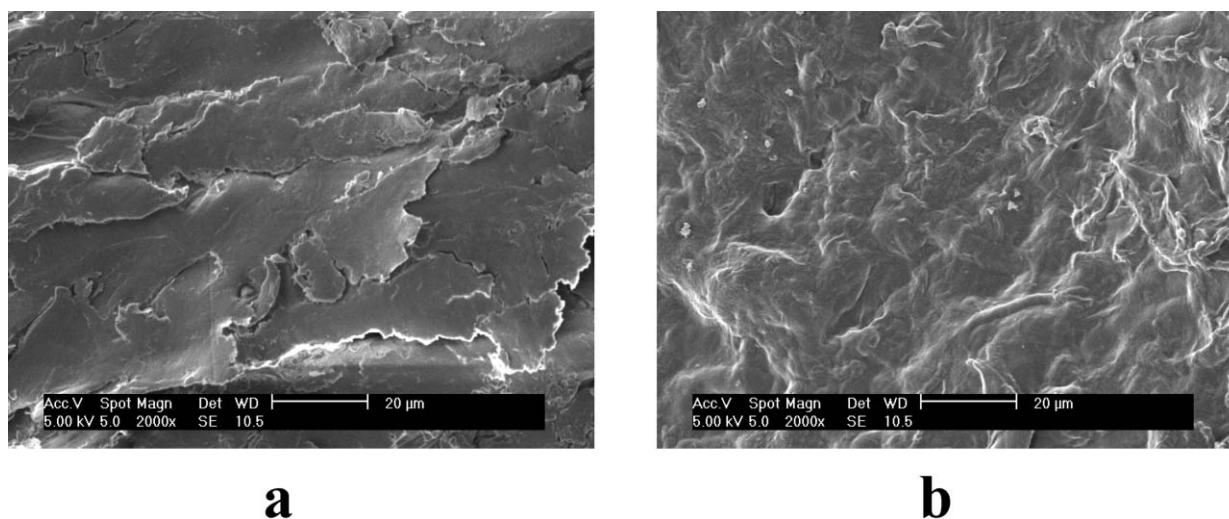


Fig. 10 SEM images of (a) ground southern yellow pine, and (b) the corresponding regenerated cellulose-rich material.

4. Conclusions

Both softwood (southern yellow pine) and hardwood (red oak) can be dissolved completely in $[C_2mim]OAc$ after mild grinding. In general, $[C_2mim]OAc$ has been shown to be a better solvent than $[C_4mim]Cl$ for the dissolution of wood. Red oak showed higher and faster dissolution than southern yellow pine. Smaller particle size and appropriate initial load of wood also result in improved dissolution. The dissolution time can be shortened by applying microwave pulse heating or ultrasound as a pretreatment prior to conventional heating. Fewer lignin-bonded carbohydrates are preferentially dissolved in the IL.

Reconstitution of most of the dissolved wood from acetone/water (1 : 1 v/v) yields a regenerated material which is proportionally richer in carbohydrates than the original wood, and lignin in free form with a similar structure to Indulin AT. As an example, when totally dissolving 5 parts of southern yellow pine particles in 100 parts of $[C_2mim]OAc$, approximately 60% of the original holocellulose was recovered in the cellulose-rich material, whereas approximately one third of the original lignin was obtained in free form and another third linked to the carbohydrates as part of the enriched reconstituted wood. Thus, partial separation of the wood components becomes possible with relative efficiency, without using toxic chemicals, and with little or no degradation of the natural polymers.

Further studies from our group will focus on how to facilitate the cleavage of the covalent bonds between lignin and carbohydrate, in order to obtain an improved or even complete separation of the constituent biopolymers. In addition, a deeper insight into the effect of variables such as the initial degree of humidity of the wood or the long term degradation of the IL will be sought.

Acknowledgements

This work was conducted under the sponsorship of BASF Corporation. We also thank the Center for Materials for Information Technology (MINT) and the Alabama Institute for Manufacturing Excellence (AIME) of The University of

Alabama for providing some of the analytical instruments used in this study.

References

- 1 C. E. Wyman, B. E. Dale, R. T. Elander, M. Holtzapfle, M. R. Ladisch and Y. Y. Lee, *Bioresour. Technol.*, 2005, **96**, 1959–1966.
- 2 G. W. Huber, S. Iborra and A. Corma, *Chem. Rev.*, 2006, **106**, 4044–4098.
- 3 P. J. Dauenhauer, J. D. Dreyer, N. J. Degenstein and L. D. Schmidt, *Angew. Chem., Int. Ed.*, 2007, **46**, 5864–5867.
- 4 T. R. Carlson, V. P. Tushar and H. W. George, *ChemSusChem*, 2008, **1**, 397–400.
- 5 G. Gellerstedt, “Pulping chemistry” in *Wood and cellulosic chemistry*, ed. D. N.-S. Hon, and N. Shiraishi, Marcel Dekker, New York, 2001, pp. 859–905.
- 6 F. S. Chakar and A. J. Ragauskas, *Ind. Crop Prod.*, 2004, **20**, 131–141.
- 7 C. Bonini, M. D’Auria, L. Emanuele, R. Ferri, R. Pucciariello and A. R. Sabia, *J. Appl. Polym. Sci.*, 2005, **98**, 1451–1456.
- 8 Y. Li and S. Sarkanen, *Macromolecules*, 2005, **38**, 2296–2306.
- 9 Y. Li and S. Sarkanen, *Macromolecules*, 2002, **35**, 9707–9715.
- 10 J. F. Kadla and S. Kubo, *Macromolecules*, 2003, **36**, 7803–7811.
- 11 W. Thielemans, E. Can, S. S. Morye and R. P. Wool, *J. Appl. Polym. Sci.*, 2002, **83**, 323–331.
- 12 *Basic research needs: catalysis for energy*, Report from the U.S. Department of Energy, Basic Energy Sciences Workshop, August 6–8, 2007 (available at http://www.er.doe.gov/bes/reports/files/CAT_rpt.pdf; last accessed: December 8, 2008).
- 13 M. E. Himmel, S. Ding, D. K. Johnson, W. S. Adney, M. R. Nimlos, J. W. Brady and T. D. Foust, *Science*, 2007, **315**, 804–807.
- 14 S. E. Lebo, Jr., J. D. Gargulak, and T. J. McNally, “Lignin” in *Kirk-Othmer Encyclopedia of Chemical Technology*, ed. J. I. Kroschwitz, and M. Howe-Grant, John Wiley & Sons, New York, 2001.
- 15 E. Sjöström, “Pulping chemistry” in *Wood chemistry: Fundamentals and applications*, ed. E. Sjöström, Academic Press, New York, 1981, pp. 104–145.
- 16 R. P. Swatloski, S. K. Spear, J. D. Holbrey and R. D. Rogers, *J. Am. Chem. Soc.*, 2002, **124**, 4974–4975.
- 17 H. Zhang, J. Wu, J. Zhang and J. He, *Macromolecules*, 2005, **38**, 8272–8277.
- 18 T. Heinze, K. Schwikal and S. Barthel, *Macromol. Biosci.*, 2005, **5**, 520–525.
- 19 D. M. Phillips, L. F. Drummy, D. G. Conrady, D. M. Fox, R. R. Naik, M. O. Stone, P. C. Trulove, H. C. De Long and R. A. Mantz, *J. Am. Chem. Soc.*, 2004, **126**, 14350–14351.
- 20 Y. Pu, *J. Wood Chem. Technol.*, 2007, **27**, 23–33.
- 21 A. Biswas, R. L. Shogren, D. G. Stevenson, J. L. Willett and P. K. Bhowmik, *Carbohydr. Polym.*, 2006, **66**, 546–550.

- 22 H. Xie, S. Zhang and S. Li, *Green Chem.*, 2006, **8**, 630–633.
- 23 Y. Wu, T. Sasaki, S. Irie and K. Sakurai, *Polymer*, 2008, **49**, 2321–2327.
- 24 H. Xie, S. Li and S. Zhang, *Green Chem.*, 2005, **7**, 606–608.
- 25 D. A. Fort, R. C. Remsing, R. P. Swatloski, P. Moyna, G. Moyna and R. D. Rogers, *Green Chem.*, 2007, **9**, 63–69.
- 26 I. Kilpeläinen, H. B. Xie, A. King, M. Granstrom, S. Heikkinen and D. S. Argyropoulos, *J. Agric. Food Chem.*, 2007, **55**, 9142–9148.
- 27 V. Myllymäki, and R. Aksela, PCT WO/2005/017001, 2005.
- 28 M. Freemantle, *Chem. Eng. News.*, 1998, **76**, 32–37.
- 29 R. C. Remsing, R. P. Swatloski, R. D. Rogers and G. Moyna, *Chem. Commun.*, 2006, 1271–1273.
- 30 T. G. A. Youngs, C. Hardacre and J. D. Holbrey, *J. Phys. Chem. B*, 2007, **111**, 3765–3774.
- 31 J. L. Anderson, J. Ding, T. Welton and D. W. Armstrong, *J. Am. Chem. Soc.*, 2002, **124**, 14247–14254.
- 32 S. Zhang, N. Sun, X. He, X. Lu and X. Zhang, *J. Phys. Chem. Ref. Data*, 2006, **35**, 1475–1517.
- 33 R. P. Swatloski, J. D. Holbrey, S. B. Memon, G. A. Caldwell, K. A. Caldwell and R. D. Rogers, *Chem Commun.*, 2004, 668–669.
- 34 K. Fukumoto, M. Yoshizawa and H. Ohno, *J. Am. Chem. Soc.*, 2005, **127**, 2398–2399.
- 35 Y. Fukaya, A. Sugimoto and H. Ohno, *Biomacromol.*, 2006, **7**, 3295–3297.
- 36 Y. Fukaya, K. Hayashi, M. Wada and H. Ohno, *Green Chem.*, 2008, **10**, 44–46.
- 37 <http://www.sigmaaldrich.com/catalog/search/ProductDetail/ALDRICH/672041> (last accessed: December 8, 2008); other catalog numbers: 672270 and 672157.
- 38 TAPPI T222om-98, Acid-insoluble lignin in wood and pulp, 1998.
- 39 T.-F. Yeh, H.-M. Chang and J. F. Kadla, *J. Agric. Food Chem.*, 2004, **52**, 1435–1439.
- 40 TAPPI Useful Methods, UM 250, Acid-soluble lignin in wood and pulp, 1991.
- 41 F. Lu and J. Ralph, *Plant*, 2003, **35**, 535–544.
- 42 T. Ikeda, K. Holtman, J. F. Kadla, H.-M. Chang and H. Jameel, *J. Agric. Food Chem.*, 2002, **50**, 129–135.
- 43 M. Fujita, and H. Harada, “Ultrastructure and formation of wood cell wall” in *Wood and cellulosic chemistry*, ed. D. N.-S. Hon, and N. Shiraishi, Marcel Dekker, New York, 2001, pp. 1–50.
- 44 S. Saka, “Chemical composition and distribution” in *Wood and cellulosic chemistry*, ed. D. N.-S. Hon, and N. Shiraishi, Marcel Dekker, New York, 2001, pp. 51–81.
- 45 J.-P. Mikkola, A. Kirilin, J.-C. Tuuf, A. Pranovich, B. Holmbom, L. M. Kustov, D. Y. Murzin and T. Salmi, *Green Chem.*, 2007, **9**, 1229–1237.
- 46 M. Lahaye, C. Rondeau-Mouro, E. Deniaud and A. Buleon, *Carbohydr. Res.*, 2003, **338**, 1559–1569.
- 47 J. S. Moulthrop, R. P. Swatloski, G. Moyna and R. D. Rogers, *Chem. Commun.*, 2005, 1557–1559.
- 48 K. E. Gutowski, G. A. Broker, H. D. Willauer, J. G. Huddleston, R. P. Swatloski, J. D. Holbrey and R. D. Rogers, *J. Am. Chem. Soc.*, 2003, **125**, 6632–6633.
- 49 R. P. Green, and G. Hough, *Chemical recovery in the alkaline pulping process*, TAPPI Press, Atlanta, 1992.
- 50 N. Labbé, T. G. Rials, S. S. Kelley, Z. M. Cheng, J.-Y. Kim and Y. Li, *Wood Sci. Technol.*, 2005, **39**, 61–77.
- 51 C. F. Liu, R. C. Sun, A. P. Zhang and J. L. Ren, *Carbohydr. Polym.*, 2007, **68**, 17–25.
- 52 P. Mansikkamäki, M. Lahtinen and K. Rissanen, *Cellulose*, 2005, **12**, 233–242.

Impact of supported ionic liquids on supported Pt catalysts†

Richard Knapp, Andreas Jentys and Johannes A. Lercher*

Received 26th January 2009, Accepted 27th February 2009

First published as an Advance Article on the web 18th March 2009

DOI: 10.1039/b901318k

Silica supported platinum catalysts coated with a thin film of 1-butyl-2,3-dimethyl-imidazolium trifluoromethane sulfonate (BDiMIIm) were investigated with respect to the interaction of the ionic liquid with the oxide support and the metal clusters. IR, inelastic neutron scattering and NMR spectroscopy indicate that the vibrations of the imidazolium ring of ionic liquid are less restricted when supported on SiO₂, while the viscosity of the supported ionic liquid increased. The presence of Pt particles enhances the electron density of the ionic liquid at the nitrogen atom inducing higher basicity. The coverage of the catalyst surface and the metal particles by the ionic liquid protects the metal against oxidation. The catalysts are active and stable for hydrogenation of ethene.

Introduction

The immobilization of organometallic complexes in thin films of supported ionic liquid has been proposed as a new concept to combine the high diversity and homogeneity of molecular catalysts with the facile separation of solid catalysts.^{1–3} As such, immobilizing an organic⁴ or aqueous phase⁵ on a support surface has already been described in 1990. The major drawback of these catalysts, however, has been that the liquid film is volatile, which limits the application at high temperatures. In addition, the stability of the catalytically active component in the aqueous phase is often insufficient.

An alternative are the recently introduced supported ionic liquid catalysts, prepared by impregnation of a porous material with an ionic liquid.⁶ The catalytically active components are immobilized in the ionic liquid and due to the low vapor pressure these catalysts can be applied in gas phase reactions.⁷ The properties of the supported catalysts can be fine-tuned by optimizing the type of ionic liquid and of the metal component. In particular, the solubility and, thus, the selectivity for different reactants can be improved by selecting the polarity of the ionic liquid. The interaction between the ionic liquid and the active component is complex showing ordering phenomena and domain formation of the ionic liquid.^{8,9} Catalysts with immobilized ionic liquids were successfully used in reactions like hydroformylation of olefins,¹ achiral hydrogenation,¹⁰ Heck-reaction¹¹ and hydroamination.^{2,3}

This work is focused on the synthesis and characterization of catalysts based on ionic liquid mediated metal nanoparticles, which allows combining different functionalities in a single material as co-catalysts and/or stabilizing agents can be easily

added into the ionic liquid phase. As active component Pt metal clusters were immobilized in supported thin films of 1-butyl-2,3-dimethyl-imidazolium trifluoromethane sulfonate. Key properties for the application as catalysts such as accessibility, mobility and local environment of the metal clusters were studied with a particular focus on the interaction between metal clusters and ionic liquids. The schematic drawing of the catalysts explored is depicted in Fig. 1.

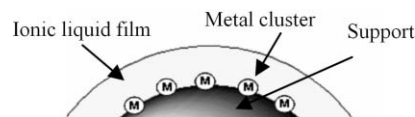


Fig. 1 Catalyst concept with metal clusters immobilized in thin films of ionic liquid.

Results

Infrared spectroscopy

The IR spectra of the catalysts and of the pure ionic liquid (prepared in KBr) are shown in Fig. 2. With pure SiO₂

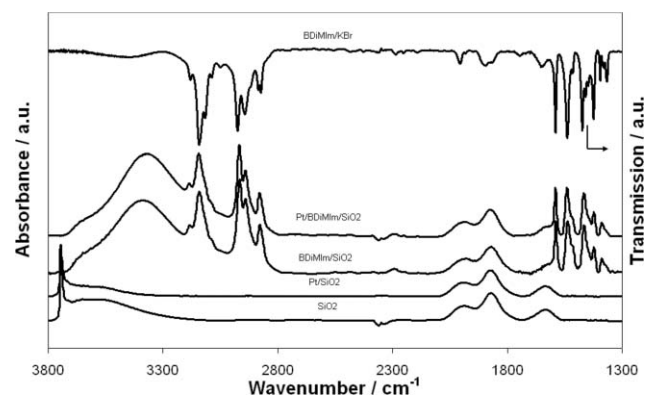


Fig. 2 IR absorption spectra of the silica support, platinum supported on silica, ionic liquid supported on silica and ionic liquid supported on Pt/SiO₂ and IR transmission spectrum of the ionic liquid in KBr.

Lehrstuhl II für Technische Chemie, Technische Universität München, Lichtenbergstr. 4, D-85747, Garching, Germany.
E-mail: johannes.lercher@ch.tum.de; Fax: +49 89 289 13544;
Tel: +49 89 289 13540

† This paper was published as part of the themed issue of contributions from the Green Solvents – Progress in Science and Application conference held in Friedrichshafen, September 2008.

support a sharp band at 3745 cm^{-1} and a broad band at 3600 cm^{-1} were observed, which are assigned to free and hydrogen bonded silanol groups. After depositing Pt on the silica support (Pt/SiO₂) the intensity of the band for silanol groups decreased by 20%. Upon adsorption of BDiMIm on SiO₂ (BDiMIm/SiO₂) and on Pt/SiO₂ (Pt/BDiMIm/SiO₂) the band corresponding to terminal SiOH groups disappeared and new bands at 3390 cm^{-1} (BDiMIm/SiO₂) and 3372 cm^{-1} (Pt/BDiMIm/SiO₂) were observed. All other bands observed in these spectra are attributed to the ionic liquid.

Symmetric and asymmetric stretching vibrations of =CH groups appear at 3184 and 3142 cm^{-1} , C–H stretching vibrations of methylene and methyl groups give absorption bands at 2967 and 2941 cm^{-1} and the methyl amino group was observed at 2878 cm^{-1} . At 1589 and 1538 cm^{-1} C=C stretching vibrations and at 1434 , 1423 and 1388 cm^{-1} C–H bending vibrations were observed. For the ionic liquid prepared in KBr bands at 2000 , 1890 and 1645 cm^{-1} were observed assigned to ring deformation vibrations and stretching vibrations of C=N.

After immobilization of the ionic liquid on SiO₂ or Pt/SiO₂ the bands at 2975 cm^{-1} (C–H stretching) and 1473 cm^{-1} (C–H bending) were shifted to lower wavenumbers (2968 and 1466 cm^{-1}) compared with the ionic liquid prepared in KBr.

Inelastic neutron scattering

The INS spectra of pure BDiMIm, BDiMIm supported on SiO₂ and BDiMIm supported on Pt/SiO₂ are shown in Fig. 3. The bands at 580 cm^{-1} , 725 cm^{-1} and 1050 cm^{-1} increased when BDiMIm is supported on SiO₂ or on Pt/SiO₂. The bands at 580 cm^{-1} and 1050 cm^{-1} were assigned to ring deformation vibrations of the imidazolium ring, the band at 725 cm^{-1} to out of plane vibrations of –CH groups of the C₅-ring. For the supported ionic liquids the band at 580 cm^{-1} was shifted to 610 cm^{-1} . Furthermore, the intensities of the bands attributed to ring deformation vibrations were slightly higher when the ionic liquid was supported on SiO₂ compared to the immobilization on Pt/SiO₂.

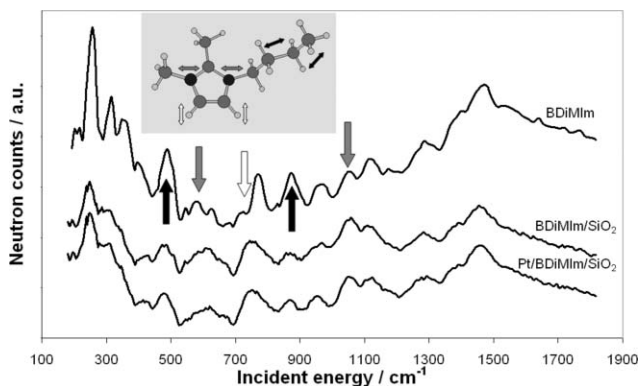


Fig. 3 INS spectra of ionic liquid, ionic liquid supported on silica and supported ionic liquid on Pt/SiO₂.

For pure BDiMIm the intensities of the bands at 490 and 880 cm^{-1} , which were assigned to the in plane vibrations of the alkyl group and stretching vibrations of the methylene groups of the butyl chain were higher compared to the supported ionic liquid. This indicates that the ring deformation led to a slightly

higher relative movement of the hydrogen atoms, while the in plane movements of the alkyl rest is more constrained (less moving) than in the free ionic liquid.

¹H MAS NMR Spectroscopy

In the ¹H MAS NMR spectra of the ionic liquid immobilized on silica (Fig. 4) a noticeable line broadening was observed relative to the pure ionic liquid (for assignments see Table 1). The highest increase in line width was observed for the peaks assigned to the methylene group at the nitrogen atom, while the smallest line broadening was observed for the terminal methyl and methylene groups of the alkyl chain. After a temperature increase to 50 °C and 70 °C , the line-width was further reduced and a high-field shift of the peak assigned to the protons of imidazolium ring was observed. This peak was also shifted by the same value (0.1 ppm) when the ionic liquid was supported on Pt/SiO₂. However, differences in line-width were not observed when BDiMIm was supported on Pt/SiO₂ compared to BDiMIm/SiO₂.

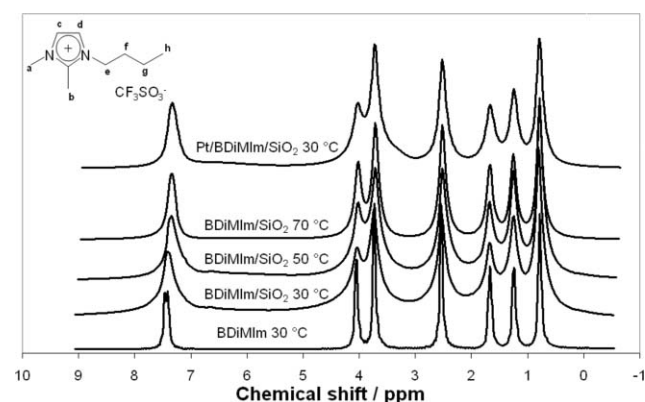


Fig. 4 Solid state ¹H NMR spectra of pure BDiMIm, BDiMIm/SiO₂ at different temperatures and Pt/BDiMIm/SiO₂.

Transmission electron microscopy

The TEM pictures of Pt clusters supported on silica and coated with 17 wt% ionic liquid at a magnification of 200000 are shown in Fig. 5b and the particle size distribution, which indicates a mean metal particle size of 2.1 nm is shown in Fig. 5a.

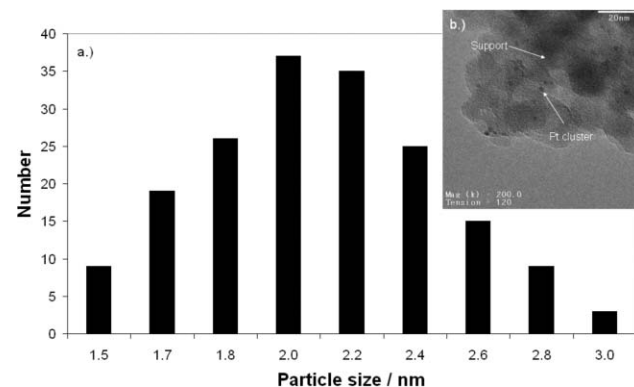


Fig. 5 Particle size distribution (a) and TEM picture (b) of an ionic liquid coated supported platinum catalyst.

Table 1 NMR peak assignment and full width at half maximum for pure BDiMIm, BDiMIm/SiO₂ at different temperatures and Pt/BDiMIm/SiO₂ (CS chemical shift/ppm; LW line-width/Hz)

Assignment	BDiMIm		BDiMIm/SiO ₂		Pt/BDiMIm/SiO ₂
	30 °C CS (LW)	30 °C CS (LW)	50 °C CS (LW)	70 °C CS (LW)	30 °C CS (LW)
c	7.46 (25)	7.40 (152)	7.34 (119)	7.35 (86)	7.32 (145)
d	7.41 (27)				
e	4.05 (30)	4.05 (125)	4.02 (102)	4.02 (82)	4.02 (124)
a	3.73 (27)	3.73 (101)	3.72 (85)	3.71 (73)	3.72 (95)
b	2.54 (27)	2.53 (101)	2.52 (82)	2.51 (76)	2.52 (90)
f	1.67 (33)	1.67 (108)	1.67 (106)	1.68 (77)	1.66 (104)
g	1.24 (35)	1.25 (104)	1.25 (80)	1.25 (70)	1.24 (101)
h	0.78 (30)	0.80 (81)	0.78 (71)	0.79 (65)	0.79 (79)

X-ray absorption near edge structure and extended X-ray absorption fine structure

To determine the influence of the ionic liquid on electronic structure of the metal clusters, Pt/SiO₂ and Pt/BDiMIm/SiO₂, coated with 17 wt% of BDiMIm, were investigated by XANES and EXAFS.

The X-ray absorption spectra at the L_{III} edge (shown in Fig. 6) show that the intensity of the peak above the edge is higher for the Pt/SiO₂ catalyst compared to Pt/BDiMIm/SiO₂ and the Pt-reference foil.

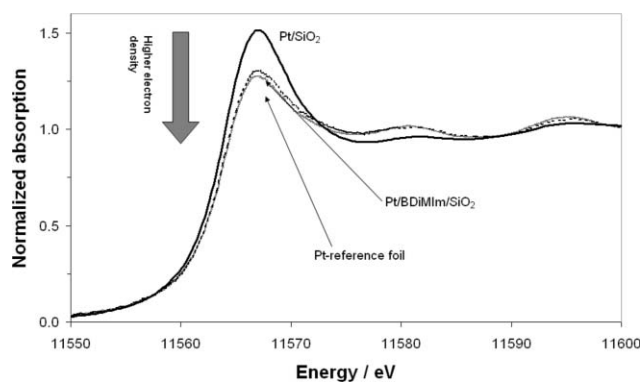
**Fig. 6** XANES of an uncoated catalyst (Pt/SiO₂), a coated catalyst (Pt/BDiMIm/SiO₂) and a Pt foil.

Fig. 7 compiles the Fourier-transformed EXAFS of the uncoated (Fig. 7a) and the coated catalyst (Fig. 7b). The number of neighbours (coordination number CN), their distance (*r*), the Debye–Waller factor (σ^2) and the zero energy correction (*E*₀) were calculated from the EXAFS and are shown in Table 2. The results indicate that oxygen neighbouring atoms can only be found for the uncoated catalyst. Also the coordination number for Pt neighbouring atoms was half compared with the coated catalyst.

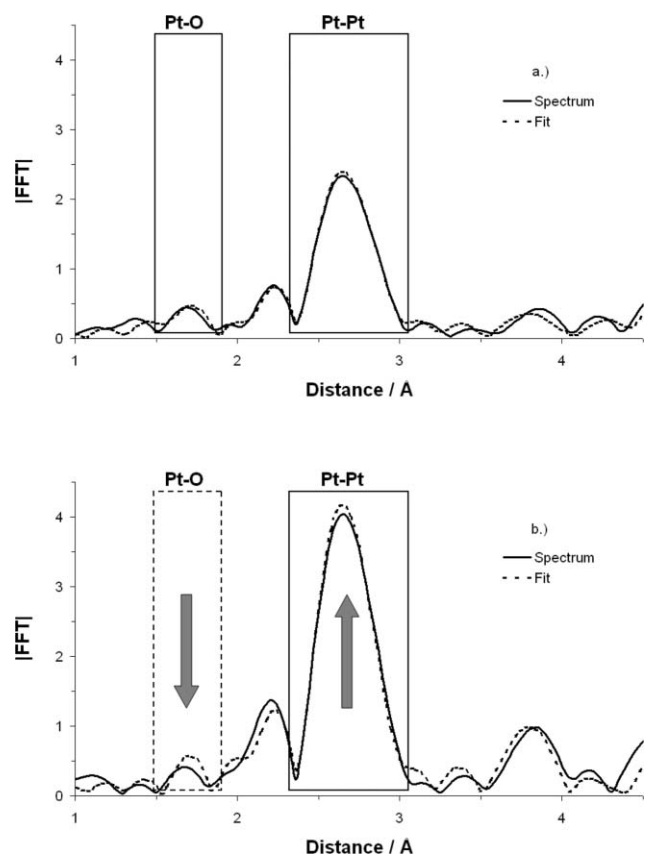
The particle size was determined from the average coordination number of the nearest metallic neighboring atoms assuming cuboctahedral geometry.¹² For Pt/SiO₂ the particle size was 0.9 nm, corresponding to a dispersion of 0.9 and for Pt/BDiMIm/SiO₂ a particle size of 1.95 nm was determined indicating a dispersion of 0.6.

Catalytic hydrogenation of ethene

The activity of the uncoated and coated catalysts as a function of the temperature is shown in Fig. 8. The reaction was zero

Table 2 EXAFS curve fitting results for Pt/SiO₂ and Pt/BDiMIm/SiO₂

	Pt/SiO ₂	Pt/BDiMIm/SiO ₂
<i>r</i> _{Pt-O} [Å]	2.05	2.15
CN _{Pt-O}	0.81	0.0
σ^2	0.0021	0.01619
<i>E</i> ₀ [eV]	16.18	18.47
<i>r</i> _{Pt-Pt} [Å]	2.77	2.76
CN _{Pt-Pt}	4.4	8.9
σ^2	0.0033	0.0033
<i>E</i> ₀ [eV]	13.23	10.98

**Fig. 7** Measured and calculated Fourier-transformed EXAFS of Pt/SiO₂ (a) and Pt/BDiMIm/SiO₂ (b).

order with respect to ethylene. The activation energy 42 kJ/mol and 40 kJ/mol, respectively, was calculated using rates from

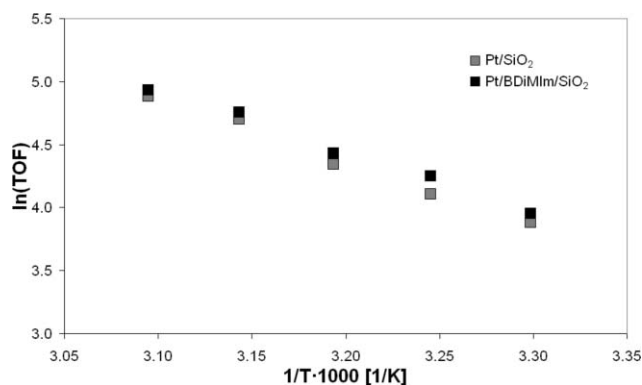


Fig. 8 Catalytic activities for Pt/SiO₂ and Pt/BDiMIm/SiO₂.

experiments with a conversion below 25%. (Note that for reactions with 0 order there is no difference between rates determined by a differential and integral analysis). The stability of the coated catalyst was followed at 70 °C after the series of kinetic experiments carried out up to 90 °C, showing a constant rate over 36 hours.

Discussion

Supported ionic liquids have been concluded to assume relative ordered states in the presence of metal organic complexes.⁹ The exact degree of coordination of the ions to the dissolved and suspended substrates are unknown, but the question arises whether or not such phenomena are confined solely to metal complexes and particles or if reacting molecules would also induce locally such phenomena, when dissolved in an IL. The most important feature of such ordering phenomena for catalysis is not the overall long range ordering, but the direct interactions determining the critical properties as sorbent and catalyst. Thus, we focus in the present case on the characterization of the interactions between the ionic liquid, the support and the Pt particles using molecular spectroscopy.

For Pt on silica the intensity of the band characteristic for SiOH groups decreased by 20% compared with the silica before impregnation. On first sight this may be attributed to dehydration of SiO₂ during the activation and reduction in hydrogen, since the treatment of SiO₂ at the same conditions (pH, Cl⁻ concentration and temperature) lead to a similar result. However, it is striking that the perturbed OH bands (indicating hydrogen bonding between OH groups) are affected most. This indicates that the Pt particles are preferentially anchored at sites with a higher SiOH concentration, *i.e.*, at parts of the support containing more defects. In contrast, the decrease of the band of the unperturbed free SiOH groups at 3740 cm⁻¹ was relatively small suggesting that the role of these OH groups in the anchoring of the Pt particles is negligible.

The disappearance of the band of terminal SiOH groups after coating SiO₂ with the ionic liquid indicates the complete coverage of the silica surface. The appearance of a new band at 3390 cm⁻¹ for BDiMIm/SiO₂ and 3372 cm⁻¹ for Pt/BDiMIm/SiO₂ characteristic of perturbed OH vibrations led us to conclude that the interactions between the ionic liquid film and the silica occurred *via* hydrogen bonds. The difference of 18 cm⁻¹ between these two bands suggests slightly stronger

hydrogen bonding when BDiMIm is supported on Pt/SiO₂. The reasons for this stronger interactions with the trifluoromethane sulfonate anions could be caused by the more pronounced interactions of 1-butyl-2,3-dimethyl-imidazolium cations with the metal particles. These interactions in turn allow a stronger coordination of anions to OH groups.

This conclusion is indirectly supported by the INS spectra. In these spectra the bands assigned to the deformation vibrations of the imidazolium ring increased in intensity. The increase in intensity is attributed to stronger relative displacements of the hydrogen atoms (stronger vibrations). The coordination of the basic CF₃SO₃⁻ anions to the weakly acidic surface hydroxyl and the stronger interaction with the metal particle allows for a stronger displacement of the C–H vibrations. The shift of the band at 580 cm⁻¹ to 610 cm⁻¹ is attributed to the enhanced deformation vibrations of the imidazolium ring.

The line broadening observed in the NMR spectra of the supported catalysts can be attributed to differences in the T₂ relaxation time that are not affected by MAS-NMR and therefore, can be used to determine the mobility of specific atomic groups.^{13–15} The immobilization of the ionic liquid on the support leads to a lower mobility of the molecules and thus to an increased viscosity. Especially the nitrogen bound methylene group was affected. This was also detected by INS as the intensities of the bands ascribed to the in plane vibrations of the alkyl groups (490 cm⁻¹) decreased for the supported ionic liquid compared with the pure BDiMIm. Differences in line width were not observed when BDiMIm was supported on Pt/SiO₂ compared to BDiMIm/SiO₂, since the amount of 1 wt% of Pt on the surface is not enough to cause a further increase in viscosity. However, for a sample with a metal loading of 5 wt% a noticeable line broadening was observed (results not reported here). After a temperature increase, the line-width was reduced, as the mobility of the molecules increased due to the thermal energy. The peak assigned to the protons of the imidazolium shifted to a higher field after increasing the temperature.

In line with IR and INS, the ¹H MAS-NMR spectra show that upon immobilization of the ionic liquid on Pt/SiO₂ the protons of the imidazolium shifted to a higher field (*i.e.* to a 0.1 ppm downwards shift) compared to the IL supported on SiO₂ only. This is attributed to an increased electron density of the imidazolium ring leading to a higher shielding of the protons. As the hydrogen bonds between the ionic liquid and the surface of the support occur *via* CF₃SO₃⁻ anions, the stronger bonding of the imidazolium ring to Pt, the higher the availability and base strength of the anion will be.

For the sample with 1 wt% metal loading TEM revealed that the particles were highly dispersed and that agglomerates of the metal clusters were not formed. The particle size determined by transmission electron microscopy (2.1 nm) was in good agreement with the particle size calculated from the EXAFS data (1.95 nm). The comparison of the XANES at the L_{III} edge of the prepared catalysts and the reference foil indicated a higher oxidation state for the uncoated Pt/SiO₂ catalyst, which was also confirmed by the EXAFS containing Pt–O contributions for the Pt/SiO₂ catalyst. The Pt cluster particle size was reduced to 0.9 nm, but the fact that the Pt–Pt distance did not increase for the Pt/SiO₂ catalyst compared with the bulk metal foil indicates that oxygen neighbouring atoms are in the outer shell of the Pt

clusters only. In contrast, the Pt particles in the coated system were in zero oxidation state, as neighbouring oxygen atoms were not found and the XANES was identical to that of bulk Pt. This illustrates that the use of the ionic liquid protects the metal clusters from oxidation under typical sample handling conditions.

Hydrogenation of ethene showed zero order in ethene and first order (concluded from preliminary measurements) in hydrogen in a temperature interval from 30 to 50 °C. This is in perfect agreement with the literature for Pt supported on silica.¹⁶ It is generally accepted that the reaction proceeds *via* the Horiuti–Polanyi mechanism.¹⁷ According to this mechanism ethene adsorbs associatively on the metal surface, while hydrogen adsorbs dissociatively. The first order in hydrogen points to a nearly simultaneous addition of hydrogen in the rate determining step. It has been shown¹⁷ that the sites for ethene and hydrogen are not identical, *i.e.*, under the conditions used the adsorption is non-competitive. The zero order in ethene indicates that the surface of the metal particles is essentially covered with ethene. This is remarkable, as the ionic liquid is present in very large excess compared to ethene. In the absence of detailed information on the heat of adsorption of the ionic liquid on metal surfaces, we speculate that the smaller size of ethene and the fact that it can form a di- σ -sorbed adsorbed state leads to a better stabilization compared with the π bonding of the imidazolium ion.

Conclusions

Detailed analysis of the supported platinum catalysts coated with a thin film of BDiMIm gave an insight into the interactions of the ionic liquid with the oxide support and the metal clusters. Spectroscopy confirmed that the vibrations of the imidazolium ring of the SiO₂ supported ionic liquid were less restricted, whereas the viscosity of the ionic liquid increased. This will have a strong impact on the diffusivity of reactants to the active sites, allowing tailoring of the selectivity towards certain products. The presence of platinum clusters further modified the electron density of the ionic liquid, which changes the polarity of the ionic liquid within certain limits and can also be used to improve the selectivity. In addition, the complete coverage of the catalyst surface including the metal particles with the ionic liquid protects the catalyst from oxidation, which can be further utilized to protect air sensitive catalysts. The similar catalytic activity of the coated catalyst for ethene hydrogenation at low temperatures shows that the ionic liquid does not block the access of hydrogen or ethane to the active sites. This is an important aspect which indicates that the interaction of the ionic liquid and the Pt surface is weaker compared to the reactant molecules and therefore, potential transport limitations resulting from a low solubility of reactants did not occur. This opens new possibilities for the selective hydrogenation of unsaturated compounds as the properties of the metal and of the reaction environment can be subtly tuned *via* the ionic liquid.

Experimental

Materials

The ionic liquid 1-butyl-2,3-dimethyl-imidazolium trifluoromethane sulfonate (BDiMIm) (99%) with a maximum water

and halide content of 47.8 and 103.1 ppm, respectively, was kindly provided by Solvent Innovation GmbH. Chloroplatinic acid hexahydrate (Pt content $\geq 37.5\%$) and methanol (99.8%) were obtained from Aldrich. Octane ($>99\%$) was purchased from Fluka. All chemicals were used as received. The silica support Aerosil 355 was provided by Degussa AG. For INS measurements SiO₂-60 from Chemie AG was used.

Preparation of the supported catalysts

The silica support was ground, sieved to 100 μm particle size and dried at 200 °C. Catalysts with immobilized metal clusters (1 wt% metal) were prepared by incipient wetness impregnation. Chloroplatinic acid hexahydrate was dissolved in the appropriate amount of bi-distilled water; the solution was trickled onto the support and stirred until the water was completely absorbed. The water was removed by freeze drying. The precursors were calcined at 400 °C for three hours in synthetic air and subsequently reduced at 250 °C for three hours in a flow of hydrogen.

For preparing the supported ionic liquid catalysts Pt/SiO₂ was added to a solution of BDiMIm dissolved in methanol. The suspension was stirred at room temperature for 10 min and the volatile components were slowly removed by freeze drying to give a free flowing grey powder (Pt/BDiMIm/SiO₂).

A silica supported ionic liquid was prepared by adding SiO₂ into a solution of BDiMIm dissolved in methanol. After stirring for 10 min, the suspension was freeze dried to give a free flowing white powder (BDiMIm/SiO₂).

Characterization

The platinum content of the supported catalysts was determined by AAS using a UNICAM 939 spectrometer. The amount of ionic liquid adsorbed on the surface was determined by elemental analysis.

The IR spectra were measured on a Bruker IFS 88 spectrometer in transmission mode. The samples were pressed into self-supporting wafers and activated in vacuum for 1 h at 150 °C. Pt containing samples were reduced *in-situ* at 250 °C and 0.8 bar hydrogen for 30 minutes. The spectra were recorded at a resolution of 4 cm^{-1} in the region from 4000 to 400 cm^{-1} . To compare the different samples, the spectra of the activated samples were normalized using the overtone and combination vibrations of silica between 2105 and 1740 cm^{-1} . For IR measurements of the pure ionic liquid, a KBr wafer was pressed and analyzed using a Jasco FT/IR-460 Plus spectrometer.

INS-Experiments were carried out at 15 K at the Be-filter detector spectrometer IN1BeF at ILL in Grenoble using a Cu (220) monochromator. The instrument resolution was between 4 cm^{-1} , at low energy transfers and 25 cm^{-1} at high energy transfers. The vibrational modes of the ionic liquid were calculated with *GAUSSIAN 03*¹⁸ and the INS spectra were calculated using *a-CLIMAX*.¹⁹

For solid state NMR, the samples were packed in 4 mm ZrO₂ rotors. ¹H MAS NMR measurements were performed on a Bruker AV500 spectrometer (B₀ = 14.1 T) with a spinning rate of 15 kHz. For temperature adjustment the bearing and drive gas stream were passed through a heat exchanger. The spectra were

recorded as the sum of 100 scans using single pulse excitation with a pulse length of 2.6 μs and recycle time of 3 s.

For transmission electron microscope images, the samples were grinded, suspended in octane and ultrasonically dispersed. Drops of the dispersions were applied on a copper-grid supported carbon film. Micrographs were recorded on a JEM-2010 Jeol transmission electron microscope operating at 120 kV.

The EXAFS spectra were collected at the beamline X1 at HASYLAB, DESY, Hamburg, Germany. The storage ring was operated at 4.5 GeV with an average current of 100 mA. The Si (311) double-crystal monochromator was detuned to 60% of the maximum intensity to minimize the intensity of higher harmonics in the X-ray beam. The catalysts were pressed into self supporting wafers (ca. 150 mg) and the X-ray absorption spectra were collected at the Pt L_{III} edge (11.564 eV) in a helium flow at liquid N₂ temperature. The EXAFS data was analysed using the *Viper* software.²⁰ For EXAFS analysis, the scattering contributions of the background were removed from the X-ray absorption by a third-order polynomial function. The oscillations were weighted with k^2 and Fourier-transformed within the limit $k = 3.5\text{--}16 \text{ \AA}^{-1}$. The local environment of the Pt atoms was determined from the EXAFS using the phase-shift and amplitude function for Pt–Pt and Pt–O calculated assuming multiple scattering processes (FEFF version 8.40).^{21,22}

The XANES data were collected in a helium flow at room temperature and analysed using the *XANES dactyloscope* software.²³ All recorded XANES spectra were normalized to unity. The position of the edge was calibrated using the spectra of a Pt reference-foil measured simultaneously.

Catalytic activity

The hydrogenation of ethylene was studied at temperatures between 30 and 50 °C with a hydrogen to ethylene ratio of 2.5:1 in a fixed bed reactor filled with 0.1 mg catalyst (diluted with SiO₂ and SiC). The products were analyzed using a Shimadzu GC-2014 gas chromatograph.

Acknowledgements

The project is funded by the BMBF (03X2012F). The authors are grateful to Max-Buchner-Stiftung for partial support. The authors acknowledge fruitful discussions in the framework of the network of excellence IDECAT. The authors would like to thank HASYLAB, Hamburg, Germany and the Institut Laue-Langevin Grenoble, France for providing beamtime at station X1 for XAFS experiments and at the IN1-BeF spectrometer to

record the INS spectra. We would like to thank Xaver Hecht and Martin Neukamm for their experimental support.

Notes and references

- 1 A. Riisager, R. Fehrmann, S. Flicker, R. van Hal, M. Haumann and P. Wasserscheid, *Angewandte Chemie-International Edition*, 2005, **44**, 815.
- 2 O. Jimenez, T. E. Muller, C. Sievers, A. Spirkl and J. A. Lercher, *Chem. Commun.*, 2006, 2974.
- 3 C. Sievers, O. Jimenez, R. Knapp, X. Lin, T. E. Muller, A. Turler, B. Wierczinski and J. A. Lercher, *J. Mol. Catal. A: Chem.*, 2008, **279**, 187.
- 4 H. L. Pelt, J. Brockhus, R. P. J. Verburg and J. J. F. Scholten, *J. Mol. Catal.*, 1985, **31**, 107.
- 5 J. P. Arhancet, M. E. Davis, J. S. Merola and B. E. Hanson, *J. Catal.*, 1990, **121**, 327.
- 6 C. P. Mehnert, E. J. Mozeleski and R. A. Cook, *Chem. Commun.*, 2002, 3010.
- 7 T. Welton, *Coord. Chem. Rev.*, 2004, **248**, 2459.
- 8 R. Atkin and G. G. Warr, *J. Am. Chem. Soc.*, 2005, **127**, 11940.
- 9 C. Sievers, O. Jimenez, T. E. Muller, S. Steuernagel and J. A. Lercher, *J. Am. Chem. Soc.*, 2006, **128**, 13990.
- 10 A. Wolfson, I. F. J. Vankelecom and P. A. Jacobs, *Tetrahedron Lett.*, 2003, **44**, 1195.
- 11 H. Hagiwara, Y. Sugawara, K. Isobe, T. Hoshi and T. Suzuki, *Org. Lett.*, 2004, **6**, 2325.
- 12 R. E. Benfield, *J. Chem. Soc. Faraday Trans.*, 1992, **88**, 1107.
- 13 A. Johansson and J. Tegenfeldt, *J. Chem. Phys.*, 1996, **104**, 5317.
- 14 A. Lauenstein and J. Tegenfeldt, *J. Phys. Chem. B*, 1997, **101**, 3311.
- 15 R. Spindler and D. F. Shriver, *J. Am. Chem. Soc.*, 1988, **110**, 3036.
- 16 R. D. Cortright, S. A. Goddard, J. E. Rekoske and J. A. Dumesic, *J. Catal.*, 1991, **127**, 342.
- 17 J. Horiuti and M. Polanyi, *Trans. Faraday Soc.*, 1934, **30**, 1164.
- 18 *Gaussian 03, Revision C.02*, M. J. Frisch, G. W. Trucks, H. B. Schlegel, G. E. Scuseria, M. A. Robb, J. R. Cheeseman, J. A. Montgomery, Jr., T. Vreven, K. N. Kudin, J. C. Burant, J. M. Millam, S. S. Iyengar, J. Tomasi, V. Barone, B. Mennucci, M. Cossi, G. Scalmani, N. Rega, G. A. Petersson, H. Nakatsuji, M. Hada, M. Ehara, K. Toyota, R. Fukuda, J. Hasegawa, M. Ishida, T. Nakajima, Y. Honda, O. Kitao, H. Nakai, M. Klene, X. Li, J. E. Knox, H. P. Hratchian, J. B. Cross, V. Bakken, C. Adamo, J. Jaramillo, R. Gomperts, R. E. Stratmann, O. Yazyev, A. J. Austin, R. Cammi, C. Pomelli, J. W. Ochterski, P. Y. Ayala, K. Morokuma, G. A. Voth, P. Salvador, J. J. Dannenberg, V. G. Zakrzewski, S. Dapprich, A. D. Daniels, M. C. Strain, O. Farkas, D. K. Malick, A. D. Rabuck, K. Raghavachari, J. B. Foresman, J. V. Ortiz, Q. Cui, A. G. Baboul, S. Clifford, J. Cioslowski, B. B. Stefanov, G. Liu, A. Liashenko, P. Piskorz, I. Komaromi, R. L. Martin, D. J. Fox, T. Keith, M. A. Al-Laham, C. Y. Peng, A. Nanayakkara, M. Challacombe, P. M. W. Gill, B. Johnson, W. Chen, M. W. Wong, C. Gonzalez, and J. A. Pople, Gaussian, Inc., Wallingford CT, 2004.
- 19 A. J. Ramirez-Cuesta, *Comput. Phys. Commun.*, 2004, **157**, 226.
- 20 K. V. Klementiev, *VIPER for Windows*, freeware: <http://www.desy.de/~klmn/viper.html>.
- 21 A. L. Ankudinov, B. Ravel, J. J. Rehr and S. D. Conradson, *Phys. Rev. B: Condens. Matter*, 1998, **58**, 7565.
- 22 A. L. Ankudinov and J. J. Rehr, *Phys. Rev. B: Condens. Matter*, 2000, **62**, 2437.
- 23 K. V. Klementiev, *XANES dactyloscope*, freeware: <http://www.desy.de/~klmn/xanda.html>.

Ibuprofen loading into mesostructured silica using liquid carbon dioxide as a solvent†

Anna Hillerström,^{*a,b} Jan van Stam^b and Martin Andersson^a

Received 2nd December 2008, Accepted 9th March 2009

First published as an Advance Article on the web 26th March 2009

DOI: 10.1039/b821281c

It has been demonstrated that the pharmaceutical molecule, Ibuprofen, can be loaded into mesoporous silica using liquid (near-critical) carbon dioxide as the solvent, and that the resulting material had a high Ibuprofen content (300 mg Ibuprofen/g SiO₂). A high enrichment (300 times) of Ibuprofen in the pores was observed in comparison to the Ibuprofen concentration in the solution. When similar experiments were performed in CO₂ (*l*) mixed with minor amounts (5 mol-%) of other organic cosolvents (cyclohexane, acetone or methanol), a significantly lower loading capacity of Ibuprofen into the mesoporous material was achieved. The drug-loaded mesoporous silica material was analyzed with Thermogravimetric Analysis (TGA), confocal Raman microscopy, X-ray Powder Diffraction (XRPD) and Scanning Electron Microscopy (SEM). It was found that the Ibuprofen loaded into the mesoporous silica host was amorphous and that Ibuprofen was present both at the surface and in the centre of the mesoporous silica particles. Furthermore, the SEM images did not reveal any large flakes of Ibuprofen molecules outside the mesoporous silica particles.

Introduction

Ordered mesostructured silica was first produced in 1992 and since then many applications for this class of material has been proposed, such as for catalysis, adsorption and separation.¹ This material is very interesting due to its tunable pore size in the mesopore range (2–50 nm), and due to its high specific surface area and large pore volume. One of the most commonly used mesoporous silica materials is the ordered hexagonal MCM-41 with a pore diameter of 3–5 nm and having a specific area of >1000 m²/g and a pore volume of >0.7 cm³/g.²

One potentially interesting application of the mesostructured silica is to use it for controlled release systems of drugs, due to the well-defined and large internal porosity of the material. These characteristics will meet the need for a prolonged and better control of the drug administration. Controlled delivery systems offer advantages, such as improved and reduced toxicity. In this study, we have used mesostructured silica of the above mentioned hexagonal MCM-41 type to study loading of a model drug molecule, Ibuprofen, using liquid carbon dioxide as the solvent. Ibuprofen is an extensively used analgesic and anti-inflammatory drug with fairly low water solubility. Also, its size (0.5 × 1.2 × 0.8 nm) is rather small in comparison to other drug molecules.³ The size of Ibuprofen makes it

suitable for inclusion in the pores of the mesostructured silica material.

It is desirable to achieve a high degree of loading of Ibuprofen to fully utilize the pores of the mesostructured silica. Hence, an effective solvent for the molecule has to be used. Previous studies have used different organic solvents to achieve the loading of Ibuprofen into mesostructured silica, while in the current study we have developed a method based on CO₂ (*l*).^{3–6} Using liquid carbon dioxide (or other liquefied gases) has several advantages over the traditional organic solvents, especially since no solvent residues will be left in the final material, which may be an issue if the material should be used in high-purity applications, such as drugs. Another advantage is that it is not necessary to add extra steps in the process for drying the final material and the material can be processed at mild conditions ($T_C = 31\text{ }^\circ\text{C}$ and $p_C = 73\text{ bar}$).⁷

The aim of this study was to investigate the loading of Ibuprofen into mesoporous silica, using liquid carbon dioxide as the solvent, with the important end-goal of maximization of the amount of Ibuprofen contained in the pores of the mesostructured silica. The solubility of Ibuprofen in the solvent was considered to be an important factor and consequently the loading efficiencies of pure CO₂ (*l*) as well as CO₂ (*l*) mixed with various cosolvents have been evaluated. The Ibuprofen-loaded samples were also analyzed with some analytical techniques. X-ray Powder Diffraction (XRPD) was used to determine the degree of crystallinity of the loaded Ibuprofen in the pores. Confocal Raman microscopy was used to confirm that Ibuprofen is loaded homogeneously into the pores. This information could also be retrieved by using Scanning Electron Microscopy (SEM), which can reveal the presence of large Ibuprofen clusters outside the mesoporous silica particles. The amount of Ibuprofen in the

^aYKI, Institute for Surface Chemistry, Box 5607, SE-114 86, Stockholm, Sweden. E-mail: anna.hillerstrom@yki.se; Fax: +46 8 20 89 98; Tel: +46 8 5010 6049

^bDepartment of Physical Chemistry, Karlstad University, SE-651 88, Karlstad, Sweden

† This paper was published as part of the themed issue of contributions from the Green Solvents - Progress in Science and Application conference held in Friedrichshafen, September 2008.

Table 1 The properties of the mesoporous silica synthesized with a spray-drying method²

BET surface area (m ² /g)	Pore volume (cm ³ /g)	Mean pore diameter (nm)
1106	0.73	2.5

mesoporous material was analyzed with a thermogravimetric analyzer (TGA).

Experimental

Materials

The used mesostructured silica (MCM-41, with a cylindrical mesoporous network) was synthesized at YKI, Institute for Surface Chemistry.² In brief, the mesoporous particles were synthesized by preparing a precursor solution by mixing tetraethoxysilane (TEOS, Purum, 98%, Fluka) in dilute hydrochloric acid (pH 2) and ethanol (99.7%, Solveco Chemicals AB, Sweden) at room temperature. The cationic surfactant, hexadecyl trimethyl ammonium bromide (CTAB, 95%, Aldrich, Germany), was dissolved in ethanol and then mixed with the hydrolyzed TEOS solution. The mesoporous particles were then formed at room temperature by spraying the solution in a spray drying equipment. This was followed by a calcination step at 550 °C for 4 hours to remove the surfactant templates. The properties of the mesoporous silica are listed in Table 1. The drug molecule in all loading studies in this article was Ibuprofen (>98%, Sigma-Aldrich, Germany). The carbon dioxide used was of industrial grade (99.7%, AGA Gas AB, Sweden) and cosolvents mixed with CO₂ (*l*) were; cyclohexane (p.a., Merck, Germany), acetone (p.a., Merck, Germany) and methanol (p.a., Merck, Germany).

Methods

Loading of Ibuprofen into SiO₂. The mesoporous particles were placed in a bag (fabric of polypropylene, PP 3333, permeability 105 DIN, Derma AB, Sweden), which was permeable for the solvent and dissolved Ibuprofen molecules but kept the mesoporous particles in one place in the reactor (see below). The amount of mesoporous particles was 0.1 g in all experiments, while the amount of Ibuprofen was varied for different loading experiments. The particles in the bag and Ibuprofen crystals (thoroughly ground in a mortar before use) were placed in a glass beaker (400 ml), which was placed in an in-house built stainless steel reactor (1.7 l) with two sapphire glass windows. The reactor was first pressurized with carbon dioxide and thereafter 200 ml CO₂ (*l*) or CO₂ (*l*) + 5 mol-% cosolvent was introduced into the glass beaker at 20 °C and 55 bar. During the loading of Ibuprofen into the mesoporous material, the solution was gently stirred at constant speed with a magnetic bar. After the loading period (15 minutes to 18 hours), the reactor was depressurized and the bag containing the mesoporous particles with Ibuprofen was retrieved.

Thermogravimetric analysis (TGA). The samples were characterized with TGA using a TGA 7 instrument (PerkinElmer Inc., USA). The temperature program used consisted of an

initial part with a heating rate of 20 °C/min from 20 °C to 95 °C, followed by an isothermal pause for 60 minutes at 95 °C, and finally heating from 95 °C up to 800 °C at a heating rate of 2 °C/min. All TGA measurements were performed under 20 ml/min flow of N₂ gas.

X-ray Powder diffraction (XRPD). All XRPD powder patterns (PANalytical X'Pert PRO, the Netherlands) were obtained with a 3050/60 theta/theta goniometer and a PW3064 spinning stage. CuK α radiation ($\lambda = 1.5418 \text{ \AA}$) was used in all experiments and the generator was operated at 45 kV and 35 mA. The powder was placed in the centre on the rotating sample holder and a diffractogram in the 2 θ range 0.5–30° was obtained with step size 0.0084°. The scan speed was 0.052°/s.

Confocal raman microscopy. The presence of Ibuprofen outside and inside the mesoporous particle was characterized by a confocal Raman Microscopy (WITec alpha 300, Germany). The instrument has a lateral resolution of 200 nm and a vertical resolution of 500 nm. A 785 nm laser was used for excitation and the spectra were recorded either approximately at the surface or in the centre of a mesoporous particle with size 5 μm . The centre of the particle was found by focusing on the surface of the particle ($z = 0 \mu\text{m}$) and then changing the focus depth to 2.5 μm (= the radius of the particle).

Scanning electron microscopy (SEM). A Scanning Electron Microscope (XL30 ESEM TMP, FEI/Philips, the Netherlands) was used to analyze the mesostructured material before and after loading of Ibuprofen into mesoporous silica in CO₂ (*l*). The microscope was operated at 15 kV electron acceleration voltage. Images were recorded at 5000X magnification using a mix of a secondary electron detector (75%) and a backscattering electron detector (25%). The samples were coated with a gold layer of ~300 Å thickness using a sputter coater (SCD 050, Baltzers Union AG, Lichtenstein) for the SEM analysis.

Results and discussion

The solubility of Ibuprofen in CO₂ (*l*) and CO₂ (*l*) with 5 mol-% of cosolvent was determined by visual inspection of sample mixtures of the solvent/-s and Ibuprofen at room temperature and 55 bar, and the solubility limit was considered to be reached when particles of Ibuprofen were visible. The dissolution of Ibuprofen appeared to occur within less than 30 minutes but the solubility test was performed for 9 hours to ascertain an equilibrium value. The solubility tests are summarized in Table 2.

The results from experiments with loading of Ibuprofen in mesoporous particles using CO₂ (*l*) is summarized in Fig. 1,

Table 2 The solubility limit of Ibuprofen in CO₂ (*l*) and CO₂ (*l*) + cosolvent

Solvent	Solubility limit (wt-%)	Solubility parameter of cosolvent (MPa ^{1/2}) ^{11a}
CO ₂ (<i>l</i>)	0.20–0.25	
CO ₂ (<i>l</i>) + cyclohexane	1.0–1.5	16.8
CO ₂ (<i>l</i>) + acetone	1.5–2.0	20.3
CO ₂ (<i>l</i>) + methanol	> 2.0	29.7

^a The solubility parameter for CO₂ (*l*) is 12 MPa^{1/2}.

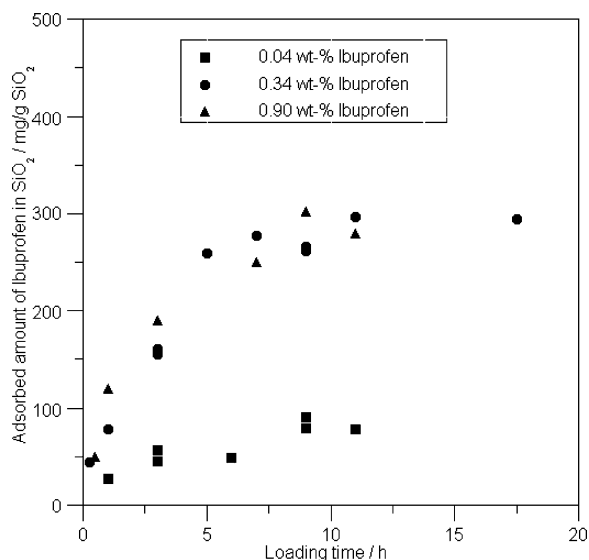


Fig. 1 Loading capacity of Ibuprofen in mesoporous SiO₂ at three different amounts of Ibuprofen in CO₂ (l) at 20 °C and 55 bar, vs loading time.

where the adsorbed amount of Ibuprofen in the particles were measured by TGA. The loading time and concentration of Ibuprofen in the CO₂ (l) was varied in the experiments and each experiment is represented by one point in the graph in Fig. 1. Three different amounts of Ibuprofen in 200 ml CO₂ (l) were evaluated: one giving a concentration *below* the solubility limit (0.04 wt-%) and two amounts with an excess of Ibuprofen present (undissolved) in the CO₂ (l) (nominal concentrations: 0.34 wt-% and 0.90 wt-%).

Firstly, as can be seen from Fig. 1, several hours (7–12 h) seems to be needed to reach the maximum (equilibrium-) loading level, both in the experiments at low and at higher concentrations of Ibuprofen. At least two factors may be relevant for influencing the time to reach the equilibrium: i) time for dissolution and ii) diffusion of dissolved Ibuprofen into the particles. As the dissolution of Ibuprofen in the solvent appeared to be very fast, as observed when performing the above solubility tests, we conclude that Ibuprofen diffusion, and not Ibuprofen dissolution, is the rate-limiting step for loading of the mesoporous particles in this system.

Secondly, a difference in maximum loaded amount was observed depending on whether the solution was saturated with Ibuprofen—which resulted in a high loading, close to 300 mg Ibuprofen/g SiO₂—or if the concentration of Ibuprofen was below this level, which then gave a much lower loading, see Fig. 1.

Similar experiments were performed by using 0.34 wt-% Ibuprofen in CO₂ (l) and a cosolvent (5 mol-%), as shown in Fig. 2. However, the addition of a cosolvent did not improve the maximum adsorbed amount of Ibuprofen in the mesoporous particles. On the contrary, using cyclohexane resulted in a slight decrease in the adsorbed amount compared to pure CO₂ (l). The maximum value in the case of CO₂ (l) + cyclohexane was approximately 200 mg Ibuprofen/g SiO₂, compared to 300 mg Ibuprofen/g SiO₂ that was obtained using only CO₂ (l). For acetone and methanol as cosolvents, a large decrease of the adsorbed amount of Ibuprofen in the mesoporous particles

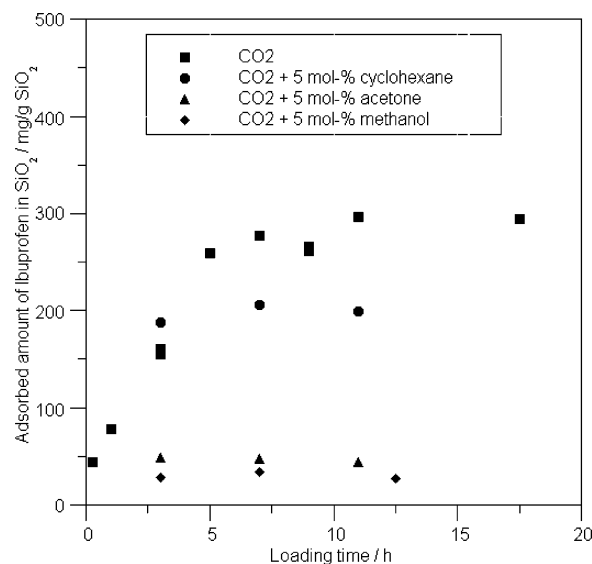


Fig. 2 Loading capacity of Ibuprofen in mesoporous SiO₂ in CO₂ (l) and CO₂ (l) + 5 mol-% cosolvent (cyclohexane, acetone or methanol), vs loading time (theoretical Ibuprofen amount in the solvent/-s 0.34 wt-%).

was observed. Only approximately 50 mg Ibuprofen/g SiO₂ was loaded into the particles in both cases.

It is interesting to note that the adsorbed amount of Ibuprofen in the SiO₂ pores is orders of magnitude higher (300 times higher for 0.04 wt-% Ibuprofen in CO₂ (l)) than if only Ibuprofen would have been deposited into the SiO₂ pores by evaporation of the solvents with dissolved Ibuprofen. The mechanisms for enrichment of Ibuprofen in the pores can be explained by two factors; i) the ability/nonability of the solvent to form hydrogen bondings with silanol groups on the walls of the silica surface and ii) a solvophobic effect.

Ibuprofen has a carboxyl group which can form a hydrogen bond with silanol groups in the mesoporous particles, hence there is a competition between Ibuprofen and solvents that have the ability to form hydrogen bonds with the silica surface. The hydrogen-bonding cosolvents that were used in this study were methanol and acetone. Apart from the effect of hydrogen bonding, these cosolvents are smaller molecules and present in a larger amount than Ibuprofen and they will hinder Ibuprofen adsorption in the SiO₂ pores. The nonhydrogen-bonding cosolvent used was cyclohexane and in this system the loading of Ibuprofen was found to be similar to the loading in only CO₂ (l).

A solvophobic effect will also contribute to enrichment of Ibuprofen in the mesoporous silica if the impregnation is performed in solvents, such as CO₂ (l) and cyclohexane where the solubility of Ibuprofen is low. When a more polar cosolvent (= higher solubility parameter) is added to the solution, the solubility of Ibuprofen increases and there is a smaller driving force for the substance to enter the pores (in other words there is a smaller tendency of Ibuprofen to leave the solvent and absorb at the hydrogen binding sites in the SiO₂). Liquid carbon dioxide has a much lower solubility parameter (approximately 12 MPa^{1/2}) than the cosolvents used within this study and is therefore a very nonpolar solvent (= a low amount of Ibuprofen is dissolved).⁸ Of the solvents evaluated the solubility

of Ibuprofen was also found to be lowest in CO₂ (l) as can be seen in Table 2.

The maximum adsorbed amount of Ibuprofen in the mesoporous particles using liquid carbon dioxide are well comparable to other studies in the literature where different organic solvents have been used as a solvent. Studies using hexane as a solvent reports 300 mg Ibuprofen/g SiO₂ in one report and 590 mg Ibuprofen/g SiO₂ in another report.^{3,5} A study using cyclohexane as the solvent reports 250 mg Ibuprofen/g SiO₂.⁶ Furthermore, in a study where solvents with the ability to form hydrogen bonds with the mesoporous silica were used, a lower loading of Ibuprofen in the pores was observed (DMA = 0 mg/g, DMSO = 25.5 mg/g, DMF = 47 mg/g and ethanol = 184 mg/g) in comparison to using hexane as the solvent.⁵ The Ibuprofen concentration in the solvents in this study were 6.5 wt-%. The results from this study are in agreement with our findings of loading experiments performed in CO₂ and a hydrogen bonding cosolvent.

Even though the results are well comparable to similar experiments using hexane or cyclohexane as the solvent, the pores of the mesoporous material are not completely filled. The maximum theoretical amount of Ibuprofen adsorbed in the mesoporous material is 880 mg/g from calculations using the crystal density of Ibuprofen.⁹ The difference between the experimental value and the theoretical value can be explained by the fact that Ibuprofen molecules do not have the possibility to pack as efficiently in the pores as expected from the crystal density. We know (see below) that the packing arrangement of Ibuprofen in the pores is not crystalline. Also, some of the pores may be blocked by other Ibuprofen molecules, hindering new molecules to enter the pore.

In addition, it was necessary to confirm whether Ibuprofen is adsorbed into the pores of SiO₂ or whether it possibly could simply be adsorbed at the outer surface of the particles. This was done by comparing the TGA curves for pure Ibuprofen and Ibuprofen loaded into SiO₂. Pure Ibuprofen showed an onset temperature in the curve at 180 °C, while the onset temperature for Ibuprofen in the mesoporous SiO₂ was at a higher temperature (350 °C). When going from low to high loading concentrations of Ibuprofen in the mesoporous SiO₂, the curve from TGA changed from a sharp transition point for the onset temperature (at 350 °C) to a smooth transition point (starting already at 180 °C) for the onset temperature. The smooth transition in the TGA curve indicates that Ibuprofen molecules present on the outside of the particle are evaporated at a lower temperature (similar to the observed evaporation temperature for pure Ibuprofen) as compared to molecules present in the pores. This difference can be understood in terms of the restriction of molecular motion of Ibuprofen in the pores in combination with the attractive forces between the pore wall and the Ibuprofen molecule. Effectively, this leads to a lower vapor pressure of Ibuprofen when present in the pores and, hence, to a higher evaporation temperature. The above results suggest that Ibuprofen was also present on the outside of the particles at a high degree of loading in the mesoporous SiO₂. To further investigate this, two different analytical techniques were used, (see below).

Samples were prepared for XRPD and the diffractograms are shown in Fig. 3. The mesoporous particles have three

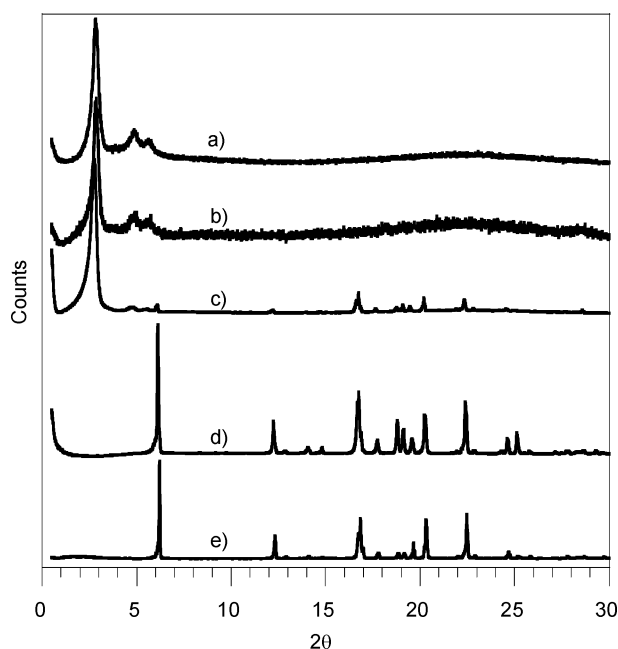


Fig. 3 XRPD measurements of a) mesoporous SiO₂, b) 177 mg Ibuprofen/g SiO₂ loaded in CO₂ (l), c) 150 mg Ibuprofen/g SiO₂, crystalline powder physically mixed with mesoporous SiO₂, d) Ibuprofen treated in CO₂ (l) and e) Ibuprofen.

specific peaks in the lower part of the measured 2θ range, while pure Ibuprofen crystalline powder has several peaks at various positions along the diffractogram. When particles that were loaded with Ibuprofen (177 mg Ibuprofen/g SiO₂) were analyzed, the diffractogram was similar to the diffractogram for the mesostructured particles, e.g., the material was amorphous, see Fig. 3b. On the other hand, the diffractogram for a physical mixture of Ibuprofen and mesoporous SiO₂ in a relevant ratio (150 mg Ibuprofen/g SiO₂, mortared with the particles) showed the typical XRPD powder pattern of Ibuprofen, see Fig. 3c. For all samples with mesoporous SiO₂ the strongest peak from SiO₂ was used as an internal standard for easier comparison of the different samples. The intensities of these diffractograms were normalized so that the strongest peak from the SiO₂ was equally strong in each diffractogram.

Due to the narrow pore diameter (2.5 nm) in the mesoporous material it is not possible for Ibuprofen (1 nm long) to crystallize within the pores. According to ref. 10, substances in pores can form a crystalline structure if the average pore diameter is 20 times larger than the molecular dimensions of the substance itself, which is not the case for our particles.¹⁰ For Ibuprofen this would correspond to a pore diameter of the mesoporous silica larger than 20 nm. However, if all Ibuprofen molecules were present outside of the pores, and in crystalline form, the material would have given rise to XRPD peaks similar to the ones obtained for the sample where SiO₂ and Ibuprofen were mortared together (Fig. 3c). In order to verify that Ibuprofen would precipitate in the crystalline state, Ibuprofen was dissolved in CO₂ (l) and subsequent precipitated after evaporation of the solvent. The obtained material was thereafter analyzed with XRPD and it was found that the formed material was in its crystalline form, as expected (Fig. 3d). Therefore, if all

Ibuprofen would have been deposited outside the mesoporous SiO₂ after loading in CO₂ (*l*) there would have been peaks from crystalline Ibuprofen in the XRPD diffractogram. Hence, it is possible to conclude that Ibuprofen has been loaded into the pores in amorphous form when CO₂ (*l*) (without/with cosolvents) has been used as the solvent. Naturally, also a thin layer of Ibuprofen will be covering the outer surface of the particles.

Confocal Raman microscopy was also employed to obtain a spectrum from the surface and in the centre of a mesoporous particle loaded with Ibuprofen. The spectra are shown in Fig. 4, where also the spectrum of pure Ibuprofen is included as a reference. Clearly, there is Ibuprofen at the surface and in the centre of the particle. No statistics were obtained for the Raman spectra but the results are in good agreement with the results from XRPD and SEM.

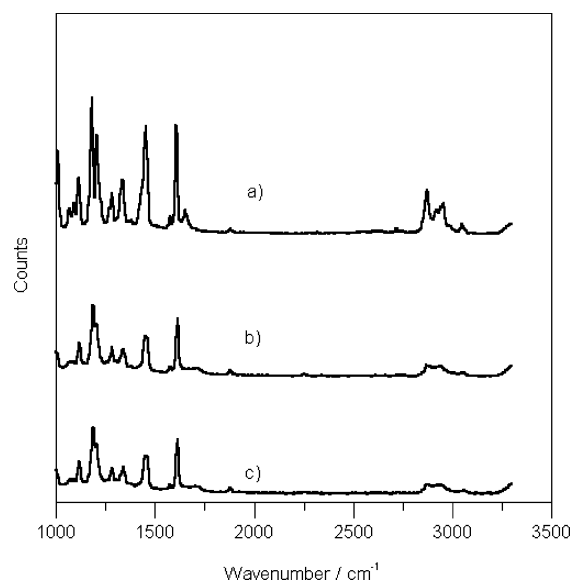


Fig. 4 Raman spectra of a) Ibuprofen, b) the surface of a mesoporous SiO₂ particle loaded with Ibuprofen (140 mg/g) in CO₂ (*l*) and c) the centre of the same particle. Note that the analysis depth is ca 500 nm.

To further verify the fact that no large Ibuprofen particles were deposited on the outside of the particles, SEM studies were carried out. The size of Ibuprofen powder after mortaring was approximately 20–50 μm and lower magnifications SEM micrographs (not shown) of samples with Ibuprofen and mesoporous silica after loading of Ibuprofen did not reveal any large Ibuprofen flakes in the sample. The particles (see Fig. 5) have

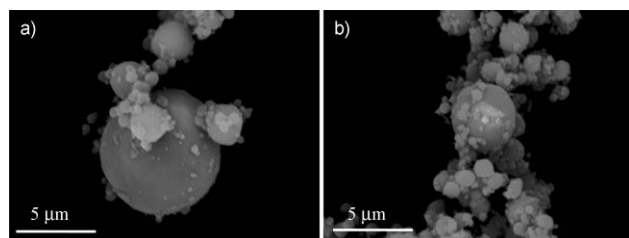


Fig. 5 SEM-images of a) mesoporous SiO₂ and b) Ibuprofen loaded in mesoporous SiO₂ (177 mg Ibuprofen/g SiO₂) in CO₂ (*l*). No Ibuprofen flakes were visible outside the mesoporous SiO₂ in b).

a similar morphology before and after the loading in CO₂ (*l*) which is an additional proof that Ibuprofen has entered inside the pores and without distorting the shape of the mesoporous silica particles.

Conclusions

The solubility of Ibuprofen in CO₂ (*l*) is low (0.20–0.25 wt %), but despite this, a high loading capacity of Ibuprofen into the mesostructured silica (300 mg Ibuprofen/g SiO₂) can be achieved by exposing mesoporous silica particles to a saturated solution of Ibuprofen for several hours (7–12 h).

On the other hand, when introducing a more polar cosolvent to liquid carbon dioxide, more Ibuprofen is dissolved. This results in a lower loading capacity of Ibuprofen into the pores than when using CO₂ (*l*) alone. In cases where the cosolvent can form hydrogen bonds with mesoporous material there will be a competition between the cosolvent and Ibuprofen to adsorb on the SiO₂ surface. This will result in a lowering of the loading capacity of Ibuprofen, at the conditions studied in this article, where the cosolvents were present in much higher concentration than Ibuprofen, and were also smaller in size (quicker diffusion).

Moreover it has been shown by using XRPD that the loaded Ibuprofen molecules are in an amorphous state, most likely due to the fact that the pores in the mesoporous silica are too narrow for crystallization of Ibuprofen to occur.

Finally, this study has also shown the potential of using CO₂ (*l*) for loading of Ibuprofen into mesoporous SiO₂ in the near-critical region, avoiding the use of supercritical CO₂, which would require a more energy-intensive process.

Acknowledgements

The Swedish Knowledge Foundation and Linde Gas/AGA AB are thanked for financial support of this research. Malin Sörensen at YKI is thanked for providing the mesoporous silica material.

Notes and references

- 1 C. T. Kresge, M. E. Leonowicz, W. J. Roth, J. C. Vartuli and J. S. Beck, *Nature (London, United Kingdom)*, 1992, **359**, 710–712;
- 2 J. S. Beck, J. C. Vartuli, W. J. Roth, M. E. Leonowicz, C. T. Kresge, K. D. Schmitt, C. T. W. Chu, D. H. Olson and E. W. Sheppard, and *et al.*, *J Am Chem Soc*, 1992, **114**, 10834–10843;
- 3 A. Taguchi and F. Schueth, *Microporous Mesoporous Mater.*, 2004, **77**, 1–45;
- 4 X. Feng, G. E. Fryxell, L. Q. Wang, A. Y. Kim, J. Liu and K. M. Kemner, *Science (Washington, D. C.)*, 1997, **276**, 923–926;
- 5 A. Bibby and L. Mercier, *Green Chemistry*, 2003, **5**, 15–19.
- 6 N. Andersson, P. C. A. Alberius, J. Skov Pedersen and L. Bergstroem, *Microporous Mesoporous Mater.*, 2004, **72**, 175–183.
- 7 M. Vallet-Regi, A. Ramila, R. P. del Real and J. Perez-Pariente, *Chem Mater*, 2001, **13**, 308–311.
- 8 T. Azaies, C. Tourne-Peteilh, F. Aussenac, N. Baccile, C. Coelho, J.-M. Devoisselle and F. Babonneau, *Chem Mater*, 2006, **18**, 6382–6390;
- 9 T. Heikkilae, J. Salonen, J. Tuura, M. S. Hamdy, G. Mul, N. Kumar, T. Salmi, D. Y. Murzin, L. Laitinen, A. M. Kaukonen, J. Hirvonen and V. P. Lehto, *Int J Pharm*, 2007, **331**, 133–138;
- 10 J. Andersson, J. Rosenholm, S. Areva and M. Linden, *Chem Mater*, 2004, **16**, 4160–4167.

-
- 5 C. Charnay, S. Begu, C. Tourne-Peteilh, L. Nicole, D. A. Lerner and J. M. Devoisselle, *European Journal of Pharmaceutics and Biopharmaceutics*, 2004, **57**, 533–540.
- 6 M. H. Sørensen, Y. Samoshina, P. M. Claesson and P. C. A. Alberius, *J. Dispersion Sci. Technol.*, 2009, **30**, 6.
- 7 H. M. Woods, M. M. C. G. Silva, C. Nouvel, K. M. Shakesheff and S. M. Howdle, *J Mater Chem*, 2004, **14**, 1663–1678; O. R. Davies, A. L. Lewis, M. J. Whitaker, H. Tai, K. M. Shakesheff and S. M. Howdle, *Adv. Drug Delivery Rev.*, 2008, **60**, 373–387.
- 8 S. R. Allada, *Ind. Eng. Chem. Proc. Des. Dev.*, 1984, **23**, 344–348.
- 9 N. Shankland, C. C. Wilson, A. J. Florence and P. J. Cox, *Acta Crystallographica, Section C Crystal Structure Communications*, 1997, **C53**, 951–954.
- 10 M. Sliwinska-Bartkowiak, G. Dudziak, R. Gras, R. Sikorski, R. Radhakrishnan and K. E. Gubbins, *Colloids Surf. A: Physicochemical and Engineering Aspects*, 2001, **187–188**, 523–529.
- 11 J. Brandrup and E. Immergut, *Polymer Handbook, Third Edition*, John Wiley & Sons, New York, 1989.

Pressurized liquid extraction of betulin and antioxidants from birch bark†

Michelle Co,^a Pirjo Koskela,^a Peter Eklund-Åkergrén,^a Keerthi Srinivas,^b Jerry W. King,^b Per J. R. Sjöberg^a and Charlotta Turner^{*a}

Received 10th November 2008, Accepted 3rd April 2009

First published as an Advance Article on the web 17th April 2009

DOI: 10.1039/b819965e

Pressurized hot (subcritical) water and ethanol were used to extract betulin and antioxidants from birch bark. Betulin was found to be the major compound (around 26% (w/w)), which was able to be extracted with ethanol (120 °C, 50 bar, 15 minutes) but not with water at any of the temperatures tested (40–180 °C, 50 bar). The obtained extraction result for betulin is supported by theoretical solvation parameter calculations. Furthermore, high antioxidant activity of the extract was obtained using both ethanol and water as solvent. The antioxidant activity, as determined by a DPPH (2,2-diphenyl-1-picrylhydrazyl) assay, was found to be highest for the water extract of finely ground bark and it markedly increased with elevated extraction temperatures (90–180 °C). To elucidate if this was due to increased extraction efficiency or chemical reactions, a set of experiments was performed in which the samples were pre-treated with water at different temperatures before extraction. Results from liquid chromatography showed some differences in molecular composition between samples pre-treated at ambient and 180 °C, respectively. However, more detailed studies have to be performed to distinguish between hot-water extraction and reaction kinetics.

Introduction

Daily, tons of different kind of wastes are mounting high in the backyard of the forestry¹ and agricultural industries, which are being discarded or used as an energy source.² For example, a Swedish paper pulp industry, Skutskär Stora Enso, has about 750 tonnes of bark waste daily. Bark from trees has always been of interest as a source of drugs against minor and severe ailments. Over the last decade, scientists have been intrigued by the chemicals in birch bark, and both biological and medical studies have been performed on birch bark extracts. Like many tree barks, birch bark contains secondary metabolites, such as triterpenoids and their derivatives,³ which have shown positive effects as anti-cancer,⁴ anti-HIV,^{4,5} anti-inflammatory⁶ and anti-microbial agents.⁷ Thus, birch bark compounds could be valuable in applications such as food additives to prevent or delay oxidative degradation or as potential drugs. The range of biologically-active compounds in trees depends on which season they are harvested and geographical location,^{8,9} which should be taken into account prior to analyzing the obtained results. Birch bark has already been utilized in the cosmetic industry for years, and recently clinical tests have been carried out to explore which

compounds in birch bark can be used as drugs to treat or prevent certain lines of cancer.¹⁰

Betulin (lup-20(29)-ene-3,28-diol) (Fig. 1) is a secondary metabolite and the major compound in birch bark.¹¹ Its chemical and biological properties have been well characterized, revealing activity toward diseases such as cancers,¹² HIV,¹³ and fungal infections.¹⁴ Betulin is easily transformed to betulinic acid, which is an even more active substance with regard to the treatment of cancers.¹⁴

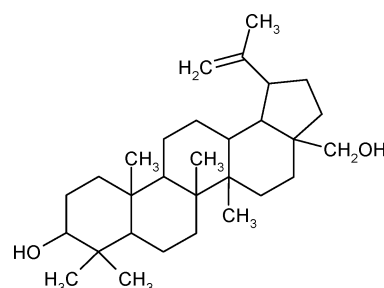


Fig. 1 The chemical structure of betulin ($M_w = 442.72 \text{ g mol}^{-1}$).

Birch bark is known for its antioxidant activity.^{9,15,16} Antioxidants are defined as substances that, even at low concentration, significantly delay or prevent oxidation of easily oxidizable substrates.¹⁷ Synthetic antioxidants such as butylated hydroxyanisole (BHA), butylated hydroxytoluene (BHT) and *tert*-butylhydroquinone (TBHQ) are commonly used in food industries to prevent or delay oxidative degradation. However, accumulation of synthetic antioxidants in the body can cause severe liver damage and give rise to carcinogenic effects.¹⁸ During recent years, natural sources of antioxidants have been studied to replace the synthetic ones.¹⁹ Extraction of antioxidative

^aAnalytical Chemistry Group, Department of Physical and Analytical Chemistry, Uppsala University, P.O. Box 599, SE-75124, Uppsala, Sweden. E-mail: charlotta.turner@kemi.uu.se; Tel: +46 18 471 3681

^bCritical Fluids Technology & Separations Laboratory, Department of Chemical Engineering, University of Arkansas, 3202 Bell Engineering Center, Fayetteville, AR, 72701, USA

† This paper was published as part of the themed issue of contributions from the Green Solvents – Progress in Science and Application conference held in Friedrichshafen, September 2008.

compounds from birch bark, especially if low-toxicity solvents are used, could potentially be an ecologically and economically efficient way to increase the value of this voluminous biomass waste.

Traditional extraction techniques have been applied for small organic molecules such as betulin and antioxidant compounds mainly using methanol as a solvent. However, the extraction process is usually time consuming and tedious.²⁰ Hence, it would be desirable to replace this with more environmentally sustainable “green” extraction techniques. Pressurized liquid extraction (PLE) is an extraction technique that utilizes elevated temperatures and pressures to extract the target components from a sample matrix.^{21,22} By using a liquid solvent at temperatures and pressures above its boiling point, the extraction process becomes more efficient due to faster diffusion rates, higher thermal energy and solvent strength, as well as lower viscosity and surface tension, compared to using the same solvent at ambient temperature. This implies that extraction times can be significantly shortened and solvent volume reduced. Furthermore, the solvent strength can easily be changed by varying the temperature.

The aim of this study was to optimize the extraction efficiency of both betulin and antioxidative compounds in birch bark using water and ethanol as “sustainable” solvents. The importance of extraction temperature, extraction time and sample pre-treatment was investigated.

Results and discussion

Betulin extraction

In this study, water and ethanol were chosen as potential extraction solvents.²³ When the temperature of water and ethanol is increased under constant pressure, their respective dielectric constants decrease, thereby reducing their polarity as extraction solvents. These polarity changes are more pronounced for water than for ethanol, which only shows minor changes. For example, liquid water's dielectric constant decreases from 80 to 38 as its temperature is increased from 25 to 180 °C. This results in water exhibiting a dielectric constant similar to that of methanol and ethanol at ambient temperature.²⁴ Hence, it seemed reasonable that both ethanol and water at elevated temperature and pressure should work as good solvents for betulin, since conventional methods are based on methanol at ambient temperature.

An experimental design was used to optimize the pressurized liquid extraction method, *i.e.* the temperature and the extraction time were varied as described in the Experimental. When using ethanol as a solvent, the extracted amount of betulin is mostly influenced by the temperature, showing an increase up to 120 °C and then it reached a plateau (Fig. 2). Furthermore, the results indicate that the number of extraction cycles has a low influence on the amount of extracted betulin, at least at the highest temperature tested. Those findings are further supported by statistical calculations from the response surface design (Table 1). The *p*-values show that the change in temperature caused significant differences and the number of 5 min extraction cycles did not, within the range investigated. The design was able to explain 84% of the variation.

Despite the similar dielectric constant for water at 180 °C and methanol at ambient temperature, no detectable amount

Table 1 Effect of temperature and number of extraction cycles using pressurized hot ethanol for betulin extraction^a

Factor	Coefficient	<i>t</i> -test	<i>p</i> -value
<i>T</i>	7.378	6.531	0.001
<i>C</i>	2.555	2.261	n.s.
<i>T</i> × <i>T</i>	−5.802	−3.424	0.014
<i>C</i> × <i>C</i>	0.283	0.167	n.s.
<i>T</i> × <i>C</i>	−1.925	−1.391	n.s.

^a SD = 2.767, *R*-Square adjusted (%) = 83.9, n.s. = not significant; *T* = temperature; *C* = cycles.

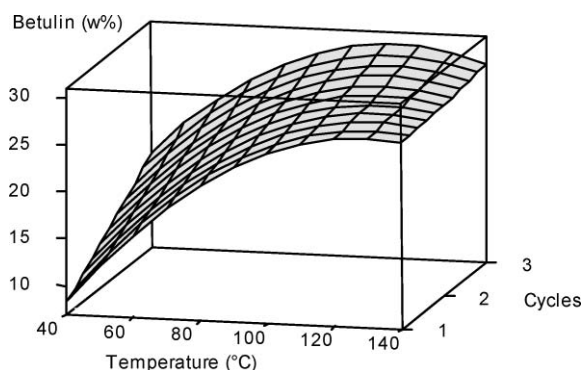


Fig. 2 A response surface plot showing betulin amount extracted (wt% of the bark) versus extraction temperature (°C) and number of 5 min extraction cycles using ethanol as a solvent.

of betulin was extracted when using water as a solvent at any of the temperatures investigated (80–180 °C). Hence, not surprisingly, the dielectric constant is only an approximate measure of the solvation properties. For this reason, we have calculated and utilized the solubility parameter concept²⁵ to better estimate the relative solubility of betulin in hot water and ethanol, and thereby rationalize the observed extraction results. Fig. 3 shows the relative solubility parameter as a function of temperature for betulin, water and ethanol. For both solvents, there is a gradual decrease in their respective solubility parameter with increasing temperature, while betulin's solubility parameter decreases to a lesser degree. This decrease in their respective solubility parameters is a reflection of the overall loss of the cohesive energy density of the components, and particularly their hydrogen bonding properties²⁶ As shown

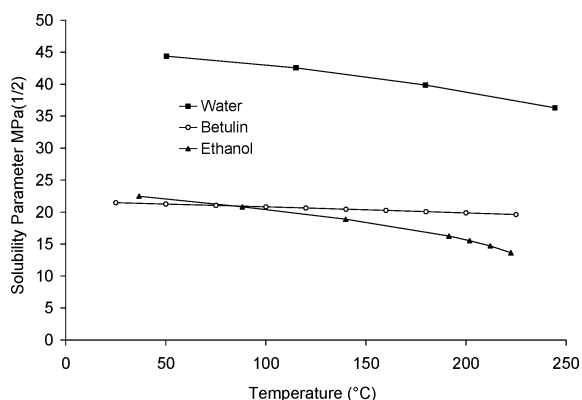


Fig. 3 Solubility parameters (MPa^(1/2)) as a function of temperature (°C) for betulin, ethanol and water.

in Fig. 3, the solubility parameter curves for ethanol and betulin are fairly close, indicating mutual miscibility and higher solubility than would be expected in the water–betulin case. As a rule of thumb, the differences between the curves should be a maximum of around four units to obtain miscibility.²⁵ Hence, these theoretical data confirm our results, where betulin was not extracted using water as a solvent. The solubility parameters for betulin and ethanol intersect theoretically at approximately 90 °C, a temperature which should be favorable for the extraction of betulin from birch bark. This temperature is not far from the experimentally obtained optimal temperature (120 °C). An explanation for the slightly higher temperature required for the extraction is that a higher temperature will help in disrupting the sample matrix and desorb the analytes, as well as give faster diffusion rates of the analytes from the matrix.

In summary, the obtained results show that the optimal parameters for extracting betulin from birch bark are ethanol at 120 °C, 50 bar, two 5 min extraction cycles and a preheating step of 5 minutes. A total extraction time of 15 minutes results in a betulin content of 20–30% (w/w) depending on type of birch bark, which corresponds well with data in the literature.²⁷

Antioxidant activity

Fig. 4 shows a chromatogram for a birch bark ethanol extract. The main compound in the ethanol extract, eluted at 13.2 minutes, corresponds to betulin. As can be seen, a number of other peaks are also visible in the chromatogram monitored at 209 nm, of which some could possibly be antioxidants. One of our overall goals is to extract valuable compounds that can be retrieved from different biomass waste sources. Antioxidants are an example of such a class of compounds. A commonly used assay for measuring antioxidant activity in plant extracts is the DPPH (2,2-diphenyl-1-picrylhydrazyl) radical scavenging method,^{28,29} which was also used in this study.

An experimental design was applied using ethanol and water at temperatures of 80, 130 and 180 °C to extract antioxidative compounds from birch bark. Results indicated significant antioxidant activity in both ethanol and water extracts, measured as EC₅₀ values (µg bark/µg DPPH). A lower EC₅₀ value indicates a higher antioxidant activity. A general trend was observed, showing higher antioxidant activity with increased extraction temperature for both ethanol and water as extraction solvent (Fig. 5). The number of extraction cycles (*i.e.* extraction time 5, 10 or 15 minutes) has less influence (data not shown). Pure betulin did not demonstrate any significant antioxidant activity.

Sample size and extraction efficiency

To gain more insight about how the particle size of birch bark affects the yield of antioxidants, a set of experiments was conducted using long bark slices (11 cm × 1 cm), square pieces (1 cm × 1 cm) as well as finely ground bark. The respective samples were put into extraction cells, and ethanol was used as a solvent at 130 °C. As expected, the antioxidant activity was highest in the sample extracts from finely ground bark (Table 2). This increase in extraction efficiency is probably due to the higher sample surface area giving shorter diffusion paths.

Table 2 Effect of sample particle size on antioxidant activity found in extracts from inner and outer layers of birch bark. Ethanol was the extraction solvent and the extraction conditions were 130 °C, 50 bar and an extraction time of 3 × 5 min

Experiment # (n = 3)	Birch layer type	Particle size	EC ₅₀ value (µg bark/µg DPPH)	RSD (%)
1	Inner	Squares	57	8
2	Inner	Finely ground	37	6
3	Outer	Long slices	9	9
4	Outer	Finely ground	5	15

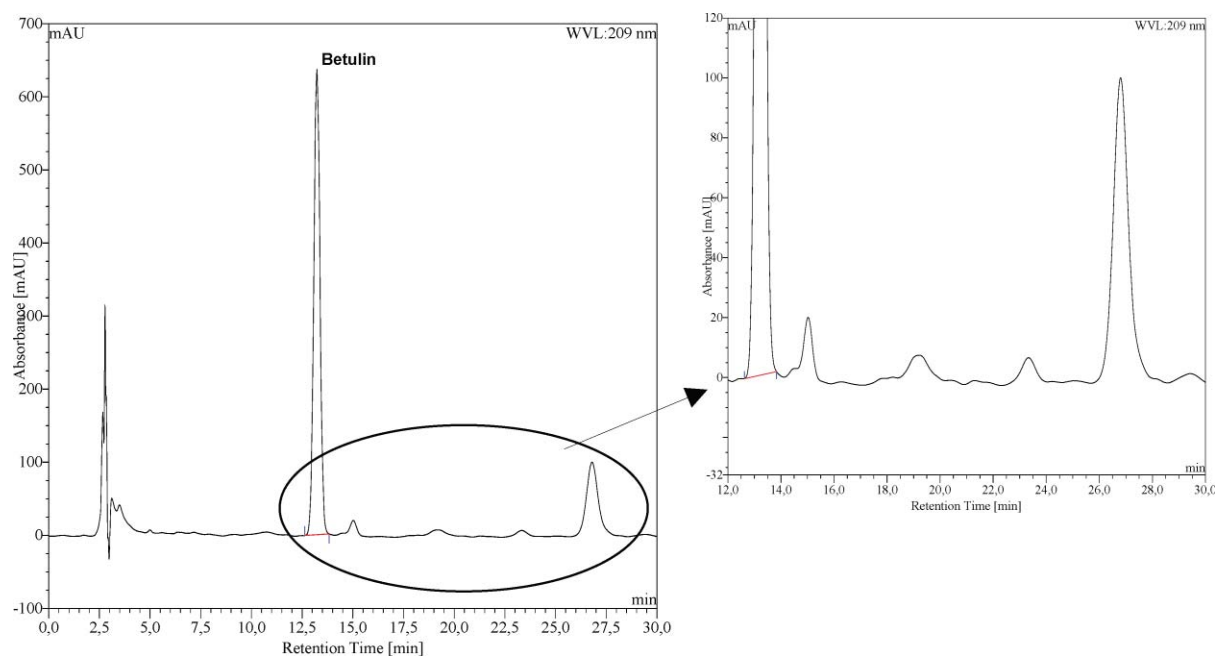


Fig. 4 A chromatogram of an ethanol extract of birch bark. In the inset a number of minor components are shown.

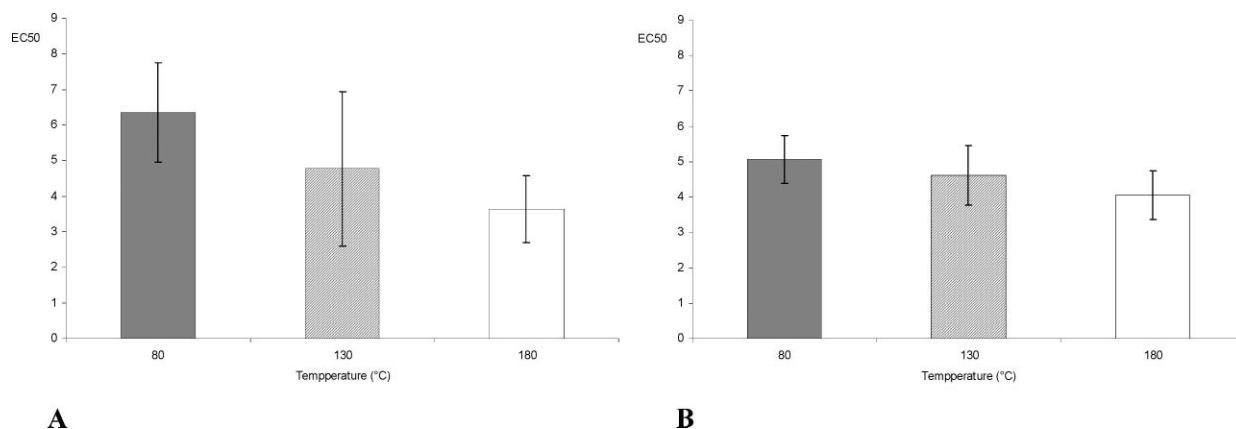


Fig. 5 Histogram showing EC_{50} values versus extraction temperature, for ethanol (A) and water (B) as extraction solvents, respectively (grey = 80 °C, stripes = 130 °C and white = 180 °C). Error bars = \pm RSD (%) and $n = 6$.

However, exposing the sample more to the air might degrade the antioxidants, hence it is advisable to perform the extraction soon after grinding the sample.

In general, a higher antioxidant activity is expected in samples that are more colorful. The inner layer of birch bark has a brown reddish color, and it could therefore be assumed to have higher antioxidant activity compared to the outmost layer, which is white. In order to verify this assumption, slices of bark pieces were divided into inner (soft, red) and outer (more tough, white) prior to extraction. Surprisingly, the results in Table 2 show that the outmost layer of the birch bark contains more antioxidants than the inner layer. The high antioxidant activity in the outmost layer of birch bark might have the function to protect the tree from herbivore and parasite attacks. Furthermore, it is important to keep in consideration that different species of trees hold different amounts and kinds of antioxidative compounds. In some other tree species, higher antioxidant activity has been found in the inner layer of bark.^{30,31}

Stability of the antioxidants during extraction

In general, antioxidants in plants are polyphenols, and they have proved to be antioxidants in many studies. An important question to pose is if the antioxidants are stable in the extraction solvent during the extraction at high temperatures. As shown in Fig. 5, the antioxidant activity increases continuously with increasing extraction temperature (EC_{50} values decrease). This observed result could be rationalized with higher concentration (*i.e.* yield) of antioxidants being extracted as the extraction temperature is increased, and/or with a temperature-induced chemical reaction that produces additional compounds exhibiting higher antioxidant activity. For instance, by hydrolyzing glycoside molecules, hydroxyl groups are made available that may result in a higher antioxidant capacity of the molecules.³²

To investigate these possibilities, pre-treatment of samples was performed prior to extraction with water at 80 or 180 °C, respectively. The results were compared with those obtained for samples that were pre-treated with water at ambient temperature.

The antioxidant activity was found to be highest in extracts obtained after pre-treating the samples at 180 °C (see Table 3). Unfortunately, the results are inconclusive. The increased an-

Table 3 Comparison of EC_{50} values of extracts using different pre-treatment methods prior to extraction

Experiment # ($n = 3$)	Pre-treatment temperature/°C	Extraction temperature/°C	EC_{50} value (μg bark/ μg DPPH)	RSD (%)
1	ambient	80	93	12
2	ambient	180	16	9
3	180	80	14	11
4	180	180	2	20

tiioxidant activity in the samples that have been pre-treated with water at 180 °C could be a result of water being quite efficient in removing antioxidants from the sample matrix into the extraction solvent. The following cooling of the samples to ambient temperature probably only resulted in some of the extracted compounds being precipitated onto the sample matrix surface, thus making them easier to extract compared to from their original location inside the sample matrix. Hence, a more detailed study of chromatography data was undertaken.

Chromatograms were recorded at 300 nm (Fig. 6), since polyphenols have their maximum absorbance around this wavelength. Results for the differently pre-treated samples revealed that there were compounds appearing only, or in relatively higher abundance, in extracts from samples pre-treated at 180 °C (marked with *). These peaks could, to some extent, be explained by chemical reactions taking place during the pre-treatment, since these peaks were not found (or were in lower abundance) in the samples pre-treated at ambient temperature and then extracted at 180 °C. There were also some peaks of higher relative abundances in samples pre-treated at ambient temperature (marked with X), which could be compounds that degraded in the high-temperature pre-treated samples.

In conclusion, as far as we know at this point, the best method for extracting antioxidants from birch bark is to use the highest temperature tested, *i.e.* 180 °C, with either ethanol or water as extraction solvent, for 2 cycles of 5 minutes each, plus an initial heat-up time of 8 minutes and 50 bar pressure. However, caution has to be taken with regard to antioxidant degradation during extraction, unless the objective is to produce extracts of as high antioxidant activity as possible.

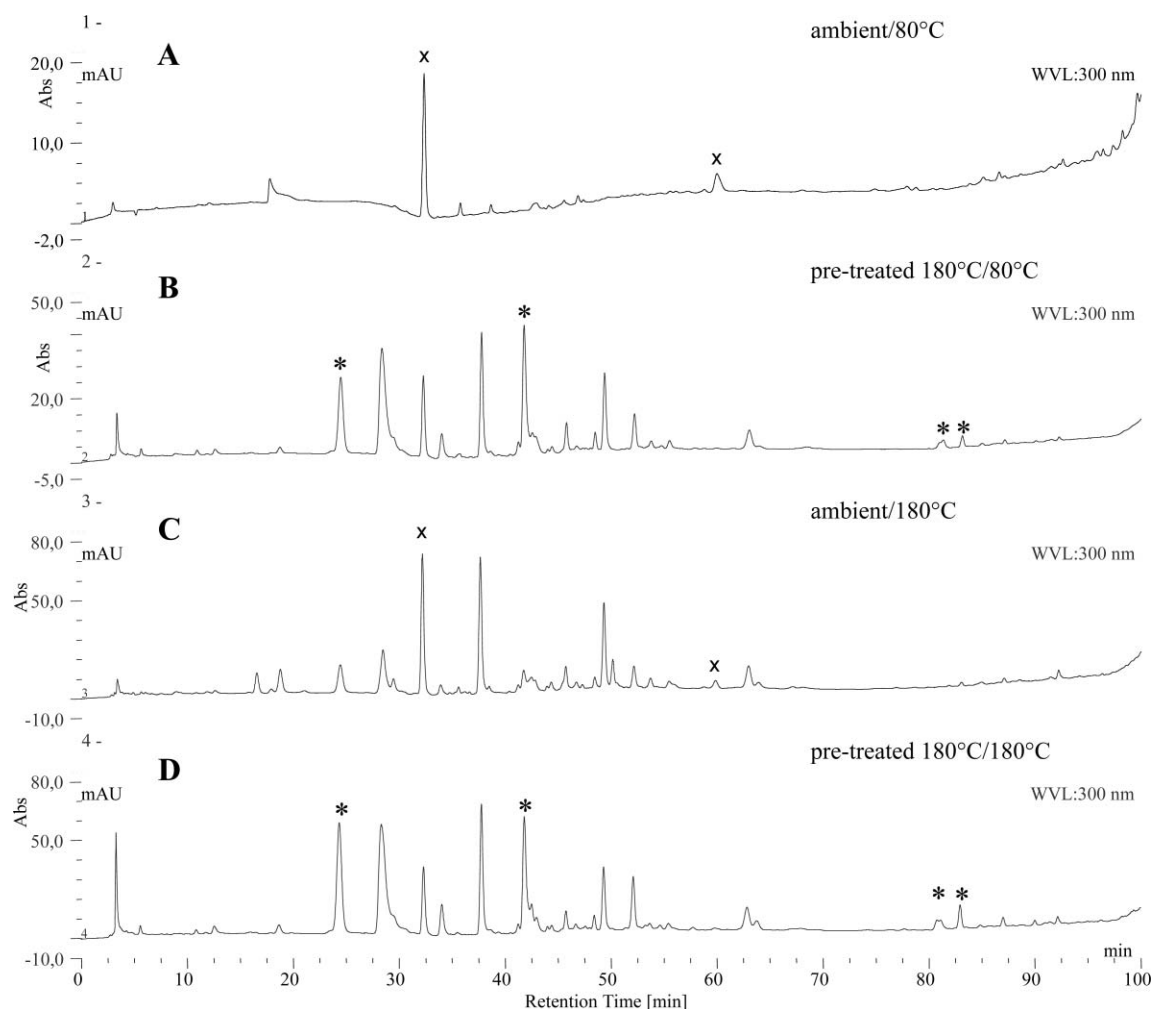


Fig. 6 Chromatograms of pre-treated water extracts at ambient temperature then extracted at 80 °C (A); pre-treated at 180 °C then extracted at 80 °C (B); pre-treated at ambient temperature then extracted at 180 °C (C); pre-treated at 180 °C then extracted at 180 °C (D).

Experimental

Equipment

The extraction procedure was performed in a pressurized liquid extraction system (ASE-200™, Dionex Corporation, Sunnyvale, CA, USA), using 11 ml extraction cells. For extract analysis, a high performance liquid chromatography (HPLC) system from Dionex (Ultimate 3000™) was used with a photodiode array detector. Data was collected and processed with a Chromeleon™ program (Dionex). The antioxidant activity measurements were conducted with an ultraviolet spectrometer (UNICAM 5625 UV/VIS, Cambridge, England).

Chemicals and material

Betulin (98%) standard and 2,2-diphenyl-1-picrylhydrazyl (DPPH, 90%) were purchased from Sigma–Aldrich Chemical Corporation (Madrid, Spain). For HPLC analysis, HPLC-grade methanol solvent (E. Merck, Darmstadt, Germany) was used. For extraction, ethanol (Etax 99.7%) was obtained from Solveco (Rajamäki, Finland) and ultra pure water from a Milli-Q system (Millipore, SA 67180, Molsheim, France).

Birch bark (*Betula pendula* and *Betula pubescens*) was collected in the area around Sundsvall in northern Sweden and in Kalmar in the southeast of Sweden, respectively. Bark samples were dried at ambient temperature before being ground into small particles (0.5–5 mm) with a kitchen grinder. When different layers of the bark were studied, the outer layer was removed by carefully removing the white thin skin. The water content was determined prior to extraction by drying overnight in an oven at 110 °C. The water content in birch bark was found to be around 30% (w/w) for bark collected around Sundsvall and around 40% (w/w) for bark collected in Kalmar. Betulin content was calculated based on dry weight, but antioxidant activity was not.

Experimental design

A response surface design was used in this study to optimize the extraction of betulin and antioxidants. For betulin, the number of extraction cycles was varied between 1, 2 and 3 and the temperature between 40, 90 and 140 °C. For antioxidants determination, the number of extraction cycles was varied between 1, 2 and 3 and the temperature between 80, 130 and 180 °C. The design contained many middle points (>10) to ensure statistical reliability. Further, the design was applied for

both water and ethanol as extraction solvents. Results were considered statistically significant when the *p*-values were below 0.05, *i.e.* 95% confidence level.

Extraction procedure

Approximately 1 g of finely ground birch bark samples (except if otherwise noted) were weighed into 11 ml extraction cells and the extraction temperature was varied between 40 and 180 °C keeping the pressure constant at 50 bar. The number of extraction cycles was varied between 1 and 3, and each cycle was 5 minutes of extraction, whereas the flush volume was kept at 60% (*i.e.* 60% of the extraction solvent in the cell was replaced in-between each extraction cycle with fresh solvent), and with a final purging using nitrogen gas for 2 minutes.

Extraction procedure for stability studies

Birch bark samples (finely ground) with added water were preheated to 180 °C during 15 min (by using the ASE in “manual” mode) followed by “reaction” during 15 min under 50 bar pressure. Thereafter, the extraction cell was cooled to ambient temperature for 4 hours prior to extraction at 80 or 180 °C, respectively. Control samples (pre-treatment at ambient temperature) were processed the same way, except that the oven was not switched on.

Antioxidant activity determination

The EC₅₀ value is calculated from the DPPH assay as the amount of sample that is required to neutralize half of the amount of DPPH initially added.

The antioxidant determination procedure was performed as described by Brand-Williams *et al.*³³ and Herrero *et al.*³⁴ The DPPH free radical is reduced by receiving a hydrogen atom from the antioxidants. A DPPH stock solution (0.30–0.40 mg ml⁻¹) was prepared fresh daily in degassed methanol. The DPPH working solutions used with the extracts were diluted 10 times with degassed methanol from stock solution to a concentration of 30–40 µg ml⁻¹. Different amounts (20, 200 and 400 µl) of extracts were evaporated (Reacti-Therm Heating/Stirring module, Pierce 18971) to dryness before 4 ml of DPPH working solution was added. The DPPH reaction was conducted in darkness at ambient temperature for 4 hours before measuring the absorption at 516 nm. This relatively long reaction time was used to make sure that the end point of the reaction was reached for most of the antioxidants.³³ The blank sample (pure extraction solvent) was treated in the same way as the birch bark extracts.

A graph with a negative slope was obtained with the absorption of the remaining DPPH radical as a function of the extract concentration. From this curve, the amount of birch bark needed to neutralize half the amount of added DPPH was calculated using the equation of the line. EC₅₀ values were calculated as µg bark/µg DPPH.

HPLC separation procedures

Betulin

For betulin analysis, a Waters C18, 150 mm × 3 mm column was used with isocratic separation using 99.8% methanol. The

ultra violet detection was set to 209 nm and the flow rate was 1 ml min⁻¹.

Other compounds

Betulin and other unidentified compounds were detected at 209 nm, on a Gemini 3 µm C6-phenyl column (150 mm × 2.0 mm i.d) using isocratic elution with a mobile phase containing 85% methanol, 15% Millipore water, and 0.1% formic acid. The flow rate was 150 µl min⁻¹.

Pre-treated bark extracts

Gradient separation of water extracts from pre-treated birch bark was performed using the same Gemini C6-phenyl column as above. The mobile phase was Millipore water (A) and methanol (B), both containing 0.1 vol% formic acid, and the flow rate was 100 µl min⁻¹. The detection wavelength was set to 300 nm. Initially, the separation started with an isocratic part, 0–10 min, 1% B; then a linear gradient 10–40 min, 1–35% B; followed by a second isocratic part, 40–65 min, 35% B; a second linear gradient part started, 65–90 min, 35–60% B; and finished with a third isocratic part, 90–100 min, 60% B.

Calculation of the solubility parameter

Initial solubility parameters for the solvents used in this study, pressurized hot water and ethanol, were calculated using the method of Giddings³⁵ based on the law of corresponding states correlation for reduced parameters. The solubility parameter for betulin was calculated using the group contribution method of Fedors³⁶ and corrected for temperature dependence *via* the Jayasri and Yaseen³⁷ homographic approach. Critical property data was estimated by a group contribution using Joback's method³⁸

Conclusions

Pressurized liquid extraction using water or ethanol as solvent provides a gentle, fast, efficient, and environmentally friendly method for the extraction of birch bark. Both betulin and compounds exhibiting antioxidant activity were extracted using hot pressurized ethanol. Ethanol was found to be an appropriate solvent for betulin extractions based on solubility considerations. Extractions conducted for 15 minutes at 50 bar of applied pressure, and at a temperature of around 120 °C, proved highly effective in removing betulin from birch bark. Antioxidative compounds were extracted with both water and ethanol. Further, experiments conducted on ground barks and bark samples having different configurations yielded extracts exhibiting antioxidant activity. Higher temperature resulted in higher antioxidant activity for both ethanol and water, giving an EC₅₀ value of around 4 µg bark/µg DPPH at 180 °C. Preliminary studies showed that pre-treating the bark at either 80 or 180 °C slightly changed the relative abundance of compounds in these extracts compared to in ambient-temperature pre-treated bark extracts, most likely due to accelerated hydrolysis reactions in hot water. However, more research is needed to study extraction and reaction kinetics in pressurized hot water, which should

also include mass spectrometric analyses to identify the different molecular species in the extracts.

Acknowledgements

The Swedish Research Council for Environment, Agricultural Sciences and Spatial Planning (FORMAS, 209-2006-1346); the Swedish Research Council (VR, 2006-4084); the Swedish International Development Cooperation Agency (SIDA, SWE-2005-473) and the Swedish Foundation for Strategic Research (SSF, 2005:0073/13) are greatly acknowledged. Kerstin Sunnerheim and Hans Elofsson are acknowledged for providing birch bark samples.

References

- D. B. Turley, Q. Chaudhry, R. W. Watkins, J. H. Clark and F. E. I. Deswarte, *Ind. Crops Prod.*, 2006, **24**, 238–243.
- A. Ferm, *Biomass Bioenergy*, 1993, **4**, 391–404.
- P. A. Krasutsky, *Nat. Prod. Rep.*, 2006, **23**, 919–942.
- T. G. Tolstikova, I. V. Sorokina, G. A. Tolstikov, A. G. Tolstikov and O. B. Flekhter, *Russ. J. Bioorg. Chem.*, 2006, **32**, 261–276.
- T. G. Tolstikova, I. V. Sorokina, G. A. Tolstikov, A. G. Tolstikov and O. B. Flekhter, *Russ. J. Bioorg. Chem.*, 2006, **32**, 37–49.
- N. I. Pavlova, O. V. Savinova, S. N. Nikolaeva, E. I. Boreko and O. B. Flekhter, *Fitoterapia*, 2003, **74**, 489–492.
- P. Dzubak, M. Hajdich, D. Vydra, A. Hustova, M. Kvasnica, D. Biedermann, L. Markova, M. Urban and J. Sarek, *Nat. Prod. Rep.*, 2006, **23**, 394–411.
- I. Habiaryemye, T. Stevanovic-Janezic, B. Riedl, F. X. Garneau, F. I. Jean and J. Wood, *Chem. Technol.*, 2002, **22**, 83–91.
- E. Hiltunen, T. T. Pakkanen and L. Alvila, *Holzforschung*, 2006, **60**, 519–527.
- M. Urban, J. Sarek, M. Kvasnica, I. Tislerova and M. Hajdich, *J. Nat. Prod.*, 2007, **70**, 526–532.
- S. Alakurtti, T. Mäkelä, S. Koskimies and J. Yli-Kauhaluoma, *Eur. J. Pharm. Sci.*, 2006, **29**, 1–13.
- S. H. Oh, J. E. Choi and S. C. Lim, *Toxicology*, 2006, **220**, 1–12.
- I. C. Sun, J. K. Shen, H. K. Wang, L. M. Cosentino and K. H. Lee, *Bioorg. Med. Chem. Lett.*, 1998, **8**, 1267–1272.
- R. H. Cichewicz and S. A. Kouzi, *Med. Res. Rev.*, 2004, **24**, 90–114.
- S. Burda and W. Oleszek, *J. Agric. Food Chem.*, 2001, **49**, 2774–2779.
- M. P. Kähkönen, A. I. Hopia, H. J. Vuorela, J. P. Rauha, K. Pihlaja, T. S. Kujala and M. Heinonen, *J. Agric. Food Chem.*, 1999, **47**, 3954–3962.
- B. Halliwell, *Free Radical Res.*, 1990, **9**, 1–32.
- N. Ito, M. Hirose, S. Fukushima, H. Tsuda, T. Shirai and M. Tatematsu, *Food Chem. Toxicol.*, 1986, **24**, 1071–1082.
- R. Scherer and H. T. Godoy, *Food Chem.*, 2009, **112**, 654–658.
- R. Julkunen-Tiitto, M. Rousi, J. Bryant, S. Sorsa, M. Keinänen and H. Sikanen, *Trees - Struct. Func.*, 1996, **11**, 16–22.
- I. Rodríguez-Meizoso, F. R. Marin, M. Herrero, F. J. Señorans, G. Reglero, A. Cifuentes and E. Ibáñez, *J. Pharm. Biomed. Anal.*, 2006, **41**, 1560–1565.
- Y. Jiang, S. P. Li, H. T. Chang, Y. T. Wang and P. F. Tu, *J. Chromatogr. A*, 2006, **1108**, 268–272.
- G. L. Zhao and W. D. Yan, *J. Chem. Eng. Data*, 2007, **52**, 2365–2367.
- Y. Yang, M. Belghazi, A. Lagadec, D. J. Miller and S. B. Hawthorne, *J. Chromatogr. A*, 1998, **810**, 149–159.
- C. M. Hansen, *Solubility Parameters—User's Handbook*, CRC Press, Boca Raton, Florida, 2007.
- C. Panayiotou, *Fluid Phase Equilib.*, 1997, **131**, 21–35.
- P. Jaaskelainen, *Pap. Puu-pap. Tim.*, 1981, **63**, 599–603.
- D. J. Huang, B. X. Ou and R. L. Prior, *J. Agric. Food Chem.*, 2005, **53**, 1841–1856.
- M. Ozgen, R. N. Reese, A. Z. Tulio, J. C. Scheerens and A. R. Miller, *J. Agric. Food Chem.*, 2006, **54**, 1151–1157.
- E. Smite, L. N. Lundgren and R. Andersson, *Phytochemistry*, 1993, **32**, 365–369.
- E. Smite, H. Pan and L. N. Lundgren, *Phytochemistry*, 1995, **40**, 341–343.
- R. Briante, F. La Cara, M. P. Tonziello, F. Febbraio and R. Nucci, *J. Agric. Food Chem.*, 2001, **49**, 3198–3203.
- W. Brand-Williams, M. E. Cuvelier and C. Berset, *Food Sci. Technol. (N. Y.)*, 1995, **28**, 25–30.
- M. Herrero, P. J. Martín-Álvarez, F. J. Señorans, A. Cifuentes and E. Ibáñez, *Food Chem.*, 2005, **93**, 417–423.
- J. W. King, K. Srinivas J. M del Valle and J. C de la Fuente, in *The 8th International Symposium on Supercritical Fluids (ISSF 2006)*, Kyoto, Japan, November 5–8, 2006, pp. 1–8.
- R. F. Fedors, *Polym. Eng. Sci.*, 1974, **14**, 147–154.
- A. Jayasri and M. Yaseen, *J. Coatings Technol.*, 1980, **52**, 41–45.
- K. G. Joback and R. C. Reid, *Chem. Eng. Commun.*, 1987, **57**, 233–243.

Green chemistry at ACHEMA 2009—from mnemonics to success stories

DOI: 10.1039/b907241c

In 2008, an article in this journal summarized the 24 principles of green engineering and green chemistry in the mnemonic “IMPROVEMENTS PRODUCTIVELY” (S. Y. Tang, R. A. Bourne, R. L. Smith and M. Poliakoff, *Green Chem.*, **10**, 268, DOI: 10.1039/b719469m). Among the principles mentioned were, for example, Efficient use of mass, energy, space and time, Easy to separate by design, Catalytic reagents and In-process monitoring.

ACHEMA 2009, the International Exhibition Congress on Chemical Engineering, Environmental Protection and Biotechnology, will open its doors on May 11 in Frankfurt. A key feature of the concept of this market place for innovation in chemical technologies will once again be the very close interaction between the exhibition and the congress. Congress sessions are exclusively devoted to technologies which are either already on display at the exhibition booths or on the verge of being displayed there in the very near future. In the 2009 edition of ACHEMA, a large number of contributions related to green chemistry have made this difficult step into the program sessions—and, among them, the visitor will recognize many of the topics included in the mnemonic:

- **Advanced Fluids in Process Engineering.** The program consists of 9 sessions with 47 contributions overall. It will be opened by Martyn Poliakoff who will report on “Multiphase Catalysis in Supercritical Fluids”. Many contributions are related to advanced fluids including their application in bio-reactions. Ionic liquids are a central point that also embraces

topics like the production of nanosystems in the session on Nanotechnologies/Nanomaterials. The risk assessment of ionic liquids will be addressed as well.

- The session **Processes for the Production of Active Pharmaceutical Ingredients** also includes new reaction technologies, e.g. catalysts for continuous production.

- **Microchemical Engineering** is a process technology for easier and safer operation of chemical reactions, for example highly exothermic or photochemical reactions. There is a close interaction between concepts of **Process Intensification** and the concepts of green technologies. **Reactions and Processes with Non-Classical Energy Input** is another example.

- **High-throughput Technologies** have developed into a powerful tool for the design of new materials, including catalysts.

- **Formulation Technologies** have not been addressed very intensively in discussions about green technologies up to now, but this topic is expected to be of increasing importance, environmentally friendly surfactants being just one example.

Innovation cycles are becoming shorter—this will hold true in the future despite the present economic crisis. In fact innovation may be the key factor for success in the market right now, but it will prove even more to be a prerequisite for finding our way out of the crisis. Innovation does not just consist of a brilliant idea—it comprises the whole process from the first idea to market entry. This process must be actively managed. For green technologies this may be even

more important, as in some cases at least in the past they have not been mainstream. For such new concepts that compete with established mainstream technologies, active management means attracting the awareness of funding institutions, but what may be even more important is creating targeted discussion forums. The congress series Green Solvents, the Congress on Ionic Liquids (COIL) and IMRET (International Conference on Microreaction Technology) are successful examples of how DECHEMA established such platforms for a discussion about implementation.

It is the merit of this journal and especially of the article IMPROVEMENTS PRODUCTIVELY to describe the principles of Green Engineering and Green Chemistry very clearly for everybody. It might seem presumptuous to add a 25th principle, but there is an important aspect which is implicitly related to some of the chemical engineering principles, but not explicitly mentioned: the potential of a new chemical process to be scaled-up—either conventionally in large-scale reactors or by numbering up microreactors. Whatever scale-up approach may be the best, it will be a point of discussion at ACHEMA—just like all aspects related to apparatus and technology in green engineering and green chemistry.

We very much hope to welcome many green chemists and technologists to Frankfurt.

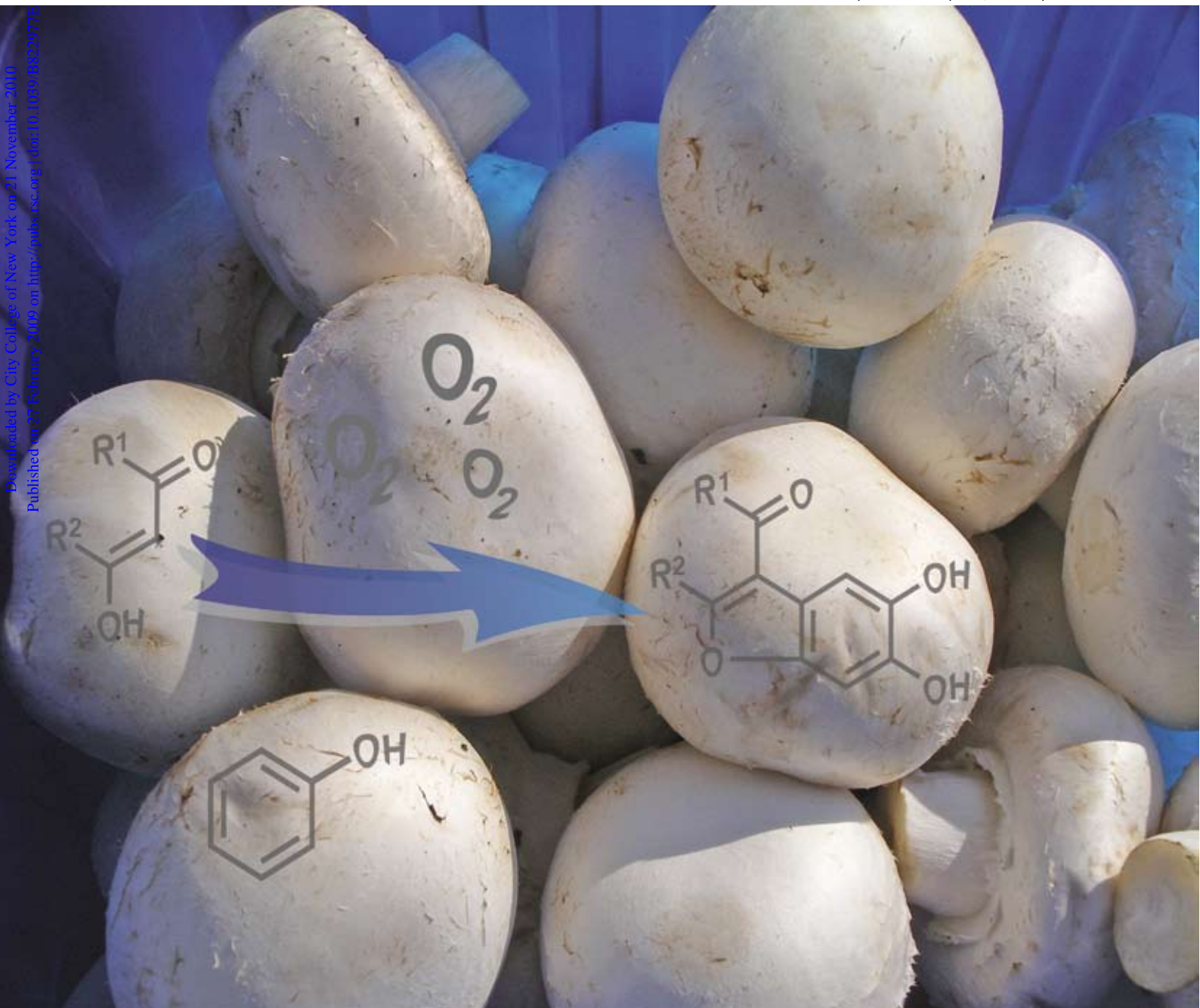
Kurt Wagemann
DECHEMA e.V.

Green Chemistry

Cutting-edge research for a greener sustainable future

www.rsc.org/greenchem

Volume 11 | Number 5 | May 2009 | Pages 593–740



Downloaded by City College of New York on 21 November 2015
Published on 27 February 2009 on <http://pubs.rsc.org> (doi:10.1039/B822977E)

ISSN 1463-9262

Beifuss *et al.*
Domino reaction catalyzed by *Agaricus bisporus*
Ley *et al.*
Transfer hydrogenation of ketones as a continuous flow process

Dorgan *et al.*
Surface esterification of nanoparticles
Franco *et al.*
New green lubricating grease formulations

RSC Publishing

Combined action of enzymes: the first domino reaction catalyzed by *Agaricus bisporus*

Heiko Leutbecher, Szilvia Hajdok, Christina Braunberger, Melanie Neumann, Sabine Mika, Jürgen Conrad and Uwe Beifuss*

Received 24th December 2008, Accepted 18th February 2009

First published as an Advance Article on the web 27th February 2009

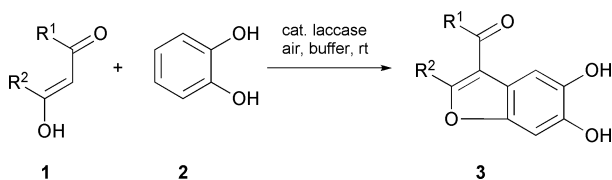
DOI: 10.1039/b822977e

The enzymes tyrosinase and laccase from a crude extract of the button mushroom (*Agaricus bisporus*) can be employed to catalyze the domino reaction between phenol and various cyclic 1,3-dicarbonyls using atmospheric oxygen as the oxidizing agent and yielding annulated benzofuranes in a highly efficient and sustainable manner.

Enzyme-catalyzed reactions are gaining more and more importance in organic synthesis since they may often be conducted in a highly efficient and environmentally friendly fashion in aqueous solutions at room temperature.¹ In the chemical industry they are not only used in the synthesis of fine chemicals, but can also be applied for the production of bulk chemicals.²

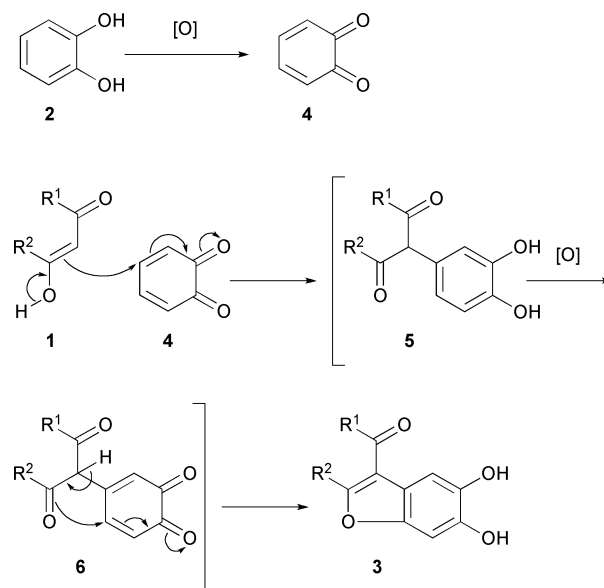
While a multitude of enzyme-catalyzed single-step transformations is known, relatively few domino reactions initiated by enzymes have been described,^{3,4} and there are even fewer examples of the combined use of several enzymes in domino processes.⁵

Recently we have been able to transform the cyclic 1,3-dicarbonyls **1** with various catechols **2** into coumestanes and related *O*-heterocycles **3** using a laccase-catalyzed reaction with atmospheric oxygen as the oxidizing agent (Scheme 1).⁶ The main characteristics of these reactions are that they can be easily performed under mild reaction conditions, that they use an ecologically benign and infinitely available oxidizing agent, and that their products can be separated and purified in a very simple way. Due to their phytoestrogenic, antibacterial, antifungal and antihepatotoxic effects, such heterocycles have an interesting biological profile.⁷



It is assumed that the first step of the domino process is the laccase-catalyzed oxidation of the catechol **2** with O₂ to *o*-benzoquinone **4**, which then undergoes an intermolecular 1,4-addition with the enol of the 1,3-dicarbonyl **1** as a nucleophile

to yield **5** (not isolable). A second laccase-catalyzed oxidation occurs (**5** → **6**) followed by a second 1,4-addition proceeding intramolecularly and forming the heterocycle **3**. Altogether, a domino oxidation/1,4-addition/oxidation/1,4-addition process has taken place (Scheme 2).



Scheme 2 Proposed mechanism of the domino reaction.

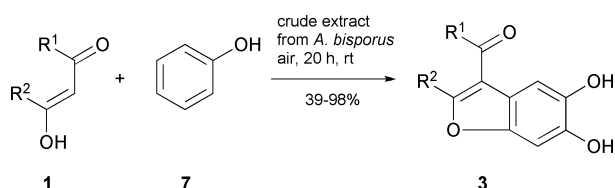
Unfortunately, phenols that are more easily accessible than the corresponding catechols cannot be used as the starting material for this reaction since laccases are unable to catalyze the phenol to catechol oxidation.⁸ In order to directly employ phenols they would first have to undergo oxidation to the catechols. Since this reaction was supposed to be run in the presence of laccase in the same reaction flask using atmospheric oxygen as the oxidant, we restricted our search to suitable oxidizing enzymes. Amongst others, we came across tyrosinases, which are known for their ability to catalyze the O₂ oxidation of phenols to catechols.⁹

And there was another reason for combining the tyrosinase with a laccase: both enzymes co-occur in various fungi, including the cultivated and thus easily and abundantly accessible button mushroom (*Agaricus bisporus*) making it a very inexpensive source of both enzymes.¹⁰ The fact that *A. bisporus* contains tyrosinase and laccase, among other enzymes, has long been known but—apart from a few studies on the oxidative degradation of phenolic compounds in industrial effluents¹¹—rarely been exploited. As far as we know no defined chemical

Bioorganische Chemie, Institut für Chemie, Universität Hohenheim, Garbenstr. 30, D-70599, Stuttgart, Germany.
E-mail: ubeifuss@uni-hohenheim.de; Fax: (+49) 711 459 22951;
Tel: (+49) 711 459 22171

transformation, let alone a domino reaction, has been reported using a crude extract from *A. bisporus* as the catalyst. However, there have been numerous reports on various reactions with either pure tyrosinases^{9,12} or pure laccases.¹³ There are also several examples of tyrosinase or laccase catalyzed oxidations followed by chemical transformations.^{6,14}

Here, we report the first example of the combined action of a tyrosinase and a laccase for a domino process. We have found that the efficient and sustainable reaction between the phenol (**7**) and the cyclic 1,3-dicarbonyls **1a–g** using a crude extract from the fruiting bodies of *A. bisporus* as the catalyst and atmospheric oxygen as the oxidant resulted in the selective formation of coumestanes and related *O*-heterocycles (**3a–g**) (Scheme 3).



First, we developed a very simple procedure for the preparation of a crude extract from *A. bisporus*. The fruiting bodies were homogenized with 0.2 M phosphate buffer (pH = 6.0) and filtered at 4 °C.† The supernatant obtained after centrifugation was used directly and without further purification to perform the transformations: the 1,3-dicarbonyls **1a–g** were stirred with a small excess of the phenol (**7**) under air at room temperature for 20 h (Scheme 3, Table 1).‡

We assume that the monooxygenase tyrosinase initially catalyzes the oxidation of the phenol (**7**) to achieve the catechol (**2**), which can be detected by thin-layer chromatography during the reaction. Tyrosinase- and/or laccase-catalyzed oxidation of **2** follows to give the *o*-quinone (**4**), which then reacts with **1a–g** to produce the *O*-heterocycles **3a–g**. Presumably, the domino reaction between **4** and **1a–g** follows the mechanism described above (Scheme 2).

Different 1,3-dicarbonyls **1** (Fig. 1) were reacted with **7**. Reactions were accomplished with the cyclic 1,3-diketones **1a** and **1b** (Table 1, entry 1 and 2), the 6-substituted 4-hydroxy-2*H*-pyran-2-ones **1c** and **1d** (Table 1, entry 3 and 4) as well as the substituted 4-hydroxy-2*H*-chromen-2-ones **1e–g** (Table 1, entries 5–7). The heterocycles **3a–g** (Fig. 2) were obtained as the sole reaction products with yields ranging from 39 to 98%.§ The

Table 1 Reaction of **7** with **1a–g** to yield **3a–g**

Entry	7 (equiv.)	1,3-Dicarbonyl 1	3	Yield (%)
1	1.2 ^a	a	a	44 ^b
2	1.3	b	b	39
3	1.3	c	c	48
4	2.2 ^a	d	d	66 ^c
5	1.1	e	e	88
6	1.2	f	f	98
7	1.3	g	g	72 ^b

^a The reaction was run in a buffer/acetone mixture (v/v = 10:1). ^b Yield after recrystallization of the crude product. ^c **3d** was transformed into the corresponding bisacetate with 71% yield.

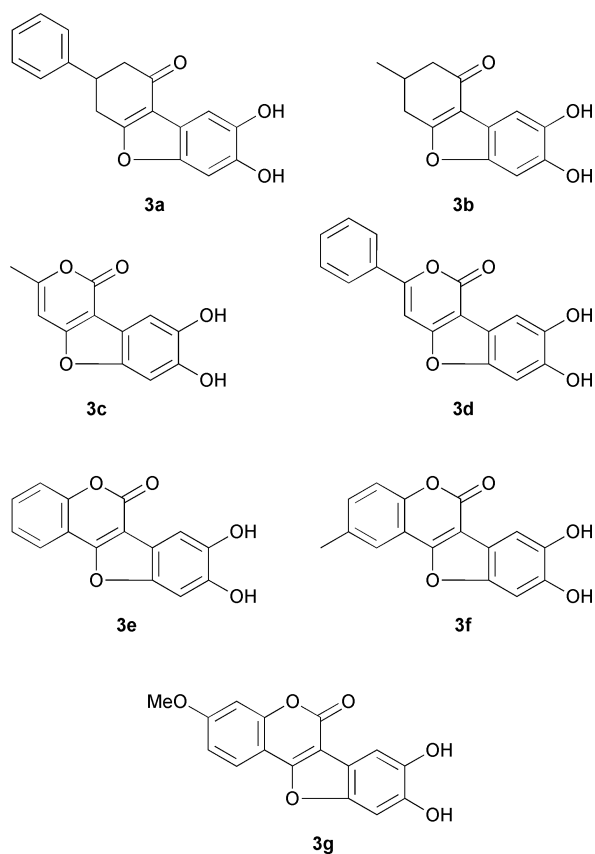
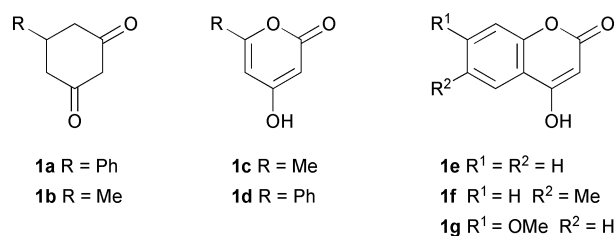


Fig. 2 Products **3a–g** of the domino reaction between **1a–g** with **7**.

highest yields were observed with the reactions involving **1e–g**. The 8,9-dihydroxy-6*H*-benzofuro[3,2-*c*]chromen-6-one **3e**, for example, was obtained with 88%, **3f** with 98% and **3g** with 72% yield. The work-up of the reaction mixture was as easy as the reaction process itself, since the crude products could be obtained from the reaction mixture by a simple salting-out procedure.

Following the extraction of the crude products with a suitable solvent (ethanol or acetone), filtration and removal of the solvent *in vacuo*, compounds with a purity of 90–95% were obtained (¹H NMR). Only three of them needed to be further purified through recrystallization (**3a** and **3g**) or transformation into the bisacetate (**3d**). Using non-polar solvents for the extraction step led to lower yields, while more polar solvents led to less pure products. All 1,3-dicarbonyls could be reacted with 1.1 to 1.3 equiv. of **7**, except **1d**. In the latter case 2.2 equiv. of **7** were required to achieve a complete transformation (Table 1, entry 4).

In order to elucidate the role that both enzymes play in this domino reaction, several additional experiments were conducted. In one experiment we tried to react **7** and **1e** under standard reaction conditions (0.5 mmol **1e**, 0.55 mmol **7**, 45 mL 0.2 M phosphate buffer pH = 6.0, 20 h at room temperature) using a commercial preparation of laccase from *A. bisporus* (Fluka): not even a trace of the heterocycle **3e** could be detected, and **1e** was quantitatively recovered after 20 h. Under the standard conditions specified above, **7** was completely transformed into products that could not be identified; they are supposed to be oligomeric and polymeric products of oxidative phenol coupling. From earlier studies we knew that the oxidative reaction of catechol (**2**) with **1e** forming **3e** is catalyzed by laccase.⁶ Consequently, the laccase is not able to catalyze the oxidation of phenol (**7**) to catechol (**2**). In another control experiment, **7** and **1e** were reacted with 7425 U of a commercially available tyrosinase from cultivated mushroom (Sigma) under standard reaction conditions. Although the product **3e** could be isolated after 20 h, the 49% yield was considerably lower than that obtained from the reaction with the crude extract from *A. bisporus* (88%; Table 1, entry 5). This is even more astonishing since the activity of the commercial preparation of tyrosinase was higher by a factor of 1.5 than that of the tyrosinase in the crude fungal extracts (4815 U). ¶ The experiment demonstrates the superiority of the laccase/tyrosinase combination over tyrosinase alone, which might be due to the fact that the laccase co-operates in the oxidation of the catechol (**2**) forming the *o*-quinone (**4**). This interpretation is supported by the result of the reaction between **1e** and **7**, where 41.7 U of pure laccase (from *Agaricus bisporus*, Fluka) ¶ was added to pure tyrosinase (from mushroom, Sigma) of the same activity as in the second control experiment (7425 U). Under these conditions **3e** was isolated with 69% yield after 20 h. If **1e** and **7** were reacted with 4815 U tyrosinase (activity of the mushroom extract) and 110 U pure laccase, side reactions are observed, and the yield of **3e** drops to 59%.

In summary, a crude extract from *A. bisporus*, which can be produced by a most simple procedure, was demonstrated to catalyze the efficient and sustainable synthesis of annulated benzofuranes **3** under mild reaction conditions by reacting phenol (**7**) with the 1,3-dicarbonyls **1** using oxygen as an oxidant.

Acknowledgements

This work was performed within the Collaborative Centre SFB 706 (Selective Catalytic Oxidations Using Molecular Oxygen; Stuttgart) and funded by the German Research Foundation.

Notes and references

† Preparation of the mushroom extract: fresh commercial mushrooms (64 g) were homogenized in ice-cold 0.2 M phosphate buffer pH 6.0 (500 mL). After filtering, the homogenate was centrifuged (4185 × *g* for 5 min). The collected supernatants were directly used as medium for the reaction of **7** with **1a–g**. The mushroom extract can be stored at –20 °C.

‡ General procedure for synthesis of **3a–g**: 1.0 equiv. **1** (0.5 mmol) [**1a** (0.3 mmol), **1d** (0.2 mmol) respectively] and 1.1 to 2.2 equivs. **7** (see Table 1) were dissolved in 45 mL of mushroom extract. For **1a** and **1d** 4.5 mL of acetone were added. The reaction mixture was stirred vigorously at room temperature for 20 h while complete consumption of the substrates occurred. The mixture was saturated with sodium chloride

and filtered through a buchner funnel. The filter cake was washed with 15% sodium chloride solution (75 mL) and water (20 mL) and dried at room temperature. The fine powdered crude product was extracted with 150 mL of boiling acetone (**3a–d**) or ethanol (**3e–g**), respectively. After filtration the solvent was evaporated *in vacuo* to yield nearly pure heterocycles **3a–g**. **3a** was recrystallized from acetone and **3g** from a mixture of ethanol/H₂O. **3d** (108 mg, 0.37 mmol) was dissolved in 2 mL (1.96 g, 24.7 mmol) of pyridine, treated with 250 µL (270 mg, 2.6 mmol) acetic anhydride and 7 mg (0.06 mmol, 15 mol%) of DMAP. The reaction mixture was stirred for 2.5 h and 14 mL of 2 M HCl were added. The precipitate (99 mg of **8d**, 71%) was collected by filtration, washed with saturated sodium bicarbonate solution and water, dried and recrystallized from ethanol.

§ Selected analytical data for 3,4-dihydro-7,8-dihydroxy-3-phenyl-dibenzofuran-1(2*H*)-one (**3a**): λ_{max}(CH₃CN)/nm 299 (lg ε 3.94), 238 (4.28) and 207 (4.61); ν_{max}(atr)/cm⁻¹ 3433 and 3107 (OH), 1630 (C=O), 1615, 1580 and 1518 (C=C), 1437 (CH₂), 1286 (OH), 1270 and 1040 (C–O), 869, 771 and 698 (=C–H); δ_H(300 MHz; DMSO-*d*₆) 2.58 (dd, ²J_{2-HA,2-HB} = 16.2 Hz, ³J_{2-HA,3-H} = 3.9 Hz, 1H, 2-H_A), 2.94 (dd, ²J_{2-HB,2-HA} = 16.2 Hz, ³J_{2-HB,3-H} = 12.3 Hz, 1H, 2-H_B), 3.16–3.30 (m, 2H, 4-H₂), 3.60–3.74 (m, 1H, 3-H), 7.01 (s, 1H, 6-H or 9-H), 7.26 (s, 1H, 6-H or 9-H), 7.27 (t, ³J_{4-H,3-H} = ³J_{4-H,5-H} = 7.5 Hz, 1H, 4'-H), 7.36 (t, ³J_{3-H,2'-H} = ³J_{5-H,4'-H} = ³J_{5-H,4'-H} = ³J_{5-H,6'-H} = 7.3 Hz, 2H, 3'-H and 5'-H), 7.43 (d, ³J_{2'-H,3'-H} = ³J_{6'-H,5'-H} = 7.2 Hz, 2H, 2'-H and 6'-H), 9.14 (s, 1H, OH), 9.17 (s, 1H, OH); δ_C(75 MHz; DMSO-*d*₆) 31.36 (C-4), 41.03 (C-3), 45.33 (C-2), 99.23, 106.11 (C-6 or C-9), 114.96 (C-9a), 116.22 (C-9b), 127.55 (C-4'), 127.79 (C-2' and C-6'), 129.27 (C-3' and C-5'), 143.79 (C-1'), 144.53, 145.21, 149.02 (C-5a, C-7 or C-8), 169.66 (C-4a), 193.74 (C-1); m/z(EI, 70 eV) 294.0903 (M⁺, 100%, C₁₈H₁₄O₄ requires 294.0892), 252 (10), 190 (98), 162 (53), 134 (5), 92 (5), 69 (4). Selected analytical data for 3,4-dihydro-7,8-dihydroxy-3-methyl-dibenzofuran-1(2*H*)-one (**3b**): (found: C, 66.97; H, 5.02. C₁₉H₁₆O₄ requires C, 67.23; H, 5.21%); λ_{max}(CH₃CN)/nm 299 (lg ε 3.91), 237 (4.22) and 207 (4.47); ν_{max}(atr)/cm⁻¹ 3470 and 3119 (OH), 1628 (C=O), 1578 and 1518 (C=C), 1293 (OH), 1247 and 1040 (C–O), 876 and 810 (=C–H); δ_H(300 MHz; DMSO-*d*₆) 1.13 (d, ³J_{3-H,3-H} = 6.3 Hz, 3H, 3-CH₃), 2.32 (dd, ²J_{2-HA,2-HB} = 16.5 Hz, ³J_{2-HA,3-H} = 12.3 Hz, 1H, 2-H_A), 2.43 (m, 1H, 3-H), 2.45 (dd, ²J_{2-HB,2-HA} = 16.2 Hz, ³J_{2-HB,3-H} = 3.0 Hz, 1H, 2-H_B), 2.71 (dd, ²J_{4-HA,4-HB} = 17.4 Hz, ³J_{4-HA,3-H} = 9.3 Hz, 1H, 4-H_A), 3.04 (dd, ²J_{4-HB,4-HA} = 17.5 Hz, ³J_{4-HB,3-H} = 4.7 Hz, 1H, 4-H_B), 6.98 (s, 1H, 6-H or 9-H), 7.22 (s, 1H, 6-H or 9-H), 9.09 (s, 1H, OH), 9.13 (s, 1H, OH); δ_C(75 MHz; DMSO-*d*₆) 21.37 (3-CH₃), 30.97 (C-3), 31.65 (C-4), 46.34 (C-2), 99.17, 106.07 (C-6 or C-9), 115.03 (C-9a), 115.98 (C-9b), 144.41, 145.06, 148.88 (C-5a, C-7 or C-8), 170.02 (C-4a), 194.63 (C-1); m/z(EI, 70 eV) 232 (M⁺, 100%), 217 (M⁺ – CH₃, 2), 190 (52), 162 (49), 134 (4), 92 (4), 69 (4).

¶ Tyrosinase activity was determined following a modified procedure taken from ref. 10: a 1 mM solution of tyrosine (2 mL) in 0.1 M phosphate buffer (pH = 6.0) was mixed with (a) a solution of commercially available tyrosinase (from mushroom, Sigma) in phosphate buffer (1 mL) or (b) with crude mushroom extract (1 mL). The change in absorption was followed *via* UV-spectroscopy (λ = 310 nm). One unit was defined as a change in absorption of 0.001 at pH = 6.0 at room temperature. The activity of the crude mushroom extract amounted to 107 U mL⁻¹. The activity of commercial tyrosinase amounted to 165 U mL⁻¹ in a total volume of 45 mL reaction mixture.

|| Laccase activity was determined following a modified procedure taken from E. J. Land, *J. Chem. Soc., Faraday Trans.*, 1993, **89**, 803–810 and M. Felici, F. Artemi, M. Luna, M. Speranza, *J. Chromatogr. A*, 1985, **320**, 435–439. A 1.18 M solution of catechol (0.3 mL) in 0.2 M phosphate buffer (pH = 6.0) was diluted with 0.2 M phosphate buffer (2.5 mL, pH = 6.0) and treated with a solution of laccase in the same buffer (0.2 mL). The change in absorption was followed *via* UV-spectroscopy (λ = 390 nm). One unit was defined as the amount of laccase that converts 1 µmol of catechol per minute at pH = 6.0 at room temperature. The activity of laccase amounted to 0.926 U mL⁻¹ in the reaction mixture for the reaction of **1e** with **7** (total volume of 45 mL). The laccase activity in the mushroom extract cannot be determined with the laccase-specific syringaldazine,¹⁰ since the laccase activity is below the detection limits of this assay. However, the total activity (tyrosinase and laccase) of the extract concerning the oxidation of catechol significantly exceeds that of the tyrosinase activity of the mushroom extract; the latter can be estimated by determining the activity of pure tyrosinase with both catechol and tyrosine and by using these values to derive the tyrosinase activity of the mushroom extract, which was determined through the reaction with tyrosine, from the tyrosinase

activity towards the other substrate. The activity of the laccase added in the third control experiment is below the detection limit of the syringaldazine assay, too.

- 1 K. Faber, *Biotransformations in Organic Chemistry*, Springer, Berlin, 5th edn, 2004.
- 2 A. Liese, K. Seelbach, A. Buchholz, J. Haberland and A. J. J. Straathof, in *Industrial Biotransformations*, ed. A. Liese, K. Seelbach, and C. Wandrey, Wiley-VCH, Weinheim, 2nd edn, 2006, ch. 6 and 7, pp. 147–520.
- 3 L. F. Tietze and A. Modi, *Med. Res. Rev.*, 2000, **20**, 304–322; L. F. Tietze, *Chem. Rev.*, 1996, **96**, 115–136; L. F. Tietze and U. Beifuss, *Angew. Chem., Int. Ed. Engl.*, 1993, **32**, 131–163.
- 4 S. M. Glueck, S. F. Mayer, W. Kroutil and K. Faber, *Pure Appl. Chem.*, 2002, **74**, 2253–2257; S. F. Mayer, W. Kroutil and K. Faber, *Chem. Soc. Rev.*, 2001, **30**, 332–339.
- 5 E. Garcia-Junceda, *Multi-Step Enzyme Catalysis*, Wiley-VCH, Weinheim, 2008.
- 6 Sz. Hajdok, H. Leutbecher, G. Greiner, J. Conrad and U. Beifuss, *Tetrahedron Lett.*, 2007, **48**, 5073–5076; H. Leutbecher, J. Conrad, I. Klaiher and U. Beifuss, *Synlett*, 2005, 3126–3130.
- 7 A. J. M. da Silva, P. A. Melo, N. M. V. Silva, F. V. Brito, C. D. Buarque, D. V. de Souza, V. P. Rodrigues, E. S. C. Pocas, F. Noel, E. X. Albuquerque and P. R. R. Costa, *Bioorg. Med. Chem. Lett.*, 2001, **11**, 283–286; K. W. Gaido, L. S. Leonard and S. Lovell, *Toxicol. Appl. Pharmacol.*, 1997, **143**, 205–212; N. A. Pereira, B. M. R. Pereira, M. C. do Nascimento, J. P. Parente and W. B. Mors, *Planta Med.*, 1994, **60**, 99–100; S. M. Wong, S. Antus, A. Gottsegen, B. Fessler, G. S. Rao, J. Sonnenbichler and H. Wagner, *Arzneim.-Forsch.*, 1988, **38**, 661–665; H. Wagner, B. Geyer, Y. Kiso, H. Hikino and G. S. Rao, *Planta Med.*, 1986, **52**, 370–374.
- 8 Laccases (EC 1.10.13.2) belong to the enzyme class of oxidoreductases which catalyze the oxidation of substrates without incorporation of molecular oxygen. In contrast, monooxygenases and dioxygenases (EC 1.13 and EC 1.14) catalyze the incorporation of one and two O-atoms, respectively, into the substrate: C. Hoh and M. V. Filho, in *Industrial Biotransformations*, ed. A. Liese, K. Seelbach and C. Wandrey, Wiley-VCH, Weinheim, 2nd edn, 2006, ch. 2, pp. 37–62.
- 9 R. Z. Kazandjian and A. M. Klivanov, *J. Am. Chem. Soc.*, 1985, **107**, 5448–5450.
- 10 X. Zhang and W. H. Flurkey, *J. Food Sci.*, 1997, **62**, 97–100; B. Ratcliffe, W. H. Flurkey, J. Kuglin and R. Dawley, *J. Food Sci.*, 1994, **59**, 824–827.
- 11 S. C. Atlow, L. Bonadonna-Aparo and A. M. Klivanov, *Biotechnol. Bioeng.*, 1984, **26**, 599–603.
- 12 S.-Y. Seo, V. K. Sharma and N. Sharma, *J. Agric. Food Chem.*, 2003, **51**, 2837–2853; E. S. Krol and J. L. Bolton, *Chem. Biol. Interact.*, 1997, **104**, 11–27; S. G. Burton, *Catal. Today*, 1994, **22**, 459–487.
- 13 F. Sagui, C. Chirivi, G. Fontana, S. Nicotra, D. Passarella, S. Riva and B. Danieli, *Tetrahedron*, 2009, **65**, 312–317; S. Nicotra, A. Intra, G. Ottolina, S. Riva and B. Danieli, *Tetrahedron: Asymmetry*, 2004, **15**, 2927–2931; S. Nicotra, M. R. Cramarossa, A. Mucci, U. M. Pagnoni, S. Riva and L. Forti, *Tetrahedron*, 2004, **60**, 595–600; S. G. Burton, *Curr. Org. Chem.*, 2003, **7**, 1317–1331; F. Carunchio, C. Crescenzi, A. M. Girelli, A. Messina and A. M. Tarola, *Talanta*, 2001, **55**, 189–200; M. Fabbrini, C. Galli, P. Gentili and D. Macchitella, *Tetrahedron Lett.*, 2001, **42**, 7551–7553; A. Potthast, T. Rosenau, C. L. Chen and J. S. Gratzl, *J. Mol. Catal. A: Chem.*, 1996, **108**, 5–9; R. Bourbonnais and M. G. Paice, *FEBS Lett.*, 1990, **267**, 99–102.
- 14 S. Witayakran and A. J. Ragauskas, *Green Chem.*, 2007, **9**, 475–480; S. Witayakran, L. Gelbaum and A. J. Ragauskas, *Tetrahedron*, 2007, **63**, 10958–10962; S. Witayakran, A. Zettili and A. J. Ragauskas, *Tetrahedron Lett.*, 2007, **48**, 2983–2987; H. M. Bialk, C. Hedman, A. Castillo and J. A. Pedersen, *Environ. Sci. Technol.*, 2007, **41**, 3593–3600; T. H. J. Niedermeyer, A. Mikolasch and M. Lalk, *J. Org. Chem.*, 2005, **70**, 2002–2008; R. Pilz, E. Hammer, F. Schauer and U. Kragl, *Appl. Microbiol. Biotechnol.*, 2003, **60**, 708–712; G. H. Müller, A. Lang, D. R. Seithel and H. Waldmann, *Chem. Eur. J.*, 1998, **4**, 2513–2522; G. H. Müller and H. Waldmann, *Tetrahedron Lett.*, 1996, **37**, 3833–3836; U. T. Bhalerao, C. M. Krishna and G. Pandey, *J. Chem. Soc., Chem. Commun.*, 1992, 1176–1177; M. Miessner, O. Crescenzi, A. Napolitano, G. Prota, S. O. Andersen and M. G. Peter, *Helv. Chim. Acta*, 1991, **74**, 1205–1212; M. Sugumaran, H. Dali and V. Semensi, *Bioorg. Chem.*, 1990, **18**, 144–153; G. Pandey, C. Muralikrishna and U. T. Bhalerao, *Tetrahedron*, 1989, **45**, 6867–6874; U. T. Bhalerao, C. Muralikrishna and G. Pandey, *Synth. Commun.*, 1989, **19**, 1303–1307; M. Sugumaran, H. Dali, V. Semensi and B. Hennigan, *J. Biol. Chem.*, 1987, **262**, 10546–10549.

Decorating in green: surface esterification of carbon and cellulosic nanoparticles†

Margaret J. Sobkowicz, Birgit Braun and John R. Dorgan

Received 1st October 2008, Accepted 25th February 2009

First published as an Advance Article on the web 4th March 2009

DOI: 10.1039/b817223d

Fischer esterification of surface hydroxyl groups on multi-walled carbon nanotubes, carbon nanospheres, and cellulosic nanowhiskers using acetic and butyric acid is presented as a green approach to decorate the surfaces of nanoparticles.

Nanoparticles are of great interest in a variety of applications.^{1–5} Here, a one-step acid-catalyzed esterification (Fischer esterification) is established as a green alternative to reactions commonly employed. Advantages include less expensive and less toxic reagents, better atom efficiency,⁶ and the potential use of renewable organic acids.

Carbon nanospheres (CNS) derived from renewable cellulose have potential in polymer nanocomposite applications.^{7,8} CNS are chemically similar to multiwalled carbon nanotubes (MWCNT) of comparable diameter, as the surface chemical reactivity predominantly depends on curvature.^{9,10} Several thorough reviews are available about existing surface functionalization methods for carbon nanotubes (CNTs).^{11,12} Most of the techniques employ hazardous and reactive compounds in numerous reaction steps.

Cellulosic nanowhiskers (CNW) are nanoparticles derived from biomass;^{13,14} they are commonly isolated by hydrochloric¹⁵ or sulfuric acid¹⁶ hydrolysis. Methods to increase the hydrophobicity are documented in the literature; again, many of them utilize toxic chemicals as well as multiple processes.^{17–21}

Fischer esterification consists of heating a carboxylic acid and alcohol mixture with a strong acid catalyst.²² The reaction is fully reversible; to favor ester formation either an excess of one of the reagents, high levels of catalyst, removal of water, or a combination of these measures is necessary.²² Previous kinetics experiments have shown that rate constants approach an asymptotic limit as the monobasic acid chain length increases. While the rate initially depends strongly on the alkyl length, the plateau value is reached for butyric acid.²²

Surface modifications of carbon nanostructures in this study were conducted at 105 °C for up to 24 h after sonication in 90 wt% organic acid (acetic and butyric). Hydrochloric acid was added as a catalyst. Surface modification of CNW occurs simultaneously with the isolation from cotton linter. Purification was accomplished by repeated centrifugation and replacement

of the supernatant with water. Further experimental details for both procedures can be found in the ESI.†

Fig. 1 shows representative TEM images of MWCNT and CNS prior to surface functionalization; diameters are about 30 nm and 40 nm, respectively. The insets of Fig. 1 show the graphitic multilayer sidewalls of each nanostructure. Walls are observed to be about 10 nm thick, corresponding to approximately 30 graphene layers.

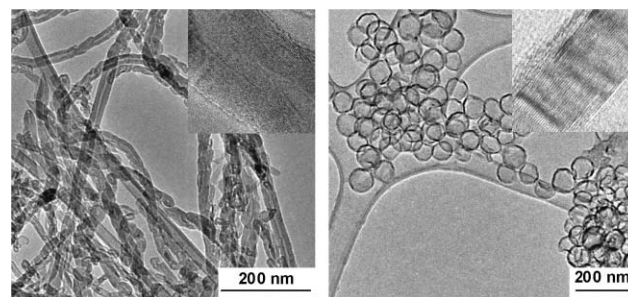


Fig. 1 TEM images of (left) MWCNT and (right) CNS. Insets are close-up images of the graphitic sidewalls of each structure.

Individual CNW isolated from cotton are reported to be 100–200 nm long with aspect ratios of around 10.¹³ Similar dimensions are observed irrespective of the acid system employed for isolation and functionalization as shown in TEM images in Fig. 2. Following the approach described in a previous study,²³ the average lengths and diameters can also be determined using multi-angle laser-light scattering (MALLS). It is found that while the number-average lengths L_n and diameters d_n are similar for all acid systems investigated ($L_n = 230$ to 260 nm, $d_n = 35$ –45 nm), the polydispersity of the diameter size distribution (ratio of weight to number average dimensions) decreased from 3.0 for CNW isolated using hydrochloric acid (CNW-HA) to 2.5 for the acetic/hydrochloric acid system (CNW-AA) and even further to 2.1 when butyric/hydrochloric acid is used (CNW-BA). This reduction in polydispersity indicates a higher degree of

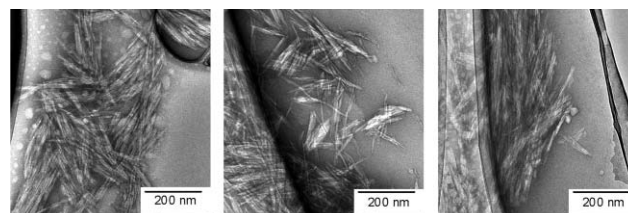


Fig. 2 TEM images of CNW isolated (left) by hydrochloric acid hydrolysis, (center) by acetic/hydrochloric acid hydrolysis, and (right) using butyric/hydrochloric acid hydrolysis.

Department of Chemical Engineering, Colorado School of Mines, Golden, CO, USA. E-mail: jdorgan@mines.edu; Fax: +1 303 273 3730; Tel: +1 303 273 3539

† Electronic supplementary information (ESI) available: Experimental details. See DOI: 10.1039/b817223d

individualization as the surface functionality molecular weight increases.

Fig. 3 shows FT-IR spectra for untreated (MWCNT-OH), acetic acid (MWCNT-AA) and butyric acid (MWCNT-BA) functionalized carbon nanotubes and nanospheres (CNS, CNS-AA, CNS-BA, respectively). All spectra are normalized to the C=C graphite peak at 1580 cm⁻¹. The most striking feature is the CH₂ and CH₃ stretch peaks that appear near 2900 cm⁻¹ after esterification. In the case of MWCNTs, the hydroxyl peak at around 3400 cm⁻¹ vanishes almost completely after acetylation. The persistence of the hydroxyl peak in MWCNT-BA reflects the difference in reactivity between the two organic acids, butyric being less reactive than acetic. Contributions from other hydroxyl-terminated moieties, such as surface carboxylic acids, as well as lower overall reactivity explains the presence of the hydroxyl peak in the CNS spectra.

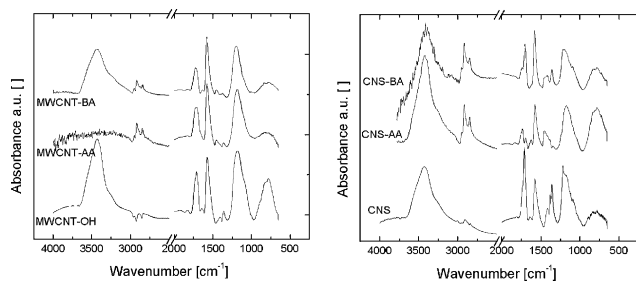


Fig. 3 FT-IR spectra from (left) MWCNT-OH, MWCNT-AA, MWCNT-BA and (right) CNS, CNS-AA, CNS-BA.

For CNW, the band resulting from the stretch of the ester carbonyl carbon²⁴ at 1736 cm⁻¹ is clearly present in the FT-IR spectra of CNW-AA and CNW-BA shown in Fig. 4 (left). Little variation of intensity is observed for the hydroxyl stretch peak centered around 3400 cm⁻¹ since the majority of these groups are located in the interior of the nanocrystallites. To estimate surface coverage, the 1736 cm⁻¹ signal is normalized by the absorbance peak at 1162 cm⁻¹ corresponding to the C–O–C stretch of the ring structure of the cellulose repeat unit.^{25,26} Determination of the applicable molar absorptivity ratios is performed using cellulose acetate, cellulose acetate butyrate and cellulose acetate propionate of known compositions. Spectral evaluation in conjunction with average dimensions obtained by MALLS allows estimation of the average degree of surface substitution; values are summarized in Table 1. No statistical difference is observed between acetic and butyric acid treated CNW. Because only half of the hydroxyl groups of a surface cellulose molecule in CNW are accessible,¹⁸ the maximum degree

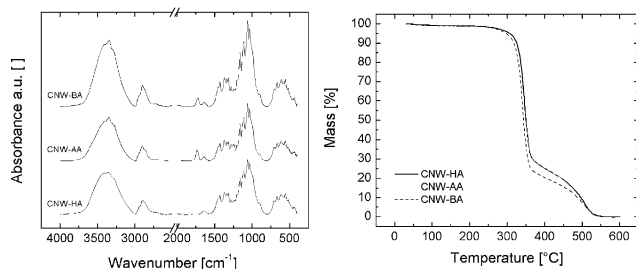


Fig. 4 FT-IR spectra obtained from CNW-HA, CNW-AA, and CNW-BA (left). Mass loss as a function of temperature for CNW (right).

Table 1 Estimated surface substitution for various substrates

Carbon nanostructures		
Sample	Mass loss ^a [%]	Surface substitution [mole % carbon]
MWCNT-AA	2.62 ± 0.70	13.7 ± 3.6
MWCNT-BA	1.99 ± 0.70	07.0 ± 2.4
CNS-AA	3.20 ± 0.70	11.9 ± 2.5
CNS-BA	2.80 ± 0.70	7.0 ± 1.7
Cellulose nanowhiskers		
Sample	Overall substitution [ester per repeat unit]	Surface substitution [ester per surface repeat unit]
CNW-AA	0.06	0.83 ± 0.39
CNW-BA	0.09	0.91 ± 0.30

^a At 400 °C

of substitution is 1.5. The values in Table 1 suggest that slightly more than half of all surface hydroxyl groups are substituted by acetate or butyrate groups under the reaction conditions employed. Fig. 4 (right) demonstrates that the thermal stability in air, which is a crucial factor for nanocomposite formation, is unaltered for surface-esterified CNW.

Fig. 5 presents mass loss as a function of temperature in air for CNS and MWCNT before and after surface treatment. The native CNS are stable up to 500 °C, whereas MWCNT gradually decompose starting at 400 °C. Acetylated and butylated CNS and MWCNT lose mass at lower temperatures associated with oxidation of surface groups. Table 1 shows the fraction of mass lost by 400 °C in each functionalized carbon structure relative to the untreated carbon. The mole fraction of functionalized surface carbon, assuming that all surface functionality is burned off by 400 °C, is calculated based on mass loss of the native substrate, average dimensions of the particles, and molecular weight of relevant functional groups.

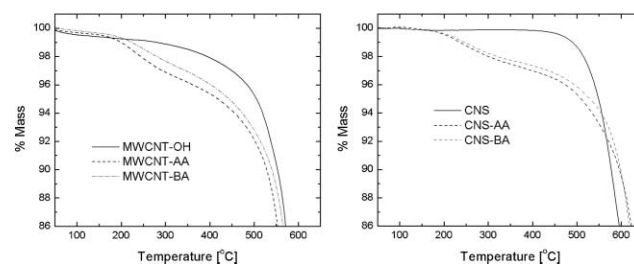


Fig. 5 TGA scans of (left) MWCNT-OH, MWCNT-AA, MWCNT-BA and (right) CNS, CNS-AA, CNS-BA.

For both carbon nanoparticles, butyric acid treatment results in less overall functionality, attributable both to the reduced reactivity of the longer chain organic acid²² and the lower molar concentration of butyric acid used (see ESI†). In terms of moles of functionalized carbon, the measured amount of acetate groups indicates that about half of the manufacturer-reported 1.76 wt% hydroxyl groups on the MWCNT-OH are successfully esterified.

For carbon nanostructures, the amount of functionalized surface carbon was determined utilizing TGA data. On both

spheres and tubes, the amount of butyrate groups (7 mol%) grafted to the surface was less than acetate groups (~12–14 mol%); this conclusion is in agreement with FT-IR spectral evidence. Combination of FT-IR data with average dimensions allows estimation of the surface substitution for CNW; values are similar for both acids and reached slightly more than 50% of available surface hydroxyl groups. This one-step surface treatment has the added benefits of using less expensive and less toxic reagents, achieving better atom efficiency, and using renewable organic acids. As such, it represents a greener approach to surface functionalization than many widely reported methods.

Acknowledgements

This research was supported by National Research Initiative Competitive Grant 2006-35504-16618 from the USDA Cooperative State Research, Education, and Extension Service and by the National Science Foundation through grant CMMI-0700869.

Notes and references

- S. Hrapovic, Y. Liu, K. B. Male and J. H. T. Luong, *Anal. Chem.*, 2004, **76**, 1083–1088.
- A. Wieckowski, E. R. Savinova and C. G. Vayenas, *Catalysis and Electrocatalysis at Nanoparticle Surfaces*, Marcel Dekker, New York, 2003, p. 970.
- T. Hegmann, H. Qi and V. M. Marx, *J. Inorg. Organomet. Polym.*, 2007, **17**(3), 483–508.
- G. Reiss and A. Hutten, *Nat. Mater.*, 2005, **4**, 725–726.
- R. Krishnamoorti and R. A. Vaia, *Polymer Nanocomposites*, ACS Symposium Series 804, ed. A. Society, Oxford University Press, San Francisco, CA, vol. 1. 2000, pp. 1–223.
- P. T. Anastas, J. C. Warner, *Green Chemistry: Theory and Practice*, 1998, Oxford University Press, New York, p. 148.
- A. M. Herring, J. T. McKinnon, B. D. McCloskey, J. Filley, K. W. Gneshin, R. A. Pavelka, H.-J. Kleebe and D. J. Aldrich, *J. Am. Chem. Soc.*, 2003, **125**, 9916–9917.
- M. J. Sobkowicz, J. R. Dorgan, K. W. Gneshin, A. M. Herring and J. T. McKinnon, *Carbon*, 2008, **47**, 622–628.
- J. Liu, A. G. Rinzler, H. Dai, J. H. Hafner, R. K. Bradley, P. J. Boul, A. Lu, T. Iverson, K. Shelimov, C. B. Huffman, F. Rodriguez-Macias, Y.-S. Shon, L. T. Randall, D. T. Colbert and R. E. Smalley, *Science*, 1998, **280**, 1253–1256.
- J. L. Bahr and J. M. Tour, *J. Mater. Chem.*, 2002, **12**, 1952–1958.
- D. Tasis, N. Tagmatarchis, A. Bianco and M. Prato, *Chem. Rev.*, 2006, **106**, 1105–1136.
- S. Niyogi, M. A. Hamon, H. Hu, B. Zhao, P. Bhowmik, R. Sen, M. E. Itkis and R. C. Haddon, *Acc. Chem. Res.*, 2002, **35**(12), 1105–1113.
- M. A. Samir, S. A. F. Alloin and A. Dufresne, *Biomacromolecules*, 2005, **6**, 612–626.
- A. Šturcová, G. R. Davies and S. J. Eichhorn, *Biomacromolecules*, 2005, **6**, 1055–1061.
- O. A. Battista and P. A. Smith, *Ind. Eng. Chem.*, 1962, **54**(9), 20–29.
- B. G. Rånby, *Faraday Discuss.*, 1951, **11**, 158–164.
- L. Heux, G. Chauve and C. Bonini, *Langmuir*, 2000, **16**, 8210–8212.
- C. Goussé, H. Chancy, G. Excoffier, L. Soubeyrand and E. Fleury, *Polymer*, 2002, **43**, 2645–2651.
- H. Yuan, Y. Nishiyama, M. Wada and S. Kuga, *Biomacromolecules*, 2006, **7**, 696–700.
- J. Araki, M. Wada and S. Kuga, *Langmuir*, 2001, **17**, 21–27.
- K. G. Nair and A. Dufresne, *Biomacromolecules*, 2003, **4**, 1835–1842.
- P. J. Flory, *Principles of Polymer Chemistry*, Cornell University Press, Ithaca and London, 1953.
- B. Braun, J. R. Dorgan and J. Chandler, *Biomacromolecules*, 2008, **9**, 1255–1263.
- M. O. Adabajo, R. L. Frost, J. T. Klopogge and S. Kotot, *Spectrochim. Acta, Part A*, 2006, **64**, 448–453.
- R. G. Zhibankov, *Infrared spectra of cellulose and its derivatives*, Consultants Bureau, New York, 1966, p. 333.
- D. Oldak, H. Kaczmarek, T. Buffeteau and C. Sourisseau, *J. Mater. Sci.*, 2005, **40**, 4189–4198.

An efficient and transition metal free protocol for the transfer hydrogenation of ketones as a continuous flow process†

Jörg Sedelmeier, Steven V. Ley* and Ian R. Baxendale

Received 4th December 2008, Accepted 4th March 2009

First published as an Advance Article on the web 12th March 2009

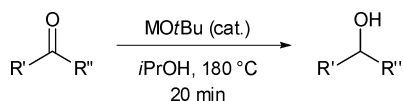
DOI: 10.1039/b821752a

We report the efficient reduction of a selection of ketones to the corresponding secondary alcohols using only catalytic amounts of LiOtBu in *i*PrOH facilitated by using a continuous flow reactor.

The development of new and improved chemical processing techniques that are both economically viable with greater environmental compatibility are of paramount importance to the chemical industry. The ability to conduct both complex and routine chemical transformations in a safe, reproducible and scalable fashion without recourse to costly route modification or redevelopment is highly desirable. The introduction of continuous flow reactor technologies^{1,2} offers the ability to rapidly test, optimise and create scalable syntheses using a single bench top device. Furthermore, the intrinsic design of these microreactors and their high temperature and pressure tolerances enables utilisation of enhanced reaction conditions that were previously difficult to evaluate.

The formation of secondary alcohols through the direct reduction of the precursor ketone typically requires either stoichiometric amounts of a hydride donor or a combination of a transition metal catalyst and a molecular hydrogen source. Recently, Adolffson reported upon an alternative protocol that excluded the use of expensive and toxic metal complexes, and avoided the need for molecular hydrogen.³ Instead, a combination of inexpensive LiOtPr and *i*PrOH was used. Expanding upon this idea we have developed a simple and highly efficient continuous flow process for the alkali metal catalysed reduction of ketones which makes potential scale up, with regard to industrial application, very straightforward.

We have previously shown that there is a significant benefit attained from the rapid co-evaluation of new high temperature reactions using microwave heating techniques and their subsequent translation into flow chemistry processes.⁴ Consequently, our initial screening involved heating an *i*PrOH solution of 4-methoxy acetophenone in a sealed vial under microwave irradiation to 180 °C for 20 minutes (Scheme 1).



Scheme 1 Alkali metal *tert*-butoxide catalysed reduction of ketones.

Innovative Technology Centre, Department of Chemistry, University of Cambridge, Lensfield Road, Cambridge, UK CB2 1EW.
E-mail: svl1000@cam.ac.uk

† Electronic supplementary information (ESI) available: ¹H and ¹³C NMR spectra for the alcohols. See DOI: 10.1039/b821752a

This study revealed that the nature of the alkali metal ion had a significant influence on the rate of the resulting reduction. LiOtBu was superior to the corresponding Na or K salts, producing the secondary alcohol in excellent yield. In these initial transformations a reproducible 94% isolated yield of the desired alcohol was achieved using only 10 mol% of LiOtBu. Of significant developmental interest was that stock solutions of the appropriate ketone and base could be prepared in advance under aerobic conditions using standard laboratory grade *i*PrOH.

This procedure was then directly transferred to a small footprint, continuous flow through reactor. We selected an experimental prototype unit from ThalesNano (X-Cube™ Flow Reactor)⁵ for our investigation (Fig. 1).⁶ The X-Cube system consists of a stand-alone Knauer K120 HPLC pump providing a continuous flow stream of reactants or solvent to the reactor. The main reactor itself comprises an integrated back-pressure regulator (200 bar max.) and detector, a heating module (350 °C max.) that encompasses an exchangeable stainless steel coil (various reactor cells can be inserted to give different reactor volumes of 4, 8 and 16 mL). A heat exchanger is also positioned at the exit of the reactor to rapidly cool the exiting flow stream. Use of an in-line cartridge⁷ containing an excess of tosylhydrazine resin allows the scavenging of any residual ketone. For the examples described in this article no attempt was made to recover the ketone, although in practice more valuable starting materials could be subsequently released from the resin *via* a mild hydrolysis procedure.⁸

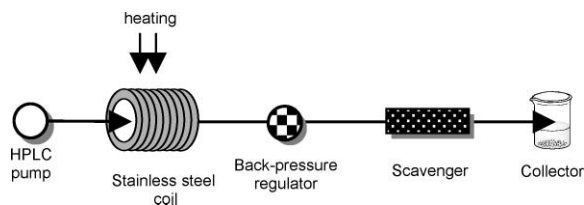


Fig. 1 Pictorial description of the flow reactor configuration.

The control of the reaction parameters (flow rate, temperature and pressure) can be programmed, monitored and modified through a basic keypad user interface.

An initial screening of conditions was performed, which included reaction temperature, internal pressure, reagent concentration and residence time (flow rate). Optimal conversions were achieved using a 0.3–0.4 M concentration of ketone in *i*PrOH at 180 °C and a back-pressure of 160 bar. Increasing the temperature to 200 °C gave no additional benefits in conversion or reaction rates. The relatively high back-pressure employed

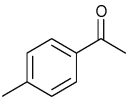
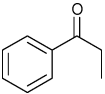
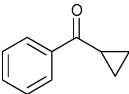
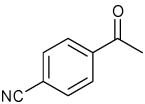
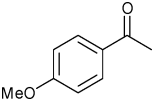
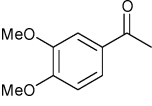
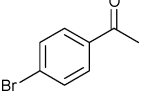
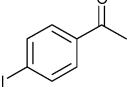
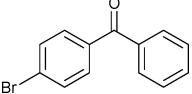
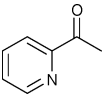
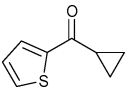
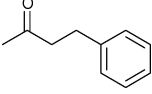
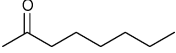
was required in order to maintain the *i*PrOH in the liquid phase at the elevated reaction temperatures, thus avoiding deposition and decomposition of the starting material, which eventually leads to the blockage of the system. The necessary residence time (flow rate) was substrate dependent and ranged between 20–30 minutes. Using these conditions a variety of ketones were readily reduced to the corresponding alcohols in high yield and excellent purity following tosyl-hydrazine resin scavenging (Table 1). The products required no additional purification following evaporation of solvent, which was pure enough to be recovered and reused.

In general the reductions proceed smoothly for substrates bearing electron-donating as well as electron-withdrawing substituents. Simple ketones (entries 1–3) reacted to the corresponding alcohols without difficulties. The presence of electron-withdrawing groups that increase the electrophilicity of the carbonyl (entries 4, 7 and 8) enabled shortening of the residence times from 30 to 20 minutes. The cyano functionalised acetophenone (entry 4) was smoothly reduced to the corresponding alcohol without affecting the nitrile functionality. In addition, the electron donating methoxy substituted acetophenones (entries 5 and 6) afforded the respective alcohols in good yield although longer residence times were required. Substrates possessing a halogen (entries 7–9) were also readily transformed; however, in the case of 4-iodo acetophenone and 4-bromo benzophenone, partial dehalogenation (6% and 5%) was also observed. The flow conditions proved to be suitable for the reduction of aliphatic (entries 12 and 13) and heteroaromatic ketones (entries 10 and 11), giving the expected products in excellent yields. Not all substrates tested reacted as efficiently. Substrates with hydroxy or amino moieties as well as easily enolisable carbonyls such as 3-chloro-4-nitro acetophenone and β -keto esters gave no conversion. The attempted reduction of ethyl 2-benzoylacetate gave the transesterified product exclusively.

The flow process easily allows for both the rapid optimisation of the reaction employing small injection aliquots of substrates as well as for scale up. Larger quantities of material can be easily prepared by running the system under steady state operation as a continuous flow process generating multi-gram batches. For example, processing a 0.3 M solution of 4-methoxy acetophenone (14.3 g, 95.2 mmol) at a flow rate of 0.53 mL min⁻¹ using a reactor volume of 16 mL generates 12.6 g (82.9 mmol) of material over a 10 h period. In the case of the large batch experiment the in-line scavenging procedure was slightly modified. First the *i*PrOH and the by-product acetone were evaporated, then the residue re-dissolved in *i*PrOH followed by addition of the tosyl-hydrazine scavenger (7.0 g, 2.84 mmol g⁻¹). The suspension was then vortexed on an orbital shaker for 1 h, and the resin removed by filtration. Following evaporation of the solvent the product was isolated in excellent purity.

In summary, we have devised a simple, efficient and transition metal free transfer hydrogenation protocol for use under flow conditions. The reaction is performed using a cheap and safe reaction medium, delivering secondary alcohol products in high yields and excellent purities following only evaporation and recovery of the solvent. The combination of the simple experimental conditions and the flow processing capabilities of

Table 1 Lithium *tert*-butoxide catalysed transfer hydrogenation^a

Entry	Substrate	Residence time/min	Conversion ^b [%]
1		30	96 (94)
2		30	96 (91)
3		30	93 (92)
4		20	98
5		30	93 (87)
6		30	85
7		20	98
8		20	96 ^c
9		30	(92) ^d
10		30	99 (97)
11		30	89 (88)
12		30	84
13		30	95 (90)

^a Reaction conditions: the reaction solution (0.3–0.4 M) containing LiO*t*Bu (10 mol%) and the appropriate ketone in *i*PrOH was continuously pumped through the X-Cube™ at 180 °C for the indicated residence time. After complete injection of the reaction mixture, the system was purged with pure *i*PrOH. ^b Conversions determined by ¹H-NMR. Yields are given in parentheses. ^c 6% dehalogenated alcohol was observed. ^d An additional 5% dehalogenated alcohol was also isolated.

the reactor permits easy scale up, rendering this approach of high relevance for industrial application. The total volumes of solvent and reagents used in the flow reactions are significantly less than the batch mode process. Moreover, this reduction procedure does not involve the hazards associated with other batch mode reduction processes, such as with hydride reagents or high pressure hydrogenations and the use of toxic metal catalysts.

Experimental

Typical procedure

LiO^tBu (0.05 mmol) and ketone (0.50 mmol) were dissolved in *i*PrOH (1.5 mL) at room temperature under atmospheric conditions. The resulting solution was pumped continuously into the X-Cube™ and heated to 180 °C for the appropriate residence time. After the reaction mixture exited the system, the solvent was removed under reduced pressure.

Acknowledgements

The authors would like to thank the DAAD for a postdoctoral fellowship (JS), the EPSRC for funding (IRB) and the BP 1702 Professorship (SVL).

Notes and references

- 1 I. R. Baxendale, J. J. Hayward, S. Lanners, S. V. Ley, C. D. Smith, *Organic Chemistry in Microreactors: Heterogeneous Reactions in Microreactors in Organic Synthesis and Catalysis*, ed. T. Wirth, Wiley-VCH, Weinheim, 2008, Chapter 4.2, pp. 84–122.
- 2 (a) T. Fukuyama, M. T. Rahman, M. Sato and I. Ryu, *Synlett*, 2008, 151; (b) H. R. Sahoo, J. G. Kralj and K. F. Jensen, *Angew. Chem., Int. Ed.*, 2007, **46**, 5704; (c) P. Hodge, *Ind. Eng. Chem. Res.*, 2005, **44**, 8542; (d) K. Jähnisch, V. Hessel, H. Löwe and M. Baerns, *Angew. Chem., Int. Ed.*, 2004, **43**, 406; (e) G. Jas and A. Kirschning, *Chem.–Eur. J.*, 2003, **9**, 5708; (f) I. R. Baxendale, C. M. Griffiths-Jones, S. V. Ley and G. K. Tranmer, *Synlett*, 2006, **3**, 427; (g) I. R. Baxendale, J. Deeley, C. M. Griffiths-Jones, S. V. Ley, S. Saaby and G. K. Tranmer, *Chem. Commun.*, 2006, **24**, 2566.
- 3 J. Ekström, J. Wettergren and H. Adolfsson, *Adv. Synth. Catal.*, 2007, **349**, 1609.
- 4 (a) I. R. Baxendale, J. J. Hayward and S. V. Ley, *Comb. Chem. High Throughput Screening*, 2007, **35**, 802; (b) C. J. Smith, F. J. Iglesias-Sigüenza, I. R. Baxendale and S. V. Ley, *Org. Biomol. Chem.*, 2007, **5**, 2758; (c) I. R. Baxendale, C. M. Griffiths-Jones, S. V. Ley and G. K. Tranmer, *Chem.–Eur. J.*, 2006, **12**, 4407; (d) S. Saaby, I. R. Baxendale and S. V. Ley, *Org. Biomol. Chem.*, 2005, **3**, 3365.
- 5 T. N. Glasnov, S. Findenig and O. Kappe, *Chem.–Eur. J.*, 2009, **15**, 1001.
- 6 <http://www.thalesnano.com/>.
- 7 An Omnifit Column 6.6 mm × 10 cm with two fixed end connectors was filled with tosyl-hydrazine resin (Biotage Cat. No. 800270 loading 2.84 mmol g⁻¹).
- 8 D. W. Emerson, R. R. Emerson, S. C. Joshi, E. M. Sorensen and J. E. Turek, *J. Org. Chem.*, 1979, **44**, 4634.

Development of new green lubricating grease formulations based on cellulosic derivatives and castor oil

R. Sánchez, J. M. Franco,* M. A. Delgado, C. Valencia and C. Gallegos

Received 19th November 2008, Accepted 30th January 2009

First published as an Advance Article on the web 25th February 2009

DOI: 10.1039/b820547g

Environmentally friendly lubricating greases may be produced by solely replacing the mineral base oil for vegetable oil. However, the substitution of traditional metallic soaps by biodegradable and renewable thickeners is, up to now, much less considered. This work is focused on the development of new oleogels, using castor oil and cellulose derivatives, which could be potentially used as biodegradable lubricating greases. Thermal and thermo-rheological behaviours of these materials were characterised by means of TGA analysis and SAOS measurements, in order to evaluate the evolution of oleogel microstructure with temperature. Moreover, both roll-stability and leakage tendency standard tests, usually performed in the grease industry, were used to evaluate the mechanical resistance of each sample. The evolution of biogrease linear viscoelasticity functions with frequency is quite similar to that found for traditional lithium lubricating greases. However, the influence of temperature on biogreases linear viscoelasticity functions is less important than that found for traditional greases. In general, the biogrease samples studied show both slightly lower mechanical stability and higher leakage tendency than traditional lubricating greases. The use of a blend of ethyl and methyl cellulose as thickener provides a mechanical stability comparable to that found for commercial greases.

Introduction

It is well known that the use of renewable resources for different industrial applications has a remarkable importance in our society, due to its positive effect on the environment. Among these renewable resources, cellulose derivatives and vegetable oils are increasingly taken into account. Thus, for instance, cellulose has been used in biocomposites for packaging applications,¹ whilst vegetable oils have been employed as biodegradable raw material in a wide range of new applications.²⁻⁴

From a general perspective, there is a marked tendency to increase the use of eco-friendly consumer products, as a result of government regulations or due to increasing public concern for a pollution-free environment.⁵ More particularly, the lubricant industry and its customers are keen on products that do not diminish the world finite resources of mineral hydrocarbons and/or exert minimal adverse impact on the environment.⁶⁻⁸ In this sense, every year millions of tonnes of engine, industrial and hydraulic oils leak into the ground or waterways, or are disposed of in the environment.⁶ Mineral-based oils can contaminate groundwater for up to 100 year, which may inhibit trees' growth and be toxic to aquatic life.⁶ In addition to this, large amounts of money have been spent to clean up accidental oil spills.^{5,9} To minimise the contamination damage that petroleum-based products cause in the environment, there has been an increasing demand for green products suitable to be used as lubricants,⁶

where cellulose-based oleogels may play an important role as environmentally friendly substitutes.

Oleogels are gel systems obtained with a gelling agent and a hydrophobic liquid. In previous studies,^{10,11} organogelators like ethylcellulose, cholesterol, sorbitan monostearate and lanolin alcohols were tested with several organic solvents, including vegetable oils. The main advantages of these gels are that they do not require extensive manufacturing expertise to be produced,¹¹ in contrast to traditional soap-based lubricating greases which require a particular and rather sophisticated technology with several processing stages,¹²⁻¹⁴ and they can exhibit permanent rigid networks or transient thermoreversible semiflexible meshes.¹⁰

Over the last fifteen years, there has been an increasing interest on these oleogels.^{11,15,16} Among their potential applications, biodegradable oleogels could be used as lubricating greases. In a previous work,¹⁷ the possibility of using oleogels based on sorbitan monostearate (SMS) and castor oil for lubricating purposes was explored. However, in spite of the promising rheological characteristics found, the use of SMS as organogellator confers to the final product some limitations, mainly related to the maximum working temperature that can be reached and to its rather poor mechanical stability.

Although some work concerning biogreases development has been previously carried out by other authors,^{18,19} it has been mainly focused on the replacement of mineral oil by vegetable oil. Among the vegetable oils, the castor oil is being occasionally used for lubricant purposes due to its high viscosity and good performance characteristics at low temperatures.²⁰ However, the research of new biodegradable thickeners, as substitutes for metal soaps or polyurea, is up to now much less explored. In this work, the use of cellulose derivatives, aiming

Departamento de Ingeniería Química, Facultad de Ciencias Experimentales, Campus de "El Carmen", Universidad de Huelva, 21071, Huelva, Spain. E-mail: franco@uhu.es; Fax: +34 959219983; Tel: +34 959219995

Table 1 Fatty acid composition of the castor oil used to prepare oleogels

Fatty acid	%
Palmitic acid (C16:0)	2.6
Stearic acid (C18:0)	2.7
Oleic acid (C18:1)	6.3
Linoleic acid (C18:2)	10.8
Ricinoleic acid (12-hidroxi C18:1)	77.6

to obtain biodegradable lubricating greases completely based on natural products, is reported. The performance of these cellulose derivatives-based oleogels was investigated through rheological, thermal, and standard mechanical tests.

Materials and methods

Materials

Castor oil (211 cSt at 40 °C, Guinama, Spain) was selected as the biodegradable lubricating oil. The fatty acid composition of castor oil is shown in Table 1. Ethyl cellulose (M_n 66000 g/mol; 49% ethoxy content), methyl cellulose (M_n 40000 g/mol; 32% methoxy content), cellulose acetate (M_n 50000 g/mol; 39.7% acetyl content), and α -cellulose, all of them from Sigma-Aldrich, were used as gelling agents to prepare different oleogel formulations. Standard lithium 12-hydroxystearate lubricating greases (14–20% lithium soap) of similar NLGI grade were used as reference systems. 12-hydroxystearic acid, lithium hydroxide, and paraffinic (334 cSt at 40 °C) and naphthenic (115 cSt at 40 °C) mineral oils were kindly supplied by Verkol Lubricantes S.A. (Spain).

Manufacture of oleogel formulations

Castor oil and cellulose derivatives were mixed using a PolyLab-Rheomix 3000p (Haake, Germany), which consists of a batch mixer fitted with two counter-rotating rollers. Specifically, the chamber (310 cm³) was first filled with the corresponding amount of oil in the blend. The cellulose derivative was then slowly added to the castor oil. Batches of 250 g oleogel were prepared. A constant rotational speed (50 rpm) was applied to this mixture, for 30 minutes, at room temperature. The mixture was previously heated, up to 150 °C, only for samples containing ethyl cellulose, and then cooled by natural convection. The reason for using this type of mixing device is due to the high viscosity of these formulations, especially during the first stages.

Specific thickener concentrations are required to obtain stable oleogels, with visual appearance similar to traditional lubricating greases, depending on the cellulose derivative employed. In the case of formulations without ethyl cellulose, stable oleogel formulations were achieved by dispersing, at room temperature, 35% w/w methyl cellulose (COMC35), 35% w/w cellulose acetate (COAC35), or 25% w/w α -cellulose (CO α C25), respectively, in castor oil. Lower cellulose derivative concentrations yield low consistency indexes (NLGI grade 000) and low physical stability, evidenced by an apparent oil separation after several days of ageing. On the other hand, higher cellulose derivative concentrations than those previously mentioned provide highly strong oleogels, with physical appearance

very different to traditional lubricating greases. In the case of formulations prepared by adding 2% w/w ethyl cellulose, stable oleogel samples were obtained with 25% and 30% w/w methyl cellulose (COECMC25 and COECMC30), and 20% w/w α -cellulose (COEC α C20). Cellulose acetate does not seem to be compatible with ethyl cellulose, and does not produce a gel-like material that could be considered a lubricating grease.

Gas chromatography (GC)

GC analysis was performed with an Agilent 6890 chromatograph equipped with a flame-ionization detector in order to determine the fatty acid profile in castor oil. C₁₄–C₂₄ FAMES provided standards were used.

Thermogravimetric analysis (TGA)

Thermogravimetric analyses were carried out by using a Q-50 TA Instrument under N₂ and O₂ purge. Approximately, 15 mg of each sample were placed on a Pt pan, and heated from 30 °C to 500 °C at 10 °C/min.

Rheological characterization

Rheological characterization of oleogels was carried out with two controlled-stress rheometers (RS-150 and Rheoscope, ThermoHaake, Germany). Small-amplitude oscillatory shear (SAOS) tests were performed inside the linear viscoelastic region, using a serrated plate-plate geometry (35 mm, 1 mm gap, relative roughness 0.4), in a frequency range of 10⁻²–10² rad/s, and temperatures comprised between 0 and 225 °C. At least two replicates of each test were performed on fresh samples.

Penetration and mechanical stability tests

Both unworked and worked penetration indexes were determined according to the ASTM D 1403 standard, by using a Seta Universal penetrometer, model 17000-2, with one-quarter cone geometry (Stanhope-Seta, UK). The one-quarter scale penetration values were converted into the equivalent full-scale cone penetration values, following the ASTM D 217 standard. Samples were worked during 2 hours in a Roll Stability Tester, model 19400-3 (Stanhope-Seta, UK) according to the ASTM D 1831 standard, and penetration measurements were carried out, once again, immediately after this rolling test.

Leakage tendencies in wheel bearings

Oleogel leakage tendencies in wheel bearings were determined in a Petrotest equipment, model 17-0450 (Germany), according to the ASTM D 1263 standard. This test method covers the evaluation of the leakage tendencies of lubricating greases when they are tested under specific simulated wheel bearing conditions. The sample is distributed in a modified front-wheel hub and spindle assembly. The hub is rotated at a speed of 660 ± 30 rpm for 6 hours ± 5 minutes, at a spindle temperature which is raised to and then maintained at 105 ± 1.2 °C. Leakage of the sample is measured, and the condition of the bearing surface is checked at the end of the test.

Table 2 Characteristic parameters obtained from TGA measurements

Sample	Atmosphere	T _{range}		T _{max} (°C)	Residue (%)
		T _{onset} (°C)	T _{final} (°C)		
COMC35	N ₂	353	401	370	3.0
	O ₂	334	—	360	5.9
COAC35	N ₂	348	412	376	4.6
	O ₂	338	—	367	10.8
COαC25	N ₂	341	413	368	3.8
	O ₂	283	—	367	4.1
COECMC25	N ₂	354	402	377	3.0
	O ₂	348	—	368	5.4
COECMC30	N ₂	351	399	378	3.7
	O ₂	330	—	362	7.5
COECαC20	N ₂	347	417	388	3.2
	O ₂	313	—	364	8.3
COLi	N ₂	329	403	362	0.3
	O ₂	321	—	357	14.3
Standard paraffinic oil-based grease	N ₂	188	—	245	3.8
	O ₂	181	—	245	1.3

Results and discussion

Oleogel formulations without ethyl cellulose

Fig. 1 shows oleogel weight loss with temperature, using N₂ flux, for a selected formulation containing α-cellulose as thickener. Its derivative function is also shown in this figure. Table 2 shows the most characteristic parameters obtained from this thermogravimetric analysis for all the oleogel formulations studied. In general, the thermal decomposition of the oleogels studied takes place in one single stage, comprised between 340 and 415 °C, approximately. The thermal stability of oleogels has been estimated from the onset temperature (T_{onset}), which is determined from the interception between the slope of the first region, where the sample weight is approximately constant, and the slope of the region where sample weight loss rate is maximum. The sample containing α-cellulose displays a slightly lower thermal stability (lower T_{onset}), being its maximum decomposition rate reached at lower temperature (T_{max}). The oleogel containing methyl cellulose shows the highest T_{onset} value, although the sample that exhibits the maximum decomposition

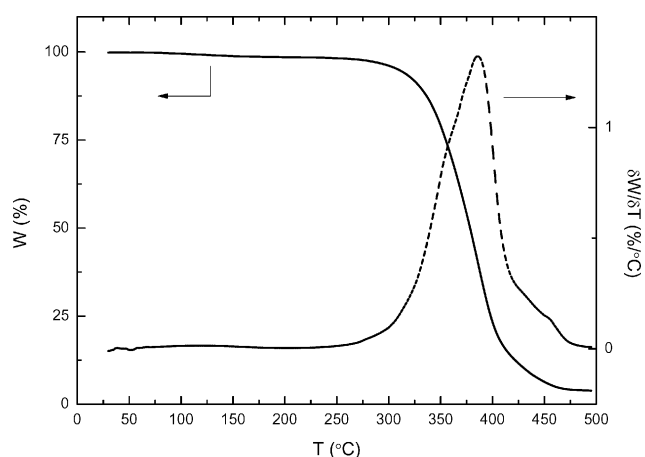


Fig. 1 TGA thermogram for a selected oleogel (COαC25). Test performed under nitrogen atmosphere.

rate at a higher temperature is the oleogel prepared with acetate cellulose, which also contains a larger amount of residues. In general, oleogels based in cellulose derivatives show slightly higher T_{onset} and T_{max} values than a standard grease prepared with the same castor oil and a lithium soap (sample COLi), and much higher values than the standard grease prepared with a mineral paraffinic oil, fact that can be explained by considering the lower volatility of castor oil.

Oleogel weight loss with temperature for the same samples, using oxygen flux during the thermogravimetric analysis, shows that the onset temperatures are always significantly lower than the ones obtained using nitrogen, especially in the case of the sample prepared with α-cellulose, which shows a T_{onset} even lower than COLi sample. In addition, the maximum decomposition rate is also reached at lower temperature. An increase in the residual content using an oxygen atmosphere is apparent. These effects must be attributed to different oxidative processes occurred in both the cellulose derivatives^{21,22} and the castor oil.²³ It is well known that other vegetable oils not containing hydroxyl groups in the predominant fatty acids, for instance soy or sunflower oils, are more resistant to oxidation than castor oil.²⁰ However, the high viscosity provided by the castor oil is crucial to reduce both the oil separation and the leakage tendency of oleogels. In any case, more work is needed to find a balance between the benefits of oil viscosity and resistance to oxidation.

Figs. 2 and 3 show the evolution of the linear viscoelasticity functions with frequency, as a function of temperature, for the different samples studied. This evolution is similar to those found for traditional lubricating greases.^{24,25} As can be observed, G' is always higher than G'' in the whole frequency range studied, except for the formulation that contain cellulose acetate at 225 °C, which displays a crossover between both viscoelastic functions at high frequencies. The plateau region of the mechanical spectrum is always noticed, which is not qualitatively affected by temperature, oppositely to the behaviour found for most of standard greases.²⁶ Moreover, oleogel elastic network seems to resist higher temperatures than metallic soap-based greases. Thus, standard grease elastic network vanishes above the soap melting point, that is, around 200 °C in the case of lithium greases.

The oleogel sample containing methyl cellulose shows a continuous decrease in G' by increasing temperature, above all in the range 25–75 °C (Fig. 2a). The loss modulus, G'', also decreases with temperature, but to a lesser extent. As a consequence, the loss tangent (tanδ=G''/G') generally increases with temperature, excepting at 225 °C, due to an important decrease in G'' values (Fig. 3a).

On the contrary, the cellulose acetate-based formulation displays a completely different behaviour. The values of both moduli slightly increase with temperature (Fig. 2b). However, the rheological behaviour drastically changes at 225 °C, due to cellulose acetate melting,²⁷ yielding the above mentioned crossover between both viscoelastic functions. The evolution of the loss tangent with frequency is almost independent of the temperature excepting, obviously, at 225 °C (Fig. 3b).

Finally, the oleogel sample containing α-cellulose shows a thermo-rheological behaviour relatively similar to that of the formulation containing methyl cellulose. However, in this case, the storage modulus is less affected by temperature (Fig. 2c).

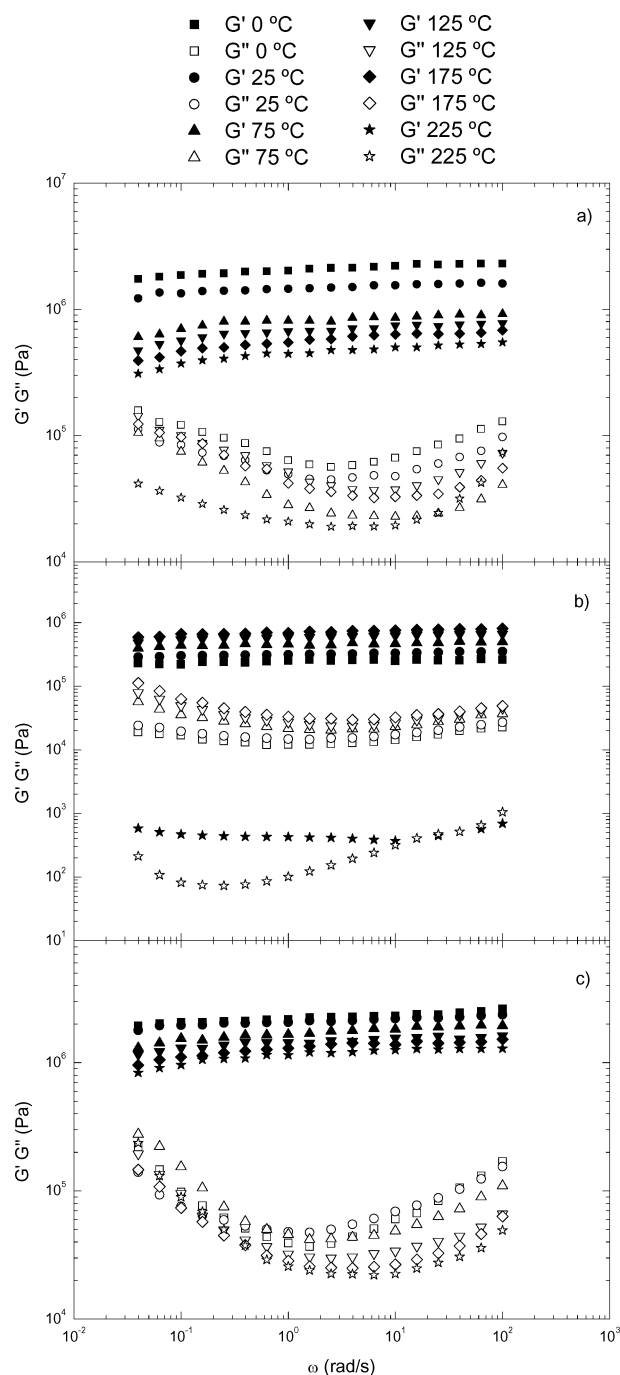


Fig. 2 Evolution of the storage and loss moduli with frequency for a) COMC35, b) COAC35 and c) CO α C25, at different temperatures.

Moreover, the loss modulus continuously decreases with temperature, although a tendency to reach similar values at low frequencies is apparent. The loss tangent is slightly influenced by temperature (Fig. 3c). The small influence of temperature on oleogel loss tangent is, thus, rather general, and is also an important characteristic of these materials, not found in traditional lithium greases.²⁶

The plateau modulus, G_N^0 , is a characteristic parameter of the plateau region of the mechanical spectrum. For polymeric systems, it is defined as the extrapolation, at high frequencies, of the contribution of entanglements to G' .²⁸ Similarly to the be-

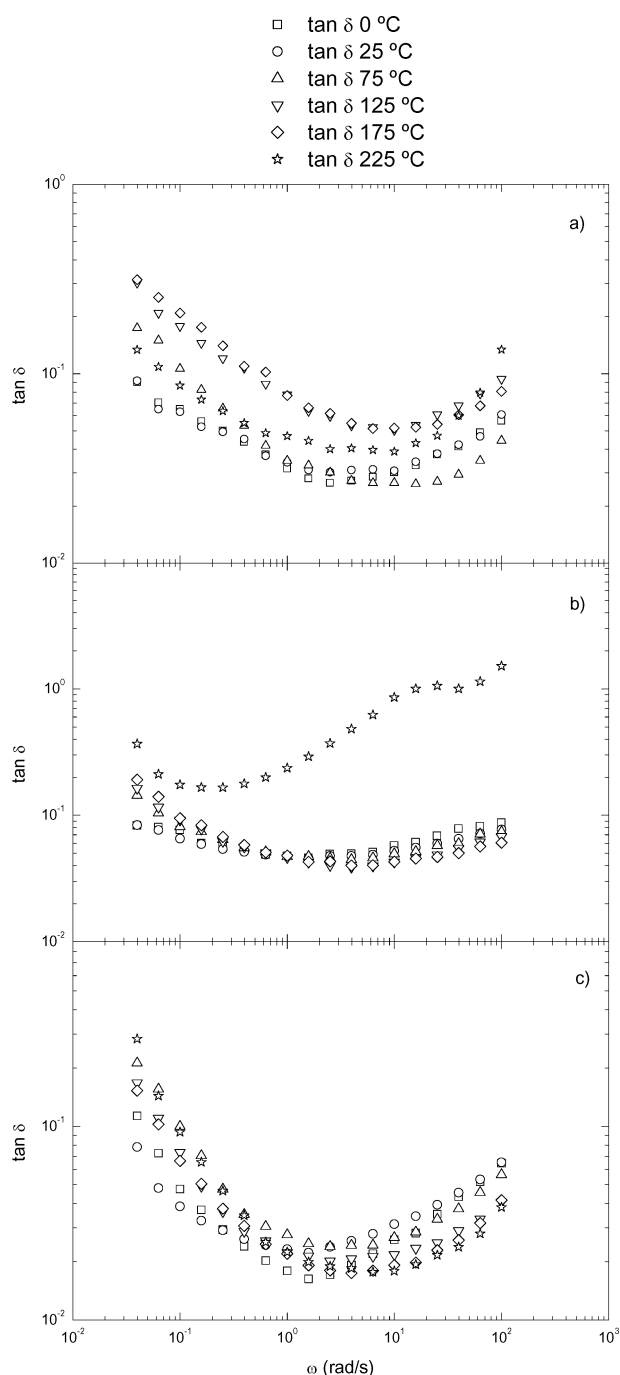


Fig. 3 Evolution of the loss tangent with frequency for a) COMC35, b) COAC35 and c) CO α C25, at different temperatures.

haviour found for traditional lubricating greases,²⁶ the oleogels studied in this research are not thermo-rheologically simple materials and, therefore, the time-temperature superposition principle is not applicable. This means that the value of the plateau modulus is not unique for a given system but a function of temperature. Thus, the evolution of G_N^0 with temperature has been fitted successfully (see Fig. 4 for a selected formulation) to an Arrhenius-like equation ($R^2 > 0.988$):

$$G_N^0 = A \cdot e^{\frac{E_a}{R} \left(\frac{1}{T} \right)} \quad (1)$$

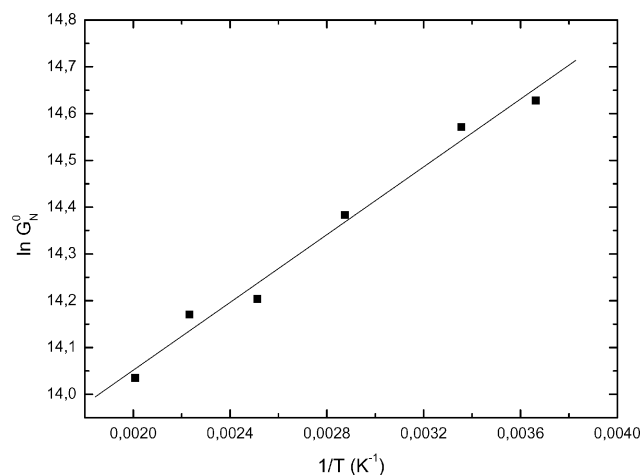


Fig. 4 Evolution of the plateau modulus (square symbols) with temperature, and Arrhenius' fitting (solid line), for a selected oleogel (CO α C25).

where E_a is the activation energy (J/mol), R is the gas constant (8.314 J/mol K), T is the absolute temperature (K), and A is the pre-exponential factor (Pa).

Table 3 shows equation (1) fitting parameters for the oleogels studied. The sample containing methyl cellulose as thickener shows the highest activation energy, since the plateau modulus is more affected by temperature than, for instance, the oleogel prepared with α -cellulose. On the other hand, the sample prepared with acetate cellulose shows a negative value of this activation energy, due to the fact that, as was previously mentioned, the plateau modulus increases with temperature (excluding the measurement carried out at 225 °C).

Oleogel formulations containing ethyl cellulose

The oleogel formulations studied in the previous section, which include just one cellulose derivative, present two important disadvantages in relation to traditional lubricating greases. First, these oleogels may be considered as strong gels, with values of the SAOS functions more than one decade higher than traditional lubricating greases,^{24–26} which is attributed to the high thickener content required to achieve stable formulations. However, these gels are highly susceptible to shear, showing, for instance, lower mechanical stability than lithium greases, in spite of the higher values of the oleogel SAOS functions. On the other hand, a certain degree of oil phase separation is apparent (oil bleeding), especially when samples are submitted to severe working conditions, due to the rigidity of the gel network. In order to minimize these adverse effects, ethyl cellulose (2% w/w)

Table 3 Activation energy values, from equation (1), for the different oleogel samples studied

Sample	E_a (J/mol)
COMC35	6978
COAC35	–6099
CO α C25	3011
COECMC25	18655
COECMC30	4505
COEC α C20	1814

was dispersed in castor oil, above its glass transition temperature (~ 150 °C). Further on, the sample was cooled. The result was a very homogeneous gel-like oil phase, much more viscous than the castor oil. Afterwards, the standard protocol was followed to mix the oil phase with the other cellulose derivative. As mentioned in the experimental section, stable oleogel samples were obtained by adding 25% and 30% w/w methyl cellulose and 20% w/w α -cellulose when ethyl cellulose was also included in the formulation. Therefore, the use of ethyl cellulose allows us to reduce the thickener content in the oleogel, and inhibits oil phase separation, even when the sample is submitted to severe working conditions. The use of a high-viscosity vegetable oil like the castor oil reinforces the role of ethyl cellulose.

As can be seen in Table 2, the sample prepared with methyl cellulose has better thermal stability (i.e. higher T_{onset} than oleogel prepared with α -cellulose), and very similar to that shown by the oleogel prepared with this thickener but without ethyl cellulose. The temperature for maximum decomposition rate is, in general, much higher than for samples formulated without ethyl cellulose when using nitrogen flux during the test. This effect is probably due to the modification that the ethyl cellulose exerts in the properties of castor oil. Once again, the onset and maximum decomposition rate temperatures decrease when the test is carried under oxygen instead of N_2 atmosphere, yielding similar values to those found for COLi sample, especially in the case of the α -cellulose-containing oleogel.

Figs. 5 and 6 show the evolution of the SAOS functions with frequency for oleogels including ethyl cellulose in their formulations, in a temperature range of 0–225 °C. The linear viscoelasticity range was not experimentally observed, at temperatures higher than 100 °C, for the oleogel containing 25% w/w methyl cellulose. The mechanical spectra of these oleogels are qualitatively similar to those previously shown for oleogels without ethyl cellulose, but, as intended, significantly lower values of the SAOS functions were obtained. The linear viscoelasticity functions of the sample containing 2% ethyl cellulose and 25% methyl cellulose are highly influenced by temperature (see Figs. 5a and 6a). G' and G'' values decrease one decade in the whole frequency studied, whilst the loss tangent slightly increases as temperature is raised from 0 to 100 °C. On the other hand, the formulation that contains 2% ethyl cellulose and 30% methyl cellulose is much less affected by temperature (see Fig. 5b), a qualitatively similar behaviour to that found for the formulation which includes only methyl cellulose as thickener. Finally, the influence of temperature on the linear viscoelasticity functions of the oleogel sample containing 2% ethyl cellulose and 20% α -cellulose is more complex. Thus, although the storage modulus slightly decreases as temperature increases, the loss modulus at 0 and 25 °C shows a minimum value at low frequency, which is shifted to higher frequencies when temperature is raised above 75 °C. Above this temperature, the behaviour is quite similar to that found for the sample without ethyl cellulose, where G'' is almost independent of temperature (see Fig. 5c).

The influence of temperature on the SAOS functions of the oleogel formulations containing ethyl cellulose can also be evaluated by comparing the activation energy values obtained from equation (1) (see Table 3). In this sense, ethyl cellulose

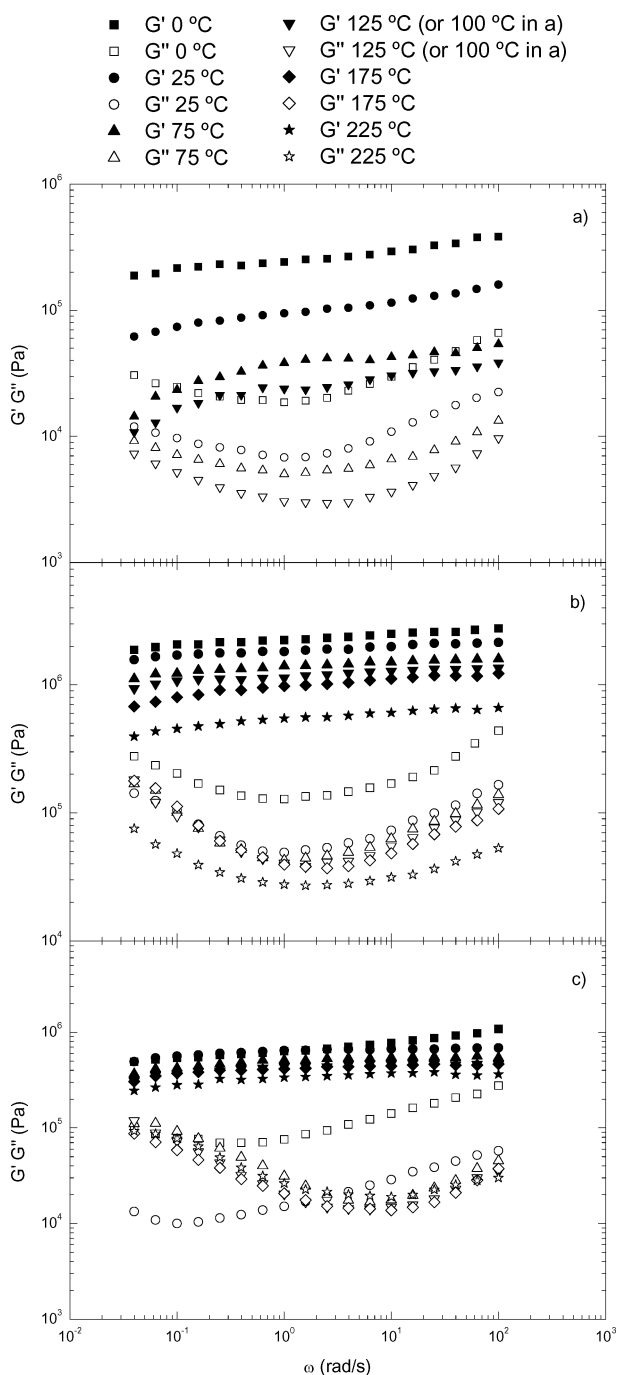


Fig. 5 Evolution of the storage and loss moduli with frequency for a) COECMC25, b) COECMC30 and c) COEC α C20, at different temperatures.

addition increases significantly the activation energy for samples containing 25% methyl cellulose, probably related to the rather low methyl cellulose concentration in the formulation. On the contrary, an important reduction in E_a values can be observed for samples with 30% methyl cellulose or 20% α -cellulose. Therefore, it may be concluded that the presence of ethyl cellulose in the formulation dampens significantly the thermal susceptibility of these oleogels, when formulations containing similar total concentrations of cellulose derivatives are compared.

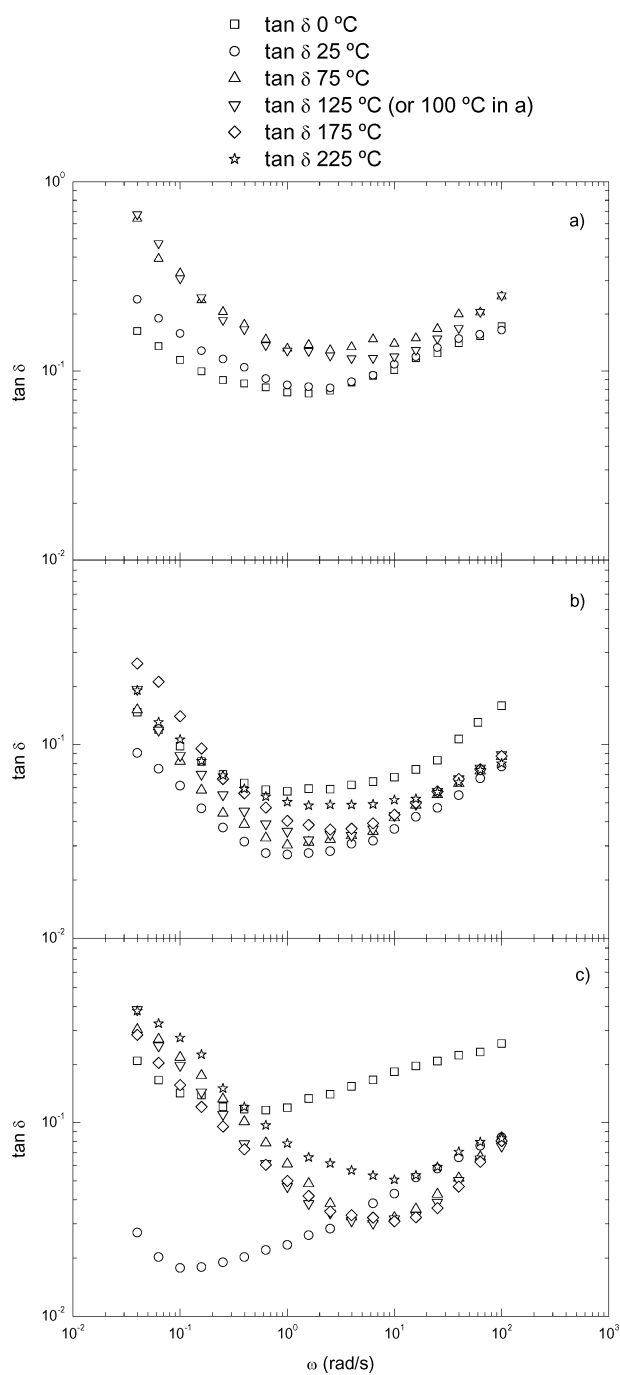


Fig. 6 Evolution of the loss tangent with frequency for a) COECMC25, b) COECMC30 and c) COEC α C20, at different temperatures.

Penetration, mechanical stability and leakage tests

Penetration values of unworked samples are traditionally converted to NLGI grades, in order to classify greases according to its consistency degree (between 000 and 6). The most commonly used greases are those with NLGI grade 2.²⁹ Softer grades, especially 0 and 1, are sometimes used for improved pumpability or low-temperature applications, while higher consistency indexes are used for certain high-speed bearings.²⁹ Table 4 collects unworked penetration values for the different oleogels studied, as well as the values obtained once the samples were submitted

Table 4 Penetration and leakage values for different oleogels, lithium soap/castor oil grease, and standard lubricating greases

Sample	Unworked penetration (dmm)	NLGI grade	Worked penetration (dmm)	Penetration variation (dmm)	Leakage (%)
COMC35	279	2	320	41	14.6
COAC35	388	00–0	459	71	26.4
CO α C25	324	1	354	30	21.7
COECMC25	380	0	422	42	49.4
COECMC30	324	1–2	347	23	37.5
COEC α C20	257	2–3	395	138	46.5
COLi	242	3	260	18	0.4
Standard paraffinic oil-based grease	303	1–2	305	2	1.2
Standard naphthenic oil-based grease	274	2	289	15	0.8

to the standard roll-stability test. In addition, the penetration values for selected (NLGI grades 1–3) lithium greases,^{30,31} prepared with either a mineral (paraffinic or naphthenic) oil or the same castor oil used to formulate the oleogels studied in this work (sample COLi), are also included for the sake of comparison. In general, the mechanical stability of the oleogels studied, which is inversely proportional to the penetration increment after working, is slightly lower than for lithium greases. Only the blend consisting of ethyl and methyl cellulose (2 and 30%, respectively) provides low enough penetration increment values, comparable to those found for commercial greases. In addition to this, the combination of ethyl cellulose and α -cellulose increases the NLGI grade of the oleogel, but, however, reduces its mechanical stability.

The main negative aspect of the oleogels containing cellulose derivatives is the high level of leakage found when they are subjected to the leakage standard test, at 105 °C (Table 4). The presence of ethyl cellulose in the formulation increases leakage, since the sol-gel transition of ethyl cellulose in oil is around 60 °C. However, when the same standard test was carried out by setting the spindle temperature at 25 °C, the leakage values obtained were $1.4 \pm 0.2\%$ for formulations with ethyl cellulose, which indicates that these oleogels show relatively low leakage tendencies when moderate temperature working conditions are applied.

Conclusions

In this work, the appropriateness of cellulose derivatives to form oleogels in a castor oil continuous phase, in order to obtain new biodegradable lubricating grease formulations completely based on natural products, was investigated. Some cellulose derivatives, like methylcellulose and α -cellulose, at concentrations of 35% and 25% w/w respectively, yield oleogels with suitable thermal and rheological properties. In general, oleogel thermal decompositions take place in one single stage, showing improved thermal stabilities and maximum decomposition rate temperatures than traditional greases based on mineral paraffinic oil and lithium soap. The evolution of the linear viscoelasticity functions with frequency is qualitatively similar to that found for traditional lithium lubricating grease, being the values of SAOS moduli more than one decade higher. In addition, the temperature dependence of the linear viscoelasticity functions of the oleogels studied is less important, which may represent an important advantage. The addition of ethyl cellulose to the oleogel allows lower amounts of other cellulose derivatives, and

reduces significantly oil phase separation, by increasing castor oil viscosity. On the other hand, the presence of ethyl cellulose in the formulation provides higher values of the maximum decomposition rate temperature, and dampens the temperature dependence of the linear viscoelasticity functions. In general, the oleogel formulations studied show both slightly lower mechanical stability and higher leakage tendency, mainly at high temperature, than traditional lubricating greases. However, blends of ethyl and methyl cellulose (i.e. 2% and 30%wt., respectively) provide a mechanical stability comparable to that found for commercial greases.

Acknowledgements

This work is part of two research projects (CTQ2007–60463/PPQ and TEP-367) sponsored by a MEC-FEDER Programme and the “Consejería de Innovación, Ciencia y Empresa de la Junta de Andalucía” (“Projects of Excellence” Programme), respectively. One of the authors (R. Sánchez) has received a Ph.D. Research Grant from the “Consejería de Innovación, Ciencia y Empresa (Junta de Andalucía)”. The authors gratefully acknowledge their financial support.

References

- 1 A. P. Kumar and R. P. Singh, *Bioresour. Technol.*, 2008, **99**, 8803–8809.
- 2 S. Gryglewicz, W. Piechocki and G. Gryglewicz, *Bioresour. Technol.*, 2003, **87**, 35–39.
- 3 L. A. T. Honary, *Bioresour. Technol.*, 1996, **56**, 41–47.
- 4 S. L. Dmytryshyn, A. K. Dalai, S. T. Chaudhari, H. K. Mishra and M. J. Reaney, *Bioresour. Technol.*, 2004, **92**, 55–64.
- 5 A. Adhvaryu and S. Z. Erhan, *Ind. Crops Prod.*, 2002, **15**, 247–254.
- 6 B. Wilson, *Ind. Lubric. Tribol.*, 1998, **50**, 6–15.
- 7 Md. Nurun Nabi, Md. Shamim Akter and Md. Zaglul Shahadat, *Bioresour. Technol.*, 2006, **97**, 372–378.
- 8 S. Boyde, *Green Chem.*, 2002, **4**, 293–307.
- 9 J. K. Adesodun and J. S. C. Mbagwu, *Bioresour. Technol.*, 2008, **99**, 5659–5665.
- 10 I. F. Almeida and M. F. Bahia, *Rheo.pt.*, 2005, **5**, 12–18.
- 11 I. F. Almeida and M. F. Bahia, *Int. J. Pharm.*, 2006, **327**, 73–77.
- 12 Yu L. Ishchuk, *Lubricating Grease Manufacturing Technology*, New Age Int., New Delhi, 2005.
- 13 M. A. Delgado, M. C. Sánchez, C. Valencia, J. M. Franco and C. Gallegos, *Chem. Eng. Res. Des.*, 2005, **83**, 1085–1092.
- 14 J. M. Franco, M. Delgado, C. Valencia, M. C. Sánchez and C. Gallegos, *Chem. Eng. Sci.*, 2005, **60**, 2409–2418.
- 15 M. A. Ruíz Martínez, M. Muñoz de Benavides, M. E. Morales Hernández and V. Gallardo Lara, *Il Farmaco*, 2003, **58**, 1289–1294.

- 16 A. Bot, Y. S. J. Veldhuizen, R. den Adel and E. C. Roijers, *Food Hydrocolloid*, 2009, **23**, 1184–1189.
- 17 R. Sánchez, J. M. Franco, M. A. Delgado, C. Valencia and C. Gallegos, *Chem. Eng. Res. Des.*, 2008, **86**, 1073–1082.
- 18 A. Adhvaryu, C. Sung and S. Z. Erhan, *Ind. Crops Prod.*, 2005, **21**, 285–291.
- 19 W. H. Dresel, *Ind. Crops Prod.*, 1994, **2**, 281–288.
- 20 S. Asadauskas, J. M. Perez and J. L. Duda, *Lubric. Eng.*, 1997, **12**, 35–41.
- 21 B. Azambre, O. Heintz, A. Krzton, J. Zawadzki and J. V. Weber, *J. Anal. Appl. Pyrol.*, 2000, **55**, 105–117.
- 22 D. Cancellieri, E. Leoni and J. L. Rossi, *Thermochim. Acta*, 2005, **438**, 41–50.
- 23 N. J. Fox and G. W. Stachowiak, *Tribol Int.*, 2007, **40**, 1035–1046.
- 24 J. M. Madiedo, J. M. Franco, C. Valencia and C. Gallegos, *J. Tribol.*, 2000, **122**, 590–596.
- 25 J. E. Martín-Alfonso, C. Valencia, M. C. Sánchez, J. M. Franco and C. Gallegos, *Eur. Polym. J.*, 2007, **43**, 139–149.
- 26 M. A. Delgado, C. Valencia, M. C. Sánchez, J. M. Franco and C. Gallegos, *Tribol. Lett.*, 2006, **23**, 47–54.
- 27 M. Scandola and G. Ceccorulli, *Polymer*, 1985, **26**, 1953–1957.
- 28 M. Baumgaertel, M. E. de Rosa, J. Machado, M. Masse and H. H. Winter, *Rheol. Acta*, 1992, **31**, 78–82.
- 29 *NLGI, Lubricating Greases Guide*, National Lubricating Grease Institute, Kansas City, MO, 1994.
- 30 M. A. Delgado, C. Valencia, M. C. Sánchez, J. M. Franco and C. Gallegos, *Ind. Eng. Chem. Res.*, 2006, **45**, 1902–1910.
- 31 J. E. Martín-Alfonso, C. Valencia, M. C. Sánchez, J. M. Franco and C. Gallegos, *Ind. Eng. Chem. Res.*, 2009, DOI: 10.1021/ie01359g.

Kinetics and solvent effects in the synthesis of ionic liquids: imidazolium

Jay C. Schleicher† and Aaron M. Scurto*

Received 19th May 2008, Accepted 5th February 2009

First published as an Advance Article on the web 26th February 2009

DOI: 10.1039/b808364a

Ionic liquids (ILs) are being considered as a promising class of potentially environmentally-friendly (“green”) solvents and materials for use in a variety of applications. However, ionic liquids are conventionally synthesized by batch, without known kinetics, in non-sustainable solvents. For ILs to be a truly “green” technology for widespread use, they must themselves be made in a correspondingly benign manner for low cost, as enabled by process development. This investigation will illustrate the kinetics and large solvent effects in the synthesis of 1-hexyl-3-methyl-imidazolium bromide in 10 different solvents: acetone, acetonitrile, 2-butanone, chlorobenzene, dichloromethane, dimethyl sulfoxide (DMSO), ethyl formate, ethyl lactate, methanol, and cyclopentanone. The kinetic rate constant for the synthesis in DMSO is over an order-of-magnitude larger than that in methanol. While the kinetic rate of these type of S_N2 reactions is generally known to increase with solvent “polarity”, multi-parameter solvent descriptors, *e.g.* of Kamlet and Taft, are required to quantify these effects in a Linear Solvation Energy Relationship. These relationships are used with environmental and toxicity databases, such as the Rowan Solvent Selection Table, to rapidly optimize the solvent for favorable kinetics and minimal human and environmental impact.

1. Introduction

Ionic liquids (ILs) have been touted as the next great class of environmentally-friendly solvents due to their molecularly “tunable” properties and lack of volatility. New applications are being developed at a rapid pace. ILs have shown promise in enhancing catalytic activity, selectivity, stability and ability for recycling in various catalyzed reaction systems, such as hydroformylation reactions,^{1,2} and even in a wide range of biocatalytic transformations.³ ILs have a number of uses in various separation process. For instance, ILs can “break” a number of azeotropes;⁴ separate gases,⁵ including refrigerant gases;⁶ desulfurize diesel fuel;⁷ dissolve and process cellulose and other carbohydrates;⁸ are involved commercially in a biphasic acid scavenging processes;⁹ *etc.* In the field of analytical chemistry, ILs can be used as stationary phases in chromatography and other separation and detection techniques.¹⁰ ILs have a long history in the field of electrochemistry¹¹ with more recent examples in electro-nanomaterial technologies.¹² Active pharmaceutical ingredients (APIs) have been re-formulated as ionic liquids themselves¹³ to overcome difficulties with solid-state polymorphic forms and other processing challenges, *etc.*

Despite all of the numerous chemistries and applications possible, reports of the synthesis of ionic liquids often include the *very* solvents that they will purportedly replace. Solvents such

as dichloromethane, 1,1,1-trichloroethane, petroleum ether, toluene, *etc.* have all been used in their synthesis.^{14–18} Moreover, ILs are often too costly to be utilized as an alternative solvent in many large-scale industrial processes.¹⁹ This is primarily due to small batch production and nearly non-existent kinetic and thermodynamic data of their synthesis that has resulted in little emphasis on reaction engineering and process intensification in the literature. For ionic liquids to be truly “green” and to be used ubiquitously, they must be made in a corresponding benign way in potentially large quantities and for low cost.

1.1. Reactions: solvent or solvent-less?

Is a solvent necessary for the synthesis of ionic liquids? Would not a neat reaction be preferred over even an environmentally-benign solvent? Typically, quaternization reactions are highly exothermic reactions. It has been reported that the heat of reaction for 1-methylimidazole and 1-bromobutane is -96 kJ mol^{-1} by Waterkamp *et al.*²⁰ They estimated the adiabatic temperature for a run-away reaction for this system to be $48 \text{ }^\circ\text{C}$ and greater.²⁰ This amount of heat release can cause a number of safety concerns along with poor quality product. Burrell *et al.*²¹ investigated synthesis of larger scale quantities ($\sim 1 \text{ kg}$) of ILs and warn: “*Caution: [this] reaction is exothermic and cooling is advisable for large scale reactions*”. In a controlled experiment in our laboratory, when 200 mL of 1-methylimidazole were mixed at room temperature with 200 mL of 1-bromoethane in a 500 mL round-bottom flask, the mixture began to over-boil within approximately 15 minutes. However, a solvent would help dissipate and manage much of the heat generated on both a laboratory scale and larger.

Department of Chemical and Petroleum Engineering, Department of Chemistry, and NSF-ERC Center for Environmentally Beneficial Catalysis, University of Kansas, Lawrence, KS 66045, USA.
E-mail: ascurto@ku.edu; Fax: +1 (785) 864 4967; Tel: +1 (785) 864 4947

† Current address: GE, Inc., 1233 West Loop South, Houston, TX 77027, USA

In addition, many ILs or their intermediates can often be quite viscous.^{22,23} Thus, as the reaction proceeds, uniform mixing for heat and mass transport issues may become a concern.²⁴ By using solvents, the viscosity can be kept relatively low.²⁵ Moreover, some ILs or their intermediates are actually higher melting-point solids, which would require much different processing techniques than for liquid solutions. For instance, the liquid-phase reaction between 1-methylimidazole and 1-bromoethane, mentioned above for its exothermicity, forms a solid compound at room-temperature and melts to a viscous liquid at 76 °C.²⁶ By using a solvent, the product can be kept in a relatively low-viscosity liquid solution that can be more easily processed. As will be shown in the following sections, the reaction kinetics can actually be faster in some solvents than in the neat reaction.

1.2. Overview

The current study quantitatively examines the solvent effects on the kinetics in the synthesis of a model ionic liquid, 1-hexyl-3-methylimidazolium bromide [HMIm][Br] in a wide variety of conventional and low-toxicity organic solvents. This contribution will demonstrate that safer/more-benign solvents can be utilized for producing ILs, while maintaining a high rate of reaction. Solvent selection was determined by understanding the effect of polarity on the kinetic rate constant through correlation with Kamlet Taft (*KT*) polarity parameters²⁷ in a Linear Solvation Energy Relationship (LSER). These correlations, along with solvent toxicity and environmental impact data, then enabled the rapid optimization of solvents for both productivity and low impact. These results will allow larger-scale production of ILs, which will ultimately decrease their cost.

2. Background

2.1. Ionic liquid synthesis

ILs are most commonly synthesized by a quaternization reaction of a substituted amine (or phosphine, *N*-heterocycles, *etc.*) with alkyl halides^{28–32} (see Fig. 1), which is followed by anion exchange if necessary. Throughout the quaternization reaction, two neutral reactants form oppositely charged ions through a polar transition state. The rate of reaction is influenced heavily by the “polarity” of the reaction mixture or solvent.^{33,34} This was first demonstrated by Menshutkin over a century ago while studying nucleophilic substitution reactions (*S_N2*) between amines with haloalkanes in 23 solvents.^{27,35} As will be discussed below, solvent “polarity” can be further described by several different features. Over the past century, a large number of studies have been performed examining the solvent effects on the transition state in the formation of ionic compounds. This investigation will illustrate the large difference in reaction kinetics in different solvents for the synthesis of 1-alkyl-3-methylimidazolium ionic salts and liquids.

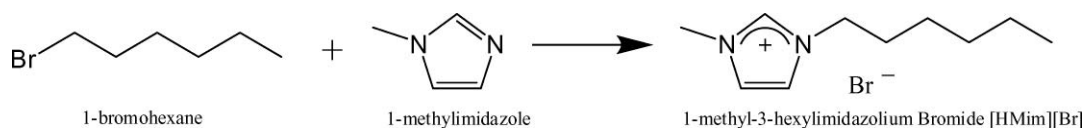


Fig. 1 Reaction between 1-methylimidazole and 1-bromohexane forming 1-hexyl-3-methylimidazolium bromide [HMIm][Br].

2.2. IL process development

From the literature, only a few studies have examined reaction engineering or process intensification for the production of ILs. The issue of heat removal from a neat reaction may be aided by proper reactor engineering solutions. For instance, Waterkamp *et al.*²⁰ have used micro-reactors to produce 1-butyl-3-methyl-imidazolium bromide, as micro-reactors have high surface area for heat removal. Minnich *et al.*³⁶ investigated the kinetics of producing 1-ethyl-3-methylimidazolium ethylsulfate for use in micro-reactors. However, micro-reactors can only be used for liquids and require adequate pumping for the high-viscosity liquefied product. Varma and Namboodiri³⁷ and Deetlefs and Seddon³⁸ have shown that ILs can be synthesized more rapidly using microwave radiation which decreases the relative reaction times. Leveque *et al.*³⁹ have found that ultrasonic irradiation is a useful tool for making a large number of ILs in a one-pot synthesis method. Grosse-Böwing and Jess have reported the bimolecular kinetic constants for the production of 1-butyl-3-methyl-imidazolium chloride.⁴⁰ Recently, they have described some of the important reactor engineering properties for the neat synthesis of 1-ethyl-3-methyl-imidazolium ethylsulfate ionic liquids.⁴¹

2.3. “Green”/sustainable solvent selection

Many factors are involved in the selection of an “appropriate” solvent⁴² for syntheses based upon principles of “green”/sustainable chemistry and engineering.^{43,44} For the production of any chemical, high kinetic rates are preferred. Facile and low-energy separations are needed to purify the ionic liquid. The human and environmental impact, especially of the solvent, is an important aspect in designing safer and more sustainable processes. However, as will be shown below, some of the more benign solvents may yield slow reaction rates and energy-intensive separations processes. Thus, a balance must be made between the inherent toxicity for a given solvent with the desired rates of reaction to produce ILs, and any subsequent processing. Life-cycle assessment (LCA)^{45–47} is a methodology to determine the effect of various process parameters on the required energy, environmental impact, and profitability for the process from cradle-to-grave. Kralisch *et al.*^{48,49} employed a modified LCA to analyze the synthesis of several ionic liquids and catalytic processes in them, based upon preliminary or estimated data. For instance, the energy inputs to create the starting materials for imidazolium based ILs are larger than for pyridinium and quaternary ammonium ILs. Increasing the temperature of the synthesis initially decreases the overall impact, but reaches a minimum below 100 °C. While all of the aforementioned aspects of sustainable processes are important, this contribution will focus on the solvents of ionic liquid synthesis, efficiency of the reaction kinetics, and address the issue of separations.

There are many different ways that solvents can be classified as to their effect on humans and the environment. The US Food and Drug Administration (FDA) typically uses a system of three classes: 1 through 3; in addition to Generally-Regarded-as-Safe (GRAS) solvents.^{50–52} Under these guidelines any Class 1 solvent shall not be used in the production of pharmaceuticals as they are known or suspected human carcinogens. Class 2 solvents have been deemed toxic and should be limited in the production of pharmaceuticals. However, the effects from exposure are reversible and acceptable limits have been established (permitted daily exposure (PDE)). Class 3 solvents are accepted in the production of pharmaceuticals and have low toxicity. GRAS solvents are preferred solvents, which are accepted in the production of pharmaceuticals, and some have been deemed safe as food additives.

While the FDA guidelines are a good indication of human toxicity, they do not include aspects of environmental impact such as aquatic toxicity, smog emissions, biodegradation potential, global warming potential, *etc.* In addition, the weighting of these different measures of toxicity and environmental impact is also an important issue. One method which takes a large number of health and environmental concerns into consideration is the Rowan Solvent Selection Table (RSST).^{53,54} Originally, the various indicators were weighted to yield an objective function, called the Pharmaceutical Index, which combines human toxicity indices, *i.e.* ingestion, inhalation, and carcinogen toxicities, with environmental effects, *e.g.* aquatic toxicity, soil absorption, ozone depletion, smog formation, *etc.* While the weighting of these different parameters can be discussed, debated and modified, the results do give a good indication of the relative effect on people and the environment. The RSST will be used extensively in this study.

Another useful guide for determining solvent selection is the GlaxoSmithKline (GSK) solvent selection table, which is based on the “International Conference on Harmonization of Technical Requirements for Registration of Pharmaceuticals for Human Use” (ICH guidelines).⁵⁵ In this solvent selection table there are nine assessments which are examined for solvent selection, and include: incineration, recyclability, volatile organic compounds (VOC’s), bio-treatment, environmental impact on air, environmental impact of water, health hazards, exposure potential, and safety hazards.⁵⁵ Each assessment is equally weighed in the ranking of solvents.

While the solvents with the lowest impact on humans and the environment could be chosen at the outset, the kinetics of the synthesis and subsequent separations may actually result in a much worse net effect. In order to expedite solvent screening, a method has been utilized here to correlate and predict solvent performance (kinetics) based upon linear solvation energy relationship (LSER) regression using Kamlet Taft (*KT*) parameters for the individual solvents.

2.4. Kamlet Taft polarity scales and LSER

Rates of reaction in the production of ionic liquids are highly dependent on the solvent media. A method to quantitatively correlate and predict the kinetics based upon the properties of the solvent, such as polarity, would be highly useful. The term “polarity” embodies a number of different concepts,

including dipole moment, dielectric constant, hydrogen bond accepting ability, polarizability, *etc.* While one-parameter scales for polarity, such as the $E_T(30)$ scale^{27,56,57} can approximate qualitative trends, they often cannot be used to quantitatively correlate reaction rates. Kamlet Taft (*KT*) parameters differentiate various aspects of “polarity”, *viz.* acidity (α), basicity (β), and dipolarity/polarizability (π^*). Acidity, α , is a measure of the solvent’s ability to donate a proton in a solvent-to-solute hydrogen bond,⁵⁸ β is the measure of the solvent’s ability to accept a proton in a solvent-to-solute hydrogen bond,⁵⁹ and π^* is a measure of the solvent’s ability to stabilize a charge or dipole.^{60,61} The *KT* parameters of the solvent can be used to correlate and predict kinetic rate constants in different solvents using a Linear Solvation Energy Relationship (LSER). The LSER method regresses parameters to correlate the kinetic rate constants, k , with the solvent-dependent physicochemical properties: α , β , and π^* :²⁷

$$\ln k = \ln k^0 + a\alpha + b\beta + p(\pi^* - d\delta) \quad (1)$$

The regressed coefficients, a , b , p , and d will indicate the magnitude and direction (positive or negative) the polarity parameter contributes to the kinetic rate. δ is the polarizability correction term which is equal to 0.0 for non-chlorinated solvents, 0.5 for polychlorinated solvents, and 1.0 for aromatic solvents.⁶²

3. Results and discussion

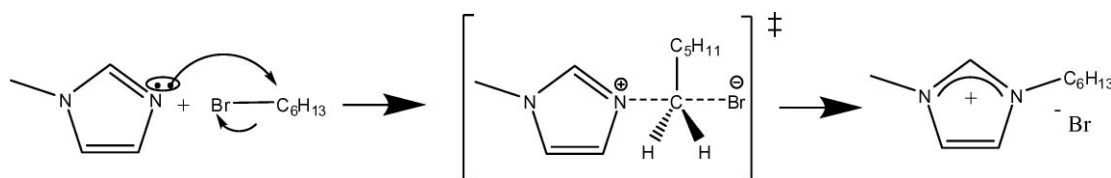
3.1. Solvent effects on kinetics

Initially, this study focused on five traditional organic solvents for the reaction of 1-methylimidazole with 1-bromohexane to form the ionic liquid [HMIm][Br]. The initial solvents (acetonitrile, acetone, methanol, dichloromethane, and chlorobenzene) have a wide range of polarity and different levels of toxicity and environmental impact factors that will be discussed below. For each reaction, the mole ratio of reactants to solvent was maintained at 1 : 1 : 20 to avoid concentration effects on the bulk polarity from the reactant and/or product. Each reaction was conducted at three different temperatures: 25 °C, 40 °C, and 60 °C, yielding insight to the transition state and activation parameters. For the chlorobenzene system, the mixture splits into two phases (IL-rich and reactant/solvent-rich) after ~6% conversion. While the developing reaction may occur in either phase, 1-bromohexane is relatively insoluble (immiscible) in the ionic liquid. Thus, little reaction is believed to occur in the IL phase and the overall rate reported here is also the rate in the solvent phase. The change of concentration with time for the synthesis of [HMIm][Br] in acetonitrile at 40 °C is shown in Fig. 3 as an example. All rates of reaction at 40 °C were regressed non-linearly assuming 2nd order kinetics and are presented in Table 1, along with the *KT* parameters and $E_T(30)$ values; for reference, the *KT* parameters of the reactants and IL product are also given. It was anticipated from the well-known work of Menshutkin³⁵ and general S_N2 reactions that the kinetic rate would increase with increasing polarity. From the five initial solvents, the rate of reaction is the greatest in acetonitrile, and is more than one order of magnitude higher than that of methanol. Methanol was the slowest despite being considered one of the

Table 1 Rate constants at 40 °C, KT parameters and $E_T(30)$ values for all solvents examined^a

Solvent	$k \times 10^6 / \text{M}^{-1} \text{s}^{-1}$ 40 °C	Kamlet Taft parameters			$E_T(30) / \text{kcal mol}^{-1}$
		α	β	π^*	
Dimethyl sulfoxide	77.89 ± 1.72	-0.013 ± 0.003	0.724 ± 0.009	1.032 ± 0.004	45.11 ± 0.02
Acetonitrile	21.56 ± 0.21	0.230 ± 0.009	0.376 ± 0.012	0.787 ± 0.012	45.62 ± 0.02
Cyclopentanone	15.11 ± 0.11	-0.085 ± 0.005	0.565 ± 0.004	0.748 ± 0.003	39.85 ± 0.01
Acetone	12.67 ± 0.06	0.110 ± 0.002	0.523 ± 0.012	0.715 ± 0.002	42.58 ± 0.03
2-Butanone	11.56 ± 0.08	0.053 ± 0.004	0.568 ± 0.004	0.675 ± 0.002	41.06 ± 0.06
Dichloromethane	8.47 ± 0.11	0.042 ± 0.003	-0.020 ± 0.014	0.790 ± 0.004	40.88 ± 0.02
Ethyl formate	7.97 ± 0.14	0.094 ± 0.035	0.412 ± 0.075	0.570 ± 0.042	40.19 ± 0.11
Chlorobenzene ^b	3.64 ± 0.11 ^b	0.051 ± 0.004	0.080 ± 0.009	0.624 ± 0.004	36.91 ± 0.02
Ethyl lactate	2.86 ± 0.06	0.642 ± 0.004	0.633 ± 0.010	0.689 ± 0.002	51.01 ± 0.04
Methanol	2.03 ± 0.08	0.909 ± 0.006	0.629 ± 0.009	0.697 ± 0.006	55.53 ± 0.04
1-Methylimidazole	—	0.232 ± 0.012	0.712 ± 0.016	0.961 ± 0.014	44.85 ± 0.01
1-Bromohexane	—	0.014 ± 0.07	-0.009 ± 0.011	0.500 ± 0.01	37.9 ± 0.70
[HMIm][Br]	—	0.453 ± 0.069	0.562 ± 0.066	0.983 ± 0.037	50.49 ± 0.18

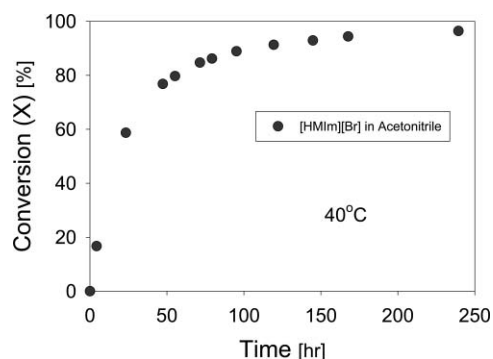
^a All rates of reaction at 40 °C were conducted at a 1 : 1 : 20 mole ratio (1-methylimidazole : 1-bromohexane : solvent). ^b Mixture split into two phases during reaction and the reported kinetic constants assume that the reaction does not occur in the IL-rich phase due to poor solubility of 1-bromohexane.

**Fig. 2** Transition state for the reaction between 1-methylimidazole and 1-bromohexane.

most “polar.” Thus, simple heuristics of increasing polarity to increase kinetic rate is not always qualitatively valid. The reaction in acetonitrile is even greater than in the neat reaction without solvent. The natural log of k was fit to the LSER coefficients based on the KT parameters (acidity α , basicity β , and dipolarizability π^*):

$$\ln k = -62.08 - 3.79\alpha + 20.89\beta + 56.36(\pi^* - 0.23\delta) \quad (2)$$

$$R^2 = 0.99$$

**Fig. 3** Concentration versus time for the formation of [HMIm][Br] in acetonitrile at 40 °C.

From the regression it is seen that the π^* parameter (dipolarity/polarizability) has the largest positive effect on the reaction rate, followed by the β parameter (basicity). The α parameter (acidity) has a negative effect on the rate of reaction. This relationship of 5 solvents with a wide variety of polarity then allows us to optimize the rate at least qualitatively: solvents with large β

and π^* and a small α should be chosen, *i.e.* high dipolarity and hydrogen bond acceptor/electron donor capability, and small hydrogen bond donating/electron accepting ability.

The general effects of polarity on the synthesis of imidazolium based ILs as determined from the solvent subset can now be used to aid the choice of other solvents with lower toxicity and environmental impact. From eqn (2) and KT parameters, five additional solvents were selected among Class 3 and GRAS solvents: ethyl formate, ethyl lactate (also a bio-renewable solvent^{63,64}), dimethyl sulfoxide, 2-butanone, and cyclopentanone. The results for the 10 solvents are presented in Table 1 along with the experimentally measured KT and $E_T(30)$ parameters. A majority of the new solvents did not have a complete set of parameters based on one set of solvatochromic probes.

A single parameter correlation for all ten solvents using the $E_T(30)$ scale is inadequate at qualitative and quantitative correlation, as shown in Fig. 4. The $E_T(30)$ scale only embodies one aspect of polarity important in this reaction. This result was also seen by Abraham *et al.*⁶⁵ who worked with a trimethylamine/*p*-nitrobenzyl chloride system. A similar conclusion was obtained by Skrzypczak and Neta³⁴ studying the reaction of 1,2-dimethylimidazole and benzylbromide.

The LSER analysis, now for all 10 solvents, was regressed against the kinetic rate constant:

$$\ln k = -14.72 - 2.07\alpha + 0.07\beta + 4.99(\pi^* - 0.20\delta) \quad R^2 = 0.95 \quad (3)$$

and the results are given in Fig. 5. The rates of reactions are heavily influenced by the solvent choice, and can be predicted fairly accurately using KT parameters in a LSER regression. This phenomena can qualitatively be explained by the solvation

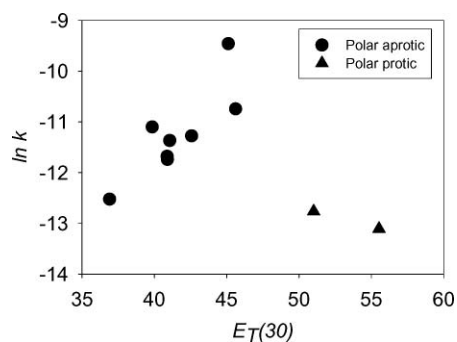


Fig. 4 Correlation of kinetic constant, k , with the $E_T(30)$ polarity scale for all solvents examined.

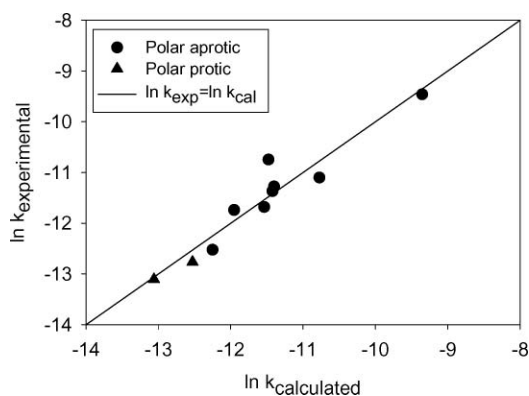


Fig. 5 LSER (eqn (7)) results for the 10 solvents used in this study at 40 °C.

scheme of Hughes and Ingold.^{27,66–68} For the alkylation of 1-methylimidazole with haloalkanes, two neutral reactants form

a transition state of significant charge separation, followed by full charge separation in the product cation and anion (Fig. 2). As seen in Table 1 for the polar aprotic solvents, an increase in the solvent polarity (π^* and $E_T(30)$) results in an increase in the rate of reaction. Following Hughes and Ingold's^{66,68} interpretation, the reaction is dominated by the degree of charge existing at the transition state. Solvents with higher dipolarity and basic character can stabilize better the charged transition state. However, polar protic solvents retard the reaction rate despite their high dipolarity. They form hydrogen bonds with the lone pair of electrons on the nitrogen of 1-methylimidazole, thus inhibiting nucleophilic attack on the haloalkane.

These effect of polarity on the kinetics may also be viewed by analysis of the Arrhenius⁶⁹ and Eyring^{70,71} parameters. The Eyring equation is given by:

$$k = \frac{k_B T}{h} \exp\left(-\frac{\Delta H^\ddagger}{RT}\right) \exp\left(\frac{\Delta S^\ddagger}{R}\right) \quad (4)$$

where k_B is the Boltzmann's constant, T is temperature, h is the Plank's constant, R is the gas rate constant, ΔH^\ddagger is the enthalpy of activation, and ΔS^\ddagger is the entropy of activation.

The Arrhenius equation is given by:

$$k = k_0 \exp\left(-\frac{E_a}{RT}\right) \quad (5)$$

where E_a is the activation energy and k_0 is the pre-exponential term.

Table 2 summarizes the parameters for each of the models determined from the kinetic constants at 25 °C, 40 °C, and 60 °C, unless otherwise specified. The values for ΔH^\ddagger are similar between the two major solvent types: polar aprotic solvents and

Table 2 Rates of reaction and kinetic parameters

Solvent	$k \times 10^6 / \text{M}^{-1} \text{s}^{-1}$			$k_0 \times 10^{-6} / \text{M}^{-1} \text{s}^{-1}$	$E_a / \text{kJ mol}^{-1}$	$\Delta H^\ddagger / \text{kJ mol}^{-1}$	$\Delta S^\ddagger / \text{J mol}^{-1} \text{K}^{-1}$
	25 °C	40 °C	60 °C				
DMSO	22.22 ± 0.11	77.89 ± 1.72	322.31 ± 3.53^a	2.51	63.05	60.43	-131.19
Acetonitrile	6.03 ± 0.14	21.56 ± 0.21	110.64 ± 1.42	6.51	68.73	66.11	-123.26
Cyclopentanone	3.75 ± 0.03	15.11 ± 0.11	76.11 ± 1.72	10.4	71.00	68.38	-119.37
Acetone	3.69 ± 0.17	12.67 ± 0.06	63.67 ± 0.61	2.20	67.26	64.64	-132.30
2-Butanone	2.69 ± 0.03	11.56 ± 0.08	53.75 ± 0.28	6.25	70.50	67.88	-123.60
Dichloromethane	2.28 ± 0.11	8.47 ± 0.11	— ^b	1.85	67.98	65.44	-133.45
Ethyl formate	1.61 ± 0.03	7.97 ± 0.14	— ^b	507	82.75	80.21	-86.78
Chlorobenzene ^c	1.11 ± 0.06	3.64 ± 0.11	24.64 ± 1.39	7.51	73.43	70.81	-122.07
Ethyl lactate	0.53 ± 0.03	2.86 ± 0.06	20.28 ± 0.28	636	86.05	83.43	-85.18
Methanol	0.42 ± 0.03	2.03 ± 0.08	17.14 ± 0.11	987	87.85	85.24	-81.52
Neat ^{c,d}	4.53 ± 0.04	17.63 ± 0.06	106.34 ± 13.2	51.2	74.57	71.95	-106.12

^a Reaction conducted at 1 : 1 : 80 mole ratio 1-methylimidazole : 1-bromohexane : dimethyl sulfoxide due to high exothermicity of more concentrated solutions. ^b Exceeds boiling point of solvent. ^c Mixture split into two phases during reaction and the reported kinetic constants assume that the reaction does not occur in the IL-rich phase due to poor solubility of 1-bromohexane. ^d 1-methylimidazole : 1-bromohexane = 1 : 1 by mole.

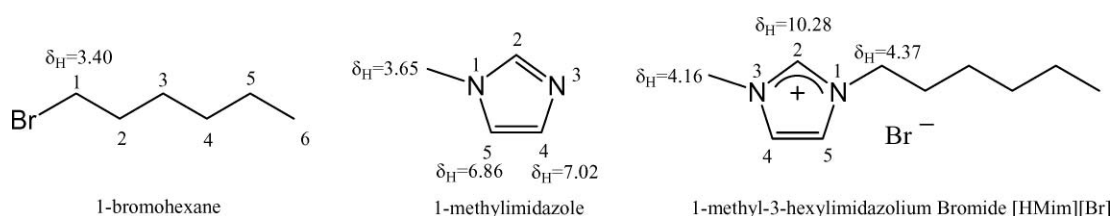


Fig. 6 ¹H NMR chemical shifts for reactants and product.

polar protic solvents (methanol, ethyl lactate). The values of ΔH^\ddagger for the polar protic solvents are approximately 20 kJ mol⁻¹ greater than the polar aprotic solvents. The kinetic parameters in ethyl formate (EF) are similar to those of the polar protic solvents, despite EF having a low acidity (α parameter). Ethyl formate is susceptible to water, base, acid, and salt catalyzed hydrolysis and decomposition⁷²⁻⁷⁶ to products with higher α values, such as ethanol, formic acid, *etc.* Haberfield *et al.*⁷⁷ suggest, for general S_N2 reactions, that the difference between the ΔH^\ddagger for protic solvents may be due to stabilization of the reactants relative to aprotic solvents, thus increasing the energy difference between the reactants and the transition state. Additional energy would be needed to break the hydrogen bonds between the solvent and 1-methylimidazole in order for the reaction to occur. Hydrogen bond strengths can vary between 2–20 kJ mol⁻¹,⁷⁸ which is of the same order as the difference in ΔH^\ddagger between the polar protic and aprotic solvent classes. Moreover, the ΔS^\ddagger for the polar protic solvents is approximately 40 J mol⁻¹ K⁻¹ more (less negative) than the polar aprotic solvents. Hydrogen bonding between the 1-methylimidazole and the solvent would induce a more-ordered ground state, *i.e.* lower entropy. Thus, the degree of order in the transition state is closer to the ground state with protic solvents.

The current example uses 1-bromohexane as the alkylation agent. Many applications with ionic liquids, *e.g.* catalysis, are adversely affected by the presence of halide and its removal after anion-exchange is often tedious. As such, several alternative halide-free alkylation techniques have emerged. Bonhôte *et al.*⁷⁹ have used ethyl triflate and ethyl trifluoroacetates for the alkylation of 1-methylimidazole. Ue *et al.*⁸⁰ have used the alkylation of 1-ethylimidazole with dimethyl carbonate. Lectercq *et al.*⁸¹ have used a complex mechanism involving the reaction between tetrahydrofuran or 1,4-dioxane, with triflic anhydride to form a diester that is then reacted with an N-substituted imidazole. Holbrey *et al.*¹⁶ used an alkylation technique between dimethyl sulfate or diethyl sulfate with N-substituted imidazole to form imidazolium alkyl sulfate ILs. Yoshizawa *et al.*⁸² have synthesized a number of zwitterionic type ILs by reacting imidazoles with 1,3-propanesultone. The kinetic rates and effects of solvents of several of these alternative alkylations are under investigation.

3.2. Diffusion limited kinetic constant

The diffusion-limited rate constant was calculated for comparison to the intrinsic kinetic rate constants. The binary diffusion coefficients for 1-methylimidazole and 1-bromohexane in dimethyl sulfoxide (DMSO) have been determined at 25 °C in another study in our laboratory⁸³ and is illustrated in Table 3. DMSO was chosen as a model solvent as it simultaneously produces the largest kinetic rate of synthesis and is the most viscous solvent studied. Thus, the reaction in DMSO should be the nearest to the diffusional limited regime. As shown in the table, 1-methylimidazole diffuses slightly faster than 1-bromohexane.

The analysis for the diffusion-limited rate constant for a reaction in a homogeneous medium is given by:⁷⁸

$$k_d = 4\pi R^* D N_A \quad (6)$$

Table 3 Calculating the k_d in DMSO for the reaction between 1-methylimidazole and 1-bromohexane

D_a (1-methylimidazole) ^a	6.10×10^{-10}	m ² s ⁻¹
D_b (1-bromohexane) ^a	5.90×10^{-10}	m ² s ⁻¹
$D = (D_a + D_b)$	1.20×10^{-9}	m ² s ⁻¹
Viscosity (DMSO) ^b	1.987×10^{-3}	kg m ⁻¹ s ⁻¹
R_a	1.80×10^{-10}	m
R_b	1.86×10^{-10}	m
$R^* = (R_a + R_b)/2$	1.83×10^{-10}	m
k_d	1.66×10^9	M ⁻¹ s ⁻¹
k (at 25 °C)	2.22×10^{-5}	M ⁻¹ s ⁻¹

^a D_a and D_b are binary diffusion coefficients in DMSO at 25 °C from ref. 83. ^b Taken from ref. 92.

where k_d is the diffusion-controlled rate constant, R^* is the distance at which the reaction occurs (assumed to be the average distance between the reactants hydrodynamic radii), D is the sum of the reactants diffusion coefficients at the concentration of the reaction, and N_A is Avogadro's constant. Using the Stokes–Einstein equation, the hydrodynamic radii for each molecule can be calculated by:⁷⁸

$$R_a = \frac{k_B T}{6\pi\eta D_a} \quad \text{and} \quad R_b = \frac{k_B T}{6\pi\eta D_b} \quad (7)$$

where R_a and R_b are the hydrodynamic radii, k_B is the Boltzmann constant, T is the temperature in K, η is the viscosity of the media, and D_a and D_b are the diffusion coefficient for each species in the solvent media. The equations above assume a hard sphere model for the hydrodynamic radius and yield an approximation of the relative rate in a diffusion-limited regime. The viscosity of the media is assumed to be the viscosity of pure DMSO and the diffusion coefficient in dilute conditions is assumed to be representative of the actual reaction. Details of the analysis are given in Table 3. The kinetic constant in a diffusion-controlled regime, k_d , is estimated to be 1.66×10^9 M⁻¹ s⁻¹, which is 14 orders of magnitude greater than the reported intrinsic rate constant. The speed of these S_N2 reactions requires more than just the reactants coming into proximity as suggested by the solvent effects discussed above. As expected, the kinetics rates reported here truly reflect the intrinsic kinetics and indicate that methods to increase mass transfer within the solution, such as stirring, *etc.*, are more important for heat transfer issues than mass transfer.

3.3. Green/sustainable solvent selection

Table 4 lists the solvents in order of decreasing rate of reaction for 1-bromohexane with 1-methylimidazole (DMSO is the fastest and methanol the slowest). For solvents that have not been examined in the Rowan Solvent Table, the closest related solvent was used: methyl formate for ethyl formate, methyl lactate for ethyl lactate, cyclohexanone for cyclopentanone, and *o*-dichlorobenzene for chlorobenzene. According to the index, the top 5 most benign solvents of the 10 studied are: DMSO > methyl(ethyl) lactate > acetone > methanol > methyl (ethyl) formate. The GSK solvent selection guide yielded similar conclusions with the top 3 benign solvent choices being: DMSO > acetone > methanol. However, the best solvents for the highest kinetic rates are: DMSO > acetonitrile > cyclopentanone > acetone > 2-butanone. On first inspection, DMSO may seem

Table 4 Abbreviated results adapted from the RSST for determining the pharmaceutical index

Solvent	Index ^a	Inhalation TLV (ppm) ^b	Ingestion/ mg kg ⁻¹ rat ^b	Carcinogen [0–5] ^b	Aquatic/ mg L ⁻¹ fish ^b	Soil adsorption coefficient ^b	Smog formation ^b	Oct/water partitioning coefficient ^b
DMSO	0.42	1000	14 500	0	66 901	0.65	0.00	-1.35
Acetonitrile	3.21	40	3800	0	4111	0.65	0.00	-0.34
Cyclohexanone ^c	5.37	50	1800	3	754	1.18	0.53	0.81
Acetone	2.15	500	5800	1	6967	0.30	0.18	-0.24
2-Butanone	4.00	200	2737	2	3173	0.58	0.51	0.29
Dichloromethane	5.36	50	1600	3	428	1.38	0.03	1.34
Methyl formate ^c	3.11	100	475	1	6260	0.33	0.00	0.03
Methyl lactate ^c	1.57	1000	2000	0	29 583	0.00	0.00	-0.67
Methanol	2.52	200	5628	0	8403	0.00	0.21	-0.77

^a Pharmaceutical index weighting. ^b Values taken from ref. 53,54. ^c Analogues of solvents used in the kinetic analysis.

Table 5 Boiling points, latent heats, sensible heats and total energy obtained for energy analysis

Solvent	Molecular weight/g mol ⁻¹	Boiling point, T _b /°C ^a	$\Delta H^{\text{vap}}(T_b)^a$ / kJ mol ⁻¹	C _p at 25 °C ^a / J g ⁻¹ K ⁻¹	Sensible heat ^b / kJ mol ⁻¹	Total heat ^c / kJ mol ⁻¹
Dimethyl sulfoxide	78.13	189.0	43.1	1.958	22.79	65.89
Acetonitrile	41.05	81.7	29.75	2.229	3.84	33.59
Cyclopentanone	98.14	130.6	36.35	1.840	16.43	52.78
Acetone	58.08	56.1	29.1	2.175	2.06	31.16
2-butanone	72.1	79.6	31.3	2.201	6.35	37.65
Dichloromethane	84.93	40.0	28.06	1.192	0.0	28.06
Ethyl formate	74.08	54.4	29.91	2.015	2.09	32.00
Chlorobenzene	147.01	131.7	35.19	1.334	17.85	53.04
Ethyl lactate	118.13	154.5	52.5 ^c	2.150	28.70	81.20
Methanol	32.04	64.6	35.21	2.531	2.00	37.21

^a Taken from ref. 92. ^b Sensible heat = C_p(T_b - 40 °C). ^c Ref. 93.

the ideal solvent to produce [HMIIm][Br]: the highest reaction rate and lowest toxicity/environmental impact. However, what is not considered here is the energy to separate the solvent from the IL using distillation/evaporation. Consideration of the boiling point and heat of vaporization may yield a peripheral energy analysis. In actual distillation/evaporation, one would need to consider the phase equilibrium thermodynamics (activity coefficients, *etc.*) to design the separation train and energy requirements; these are often more than simply the sensible heat and latent heat of vaporization.⁵⁵ Table 5 lists the boiling points, heats of vaporization, sensible heat, and the total energy for the solvents investigated. As seen in Table 5, DMSO's boiling point and heat of vaporization (thus energy requirement) is quite high compared to the other solvents in the table. This excess energy would result in higher energy usage and, thus, more pollution, which in turn would worsen the actual measure of toxicity and environmental impact of the solvent. Based on comparison of the reaction rates, the solvents' Index, and a scan of the energy requirements of separation, *acetone* appears to possess an optimal combination of properties for use, at least on the bench-scale, if not on an industrial scale. In addition, acetone is relatively inexpensive, can be purchased on a large scale, and can be produced by bio-renewable methods (ABE fermentation).⁸⁴

Other means of separation should also be considered for a complete analysis. These techniques range from liquid extraction to more recent techniques using low to moderate pressure of CO₂ to induce phase splitting.^{85–87} CO₂ has been found to induce a

broad range of IL–solvent mixtures to split into an IL-rich and solvent-rich phase that can be decanted, or, at higher pressures, extracted by near- or supercritical CO₂. Scurto⁸⁸ indicates that depending on the needed purity, the energy needed to power a compressor for a CO₂ separation process may be competitive with the energy (heat) requirements for evaporation/distillation, even with relatively high volatility solvents such as methanol.

4. Experimental

4.1. Kinetic measurements

The reaction of 1-methylimidazole and haloalkanes with different solvents was conducted at three different temperatures using a multi-well reactor block from Chemglass, Inc. (model number CG-1991–03) which holds 16 standard 20 mL scintillation vials. The temperature and stirring of the reactor block was maintained using an IKAMAG RET basic hotplate equipped with an ETS-D4 fuzzy logic temperature controller that maintained the temperature to ±1 °C. Reactants were carefully weighed to 0.01 mg in 20 mL scintillation vials and a magnetic stir bar was placed in each vial. The vials were then placed in the reactor block and samples were drawn from each vial and placed in NMR tubes containing deuterated chloroform at room temperature. The samples were quickly analyzed using a Bruker 400 MHz Nuclear Magnetic Resonance (NMR) spectrometer. Typically, the time duration between sample extraction and

NMR analysis was less than 5 minutes; further conversion during this time was negligible due to the relatively slower kinetic rates at ambient conditions, and the more dilute concentrations after adding deuterated chloroform. The conversion over time was determined by following the disappearance of the reactant and appearance of the product peaks on the NMR spectrum.

The methyl peaks for the reactant, 1-methylimidazole and the corresponding methyl peaks for [HMIm][Br] at $\delta_{\text{H}} \sim 3.65$ ppm and $\delta_{\text{H}} \sim 4.16$ ppm, respectively (see Fig. 6), are integrated to determine the fractional conversion, X , using the following equation:

$$X = \frac{C_{\text{MIm}}^0 - C_{\text{MIm}}}{C_{\text{MIm}}^0} = \frac{N_{\text{IL}}}{N_{\text{MIm}}^0} = \frac{N_{\text{IL}}}{N_{\text{MIm}} + N_{\text{IL}}} = \frac{I_{\delta_{\text{H}} 4.16}}{I_{\delta_{\text{H}} 4.16} + I_{\delta_{\text{H}} 3.65}} \quad (8)$$

where N is the number of moles of each species at any point in time, N^0 is initial amounts of limiting reactant, and I is the peak area at each of the chemical shifts being analyzed. Alternatively, the conversion could be determined based on the difference in the methylene peak next to the bromine ($\delta_{\text{H}} 3.40$ ppm) or the imidazolium ring ($\delta_{\text{H}} 4.37$ ppm); see Fig. 6. When the individual solvent peaks overlap with these peaks in the NMR spectra, the peaks at $\delta_{\text{H}} 7.02$ ppm and $\delta_{\text{H}} 10.28$ ppm were used for calculating conversion, which correspond to the hydrogen in position number 5 on the 1-methylimidazole and the hydrogen in position number 2 on the [HMIm][Br]; see Fig. 6. For further details of the NMR technique, see Schleicher.⁸⁹ The accuracy of this method to determine X has been estimated to $\pm 1\%$.

The reaction rates were confirmed to be 2nd order/bimolecular according to the expression:

$$r_{\text{IL}} = -r_{\text{MIm}} = -r_{\text{BrHex}} = -\left(\frac{\partial C_{\text{MIm}}}{\partial t}\right) = k C_{\text{MIm}} C_{\text{BrHex}} \quad (9)$$

or alternatively:⁹⁰

$$r_{\text{IL}} = -r_{\text{MIm}} = C_{\text{MIm}}^0 \left(\frac{\partial X}{\partial t}\right) = k (C_{\text{MIm}}^0 - C_{\text{MIm}}^0 X)(C_{\text{BrHex}}^0 - C_{\text{MIm}}^0 X) \quad (10)$$

where r is the reaction rate based on component i , k the kinetic constant, C_i^0 the initial concentrations of the components (molarity), and X is the fractional conversion (eqn (8)).

When the initial concentrations of the two reactants are equal (1 : 1 stoichiometry), eqn (10) becomes:

$$r_{\text{IL}} = -r_{\text{MIm}} = C_{\text{MIm}}^0 \left(\frac{\partial X}{\partial t}\right) = k (C_{\text{MIm}}^0)^2 (1 - X)^2 \quad (11)$$

$$\frac{X}{C_{\text{MIm}}^0 (1 - X)} = kt$$

While the kinetic constant could be obtained by graphing the experimental data to a linearized form of eqn (11), this often introduces unnecessary errors or undue emphasis on certain time regimes. A non-linear regression technique is used here in the software SigmaPlot 2000.

4.2. Kamlet Taft measurements

Many different solvatochromic probes can be used to determine the KT parameters. Different sets of dyes produce slightly

different results and, thus, comparison with other studies should be made only with similar dye sets.^{58-60,91} In this study, the solvatochromic probes: *N,N*-diethyl-4-nitroaniline, 4-nitroaniline, and Reichardt's dye, were used to calculate the three solvent parameters α , β , and π^* . All KT parameters and $E_T(30)$ values were obtained from solutions with the appropriate dyes using a Varian Cary 300 Bio Ultra violet-Visible (UV-Vis) Spectrophotometer, with a dual cell Peltier accessory temperature controller. The temperature was maintained at the standard 25 °C. The wavelengths of maximum absorption of the dyes are related to the KT parameters using the standard formulas.²⁷ The LSER coefficients were regressed using the non-linear optimization techniques in the software: Sigma-Plot 2000 version 6.0.

4.3. Materials

Reagents: 1-methylimidazole (>99%), 1-chlorohexane (95%), 1-iodohexane (>98%), and 1-bromopropane (99%) were obtained from Acros Organics, while 1-bromohexane (>99%), 1-bromopentane (99%), 2-bromopentane (95%), 1-bromo-3-methylbutane (96%), 2-bromo-2-methylbutane (95%), and 1-bromodecane (98%) were obtained from Sigma Aldrich. Solvents: acetonitrile (>99.9%), acetone (>99.9%), methanol (>99.9%), chlorobenzene (99.9%), dichloromethane (99.8%), dimethyl sulfoxide (>99%), cyclopentanone (>99%), ethyl lactate (>98%), 2-butanone (>99.7%), and cyclohexane (>99.9%) were all obtained from Sigma Aldrich, while ethyl formate (>98%) was purchased from Acros Organics. Solvatochromic probes: 4-nitroaniline (>99%) was purchased from Sigma Aldrich, *N,N*-diethyl-4-nitroaniline (97%) was purchased from Oakwood Products Inc., and Reichardt's Dye (>90%) was purchased from Fluka. All starting materials were distilled and kept under argon gas prior to use. All solvents were dried using 3 Å or 4 Å molecular sieves. The solvatochromic probes Reichardt's Dye, 4-nitroaniline, and *N,N*-diethyl-4-nitroaniline were used as received.

5. Conclusion

The kinetic rate constants for the reaction of 1-bromohexane with 1-methylimidazole have been determined in 10 solvents at 25 °C, 40 °C, and 60 °C. Kamlet-Taft parameters in a LSER regression can quantitatively correlate the kinetics of reaction with the parameters of the solvent. For imidazolium based ILs, reaction rates increase with solvents containing high dipolarity/polarizability and basicity with low acidity. Estimation of the diffusion-limited rate constant confirms that the measured reactions rates represent the intrinsic kinetics. Using the kinetic data, the toxicological and environmental data, and the volatility of the solvents, a method has been proposed to determine the optimal solvents for the synthesis of ILs. Acetone has been shown to possess a number of optimal attributes for the production of ionic liquids.

Acknowledgements

This material is based upon work supported by the US National Science Foundation under Grant No. CBET-0626313. The author (AMS) appreciates the support of the DuPont Young

Professor Award. Ms Silvia Nwosu is kindly thanked for some experimental assistance.

References

- 1 A. Ahosseini, W. Ren and A. M. Scurto, *Chim. Oggi*, 2007, **25**, 40–42.
- 2 M. Haumann and A. Riisager, *Chem. Rev.*, 2008.
- 3 R. A. Sheldon, R. M. Lu, M. J. Sorgedraeger, F. v. Rantwijk and K. R. Seddon, *Green Chem.*, 2002, **4**, 147–151.
- 4 C. Jork, M. Seiler, Y.-A. Beste and W. Arlt, *J. Chem. Eng. Data*, 2004, **49**, 852–857.
- 5 J. L. Anderson, J. K. Dixon and J. F. Brennecke, *Acc. Chem. Res.*, 2007, **40**, 1208–1216.
- 6 M. B. Shiflett and A. Yokozeki, *Chim. Oggi*, 2006, **24**, 28–30.
- 7 A. Bösmann, L. Datsevich, A. Jess, A. Lauter, C. Schmitz and P. Wasserscheid, *Chem. Commun.*, 2001, 2494–2495.
- 8 S. Murugesan and R. J. Linhardt, *Curr. Org. Synth.*, 2005, **2**, 437–451.
- 9 R. D. Rogers, and K. R. Seddon, *Ionic Liquids IIIB: Fundamentals, Progress, Challenges, and Opportunities: Transformations and Processes*, 2005.
- 10 M. Koel, *Crit. Rev. Anal. Chem.*, 2005, **35**, 177–192.
- 11 R. J. Gale and R. A. Osteryoung, *J. Electrochem. Soc.*, 1980, **127**, 2167–2172.
- 12 J. N. Barisci, G. G. Wallace, D. R. MacFarlane and R. H. Baughman, *Electrochem. Commun.*, 2004, **6**, 22–27.
- 13 W. L. Hough, M. Smiglak, H. Rodriguez, R. P. Swatloski, S. K. Spear, D. T. Daly, J. Pernak, J. E. Grisel, R. D. Carliss, M. D. Soutullo, J. H. Davis and R. D. Rogers, *New J. Chem.*, 2007, **31**, 1429–1436.
- 14 P. Bonhôte, A. P. Dias, N. Papageorgiou, K. Kalyanasundaram and M. Gratzel, *Inorg. Chem.*, 1996, **35**, 1168–1178.
- 15 S. V. Dzyuba and R. A. Bartsch, *PhysChemPhys*, 2002, **3**, 161–167.
- 16 J. D. Holbrey, W. M. Reichert, R. P. Swatloski, G. A. Broker, W. R. Pitner, K. R. Seddon and R. D. Rogers, *Green Chem.*, 2002, **5**, 407–413.
- 17 D. R. MacFarlane, J. Golding, S. Forsyth, M. Forsyth and G. B. Deacon, *Chem. Commun.*, 2001, 1430–1431.
- 18 J. S. Wilkes, J. A. Levisky, R. A. Wilson and C. L. Hussey, *Inorg. Chem.*, 1982, **21**, 1263–1264.
- 19 J. F. Brennecke and E. J. Maginn, *AIChE J.*, 2001, **47**, 2384–2389.
- 20 D. A. Waterkamp, M. Heiland, M. Schluter, J. C. Sauvageau, T. Beyersdorff and J. Thoming, *Green Chem.*, 2007, **9**, 1084–1090.
- 21 A. K. Burrell, R. E. Del Sesto, S. N. Baker, T. M. McCleskey and G. A. Baker, *Green Chem.*, 2007, **9**, 809–809.
- 22 K. R. Harris, M. Kanakubo and L. A. Woolf, *J. Chem. Eng. Data*, 2006, **51**, 1161–1167.
- 23 J. M. Crosthwaite, M. J. Muldoon, J. K. Dixon, J. L. Anderson and J. F. Brennecke, *J. Chem. Thermodyn.*, 2005, **37**, 559–568.
- 24 K. Kunkel and G. Maas, *Eur. J. Org. Chem.*, 2007, 3746–3757.
- 25 E. J. Gonzalez, B. Gonzalez, N. Calvar and A. Dominguez, *J. Chem. Eng. Data*, 2007, **52**, 1641–1648.
- 26 E. A. Turner, C. C. Pye and R. D. Singer, *J. Phys. Chem. A*, 2003, **107**, 2277–2288.
- 27 C. Reichardt, *Solvent and Solvent Effects in Organic Chemistry* 3edn., Wiley-VCH, Weinheim, Germany, 2003.
- 28 L. W. Deady and D. C. Stillman, *Aust. J. Chem.*, 1976, **29**, 1745–1748.
- 29 Y. Gao and J. M. Shreeve, *Synthesis*, 2004, 1072–1082.
- 30 M. M. Kabachnik, Y. A. Khomutova and I. P. Beletskaya, *Russ. J. Org. Chem.*, 1999, **35**, 26–27.
- 31 J. Ropponen, M. Lahtinen, S. Busi, M. Nissinen, E. Kolehmainen and K. Rissanen, *New J. Chem.*, 2004, **28**, 1426–1430.
- 32 J. Sun, D. R. MacFarlane and M. Forsyth, *Sol. State Ionics*, 1997, **3**, 356–362.
- 33 T. Neveca and V. Bekarek, *Acta Univ. Palack. Olomuc. Fac. Rerum Natur. Chemica XXXI*, 1992, **108**, 33–37.
- 34 A. Skrzypczak and P. Neta, *Int. J. Chem. Kinet.*, 2004, **36**, 253–258.
- 35 N. Menshutkin, *Z. Phys. Chem*, 1890, **5**, 589.
- 36 C. B. Minnich, L. Küpper, M. A. Liauw and L. Greiner, *Catal. Today*, 2007, **126**, 191–195.
- 37 R. S. Varma and V. V. Namboodiri, *Chem. Commun.*, 2001, **7**, 643–644.
- 38 M. Deetlefs and K. R. Seddon, *Green Chem.*, 2003, **5**, 181–186.
- 39 J.-M. Leveque, G. Cravotto, L. Boffa, W. Bonrath and M. Draye, *Synlett*, 2007, 2065–2068.
- 40 A. Grosse-Böwing and A. Jess, *Green Chem.*, 2005, **7**, 230–235.
- 41 A. Grosse-Böwing and A. Jess, *Chem. Eng. Sci.*, 2007, **62**, 1760–1769.
- 42 P. T. Anastas, *Clean Solvents*, 2002, **819**, 1–9.
- 43 P. Anastas, and J. C. Warner, *Green Chemistry: Theory and Practice*, Oxford University Press, New York, USA, 1998.
- 44 P. T. Anastas, *Environ. Sci. Technol.*, 2003, **37**, 423a.
- 45 G. Koller, U. Fischer and K. Hungerbühler, *Ind. Eng. Chem. Res.*, 2000, **39**, 960–972.
- 46 R. L. Lankey and P. T. Anastas, *Ind. Eng. Chem. Res.*, 2002, **41**, 4498–4502.
- 47 W. McDonough, M. Braungart, P. T. Anastas and J. B. Zimmerman, *Environ. Sci. Technol.*, 2003, **37**, 434a–441a.
- 48 D. Kralisch, D. Reinhardt and G. Kreisel, *Green Chem.*, 2007, **9**, 1308–1318.
- 49 D. Kralisch, A. Stark, S. Korsten, G. Kreisel and B. Ondruschka, *Green Chem.*, 2005, **7**, 301–309.
- 50 P. G. Jessop, R. Stanley, R. A. Brown, C. A. Eckert, C. L. Liotta, T. T. Ngo and P. Pollet, *Green Chem.*, 2003, **5**, 123–128.
- 51 U.S. FDA, 2007, <http://vm.cfsan.fda.gov/~dms/efafus.html>.
- 52 U.S. FDA, CFSAN/Office of Food Additive Safety, 2006, <http://www.cfsan.fda.gov/~dms/opa-appa.html#ftnE>.
- 53 Rowan University, <http://www.rowan.edu/greenengineering>, accessed: January 20, 2008.
- 54 C. S. Slater and M. J. Savelski, *J. Environ. Sci. Health Part A*, 2007, **42**, 1595–1605.
- 55 *Corporate Environment and Safety Product Stewardship Guide: Solvent Selection Guidelines*, GlaxoSmithKline(GSK) pharmaceuticals, 2003.
- 56 M. J. Muldoon, C. M. Gordon and I. R. Dunkin, *J. Chem. Soc. Perkin Trans. 2*, 2001, 433–435.
- 57 C. Reichardt, *Green Chem.*, 2005, **7**, 339–351.
- 58 M. J. Kamlet and R. W. Taft, *J. Am. Chem. Soc.*, 1976, 2886–2894.
- 59 M. J. Kamlet and R. W. Taft, *J. Am. Chem. Soc.*, 1976, 377–383.
- 60 M. J. Kamlet, J. L. Abboud and R. W. Taft, *J. Am. Chem. Soc.*, 1977, **99**, 6027–6037.
- 61 C. Laurence, P. Nicolet and M. T. Dalati, *J. Phys. Chem.*, 1994, 5807–5816.
- 62 M. J. Kamlet, J. M. Abboud, M. H. Abraham and R. W. Taft, *J. Org. Chem.*, 1983, 2877–2887.
- 63 J. McLaren, *J. Chem. Technol. Biotechnol.*, 2000, 927–932.
- 64 D. Wilke, *Appl. Microbiol. Biotechnol.*, 1999, 135–145.
- 65 M. H. Abraham, *Prog. Phys. Org. Chem.*, 1974, **11**, 1–87.
- 66 E. D. Hughes, *Trans. Faraday Soc.*, 1941, **37**, 603–637.
- 67 E. D. Hughes, M. L. Dhar, C. K. Ingold, A. M. M. Mandour, G. A. Maw and L. I. Woolf, *J. Chem. Soc.*, 1948, 2093–2119.
- 68 E. D. Hughes and C. K. Ingold, *J. Chem. Soc.*, 1935, 244–255.
- 69 Arrhenius, *Z. Physik. Chem.*, 1889, **4**, 226.
- 70 H. Eyring, *Chem. Rev.*, 1935, **17**, 65–77.
- 71 H. Eyring, *J. Chem. Phys.*, 1935, **3**, 107–115.
- 72 U. A. Chaudry and P. L. A. Popelier, *J. Phys. Chem. A*, 2003, **107**, 4578–4582.
- 73 J. F. Mata-Segreda, *Int. J. Chem. Kinet.*, 2000, **32**, 67–71.
- 74 D. Stefanidis and W. P. Jencks, *J. Am. Chem. Soc.*, 1993, **115**, 6045–6050.
- 75 L. Singh, R. T. Singh and R. C. Jha, *J. Indian Chem. Soc.*, 1981, **58**, 966–969.
- 76 A. B. Manning, *J. Chem. Soc.*, 1921, **119**, 2079–2087.
- 77 P. Haberfield, A. Nudelman, A. Bloom, R. Bloom and H. Ginsberg, *J. Org. Chem.*, 1971, **36**, 1792–1795.
- 78 P. Atkins, *Physical Chemistry 6th Edition*, W.H. Freeman and Company, New York, 1998.
- 79 P. Bonhôte, A.-P. Dias, N. Papageorgiou, K. Kalyanasundaram and M. Gratzel, *Inorg. Chem.*, 1996, **35**, 1168–1178.
- 80 M. Ue, M. Takeda, T. Takahashi and M. Takehara, *Electrochem. Solid-State Lett.*, 2002, **5**, A119–A121.
- 81 L. Leclercq, I. Suisse, G. Nowogrocki and F. Agbossou-Niedercorn, *Green Chem.*, 2007, **9**, 1097–1103.
- 82 M. Yoshizawa, M. Hirao, K. Ito-Akita and H. Ohno, *J. Mater. Chem.*, 2001, **11**, 1057–1062.
- 83 J. Schleicher, A. Ahosseini and A. M. Scurto, *manuscript in preparation*, 2008.

-
- 84 V. V. Zverlov, O. Berezina, G. A. Velikodvotskaya and W. H. Schwarz, *Appl. Microbiol. Biotechnol.*, 2006, **71**, 587–597.
- 85 S. N. V. K. Aki, A. M. Scurto and J. F. Brennecke, *Ind. Eng. Chem. Res.*, 2006, **45**, 5574–5585.
- 86 A. M. Scurto, S. N. V. K. Aki and J. F. Brennecke, *J. Am. Chem. Soc.*, 2002, **124**, 10276–10277.
- 87 A. M. Scurto, S. N. V. K. Aki and J. F. Brennecke, *Chem. Commun.*, 2003, 572–573.
- 88 A. M. Scurto, Ph.D. Dissertation, University of Notre Dame, 2002.
- 89 J. Schleicher, MS Thesis, University of Kansas, 2007.
- 90 O. Levenspiel, *Chemical Reaction Engineering*, Wiley, New York, USA, 1998.
- 91 M. J. Kamlet, T. N. Hall, J. Boykin and R. W. Taft, *J. Org. Chem.*, 1979, **44**, 2599–2604.
- 92 D. Lide, *CRC Handbook of Chemistry and Physics 88th edn.*, CRC Press, Boca Raton, 2007.
- 93 M. Temprado and J. S. Chickos, *Thermochim. Acta*, 2005, **435**, 49–56.

A novel glycerol valorization route: chemoselective dehydrogenation catalyzed by iridium derivatives

Erica Farnetti,^{a,b} Jan Kašpar^{a,b} and Corrado Crotti^{*b,c}

Received 10th November 2008, Accepted 29th January 2009

First published as an Advance Article on the web 18th February 2009

DOI: 10.1039/b819870e

Organoiridium derivatives of the type Ir(diene)(N-N)X (diene = 1,5-hexadiene, 1,5-cyclooctadiene; N-N = 2,2'-bipyridine, 1,10-phenanthroline and substituted derivatives; X = Cl, I) catalyze the hydrogen transfer reaction from glycerol to acetophenone, yielding dihydroxyacetone and phenylethanol. The catalytic reactions are performed at temperatures of 100 °C or higher, in the presence of a basic cocatalyst. The effect of experimental conditions on overall conversion and catalyst lifetime is discussed, as well as on the degradation of dihydroxyacetone, which can lead to an apparent decrease of selectivity of the catalytic reaction.

Introduction

In recent years sustainability has become an imperative issue, forcing both academic and industrial scientists towards the design of more environmentally friendly and atom efficient chemical processes. A considerable number of new synthetic methods has been proposed which meet the requirements of the twelve principles of green chemistry as stated by Anastas and Kirchoff.¹ One of the crucial points is represented by the use of renewables which are destined to increasingly replace fossil fuels as a carbon source. In this respect, the interest of several scientists has been recently attracted by glycerol, a renewable raw material² which is characterized by unique properties: it is a nontoxic, edible and biodegradable compound and its nature as a polyfunctional molecule allows a variety of possible transformations.

At present, the availability of glycerol is increasing due to the expanding manufacture of the biodiesel fuel obtained by methanol transesterification of seed oils, a process which generates about 10% weight of glycerol as a side-product. At the same time, first generation biofuel production from edible seeds is already causing unacceptable consequences on food costs, *i.e.* the food vs. fuel dilemma.³ However, second generation biofuels based on alternative sources (lignocellulosic materials, microalgae, inedible seeds such as *Jatropha curcas*), which combine highly efficient production with environmental and ethical sustainability, are expected to use the same industrial route as the economic feasibility of the direct conversion of biomass to second generation fuels is still far away.

On the whole, the large surplus of glycerol in association with its high functionalization makes it one of the most promising platform chemicals of the near future. Under the influence

of suitable catalysts, glycerol can undergo a large number of chemical transformations to products of commercial value. Among the processes under current investigation hydrogenolysis leading to 1,2- or 1,3-propanediol, reforming to CO and H₂, carboxylation to give glycerol carbonate, dehydration to acrolein and oxidation seem the most promising.⁴

Glycerol oxidation can lead to a large variety of products (Scheme 1), many of which have commercial relevance. In most cases, however, the process is far from being satisfactory as the selective transformation of one single hydroxyl group has proven a hard task to be accomplished. Oxidation of the primary hydroxyl groups to form glyceric acid and subsequently tartronic acid is catalyzed by platinum group metals supported over carbon or ceria, however the selectivity observed is often affected by low catalyst stability.⁵ Selective oxidation of the secondary hydroxyl group of glycerol yields dihydroxyacetone (DHA), an important synthon in organic synthesis⁶ and itself a commercially valuable chemical used as a component in artificial tanning preparations. At present DHA is produced by microbial fermentation of glycerol with *Gluconobacter oxydans*⁷ or by electrocatalytic oxidation in the presence of TEMPO,⁸ whereas heterogeneous catalysts mostly prefer to affect primary OH groups, with some notable exceptions such as bismuth-promoted platinum.⁹ Finally, oxidation of all three alcoholic groups of glycerol yields mesoxalic acid, a reaction which is preferably catalyzed by platinum-based heterogeneous catalysts.¹⁰

A possible environmentally friendly route to glycerol oxidation is represented by dehydrogenation *via* a hydrogen transfer reaction. In the last few decades, transfer hydrogenation has been developed as an efficient reduction method for organic substrates, generally ketones, aldehydes and imines (Scheme 2).¹¹ These reactions are homogeneously catalyzed by transition metal derivatives, with the hydrogen donors generally employed being formic acid and 2-propanol.

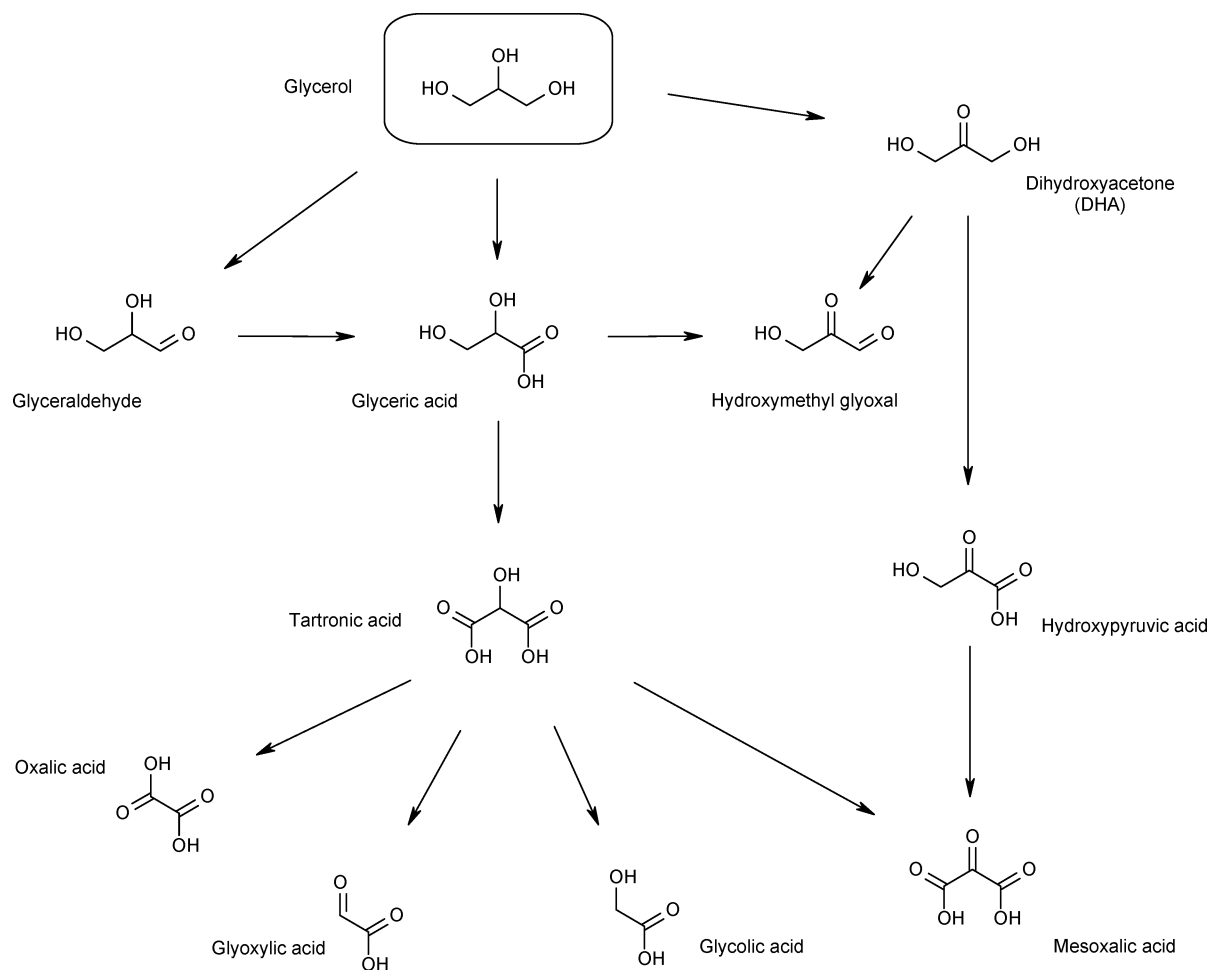
Glycerol can be envisaged as a disubstituted 2-propanol, therefore we reasoned that it should be possible to perform a transfer dehydrogenation of glycerol in the presence of a suitable catalyst and an appropriate hydrogen acceptor. In principle, both primary and secondary hydroxyl groups of glycerol can undergo

^aDipartimento di Scienze Chimiche, Università di Trieste, Via Giorgieri 1, 34127, Trieste, Italy

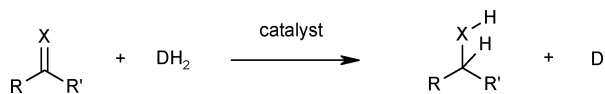
^bINCA research unit Trieste, Italy

^cCNR-Istituto Struttura della Materia, Unità staccata di Trieste, S.S.14, Km163.5, 34012, Basovizza, Trieste, Italy.

E-mail: crotti@ism.cnr.it; Fax: +39 040 226870; Tel: +39 040 9221091



Scheme 1 Products of glycerol oxidation.



Scheme 2 Transfer hydrogenation.

dehydrogenation, however, according to the relative oxidation potentials of secondary vs. primary alcohols¹² the hydrogen transfer is expected to selectively occur from the secondary hydroxyl group, yielding DHA as a dehydrogenation product.

To our knowledge, no report regarding transfer dehydrogenation of glycerol has appeared in the literature until now. We therefore applied our previous experience in hydrogen transfer reactions catalyzed by organoderivatives of platinum group metals, especially iridium¹³ to study selective glycerol dehydrogenation.

Here we describe the results obtained in the dehydrogenation of glycerol catalyzed by the compounds Ir(diene)(N-N)X (diene = 1,5-hexadiene (hd), 1,5-cyclooctadiene (cod); N-N = 2,2'-bipyridine, 1,10-phenanthroline and substituted derivatives; X = Cl, I).

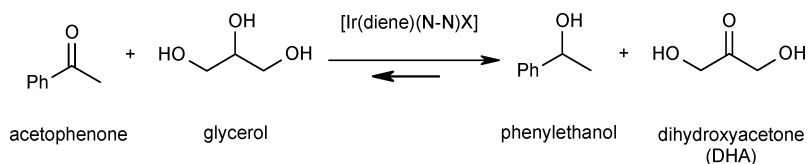
Results and discussion

Iridium derivatives of the type Ir(diene)(N-N)X are well known transfer hydrogenation catalysts for the reduction of various

unsaturated substrates. When a ketone is used as a hydrogen acceptor, the hydrogen transfer reaction is actually an equilibrium between the hydrogen donor (an alcohol such as 2-propanol or cyclopentanol) and the acceptor molecule: this equilibrium can be driven to the products side by use of a large excess of one of the reactants, a situation which is generally obtained by using the hydrogen donor (alcohol) as a solvent for the reaction mixture.

In our initial approach to transfer dehydrogenation of glycerol we chose as the acceptor molecule acetophenone, a model substrate which has often been employed in catalytic reduction studies (Scheme 3). Initial tests performed using an excess of glycerol together with a cosolvent (*e.g.* dioxane) gave encouraging results, whereas reactions performed in the absence of a cosolvent evidenced some difficulties concerning, for example, solubility of catalysts. However, as the latter option looked more coherent with the green chemistry principles, we decided to limit our investigations to the reactions performed in the absence of a cosolvent.

A first series of reactions was performed using Ir(diene)(Me₄phen)Cl and Ir(diene)(Me₂bipy)Cl (diene = hd or cod; Me₄phen = 3,4,7,8-tetramethyl-1,10-phenanthroline; Me₂bipy = 4,4'-dimethyl-2,2'-bipyridine) and 2 equivalents of NaOH, the basic cocatalyst generally employed in transfer hydrogenation: after 1 h at 100 °C the analysis of the reaction mixture revealed that glycerol was behaving as a hydrogen



Scheme 3 Transfer dehydrogenation of glycerol.

Table 1 Hydrogen transfer reduction of acetophenone by glycerol catalyzed by Ir(diene)(N-N)Cl^a

Entry	Catalyst	Conv. (%) ^b
1	Ir(hd)(Me ₄ phen)Cl	26
2	Ir(cod)(Me ₄ phen)Cl	4
3	Ir(hd)(Me ₂ bipy)Cl	25
4	Ir(cod)(Me ₂ bipy)Cl	6

^a Experimental conditions: [Ir] = 3.0 × 10⁻³ M; [acetophenone]/[Ir] = 100; T = 100 °C; reaction time = 1 h; base = NaOH; [base]/[Ir] = 2.
^b Calculated as % acetophenone reduced to phenylethanol.

Table 2 Hydrogen transfer reduction of acetophenone by glycerol catalyzed by Ir(hd)(Me₄phen)Cl^a

Entry	Base	K _b	[base]/[Ir]	Conv. (%) ^b	DHA yield (sel.) (%) ^c
1	—	—	—	0	—
2	NaOH	55	2	26	8 (30)
3	K ₂ CO ₃	2 × 10 ⁻⁴	2	33	13 (39)
4	NaHCO ₃	2 × 10 ⁻⁸	2	21	7 (35)
5	NaCO ₂ CH ₃	6 × 10 ⁻¹⁰	2	8	6 (76)
6	Na ₂ C ₂ O ₄	2 × 10 ⁻¹⁰	2	13	8 (58)
7	K ₂ CO ₃	2 × 10 ⁻⁴	1	30	10 (34)
8	K ₂ CO ₃	2 × 10 ⁻⁴	4	35	11 (31)

^a Experimental conditions: [Ir] = 3.0 × 10⁻³ M; [acetophenone]/[Ir] = 100; T = 100 °C; reaction time = 1 h. ^b Calculated as % acetophenone reduced to phenylethanol. ^c DHA yield %: calculated on the basis of the initial acetophenone; sel. %: calculated on the basis of the Conversion.

donor, partially reducing acetophenone to phenylethanol. When the reaction was performed in the absence of either metal catalyst or NaOH, no traces of phenylethanol were observed. These findings confirm on one hand that NaOH does not promote hydrogen transfer from the alcohol to the ketone in the present conditions, on the other the need for the presence of both a catalyst and a base. Notably, the presence of the base also suppressed formation of ketals arising from the condensation of acetophenone with glycerol that was observed in the blank experiments. A comparison between cod and hd-derivatives is reported in Table 1: the hexadiene catalysts are superior to those with cyclooctadiene in both cases, with phenylethanol yields of 25–26% (hd catalysts) vs. 4–6% (cod catalysts). Such a difference in catalytic activity as a function of the diene is coherent with previously reported trends in transfer hydrogenation of ketones.^{13a} On the other hand an effect of the lower solubility in glycerol of the cod complexes compared to the hd ones cannot be disregarded.

In the final reaction mixtures dihydroxyacetone was always detected among the products, however the relative amount was always lower than that of phenylethanol: with 25–26% of acetophenone reduction, DHA yield was only 8% of the initial acetophenone, resulting in a selectivity in DHA of 30%; on the other hand, other dehydrogenation products of glycerol (e.g. glyceraldehyde) were never detected in the final reaction mixtures.

As an alternative approach, weaker bases were considered as possible cocatalysts. Actually, a first reaction performed using K₂CO₃ in the place of NaOH gave even better results both as conversion (33 vs. 26%) and selectivity in DHA (39 vs. 30%). The results of a series of reactions using different bases are reported in Table 2. From these data, apart from entry 2 concerning NaOH, a significant correlation between cocatalyst basicity and conversion is observed, *i.e.* the lower the K_b value, the lower the extent of acetophenone reduction (see Table 2, entries 3–6). On the other hand, the selectivity in DHA formation does not show an analogous, clear correlation upon the strength of the base: apparently the higher the conversion, the lower the DHA selectivity.

Interestingly, when sodium acetate was used as cocatalyst at 120 °C higher conversion (26%) was achieved, but lower selectivity (52%) compared to the reaction at 100 °C (Table 2, entry 5). With regard to cocatalyst concentration, the data reported in entries 3, 7 and 8 of Table 2 evidence that an increase of [K₂CO₃]/[Ir] ratio produces a moderate increase of conversion, leaving the yield of DHA nearly unaffected.

A comparison of catalytic activity and selectivity using iridium-hexadiene complexes with different ligands was made using K₂CO₃ as a basic cocatalyst. Table 3 reports the data concerning chloro complexes which differ in the nature of the nitrogen ligand (entries 1–4; Me₂phen = 4,7-dimethyl-1,10-phenanthroline; bipy = 2,2'-bipyridine); two results regarding iodo derivatives are included to evaluate the halogen effect (compare entries 1, 5 and 2, 6); in the table conversions and selectivities are shown at two different reaction times (30 and 60 min) to enable easier comparison. Chloro derivatives prove to be more active; on the other hand, selectivity in DHA formation is higher when iodo compounds are employed, *i.e.* once more a lower reaction conversion corresponds to better selectivity. The four chloro complexes with different nitrogen ligands (the derivative with unsubstituted phenanthroline was not examined due to its low solubility) display similar catalytic activities with highest conversion observed with the Me₂phen catalyst (36% conversion in 30 min and 39% in 60 min). In previous studies, the activity of analogous series of catalysts in hydrogen transfer reactions had been shown to be influenced by the donor ability of the nitrogen ligands,^{13–15} in other words, better electron releasing ligands gave rise to more active catalysts. In the present studies no such dependence is evidenced as the best donor ligand leads to the lowest conversion, although the differences observed are barely significant. A prompt rationalization of such data is not obvious as several factors are likely to affect the extent of acetophenone reduction, *i.e.* catalyst solubility, the effect of

Table 3 Hydrogen transfer reduction of acetophenone by glycerol catalyzed by Ir(hd)(N-N)X complexes^a

Entry	Catalyst	30 min reaction time		60 min reaction time	
		Conv. (%) ^b	DHA yield (sel.) (%) ^c	Conv. (%) ^b	DHA yield (sel.) (%) ^c
1	Ir(hd)(Me ₄ phen)Cl	28	13 (47)	33	13 (39)
2	Ir(hd)(Me ₂ phen)Cl	36	17 (47)	39	13 (34)
3	Ir(hd)(Me ₂ bipy)Cl	31	13 (41)	33	11 (33)
4	Ir(hd)(bipy)Cl	28	12 (42)	31	12 (38)
5	Ir(hd)(Me ₄ phen)I	17	11 (68)	21	11 (50)
6	Ir(hd)(Me ₂ phen)I	13	12 (92)	18	12 (67)

^a Experimental conditions: [Ir] = 3.0 × 10⁻³ M; [acetophenone]/[Ir] = 100; T = 100 °C; base = K₂CO₃; [base]/[Ir] = 2. ^b Calculated as % acetophenone reduced to phenylethanol. ^c DHA yield %: calculated on the basis of the initial acetophenone; sel. %: calculated on the basis of the conversion.

ligands steric hindrance on the coordination of the reactants and products, kinetics of catalyst deactivation (*vide infra*) etc. A final remark about the data reported in Table 3 regards the selectivity in DHA formation which decreases at longer reaction times.

In order to have a clearer view on the observed trend of DHA selectivity we studied in the detail the evolution of conversion and DHA yield as a function of reaction time and temperature; the results are listed in Table 4.

The data regarding the reactions at 100 °C (Table 4, entries 1–5) clearly show that initially the catalytic reaction is fast and very selective with respect to DHA formation; then, after 15 min a pronounced decrease in rate of acetophenone consumption is observed; no significant acetophenone reduction takes place after 60 min. On the other hand, the conversion is significantly increased by a moderate temperature increase (Table 4, entries 3, 6 and 7) whereas at lower temperature (80 °C) the reaction rate is negligible.

As far as the DHA selectivity is concerned, we observe a different behaviour: at 100 °C (Table 4, entries 1–5 and Fig. 1, (▲) markers) there is nearly linear apparent dependence on the conversion, *i.e.* the higher the conversion, the lower the selectivity.

The same trend in conversion *vs.* DHA selectivity was found (i) for the same reactions carried out at 110 °C (Fig. 1, (●) markers), and (ii) again at 100 °C but with the catalyst Ir(hd)(Me₄phen)I (Fig. 1, (◆) markers). Remarkably, all the trends reported in Fig. 1 clearly suggest a 100% selectivity for DHA formation at initial stages of the reaction.

Table 4 Hydrogen transfer reduction of acetophenone by glycerol catalyzed by Ir(hd)(Me₄phen)Cl^a

Entry	Reaction time/min	T/°C	Conv. (%) ^b	DHA yield (sel.) (%) ^c
1	5	100	15	11 (77)
2	15	100	26	13 (53)
3	30	100	28	13 (47)
4	60	100	33	13 (39)
5	180	100	34	12 (34)
6	30	110	37	14 (37)
7	30	120	47	12 (24)

^a Experimental conditions: [Ir] = 3.0 × 10⁻³ M; [acetophenone]/[Ir] = 100; T = 100 °C; base = K₂CO₃; [base]/[Ir] = 2. ^b Calculated as % acetophenone reduced to phenylethanol. ^c DHA yield %: calculated on the basis of the initial acetophenone; sel. %: calculated on the basis of the conversion.

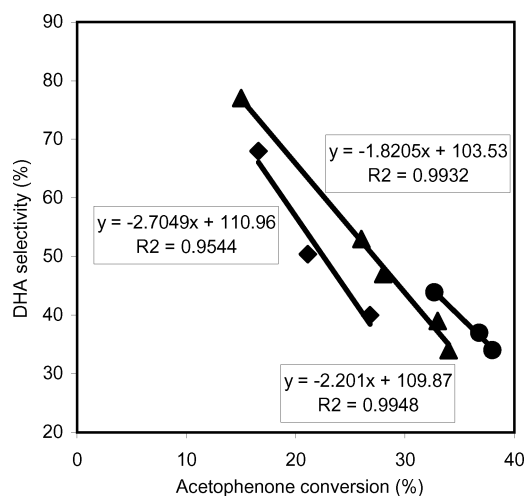


Fig. 1 DHA sel. *vs.* acetophenone conv.; exp. conditions: [Ir] = 3.0 × 10⁻³ M; [acetophenone]/[Ir] = 100; base = K₂CO₃; [base]/[Ir] = 2; (–▲–): cat. = Ir(hd)(Me₄phen)Cl, T = 100 °C; (–●–): cat. = Ir(hd)(Me₄phen)Cl, T = 110 °C; (–◆–): cat. = Ir(hd)(Me₄phen)I, T = 100 °C; the calculated equations and R² for each of the linear correlations are shown in the boxes.

In summary, the above reported data suggest that dehydrogenation of glycerol yields DHA as the only product which, however, partially disappears from the reaction mixture owing to further reactions. Several features suggest the decomposition of DHA, *i.e.* the trend at low conversion values in Fig. 1; the actual decrease in DHA yield at longer reaction times (Table 3, entries 2 and 3, reaction times 30 and 60 min; Table 4, entries 4 and 5); the analogous behaviour obtained with different catalysts and different temperatures.

The occurrence of DHA decomposition was confirmed by performing a series of test reactions in the same experimental conditions of the catalytic reactions but without a catalyst. In the first test we loaded a Schlenk tube with 0.88 mmols of acetophenone, 0.43 of phenylethanol and 0.43 of DHA: *i.e.*, the amounts calculated on an hypothesis of 33% conversion and 100% DHA selectivity. After 1 h at 100 °C, in the presence of K₂CO₃, we detected only 0.16 mmols of DHA in the reaction mixture which corresponds exactly to what found at the end of the catalytic reaction in the same experimental conditions. In other words, 60% of the initial DHA in the test reaction underwent decomposition. No decomposition products were detected by GC/MS in the final reaction mixture; attempts to

identify the products by NMR spectroscopy were frustrated by the presence of too many resonances.

Further tests were devoted to check the dependence of DHA decomposition on the base strength, showing an increase of decomposition for stronger bases. In the absence of basic cocatalyst at 100 °C only 10% of DHA was lost; however, thermal decomposition was progressively affected by an increase in reaction temperature: up to 90% of DHA was decomposed in 1 h at 160 °C. As in the catalytic reactions, in absence of bases, significant amounts of ketals were detected by the reaction of glycerol with acetophenone.

In summary, DHA decomposition promoted by temperature and a basic cocatalyst explains the DHA selectivity dependence on cocatalyst basicity, [base]/[Ir] ratio, temperature and reaction time and, more generally, the decrease of selectivity with the increase of conversion.

Actually, instability of DHA towards thermal degradation is well known,¹⁶ whereas effects of a strong base on DHA formation were not evidenced,^{5a,8} even if condensation reactions of DHA in basic media were previously reported leading to complex mixtures of higher carbohydrates even at temperatures as low as 30 °C;¹⁷ similar condensation reactions are likely to take place also in our hydrogen transfer conditions.

Further comments are due to the observed decrease of acetophenone reduction with time, which can be rationalized in terms of catalyst deactivation. Similar deactivations of iridium-based hydrogen transfer catalysts have been previously observed;¹⁸ they can be explained in terms of irreversible processes caused by either high temperature or reactions with the cocatalyst (or both) and they represent a major weak point of such catalytic systems. Furthermore, also the presence of significant amounts of water in the reaction medium due to the hygroscopicity of the glycerol is expected to have a detrimental effect on the lifetime of the catalyst. Previously reported deactivations caused a less pronounced decrease of catalytic activity, but the experimental conditions used were milder (lower temperature and/or absence of basic cocatalyst) than those employed in the present investigation.

Conclusions

The hydrogen transfer from glycerol to acetophenone is catalyzed by Ir(diene)(N-N)X; the reaction is performed at 100 °C in pure glycerol. As foreseen on the basis of thermodynamic data, glycerol dehydrogenation does selectively occur at the secondary hydroxyl group to give dihydroxyacetone, whereas acetophenone is reduced to phenylethanol. To the best of our knowledge, this study is the first example of a transfer dehydrogenation of glycerol, a reaction which represents an interesting green route to glycerol valorization. However, the selectivity is lowered by further reactions of DHA which are promoted by the basic cocatalyst. Further, thermal degradation of DHA, which becomes significant above 100 °C, prevents the use of higher reaction temperatures which might allow avoidance of the basic cocatalyst. Even though the experimental conditions required by the catalysts used in the present study affect the observed selectivity, we have demonstrated that the route of chemoselective glycerol oxydation *via* hydrogen transfer to a

suitable acceptor is feasible, thus opening future perspectives in this field.

Experimental section

General

All the reactions and manipulations were routinely performed under an argon atmosphere using standard Schlenk tube techniques.

Methanol was distilled over CaO; dioxane was distilled over sodium benzophenone ketyl just prior to use. Naphthalene (GC standard) was purified by recrystallization from ethanol. All the other chemicals were reagent grade and were used as received by commercial suppliers.

Iridium chloride hydrate was a loan from Johnson Matthey PLC and it was used as received.

Instrumental

¹H and ¹³C NMR spectra were recorded on a JEOL EX400 spectrometer operating at 399.77 and 100.54 MHz, respectively. Infrared spectra were recorded in Nujol mull on a FT-IR Perkin Elmer System 2000 spectrometer.

Chemical yields of the catalytic reactions were determined by GC on a Hewlett-Packard 5890 Series II gas chromatograph equipped with a Rtx-5 capillary column, using naphthalene as an internal standard. Alternatively, analysis of the reaction products were performed on a Hewlett-Packard 5890 Series II GC instrument coupled to a Hewlett-Packard 5971A Mass Selective Detector equipped with a Rtx-5MS column.

Synthesis of Ir(cod)(N-N)Cl, Ir(hd)(N-N)Cl and Ir(hd)(N-N)I

The compounds were prepared according to previously described methods.^{19,13a}

Procedure for the catalytic reactions

The experimental procedure for the hydrogen transfer reactions performed using glycerol as a solvent, without addition of a cosolvent, was carefully set up in order to overcome operative difficulties (*e.g.* high solvent viscosity, low solubility of catalysts and GC standards) and at the same time to guarantee excellent reproducibility.

In a typical catalytic reaction, 4.0 mL of glycerol were introduced in a Schlenk tube equipped with an argon inlet and deaerated by bubbling argon for 15 min. After addition of the catalyst (0.012 mmol), the reaction vessel was closed with a serum cap and heated with vigorous stirring to 100 °C (or other chosen reaction temperature) in a thermostatted oil bath. When the final temperature was reached, addition by microsyringe of 1.2 mmol of acetophenone ([sub]/[Ir] = 100) was followed by addition of 0.024 mmol of K₂CO_{3(aq)} or other basic cocatalyst ([base]/[Ir] = 2), which started the catalytic reaction.

Use of a condenser was avoided in order to minimize evaporation of acetophenone and of its reduction product phenylethanol (as evidenced in preliminary reactions). After the desired reaction time, the Schlenk tube was cooled under

running water and 10 mL of methanol containing the GC standard naphthalene were added. The resulting solution was analyzed as described in the next paragraph.

Determination of the reaction products

Determination of the composition of the final reaction mixture was made by GC and GC/MS. Qualitative analysis was accomplished by GC/MS using where possible authentic samples for comparison. Quantitative evaluation of product distribution was performed by GC with the aid of an internal standard reference (naphthalene), using response factors determined by use of standard solutions; several specimens of such standard solutions at different concentrations allowed quantitative analysis which were reproducible within $\pm 1\%$.

In the quantitative analysis of the catalytic reactions, the sum of final amounts of acetophenone and phenylethanol exactly corresponded to the amount of acetophenone initially loaded; moreover, no other product derived from acetophenone was detected.

Acknowledgements

Johnson Matthey PLC is gratefully acknowledged for a generous loan of iridium chloride. The Interuniversity Consortium, Chemistry for the Environment (INCA) is acknowledged.

Notes and references

- 1 P. T. Anastas and M. M. Kirchhoff, *Acc. Chem. Res.*, 2002, **35**, 686.
- 2 (a) R. A. Sheldon, *Chem. Commun.*, 2008, 3352; (b) P. Gallezot, *Green Chem.*, 2007, **9**, 295.
- 3 R. Luque, L. Herrero-Davila, J. M. Campelo, J. H. Clark, J. M. Hidalgo, D. Luna, J. M. Marinas and A. A. Romero, *Energy Environ. Sci.*, 2008, **1**, 542.
- 4 (a) M. Pagliaro, R. Ciriminna, H. Kimura, M. Rossi and C. Della Pina, *Angew. Chem., Int. Ed.*, 2007, **46**, 4434; (b) A. Behr, J. Eilting, K. Irawadi, J. Leschinski and F. Lindner, *Green Chem.*, 2008, **10**, 13; (c) C.-H. Zhou, J. N. Beltramini, Y.-X. Fan and G. Q. Lu, *Chem. Soc. Rev.*, 2008, **37**, 527.
- 5 (a) R. Garcia, M. Besson and P. Gallezot, *Appl. Catal. A*, 1995, **127**, 165; (b) P. Gallezot, *Appl. Catal., A*, 1995, **133**, 179; (c) N. Dimitralos, J. A. Lopez-Sanchez, D. Lennon, F. Porta, L. Prati and A. Villa, *Catal. Lett.*, 2006, **108**, 147; (d) S. Carrettin, P. McMorn, P. Johnston, K. Griffin, C. J. Kiely and G. J. Hutchings, *Phys. Chem. Chem. Phys.*, 2003, **5**, 1329; (e) S. Carrettin, P. McMorn, P. Johnston, K. Griffin, C. J. Kiely, C. A. Attard and G. J. Hutchings, *Top. Catal.*, 2004, **27**, 131.
- 6 (a) H. Kimura and K. Tsuto, *J. Am. Oil Chem. Soc.*, 1993, **70**, 1027; (b) A. N. Zelikin and D. Putnam, *Macromolecules*, 2005, **38**, 5532.
- 7 D. Hekmat, R. Bauer and V. Neff, *Process Biochem.*, 2007, **42**, 71.
- 8 R. Ciriminna, G. Palmisano, C. Della Pina, M. Rossi and M. Pagliaro, *Tetrahedron Lett.*, 2006, **47**, 6993.
- 9 (a) H. Kimura, K. Tsuto, T. Wakisaka, Y. Kazumi and Y. Inaya, *Appl. Catal., A*, 1993, **96**, 217; (b) H. Kimura, *Appl. Catal., A*, 1993, **105**, 147.
- 10 (a) P. Fordham, M. Besson and P. Gallezot, *Catal. Lett.*, 1997, **46**, 195; (b) H. Kimura, *Polym. Adv. Technol.*, 2001, **12**, 697.
- 11 (a) G. Brieger and T. J. Nestruck, *Chem. Rev.*, 1974, **74**, 567; (b) J.-E. Bäckvall, *J. Organomet. Chem.*, 2002, **652**, 105; (c) S. Gladiali, and E. Alberico, in *Transition Metals for Organic Synthesis*, ed. M. Beller, C. Bolm, Wiley-VCH, Weinheim, 2nd edn, 2004, ch. 1.3, pp. 145–166; (d) S. Gladiali and E. Alberico, *Chem. Soc. Rev.*, 2006, **35**, 226.
- 12 H. Adkins, R. M. Eloffson, A. G. Rossow and C. C. Robinson, *J. Am. Chem. Soc.*, 1949, **71**, 3622.
- 13 (a) E. Farnetti, F. Vinzi and G. Mestroni, *J. Mol. Catal.*, 1984, **24**, 147; (b) E. Farnetti, J. Kaspar and M. Graziani, *J. Mol. Catal.*, 1990, **63**, 5; (c) C. Bianchini, E. Farnetti, M. Graziani, G. Nardin, A. Vacca and F. Zanolini, *J. Am. Chem. Soc.*, 1990, **112**, 9190; (d) C. Bianchini, E. Farnetti, M. Graziani, M. Peruzzini and A. Polo, *Organometallics*, 1993, **12**, 3753.
- 14 F. Vinzi, G. Zassinovich and G. Mestroni, *J. Mol. Catal.*, 1983, **18**, 359.
- 15 C. Crotti, E. Farnetti, S. Filipuzzi, M. Stener, E. Zangrando and P. Moras, *Dalton Trans.*, 2007, 133 and references cited therein.
- 16 (a) Y. Zhu, D. Youssef, C. Porte, A. Rannou, M. P. Delplancke-Ogletree and B. Loi Mi Lung-Somarrriba, *J. Cryst. Growth*, 2003, **257**, 370; (b) R. K. Chaudhari, *Surfactant Science Series*, 2007, **135**, 325.
- 17 (a) C. D. Gutsche, D. Redmore, R. S. Buriks, K. A. Nowotny, H. Grassner and C. W. Ambruster, *J. Am. Chem. Soc.*, 1967, **89**, 1235; (b) M. Fleming, K. J. Kenneth and J. C. Williams, *Sugar J.*, 1971, **33**, 21.
- 18 B. Milani, C. Crotti and E. Farnetti, *Dalton Trans.*, 2008, 4659 and references cited therein.
- 19 G. Mestroni, A. Camus and G. Zassinovich, *J. Organomet. Chem.*, 1974, **73**, 119.

Continuous synthesis of glycerol acetates in supercritical carbon dioxide using Amberlyst 15[®]

Marzieh Rezayat and Hassan S. Ghaziaskar*

Received 9th September 2008, Accepted 14th January 2009

First published as an Advance Article on the web 18th February 2009

DOI: 10.1039/b815674c

Continuous esterification of glycerol with acetic acid was investigated in supercritical carbon dioxide (scCO₂) using Amberlyst 15[®] as a heterogeneous catalyst. The effect of pressure at (65–300) bar on the substrate conversion and the reaction yield and selectivity was studied. With increasing pressure, the percent of total yield and conversion remain almost unaffected and the selectivity of monoacetin synthesis increases while the selectivity for triacetin stays relatively unchanged. The effect of temperature on the yield, conversion, and the selectivity at (100–150) °C was also investigated. With increasing temperature from 100 to 140 °C, the selectivity for monoacetin decreases while for tri- and diacetin slightly increases. In contrast, with further increase in temperature, from 140 °C to 150 °C, the selectivity of monoacetin synthesis increases while that of diacetin decreases. By increasing the molar ratio of acetic acid to glycerol to 24, a selectivity of 100% was achieved for 2 h while the yield was 41% for the continuous triacetin synthesis in scCO₂. When neat scCO₂ as solvent with no catalyst was used, only monoacetin with 29% conversion was synthesized. The catalyst durability was also studied by monitoring the reaction for 25 h. The results show that the catalyst retains its activity even for 25 h but the selectivity for triacetin synthesis declines from 100% to about 60%.

Introduction

Esters have a wide variety of applications as solvents, as emulsifying and stabilizing compounds, and as raw materials in food, and the cosmetic and pharmaceutical industries.¹ Acetins are mono-, di-, and tri-esters of glycerol acetates. Monoacetin or glycerol monoacetate are used in the manufacture of explosives, in tanning, and as solvents for dyes. Diacetin or glycerol diacetate is used as a plasticizer and softening agent and solvent.² Glycerol triacetate or triacetin is used as a solvent for dissolving or diluting drugs and organic compounds. Also it is used as an antimicrobial and emulsifying agent in cigarette filters.^{3,4} Triacetin is used especially in the pharmaceutical industries as a skin pH controller for treatment of skin disorders and some pathological diseases and is used as a drug delivery compound.^{5,6}

Glycerol acetates have been synthesized *via* esterification of glycerol with acetic acid or acetic anhydride with or without a homogeneous or heterogeneous catalyst using an organic solvent and in batch or continuous processes.^{7–9} Usually, the produced esters are accompanied with some by-products, which a change in their color and odor so that it makes their purification difficult and costly. As a result, selective synthesis of the esters with high purity has been a great challenge for some researchers.^{10,11}

In recent years, considerable attention has been paid to replacing fossil fuels with bio-diesel, because of its presumed environmental and economic benefits compared to petroleum. Bio-diesel is produced by transesterification of vegetable oil where

glycerol is the main by-product.^{12,13} It is reported that 1 kg of crude glycerol is formed for every 9 kg of bio-diesel produced.¹⁴ It is therefore a reasonable scientific and technological task to find new or improved methods for the conversion of this huge pile of relatively low price glycerol to valuable products. For example, Suppes *et al.* have reported dehydration of glycerol *via* catalytic reactive distillation to produce acetol.¹⁴ Also the synthesis of acrolein from dehydration of glycerol in sub- and supercritical water has been reported.^{15,16} Indeed, some articles have focused on the esterification of glycerol with fatty acids using a catalyst, especially, heterogeneous catalyst to get the desired esters.^{17–19} Mota *et al.* have done the esterification of glycerol with acetic acid in the presence of different solid acid catalysts in a free solvent medium under reflux.²⁰ According to their report, the esterification achieved 97% conversion at 30 min of reaction time in the presence of Amberlyst 15[®] with selectivity for mono-, di-, and triacetin of 31%, 54% and 13%, respectively.

Other researchers have resorted to supercritical carbon dioxide (scCO₂) as a solvent to replace organic ones. Esterification of glycerol with lauric acid over a heterogeneous catalyst has excellent conversion in scCO₂, compared to the use of mesitylene as solvent.¹ Sugi *et al.* have explained that it is mainly due to the decrease in coke formation and removal of the water formed from the catalyst acidic sites by scCO₂. Because scCO₂ is non-flammable, inexpensive, and environmentally safe and it has moderate critical conditions ($t_c = 31.2$ °C, $p_c = 73.8$ bar), scCO₂ is a preferred solvent.²¹

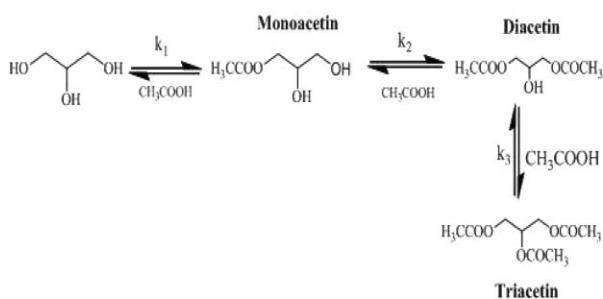
There are only a few published papers involving continuous acid-catalyst reactions in scCO₂. Most researchers have used this system when one or more of the substrates are gaseous, such as in

Department of Chemistry, Isfahan University of Technology, Isfahan, 84156-83111, I. R. Iran. E-mail: ghazi@cc.iut.ac.ir; Fax: +98-311-3913260

hydroformylation,²² hydrogenation,^{23,24,25} and partial oxidation of alcohols.²⁶ The main reason is the greater miscibility of gases in scCO₂ leading to higher reaction rates.

However, investigations have shown that tuning of the pressure of the reactions, when none of the substrates are gases, could change the selectivity and the yield to a high extent. For example, etherification of n-terminal diols in scCO₂, over Amberlyst 15[®] as a solid catalyst, could switch dramatically between mono- and bis-ethers, while the pressure was increased from 50 bar to 200 bar.²⁷ Also, Han *et al.* reported esterification of ethylene glycol with propionic acid in scCO₂ in the presence of *p*-toluene sulfonic acid as a catalyst in a batch mode. They showed that with increasing pressure, the yield and selectivity of the diester increased, while those of the monoester decreased. They claimed that the distribution of reactants and products between the vapor and liquid phase at high pressure is the main reason.²⁸

In this work, we have investigated the synthesis of glycerol esters in scCO₂ by a continuous esterification of glycerol with acetic acid in the presence of Amberlyst 15[®] as a strong solid-acid catalyst, as shown in Scheme 1. It should be noted that the boiling points of mono-, di-, and triacetin are close to each other. Specially, the boiling points of di- and triacetin are very similar, making their separation by conventional processes very difficult and costly.



Scheme 1 Synthesis of glycerol esters in three reversible steps.

Experimental

As shown in Fig. 1 a continuous flow apparatus was used to carry out the esterification reaction. The details of the system are described elsewhere.²⁹ The catalytic bed reactor, used in most

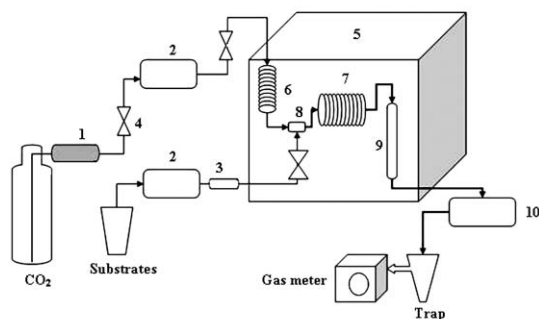


Fig. 1 The schematic diagram of the setup used for the esterification reaction; 1, molecular sieve trap; 2, liquid pump; 3, check valve; 4, needle valve; 5, air oven; 6, preheating coil; 7, static mixer; 8, T connector; 9, catalytic bed reactor; 10, back pressure regulator.

of our experiments was a 10 mm (i.d.), 316-stainless steel tubing with an internal volume of about 19 mL, containing about 9.5 g of dried catalyst (Amberlyst 15[®]), placed in an air oven with a temperature controller (± 1 °C) throughout the experiment.

To be sure that the catalyst is completely dried, a flow of scCO₂ at 100 °C was passed over the catalyst for about 1 h.⁸ When the system was set at the desired pressure and temperature, a HPLC pump (PU-980), continuously and at a constant flow rate, pumped a homogenized mixture of liquid glycerol and acetic acid, premixed in the desired molar ratio. Meanwhile another HPLC pump introduced liquid CO₂ into the system at a set flow rate. The two flows met each other in a 1/8 inch (o.d.) tubular mixer, 1.8 m long, filled with glass beads (mesh of 20–40) and then the mixture passed over the catalyst bed. Each sample was collected in a cold trap, at different time intervals and analyzed by GC-FID.

Analytical method

Analysis of the samples was carried out using a GC-FID (Agilent Technologies model 6890 N). The carrier gas was helium and the capillary column of HP-5 (with 30 m length, 0.25 mm i.d., and 0.25 μ m of film thickness) was used.

The temperature program was used for the analysis. The GC injection port and the detector temperature were set at 240 and 260 °C, respectively. The initial column temperature was set at 70 °C for 2 min and programmed from 70 °C to 150 °C for 1.5 min at the rate of 45 °C min⁻¹ and from 150 °C to 180 °C at the rate of 8 °C min⁻¹ and from 180 to 240 °C at the rate of 35 °C min⁻¹. The quantification was performed by injecting some standard ester solutions containing an internal standard and integrating their peak areas to establish the calibration curve. Since we could not find commercial monoacetin, it was synthesized *via* a previously reported method.³⁰ The identification of the products in all experiments was carried out by GC-MS (Trio 1000, Fisons Instruments, model 8060).

The yield, conversion, and selectivity for each sample are calculated as follows:

$$\text{Yield} = \frac{\text{Total moles of detected esters}}{\text{Total moles of glycerol in the feed solution}} \times 100$$

$$\text{Conversion} = \frac{\text{Total moles of detected esters}}{\text{Moles of detected esters and glycerol in exit flow}} \times 100$$

$$\text{Selectivity} = \frac{\text{Moles of each ester}}{\text{Total moles of detected esters in exit flow}} \times 100$$

Materials

Carbon dioxide with a purity of 99.95% was supplied from ZamZam Co. Ltd (Isfahan, Iran). Acetic acid (purity > 99%) and Amberlyst 15[®] was purchased from Merck. The catalyst capacity²⁶ was calculated as 4.64 meq g⁻¹. Triacetin (glycerol triacetate, purity > 99%) and diacetin (glycerol diacetate, purity = 50% verified by GC analysis) were purchased from Fluka. Absolute ethanol was purchased from Temad Co. (purity > 99%,

Tehran, Iran). Glycerol was purchased from Hopkin & Williams; 1-hexanol was purchased from Riedel-deHaën (purity > 98%).

Results and discussion

The esterification reaction of glycerol with acetic acid proceeds in three consecutive reversible steps as shown in Scheme 1. The effect of pressure, temperature, and molar ratio of acetic acid to glycerol has been investigated for the reaction over Amberlyst 15[®] as a heterogeneous strong acid-catalyst in scCO₂. In addition, we studied the catalyst reusability and the reactor length at two different molar ratio of substrates. The reaction was also performed in scCO₂ in the absence of the catalyst and only the reactor was packed with crushed glass with almost the same grain size as the catalyst. The conversion, yield, and selectivity of the reactions have been reported. All data reported in Fig. 5, 6, and 7 are the equilibrium data, taken after the continuous system has reached a steady state that is about 120 min after the start of the reaction.

Effect of pressure

The effect of pressure on the esterification of glycerol with acetic acid and the formation of tri-, di-, and monoacetic acid in a continuous flow reactor at (65–300) bar using Amberlyst 15[®] is shown in Fig. 2–4 at different time from the start of the reaction. All the experiments were carried out at 100 °C. The molar ratio of acetic acid to glycerol was equal to 3 and the flow rate of liquid CO₂ (at 0 °C) and substrates was 1.2 mL min⁻¹ and 0.2 mL min⁻¹, respectively.

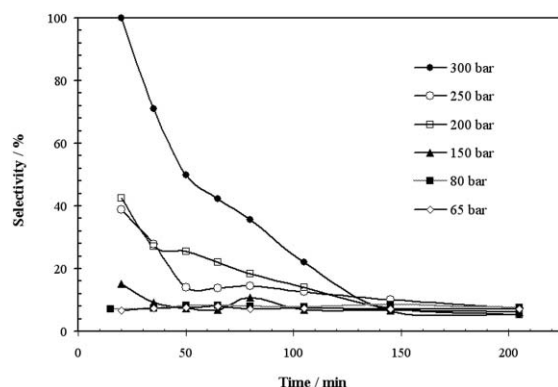


Fig. 2 Variation of the triacetin selectivity in the continuous esterification of glycerol with acetic acid versus time using Amberlyst 15[®] (9.5 g) as catalyst at a temperature of 100 °C and acid/glycerol ratio of three at different pressures.

These data show that the effect of pressure on the selectivity of tri- and monoacetic acid is more significant at the beginning of the reaction, where the selectivity of diacetin has less variation in time at different pressures. The highest variation takes place in the first 60 min. In addition, with increasing the system pressure, a longer time is needed for the esterification reaction to reach equilibrium. Due to higher solubility of the products at the higher pressures, scCO₂ can extract products from the catalyst bed and postpone the equilibration time.²⁸ This phenomena also affects the selectivity of produced esters at different times before the equilibrium is established. The greater solubility of

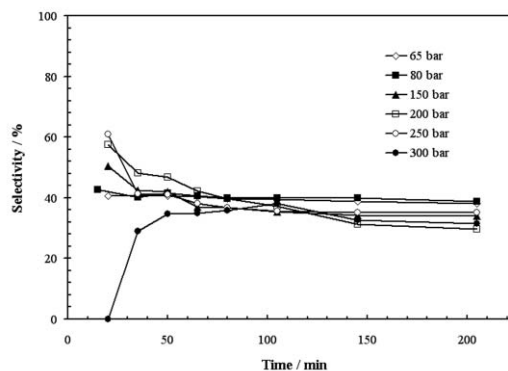


Fig. 3 Variation of the diacetin selectivity in continuous esterification of glycerol with acetic acid versus time using Amberlyst 15[®] (9.5 g) as catalyst at a temperature of 100 °C and acid/glycerol ratio of three at different pressures.

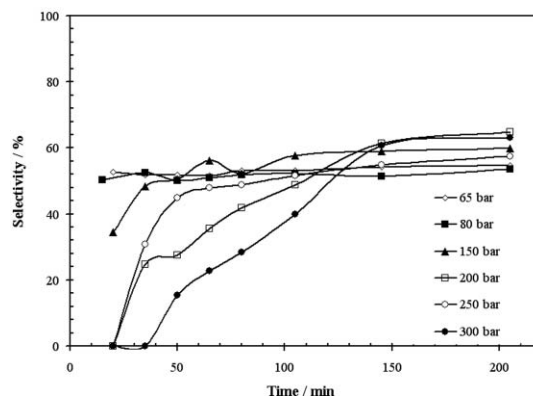


Fig. 4 Variation of the monoacetic acid selectivity in continuous esterification of glycerol with acetic acid versus time using Amberlyst 15[®] (9.5 g) as catalyst at a temperature of 100 °C and acid/glycerol ratio of three at different pressures.

products in scCO₂ at high pressures drives the esterification towards the selective synthesis of triacetin. In addition, dryness of the catalyst at the beginning of the reaction helps the forward reaction proceed to completion and triacetin is formed selectively. As time passes, since the synthesis of one mole triacetin is associated with three moles of water, the catalyst absorbs water and as a result, the reverse reaction to monoacetic acid lowers the selectivity.

The data reported in Fig. 5 is the equilibrium data shown in Fig. 2–4 and taken after the continuous system has reached to the equilibrium state where the selectivity does not change versus time. It seems the esterification reaction was found to be relatively unaffected by changes in the system pressure. As shown in Fig. 5 the total yield was not seen to be very sensitive to change in the system pressure. Moreover, the conversion was about 92% at different pressures. With increasing the pressure, a slight increase in monoacetic acid formation and a slight decrease in the diacetin formation are observed. Increasing the system pressure increases the scCO₂ density and as a result, the solubility of the monoacetic acid (*i.e.* more polar) in scCO₂ increases. The produced monoacetic acid at this condition could be extracted by scCO₂ from the catalyst bed where the esterification takes place.

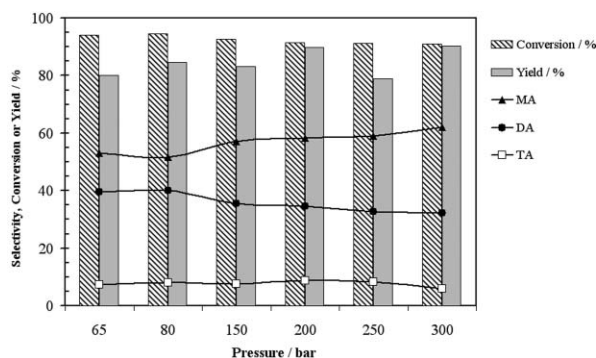


Fig. 5 The effect of increasing pressure on the conversion, yield, and product selectivity in the continuous esterification of glycerol with acetic acid at a temperature of 100 °C using Amberlyst 15[®] (9.5 g) as catalyst.

Effect of temperature

The effect of temperature on the esterification of glycerol with acetic acid in the range of (100–150) °C at 200 bar, with a molar ratio of acetic acid to glycerol of 3 and a flow rate of liquid CO₂ (at 0 °C) and substrates of 1.2 mL min⁻¹ and 0.2 mL min⁻¹, respectively, in the presence of Amberlyst 15[®], is shown in Fig. 6. The conversion was nearly constant at 91%. But the total yield of the esterification decreased continually with increasing temperature as shown in Fig. 6.

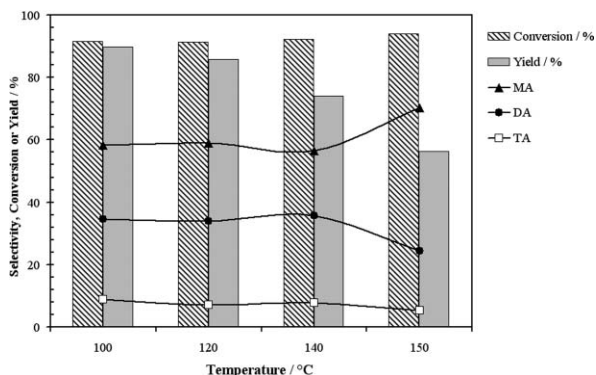


Fig. 6 The effect of increasing temperature on the conversion, yield, and products selectivity in the continuous esterification of glycerol with acetic acid using Amberlyst 15[®] (9.5 g) as catalyst at a pressure of 200 bar.

The decrease in the total yield with raising the system temperature might be due to the reduction of the catalyst activity that is happening *via* lose of the catalyst active sites at high temperatures by desulfonation of the catalyst.³¹ It has been reported that the Amberlyst 15[®] activity at 200 bar and 150 °C in an alkylation reaction in scCO₂, was about 10% lower compared to the untreated one. Moreover, at high temperatures scCO₂ density is reduced and as a result the amount of water that could be extracted out of the catalyst bed is diminished. Since the process is reversible and coproduced water would affect the equilibrium the yield of the reaction is lowered at the higher temperatures.

At temperatures above 140 °C, the selectivity for monoacetin formation increases while that for diacetin formation decreases and remains nearly constant for triacetin.

The change in selectivity could be related to the hydrolysis of diacetin to monoacetin as a decrease in the solubility of the produced esters in the presence of the water formed in scCO₂ when the system temperature is increased.

Effect of molar ratios of the substrates

In order to investigate the effect of molar ratio of acetic acid to glycerol on the yield and selectivity of the produced esters, the molar ratio was varied from 1.5 to 24 while other variables were kept constant (200 bar and 110 °C). The results are shown in Fig. 7.

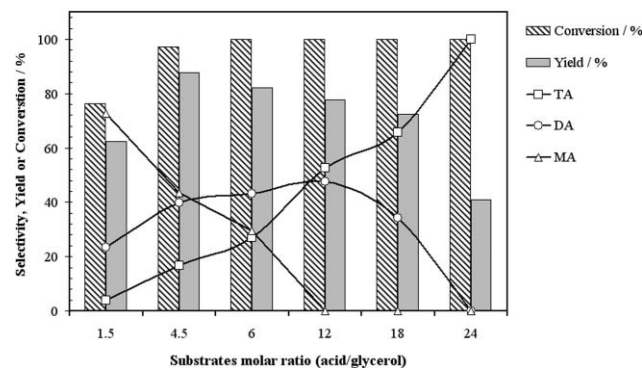


Fig. 7 The effect of increasing acetic acid to glycerol molar ratio on the conversion, yield and product selectivity in continuous esterification reaction using Amberlyst 15[®] (9.5 g) at 110 °C and 200 bar.

Except for the molar ratio of 1.5, the conversion of esterification reaction was 100 percent in all molar ratios studied. On the other hand, the total yield appears to have a maximum at molar ratio of 4.5 and a further increase in acetic acid concentration is accompanied by a decrease in the total reaction yield. The rise in total yield observed when the molar ratio is increased from 1.5 to 4.5 is thought to be related to the role of acetic acid, not only as an excess reactant, forcing the esterification reaction forward, but as a co-solvent in scCO₂. With further increase of the molar ratio, the selectivity for triacetin increases while it significantly decreases for monoacetin and diacetin. Fig. 6 shows that at the molar ratio of 24 the yield reaches a low level. However, the higher acetic acid concentration drives the esterification reaction towards triacetin production with 100% selectivity up to 120 min after the start of the reaction.

More information about the Amberlyst 15[®] performance in this reaction could be found by comparing the yield with the conversion data in all the experiments. The difference between these data could be related to the amount of the fed glycerol that is not taking part in the reaction. It seems that there is an interaction between glycerol and the catalyst active sites causing a decrease in the number of free glycerol molecules for the reaction with the protonated acetic acid over the catalyst surface.¹⁸ Since the catalyst capacity for the adsorption of glycerol and the amount of the catalyst used in all the experiments are more or less the same, the yield is decreased while the molar ratio of the substrates increased.

The influence of the acetic acid concentration on the selectivity of the esters formed shows the esterification equilibrium of the glycerol with acetic acid using Amberlyst 15[®] in scCO₂ could be progressed in three consecutive reversible reactions.

Table 1 Influence of the reactor length on the conversion, yield, and the product selectivity of the esterification of glycerol with acetic acid in scCO_2 ^a using Amberlyst 15[®]

Reactor length (cm)	Conversion (%)	Yield (%)	TA (%)	DA (%)	MA (%)
25	100	41	100	0	0
100	100	48	82	19	0

^a At 200 bar, 110 °C; the flow rate of scCO_2 and reagents was 1.2 and 0.2 mL min^{-1} , respectively; the acid/glycerol ratio was 24.

Therefore, the greater acetic acid concentration as a substrate could promote diacetin to triacetin conversion. Further studies are going on in our research group to increase the yield of the esterification reaction while keeping the high selectivity of triacetin synthesis at 100% for a longer time.

Effect of the reactor length

One of the ways considered to maximize the yield was to increase substrate–catalyst contact time. Table 1 presents the effect of increasing the length of the reactor tube on the yield and the selectivity of products while maintaining the same amount of the catalyst, the volume of the reactor, and the flow rate of scCO_2 . At a four-fold reactor length, the selectivity of triacetin synthesis was unexpectedly lower while the total yield increased 17% as illustrated in Table 1. It seems that difficulty in removal of water formed in the esterification reaction when a longer reactor is used enhances the reverse hydrolysis reaction of triacetin to diacetin.

Effect of the catalyst and its reusability

Finally, the esterification of glycerol with acetic acid at 200 bar and 110 °C was performed in scCO_2 as solvent with and without the catalyst when the molar ratio of the acid to the alcohol was 24. The results are shown in Table 2. When scCO_2 is used as solvent in the absence of the catalyst, the total yield was 29%, but the selectivity of monoacetin synthesis was 100%. In fact, CO_2 can function in this reaction, in addition to all the factors already mentioned, as a Lewis acid, even a Brønsted acid in high pressures and in the presence of water to catalyze the reaction.³² Alternatively, the reaction under the same conditions in the presence of the catalyst, leads to 100% selective synthesis of triacetin. This confirmed the importance of the catalyst in this esterification reaction.

Table 2 Influence of the catalyst and scCO_2 alone on the yield, conversion, and product selectivity of the esterification of glycerol with acetic acid at scCO_2 ^a

Condition	Conversion (%)	Yield (%)	TA (%)	DA (%)	MA (%)
1 ^b	35	29	0	0	100
2 ^c	100	41	100	0	0

^a At 200 bar, 110 °C; the flow rate of scCO_2 and substrates was 1.2 and 0.2 mL min^{-1} , respectively; the acid/glycerol ratio was 24. ^b The catalyst reactor was loaded with crushed glass or finely crushed ceramic Raschig rings (16/20 mesh). ^c The catalyst reactor was loaded with dried Amberlyst 15[®].

Table 3 Influence of the catalyst reusability on the yield, conversion, and product selectivity of the esterification of glycerol with acetic acid in scCO_2 ^a

Times catalyst recycled	Conversion (%)	Yield (%)	TA (%)	DA (%)	MA (%)
3 ^b	100	82	27	42	31
3 ^c	100	49	92	8	0

^a At 200 bar, 110 °C; the flow rate of scCO_2 and reagents was 1.2 and 0.2 mL min^{-1} , respectively. ^b The acid/glycerol ratio was 6.0 ^c The acid/glycerol ratio was 24.

We also evaluated the reusability of the catalyst (Amberlyst 15[®]). Since the substrates and products have a good solubility in absolute ethanol, this solvent was used for removal of the unreacted substrates from the catalyst surface using a Soxhlet extraction apparatus. Analysis of the extract by GC-FID and FT-IR spectroscopy confirmed that nearly all of the materials desorbed from the catalyst surface were glycerol. The washed catalyst was subsequently re-used in its dried form to investigate the reusability of the catalyst for the esterification reaction.

Table 3 shows that the recycled catalyst, after three times of usage, has clearly retained its activity in this reaction. However, the selectivity of triacetin synthesis for the molar ratio of 24 was decreased to 91.6%.

Finally as shown in Fig. 8, the catalyst stability was investigated by following the reaction at the optimum reaction condition for 25 h. The results revealed that the catalyst was still active over a long period. Nevertheless, after about 5 hours the system reaches a steady state in which the selectivity for triacetin declines to about 60% while that of diacetin rises to about 40% with no monoacetin among the products. Even at

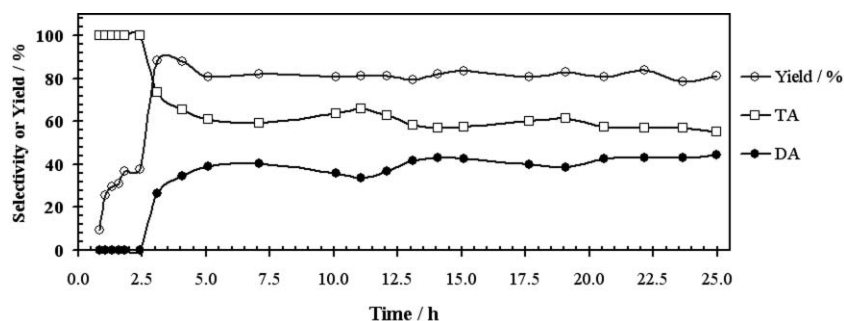


Fig. 8 Time variation in percent yield and selectivity of tri- and diacetin over a period of 25 h in continuous esterification of glycerol with acetic acid over Amberlyst 15[®] in scCO_2 , at a pressure of 200 bar, a temperature of 110 °C, and acid/glycerol ratio of 24.

this stage the selectivity for triacetin in the reaction performed in scCO₂ is about 4.6 times the reaction under reflux using the same catalyst.³³

Conclusion

The results show that the use of scCO₂, the molar ratio of the substrates, and the catalyst play a major role in tailoring the yield and selectivity in the esterification reaction of glycerol with acetic acid. However, the pressure and temperature in the synthesis of the acetins do not have a significant contribution. The continuous flow esterification of glycerol with acetic acid using Amberlyst 15[®] while the molar ratio, pressure, and temperature are 24, 200 bar and 110 °C, respectively, has shown the real advantage of 100% selectivity for triacetin synthesis for about 120 min. However, the selectivity of triacetin was diminished when the reaction is performed for a longer time. Moreover, the results of the catalyst reusability show that, the adsorption of glycerol over the catalyst was due to a physical interaction.

This work has demonstrated that the esterification could be performed without the catalyst at the molar ratio, pressure, and temperature of 24, 200 bar, and 110 °C, respectively, with 100% selectivity of the reaction towards monoacetin synthesis.

In short, the controlling of the yield and selectivity of the produced esters in the continuous esterification reaction of glycerol with acetic acid using Amberlyst 15[®] under scCO₂ was affected by Lewis acidity of CO₂, removal of the formed water from the catalyst surface, the amount of the product solubility in scCO₂, and the adsorption of glycerol by the active sites of the catalyst.

Acknowledgements

This work has been supported by IUT. The comments and critical review of Professor M. Yalpani is greatly acknowledged.

Notes and references

- 1 A. Sakthivel, R. Nakamura, K. Kamura and Y. Sugi, *J. Supercrit. Fluids*, 2007, **42**, 219–225.
- 2 J. C. Kern, *Encyclopedia of Chemical Technology*, 3rd ed., 1978, Vol. 11, p. 931.
- 3 *US Pat.*, 5 777 157, 1998.
- 4 *CN Pat.*, 1 194 997, 1998.
- 5 *US Pub.*, 2004/0091506A1, 2004.
- 6 *US Pat.*, 5 601 839, 1997.
- 7 J. B. Senderens, *Chem. Abs.*, 1914, **8**, 1752².
- 8 *US Pat.*, 4 381 407, 1983; G. Janzso, L. Cegledi, L. Manya and J. Kocsis, *Chem. Abs.*, 1992, **116**, 173576j.
- 9 *US Pat.* 6 586 609 B2, 2003; *JP Pat.* 8 027 061, 1996; B. Ding and Z.-guo Wang, *Chem. Abs.*, 2003, **138**, 273232s.
- 10 *US Pat.*, 5 434 280, 1995.
- 11 F. H. Mattson and R. A. Volpenhein, *J. lipid Research*, 1962, **3**, 281–296.
- 12 H. E. Hoydonckx, D. E. De Vos, S. A. Chavan and P. A. Jacobs, *Topics in Catalysis*, 2004, **27**, 83–96.
- 13 A. Demirbas, *Energy Convers. Manage.*, 2006, **47**, 2271–2282.
- 14 C. W. Chiu, M. A. Dasari, G. J. Suppes and W. R. Sutterlin, *AIChE*, 2006, **52**, 3543–3547.
- 15 M. Watanabe, T. Iida, Y. Aizawa, T. M. Aida and H. Inomata, *Bioresour. Technol.*, 2007, **98**, 1285–1290.
- 16 Y. Pouilloux, S. Métayer and J. Barrault, *C. R. Acad. Sci. Paris, Série IIc, Chimie/Chem.*, 2000, **3**, 589–594.
- 17 I. Díaz, F. Mohino, T. Blasco, E. Sastre and J. Pérez-Pariente, *Micropor. Mesopor. Mater.*, 2005, **80**, 33–42.
- 18 Y. Pouilloux, S. Abro, C. Vanhove and J. Barrault, *J. Mol. Catal. A-Chem.*, 1999, **149**, 243–254.
- 19 I. Díaz, F. Mohino, J. Pérez-Pariente and E. Sastre, *Appl. Catal. A: Gen.*, 2003, **242**, 161–169.
- 20 V. L. C. Gonçalves, B. P. Pinto, J. C. Silva and C. J. A. Mota, *Catal. Today*, 2008, **133–135**, 673–677.
- 21 R. S. Oakes, A. A. Clifford and C. M. Rayner, *J. Chem. Soc. Perkin. Trans.*, 2001, **1**, 917–941.
- 22 O. Hemminger, A. Marteel, M. R. Mason, J. A. Davies, A. R. Tadd and M. A. Abraham, *Green Chem.*, 2002, **4**, 507–512.
- 23 M. G. Hitzler, F. R. Smail, S. K. Ross and M. Poliakoff, *Org. Process Res. Dev.*, 1998, **2**, 137–146.
- 24 P. Stephenson, P. Licence, S. K. Ross and M. Poliakoff, *Green Chem.*, 2004, **6**, 521–523.
- 25 J. R. Hyde, P. Licence, D. Carter and M. Poliakoff, *Appl. Catal. A Gen.*, 2001, **222**, 119–131.
- 26 G. Jenzer, D. Sueur, T. Mallat and A. Baiker, *Chem. Commun.*, 2000, **22**, 2247–2248.
- 27 P. Licence, W. K. Gary, M. Sokolva and M. Poliakoff, *J. Am. Chem. Soc.*, 2005, **127**, 293–298.
- 28 J. Zhang, T. Jiang, B. Han, A. Zhu, X. Ma, Y. Zhou, L. Bai, H. Xiang and Y. Li, *J. Phys. Chem.*, 2007, **111**, 5322–5325.
- 29 H. S. Ghaziaskar, A. Daneshfar and L. Calvo, *Green Chem.*, 2006, **8**, 576–581.
- 30 C. C. Yu, Y. S. Lee, B. S. Cheon and S. H. Lee, *Bull. Korean Chem. Soc.*, 2003, **24**, 1229–1231.
- 31 R. Amandi, P. Licence, S. K. Ross, O. Altonen and M. Poliakoff, *Org. Process Res. Dev.*, 2005, **9**, 451–456.
- 32 E. J. Beckman, *Chem. Commun.*, 2004, 1885–1888.
- 33 V. L. C. Gonçalves, B. P. Pinto, J. C. Silva and C. J. A. Mota, *Catalysis Today*, 2008, **133–135**, 673–677.

Regioselective catalytic hydrogenation of citral with ionic liquids as reaction modifiers

Jürgen Arras, Martin Steffan, Yalda Shayeghi, Dominik Ruppert and Peter Claus*

Received 24th December 2008, Accepted 5th February 2009

First published as an Advance Article on the web 27th February 2009

DOI: 10.1039/b822992a

Silica and polyaniline supported palladium catalysts prepared by different techniques (incipient-wetness impregnation, deposition precipitation) using Pd(OAc)₂ or H₂PdCl₄ as precursors were studied in the liquid-phase hydrogenation of citral under addition of several ionic liquids ([BMIM][NTf₂], [BMIM][PF₆], [BMPL][NTf₂], [BMIM][DCA], [BMPL][DCA], [B3MPYR][DCA]) either as catalyst coating or as additive. By an incipient-wetness technique, the catalysts were coated with a mixture of IL in acetone. The catalysts were characterized by nitrogen physisorption, whereby a decrease of surface area and pore volume was detected by the IL coated catalysts. Furthermore, ICP-OES, TEM and IR spectroscopy were performed to analyze metal content, particle size and coverage of the catalyst with ionic liquid. Citral hydrogenation was performed at 323 K and under 2.0 MPa H₂ in an autoclave with off-line GC analysis of the product mixtures. Beside stirrer speed, catalyst mass and citral concentration, the type and quantity of ionic liquid were also varied to elucidate their influence on activity and selectivity of the Pd/SiO₂ catalysed citral hydrogenation. The results show that treatment of the catalyst with ionic liquids— independent of catalyst coating or additive— leads to a selectivity enhancement of the desired product, citronellal. With [PF₆]⁻ or [NTf₂]⁻ as the IL anion, maximum selectivities were (60 ± 2)% at 70% conversion. In particular, dicyanamide (DCA) containing ionic liquids allow, under optimised conditions, the quantitative one-pot synthesis of citronellal, at least if the Pd/SiO₂ catalyst was coated with 29 wt% [B3MPYR][DCA]. By using polyaniline supported Pd catalysts and [BMIM][DCA] as additive, the consecutive hydrogenation towards dihydrocitronellal was less pronounced and the influence of metal precursor, support material and preparation technique of the catalyst could be excluded. Hydrogenation of pure citral on [BMIM][DCA] coated palladium catalysts offers a solvent-free, green route to citronellal in reasonable selectivities (*S* = 86%).

1. Introduction

Regioselective hydrogenations of multifunctional substrates are widely used for the study of factors determining activity and selectivity on supported metal catalysts.¹ α,β -Unsaturated aldehydes contain at least one carbonyl in conjugation an olefinic bond, which results in a heterogeneously catalysed competitive hydrogenation towards saturated aldehydes and unsaturated alcohols.^{2–5} Citral belongs to this class of compounds and has additionally an isolated double bond. The liquid phase hydrogenation of citral leads to valuable flavouring compounds like citronellal, geraniol, nerol and citronellol (Scheme 1).

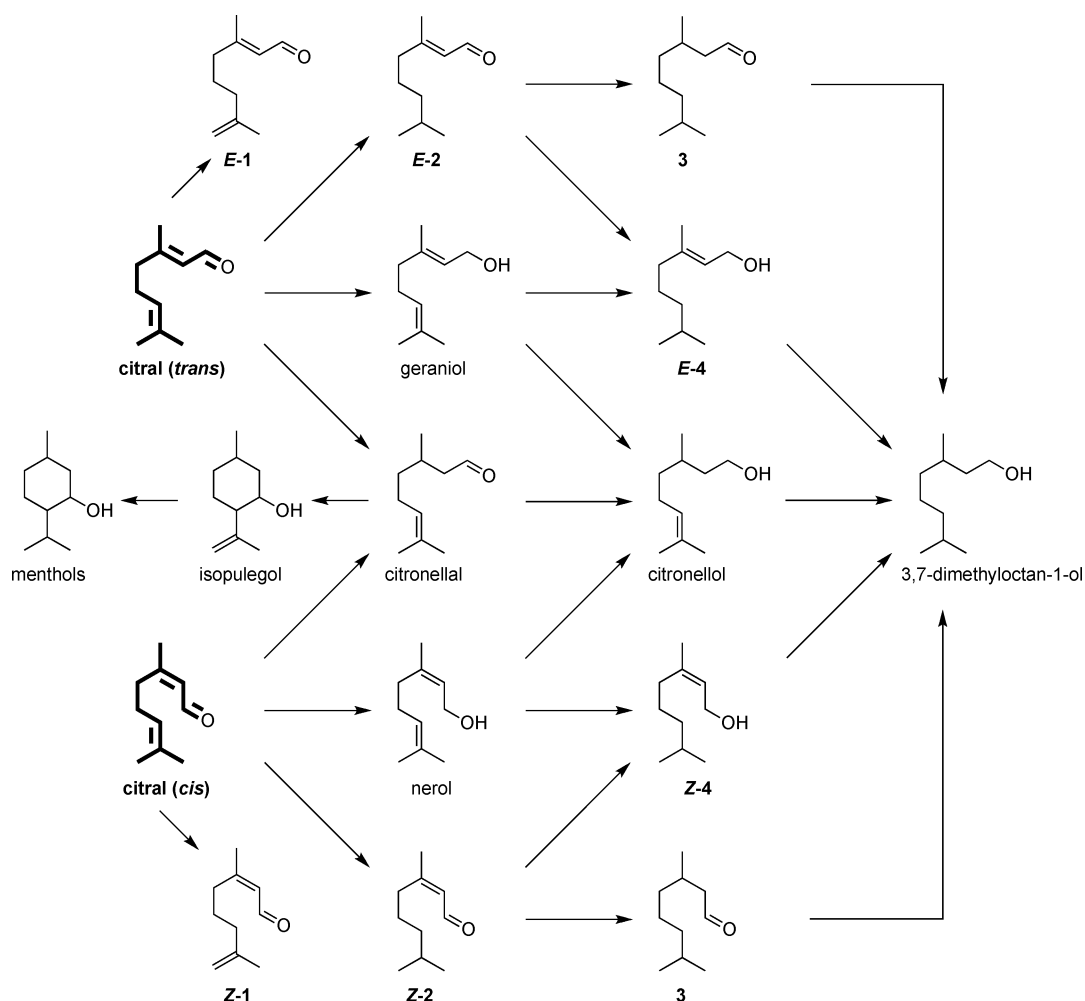
Several active metals, such as palladium,^{6,7} ruthenium,⁸ platinum,^{9,10} gold,¹¹ and bimetallic rhodium-tin,¹² nickel-tin¹³ or silver-indium¹³ supported on carbon or metal oxides, were studied in citral hydrogenation conducted in liquid phase, whereby different consecutive products were obtained. Selectivity can also be controlled by introducing electron-conducting

materials like polyaniline as the catalyst support.^{14,15} By choosing palladium, a consecutive hydrogenation could be considered, whereby dihydrocitronellal and 3,7-dimethyloctan-1-ol are obtained at higher conversion. In industrial applications, the selective hydrogenation of citral towards citronellal is catalysed by palladium on carbon¹⁶ which is usually performed in a bubble reactor with structured packings.¹⁷ Yields of citronellal >90% were obtained by using methanol as solvent and trimethylamine as a base (citral:CH₃OH:N(CH₃)₃ = 70:27:3 w/w).¹⁶

Ionic liquids (ILs) are low-melting salts with negligible vapour pressure and their application is a field of growing interest. In catalysis, ILs have been introduced in several ways,¹⁸ e.g. as solvent, as stabilizer for metallic nanoparticles¹⁹ and as supported ionic liquid phase (SILP catalysts).²⁰ The latter offers the opportunity to combine the advantages both of homogeneous and heterogeneous catalysis, as described for olefin hydrogenation,²¹ olefin hydroformylation²² and methanol carbonylation.²³ Hereby, transition metal complexes are dissolved in a thin layer of ionic liquid, which is immobilized on microporous silica.

The application of ionic liquids as coating for nickel/silica-catalysts (SCILL: solid catalyst with ionic liquid layer) was shown for the liquid-phase hydrogenation of cyclooctadiene,

Ernst-Berl-Institut, Chemical Technology II, Department of Chemistry, Technische Universität Darmstadt, Petersenstr. 20, 64287 Darmstadt, Germany. E-mail: claus@ct.chemie.tu-darmstadt.de; Fax: +49 6151 16 4788; Tel: +49 6151 16 5369



Scheme 1 Reaction network of citral hydrogenation, 3,7-dimethyl-2,7-octadienal (**1**), 3,7-dimethyl-2-octenal (**2**), dihydrocitronellal (**3**), 3,7-dimethyl-2-octen-1-ol (**4**).

leading to an enhanced selectivity towards cyclooctene in comparison to the IL-free catalysts.²⁴ It was assumed that the chosen IL ([BMIM][*n*-C₈H₁₇OSO₃]) shows a promoting effect. Furthermore, leaching of the IL into the organic solution was not detected.

In the selective hydrogenation of citral, ILs were used as bulk solvents, whereby a commercial Pd/C catalyst showed maximum selectivity towards citronellal by using [EMIM][NTf₂] and a quantitative yield of citronellal was obtained.²⁵ Although citral hydrogenation in toluene with Pd/C gave mixtures of citronellal and further side and consecutive products, the reaction rate was faster with organic solvents due to a higher hydrogen solubility than for ionic liquids.^{26,27} The catalytic system was multiply recycled and product extraction is still necessary.

The selectivity pattern of monometallic Pd/Al₂O₃ or bimetallic Ni-Sn/Al₂O₃ in citral hydrogenation could not be modified by replacing the organic solvent (*n*-hexane) with IL ([BMIM][NTf₂]).¹³ Product selectivities at equal citral conversion level were in the same range, whereby the reaction rate was lowered in presence of bulk IL.

The concept of supported ionic liquid catalysts, named SILCA, was extensively studied in the selective hydrogenation of citral.^{28,29} During preparation of the activated carbon cloth

(ACC) supported palladium catalysts, ILs were used as a nanoparticle stabilizer. The selectivity towards citronellal and dihydrocitronellal was controlled by varying the anion of the ILs ([PF₆]⁻ or [BF₄]⁻), but product mixtures were still present.

Recently, we could show that applying a dicyanamide containing ionic liquid ([BMIM][DCA]) on supported palladium catalysts leads to high selectivities towards citronellal in citral hydrogenation.³⁰ By treating a conventional Pd/C catalyst with minor amounts of ionic liquids prior to reaction, a quantitative citronellal yield was obtained. The ionic liquid covers the palladium nanoparticles, as shown in Fig. 1.

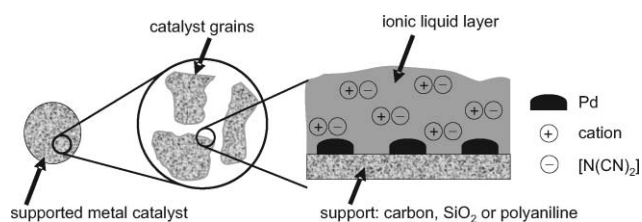


Fig. 1 Supposed structure of an IL coated solid catalyst.

The aim of this investigation was to study reaction variables (catalyst mass, citral concentration, stirrer speed) on the course of citral hydrogenation by using ionic liquids as catalyst coating or as additive for supported catalysts. Furthermore, influences of catalyst precursor and preparation route were studied and pure citral was also applied for hydrogenation. Focusing on dicyanamide ionic liquids, further cations ([BMPL]⁺ and [B3MPYR]⁺) were investigated to validate their influence on selectivity and activity. Catalyst characterization by IR spectroscopy and pulse CO chemisorption will give information about the interaction of the ionic liquid with the silica supported palladium catalyst.

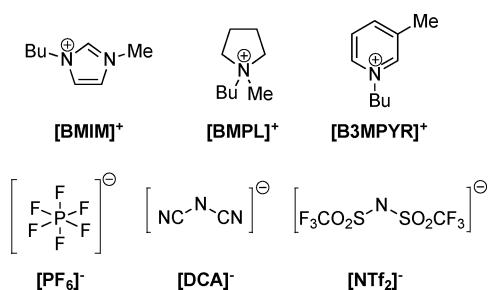
2. Experimental

2.1. Catalyst preparation

2.1.1. Pd/SiO₂ via incipient-wetness. Pd/SiO₂ (*w*_{Pd} = 5wt%) was obtained via incipient-wetness impregnation of the silica support (9.5 g, silica gel 100, Merck, pre-dried at 473 K for 2 h) with a 1.1 g portion of Pd(OAc)₂ (Evonik-Degussa) dissolved in 40 mL acetone (Merck), whereby the support was impregnated in five steps. After drying (RT overnight, then at 353 K for 2 h), the catalyst was reduced in a flow of hydrogen at 373 K for 1 h.

2.1.2. Pd/PANI via deposition-precipitation. Polyaniline (11.5 g, *M*_w = 65 kg/mol, Aldrich) was suspended at room temperature in water (100 mL) and the pH was raised to 11 by adding aqueous sodium carbonate (5 mL, 10wt%) dropwise. Then, an aqueous solution of dihydrogentetrachloropalladate (2.5 g, Heraeus, 20wt% Pd) was diluted with water to 20 mL and added to the suspension. The solution was heated to 363 K and the pH was held constant at 7 with aqueous sodium hydroxide (10wt%). After 15 min, it was cooled to 353 K; aqueous sodium hydroxide (5.8 mL, 10wt%) and formaldehyde (1.2 mL, 37wt% in water) were then added for reducing. After filtering, washing with water (5 × 10 mL) and drying, a black powder was obtained.

2.1.3. Preparation of IL coated catalysts. The ionic liquid (0.3 g) ([BMIM][NTf₂] = 1-butyl-3-methylimidazolium bis(trifluoromethylsulfonyl)amide, [BMPL][NTf₂] = *N*-butyl-*N*-methylpyrrolidinium bis(trifluoromethylsulfonyl)amide, [BMIM][PF₆] = 1-butyl-3-methylimidazolium hexafluorophosphate, [BMIM][DCA] = 1-butyl-3-methylimidazolium dicyanamide, [BMPL][DCA] = *N*-butyl-*N*-methylpyrrolidinium dicyanamide, [B3MPYR][DCA] = *N*-butyl-3-methylpyridinium dicyanamide, Merck, Scheme 2) was dissolved in acetone (Merck, 2 mL) and impregnated over the Pd/SiO₂ catalyst via



Scheme 2 Cation (top) and anion (bottom) structures of ionic liquids used in this work.

incipient-wetness. The catalyst was then dried at 343 K (3 h) to remove traces of the organic solvent. The amount of ionic liquid was varied in a range between 0.04 and 1 g_{IL}/g_{catalyst}.

2.2. Catalyst characterization

2.2.1. Nitrogen physisorption. For the determination of textural properties, nitrogen physisorption was carried out on a Quantachrome Autosorb at 77 K. Prior to analysis, the catalyst samples (100 mg) were dried at 423 K for 2 h. Adsorption isotherms were recorded with increased relative pressures (multipoint-method), the specific surface area, total pore volume and pore diameter of the catalysts were calculated according to the BET³¹ and BJH³² methods, respectively.

2.2.2. Transmission electron microscopy (TEM). HRTEM was performed using a 300 kV JEOL JEM-3010 microscope equipped with a LaB₆-cathode. Samples were prepared by suspending ground catalyst powder in methanol and dripping the suspension onto a 3.2 mm copper mesh coated with a continuous carbon film.

2.2.3. Pulse CO chemisorption. In order to identify the number of surface palladium, pulse chemisorption of the catalysts was investigated on a TPD/R/O 1100 with carbon monoxide as the probe molecule. The samples (1 g) were charged in a quartz reactor and reduced at 473 K prior to analysis. The chemisorption experiment was performed at room temperature and the sample was pulsed with CO until saturation was completed. Mean particle diameters were calculated using the following equation:

$$d_{\text{Pd}} = \frac{6 \left(\frac{v_{\text{Pd}}}{a_{\text{Pd}}} \right) f_{\text{Stoch}} W_{\text{Pd}}}{\left(\frac{n_{\text{CO}}}{m_{\text{cat}}} \right) M_{\text{Pd}}} \quad (1)$$

where *v*_{Pd} represents the atomic volume and *a*_{Pd} the atomic surface area of palladium (data and equation obtained from ref. 33), *f*_{Stoch} the stoichiometry factor of CO on palladium and $\left(\frac{n_{\text{CO}}}{m_{\text{cat}}} \right)$ the chemisorbed amount of CO per catalyst mass.

2.2.4. Infrared spectroscopy. Infrared spectroscopic studies were carried out on a Paragon 1000 PC (Perkin Elmer) spectrometer in transmission mode. Prior to analysis, the solid ionic liquid coated sample was diluted with KBr and pressed to a tablet. In order to observe the influence of palladium, a Pd-free sample was prepared by incipient wetness impregnation of [BMIM][DCA] dissolved in acetone on silica, further designated as “[BMIM][DCA]/SiO₂”.

2.3. Citral hydrogenation

The hydrogenation runs were performed in a stainless steel autoclave (Parr, 300 mL) equipped with a heating jacket and magnetic stirring (impeller type). At first, the reactor was loaded with catalyst (*m*_{cat} = 0.05–0.5 g) prior to addition of the reaction mixture (20 mL citral, Merck; 80 mL *n*-hexane, Roth; 5 mL *n*-tetradecane, Merck). Then, the reactor was closed and the

Table 1 Results of nitrogen physisorption on Pd/SiO₂ catalysts with IL coating ($w_{\text{IL}} = 17 \text{ wt}\%$)

Entry	IL	Measurement	S_{BET} [m ² /g]	V_{pore} [mL/g]
1	—	prior to hydrogenation	317	0.96
2	[BMIM][NTf ₂]	prior to hydrogenation	230	0.66
3	[BMIM][PF ₆]	prior to hydrogenation	171	0.75
4	[BMPL][NTf ₂]	prior to hydrogenation	236	0.69
5	[BMPL][NTf ₂]	after hydrogenation	234	0.66
6	—	after hydrogenation	295	0.83

magnetic stirrer was tuned to its desired frequency ($n = 500$ – 1200 rpm). After flushing with argon (2.0 MPa, three times), the reaction suspension was heated up to 323 K. Charging the reactor with hydrogen (1–2 MPa) determined the start of the reaction. Periodically taken samples were analyzed by temperature programmed gas capillary chromatography (HP 6890) using an Agilent DB-Wax column ($l = 30 \text{ m}$, $d_i = 0.25 \text{ mm}$, $t_f = 0.25 \mu\text{m}$); *n*-tetradecane was used as internal standard.

If ionic liquids were used as additive, the reactor was charged with an amount of it prior to addition of the substrate solution.

3. Results and discussion

3.1. Catalyst characterisation

3.1.1. Nitrogen physisorption. In good accordance to previous findings with dicyanamide based ionic liquids,³⁰ the textural properties of the catalyst were influenced by coating it with ionic liquids based on the [NTf₂], and [PF₆] anions, respectively (Table 1). The IL-free catalyst showed a BET surface area of 317 m²/g, and a pore volume of 0.96 mL/g, whereas these parameters were lowered for all IL coated catalysts prior to hydrogenation. As indicated by a post-hydrogenation analysis with the [BMPL][NTf₂] coated catalyst, the pore sizes remained on the same level. A slight decrease in surface area and pore volume was observed with an IL-free catalyst after citral hydrogenation. It can be assumed that the deposition of the ionic liquid into the pores remains stable, possibly by covering the catalytically active palladium nanoparticles.

3.1.2. Transmission electron microscopy (TEM). TEM analysis of the prepared Pd/PANI catalyst also revealed a high distribution of palladium nanoparticles, as depicted in Fig. 2. A thorough measurement of the particle sizes gave a mean diameter of $(3.1 \pm 0.8) \text{ nm}$, where a spherical particle shape was assumed. Pd/SiO₂ exhibits an average palladium particle size between 5 and 10 nm, as described elsewhere.³⁰

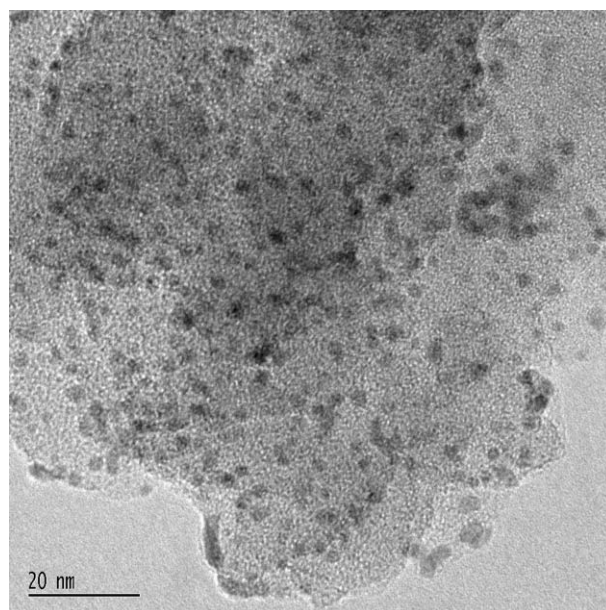
3.1.3. CO pulse chemisorption of Pd/SiO₂ and Pd/SiO₂ modified by [BMIM][DCA]. Pulse chemisorption results showed a decrease in CO uptake if the IL-free Pd/SiO₂ ($\sim 58 \mu\text{mol CO/g}_{\text{cat}}$) was treated with [BMIM][DCA] ($\sim 10 \mu\text{mol CO/g}_{\text{cat}}$) and imply that the chosen ionic liquid modifies the adsorption characteristics of CO on palladium (Table 2). Assuming a linear coordination of CO on palladium, the mean particle diameter is 9 nm for the IL-free Pd/SiO₂ and in good agreement with observations by TEM.³⁰

The decrease of $\sim 48 \mu\text{mol CO/g}_{\text{cat}}$ can be generally attributed to the lower palladium loading (2.5 wt%) of the SCILL catalyst,

Table 2 Pulse CO chemisorption results of Pd/SiO₂ catalysts coated with or without [BMIM][DCA]

Entry	Catalyst	w_{Pd} [wt%]	$n_{\text{CO}}/m_{\text{cat}}$ [$\mu\text{mol}_{\text{CO}}/\text{g}_{\text{cat}}$]	CO/Pd ^a
1	Pd/SiO ₂	5	57.8	0.12
2	Pd/SiO ₂ -[BMIM][DCA]	2.5	9.6	0.04

^a constants: $v_{\text{Pd}} = 14.7 \text{ \AA}^3$, $a_{\text{Pd}} = 7.93 \text{ \AA}^2$, $M_{\text{Pd}} = 106.42 \text{ g mol}^{-1}$, $f_{\text{Stoich}} = 1$ (data from ref. 33).

**Fig. 2** TEM characterization of Pd/PANI.

whereas the IL-free Pd/SiO₂ had 5 wt%. Under the assumption that the shape of the palladium nanoparticles remains stable after ionic liquid impregnation, *i.e.* particle diameters are equal for the IL-free and IL-coated catalyst, the uptake of the latter one should be approximately $30 \mu\text{mol CO/g}_{\text{cat}}$, which is three times higher than the observed uptake of $\sim 10 \mu\text{mol CO/g}_{\text{cat}}$. Additionally, the relatively low solubility of CO in [BMIM][DCA] compared to molecular solvents³⁴ may also decrease the CO uptake on palladium.

3.1.4. Infrared spectroscopy. Infrared spectroscopic studies were performed on IL-free and [DCA]-coated catalysts and characteristic nitrile vibrations between 2100–2300 cm⁻¹ for the dicyanamide anion are shown on Table 3. The observed nitrile absorptions for [BMIM][DCA]/SiO₂ are comparable to IR studies on neat [EMIM][DCA] and [BMPL][DCA], respectively.³⁵ In presence of palladium (entry 2), a blue shift to higher energy of at least 15 cm⁻¹ is observed which can be interpreted as an electronic interaction between palladium and the anion. A coordination of $\text{N}(\text{CN})_2^-$ and palladium *via* the central nitrogen, which was described for $\text{Pd}\{\text{N}(\text{CN})_2\}$,³⁶ could be formed.

3.2. Citral hydrogenation with ionic liquids as catalyst additives

Compared to other metals like nickel and rhodium, palladium as the active metal favours the hydrogenation of the conjugated

Table 3 Infrared study of [BMIM][DCA] supported silica materials

Entry		$V_s + V_{as}$			Ref.
		(C–N)	$\nu_1(\text{C}\equiv\text{N})$	$\nu_2(\text{C}\equiv\text{N})$	
1	[BMIM][DCA]/SiO ₂	2235	2135	2195	this work
2	Pd/[BMIM][DCA]/SiO ₂	2260	2151	2210	this work
3	Pd ^{II} {N(CN) ₂ } ₂	2305	2190	2235	36

C=C bond of citral instead of its C=O bond; density-functional-theory (DFT) calculations predict a preferred adsorption of α,β -unsaturated aldehydes on Pd(111) than for simple alkenes.³⁷ Moreover, the η^4 adsorption mode of the conjugated C=O group on palladium is favoured due to its low four-electron repulsion leading to a poor catalyst towards C=O hydrogenation.³⁷

3.2.1. Influence of catalyst mass. Several reaction conditions, *i.e.* catalyst mass, stirring frequency, and citral concentration, were varied to determine the influence of the added [BMIM][DCA] in comparison to the IL-free Pd/SiO₂ (Table 4). Nearly full citral conversion was obtained with a catalyst mass of 500 mg and the selectivity for dihydrocitronellal ($S = 70\%$) indicates a high degree of consecutive reaction. By adding [BMIM][DCA] to the substrate solution and performing the hydrogenation under the same conditions, a decrease of citral conversion was observed ($X = 41\%$), while citronellal was obtained with very high selectivity ($S = 97\%$).

These relationships between IL-free and IL-as-additive conditions were also observed by a less amount of catalyst ($m_{\text{cat}} = 50$ mg), but the final conversions were lowered due to a higher citral/catalyst ratio. Again, by adding [BMIM][DCA] to the substrate solution, selectivity towards citronellal was enhanced ($S = 100\%$) and a poor conversion was obtained ($X = 4\%$).

For IL-free conditions, citronellal selectivity could be observed in a range between 10 and nearly 100% conversion, showing a consistent transition between the catalyst masses (Fig. 3). Hence, the selectivities at a fixed conversion are independent of the chosen catalyst mass and reaction time. Furthermore, these results are in accordance with experiments at 250 mg catalyst mass showing similar selectivity patterns both for IL coated and IL-free catalyst.³⁰

3.2.2. Influence of stirrer speed and citral concentration.

The influence of stirrer speed on the catalyst properties was examined at 500 and 1200 rpm (Table 4, entries 5 and 6), whereby 250 mg Pd/SiO₂ was introduced. Independent of the reaction conditions (IL-free or IL-additive), the conversion levels and selectivities were congruent for both stirring frequencies. There-

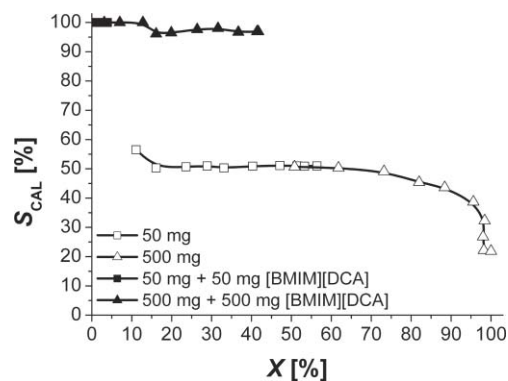


Fig. 3 S,X -plot for various Pd/SiO₂ masses in citral hydrogenation; open symbols = IL-free catalyst, close symbols = [BMIM][DCA] as catalyst additive; conditions: $c_{0,\text{citral}} = 1.1$ mol/L, $T = 323$ K, $p_{\text{H}_2} = 2.0$ MPa, $n = 1200$ rpm, $t_{\text{R}} = 6$ h.

fore, stirrer speed does not affect the catalysts performance and, thus, external film diffusion can be excluded.

For an industrial catalyst application, the chosen citral concentration (1.1 mol/L) is low. Thus, two runs—either with or without [BMIM][DCA] as additive—were carried out with pure citral (5.6 mol/L, entries 7 and 8); *n*-tetradecane was added for GC analysis and the hydrogenation was performed with 500 mg catalyst. Under IL-free conditions, the citronellal selectivity at 48% conversion is moderate due to a higher amount of isomerization of citral to **1** and other by-products like dihydrocitronellal. The lower conversion level can be attributed to higher citral/catalyst ratio. Because no solvent was added, citral may also adsorb on the acidic sites of the support material and unpreferred side-reactions took place. With the addition of [BMIM][DCA], selectivity of citronellal could be also enhanced at a comparable conversion level. The ionic liquid might be covering the acidic sites of SiO₂, which formerly catalyse the isomerisation. The considerable space-time-yield towards citronellal for the [BMIM][DCA] coated catalyst (13.4 kg_{CAL} (kg_{Pd/SiO2} h)⁻¹) is comparable to results described by Bröcker *et al.*,¹⁷ although the citral conversion did not reach 100%. Nevertheless, the use of volatile co-solvents like methanol and trimethylamine is not necessary with the introduced SCILL(DCA) concept enabling a greener route to citronellal.

3.2.3. Influence of palladium precursor and support material.

Determining influences of the choice of palladium precursor, support material and preparation route, a Pd/PANI catalyst was investigated—for the first time—in the citral hydrogenation. The

Table 4 Citral hydrogenation with Pd/SiO₂ catalysts added with [BMIM][DCA] in *n*-hexane ($T = 323$ K, $p_{\text{H}_2} = 2.0$ MPa, $t_{\text{R}} = 6$ h) under various conditions

Entry	m_{cat} [mg]	m_{IL} [mg]	$c_{0,\text{citral}}$ [mol/L]	n [rpm]	X [%]	S_{CAL} [%]	S_{DHC} [%]	S_{ISO} [%]	S_{OP} [%]
1	500	—	1.1	1200	98	22	69	1	8
2	500	500	1.1	1200	41	97	—	—	3
3	50	—	1.1	1200	53	51	12	8	30
4	50	50	1.1	1200	4	100	—	—	—
5	250	—	1.1	500	90	40	36	—	24
6	250	250	1.1	500	23	100	—	—	—
7	500	—	5.6	1200	48	43	9	11	37
8	500	250	5.6	1200	52	86	1	4	8

catalyst showed higher citronellal selectivity, with 78% at 50% conversion, than Pd/SiO₂ under IL-free conditions ($S = 50\%$ at $X = 50\%$). As depicted in Fig. 4, the course of hydrogenation gave initial citronellal selectivity of 80% and at final conversion, dihydrocitronellal was the main product ($S = 96\%$).

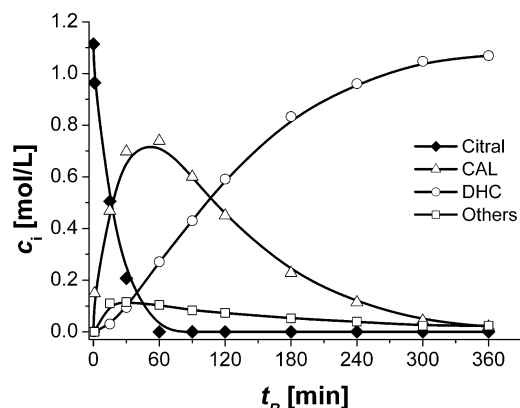


Fig. 4 c,t -plot for Pd/PANI-catalysed citral hydrogenation; conditions: $m_{\text{cat}} = 250$ mg, $c_{0,\text{citral}} = 1.1$ mol/L, $T = 323$ K, $p_{\text{H}_2} = 2.0$ MPa, $n = 1200$ rpm, $t_{\text{R}} = 6$ h.

In contrast, the addition of [BMIM][DCA] leads to a high citronellal selectivity of at least 90% (Fig. 5). Even when the substrate citral was consumed, no consecutive hydrogenation

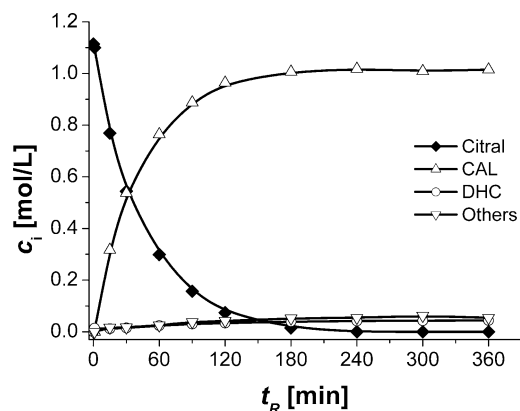


Fig. 5 c,t -plot for Pd/PANI-catalysed citral hydrogenation with [BMIM][DCA] as additive; conditions: $m_{\text{cat}} = 250$ mg, $m_{[\text{BMIM}][\text{DCA}]} = 155$ mg, $c_{0,\text{citral}} = 1.1$ mol/L, $T = 323$ K, $p_{\text{H}_2} = 2.0$ MPa, $n = 1200$ rpm, $t_{\text{R}} = 6$ h.

Table 6 Citral hydrogenation with Pd/SiO₂ and IL coated catalysts in n -hexane ($T = 323$ K, $p_{\text{H}_2} = 2.0$ MPa, $c_{0,\text{citral}} = 1.1$ mol/L, $n = 1200$ rpm, $t_{\text{R}} = 6$ h) with various ILs. Unless noted otherwise, selectivities referring to 80% citral conversion

Entry	IL	m_{cat} [mg]	w_{IL} [wt%]	X [%]	S_{CAL} [%]	S_{DHC} [%]	S_{OP} [%]	Ref.
1	—	0.2	—	79 ^a	45 ^b	19 ^b	36 ^b	33
2	[BMIM][NTf ₂]	0.24	17	74 ^a	59 ^b	15 ^b	26 ^b	38
3	[BMIM][PF ₆]	0.24	17	63 ^a	59 ^b	10 ^b	31 ^b	38
4	[BMPL][NTf ₂]	0.24	17	75 ^a	62 ^b	14 ^b	24 ^b	30,38
5	[BMIM][DCA]	0.28	10	100	81	11	8	this work
6	[B3MPYR][DCA]	0.27	7	100	82	10	8	this work
7	[B3MPYR][DCA]	0.35	29	99	98	1	1	this work
8	[BMPL][DCA]	0.28	10	100	90	3	7	this work
9	[BMPL][DCA]	0.33	24	100	99	—	1	this work

^a final citral conversion after $t_{\text{R}} = 4$ h, ^b selectivities for final conversion.

Table 5 Reaction rate constants and reaction rates under first-order kinetics of Pd/PANI catalysed citral hydrogenation with or without [BMIM][DCA] as additive

Entry	Catalyst	IL	k [min ⁻¹] ^a	r_0 [mmol L ⁻¹ s ⁻¹] ^b	r^2
1	Pd/PANI	—	0.05619 ± 0.00324	10.4 ± 0.06	0.994
2	Pd/PANI	[BMIM]-[DCA]	0.02293 ± 0.00038	0.43 ± 0.07	0.999

^a $c = c_0 \exp(-kt_{\text{R}})$, ^b $r_0 = kc_0$.

of citronellal to dihydrocitronellal took place and the product composition remained stable for two hours. The consumption of citral followed first-order kinetics, which was determined by an exponential curve fit (Table 5), whereas on Pd/PANI the initial reaction rate r_0 was higher (1.04 mmol L⁻¹ s⁻¹) than for the respective [BMIM][DCA] coated Pd/PANI catalyst (0.43 mmol L⁻¹ s⁻¹).

Despite the higher intrinsic selectivity for that catalyst, which may be attributed to another preparation route, IL treatment leads again to a selectivity enhancement showing that this concept is independent of the palladium catalyst source. As determined by nitrogen physisorption, the BET surface area of PANI (37 m²/g) is lower than for the applied SiO₂ (344 m²/g), not affecting the selectivity pattern. Moreover, these experiments show that the concept is also suitable for unconventional support materials like polyaniline.

3.3. Citral hydrogenation with ionic liquids as catalyst coating

3.3.1. Variation of fluoros anions based ionic liquids. Several ionic liquids based on fluoros containing anions were deposited with a loading of 17% on a Pd/SiO₂ catalyst to determine its influence on selectivity and activity in the hydrogenation of citral (Table 6, entries 1–4). For comparison, an experiment with IL-free Pd/SiO₂ was performed, and throughout the reactions the molar Pd/citral ratio was held constant, so a higher mass of ionic liquid coated catalyst was introduced.

Except for the [BMIM][PF₆] coated catalyst, the citral conversion level for coatings of [BMIM][NTf₂] and [BMPL][NTf₂], respectively, were in the same order as for the IL-free catalyst.³⁸ The lower hydrogen solubility in ionic liquids compared to organic solvents³⁹ does not affect the conversion level, indicating no mass transport limitation. The final citronellal selectivity

after 4 h reaction time was increased for all IL coated catalysts compared to the IL-free reaction ($S = 45\%$), whereby [BMPL][NTf₂] showed the best performance ($S = 62\%$).

Minimum amounts of fluoride present in [BMIM][PF₆] may also decrease the conversion level. It is known that citral hydrogenation is sensitive towards halides as contaminants, which was shown for chloride contamination by Hardacre *et al.*²⁵ The higher average pore diameter of [BMIM][PF₆] coated Pd/SiO₂ determined by N₂ physisorption (167 nm instead of 114 nm for Pd/SiO₂) could be interpreted by partially etching of silica by the fluoride possibly forming SiF₄.

In contrast to the dicyanamide based ionic liquids, the selectivity towards citronellal was enhanced to a lesser extent.

3.3.2. Dicyanamide containing ionic liquids. By applying dicyanamide based ionic liquids as catalyst coating, citral conversion and citronellal selectivity could be improved independent of which cation (either [BMIM]⁺, [BMPL]⁺ or [B3MPYR]⁺) was used (Table 6, entries 5–9). Moreover, nearly quantitative citronellal yield was obtained if the catalyst was loaded with 29wt% [B3MPYR][DCA]. In comparison to previous findings, the citronellal selectivity is moderately lowered due to a decreased amount of ionic liquid. With decreased IL loading, the citronellal selectivity at 80% conversion was diminished either with [BMIM][DCA] ($S = 81\%$) or [B3MPYR][DCA] ($S = 82\%$) as catalyst coating (entries 5 and 6); dihydrocitronellal was then observed as the consecutive product ($S \sim 10\%$).

In comparison with [BMIM][DCA] and [B3MPYR][DCA] at equal IL loading, experiments with 10wt% [BMPL][DCA] gave the highest selectivity towards citronellal, supporting the findings with [NTf₂]-based ILs, whereas the [BMPL]-cation showed increased selectivities compared to the [BMIM]-cation. Quantitative citronellal yield was obtained with a 24wt% [BMPL][DCA] coated catalyst (entry 9).

The latter supports the findings with [BMIM][DCA] as catalyst additive,³⁰ where an increasing amount of IL leads to increased citronellal selectivities. Obviously, it is necessary to introduce a threshold amount of DCA-IL to perform the reaction at full citronellal selectivity, facilitating a full coverage of the active sites with DCA-containing ionic liquid.

The results show that generally dicyanamide based ILs are able to act as a modifier in the citral hydrogenation with a selectivity enhancement towards citronellal. So the electronic and chemical structure of the anion plays a crucial role, affecting the mechanism of hydrogenation which may also be concluded by IR spectroscopy, whereas the blue shift ($\sim 15\text{ cm}^{-1}$) of the nitrile vibrations indicates a partial formation of DCA complexed palladium species.

Furthermore, the DCA based ionic liquids may also modify the adsorption, reaction and mass transport processes, as is known for the liquid phase hydrogenation of benzene, where suspending of the supported ruthenium catalyst in water leads to a selectivity enhancement towards the preferred cyclohexene by lowering the desorption of cyclohexene from the catalyst surface.⁴⁰ In our study, extraction experiments with ILs and solutions of citral and citronellal were performed at room temperature in order to determine the concentration of citral and citronellal in the ionic liquid. The product mixture of the organic phase was analyzed by GC and a “conversion” level

was determined under the assumption that the GC standard *n*-tetradecane is insoluble in ionic liquids. As a general trend, the solubility of citronellal in dicyanamide based ionic liquids was lower than for citral. In comparison to [BMIM][NTf₂], dicyanamide based ionic liquids gave lower solubilities indicating better desorption of citronellal from the ionic liquid layer into the organic phase.

To understand in detail the interaction of DCA based ionic liquids with active metal palladium and the reactants citral and hydrogen, respectively, further examinations are in progress.

4. Conclusion

Dicyanamide containing ionic liquids, independent of the cation, act very well as selectivity modifiers for the heterogeneously catalysed citral hydrogenation on Pd supported catalysts. Regardless of the nature and origin of the prepared Pd catalysts, excellent selectivities towards citronellal were observed by using these ILs as catalyst additive or coating, whereby consecutive and side reactions are strongly inhibited. This concept offers a greener opportunity to a solvent-less hydrogenation of citral, as experiments on neat citral at high citronellal selectivity in considerable space-time-yield have shown.

Acknowledgements

The authors want to thank Dipl.-Ing. K. Lehnert, Dipl.-Ing. F. Klasovsky and Dipl.-Ing. A. Pachulski for catalyst characterization, and Dipl.-Ing. N. Wörz for catalyst preparation. P. C. thanks the *Fonds der Chemischen Industrie* for financial support.

References

- 1 P. Claus and Y. Önal, Regioselective Hydrogenations, in *Handbook of Heterogeneous Catalysis*, ed. G. Ertl, H. Knözinger, F. Schüth and J. Weitkamp, 2nd Edition, Wiley-VCH, Weinheim, 2008, pp. 3308–3329.
- 2 P. Claus, *Top. Catal.*, 1998, **5**, 51–62.
- 3 P. Claus, *Appl. Catal. A General*, 2005, **291**, 222–229.
- 4 P. Gallezot and D. Richard, *Catal. Rev. Sci. Eng.*, 1998, **40**, 81–126.
- 5 D. Murzin, *Appl. Catal. A General*, 2005, **292**, 1–49.
- 6 M. A. Aramendia, V. Borau, C. Jimenez, J. M. Marinas, A. Porras and F. J. Urbano, *J. Catal.*, 1997, **172**, 46–54.
- 7 V. Satagopan and S. B. Chandalia, *J. Chem. Tech. Biotechnol.*, 1994, **59**, 257–263.
- 8 G. Neri, L. Mercadante, A. Donato, A. M. Visco and S. Galvagno, *Catal. Lett.*, 1994, **29**, 379–386.
- 9 U. K. Singh and M. A. Vannice, *J. Catal.*, 2001, **199**, 73–84.
- 10 S. Mukherjee and M. A. Vannice, *J. Catal.*, 2006, **243**, 108–130.
- 11 C. Milone, M. L. Tropeano, G. Gulino, G. Neri, R. Ingoglia and S. Galvagno, *Chem. Commun.*, 2002, 868–869.
- 12 M. Lucas and P. Claus, *Chem. Ing. Tech.*, 2001, **73**, 252–257.
- 13 M. Steffan, M. Lucas, A. Brandner, M. Wollny, N. Oldenburg and P. Claus, *Chem. Eng. Technol.*, 2007, **30**, 481–486.
- 14 M. Steffan, F. Klasovsky, J. Arras, C. Roth, J. Radnik, H. Hofmeister and P. Claus, *Adv. Synth. Catal.*, 2008, **350**, 1337–1348.
- 15 F. Klasovsky, M. Steffan, J. Arras, J. Radnik and P. Claus, *Open Phys. Chem. J.*, 2007, **1**, 1–4.
- 16 H. G. Göbbel, G. Wegner, H. Fuchs, S. Unverricht, and A. Salden, WO2004007414A1, 2004.
- 17 F. J. Bröcker, G. Kaibel, W. Aquila, H. Fuchs, G. Wegner, and M. Stroezel, EP0947493B1, 1999.
- 18 V. I. Parvulescu and C. Hardacre, *Chem. Rev.*, 2007, **107**, 2615–2665.
- 19 C. C. Cassol, A. P. Umpierre, G. Machado, S. I. Wolke and J. Dupont, *J. Am. Chem. Soc.*, 2005, **127**, 3298–3299.
- 20 A. Riisager, P. Wasserscheid, R. van Hal and R. Fehrmann, *J. Catal.*, 2003, **219**, 452–455.

- 21 C. P. Mehnert, E. J. Mozeleski and R. A. Cook, *Chem. Commun.*, 2002, 3010–3011.
- 22 M. Haumann and A. Riisager, *Chem. Rev.*, 2008, **108**, 1474–1497.
- 23 A. Riisager, B. Jorgensen, P. Wasserscheid and R. Fehrmann, *Chem. Commun.*, 2006, 994–996.
- 24 U. Kernchen, B. Etzold, W. Korth and A. Jess, *Chem. Eng. Technol.*, 2007, **30**, 985–994.
- 25 K. Anderson, P. Goodrich, C. Hardacre and D. W. Rooney, *Green Chem.*, 2003, **5**, 448–453.
- 26 J. L. Anthony, E. J. Maginn and J. F. Brennecke, *J. Phys. Chem. B*, 2002, **106**, 7315–7320.
- 27 P. J. Dyson, G. Laurency, C. A. Ohlin, J. Vallance and T. Welton, *Chem. Commun.*, 2003, 2418–2419.
- 28 J. P. Mikkola, P. Virtanen, H. Karhu, T. Salmi and D. Y. Murzin, *Green Chem.*, 2006, **8**, 197–205.
- 29 J. P. Mikkola, P. P. Virtanen, K. Kordas, H. Karhu and T. O. Salmi, *Appl. Catal. A General*, 2007, **328**, 68–76.
- 30 J. Arras, M. Steffan, Y. Shayeghi and P. Claus, *Chem. Commun.*, 2008, 4058–4060.
- 31 S. Brunauer, P. H. Emmett and E. Teller, *J. Am. Chem. Soc.*, 1938, **60**, 309–319.
- 32 E. P. Barrett, L. G. Joyner and P. P. Halenda, *J. Am. Chem. Soc.*, 1951, **73**, 373–380.
- 33 G. Bergeret and P. Gallezot, in *Handbook of Heterogeneous Catalysis*, eds. G. Ertl, H. Knözinger, J. Weitkamp, (Eds.), 1st edition, Wiley-VCH, Weinheim, 1999, pp. 439–441.
- 34 C. A. Ohlin, P. J. Dyson and G. Laurency, *Chem. Commun.*, 2004, 1070–1071.
- 35 D. R. MacFarlane, J. Golding, S. Forsyth, M. Forsyth and G. B. Deacon, *Chem. Commun.*, 2001, 1430–1431.
- 36 H. Köhler, M. Jeschke and H. Wusterhausen, *Z. anorg. Allg. Chem.*, 1987, **549**, 199–203.
- 37 F. Delbecq and P. Sautet, *J. Catal.*, 1995, **152**, 217–236.
- 38 J. Arras, M. Steffan, and P. Claus, *1st SynTOP Smart Synthesis and Technologies for Organic Processes*, VDI-Berichte 2039, VDI-Verlag GmbH, Düsseldorf, 2008, pp. 109–114.
- 39 P. J. Dyson, G. Laurency, A. Ohlin, J. Vallance and T. Welton, *Chem. Commun.*, 2003, 2418–2419.
- 40 E. Dietzsch, PhD thesis, TU Chemnitz, 2004; and references therein.

Inhibition of methane formation in steam reforming reactions through modification of Ni catalyst and the reactants

Xun Hu^{a,b} and Gongxuan Lu^{*a}

Received 14th August 2008, Accepted 6th February 2009

First published as an Advance Article on the web 9th March 2009

DOI: 10.1039/b814009j

Methane, a greenhouse gas and a main by-product in steam reforming reaction, can greatly diminish hydrogen yield. Modifications of both the catalyst and reactants were performed in this study to suppress methane formation. Ni/Al₂O₃ catalysts modified with a series of promoters (Li, Na, K, Mg, Fe, Co, Zn, Zr, La, Ce) were evaluated in acetic acid reforming reaction. The addition of Co, Zr, La, or Ce to Ni/Al₂O₃ promoted the methanation reaction, and consequently promoted methane formation. Conversely, alkali metal modified samples effectively inhibited methane formation, especially the Ni–K/Al₂O₃ catalyst. Moreover, the addition of alkali metal remarkably increased the number of metallic Ni sites on the catalyst surface by promoting the reduction of Ni oxides, which enhanced the catalytic activity. In addition, the presence of K on alumina also promoted stability of the Ni catalyst through suppression of coke formation. Type of fuels reformed also affected methane formation. Methane selectivity was much higher in steam reforming of the neutral fuels (ethanol, 1-propanol) than in steam reforming of the acidic fuels (acetic acid, propanoic acid). Acidification of neutral alcohols with nitric acid remarkably suppressed methane formation, which was accomplished through the suppression of the methanation reaction. Besides, the addition of nitric acid to ethanol can help eliminate coke deposition in ethanol reforming reactions, since production of the main carbon precursor, ethylene, is suppressed to a significant extent in the presence of nitric acid.

Introduction

Hydrogen production is a hot topic in the energy area because of the potential applications of hydrogen in transportation and production of electricity with fuel cell systems.^{1,2} Hydrogen can be obtained from catalytic reforming of natural gas, light hydrocarbons, and naphtha, or gasification of coal to yield syngas followed by water–gas shift conversion.^{3–6} However, the use of hydrocarbons and coal for hydrogen production fails to provide a solution to deal with the huge amount of carbon dioxide emissions produced during steam reforming processes.^{7,8} On the other hand, the depletion of fossil fuel reserves in the near future will cause serious energy problems. Therefore, the development of technology which utilizes biomass energy resources to produce hydrogen attracts much attention, due to the renewable, available, and carbon-neutral features of biomass.^{9–11}

Biomass-derived bio-oils such as alcohols and organic acids are easily obtained and are recognized as appropriate fuels for hydrogen production.^{12–14} Nevertheless, a significant amount of methane is always generated in steam reforming of alcohols or organic acids at mild temperatures.^{15–18} Methane contributes

to global warming and competes with the hydrogen atom. Generation of 1 mol of methane will result in loss of 4 mol of hydrogen in steam reforming reactions. F. Marino *et al.* point out that methane production must be reduced as much as possible to enhance the utilization efficiency of the liquid fuels for hydrogen production.¹⁹ Although by-product methane can be reformed with steam at high temperature, for example, 800 °C, steam reforming of the oxygenated hydrocarbon at this high temperature always produces a significant amount of CO.²⁰ The high concentration of CO in the effluent gas can poison the Pt anodes of the proton exchange membrane fuel cells (PEMFC).²¹ The operation of steam reforming at mild temperatures may obtain a hydrogen-rich gas with low CO concentrations, and consequently may avoid the subsequent processes of water–gas shift or partial oxidation to remove CO. Based on the above considerations, we carried out inhibition of methane formation at mild temperatures, aiming to obtain a hydrogen-rich gas with low level CO and CH₄ concentrations at the same time.

Steam reforming reactions involve a complex reaction network. The side reactions such as homogeneous decomposition of the organics and methanation of carbon oxides may lead to methane formation.^{17,18} The main reaction pathway for methane formation depends on the active metal, the promoter, the support, or the fuels reformed. Therefore, modification of the catalyst by some appropriate additives may affect the reaction pathways for methane formation, which then inhibits methane production. In this study, the typical reforming catalyst Ni/Al₂O₃ modified with alkali metal (Li, Na, K), alkaline earth (Mg), transition metal (Fe, Co, Zn, Zr), or rare earth (La, Ce)

^aState Key Laboratory for Oxo Synthesis and Selective Oxidation, Lanzhou Institute of Chemical Physics, Chinese Academy of Sciences, Lanzhou, 730000, P. R. China. E-mail: gxlu@lzb.ac.cn; Fax: +86 931 4968178

^bGraduate School of Chinese Academy of Sciences, Beijing, 100039, P. R. China

were evaluated in acetic acid reforming reactions, to select which promoters could inhibit methane formation. The promoters selected were based on their ability to; neutralize acidic sites of the support (Li, Na, K, Mg, La),^{19,22} strong interaction with Ni species (Fe, Co, Zn, Zr),^{23,24} and high oxygen mobility and storage capacity (Ce).²⁵ In addition to the catalyst, modification of the fuels reformed may be another way of affecting methane generation. Steam reforming of the different type of fuels always results in distinct product distribution, which may be related to the special properties of a given fuel, for example, its acidity. The adsorption of acidic fuel on active sites may acidize the catalyst surface, which may further impose effects on the reaction intermediate and methane formation. Therefore, this study also made an effort to modify the fuel by controlling the pH of the reactants to control methane formation.

Experimental

Catalyst preparation

Ni/Al₂O₃ catalyst was prepared by an impregnation method using Ni(NO₃)₂ · 6 H₂O as a precursor. The nickel loading was 30 wt% to Al₂O₃. Before impregnation, the support γ-Al₂O₃ was stabilized in air at 600 °C for 6 h. After impregnation, the catalyst precursor was dried at room temperature for 24 h and at 110 °C for another 24 h. Finally, the precursor was calcined at 500 °C for 4 h. The Ni–M/Al₂O₃ (M = Li, Na, K, Mg, Fe, Co, Zn, Zr, La, or Ce) catalysts were prepared by a co-impregnation method using the mixed solution containing both Ni(NO₃)₂ and M(NO₃)_x. The drying and calcination procedures were the same as for Ni/Al₂O₃. The metal loading of the promoters was selected in order to achieve an M/Al atomic ratio of 0.1. A Ni–K/Al₂O₃ catalyst with other K loading was also prepared, which would be specially indicated.

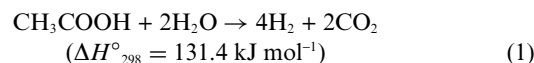
Catalytic measurements

The steam reforming reaction was carried out at atmospheric pressure in a fixed-bed continuous flow quartz reactor (i.d. 8 mm), consisting of a flow controller unit, a reactor unit, and an analysis unit. Heating of the reactor was provided by an electric furnace controlled by a programmable controller, which was connected *via* a thermocouple placed in the middle of the furnace. The temperature of the catalyst was measured by means of a K-type thermocouple placed within a quartz capillary well, running through the bed. Typically, 0.5 g catalyst diluted with an equal amount of quartz was used in each run. Prior to the experiment, the calcined catalyst was reduced *in situ* at 600 °C (heating rate 10 °C min⁻¹) for 3 h with a 50 vol% H₂/N₂ mixture (flow rate: 60 ml min⁻¹). The reaction mixture was fed into a pre-heater by a syringe pump with a liquid hourly space velocity (LHSV) of 12.1 h⁻¹ and a given steam to carbon ratio (S/C) that was determined according to different runs. The vaporized reaction mixture was then fed into the reactor using N₂ (40 ml min⁻¹) as the carrier gas. The separation and quantification of the products were attained on two on-line chromatographs equipped with a thermal-conductivity detector (TCD) and flame ionization detector (FID). For acetic acid reforming, acetic acid conversion (X_{HAC}) was calculated by dividing the total carbon in gaseous and liquid products with

carbon in the feed. Hydrogen selectivity was defined as the fraction of H₂ produced with respect to the theoretical full conversion of acetic acid to H₂ according to [Eqn (1)].

Selectivity to methane was defined by the formula: S_{CH_4} (%) = 100 × (mole of CH₄ generated)/(mole of the carbon-containing products). The method for calculating other carbon-containing product selectivities was similar to that of methane.

LHSV was defined as (volumetric flow rate of feed solution (cm³ h⁻¹))/(catalyst bed volume (cm³)), while S/C was defined by the formula: S/C = (mole of steam in feed)/(mole of carbon in feed).



Methanation reactions were carried out using two reactors. Acetic acid was firstly steam reformed at 650 °C over a Ni/Al₂O₃ catalyst in the first reactor to generate the reformat gas that contained mainly hydrogen and carbon oxides (the molar ratio between H₂, CO₂, and CO was 2 : 0.97 : 0.03), it was then introduced into the second reactor to measure the methanation activity of the catalysts. The methane yield in the methanation reaction was defined by the fraction of methane in the effluent gas of the second reactor.

Catalyst characterizations

Temperature-programmed reduction analysis (H₂-TPR) was carried out by heating a sample (50 mg) from 25 to 800 °C at 10 °C min⁻¹ in a flow of 5 vol% H₂/Ar mixture (40 ml min⁻¹). The amount of H₂ consumed was measured by a TCD.

X-ray diffraction spectra (XRD) measurements were performed on a Philips X'pert MPD instrument using Cu K α radiation in the scanning angle range of 10–80° at a scanning rate of 4° min⁻¹ at 40 mA and 50 kV.

X-ray photoelectron spectroscopy (XPS) measurements were performed on a VG ESCALAB 210 spectrometer with Mg K α radiation ($h\nu = 1253.6 \text{ eV}$). The binding energies were calibrated by the C_{1s} binding energy of 285.0 eV.

The specific surface area of the catalyst was measured by BET method on a Micromeritics ASAP 2010 apparatus at a liquid nitrogen temperature with N₂ as the absorbent at 77 K.

The amounts of carbon deposition on catalyst surface were analyzed by thermo-gravimetric analysis in a PerkinElmer TG/DTA apparatus. The catalyst was heated at 10 °C min⁻¹ under synthetic air flow and the mass loss was measured.

Results and discussion

The reaction pathways for methane formation in acetic acid reforming

Methane is a main by-product in acetic acid reforming. The occurrence and extent of the secondary reactions in the reforming process determine methane production. Firstly, methane may be a primary product that directly comes from the decomposition of acetic acid [Eqn. (2)], since acetic acid is thermally unstable, it may decompose before reaching or on the catalyst bed.²⁶ Secondly, methane may be a secondary product that comes from the methanation of carbon oxides [Eqn (3) and (4)].²⁷ These methanation reactions are highly favorable in steam reforming

processes, due to the high efficiency of the Ni catalyst for methanation of carbon oxides,^{28,29} and the high concentrations of hydrogen and carbon oxides in effluent gas. Thirdly, methane steam reforming [Eqn (5)], which acts as a factor for the elimination of methane, may occur during the acetic acid reforming process. Based on the above considerations, inhibition of acetic acid decomposition and methanation reaction as well as the promotion of methane steam reforming are regarded as possible ways of reducing methane formation.



Effects of the promoters on methane formation in acetic acid reforming

Acetic acid steam reforming was carried out over bare and modified Ni catalysts at mild temperature, 400 °C, with a LHSV of 12.1 h⁻¹ and an S/C of 7.5. Acetic acid conversion and the product distribution are summarized in Table 1, where the distinct effects of the promoters on catalytic activity and methane production are observed. Alkali metal modified samples presented a much lower methane selectivity than bare catalyst, especially the Ni-K/Al₂O₃. Methane selectivity decreased drastically from 14.7 to 1.4% with the addition of K to Ni/Al₂O₃, along with a sharp increase in hydrogen yield. Although methane production was also suppressed to some extent over Fe or Mg modified samples, these two promoters negatively affected catalytic activity. Conversely, both transition metal (Co, Zr) and rare earth (Ce, La) modified catalysts promoted the production of methane and consequently led to lower hydrogen yields. As regards Zn, its addition had a negligible effect on the production of methane.

The distinct effects of the promoters on methane formation originated from their different effects on the secondary reactions related to methane formation. The mechanisms for the inhibition effects of alkali metal on methane formation were firstly investigated using Ni/Al₂O₃ and Ni-K/Al₂O₃ as the model

Table 1 Acetic acid conversion and product distribution over bare and modified Ni catalysts: $T = 400$ °C; $S/C = 7.5$; $LHSV = 12.1$ h⁻¹; $P = 1$ atm

Catalysts	X_{HAC} (%)	Selectivity (%)					
		CH ₄	H ₂	CO ₂	CO	Acetone	Ketene
Ni/Al ₂ O ₃	67.8	14.7	66.2	68.9	2.3	3.3	2.1
Ni-Li/Al ₂ O ₃	77.6	8.3	81.2	78.4	2.1	2.8	1.4
Ni-Na/Al ₂ O ₃	93.8	4.0	89.6	90.7	1.7	1.2	—
Ni-K/Al ₂ O ₃	100	1.4	93.5	95.2	1.3	0.7	—
Ni-Mg/Al ₂ O ₃	47.8	12.3	57.6	61.2	4.6	5.1	3.3
Ni-Fe/Al ₂ O ₃	56.4	10.6	71.2	70.8	3.4	3.8	1.9
Ni-Co/Al ₂ O ₃	70.8	16.2	63.7	68.8	2.4	2.8	2.1
Ni-Zn/Al ₂ O ₃	66.9	14.4	68.8	69.1	2.5	3.0	2.5
Ni-Zr/Al ₂ O ₃	74.6	16.9	64.3	67.1	2.7	3.1	2.0
Ni-La/Al ₂ O ₃	76.9	16.7	65.4	70.1	2.1	2.5	1.8
Ni-Ce/Al ₂ O ₃	81.8	20.4	59.1	66.5	1.9	2.6	1.7

catalysts, since Ni-K/Al₂O₃ presents the most superior capacity for suppressing methane production. Methane reforming, acetic acid decomposition, and methanation reactions were conducted over Ni/Al₂O₃ and Ni-K/Al₂O₃ catalysts in sequence, due to the determination of these reactions to methane formation, as previously stated. The methane reforming reactions were conducted using the conditions: $S/C = 5$; $GHSV = 10000$ h⁻¹; $P = 1$ atm. The experimental results showed that both Ni/Al₂O₃ and Ni-K/Al₂O₃ catalysts presented negligible activity for methane reforming at 400 °C. Evidently, this result could not explain the low selectivity toward methane over Ni-K/Al₂O₃ catalyst. Acetic acid decomposition and methanation reactions were subsequently performed. For comparison, blank tests were also conducted. Methane yields at 400 °C in the reactions are depicted in Fig. 1. Acetic acid decomposition occurred homogeneously, as evidenced by the blank test. Nevertheless, in the presence of Ni/Al₂O₃ or Ni-K/Al₂O₃ catalysts, acetic acid decomposition occurred at a much higher efficiency. The catalytic activities of Ni/Al₂O₃ and Ni-K/Al₂O₃ catalysts for acetic acid decomposition were approximately comparable. That is, acetic acid decomposition was not the reaction that resulted in the low methane selectivity over Ni-K/Al₂O₃ catalyst. As for the methanation reaction, although both bare and K modified samples were active for methanation of carbon oxides, the Ni-K/Al₂O₃ catalyst presented a much lower methanation activity. Clearly, a direct relationship between the lower activity of Ni-K/Al₂O₃ in the methanation reaction and the lower methane selectivity in the steam reforming reaction could be found.

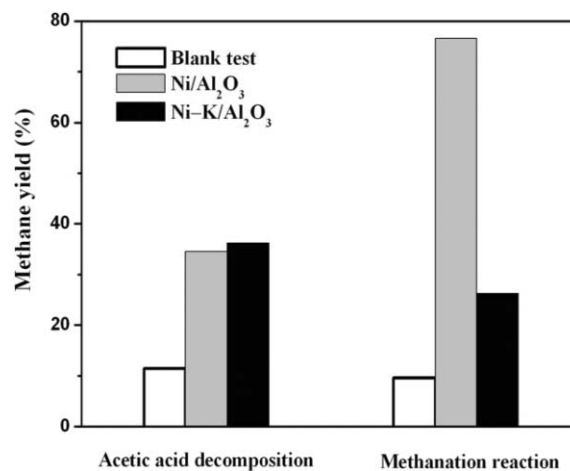


Fig. 1 Blank tests and catalytic acetic acid decomposition and methanation reactions over Ni/Al₂O₃ and Ni-K/Al₂O₃ catalysts. Acetic acid decomposition: $T = 400$ °C; $LHSV = 5.0$ h⁻¹; $P = 1$ atm. Methanation reaction: $T = 400$ °C; $n_{\text{H}_2} : n_{\text{CO}_2} : n_{\text{CO}} = 2 : 0.97 : 0.03$; $GHSV = 5000$ h⁻¹; $P = 1$ atm.

The basic characteristics of K and its electronic effect toward the metal phase favors adsorption of carbon oxides,³⁰ which in turn should favor methanation reactions. However, the addition of K to Ni/Al₂O₃ negatively affected methanation reactions. During the process of methanation, adsorbed CO₂ and H₂ reacted to form HCOOH (and/or HCOO⁻ ion) which then dehydrated to give CO *via* rapid equilibration, the CO intermediate then dissociated and hydrogenated forming the product CH₄, in which the CO dissociation step is rate-controlling.³¹ However,

CO dissociation was effectively inhibited in the presence of K species,³² which probably inhibited the reaction pathway for methane formation, leading to low methane selectivity in the steam reforming process.

Methanation and acetic acid decomposition reactions were also carried out for other modified catalysts at 400 °C. The methane yields from methanation reactions over the series of catalysts are depicted in Fig. 2. Comparing with the results presented in Table 1 and Fig. 2, we found that the methanation activities of the catalysts were in accordance with their methane selectivities in the reforming reactions. Generally, the higher the methanation activity in the methanation reaction, the higher the methane selectivity in the reforming process. Among the additives, Co, Zr, La, and Ce all promoted methanation and consequently led to higher methane selectivity. These additives are active for methanation and have been widely used as supports or promoters for methanation reactions.^{33–36} As regards acetic acid decomposition, the promoters all presented insignificant effects with the exception of Ce (results not shown). The addition of Ce to Ni/Al₂O₃ remarkably enhanced methane selectivity in acetic acid decomposition. Herein, we conclude that the promotion of Ce on both methanation and acetic acid decomposition reactions lead to the high methane selectivity over Ni–Ce/Al₂O₃ catalyst in acetic acid reforming.

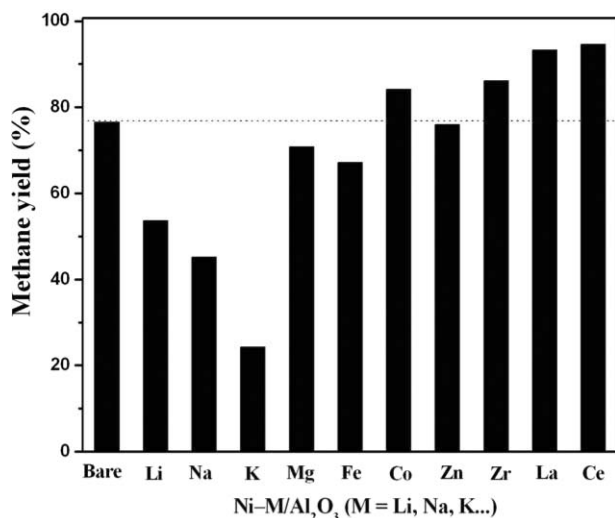


Fig. 2 Methanation activity of the bare and modified Ni catalysts: $T = 400\text{ }^{\circ}\text{C}$; $n_{\text{H}_2} : n_{\text{CO}_2} : n_{\text{CO}} = 2:0.97:0.03$; GHSV = 5000 h⁻¹; $P = 1\text{ atm}$.

Characterization of the alkali metal modified Ni/Al₂O₃ catalysts

Considering that the addition of alkali metal to Ni/Al₂O₃ catalyst can effectively suppress methane generation while promoting catalytic activity, alkali metal modified samples were further characterized. Results of H₂-TPR profiles for the bare and modified Ni/Al₂O₃ catalysts are presented in Fig. 3, where the significant effects of alkali metal on the reduction behavior of Ni species can be observed. The reduction profile of the bare Ni/Al₂O₃ catalyst was composed of a broad peak centred at 610 °C and a prolonged tail peak centred at temperatures as high as 780 °C, indicating the strong interaction of Ni species with alumina. For the Li modified sample, in addition to the two main reduction peaks in the high temperature region, a

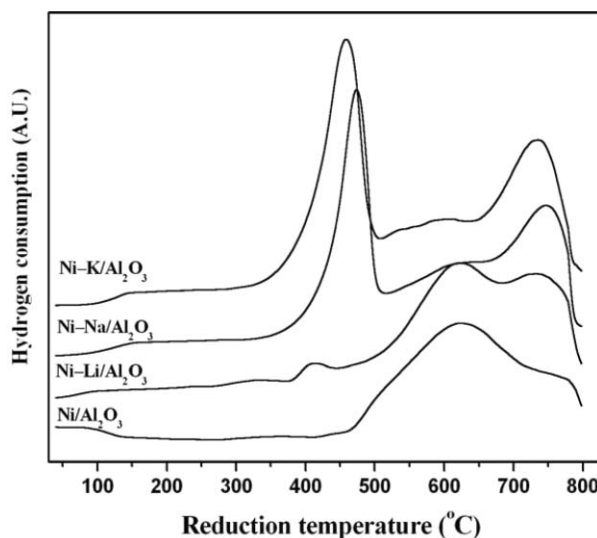


Fig. 3 H₂-TPR profiles for the bare and alkali metal modified Ni catalysts.

weak reduction peak at low temperature (*ca.* 400 °C) was observed. In Na or K modified samples, the reduction peak at *ca.* 400 °C became more remarkable, or rather, it became the main reduction peak. Evidently, the addition of Na or K to alumina significantly modified the distribution of Ni species on alumina and promoted the reduction of Ni oxides, especially the promoter K. The main reduction peak shifted downwards from 610 to 459 °C with the addition of K to Ni/Al₂O₃. In addition, the H₂-uptake for Na or K modified catalyst was much higher than that of bare catalyst. (The H₂-uptake ratio of Ni/Al₂O₃, Ni–Li/Al₂O₃, Ni–Na/Al₂O₃ and Ni–K/Al₂O₃ was 8 : 7.1 : 1.6 : 1). The alumina carrier was passivated and became less reactive toward metal oxides in the presence of alkali metals.³⁷ Therefore, more metallic Ni species appeared on the surface of the alkali metal modified samples after the reduction process.

The crystal structures of the reduced bare and modified Ni catalysts were checked using XRD techniques. Here, the reduced catalyst was the catalyst that was reduced in a hydrogen stream and then cooled to room temperature in a nitrogen stream. The diffraction patterns of the bare and modified samples were simple and comparable, as shown in Fig. 4. The peaks centred at 44.4, 51.8, and 76.3° are characteristic diffraction peaks of metallic Ni phase [JCPD 04–0850], while the peaks at 37.5, 45.9, and 66.9° are assigned to the diffraction of Al₂O₃ phase [JCPD 03–0914]. The diffractions of the alkali metal oxides are invisible, implying that they are highly dispersed on the alumina surface. The addition of alkali metal to Ni/Al₂O₃ affected the diffraction intensity of the Al₂O₃ phase. Compared with that of the bare sample, the diffraction of Al₂O₃ phase became stronger in Ni–Li/Al₂O₃ sample while it became weaker in both Ni–K/Al₂O₃ and Ni–Na/Al₂O₃ samples, indicating the different interaction of alkali metal with alumina carrier. The addition of alkali metal also affected the dispersion of metallic Ni. Ni particle sizes in the reduced catalysts were calculated by the Scherrer formula. It was found that Ni sizes in the bare and K modified samples were similar (19.7 and 18.7 nm) and a little smaller than those of the Li and Na modified samples (24.7 and 22.9 nm).

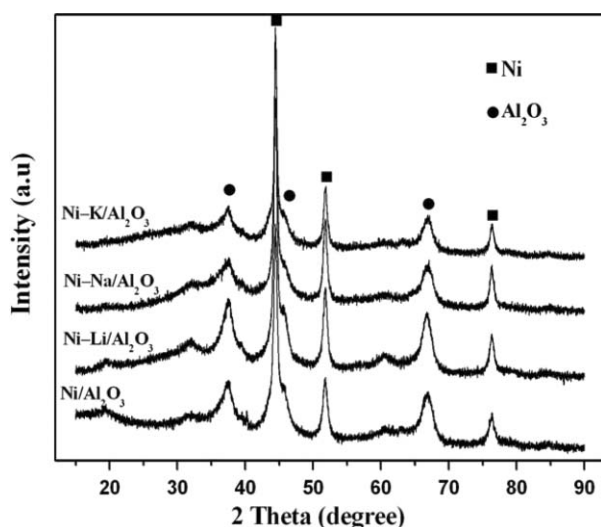


Fig. 4 XRD patterns for the bare and alkali metal modified Ni catalysts.

The XPS and BET results of reduced bare and modified samples were compiled in Table 2. The Ni $2p_{3/2}$ of the modified samples shifted to a lower region, which was induced by the electronic enrichment of metallic phase with the addition of alkali metal.³⁸ Furthermore, more metallic Ni species appeared on the surface of the modified samples (e.g. Ni-K/Al₂O₃), as is evident by the higher surface Ni/Al and Ni/O ratio. This result is in line with H₂-TPR results that show the presence of K on alumina promotes the reduction of Ni oxides. Furthermore, this result is also in accordance with the catalytic results shown in Table 1 *i.e.* that the catalytic activity of Ni-K/Al₂O₃ was the most superior. More metallic Ni species on the catalyst surface means more active sites for the reforming reaction, and higher catalytic activity is obtained. However, the BET results show that the alkali metal modified samples have relatively lower specific areas than those of the bare sample. It is probably caused by plugging some channel of the alumina carrier with the alkali metal.

Effects of K on catalytic performances of Ni catalyst

As presented above, K presents the most superior capacity for inhibiting methane formation while promoting the catalytic activity among the promoters investigated. Thus, the optimum of K loading on alumina as well as the effect of K on the catalytic stability, the coke formation, and the sintering of Ni species in the long-term experiments was further investigated. The effects of K loading on methanation and steam reforming reactions were studied first. Acetic acid conversion and methane selectivity in reforming reactions as well as the methane yields in methanation reactions were plotted as functions of K loading in Fig. 5. The addition of a small amount of K to Ni/Al₂O₃ was able to

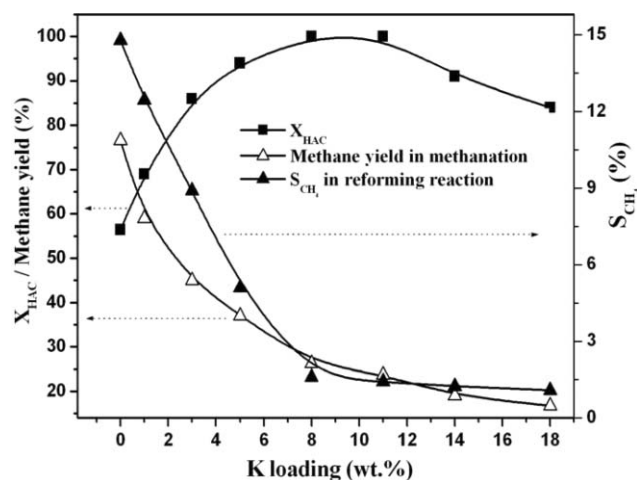


Fig. 5 Effects of K loading on catalytic activity, methane selectivity, and methanation activity of Ni-K/Al₂O₃ catalyst. Steam reforming: $T = 350\text{ }^{\circ}\text{C}$; $S/C = 7.5$; $LHSV = 12.1\text{ h}^{-1}$; $P = 1\text{ atm}$. Methanation: $T = 400\text{ }^{\circ}\text{C}$; $n_{\text{H}_2} : n_{\text{CO}_2} : n_{\text{CO}} = 2 : 0.97 : 0.03$; $GHSV = 5000\text{ h}^{-1}$; $P = 1\text{ atm}$.

remarkably improve the catalytic activity. Acetic acid conversion increased remarkably with the addition of only 3 wt% of K to alumina, and the complete conversion of acetic acid was attained with the increase of K loading to 8 wt%. Nevertheless, the further increase of K loading resulted in the loss of catalytic activity, as seen by the sharp decrease of acetic acid conversion. The reduced Ni-K/Al₂O₃ with 17 wt% of K was characterized by BET. The results showed that the specific area was only $34.3\text{ m}^2\text{ g}^{-1}$, which was much lower than that of the bare catalyst ($124.7\text{ m}^2\text{ g}^{-1}$). Evidently, too much K species on the catalyst surface blocked some pores and channels of alumina or occupied the active sites, lowering the catalytic activity. The methanation activity and methane selectivity of Ni catalyst *versus* K loading followed a similar trend. They decreased drastically with increased K loading to 8 wt%, and the further increase of K loading also led to their further decrease, but the decrease became insignificant. Taking the effects of K loading on both the catalytic activity and methane selectivity into consideration, the 8 wt% of K on alumina was regarded as the appropriate value that could maximize the catalytic activity and yet minimize the production of methane.

Stability tests were carried out under conditions that deliberately favored coke formation to assess the effect of K on carbon deposition. Steam reforming of acetic acid was performed over Ni/Al₂O₃ and Ni-K/Al₂O₃ (K loading: 8 wt%) catalysts at the low S/C of 1.5 and $600\text{ }^{\circ}\text{C}$ for 30 h, respectively. Acetic acid conversion and product distribution *versus* reaction time are depicted in Fig. 6. Ni/Al₂O₃ catalyst exhibited lower initial activity and deactivated quickly *versus* the prolonged time onstream. Furthermore, significant amounts of by-products (CO, CH₄,

Table 2 The results of XPS and BET for the bare and alkali metal modified Ni catalysts

Samples	Ni $2p_{3/2}$	M (1 s, $2p_{3/2}$)	Ni/Al	Ni/O	S_{BET} ($\text{m}^2\text{ g}^{-1}$)	V_{pore} ($\text{cm}^3\text{ g}^{-1}$)	d_{pore} (nm)
Ni/Al ₂ O ₃	852.6	—	0.121	0.0496	124.7	0.283	7.7
Ni-Li/Al ₂ O ₃	852.3	55.3	0.146	0.0549	79.7	0.206	9.3
Ni-Na/Al ₂ O ₃	852.0	1072.4	0.157	0.0564	91.6	0.238	8.9
Ni-K/Al ₂ O ₃	852.1	292.6	0.165	0.0577	96.4	0.241	8.2

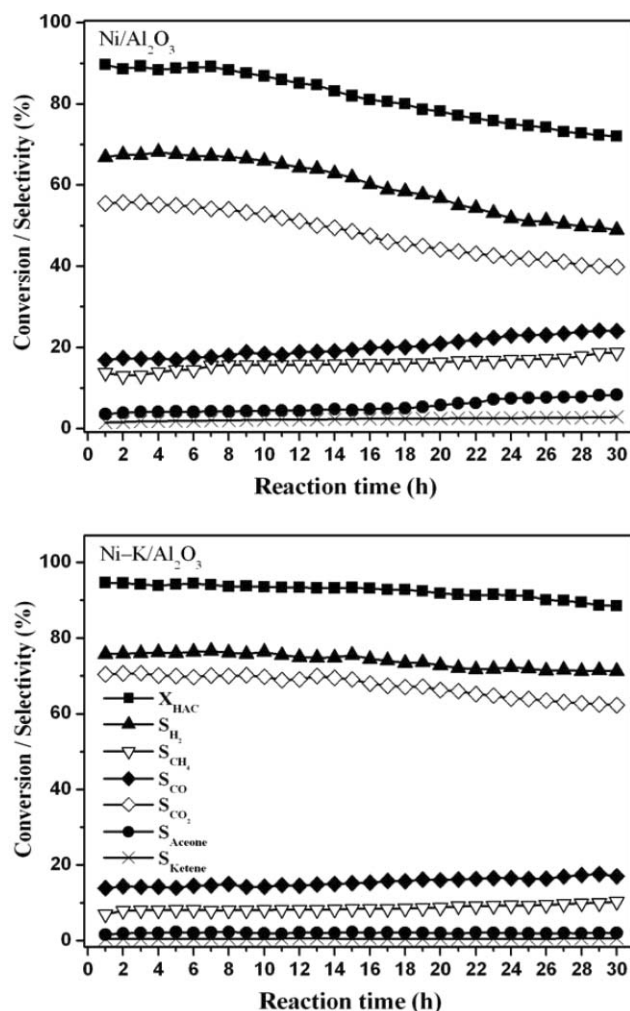


Fig. 6 Stability tests over Ni/Al₂O₃ and Ni-K/Al₂O₃ catalysts: $T = 600\text{ }^{\circ}\text{C}$; $S/C = 1.5$; $LHSV = 12.1\text{ h}^{-1}$; $P = 1\text{ atm}$.

acetone, ketene) were produced at the initial stage of the test and increased significantly at the end of the test, resulting in low hydrogen yield. Conversely, Ni-K/Al₂O₃ catalyst showed much more stable catalytic behavior. The amount of by-products were less and kept almost stable over the whole time investigated. The Ni/Al₂O₃ catalyst is subject to several deactivation mechanisms such as sintering and coking in steam reforming.³⁹ The addition of K to Ni/Al₂O₃ probably prevented the sintering of Ni species or promoted the gasification of coke deposit, as well as promoting the stability of the Ni/Al₂O₃ catalyst. We therefore characterized bare and K modified samples after stability testing using XRD and TG techniques. The XRD results for the two catalysts are shown in Fig. 7. The diffraction patterns became more complex when compared with those of freshly reduced samples. In addition to the diffraction of metallic Ni phase, strong diffraction of the graphitic carbon centred at 26.6, 43.2, and 45.6° was observed [JCPD 26-1079], indicating serious coke formation in stability tests. Although stability tests were performed at 600 °C for 30 h, no obvious sintering of Ni species occurred in the Ni-K/Al₂O₃ sample, as evidenced by the diffraction peak of metallic Ni at 44.4°. Furthermore, the addition of K to Ni/Al₂O₃ was favorable for the elimination of coke deposits. The coke formation rates over Ni/Al₂O₃ and

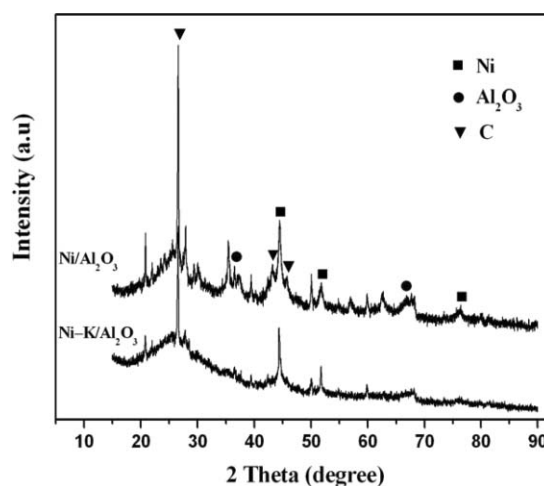


Fig. 7 XRD patterns for the Ni/Al₂O₃ and Ni-K/Al₂O₃ catalysts after the stability tests.

Ni-K/Al₂O₃ catalysts, which were calculated from TG results, in stability tests were 24.6 and 14.7 mgC g⁻¹Cat h⁻¹, respectively. This result was approximately in line with XRD results that diffraction of the graphitic carbon was much stronger in the Ni/Al₂O₃ than in the Ni-K/Al₂O₃ sample. It is commonly accepted that K is easy to leach from the solid catalyst. Thus, we also characterized the Ni-K/Al₂O₃ sample after the stability tests using XPS techniques, to check the loss of K species. The surface K/Al ratio was a little lower in the used sample (0.18) than in the freshly reduced sample (0.21), which indicated the loss of K species was not very significant under the experimental conditions employed.

Modification of the alcohols with acids to suppress methane formation

The type of fuel reformed is another factor that affects methane formation, since different fuels possess distinct properties that determine the reaction intermediate in the reforming process. Considering that both organic acid and alcohol are main components of bio-oil, in this study acetic acid, propanoic acid, ethanol, and 1-propanol were selected to investigate the effects of liquid fuel on methane production. Steam reforming of acetic acid [Eqn (1)], propanoic acid [Eqn (6)], ethanol [Eqn (7)], and 1-propanol [Eqn (8)] were carried out over Ni/Al₂O₃ catalyst in the temperature region of 300–500 °C with a LHSV of 12.1 h⁻¹ and an S/C of 6. For comparison, the methane selectivities *versus* reaction temperature were compiled in Fig. 8. The methane selectivity curves presented similar trends in steam reforming of the different fuels. The maximum amount of methane was obtained at middle temperatures whether in alcohol or acid reforming reactions, and further increases to reaction temperature resulted in the decrease of methane formation. Nevertheless, steam reforming of the organic acids (acetic acid, propanoic acid) gave remarkably lower methane selectivities than those of the alcohols (ethanol, 1-propanol). In reforming reactions, ethanol and 1-propanol solutions were neutral while acetic acid and propanoic acid solutions were acidic. Acidity of the fuels probably negatively affected methane formation. In order to prove the hypothesis, steam reforming of the neutral methanol

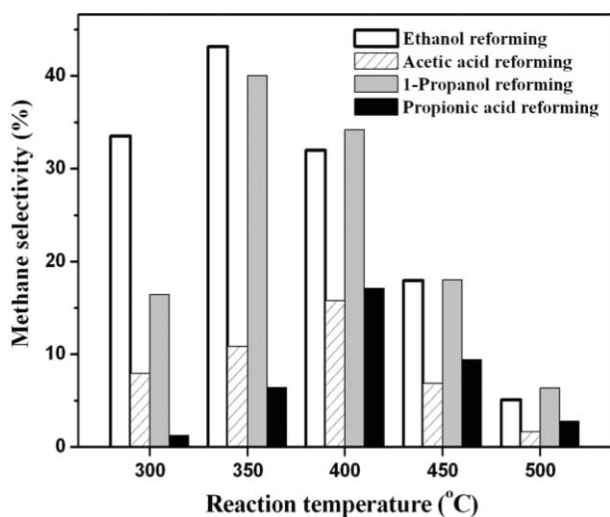
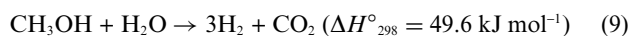
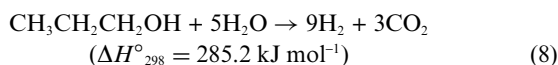
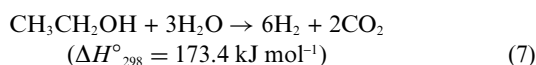
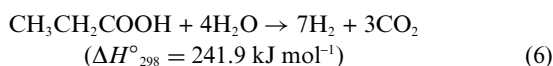


Fig. 8 Methane selectivity in steam reforming of ethanol, acetic acid, 1-propanol, and propionic acid: $S/C = 6$; $LHSV = 12.1 \text{ h}^{-1}$; $P = 1 \text{ atm}$.

[Eqn (9)] and ethanol, and acidic methanol and ethanol were performed over $\text{Ni}/\text{Al}_2\text{O}_3$ catalyst, respectively.



Herein, the acidic methanol and ethanol solutions were obtained by acidifying the reactants with inorganic acids (nitric acid, hydrochloric acid, sulfuric acid) to pH 1. Besides, acetic acid was also used to acidify the alcohol solutions, and the concentration of acetic acid in the solutions was 0.05 mol L^{-1} . Steam reforming of methanol and ethanol without any treatment, as well as acidified methanol and ethanol were carried out at $400 \text{ }^\circ\text{C}$ with a $LHSV$ of 12.1 h^{-1} and an S/C of 6, respectively. The catalytic results showed that acidification of the alcohol solutions mainly imposed effects on the production of methane, and therefore only the methane selectivities in the reforming reactions are summarized in Fig. 9. The different acids imposed distinct effects on methane generation in the reforming process. Acidification of the alcohol solutions with nitric acid remarkably suppressed methane formation and enhanced hydrogen yields whether in the methanol or ethanol reforming process. Furthermore, methane selectivity decreased further with the further increasing concentration of nitric acid in reactants. For example, at pH 0, methane selectivity in ethanol reforming was only 12.8%, which was much lower than that in neutral ethanol reforming (32.2%). In comparison, the effects of sulfuric acid and acetic acid on methane formation were negligible. Although the addition of hydrochloric acid to alcohols suppressed methane production to some extent, hydrochloric acid deactivated the $\text{Ni}/\text{Al}_2\text{O}_3$ catalyst quickly. The

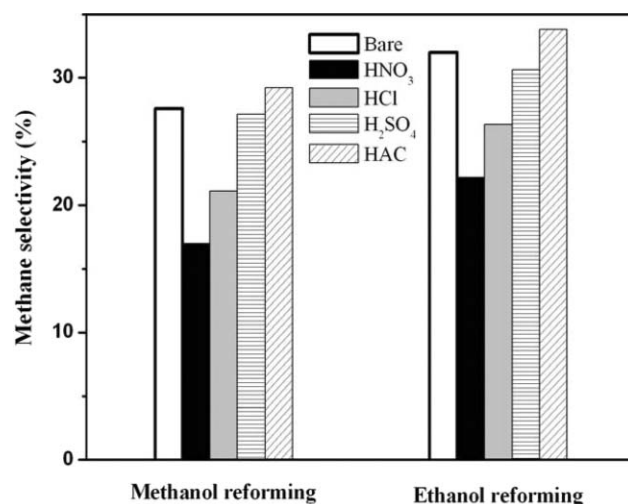


Fig. 9 Methane selectivity in steam reforming of neutral alcohols and alcohols modified with different acids: $T = 400 \text{ }^\circ\text{C}$; $S/C = 6$; $LHSV = 12.1 \text{ h}^{-1}$; $P = 1 \text{ atm}$.

Cl species in hydrochloric acid was probably adsorbed onto the active sites, poisoning the catalyst.⁴⁰

In the methanol reforming reaction, by-product methane comes mainly from the methanation reaction.⁴¹ Furthermore, in methanol decomposition, trace amounts of methane also come from the methanation of CO .⁴² Therefore, it is probable that acidification of methanol solution by nitric acid negatively affects the methanation reaction, resulting in lower methane selectivity. To verify this hypothesis, we further carried out methanation reactions in both the presence and absence of nitric acid to measure the effect of nitric acid on methanation. The experiments were performed using a gas mixture of H_2 and CO_2 (molar ratio: 3 : 1) as reactants. The introduction of nitric acid into the reactor was achieved by bubbling concentrated nitric acid into the gas mixture ($T = 20 \text{ }^\circ\text{C}$, flow rate: 80 ml min^{-1}). Composition of H_2 , CO_2 , and CH_4 in the outlet of the reactor was summarized in Fig. 10. It is very interesting that nitric acid negatively affected the methanation reaction to a significant

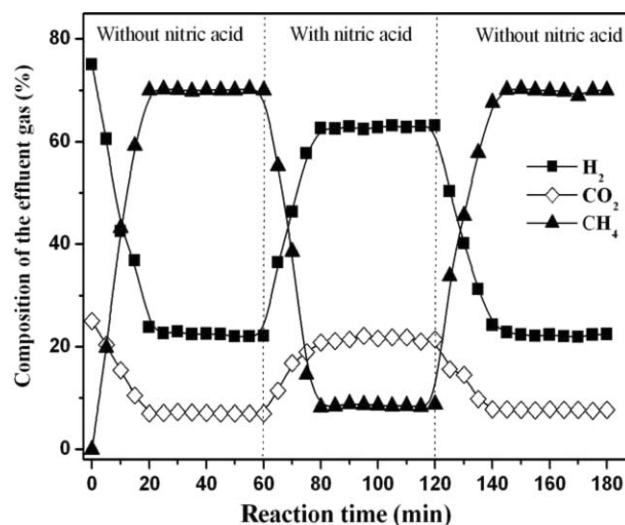


Fig. 10 Effects of nitric acid on the methanation activity of $\text{Ni}/\text{Al}_2\text{O}_3$ catalyst: $T = 400 \text{ }^\circ\text{C}$; $n_{\text{H}_2} : n_{\text{CO}_2} = 3 : 1$; $GHSV = 9600 \text{ h}^{-1}$; $P = 1 \text{ atm}$.

extent. Methane production was decreased drastically in the presence of nitric acid, while in the absence of nitric acid, methane production was restored. Nitric acid will decompose to nitrogen oxides, oxygen, and water at elevated temperatures.^{43,44} The nitric oxides may adsorb onto the metal sites, resulting in low methanation activity, or the oxygen may react with the precursor of methane, also resulting in low methane selectivity. After the methanation test, the Ni/Al₂O₃ catalyst was also characterized using XPS techniques. The results indicated that introducing nitric acid onto the catalyst surface did not lead to oxidation of metal Ni or a decrease in metallic Ni sites.

In addition to methane, nitric acid may further affect the stability of the Ni/Al₂O₃ catalyst, this was further investigated by ethanol steam reforming. Steam reforming of neutral ethanol and acidic ethanol (pH 1) were performed over a Ni/Al₂O₃ catalyst at S/C = 1.5 and 600 °C for 30 h, respectively. Ethanol conversion and product distribution *versus* reaction time are depicted in Fig. 11. The addition of nitric acid did not affect ethanol conversion at the initial stage of the experiments. Nevertheless, nitric acid affected product distribution, especially at the end of the tests. Steam reforming of neutral ethanol produced a significant amount of ethylene after 9 h onstream, while the amount of ethylene was negligible in steam reforming of acidic ethanol and increased only slightly *versus* the prolonged

reaction time. Ethylene, which is a main carbon precursor in ethanol reforming, was easily polymerized, forming polymeric coke.⁴⁵ TG results for the Ni/Al₂O₃ catalyst after the stability tests also showed that the coke formation rate was much lower in steam reforming of acidic ethanol (18.3 mgC g⁻¹Cat h⁻¹) than in steam reforming of neutral ethanol (37.4 mgC g⁻¹Cat h⁻¹).

Conclusions

Methane is one of the main by-products in steam reforming reactions. The modification of a Ni/Al₂O₃ catalyst with alkali metal can effectively reduce methane formation through inhibition of methanation reactions. The inhibition effect of K on methane formation was the most superior among the promoters investigated. Addition of a small amount of K (3 wt%) could remarkably suppress methane production and improve Ni catalyst activity, while 8 wt% of K on alumina could minimize the production of methane, and still maximize catalytic activity. Besides, the addition of K to a Ni/Al₂O₃ catalyst remarkably enhanced the stability of the Ni catalyst, due to the promotion of K on the gasification of coke deposit. Hence, a Ni-K/Al₂O₃ catalyst could be a promising reforming catalyst for producing hydrogen-rich gas with a low concentration of methane at mild temperatures.

Modification of the fuels reformed with acid is another way to suppress methane formation. The addition of nitric acid to alcohols (methanol, ethanol) remarkably suppressed methane formation, and the higher the concentration of nitric acid in alcohols, the lower the amount of methane in the reformat gas. In addition to methane, the addition of nitric acid also significantly suppressed the production of ethylene, a main carbon precursor in ethanol reforming. In summary, both modification of Ni catalyst by K species and acidification of alcohols with nitric acid can effectively eliminate methane formation and reduce coke deposition, which are important for enhancing the utilization efficiency of bio-oil derived compounds for hydrogen production.

Acknowledgements

We acknowledge the financial support of the 973 Project of China (No. G 2003CB214503, 2007CB613305 and 2009CB220003).

References

- H. Song, L. Zhang and U. S. Ozkan, *Green Chem.*, 2007, **9**, 686–694.
- V. Fierro, O. Akdim and C. Mirodatos, *Green Chem.*, 2003, **5**, 20–24.
- V. A. Goltsov, T. N. Veziroglu and L. F. Goltsova, *Int. J. Hydrogen Energy*, 2006, **31**, 153–159.
- Z. Wang, Y. Zhao, L. Cui, H. Du, P. Yao and C. Liu, *Green Chem.*, 2007, **9**, 554–559.
- D. A. Slade, A. M. Duncan, K. J. Nordheden and S. M. Stagg-Williams, *Green Chem.*, 2007, **9**, 577–581.
- A. Berman, R. K. Karn and M. Epstein, *Green Chem.*, 2007, **9**, 626–631.
- E. Ochoa-Fernandez, G. Haugen, T. Zhao, M. Ronning, I. Aartun, B. Borresen, E. Rytter, M. Ronnekleiv and D. Chen, *Green Chem.*, 2007, **9**, 654–662.
- M. Marquovich, G. W. Sonnemann, F. Castells and D. Montane, *Green Chem.*, 2002, **4**, 414–423.
- J. Rass-Hansen, C. H. Christensen, J. Sehested, S. Helveg, J. R. Rostrup-Nielsen and S. Dahl, *Green Chem.*, 2007, **9**, 1016–1021.

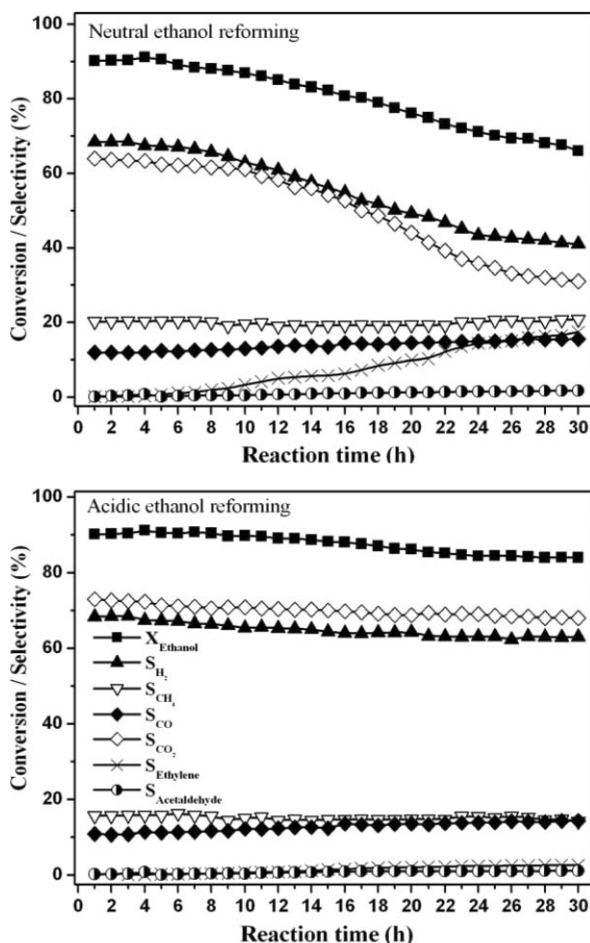


Fig. 11 Stability tests of neutral ethanol and nitric acid modified ethanol reforming over Ni/Al₂O₃ catalyst: $T = 600\text{ }^{\circ}\text{C}$; $S/C = 1.5$; $LHSV = 12.1\text{ h}^{-1}$; $P = 1\text{ atm}$.

- 10 K. Tomishige, T. Miyazawa, M. Asadullah, S. Ito and K. Kunimori, *Green Chem.*, 2003, **5**, 399–403.
- 11 J. L. Colby, P. J. Dauenhauer and L. D. Schmidt, *Green Chem.*, 2008, **10**, 773–783.
- 12 F. W. Bai, W. A. Anderson and M. Moo-Young, *Biotechnol. Adv.*, 2008, **26**, 89–105.
- 13 X. Hu and G. Lu, *Chem. Lett.*, 2006, **35**, 452–453.
- 14 N. Himeshima and Y. Amao, *Green Chem.*, 2005, **7**, 742–746.
- 15 A. Birot, F. Epron, C. Descorme and D. Duprez, *Appl. Catal. B: Environ.*, 2008, **79**, 17–25.
- 16 X. Hu and G. Lu, *Chem. Lett.*, 2008, **37**, 614–615.
- 17 A. C. Basagiannis and X. E. Verykios, *Int. J. Hydrogen Energy*, 2007, **32**, 3343–3355.
- 18 X. Hu and G. Lu, *J. Mol. Catal. A: Chem.*, 2007, **261**, 43–48.
- 19 F. Marino, M. Boveri, G. Baronetti and M. Laborde, *Int. J. Hydrogen Energy*, 2001, **26**, 665–668.
- 20 G. Rabenstein and V. Hacker, *J. Power Sources*, 2008, **185**, 1293–1304.
- 21 R. A. Dagle, Y. Wang, G. Xia, J. J. Stroh, J. Holladay and D. R. Palo, *Appl. Catal. A: Gen.*, 2007, **326**, 213–218.
- 22 H. Vidal, S. Bernal, R. Baker, G. Cifredo, D. Finol and J. Rodriguez-Izquierdo, *Appl. Catal. A: Gen.*, 2001, **208**, 111–123.
- 23 J. A. Torres, J. Llorca, A. Casanovas, M. Dominguez, J. Salvado and D. Montane, *J. Power Sources*, 2007, **169**, 158–166.
- 24 M. Yamasaki, H. Habazaki, K. Asami, K. Izumiya and K. Hashimoto, *Catal. Commun.*, 2006, **7**, 24–28.
- 25 S. Imamura, M. Shono, N. Okamoto, A. Hamada and S. Ishida, *Appl. Catal. A: Gen.*, 1996, **142**, 279–288.
- 26 J. C. Mackie and K. R. Doolan, *Int. J. Chem. Kinet.*, 1984, **16**, 525–541.
- 27 A. N. Fatsikostas, D. I. Kondarides and X. E. Verykios, *Catal. Today*, 2002, **75**, 145–155.
- 28 I. Czekaj, F. Loviat, F. Raimondi, J. Wambach, S. Biollaz and A. Wokaun, *Appl. Catal. A: Gen.*, 2007, **329**, 68–78.
- 29 C. W. Hu, J. Yao, H. Q. Yang, Y. Chen and A. M. Tian, *J. Catal.*, 1997, **166**, 1–7.
- 30 C. Qi, J. C. Amphlett and B. A. Peppley, *J. Power Sources*, 2007, **171**, 842–849.
- 31 M. R. Prairie, A. Renken, J. G. Highfield, K. R. Thampi and M. Gratzel, *J. Catal.*, 1991, **129**, 130–144.
- 32 F. Frusteri, F. Arena, G. Calogero, T. Torre and A. Parmaliana, *Catal. Commun.*, 2001, **2**, 49–56.
- 33 H. Habazaki, M. Yamasaki, B. Zhang, A. Kawashima, S. Kohno, T. Takai and K. Hashimoto, *Appl. Catal. A: Gen.*, 1998, **172**, 131–140.
- 34 M. Yamasaki, H. Habazaki, T. Yoshida, E. Akiyama, A. Kawashima, K. Asami, K. Hashimoto, M. Komori and K. Shimamura, *Appl. Catal. A: Gen.*, 1997, **163**, 187–197.
- 35 H. Ando, M. Fujiwara, Y. Matsumura, H. Miyamura and Y. Souma, *Energy Convers. Manage.*, 1995, **36**, 653–656.
- 36 A. Trovarelli, C. Deleitenburg, G. Dolcetti and J. L. Lorca, *J. Catal.*, 1995, **151**, 111–124.
- 37 J. Sehested, J. A. P. Gelten and S. Helveg, *Appl. Catal. A: Gen.*, 2006, **309**, 237–246.
- 38 Y. Yazawa, H. Yoshida, S. Komai and T. Hattori, *Appl. Catal. A: Gen.*, 2002, **233**, 113–124.
- 39 J. Sehested, *J. Catal.*, 2003, **217**, 417–426.
- 40 T. E. McMinn, F. C. Moates and J. T. Richardson, *Appl. Catal. B: Environ.*, 2001, **31**, 93–105.
- 41 C. Qi, J. C. Amphlett and B. A. Peppley, *Appl. Catal. A: Gen.*, 2006, **302**, 237–243.
- 42 D. H. Chun, Y. Xu, M. Demura, K. Kishida, D. M. Wee and T. Hirano, *J. Catal.*, 2006, **243**, 99–107.
- 43 J. N. Crowley, J. P. Burrows, G. K. Moortgat, G. Poulet and G. L. Bras, *Int. J. Chem. Kinet.*, 1993, **25**, 795–803.
- 44 W. Choi and M. Leu, *J. Phys. Chem. A*, 1998, **102**, 7618–7630.
- 45 M. Ni, D. Y. C. Leung and M. K. H. Leung, *Int. J. Hydrogen Energy*, 2007, **32**, 3238–3247.

Remarkable influence of substituent in ionic liquid in control of reaction: simple, efficient and hazardous organic solvent free procedure for the synthesis of 2-aryl benzimidazoles promoted by ionic liquid, [pmim]BF₄†

Debasree Saha, Amit Saha and Brindaban C. Ranu*

Received 5th January 2009, Accepted 11th February 2009

First published as an Advance Article on the web 4th March 2009

DOI: 10.1039/b823543k

A simple and efficient procedure for the synthesis of 2-substituted benzimidazoles has been developed by a one-pot reaction of *o*-phenylenediamine with aromatic aldehydes in the presence of an ionic liquid, 1-methyl-3-pentylimidazolium tetrafluoroborate, [pmim]BF₄ at room temperature in open air without any organic solvent. The ionic liquid is recycled. A remarkable influence of the substituent on the imidazolium unit of the ionic liquid on the outcome of the reaction is observed.

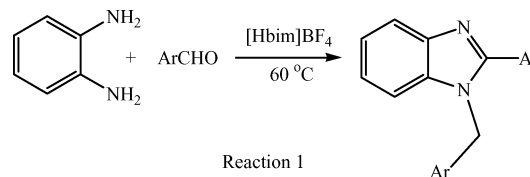
1 Introduction

The benzimidazoles have received considerable attention in recent times because of their applications as antiulcers, antihypertensives, antivirals, antifungals, anticancers and antihistamines among others.¹ In addition, they are important intermediates in many organic reactions² and act as ligands to transition metals for modeling biological systems.³ This has led to the development of several methods for the synthesis of benzimidazoles during the last few years. Two protocols are usually followed. One of them is the coupling of *o*-phenylenediamines with carboxylic acids or their derivatives⁴ and the second route involves condensation of *o*-phenylenediamine and aldehydes followed by oxidative cyclo-dehydrogenation.⁵ However, the second approach has become more popular probably because of the ease of accessibility of a variety of substituted aldehydes. The reported procedures for this protocol involved a wide spectrum of reagents including (bromodimethyl) sulfonium bromide/MeCN,^{6a} iodobenzene diacetate/1,4-dioxane,^{6b} H₂O₂/HCl in MeCN,^{6c} chlorotrimethylsilane/DMF,^{6d} I₂/KI/K₂CO₃/H₂O,^{6e} air/dioxane,^{6f} ytterbium triflate in neat,^{6g} *p*-TsOH/DMF,^{6h} Na₂S₂O₅ in neat under microwave irradiation,⁶ⁱ [(NH₄)H₂PW₁₂O₁₄] in dichloroethane,^{6j} H₂O₂/CAN,^{6k} [Hbim]BF₄,^{6l} proline,^{6m} *p*-TsOH/graphite,⁶ⁿ sodium hydrogen sulfite,^{6o} *p*-TsOH/silica gel^{6p} and ytterbium(III) perfluorooctanesulfonate.^{6q} Although these methods are quite satisfactory, many of them employed considerable amounts of hazardous organic solvents either for carrying out the reactions or for extraction and purifications (column chromatography) or for both, which are not environmentally friendly. Moreover, several of these reactions were carried out at higher temperatures and using costly reagents.

Department of Organic Chemistry, Indian Association for the Cultivation of Science, Jadavpur, Kolkata, 700 032, India. E-mail: oecbr@iacs.res.in

† Electronic supplementary information (ESI) available: Copies of ¹H NMR, ¹³C NMR and HRMS spectra of all the products listed in Table 2, copies of ¹H NMR spectra of ionic liquid, [pmim]BF₄ of the fresh and recovered (after reaction) samples and copies of ¹H NMR and HRMS spectra of compounds obtained as products listed in entries 8 and 10, Table 3. See DOI: 10.1039/b823543k

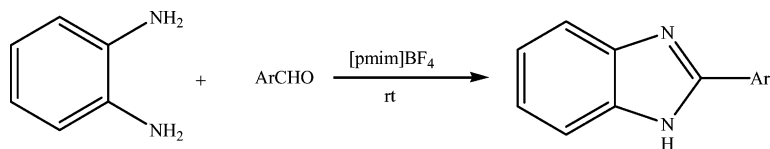
The use of large volumes of volatile hazardous organic solvents in industrial processes posed a serious threat to the environment. Thus, procedures involving alternative benign solvents in reaction, isolation and purification are of high priority in industry. The room temperature ionic liquids have been the subject of considerable interest in the context of green chemistry because of their relatively benign character, very low volatility, thermal stability, efficiency as a catalyst and promoter and reusability.⁷ As a part of our continued activities in this area,⁸ we became interested to investigate this condensation reaction using ionic liquid. From a literature search we found a recent report by Wang *et al.*^{6l} describing a reaction of *o*-phenylenediamine and aromatic aldehydes using an ionic liquid, [Hbim]BF₄ to produce 2-aryl-1-arylmethyl-benzimidazoles (Reaction 1). It was also reported that their efforts to synthesize 2-aryl benzimidazoles using this IL failed.^{6l}



Very interestingly, we discovered that a change of substituent, specifically a replacement of *N*-H by *N*-alkyl on the imidazolium unit of the ionic liquid, dramatically influences the course of the reaction. The same condensation of *o*-phenylenediamine and aromatic aldehydes when mediated by the ionic liquid, 1-methyl-3-pentylimidazolium tetrafluoroborate [pmim]BF₄ under organic solvent-free conditions produced exclusively 2-aryl benzimidazoles (Scheme 1) in contrast to 2-aryl-1-arylmethyl-benzimidazole as reported by Wang *et al.*^{6l} using [Hbim]BF₄ and the results are reported here.

2 Results and discussion

The experimental procedure is very simple. A mixture of *o*-phenylenediamine and an aromatic aldehyde was stirred at room temperature in air in the presence of an ionic liquid, [pmim]BF₄ for the required period of time (TLC). The solid



Scheme 1 Synthesis of 2-aryl benzimidazole.

Table 1 Standardisation of reaction conditions

Entry	IL	Temp./°C	Yield ^a (%)
1	[pmim]BF ₄	80	85
2	[pmim]BF ₄	25	92
3	[bmim]BF ₄	25	82
4	[pmim]Br	25	88

^a Yields refer to those of purified isolated products characterized by spectroscopic data (IR, ¹H NMR and ¹³C NMR).

product was isolated by filtration and purified by crystallization from ethanol. The ionic liquid, [pmim]BF₄ was found to give best results at room temperature (25 °C) in comparison to other imidazolium based ionic liquids such as [pmim]Br and [bmim]BF₄ as illustrated in Table 1.

The remaining ionic liquid, [pmim]BF₄ after isolation of product, was recycled for the first two subsequent reactions without any significant loss of efficiency, while the next two reactions showed some loss of efficiency in terms of yields of products (Fig. 1). To find out any change of the recovered ionic liquid from the fresh one the ¹H NMR of the two samples were checked. Both were found to be basically same except two additional spikes in the region of 2–4 ppm in the spectrum of the recovered one, probably due to contamination of trace impurities from the reaction.

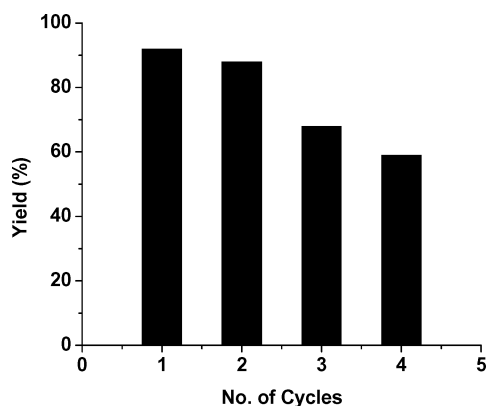


Fig. 1 Recyclability diagram for the reaction of *o*-phenylenediamine and *p*-tolualdehyde.

Several substituted aromatic aldehydes underwent condensations with *o*-phenylenediamine by this procedure to produce the corresponding 2-substituted benzimidazoles. The results were summarized in Table 2. The aldehydes with electron donating

Table 2 Synthesis of benzimidazoles

Entry	Ar	Time/h	Yield ^a (%)	Mp/°C (Lit M.P.)	Ref.
1		5	85	288 (289–291)	6b
2		6	88	242 (243–244)	9
3		6	90	264 (264–266)	6b
4		4	92	298 (299–300)	6b
5 ^b		4	92	290 (292–294)	6b
6		7	80	250 (250–251)	6b
7		5	90	207 (209)	10
8		4	94	328 (327)	10
9		6	88	224 (224–226)	6b
10 ^c		5	92	276–277 (277)	6e
11		6	80	270 (272–274)	11
12		7	82	261–263	
13		7	90	332 (330)	6e

^a Yields refer to those of purified isolated products characterized by spectroscopic data (IR, ¹H NMR and ¹³C NMR). ^b The reaction when performed in 10 mmol scale under identical reaction conditions, the corresponding product was formed in 88% yield. ^c The reaction when performed in 10 mmol scale under identical reaction conditions, the corresponding product was formed in 90% yield.

(entries 9 and 10, Table 2) as well as with electron withdrawing groups (entries 2–8, Table 2) participated in this reaction uniformly. Apparently, the nature and position of substitution on the aryl ring did not make much difference in reactivity

(entries 2, 3, 4 Table 2). The sensitive molecule like thiophen-2-aldehyde (entry 13, Table 2) produced the corresponding benzimidazole without any difficulty. The sterically hindered 9-anthraldehyde (entry 12, Table 2) also underwent reaction by this procedure. The reactions of sterically hindered aldehydes were not addressed by many of the existing methods. Significantly, when the reaction of 9-anthraldehyde and *o*-phenylenediamine was carried out using conventional reagents such as $I_2/KI/K_2CO_3/H_2O$,^{6c} $O_2/dioxane$ ^{6f} and H_2O_2/HCl ^{6e} no appreciable product was isolated by us.

The reactions, in general are high yielding. No hazardous organic solvent was used in this process. In several reactions, dialdimines were formed in small amounts (2–8%) which were separated during crystallization. Several functional groups such as Cl, Br, NO_2 , OMe and sensitive molecules like thiophene-2-carboxaldehyde are compatible with the reaction conditions. A comparison of results of reactions with a few substrates using ionic liquid, [pmim]BF₄ with those reported by Wang *et al.*^{6f} using [Hbim]BF₄ reveals that minor variations of substituents in core imidazolium ionic liquid and reaction conditions (room temperature from 60 °C) change the outcome of the reaction producing 2-aryl benzimidazole **I** by [pmim]BF₄ against 2-aryl-1-arylmethyl benzimidazole **II** by [Hbim]BF₄ without any exception. These results are summarized in Table 3. The outcome of the reaction with one substrate using a mixture of our ionic liquid, [pmim]BF₄ with [Hbim]BF₄ (Wang *et al.*^{6f}) in varying proportions has also been investigated and the results are included in entries 11–13, Table 3. Significantly, 1 : 1 and 1 : 3 mixture of these two ionic liquids led exclusively to Wang *et al.*'s product, **II**, while 3 : 1 mixture of the same ionic liquids produced 22% of our product, **I**. These results clearly indicate a general tendency towards formation of 2-aryl-1-arylmethyl benzimidazole **II** and our ionic liquid, [pmim]BF₄ is powerful enough to change the usual course of the reaction leading to **I**.

This dramatic influence of ionic liquid, although very surprising, is not unprecedented.¹²

The ionic liquid (75 mol%) works here as catalyst as well as reaction medium. Presumably, [pmim]BF₄ activates the aldehyde towards nucleophilic attack by *o*-phenylenediamine forming a monoaldimine **1** which on cyclization followed by oxidative dehydrogenation by air^{6f} leads to benzimidazole (Scheme 2).

To check the role of O₂ (air) in this process two simultaneous reactions were run with 4-chlorobenzaldehyde in air and in argon. In the presence of air the intermediate **A** undergoes oxidation to provide the product **I**, while in the presence of argon condensation of **A** with another molecule of aldehyde is facilitated leading to product **II** (Wang *et al.*'s compound^{6f}) as outlined in Scheme 3.

3 Experimental section

General

The ionic liquid, [pmim]Br was prepared following a reported procedure^{13a} and [pmim]BF₄ was then obtained by a metathesis reaction of [pmim]Br with NaBF₄ also following a reported procedure.^{13b}

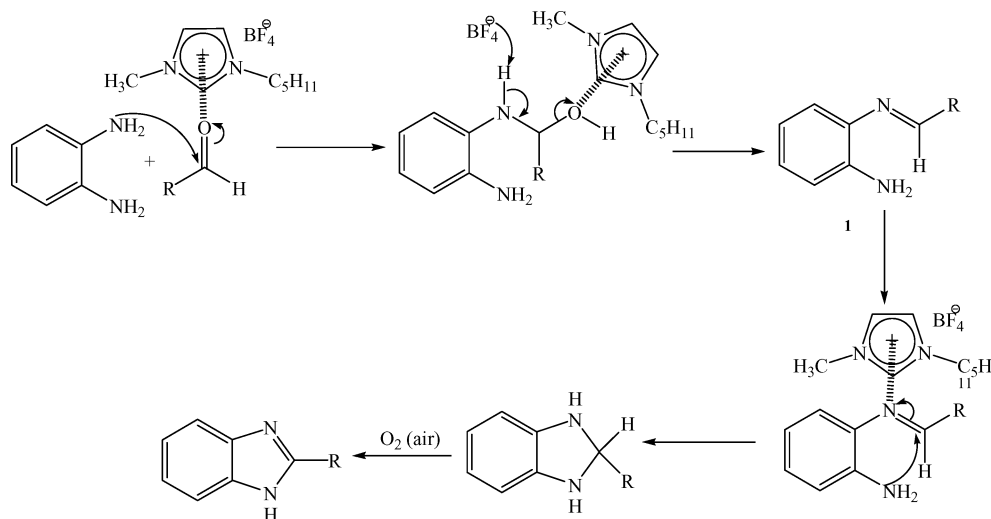
General experimental procedure for the synthesis of 2-arylbenzimidazole. Representative procedure for the condensation of *o*-phenylenediamine and *p*-tolualdehyde (entry 10, Table 2)

A mixture of *o*-phenylenediamine (108 mg, 1 mmol) and *p*-tolualdehyde (120 mg, 1 mmol) was stirred at room temperature in the presence of [pmim]BF₄ (178 mg, 0.75 mmol) in air for 5 h (monitored by TLC). After the reaction was over, H₂O (10 mL) was added and a solid product appeared. This crude product was collected by filtration and recrystallized from ethanol to afford

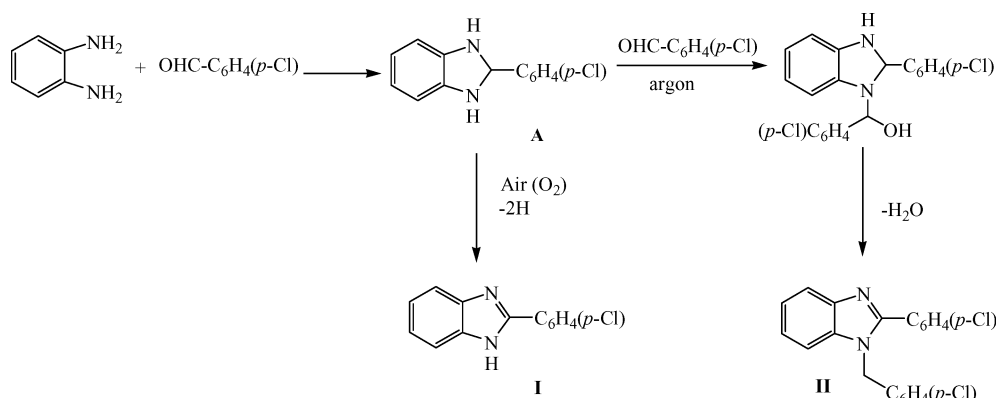
Table 3 Comparison of reaction results using [pmim]BF₄ and [Hbim]BF₄

Entry	Ar	IL	Product ratio (I : II)	Yield ^a (%)
1 ^b	C ₆ H ₅	[pmim]BF ₄	100 : 0	85
2 ^c	C ₆ H ₅	[Hbim]BF ₄	0 : 100	88
3 ^b	4-ClC ₆ H ₄	[pmim]BF ₄	100 : 0	92
4 ^c	4-ClC ₆ H ₄	[Hbim]BF ₄	0 : 100	80
5 ^b	4-H ₃ CC ₆ H ₄	[pmim]BF ₄	100 : 0	92
6 ^c	4-H ₃ CC ₆ H ₄	[Hbim]BF ₄	0 : 100	84
7 ^b	4-BrC ₆ H ₄	[pmim]BF ₄	100 : 0	92
8 ^d	4-BrC ₆ H ₄	[Hbim]BF ₄	0 : 100	86
9 ^b	4-FC ₆ H ₄	[pmim]BF ₄	100 : 0	80
10 ^d	4-FC ₆ H ₄	[Hbim]BF ₄	0 : 100	82
11 ^e	4-ClC ₆ H ₄	[pmim]BF ₄ + [Hbim]BF ₄ (1 : 1)	0 : 100	78
12 ^c	4-ClC ₆ H ₄	[pmim]BF ₄ + [Hbim]BF ₄ (1 : 3)	0 : 100	80
13 ^e	4-ClC ₆ H ₄	[pmim]BF ₄ + [Hbim]BF ₄ (3 : 1)	22 : 78	75

^a Yields refer to those of purified isolated products characterized by spectroscopic data (IR, ¹H NMR and ¹³C NMR). ^b The reaction where performed in 25 °C for the required time period as mentioned in Table 2 in the text. ^c The reaction when performed at 60 °C for the required time period as mentioned in ref. 6f. ^d The reactions were performed at 60 °C for 1 h. ^e The reactions were performed at 60 °C for 4 h.



Scheme 2 Plausible mechanism.



Scheme 3 Comparison of plausible reaction pathway in air to that in argon atmosphere.

pure 2-tolylbenzimidazole (192 mg, 92%), mp 276–277 °C (mp 277 °C^{6e}). The spectroscopic data (¹H and ¹³C NMR) are in good agreement with those reported for the authentic sample.^{6e} The ionic liquid, left in the reaction vessel was dried under vacuum and was reused for subsequent reactions.

This procedure was followed for the synthesis of all the products listed in Table 2. Although the general experimental procedure was based on 1 mmol scale reaction multimol reactions also produced similar results (entries 5 and 10, Table 2). All the products are known compounds except one (entry 12, Table 2). The known compounds were identified by comparison of their spectral data with those reported earlier (see references in Table 2). The new compound, 2-anthracen-9-yl-1H-benzimidazole (entry 12, Table 2), a pale yellow solid, mp 261–263 °C, was characterized by its IR, ¹H NMR and ¹³C NMR and HRMS spectroscopic data: IR (KBr): 3435, 3350, 2956, 2862, 1612, 1595, 1296, 1082 cm⁻¹; ¹H NMR (300 MHz, CDCl₃) δ 7.32–7.35 (m, 2H), 7.48–7.59 (m, 5H), 7.65–7.74 (m, 4H), 8.19–8.22 (d, *J* = 8.2 Hz, 2H), 8.86 (s, 1H); ¹³C NMR (75 MHz, CDCl₃) δ 114.9 (2C), 122.0 (2C), 124.8 (2C), 125.1 (2C), 125.3 (2C), 126.6 (2C), 128.2 (2C), 128.7, 130.1 (4C), 130.2, 149.0; HRMS *m/z* calculated for C₂₁H₁₄N₂ [M + H]⁺ 295.1233; found: 295.1235.

4 Conclusion

In conclusion, the present procedure using an easily available ionic liquid, [pmim]BF₄¹³ provides a very simple and efficient methodology for the synthesis of 2-aryl benzimidazoles by condensation of *o*-phenylenediamine and aromatic aldehydes. Besides mild reaction conditions (room temperature), low energy consumption, high yields, and reusability of ionic liquids, this procedure uses no hazardous organic solvents in the entire process including workup and purification. To the best of our knowledge this is the first report of condensation of aldehydes and *o*-phenylenediamine to 2-aryl-benzimidazoles, promoted by an ionic liquid without any other solvent and catalyst. Most significantly, the influence of substituent on the imidazolium unit of the ionic liquid to dictate the outcome of this reaction to produce 2-arylbenzimidazole exclusively, preventing further condensation as reported by Wang *et al.*^{6f} using [Hbim]BF₄ is remarkable and induces further investigation for useful applications.

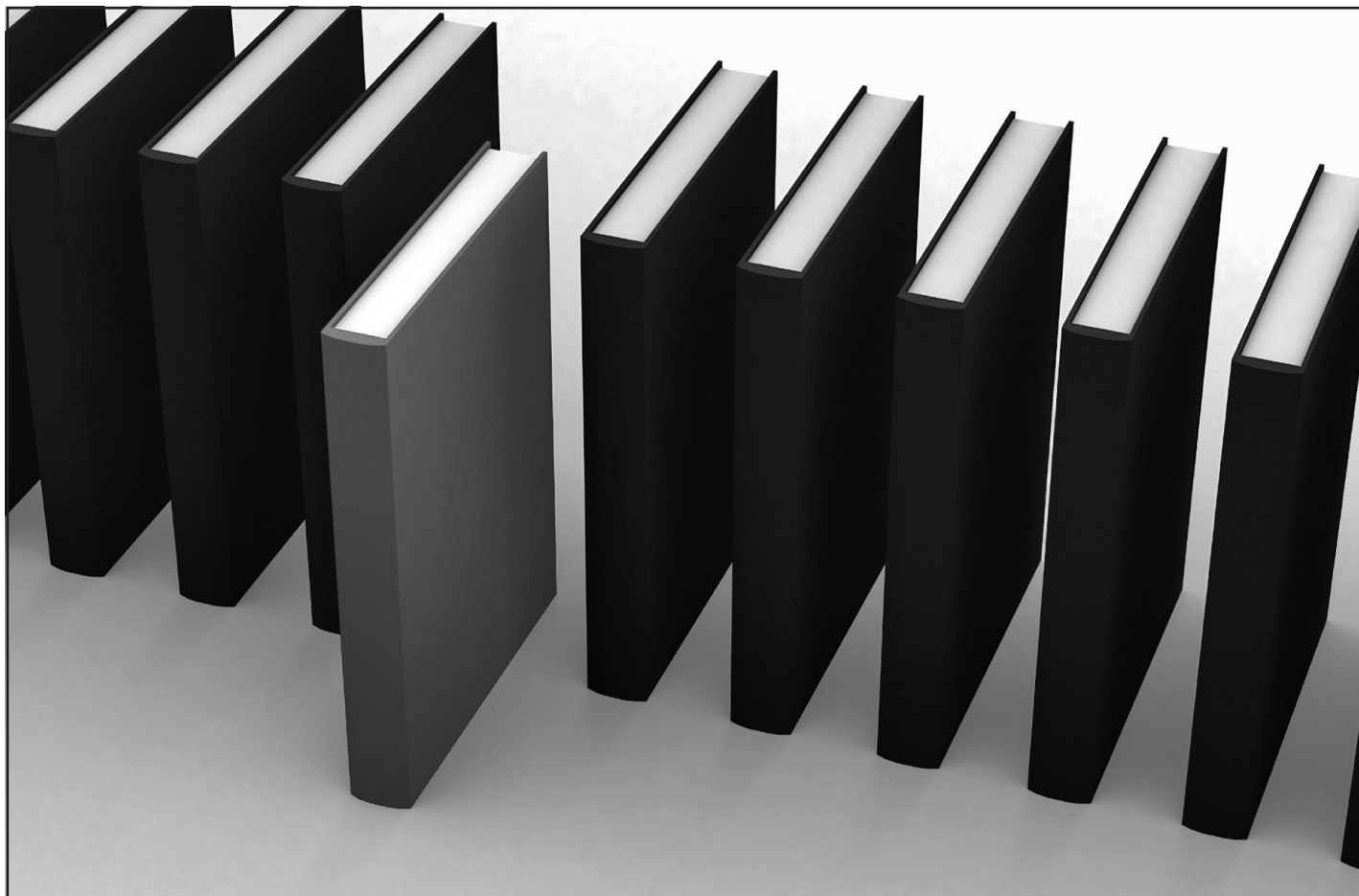
Acknowledgements

We are pleased to acknowledge the financial support from DST, New Delhi (grant no. SR/S5/GC-02/2006) for this

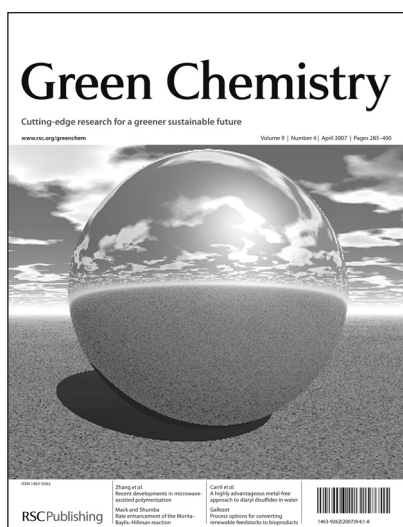
investigation. D.S. and A.S. are thankful to CSIR for their fellowships.

References

- (a) P. W. Erhardt, *J. Med. Chem.*, 1987, **30**, 231; (b) G. L. Gravalt, B. C. Baguley, W. R. Wilson and W. A. Denny, *J. Med. Chem.*, 1994, **37**, 4338; (c) K.-J. Soderlind, B. Gorodetsky, A. K. Singh, N. Bachur, G. G. Miller and J. W. Loun, *Anti-Cancer Drug Des.*, 1999, **14**, 19; (d) J. S. Kim, B. Gatto, C. Yu, A. Liu, L. F. Liu and E. J. LaVoie, *J. Med. Chem.*, 1996, **39**, 992; (e) T. Roth, M. L. Morningstar, P. L. Boyer, S. H. Hughes, R. W. Buckheit, Jr. and C. J. Michejda, *J. Med. Chem.*, 1997, **40**, 4199.
- (a) Y. Bai, J. Lu, Z. Shi and B. Yang, *Synlett*, 2001, 544; (b) E. Hasegawa, A. Yoneoka, K. Suzuki, T. Kato, T. Kitazume and K. Yangi, *Tetrahedron*, 1999, **55**, 12957.
- (a) E. Bouwman, W. L. Driessen and J. Reedjik, *Coord. Chem. Rev.*, 1990, **104**, 143; (b) M. A. Pujar and T. D. Bharamgoudar, *Transition Met. Chem.*, 1988, **13**, 423.
- (a) M. R. Grimmet, in *Comprehensive Heterocyclic Chemistry*, ed. A. R. Katritzky and C. W. Rees, 1984; *Vol. 5*, p. 457; (b) Y. Wang, K. Sarris, D. R. Sauer, and S. W. Djuric, *Tetrahedron Lett.* 2006, **47**, 4823; (c) S.-Y. Lin, Y. Isome, E. Stewart, J.-F. Liu, D. Yohannes and L. Yu, *Tetrahedron Lett.*, 2006, **47**, 2883; (d) R. N. Nadaf, S. A. Siddiqui, T. Daniel, R. J. Lahoti and K. V. Srinivasan, *J. Mol. Catal. A: Chem.*, 2004, **214**, 155.
- A. Ben-Alloum, S. Bougrin and M. Soufiaoui, *Tetrahedron Lett.*, 2003, **44**, 5935 and references cited therein.
- (a) B. Das, H. Holla and Y. Srinivas, *Tetrahedron Lett.*, 2007, **48**, 61; (b) L.-H. Du and Y.-G. Wang, *Synthesis*, 2007, 675; (c) K. Bahrami, M. M. Khodaei and I. Karianinia, *Synthesis*, 2007, 547; (d) S. V. Ryabukhin, A. S. Plaskon, D. M. Volochnyuk and A. A. Tolmachev, *Synthesis*, 2006, 3715; (e) P. Gogoi and D. Konwar, *Tetrahedron Lett.*, 2006, **47**, 79; (f) S. Lin and L. Yang, *Tetrahedron Lett.*, 2005, **46**, 4315; (g) M. Curini, F. Epifano, F. Montanari, O. Rosati and S. Taccone, *Synlett*, 2004, 1832; (h) H. Xiangming, M. Huiqiang and W. Yulu, *ARKIVOC*, 2007, 150; (i) G. Navarrete-Vazquez, H. Moreno-Diaz, S. Estrada-Soto, M. Torres-Piedra, I. Leon-Rivera, H. Tlahuext, O. Munoz-Muniz and H. Torres-Gomez, *Synth. Commun.*, 2007, **37**, 2815; (j) B. Y. Giri, B. L. A. P. Devi, K. N. Gangadhar, K. V. Lakshmi, R. B. N. Prasad, N. Lingaiah and P. S. S. Prasad, *Synth. Commun.*, 2007, **37**, 2331; (k) K. Bahrami, M. M. Khodaei and F. Naali, *J. Org. Chem.*, 2008, **73**, 6835; (l) H. Ma, Y. Wang, J. Li and J. Wang, *Heterocycles*, 2007, **71**, 135; (m) D. B. Ramachary and G. B. Reddy, *Org. Biomol. Chem.*, 2006, **4**, 4463; (n) H. Sharghi, O. Asemali and S. M. H. Tabaei, *J. Het. Chem.*, 2008, **45**, 1293; (o) X. Han, H. Ma and Y. Yang, *Russ. J. Org. Chem.*, 2008, **44**, 863; (p) M. Chakraborty, R. Mukherjee, D. Karmakar and Y. Harigaya, *Monath. Chem.*, 2007, **138**, 1279; (q) M.-G. Shen and C. Cai, *J. Fluorine Chem.*, 2007, **128**, 232.
- (a) T. Welton, *Chem. Rev.*, 1999, **99**, 2071; (b) P. Wasserscheid and W. Keim, *Angew. Chem., Int. Ed.*, 2000, **39**, 3772; (c) J. S. Wilkes, *Green Chem.*, 2002, **4**, 73; (d) V. I. Parvulescu and C. Hardacre, *Chem. Rev.*, 2007, **107**, 2615.
- (a) B. C. Ranu, A. Saha and S. Banerjee, *Eur. J. Org. Chem.*, 2008, 519; (b) B. C. Ranu, S. Banerjee and R. Jana, *Tetrahedron*, 2007, **63**, 776 and references cited therein.
- O. N. Savchenko, *Prot. Met.*, 2005, **41**, 573.
- R. G. Srivastava, *Synth. Commun.*, 1988, **18**, 1537.
- T. Itoh, *Heterocycles*, 2004, **63**, 2769.
- (a) M. J. Earle, S. P. Katdare and K. R. Seddon, *Org. Lett.*, 2004, **6**, 707; (b) B. C. Ranu and S. Banerjee, *Org. Lett.*, 2005, **7**, 3049.
- (a) V. Namboodiri and R. S. Varma, *Org. Lett.*, 2002, **4**, 3161; (b) S. Ding, M. Radosz and Y. Shen, *Macromolecules*, 2005, **38**, 5921.



'Green Chemistry book of choice'



Why not take advantage of free book chapters from the RSC? Through our 'Green Chemistry book of choice' scheme *Green Chemistry* will regularly highlight a book from the RSC eBook Collection relevant to your research interests. Read the latest chapter today by visiting the *Green Chemistry* website.

The RSC eBook Collection offers:

- Over 900 new and existing books
- Fully searchable
- Unlimited access

Why not take a look today? Go online to find out more!

RSC Publishing

www.rsc.org/greenchem

Registered Charity Number 207890



13th Annual Green Chemistry & Engineering Conference

Innovating For the Future: Progress on the Grand Challenges in the Chemical Enterprise

www.GCandE.org

JUNE 23-25, 2009 · COLLEGE PARK, MARYLAND

The 13th Annual Green Chemistry & Engineering Conference

is the premier meeting of the year for scientists, engineers, and corporate leaders engaged in the business of sustainability. If you can only attend one meeting on sustainability, this should be your top choice.

The conference will spotlight advances that have been made since the National Academy of Sciences' 2006 report, "Sustainability in the Chemical Industry: Grand Challenges and Research Needs."

Featured Speakers Include:

- **Len Sauers, Ph.D.** – Vice President, Global Sustainability, The Proctor & Gamble Company – June 24.
- **Jean-Michel Cousteau** – Founder and President, Ocean Futures Society; Executive Vice President, The Cousteau Society – June 25.
- **Presidential Green Chemistry Challenge Awards** will be presented Monday evening, June 22, before the conference in Washington, D.C. Winners will speak at the conference on June 23.

To register and reserve housing, please visit www.GCandE.org
Make your plans now to attend. We look forward to seeing you there.

green pharma summit

Implement and Operationalize
a Comprehensive Sustainability
Program to Maximize ROI



July 20-21, 2009
Ritz-Carlton • Philadelphia, PA

- **The Premier Event for Pharmaceutical Executives Looking to Achieve Efficiency Gains and Cost Savings Through Green Initiatives**
- **Extensive Agenda with Numerous Case Studies on Sustainable Green Manufacturing and Product Development**
- **Over 20 Leading Pharmaceutical and Industry Sustainability Experts**

Our Conference Commitment to Green:

- A Paperless Event-Electronic Document Distribution
- Carbon Buyback Program
- Partnering with a Green Venue
- Green Travel, Dining and Lodging Options

www.greenpharmasummit.com

Energy & Environmental Science

Linking all aspects of the chemical sciences relating to energy conversion and storage, alternative fuel technologies and environmental science

Don't miss out on your FREE access!



The current issue of *Energy & Environmental Science* is freely available online to everybody.

Free institutional online access to all 2008 and 2009 content of *Energy & Environmental Science* will be made available after a simple registration process.

Register today at www.rsc.org/ees_registration

RSC Publishing

www.rsc.org/ees

Registered Charity Number 207890